Not a drop left to drink

Robert E. Reynolds, editor

California State University Desert Studies Center

2014 Desert Symposium

April 2014

Table of contents

Front cover: snow geese at Sonny Bono National Wildlife Refuge, Salton Sea

Back cover: terns at Corvina Beach, Salton Sea

Title page: Ship Mountains from Fenner Valley

Not a drop left to drink: the field trip

Robert E. Reynolds

Redlands, California, rreynolds220@verizon.net

Day 1

Trip leaders: Robert E. Reynolds, David M. Miller, Keith Howard

What We Will See

Our route will pass through floras of the eastern Mojave Desert and, at lower elevations, those of the Colorado Desert. At Granite Pass, we enter Bristol–Danby Trough which contains closed basins that would drain to the Colorado River near Vidal, if filled. At Amboy, outcrops of Bouse Formation sediments containing the early Pliocene Lawlor Tuff (4.83 Ma) indicate that the Bristol–Danby Trough was indeed filled in the past to approximately 950 feet elevation, allowing it to connect with the Blythe Basin to the southeast. Elsewhere in the Bristol–Danby Trough, sediments containing Pleistocene vertebrate fossils suggest wetlands and vegetation supported a complex biotic community. Post-Ice Age evaporation reduced water flow along axial drainage of valleys. This allowed alluvial fans to build on slopes, to surround outlying outcrops to form inselbergs, and to overload the carrying capacity of Fenner Valley's axial drainage.

Convene at the Desert Studies Center in Zzyzx For the Day 1 240-mile trip, fill your gas tank Saturday evening and check fluids and tire pressure. Wear sturdy shoes and dress for hot or cold windy weather; bring water, hat, and sunscreen.

Proceed north to I-15. At the Zzyzx Road overpass, proceed east on I-15 to Baker.

Exit at Kelbaker Road, turn south, and proceed toward Kelso. At the first cattle guard, reset odometer to 0.0

0.0 (0.0) Cross the first cattle guard. Continue easterly on Kelbaker Road.

0.2 (0.2) The Mojave National Preserve sign on the right, elevation 935', is at the high stand of pluvial Lake Mojave. The lake was about 40 ft deep in its terminal stages about 18 to 14 ka, and very broad and shallow.

1.6 (1.4) Cross a second cattle guard. On the right skyline, Old Dad Mountain at 1:30 and the Cowhole Mountains at 2:30 flank the northern edge of Devils Playground, a region of sand ramps in the mountains and dune fields in lowlands that may be covered by flowers in the spring (Gardner, 2008). Climbing dunes bury the flanks of Little Cowhole Mountain

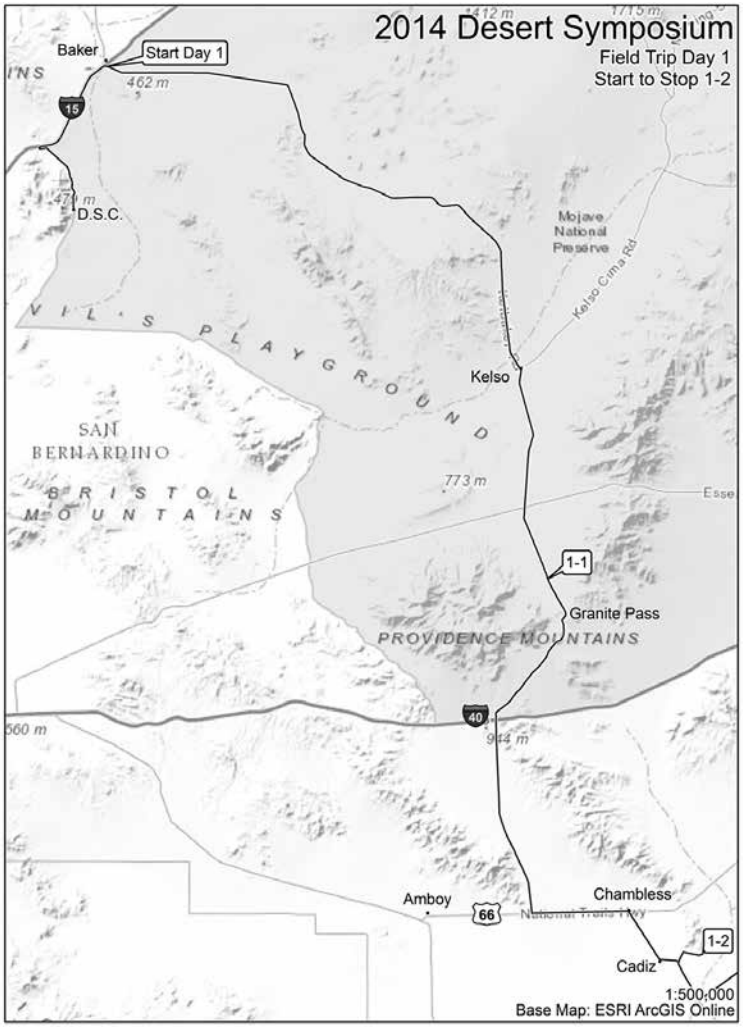

at 3:00. The dune fields came into existence when the Mojave River first began depositing in the Soda basin, supplying sand for transport. The road crosses recent fan deposits that have transported well-varnished basaltic boulders twelve miles westward from the Cima volcanic field.

5.0 (3.4) The outcrop ahead is Teutonia Quartz Monzonite. Beyond at 10:30 and at 2:00 are granitic pediment domes. The pediments lie below perched late Miocene through Pleistocene basalt flows because they erode faster (Dohrenwend and others, 1984). To the right are younger late Pleistocene basalt flows nearly coincident with the modern topography; erosion of the surrounding surface has left the flows slightly elevated.

6.6 (1.6) The road bends to the right and ascends the southern Cima volcanic field. The next nine miles we will pass prominent pediment domes. These granitic domes were tilted east by listric-normal faults, and now sit with the retreating scarp facing west and the original surface tilted east.

11.1 (4.5) Slow for an abrupt 90° curve to the right (south). Large inselbergs (isolated rocky hills rising abruptly from a flat plain) of granitic gneiss block the view on the left. These are buried by alluvial debris derived from granitic domes to the east. The road crosses an active alluvial transport surface southwest of the Cima volcanic field. Alluvial debris from floods is regularly plowed from the next two miles of road.

14.2 (3.1) Pass 17-Mile Point. The Old Government Road crosses here, at a point midway between Marl Spring and Fort Rock Spring about 17 miles to the east and Fort Soda at Soda Spring (Zzyzx) about 17 miles to the west (Casebier, 1975).

Kelbaker Road crosses a 0.17±0.06 Ma basalt flow (at road level) lying on reddened sediments, and passes the western end of higher flows that range in age from 0.17 to 0.58 Ma. Sources of these flows are vents at cinder cones located 2 miles east (Wells and Reynolds, 1990). The 0.58 Ma flow buries early to middle Pleistocene fan systems and younger flows have partly buried the 0.58 Ma flow. The basalt flow temporarily dammed all drainage from the southern part of the Cima volcanic field. The road passes through a notch cut across Precambrian rock where basalt ponded against the flank of Old Dad Mountain and the stream shifted west to cut into the older rock.

16.6 (2.4) On the left is the Black Tank flow, the youngest in the Cima field, dated by several methods as ~10,000 yr (Wells and others, 1995; Phillips, 2003). Adjacent lava tubes in older flows contain a record of accumulation of Holocene eolian dust (Reheis and others, this volume). On the right skyline between 12:00 and 6:00 are the Kelso Mountains, Radar Ridge, and Old Dad Mountain. East-tilted 10–12 Ma fanglomerates are faulted against Tertiary through Precambrian rocks (Barca, 1966). The Peach Spring Tuff (18.8 Ma) lies near the base of the fanglomerate. Neogene faults are predominantly northwest-striking, right-lateral strike-slip faults (Skirvin and Wells, 1990) but none cut the late Pleistocene basalt flows (Miller, 2012).

18.1 (1.5) Pass through a dip. On the right is a ridge of Miocene granitic boulders shed from the Cretaceous Teutonia Quartz Monzonite terrane to the east.

20.6 (2.5) Pass the junction on the left with the Aiken Cinder Mine Road, marked by a dirt pile with a sign.

21.0 (0.4) Pass a right turn toward a microwave complex on the ridge. Large landslides (Bishop, 2003) and post extensional emplacement and right lateral translation of Old Dad Mtn have been discussed (Reynolds and others, 2003).

24.0 (3.0) Pass the transmission line that runs from Hoover Dam at Boulder City, NV (west) through the Kelso Dunes past Pisgah Crater and onward to Los Angeles. Prepare for a sharp left bend in the road.

27.0 (3.0) Pass the Old Government Road running east to Cedar Canyon and Fort Rock Springs. The view east is of Kelso Wash and Cedar Wash that drain the southern New York Mountains and Mid Hills and flow through the sand dunes of the Devils Playground to enter southern Soda Lake (south of Zzyzx). The view southeast is of the prominent Providence Mountains.

35.5 (8.5) Cross Kelso Wash, here consisting of several stream threads over a broad valley bottom.

36.0 (0.5) STOP and RECONVENE in the town of Kelso at the intersection with Cima Road. Kelso Depot is to the east. The small settlement around this important railroad station and yard provided water,

gasoline, and food for travelers who, if traveling by automobile, had reached the "end of the line" in 1917. No reasonably passable road went west along the Los Angeles and Salt Lake Railroad. The only exit from Kelso Valley was north, via Cima and northwest to Valley Wells, or northeast to Searchlight, or southeast to Fenner and National Trails Highway to Needles (Thompson, 1929).

Granite Mountains, view west toward Granite Cove and Dorner's Camp. with juniper, *Opuntia*, and *Yucca*.

The Union Pacific Railroad completed laying rail to Siding # 16 (renamed Kelso) in 1905. By the end of that year, rail joined Salt Lake City, UT to San Pedro, CA. The Spanish Mission Revival style "Kelso Clubhouse & Restaurant" opened in 1924. Because of the increased efficiency of diesel engines combined with the closing of the Vulcan Iron Mine after WW II, the depot stopped most service in 1962. With dedication of the Mojave National Preserve, depot renovation began in 2002 and the building reopened in October, 2005.

Proceed south on Kelbaker Road. The Providence Mountains on the east reach 7,000 feet and support piñon and juniper forest (Gardner, 2008).

36.6 (0.6) Cattle guard. Slow to 45 mph around curve.

39.7 (3.1) Pass a left turn to the Vulcan Iron Mine, and exposures of the Bishop Ash in old alluvial fans on western slopes of the Providence Mountains (McDonald and others, 1995)

39.8 (0.1) Kelbaker Road bears south.

43.6 (3.8) Pass road west to the booming Kelso Dunes (Trexler and Melhorn, 1986), host to spring wild-flowers (Gardner, 2008) and sand-adapted animals such as the fringe-toed lizard (Presch, 2007).

44.1 (0.5) Proceed through a junction with a power line/gas line road.

44.8 (0.7) Kelbaker Road bears left (south).

47.0 (2.3) Wide west shoulder.

48.3 (1.3) Right turn to Cottonwood Spring Road.

STOP 1-1: PULL RIGHT onto shoulder. Van Curen (this volume) discusses "Monitoring air pollution in the Mojave—sources, distributions, and resources at risk." The USGS is conducting soil moisture monitoring within the Mojave Preserve to the north of Kelso, and around Cima Dome (McAuliffe and McDonald, 1995; Bedford, this volume).

48.6 (0.3) Note the light brown soil with pedogenic carbonate in a cut on the east side of the road. This pale discoloration is the most well-developed soil profile, Pleistocene in age, that we pass in the south-eastern Kelso Wash drainage basin (McDonald and others, 1995). The pale color of this soil implies less antiquity than the darker colored thick silty soils that we will see near Desert Center.

50.1 (1.5) Continue past a road on the right to Granite Cove and Dorner's Camp.

50.2 (0.1) Pass a microwave station. As we continue south, observe the development of pediments, particularly on the west (right) side of the road. Note that the tops of granite spires are concordant and mark the old (pre-Miocene) pediment surface, and stand above the more recently exhumed flat granite surfaces. We are entering the Bristol—Danby Trough, a drainage that runs southeast to the Colorado River near Vidal.

50.3 (0.1) Slow for a 30-mph curve.

51.5 (1.2) Pass the intersection east with Hidden Hills Road. The Van Winkle Mts are at 10:00.

53.7 (2.2) Pass the oval turnout on the left (east) that offers a view of the Van Winkle Mountains. Wide pediments are found on the south side of the Granite Mountains, in contrast to narrow pediments on the north side, possibly indicating tilt of the mountain block, similar to block tilting in the Cima highlands. The faults responsible for tilting are not visible, however. Support for Miocene tilt and extension in the area can be viewed from Kelbaker Road by looking southeast at the Van Winkle Hills, where a high plateau of basalt flows caps the steep-flanked hills. Farther south, these basalt flows can be shown to overlie the Peach Spring Tuff, so they are about 18 Ma in age. The Peach Spring Tuff and basalts discordantly overlie tilted basin-fill sediment, which in turn lies on granitic basement. These tilted basins, exposed along the sides of the Van Winkle Hills, demonstrate that early Miocene extensional faulting and tilt affected this general area.

53.9 (0.2) Pass a right turn to the microwave station; continue on Kelbaker Road.

54.5 (0.6) Pass a right turn to Granite Cove.

56.1 (1.6) A road on the right (west) provides a view at 10:00 of the flat surface of the granitic pediment at the south base of the Granite Mountains. These pediments are among the most spectacular in the Mojave Desert, showing deep erosion, with the concordant tops of granite spires marking the old (pre-Miocene) pediment surface standing above the more recently exhumed flat granite surfaces. Flat swaths of grus are thin veneers on pediments. The view east shows the tilted volcanics of the Van Winkle Mountains.

56.7 (1.0) Turn to look upslope along a beautifully exposed pediment that extends north toward the foot of Granite Mountains. Notice the lack of alluvial fans.

58.0 (1.3) Proceed under I-40. Miocene volcaniclastic flows and pyroclastic rocks are exposed in the Brown Buttes to the west and of the northern Marble Mountains to the east, the latter containing early Miocene volcanic domes and the Peach Spring Tuff (18.8 Ma: Glazner and Bartley, 1995). The steep west flank of the Marble Mountains is bordered by the eastern fault of the eastern California Shear Zone, which here cuts middle Quaternary deposits but apparently is not currently active (Bedford and others 2010). The fault may continue southeast toward the Iron Mountains.

62.7 (4.7) Well-developed desert pavement is visible in the saddle to the west at 10:00.

64.7 (2.0) Pass a road to Orange Blossom Wash and a microwave station.

65.4 (0.7) Near Windy Point, cross Orange Blossom Wash, which drains the Bristol Mountains and the western Granite Mountains. Jurassic granitoids to the west in the southern Bristol Mountains form dark outcrops, and the white stripes and blobs are in some places albitized granitoids (Fox and Miller, 1990) and in others are giant xenoliths of marble.

65.7 (0.3) The Hope/New Method mine is located to the west at 2:00 (Jenkins, 1995). The mine has produced a variety of uranium minerals, including rare fluoborite, a magnesium hydroxyl borate.

67.7 (2.0) At the bend in road, the Blackjack iron mine and Snowcap limestone mine are two miles west (Wright and others, 1953; Brown, 2003).

69.4 (1.7) STOP at Route 66 (National Trails Highway). Bolo Hill is to the southwest (Lerch, 1992). Bristol Lake basin is to the south. Groundwater in the western half, in the playa, is saline, while the Fenner Fan covering the eastern half of the basin contains fresh water currently used for agricultural irrigation. Clasts of opal with distinctive spherical structure suggest that the flow of Fenner Wash is in part derived from the New York and Providence Mountains around Lanfair Valley via Hackberry Wash (Reynolds and others, 1992). As Fenner Wash reaches Cadiz, it spreads to three lobes of a fan (Reynolds and others, 2003). The northern lobe is a ground water discharge (GWD) platform that was deposited into a topographic depression; the southern lobe was deposited by GWD over a near-bedrock source of fanglomerates. The central lobe of Fenner Wash contains a diverse assemblage of middle Pleistocene invertebrate and vertebrate fossils (Reynolds and Reynolds, 1992). The invertebrates (clams and snails; Reynolds and others, 2003) suggest that surface fresh water ponds were present. Thus, the wet GWD lobes of the Fenner Fan may have been active at least from middle Pleistocene time through the late Pleistocene.

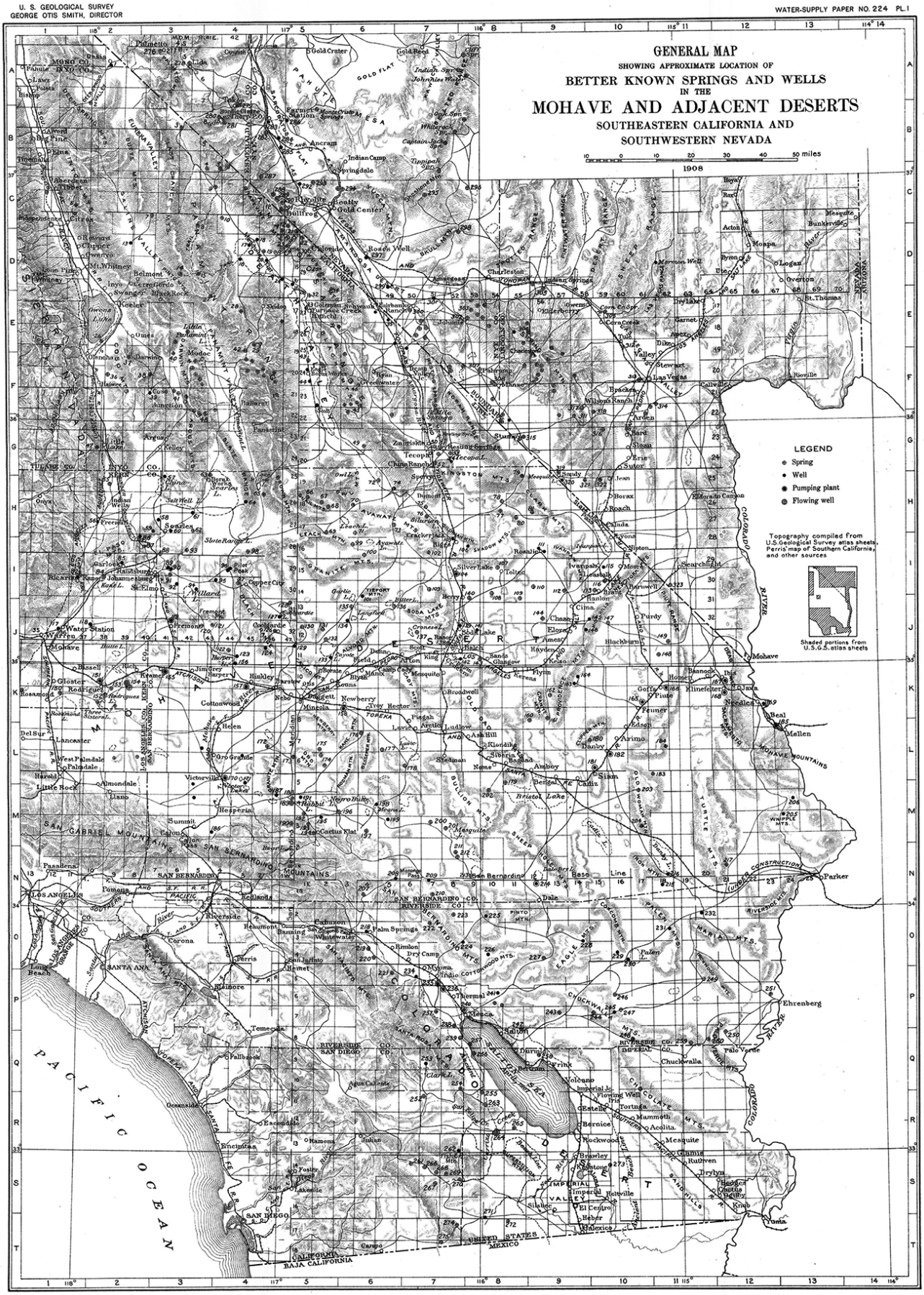
U. S. GEOLOGICAL SURVEY
GEORGE OTIS SMITH, DIRECTOR
WATER-SUPPLY PAPER NO. 224 PL. I
GENERAL MAP
SHOWING APPROXIMATE LOCATION OF
BETTER KNOWN SPRINGS AND WELLS
IN THE
MOHAVE AND ADJACENT DESERTS
SOUTHEASTERN CALIFORNIA AND
SOUTHWESTERN NEVADA
50 miles
1908
LEGEND
Spring
Well
Pumping plant
Flowing well
Topography compiled from U.S.Geological Survey atlas sheets, Perris map of Southern California, and other sources
Shaded portions from U.S.G.S. atlas sheets
PACIFIC OCEAN
CALIFORNIA
BAJA CALIFORNIA
UNITED STATES
MEXICO

The age of the Bristol Lake Basin is unknown, but several long (500 m) cores have been taken in the basin, two of which have been dated using tephra chronology (Rosen, 1991). The oldest tephra date is 3.7 million years old, but in one core there is more than 200 m of sediment below this age. The basin center core has a repeated, tilted, section at around 200 meters depth, indicating faulting in the basin center. The basin center core is also approximately 40 percent halite, with the rest being red colored mud, indicating no deep lake sediments (which would likely be green in color) through the 3.7 my record of the core (Brown and Rosen, 1995). There is very little carbonate in the basin center core, other than small calcite nodules with halite pseudomorphs. The margin of the playa is surrounded by gypsum formed by groundwater discharge (Rosen and Warren, 1990). Celestite forms at the basinward margin of the gypsum.

The evolution of the brine is currently controversial with some scientists interpreting the chemistry as needing a geothermal source to produce the current brine (Lowenstein and Risacher, 2009), and others using evidence from the age of the basin and mixing with older fluids to indicate that the composition is the result of only groundwater discharge and mineral reactions due to evaporation and concentration (Rosen, 1991; Rosen, this volume).

At the turn of the last century potable water was unavailable along many sections of the Santa Fe Railway, except as dispensed from water tenders at Amboy, a stage stop on the route to the Dale Mining District to the south (Mendenhall, 1909). East of Cadiz, along Fenner Wash at the north end of the Ship Mountains, water of excellent quality and abundance was available for travelers from railroad pumping stations at Siam and Danby. By 1921, Amboy was important enough to boast of "Water, gasoline, general supplies, and a hotel and garage accommodations" (Thompson, 1929). An oiled road crossed east over the southern Marble Mountains to Danby (gasoline and food) and Fenner (meals, gasoline and groceries). Travelers could take the southern route—"Parker cutoff"—through Cadiz Valley, or take a better road south (the Skeleton Pass Road) from Danby to the Parker Cutoff. Water was generally available at section houses along the AT&SF RR. Many travelers still preferred the longer but quicker and smoother route east to Needles, then south to Parker. Although Cadiz was the major junction of the two routes, it never boasted accommodations or supplies other than emergency water. The route south from Amboy over Sheephole Pass was very sandy on the south side of Bristol Lake and at Dale Lake, and automobiles had to "...cross it on deflated tires" (Thompson, 1929). The mines at Dale closed in 1918, and the road fell into disuse.

Amboy Crater is visible to the right (southwest), near Amboy, south of Route 66.

TURN LEFT (east) toward Chambless. The Marble Mountains are at 11:00, the Ship Mountains at 2:00, and the Old Woman Mountains are ahead on the skyline. Amboy (with gas) is behind us to the west.

74.0 (4.6) The Iron Hat mine, at 10:00, was mined in the 1940s; the iron ore (hematite and magnetite) occurred in small, shallow lenses in Cambrian? limestone (Wright and others, 1953; Bridenbecker, 2008).

76.0 (2.0) Chambless. TURN RIGHT (south) on Cadiz Road. Water from Orange Blossom Wash and Fenner Wash contributed soluble carbonates to form white ground water discharge (GWD) sediments on the east side of Cadiz Road that have been dated by optically stimulated luminescence and radiocarbon methods at about 10 ka. Fossil camel limbs support a Pleistocene age (Reynolds and others, 2003, p. 21).

79.3 (3.3) Slow: the road bends left (east) at the Cadiz railroad siding.

80.3 (1.0) TURN LEFT on dirt road toward the Latham Shale in the south Marble Mountains. The road bears right; TURN LEFT (north).

80.9 (0.6) TURN RIGHT (east) on abandoned pole line road.

81.2 (0.3) At the fork in the road, take the right branch. The left branch leads to the historic quarry in the Chambless Limestone that overlies the Latham Shale (Mount, 1980; Bridenbecker, this volume). This is one of several localities in the eastern Mojave Desert with invertebrate fossils that record an explosive radiation of life forms in earliest Cambrian time, about 530+ Ma (Finney, 2011). Trilobites and trace fossils occur in the upper portion of the Wood Canyon Formation (quartzite) and Zabriskie Quartzite that underlie the very fossiliferous (35 taxa;

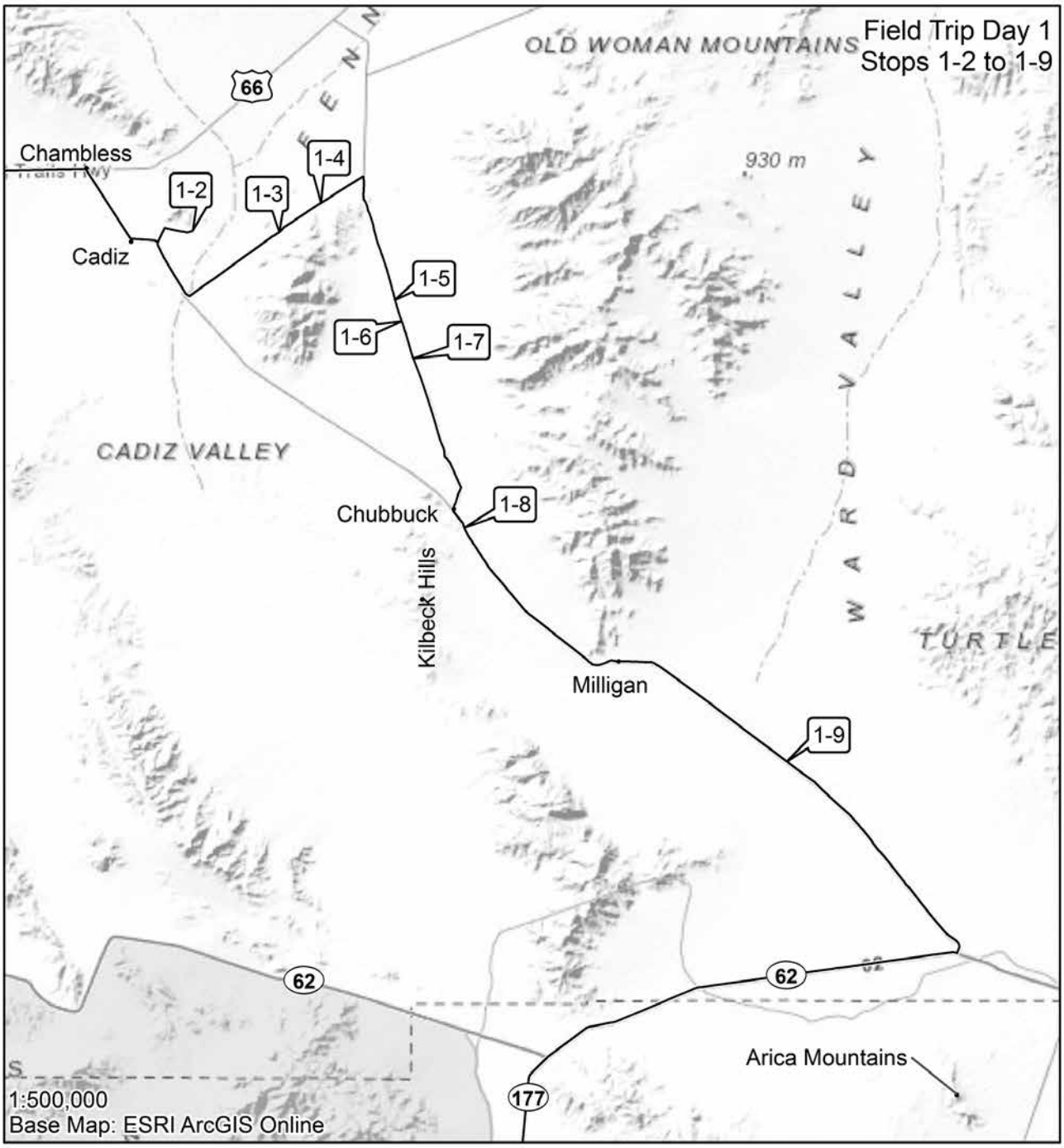

Mount, 1980) Latham Shale. The question remains: Where were the ancestors of these hard shelled invertebrates hiding in late Proterozoic time?

81.8 (0.6) BLM marker for road NS 159. The road bears left (northeast) to an outcrop.

82.1 (0.3) Wood Canyon Quartzite supports the southern tip of Marble Mountains, to the north.

82.2 (0.1) STOP, hike south to a small outcrop.

STOP 1-2. Jurassic Banded Gneiss—Southern Marble Mountains. The well-preserved upper Proterozoic and lower Paleozoic section, from Wood Canyon Quartzite through Bonanza King Formations (Bridenbecker, this volume) is intercalated with banded Jurassic gneiss similar in composition to Jurassic intrusions in the Bristol Mountains (Kenney Geoscience, 2012). RETRACE to pavement.

83.4 (1.2) TURN LEFT (south) at BLM sign 92-04.

84.1 (0. 7) Stop at pavement, TURN LEFT, cross the railroad tracks, and proceed straight (south-southeast).

86.1 (2.0), BEAR LEFT (southeast) on BLM 443 when the road forks.

86.4 (0.3) Cross west Fenner Wash.

86.5 (0.1) The road bears left (north-northeast) along a buried gas line. Note view of inselbergs ahead.

87.2 (0.7) Caution: dips at east Fenner Wash tributary. Fenner Wash drains Lanfair Valley, surrounded by the Mid Hills, Providence Mountains, and New York Mountains, and has carried distinctive spherulitic opalite from the Hackberry Mountains to the Fenner outwash one mile to the southwest of this point. The Fenner outwash contains a vertebrate fauna that may be mid-Pleistocene in age (Reynolds and Reynolds, 1992).

89.4 (2.2) View east (3:00) to a striped butte of Pennsylvanian marine sediments. To the north (left), we can see the Providence Mountains with a relatively complete Paleozoic section.

Inselbergs are northwest at 11:00. The inselbergs appear to have no bedrock pediment exposed at their bases, since they are being buried by Holocene alluvium derived from the Ship Mountains, as well as aeolian sand blown eastward from Bristol Playa. A similar scenario can be suggested for the southern Marble Mountains. However, farther northeast in Fenner Valley, the Clipper Mountains (north) and Old Woman Mountains (south) have margins with well terraced and heavily varnished fans that are being incised by drainages lateral to the Fenner wash axial drainage. The alluvial cover that buries the bases of the inselbergs reflects the reduced carrying capacity of Fenner Wash along with the influx of aeolian sand deposited by westerly winds (Lancaster, 1995) and alluvial materials derived from the Ship and Marble mountains, as well as sediment aggradation from groundwater discharge.

89.5 (0.1) Pass a road to the south that leads to metamorphosed Chambless Limestone.

90.5 (1.0) Pass caged gas line apparatus.

90.9 (0.4) The road crosses a complex of dark igneous and metamorphic rocks. PARK.

STOP 1-3. Exposure of metamorphosed lower Paleozoic rocks. Observe metamorphosed Wood Canyon Formation (the lowest-oldest of the lower Paleozoic section). Find the pebble conglomerate member which is 10% as thick as in the southern Marble Mountains 3 miles west. PROCEED northwest on the gas line road. Where the Cambrian units crop out to the south in the Kilbeck Hills and to the southeast in the Old Woman Mountains along the Scanlon thrust, they are higher in metamorphic grade and typically upside down.

91.0 (0.1) Pass a faint road to the right (south). Continue on BLM443.

92.7 (1.7) Continue on BLM 443 past a right turn (BLM 390) to the Vulcan (gold) Mine (Wright and others, 1953; Vredenburgh, this volume). The eastern margin of the valley to the southeast exhibits a thick section of early Miocene sediments with avalanche deposits (Knoll, 1993; Knoll, this volume) overlain by a thin basalt layer, more sediments, columnar basalts, and capped by the Peach Spring Tuff (18.8 Ma, Miller and others 2010). The megabreccia avalanche deposits were mined for iron ore.

Vertebrate fossils reported by Hazzard (1928) may be some of the oldest in the initial filling of mid-Tertiary extensional basins of the southeastern Mojave Block. Remains of small camels recently located in the sedimentary layer above the lowest basalt are curated in the Raymond Alf Museum. These fossils would be comparable in age to vertebrate fossils from basin filling sediments on the west side of the Little Piute Range (Reynolds and Knoll, 1992), east of the Old Woman Mountains.

93.2 (0.5) PARK. **STOP 1-4**. Vulcan Valley. View of inselbergs along the northern Ship Mountains. Each hill is supported by distinct rock types—Pennsylvanian/Permian Bird Spring Formation, Cambrian Bonanza King Formation, etc. Inselbergs to the left (north) are pinkish 18.8 Ma Peach Spring Tuff (PST) overlying basalt and hornblende-phyric andesite. Proceed northeast.

94.3 (1.1) The graded road becomes double width, with landing pads.

95.0 (0.7) TURN RIGHT (south) on NS 195, Skeleton Pass Road through the Ship Mountains. Danby Siding and Danby Mill are to the northeast.

View north through Skeleton Pass toward Fenner Valley, showing the andesite/basalt hill (MP 96.1) on the left and the hill of Peach Spring Tuff on the right.

96.0 (1.0) Stay left at the fork in the road.

96.1 (0.1) The hill on the left (east) consists of hornblende-phyric andesite overlain by vesicular basalt, in turn overlain by pinkish PST with blue schiller sanidine. Structural relations between here and Vulcan Valley (Stop 1-4) suggest that there are four north-trending, down-to-the-west faults (James and others, 1986).

96.3 (0.2) The gravel hill on the left (east) contains clasts of granitic rocks, quartz dike material, gneiss, mica schist, but no apparent Tertiary volcanics, even though the ridges north and east strike in this direction. Mapping (Knoll, this volume) suggests that these are Miocene gravels that were derived from the "structural horst" of the Old Woman Mountains to the east. The Ship Mountains Fault, four miles east at the western base of the Old Woman Mountains, separates the Miocene sedimentary and volcanic sequence from the crystalline basement complex.

96.6 (0.3) Continue south on NS 195, past the junction of NS 403 to the left (east) to Carbonate Gulch and early 1900s silver and gold mines (Vredenburgh, this volume). The Old Woman statue is at 10:00.

98.9 (2.3) Continue south on NS 195, past the junction with NS 404 to Scanlon Gulch, with silver mines worked in the early 1900s (Vredenburgh, this volume) and tungsten mines worked during World War II. The lack of varnished desert pavement in this section suggests that sediment is young and is being actively transported southwest from the Old Woman Mountains.

View west from Skeleton Pass showing basalt cap over early Miocene sediments..

99.7 (0.8) Pass a gravel bar with cobbles.

99.9 (0.2) Cross a major wash.

STOP 1-5. The west slope of the Old Woman Mountains on the left (east) exposes the Scanlon Thrust, the base of a basement-cored

fold-thrust nappe that can be traced 45 km from the Little Piute Mountains southwest through the Old Woman Mountains to the Kilbeck Hills. The thrust places inverted metamorphosed Cambrian strata and Proterozoic gneiss over a section of metamorphosed upper Paleozoic strata, all highly strained and recrystallized (Howard and others, 1987; Howard, 2002). The thrust is cut by Late Cretaceous granite and likely postdates sills of Jurassic granitoids that exhibit the same gneissic fabric as the Paleozoic strata. The upper Paleozoic rocks in turn rest structurally (on the ductile Kilbeck Fault) on a skin of tectonic schist that envelops a large Late Cretaceous pluton composed of the Old Woman Granodiorite.

100.1 (0.2) Cross a major wash.

100.8 (0.7) Pass a gravel bar with cobbles.

101.1 (0.3) **STOP 1-6**. Explore gravel bars with gneiss, schist, marble, and quartzite.

101.5 (0.4) Gravel bars with gneiss, pegmatite, marble, granite, calcsilicate rock, and schist.

101.7 0.2 Cross a major wash.

101.9 (0.2) Pass a closed route on the left (east).

102.8 (0.9) **STOP 1-7.** Gravels bars include quartzite, schist, and quartz crystal with bladed hematite inclusions. View the Cadiz Dunes Wilderness to the southwest. Caution: dip.

103.1 (0.3) Signpost. Gravel bars with marble, gneiss, schist, and quartzite.

105.2 (2.1) Road sign for NS 195.

106.4 (1.2) The white, pyramid-shaped butte due east at 9:00 consists of metamorphosed Bird Spring Fm. and Red Wall Limestone (Howard, 2002).

The Old Woman meteorite (Wasson and Willis, 1976) was discovered by prospectors in March 1976 on the ridge between Sheep Camp Spring and Brown's Wash. The second largest nickel-iron meteorite found in the United States (6070 lbs), it sparked ownership disputes between the finders, the Bureau of Land Management, the Secretary of the Department of the Interior, the State of California, the California members of the U.S. Congress, various museums in California, the Smithsonian Institution, and the Department of Justice. Ownership of the meteorite was transferred to the Smithsonian under the powers of the 1906 Antiquities Act. The Smithsonian removed a large cut for study and curation, and the main mass was returned to California where it is today on exhibit at the Bureau of Land Management's Desert Discovery Center in Barstow (Plotkin and others, 2012).

107.1 (0.7) Slow for deep wash.

109.3 (2.2) Intersection with Black Metal Mine Wash (NS 465) where there are mines for silver and lead (Wright and others, 1953; Vredenburgh, this volume).

109.4 (0.1) STOP at railroad tracks. Proceed to south side of tracks at Chubbuck (Kilbeck) Siding.

109.5 (0.1) Intersection with NS 582, Cadiz Road. TURN LEFT (east).

110.3 (0.8) Chubbuck Mill Road leads south (right) to a marble quarry.

STOP 1-8. The northern Kilbeck Hills are directly south. They contain the Scanlon Thrust and recrystallized early Proterozoic Fenner Gneiss as well as interfingering slices of Cambrian through Triassic metamorphosed sediments separated from

View east of the southern Old Woman Mountains.

structurally underlying Cretaceous Old Woman Granodiorite by the Kilbeck Fault. Detailed mapping by Eric Horringa documented the structural complexity (Howard and others, 1989). We are at Chubbuck Mill, built for the Chubbuck Limestone Mine (Vredenburgh, this volume). The road to the south reaches the Desert Group carbonate workings. Proceed southeast on Cadiz Road. Prepare yourself for dips.

A dune-filled pass near the south end of the Kilbeck Hills is the low point along the divide between Cadiz–Bristol basin and Danby basin. The divide might have restricted circulation in the Pliocene Bouse waters, which would have been only 5 to 35 m deep there.

114.5 (4.2) Slow for dip. Note reddish-brown paleosols.

117.3 (2.8) Pass the southern tip of the Old Woman Mountains. The Iron Mountains are at 2:00 across Danby Playa. The steep northeast flank of the Iron Mountains is fronted by a fault that probably extends farther northwest as the Bristol–Granite fault (Howard and Miller, 1992). Stay right at the fork; the left road has deep sand.

117.5 (0.2) Continue past BLM road NS 600 to salt evaporation ponds.

118.9 (1.4) Continue past paved crossroad south to salt evaporation ponds in western Danby Playa.

119.2 (0.3) Wooden crosses on left mark Milligan Cemetery.

119.7 (0.5) Caution: dip! Note brown paleosols. Take the right fork; the left goes to Milligan Surplus Salt works.

120.2 (0.5) Milligan Salt Plant (Vredenburgh, this volume) Refined salt is removed by truck or sometimes by rail car on the Arizona & California Railroad (ACR) which runs from Matthie, near Congress, Arizona, to Cadiz, California, south of Route 66.

120.3 (0.1) Caution: Dip! Crossroads at Milligan sign. Proceed on Cadiz Road, the middle of three branches. NS604 goes south to the salt ponds. We are crossing the western margin of the inferred Breakaway Fault to the Colorado River extensional corridor (Howard and John, 1987). Clasts of mylonitic granite in Miocene rock avalanche megabreccia deposits in the southern Turtle Mountains to the east and near the Arica Mountains to the south, both in the extensional corridor, resemble mylonitic granite in the Iron and Granite Mountains and are interpreted to have been sourced from headwalls to this fault system (Howard and John, 1987). The Colorado River extensional corridor accumulated 50 km or more of east-west extension on east-rooted normal faults that carry west-tilted fault blocks on detachment faults. Isostatic adjustments to the extensional unroofing caused the detachment faults and underlying deep-seated rocks to dome under the Whipple and Chemehuevi metamorphic core complexes (Spencer, 1984; Howard and John, 1987). The Turtle Mountains are at 11:00.

122.4 (2.1) View south of coppice dunes.

123.1 (0.7) Cross a private road for a north/south power line in central Ward Valley (no exit south).

124.4 (1.3) Pass an abandoned powerline road (no exit south to Hwy 62).

126.6 (2.4) **STOP 1-9.** Saltmarsh Siding, Danby Lake. Danby playa sediments here consist of tan silts covered by a soil profile containing carbonate kernels and root casts. Hematite-stained, cross-bedded dunes are inset within these playa strata. The elevation (630+) of highest playa sediments indicates the Pleistocene playa elevation, and vertebrate fossils (Camelops sp., Equus sp., Equus sp., (sm); Reynolds and Reynolds, 1992) suggest a late Pleistocene Rancholabrean NALMA.

Halite (NaCl), gypsum (CaSO4. 2H20), and celestine (SrS04) mineral concentrations occur to the southeast (Kupfer and others, 1957; Howard, 2002), along with curious rings of gypsum and halite apparently associated with salt tolerant plants (Reynolds and Schweich, this volume).

Note the lack of surface exposures of the Bouse Formation despite outcrops of Bouse at higher elevations north of Amboy. In this area, the Bouse Formation is inferred from marine and brackish water fossils in cores at depth (Smith, 1970; Brown and Rosen, 1992, 1995; McDougall, 2008).

127.1 (0.5) Pass a compressor station on the south side of the road.

127.7 (0.6) Coppice dunes are to the right (south).

130.7 (3.0) Dip.

131.2 (0.5) Pass a road running west to historic salt evaporation ponds.

131.8 (0.6) Dip.

132.7 (0.9) Dip. Dips continue for the next 4+ miles.

137.1 (4.4) STOP at Hwy 62. Watch for traffic, TURN RIGHT (west) toward Desert Center. Metamorphosed Mississippian to Permian strata in the Arica Mountains due south, straight ahead, are similar to those exposed in the Old Woman Mountains and Kilbeck Hills (Stone and others, 1983).

147.0 (9.9) Pass Iron Mountain Road to Colorado River Aqueduct pumping station. Colorado River water behind Parker Dam, 15 miles northeast of Parker, Az, is pumped into Gene Wash Reservoir (el: 740') and Copper Basin Reservoir (el: 1030') to gain elevation. This aqueduct carries water through a series of siphons, tunnels and open aqueduct westward. To pass through high desert mountains there are pumping stations at Iron Mountain and Hayfield (ahead). When reaching Cabazon, in San Gorgonio Pass, a tunnel (el:1680') was drilled through Mt. San Jacinto to the town of San Jacinto, where pipes carry water to Lake Mathews, near Corona, in western Riverside County.

147.6 (0.6) Road bends southwest; cross the Colorado River Aqueduct.

148.6 (1.0) Patton's camp. World War II Army exercises led by General George S. Patton were based out of several camps, now considered historical relics. Iron Mountain was one of the largest. The Granite Mountains lie to the south, the Iron Mountains to the northwest. Both are underlain by Cretaceous granitic rocks (Miller and Howard 1985) but those in the Iron Mountains are strongly mylonitized by down-to-the-west unroofing at the end of the Cretaceous.

149.1 (0.5) Riverside County line. Ahead on the skyline are the Coxcomb Mountains, another mountain range composed mainly of Cretaceous granite.

152.0 (2.9) View of pediment. Proceed south.

153.6 (1.6) Continue past a powerline road.

154.3 (0.7) Stop at the junction of Hwy 62 and 177. Proceed south on 177 toward Desert Center. At the southwest quadrant of the intersection, note pedogenic carbonate in reddish arkosic sediments.

155.3 (1.0) Slow for curve. Notice the lack of fans at the base of the hill intersecting with the pediment at 9:00 (east).

164.2 (8.9) Continue past a left turn (east) to Palen Pass.

166.0 (1.8) Continue past a right turn (west) to the Coxcomb Tunnel of the Colorado River aqueduct.

169.0 (3.0) Slow; road bends right (southwest). Pleistocene ground water deposits and greenish pond or lacustrine sediments of Palen Playa are to the left (east) at a maximum elevation of 490 feet. The source of water in Pleistocene time may have been from Palen Wash, behind us to the north, meeting strong drainage from Pinto Basin to the northwest, where Pinto Wash drains the basin surrounded by 4,000 foot peaks. It has been speculated (Reynolds and others, 2008, p. 11) that a Big Meander of the Colorado River filled Chuckwalla Basin to the east with brown silts to an elevation of more than 600 feet during mid-Pleistocene time.

171.5 (2.5) Note the Pleistocene paleosols in fanglomerate exposed in road cuts on the west side of the road.

172.5 (1.0) Desert Lily preserve. The desert lily (*Hesperocallis undulata* A. Gray) prefers dry, sandy flats below 2,000 feet. The plant's bulb lies dormant until ideal conditions are present for blooming. With appropriate weather conditions, the stem will sprout from a bulb buried two feet underground, producing a tall stalk with a cluster of white flowers.

In a manner somewhat similar to the Parry's beargrass (*Nolina parryi* S. Watson) seen at Pioneertown (Reynolds, 2012, p. 12), our evolving knowledge of the genetic relationships among plants through molecular analysis has moved the desert lily (*H. undulata* A. Gray) from Liliaceae in the broad sense as defined by Cronquist in the 1980s, to the Asparagaceae along with the agaves (Stevens, 2001+), to a separated agave family (Agaveaceae), with agaves, yuccas, and hostas (Bogler and others 2005), and

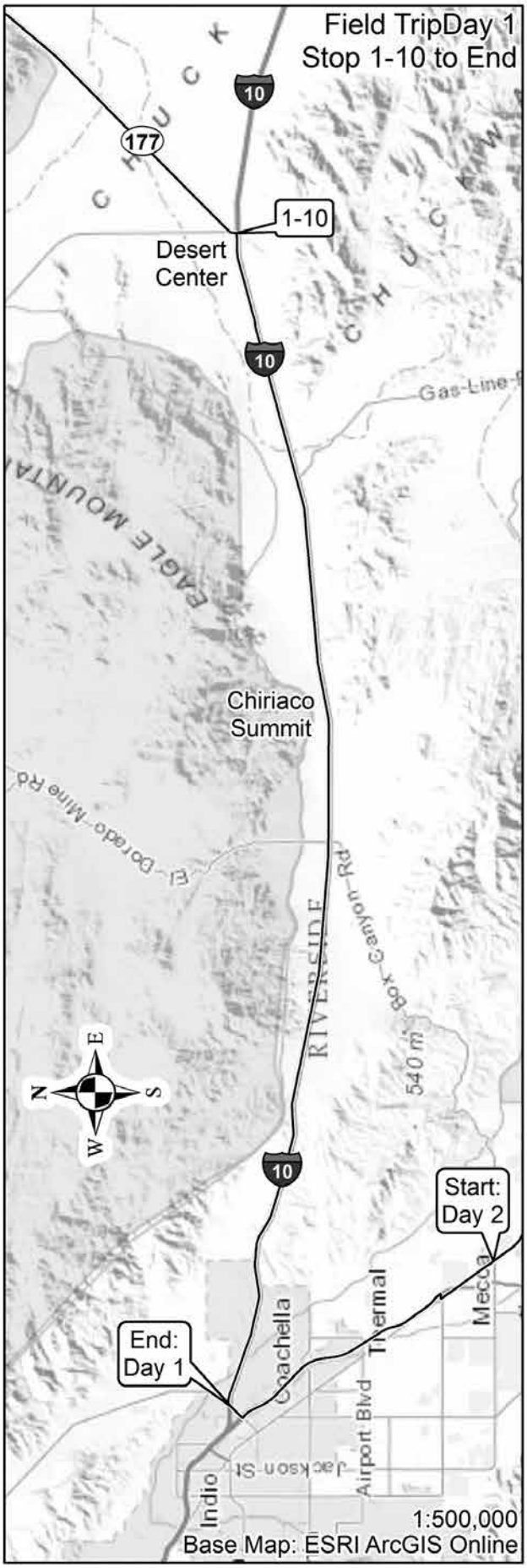

finally, perhaps, to its own family, Hesperocallidaceae (Kim and others 2010).

180.0 (7.5) Pass Oasis Road to Lake Tamarisk.

182.0 (2.0) Kaiser Road, Rte 2, enters from the right. After WWII, the Eagle Mountain iron replacement deposit in limestone and quartzite provided most of the ore for Kaiser Steel's smelter in Fontana between 1948 and 1982 (Murdoch and Webb, 1966; Dubois and Brummett, 1968; Pemberton, 1983).

North of here, drill holes reveal several hundred feet of buried clay deposits (Geopentech, 2003). Although age and origin are unknown, the clay deposits are at an elevation below the high stand of the Bouse Formation, spanning depths from ~900 to 600 ft elevation, and may represent a western arm of the water body (Reynolds and others, 2008; Spencer and others, 2008, Fig 1; Miller and others, in press [Geosphere]).

Late Pleistocene vertebrate fossils were recovered from paleosols in the western Chuckwalla Valley (Raum and Aron, this volume)

182.2 (0.2) Stop and Park prior to west bound onramp and underpass for I-10 at Desert Center.

STOP 1-10. Walk south to the many thick paleosols exposed in the walls under the overpass. Discuss the potential for paleosols to contain paleontological resources that might provide temporal constraints on Chuckwalla Valley formation.

In this area we transition from northwest-striking faults of the eastern California Shear Zone to east-striking (left-lateral) faults of the Joshua Tree terrane. Recent study by Langenheim and Powell (2009) demonstrated 6-8 km offset on many of the faults.

Proceed westbound on I-10 toward Indio.

191.7 (9.5) Pass Red Cloud Mine Road offramp. The Hayfield plant (at 2:00) pumps Colorado River Aqueduct water uphill approximately 455 feet, to an elevation of 1820 feet. From that elevation, it flows west, down grade across the northern Coachella Valley where it crosses the Twentynine Palms Highway at elevation 1615 (Reynolds, 2012, p. 14). It proceeds westward to Cabazon, where it enters the San Jacinto Tunnel at about 1,600 feet. Cross over the Salt Creek Railroad (see Day 2).

196.9 (5.2) Pass the Hayfield Road exit.

200.9 (4.0) Chiriaco Summit, formerly Shavers Summit, was renamed after Joe Chiriaco, who opened roadside services as the area was reached in 1938 by the paved Interstate Highway 10. Chiriaco served Gen. Patton's troops, and erected the Patton Memorial on the site of Camp Young, part of the World War II Desert Training Center, eventually becoming the home of the Gen. Patton Memorial Museum

204.5 (4.6) Continue past Cottonwood Springs Road, the exit to Mecca and 29 Palms. The route north to Twentynine Palms passes through interesting floral zones as it reaches the elevation of Joshua trees and huniper (Cornett, this volume). Box Canyon, to the south. was the route from Indio to Shaver's Summit before I-10 was in use.

205.0 (0.5) View of Santa Rosa Peak (8035 ft) and Toro Peak (8694 ft.). In Shavers Valley to the southwest, playa silts and clays were briefly ponded against the Clemens Well Fault or Hidden Spring Fault before breaching to flow through Box Canyon (Bridges and Meek, 1993).

219.5 (14.5) View of Mt. San Jacinto (elev. 10,834 feet) and Mt. San Gorgonio (elev. 11,503 feet). We are dropping into the Coachella Valley. Ahead, in the northern Coachella Valley of the Salton Trough, are outcrops exposing the Miocene marine Imperial Formation (6.3–4.3 Ma; Dorsey and others, 2011; McDougall and others, 1999; McDougall, 2008).). In the Super Creek area the Imperial contains older (10 Ma) reworked microfossils providing evidence of an earlier marine incursion (McDougall, 2008). To the southwest, the Imperial Formation is exposed in ABDSP (Jefferson and Lindsay 2006; Carreno and Smith, 2007). The older deposits of this marine incursion offer important information on the source of clasts from nearby highlands, as well as producing a diverse fauna of marine invertebrates (Powell, 1985, 1986, 1987; Carreno and Smith, 2007; Powell and others, 2011; LaFollette, 2012; Rugh, this volume) and fossil fish taxa (Roeder, 2005; Roeder and Huddleston, 2011; Roeder, 2012) that are related to fish populations in the Caribbean and Atlantic oceans, while the younger outcrops produce taxa that seem related to the northern Gulf of California (Roeder, 2012; Bahar, this volume).

Interstate 10 passes through the Palm Springs Formation, from which a late Pliocene / early Pleistocene fossil flora has recently been recovered northwest of Dillon Road (Raum and Aaron, this volume).

227.3 (7.8) Cross the Coachella Canal (el. 41 ft above amsl). This canal runs north, starting at the All American Canal at elevation 172 ft., 15 miles west of the Yuma, and east of El Centro. The All American Canal starts miles 16 miles north northeast of Yuma at Imperial Dam (El.: 182 ft).

228.8 (1.5) EXIT at Dillon Road.

229.0 (0.2) Stop, TURN LEFT onto Dillon Rd.

0.6 (0.6) STOP light at Harrison.

0.7 (0.1) Cross under SR 86 and TURN LEFT, enter SR 86 southbound toward Mecca. Proceed south to reach Ave. 66 (SR 195), TURN LEFT (E) on SR 195 and proceed 0.8 miles to Start Day 2 at SR 111.

What we have seen: Our Day 1 route has led us across the internally drained Soda Lake Basin, and its eastern tributary Kelso Wash. Upon entering the Bristol-Danby Trough, we reached elevations once covered by the arm of the brackish Bouse Embayment. After Bouse time (4.83 Ma) there is no evidence that the trough contained enough water to drain to the Colorado River. Fenner Wash, flowing during the Pleistocene, is now being choked be debris from adjacent slopes, and playas in the trough are being mined for salt. Finally, we dropped into the Salton Trough, to explore the complex history of marine incursion, followed by fluctuating fresh water flows from the Colorado River.

Day 2

Trip Leaders: Robert E. Reynolds, Mark Roeder, David Lynch, Paul Adams, and Victoria Langenheim

0.0 (0.0) RESET ODOMETER. from SR 86S at junction with Avenue 66 (SR 195), TURN LEFT (east) on SR 195. Proceed 0.8 miles and pull right onto the shoulder of Lincoln Street just before SR 111.

PARK and reconvene on Lincoln Street immediately west of SR 111.

0.8 (0.8) PROCEED EAST a few feet to SR 111. TURN RIGHT (southeast) on Hwy 111.

7.3 (6.5) Continue past Palm Island Drive.

7.7 (0.4) Continue past Cleveland St.

9.5 (1.8) SR 111 bears south past North Shore. We are driving about 200 m SE of and parallel to the trace of the San Andreas fault zone (Jennings, 1967).

9.7 (0.2) Bay Drive. Look left (northeast) to see a low pressure ridge of the San Andreas fault about 300 m away.

10.6 (0.9) Desert Beach Drive

11.7 (1.1) Salton Sea State Park headquarters is to the right (west). Approaching Parkside Drive, we are driving directly along the San Andreas fault. TURN LEFT (east) onto Parkside Drive. Cross railroad tracks and proceed toward Dos Palmas Spring.

13.5 (1.8) TURN RIGHT (south) on Desert Aire Drive at T intersection.

13.9 (0.4) TURN LEFT (southeast) at the stop sign onto dirt power line road.

14.6 (0.7) TURN LEFT (east) on dirt Sea Breeze Road (a sign points toward Dos Palmas Preserve). As we drive east, we are ascending a low ridge and will reach an elevation of 50 feet above sea level. This ridge is a south-trending spit that was incised on east and west sides by the high stand of Lake Cahuilla at +40 feet elevation around 16 - 14 Kya (Li, 2003). The slopes to the west and south have stepped shorelines carved by the retreat of Lake Cahuilla, and in places, are dotted with rock rings used as fish traps by Native Americans.

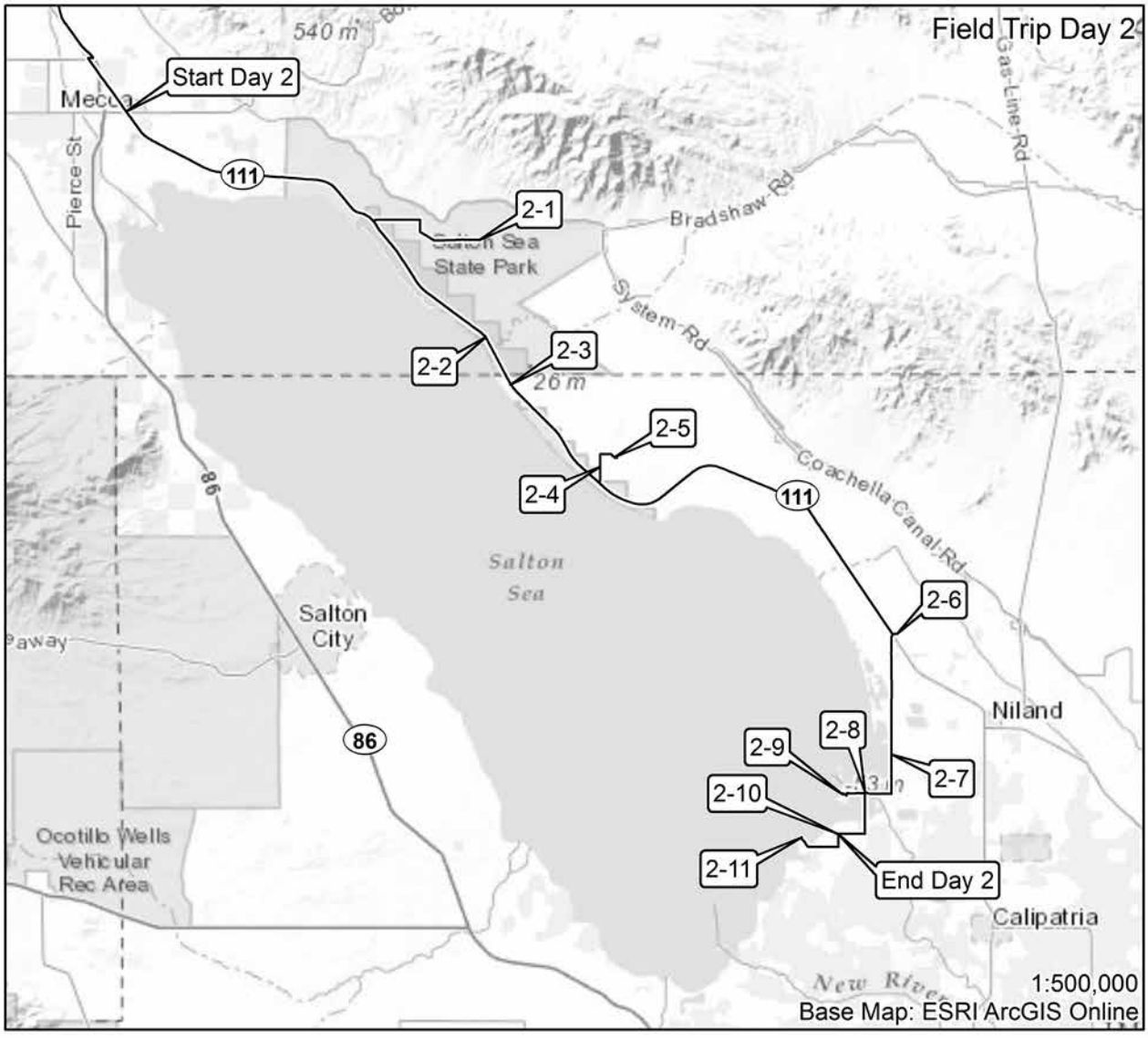

View east from ridge toward San Andreas Springs Oasis (right center) and Dos Palmas Oasis (left distance). We are +50' AMSL, about ten feet above the high stand of Lake Cahuilla.

Our route descends into a basin that was created when westerly running Salt Creek encountered sediments disrupted by the San Andreas fault. The antecedent drainage then ran southwest (to MP 27.1, Stop 2-2). See Cornett, this volume, for a review of the history and natural history of Dos Palmas Oasis.

16.3 (1.7) **STOP 2-1:** Dos Palmas gate and parking lot. San Andreas Springs Oasis is to the right (south). The Bradshaw Wagon Road to the goldfields of La Paz on the Colorado River and other "bonanzas" in Arizona was developed in the early 1860s. The route ran along Indian trails from San Bernardino east through San Timoteo Canyon and San Gorgonio Pass, past Whitewater to Agua Caliente (Palm Springs), Sand Hole, and then to Dos Palmas Oasis. The road continued east on the south side of the Chuckwalla Mountains to Clemens Well, Canyon Spring, Tabaseco Tank, and Chuckwalla Spring (Gunther, 1984) and crossed the Colorado River near the present Blythe and Mineral City (renamed Ehrenberg in 1869 after Hermann Ehrenberg, who surveyed the townsite in 1863). Ehrenberg was murdered on October 9, 1866 at Dos Palmas (Ornish, 1989).

A variation of this road, pioneered by the Frink brothers, took an even more direct route somewhat more northerly from Canyon Spring to the river. The Frinks also helped develop a lesser-used variation which ran almost directly from Dos Palmas to Yuma, passing east of the (Glamis) sand dunes. (Haenszel and Reynolds, 1975; Brunzell, 2008; Ross, 1992; Tong and Lutz, 2002).

RETRACE to SR 111.

18.1 (1.8) TURN RIGHT (northeast) at the stop sign.

Ferrum Junction and maintenance building.

18.7 (0.6) TURN RIGHT (north) onto Desert Aire Drive.

19.2 (0.5) TURN LEFT (west) on Parkside Drive.

21.0 (0.8) Stop at Hwy 111. TURN LEFT (southeast).

22.5 (1.5) Continue past the to Mecca Creek campground.

23.8 (1.3) Pass Corvina Beach.

26.4 (2.6) Ferrum Junction (after 1956, just Ferrum), immediately east, marks the junction of the Eagle Mountain Railroad (EMRR) with the Southern Pacific Railroad (SPRR). The Eagle Mountain Iron Mine was connected to the Kaiser Steel Mill in Fontana by the SPRR and the 50-mile-long EMRR that ran south from the mining town, then westerly along Salt Creek to this siding. Constructed between 1947 and 1948, the EMRR was used until 1986 to haul iron-ore in five to eight 100-car trains running each week.

Sections of the EMRR line were used in the 1966 movie "The Professionals" starring Lee Marvin, Burt Lancaster, Robert Ryan, Woody Strode, Jack Palance, Claudia Cardinale, and Ralph Bellamy. The scenes where the four men cross the border at a wooden bridge is actually the first railroad bridge north of Ferrum over the Salt Creek Wash. In 1986, the film "Tough Guys" with Burt Lancaster and Kirk Douglas was also shot on the EMRR. After filming ended, the locomotive was backed all the way from the Eagle Mountain train yard to Ferrum, where it could turn around (Eagle Mountain Railroad, 2013).

Dark scatters of iron ore remain at the siding, along with a maintenance shed that could house railroad rolling stock. This bomb-proof structure was built with walls of wooden ties stacked within vertical sections of steel track, a roof of layered steel track, thick rubber sheeting, and a thick cover of dirt.

26.9 (0.5) Prepare for a left turn. Watch traffic ahead and behind.

27.1 (0.2) TURN LEFT across CA 111 and PARK just north of the trestle between the railroad tracks and Hwy 111.

STOP 2-2: Salt Creek. Walk under the trestle about a quarter mile northeast to where the creek has incised the bank, revealing the San Andreas fault scarp (note the sharp color contrasts on either side of the fault). Salt Creek displays at least 280 m right lateral offset. RETRACE to CA 111 and continue south.

27.5 (0.4) Cross Salt Creek and continue past Salt Creek Beach and campground.

28.8 (1 .3) Cross into Imperial County.

28.6 (0.4) PARK on the right at the abandoned café.

STOP 2-3: Discussion Stop. "In the Bat Cave Buttes/ Salt Creek area of Durmid Hill, the San Andreas Fault coincides with a complex magnetic signature of high-amplitude, short-wavelength anomalies. Gravity data modeling indicates a steep dip for the San Andreas Fault, and defines a deeper basin, extending southeast, suggesting that the San Andreas Fault zone is wider than indicated by its mapped surface trace" (Langenheim, this volume). CONTINUE south on Hwy 111.

33.7 (5.1) Slow for left turn. Watch for traffic.

33.9 (0.2) TURN LEFT (north) onto Range Road. Cross railroad tracks. Proceed north

34.4 (0.5) **STOP 2 -4**: Resistant sandstone. Examine resistant beds of silty, well sorted, planar bedded sheets of fluvial sandstone. Can we locate clasts that would provide source data? The Late Pleistocene Brawley Formation mapped by Dibblee (1954, 2008) forms badlands here in the Durmid Hills and in the Superstition Hills and San Felipe Hills on the west side of the Salton Sea. Beds of the Brawley Formation are either steeply dipping, upright, or overturned ib the San Andreas fault zone in the Durmid Hills. This sedimentary unit consists of at least 2,000 feet of gray clay, silt, sand, and pebbles (Morton, 1977) and is present in the subsurface over a large portion of the Salton Trough. Sediments of the Brawley Formation range in age from about 1.1 million years to about 0.5-0.6 Ma (Kirby and others, 2007).

The Brawley Formation stratigraphy records a series of periodic inundations of the Salton Trough by waters of the Colorado River, repeatedly inundating the trough to form large freshwater to brackish lakes. The lithologic record of the Brawley Formation consists mainly of alternating lacustrine, fluvial and deltaic deposits representing the Colorado River influence, and to a lesser extent aeolian, playa (dry lake), and alluvial sediments.

Here in the Durmid Hills, marine fossils consisting of articulated remains of razor clams (*Tagulus*) and fish called a croaker (Sciaenidae). That site, about one mile from here, is evidence of marine incursion into this area during the late Pleistocene. Other papers (Roeder and Calvano, this volume; Roeder and Remeika, this volume) comment on recent paleontological finds in the Brawley Formation in the Superstition Hills and elsewhere.

34.9 (0.5) TURN RIGHT and proceed east along the berm.

35.5 (0.6) Pass the west workings of the Bertram Mine.

35.8 (0.3) **STOP 2-5**: Central workings of Bertram Mine, developed for glauberite [$Na_2Ca(SO_4)_2$] in clay nodules, thenardite [$Na_2(SO_4)$], and bloedite [$Na_2Mg(SO_4)_2{\cdot}4H_2O$]. The large white chunks dotting the diggings are thenardite, used for making paper and glass, in detergent, and as a chemical (Morton, 1977). Thenardite may condense directly from solution or by dehydration of mirabilite [Na2(SO4)·10H2O]. Note the typical sharp dissolution structures. Walk east to the deep cuts. Sediments are truncated and folded by the San Andreas fault; their colors (white, brown and gray-green) are reminiscent of the soils at Salt Creek. RETRACE to CA 111.

36.7 (0.9) TURN LEFT (south) on Range Road.

37.8 (1.1) Stop. TURN LEFT (south) on Hwy 111.

40.1 (2.3). Bombay Beach. Cross the San Andreas fault just east of Bombay Beach turnoff. Bombay Beach, at elevation -223 ft, may have the lowest elevation of any community in the United States.

42.9 (2.8) Pass Hot Mineral Spa Road.

46.0 (3.1) Pass the Border Patrol station and a turnoff to a boat ramp.

46.3 (0.3) Pass Frink Road. Frink is an unincorporated community located on the Southern Pacific Railroad at an elevation of 171 feet below sea level, and 211 feet below the high stand of Lake Cahuilla. Horace Monroe Frink had been an army scout with Carson and Fremont and was a personal friend of Brigham Young. In 1854 he and his brother homesteaded a ranch in San Timoteo Canyon, between Redlands and Riverside. The brothers also established a wagon freighting business, which included hauling supplies to Col. Washington's Base Line Survey party in 1855–1857, the Arizona mines in the 1860s, and survey and construction crews for the Southern Pacific Railroad line through San Gorgonio Pass and Imperial Valley in the early 1870s (Haenszel and Reynolds, 1975).

52.4 (6.1) Pass a sign marking the Wister Unit. Watch for traffic and prepare to turn left.

52.5 (0.1) Wister (formerly Davis) Road & Gillespie Road. Watch for traffic. TURN LEFT across railroad tracks on Gillespie Road.

52.7 (0.2) **STOP 2-6**. PARK on road shoulder. [CAUTION: respect private land]. The southern Salton Sea area has a large number of mound springs, all driven by CO_2 which rises from the hydrothermally altered carbonates of the Colorado River delta. Walk east to a large, active spring mound. The pool is about 25 m across and gently bubbles with CO2. A large area of mound springs is found 300 m north (accessed over the bridge). It consists of four elevated springs and numerous smaller structures on a foundation of aragonite + dolomite and halite. The water is at ambient temperature and slightly acidic (pH 6.5–7.0). Minerals found here are mostly carbonates and include aragonite, dolomite, halite, hydromagnesite, magnesite, nesquehonite, northupite, polyhalite, and thenardite. (See Adams and Lynch, this volume). Return to Hwy 111.

52.9 (0.2) Stop at CA 111, watch traffic. Jog southwest to Wister (formerly Davis) Road and head south.

53.5 (0.6) To the right is a seasonal campground and a road to the Mud Pots, which are one mile west.

57.5 (4.0) **STOP 2-7**: Adobe & concrete ruins on the left (east) at the junction of Adobe and Pound roads are the remains of a small dry ice factory that used CO_2 from wells across the road. Remnants of the wells are still visible (Vredenburgh, this volume).

59.0 (1.5) "Davis-Schrimpf" mud volcanoes (Lynch and Hudnut, 2008) and currently active fumaroles. The EnergySource geothermal power plant, immediately north, was installed in 2011. The mud volcanoes are on private property.

59.1 (0.1) TURN RIGHT on Schrimpf Road. There are often active beehives in this area, so roll up your windows!


Remains of the dry ice factory at Stop 2-7, December 2013.

60.1 (1.0) **STOP 2-8** at Garst Rd. Walk to discuss Mullet Island & fumaroles. DANGER: Roads may be impassable, fumaroles are boiling hot and dangerous. The fumaroles are 1.3 miles to the north and consist of three steaming hot fields of mud pots and mud volcanoes (gryphons and salses, respectively) and several that are still under water (Lynch, Hudnut and Adams 2013). They have been episodically submerged since the Salton Sea formed in 1905. In the 1930s they were popular tourist attractions, but were submerged by the rising sea in the late 1950's. They were most recently exposed in 2007. In addition to CO_2, they emit hydrogen sulfide and ammonia (Tratt and others 2011). A number of ammoniated minerals have been found in and around the gryphons and salses: boussingaultite [$(NH_4)_2Mg(SO_4)_2 \cdot 6(H_2O)$], koktaite [$(NH_4)_2Ca(SO_4)_2 \cdot (H_2O)$], lecontite [$(NH_4,K)Na(SO_4) \cdot 2(H_2O)$], mascagnite [$(NH_4)_2SO_4$], Sal ammoniac [$NH_4Cl$], and tschermigite [$NH_4AlSO_4 \cdot 12(H_2O)$]. The nitrate mineral nitratine is associated. Other minerals found at the fumaroles include sulfur, halite, gypsum, blödite, konyaite, mirabilite, thenardite, and tamarugite (Adams and Lynch, this volume).

Retrace to corner of Garst and Schrimpf Roads.

TURN SOUTH on Garst, cross the Alamo River and take an IMMEDIATE RIGHT TURN (west) on Red Island Road, and proceed to Red Island.

60.9 (0.8) Stop. TURN LEFT at stop sign. An RV camp is to the right.

61.0 (0.1) TURN RIGHT between piles of obsidian and bear right. The rhyolitic obsidian from Red Hill and Obsidian Butte contains distinctive small, white feldspar phenocrysts. Blocks and slabs are flow banded; some bands may be only 2 mm thick. Slab interfaces show stretched chill fractures, ropey structures, and transported pumice clasts.

61.1 (0.1) PARK off the road in a saddle between two obsidian buttes.

STOP 2-9: Walk a hundred yards north up the butte to see hot vents at the summit. Lynch and Adams recorded six steaming vents. From the summit, the Mullet Island land bridge and steaming fumaroles are visible.

Muffler (1990) describes the Salton Buttes as


The "Davis-Schrimpf" mud volcanoes.

Large obsidian clast in volcanic sediments at Red Hill.

> "….five small rhyolite domes extruded onto Quaternary sediments of the Colorado River delta. Rock Hill and Mullet Island are simple domes; Mullet Island is notable for its symmetrical "onion-skin" pattern of foliation, attributed to endogenous growth. Obsidian Butte consists of a central dome surrounded on all sides by a single flow. Red Island is made up of two domes, each mantled by subaqueous pyroclastic deposits. Xenoliths of basalt, partly melted granite, deltaic sediments, and their hydrothermally metamorphosed equivalents are common in the rhyolites of Obsidian Butte and Red Island. All the domes exhibit wave-cut benches carved during various stands of pre-historic Lake Cahuilla, and have been partly buried by lacustrine and aeolian deposits."

Age estimates have varied widely, from 16,000 BP (Muffler and White, 1969) to 2000 BP (Schmitt and others 2012).

The latest measurements by Schmitt and others would place the buttes in the Holocene and thus would come under official scrutiny by the USGS and CGS as geologic hazards.

There have been occasional reports of transient steam clouds and "hot vents" from Red Island and Rock Hill. Recently Lynch and Adams (this volume) identified six hot vents (~29°C) on Red Island north and two on Red Island south. RETRACE on Red Island Road to Garst Road.

61.4 (0.3) STOP at T intersection. TURN RIGHT (south) on Garst Road.

63.0 (1.6) STOP, TURN RIGHT (west) on Sinclair Road.

63.9 (0.9) Sinclair Road turns to the left (south). PROCEED STRAIGHT into Sonny Bono.

64.0 (0.1) **STOP 2-10:** Sonny Bono Salton Sea National Wildlife Refuge (US Fish and Wildlife Service). Restrooms and water here, along with a diverse number of migrant and resident bird species.

Return to Sinclair Road.

64.1 (0.1) TURN RIGHT (south) on Gentry.

64.5 (0.4) TURN RIGHT (west) on McKendry Road.

65.0 (0.5) Cross Boyle Road.

Snow geese at Sonny Bono National Wildlife Refuge.

65.6 (0.6) Bear right toward the north shore. Do not spin tires—you are driving on volcanic glass!

66.1 (0.5) PARK on the north shore of Obsidian Butte.

STOP 2-11. Discuss the Salton Trough rift basin recent volcanism, and current hydrothermal energy sources (Lindsay and Hample, 1998, Oglesby 2005; McKibben, 2008). Humans have been present in the Salton Trough for a long time, and signs of occupation remain. The oldest known petroglyphs in the United States (about 9,000 BP) are located between 10 and 40 feet above AMSL at Travertine Point, on the west side of the Salton Sea (Turner and Reynolds, 1977; Li, 2003).

Precise dating of the rhyolitic obsidian (Schmitt and others, 2012) suggest an age range of 2480 ± 470 BP but it may be older. This suggests that Native American use of this lithic source only occurred after 2400 ybp. The source of this obsidian can be recognized by the included small, white phenocrysts of feldspar. This obsidian quarry was important, and material is found at sites throughout southern California and northern Mexico. The first Spanish explorers to reach the trough in the late 1500s did not encounter Lake Cahuilla, suggesting that it disappeared due to evaporation by 1600.

Retrace on McKendry Road to Gentry Road. [aka: McNerney Rd.]

68.2 (2.0) TURN LEFT (north) on Gentry Road.

68.6 (0.4) STOP at Sonny Bono Salton Sea Wildlife Refuge Headquarters.

End of Day 2: What we have seen:

We have conducted a brief review of the sediments that fill the Salton Trough, starting with the marine

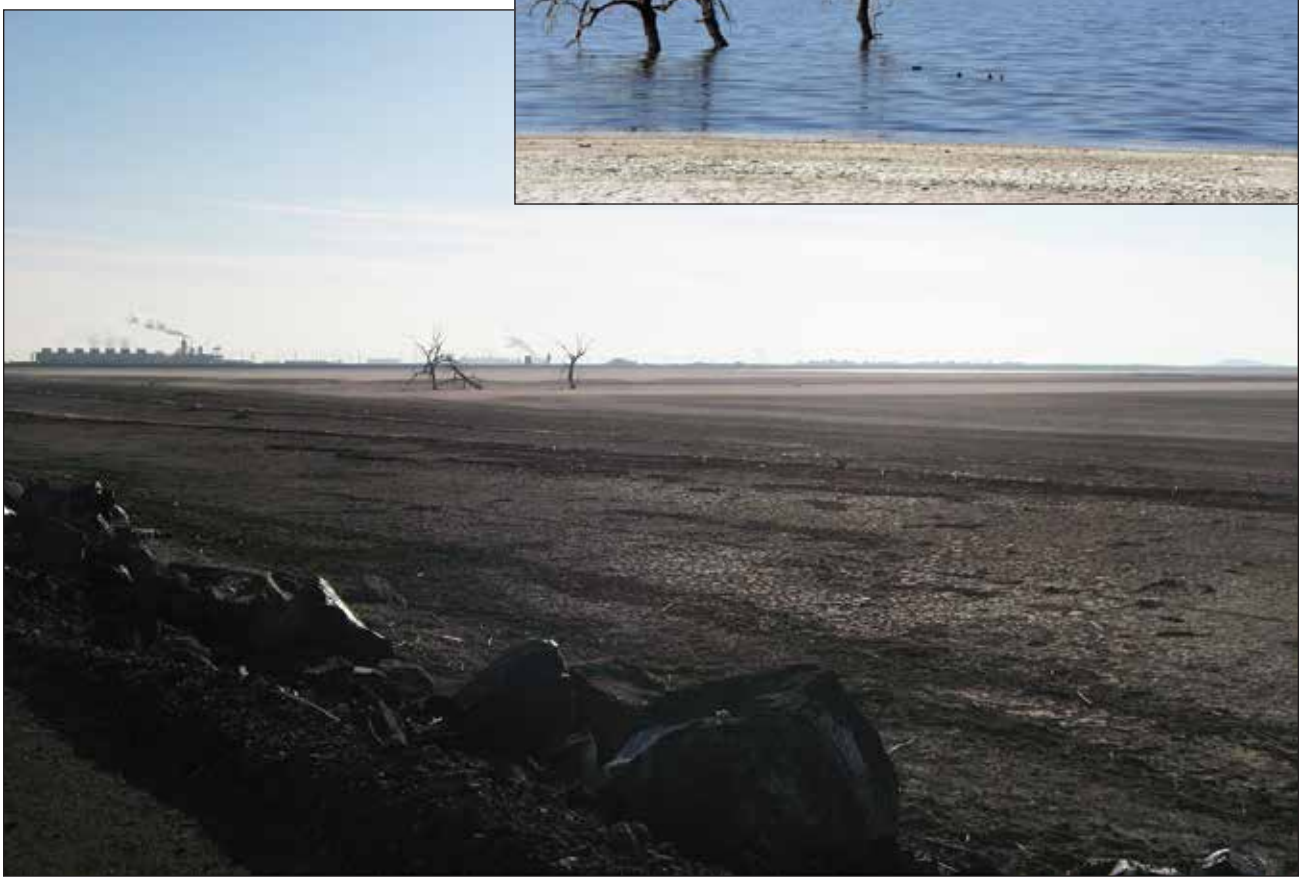

Salton Sea, view westerly from the east shoreline on Garst Road in 2006 and, below, in 2013.

Miocene - Pliocene Imperial Formation (4-7 Ma), the Plio-Pleistocene Indio Hills Formation (3-2 Ma), the fresh and marine Brawley Formation (1.1 - 0.5 Ma) and patches of fresh water Holocene Lake Cahuilla sediments that overlie the older stratigraphy. The incursion of marine sediments occurred in conjunction with activity on the San Andreas Fault, which remains active, and is a controlling structure for topography, erosion and groundwater discharge. As a mapped, active hazard along a graben, it is a recent source of rhyolitic eruptions, and continues to vent CO_2 and other gasses to the surface. Its structures produce heat for geothermal energy.

Exit route east: From the junction of Sinclair and Garst roads, drive 4.5 miles east to SR 111, then either north to Indio, or south to Brawley or Yuma.

Exit route west: Drive south on Garst Road to Barrister Road, then west on Barrister to SR 111, and south to San Diego, west to Borrego Springs (ABDSP book store, exhibits and Stout Research Center) and Temecula, or north to Indio. On all routes you will encounter Border Patrol stations.

References cited

Barca, R. A. 1966. Geology of the northern part of Old Dad Mountain quadrangle, San Bernardino County, California. California Division of Mines and Geology Map Sheet 7.

Bedford, D.R., D. M. Miller, and G. A. Phelps. 2010. Surficial geologic map of the Amboy 30' x 60' quadrangle, San Bernardino County, California. U.S. Geological Survey Scientific Investigations Map 1309, scale 1:100,000.

Bishop, Kim M. 2003. Miocene landslides within Avawatz Basin support hypothesis of a Paleozoic allochthon above Mesozoic metavolcanic rocks in the Soda and Avawatz Mountains, southeastern California. CSUF 2003 Desert Symposium Volume p. 42-47.

Bogler, D. J., C. Pires, and F.-O. Javier. 2005. Phylogeny of Agavaceae based on ndhF, rbcL, and its sequences: Implications of molecular data for classification. Aliso, 22(1), p. 311–326.

Brown, W.J., and M. R. Rosen. 1992. The depositional history of several basins in the Mojave Desert: Implications regarding a Death Valley–Colorado River hydrologic connection, *in* Old routes to the Colorado, J. Reynolds, ed. Redlands, SBCMA Special Publication 92-2, p. 77-82.

Bridenbecker, B. W. 2008. The Iron Hat (Ironclad) ore deposits, Marble Mountains, San Bernardino County, California, *in* Trough to trough: the Colorado River and the Salton Sea, R. E. Reynolds, ed. CSUF 2008 Desert Symposium volume, p. 44-47.

Bridges, D. P. and N. Meek. 1993. The upper Quaternary strata of Shavers Valley, California. SBCMA Special Publication 93-1, p. 59-61.

Brown, H. 2003. Geology, genesis, and mining of pharmaceutical and food grade calcium carbonate at the Amboy Limestone Quarry, *in* Land of Lost Lakes, the 2003 Desert Symposium Field Trip, R. E. Reynolds, ed. CSUF 2003 Desert Symposium volume, p. 49-56.

Brown, W. J. and M. R. Rosen. 1995. Was there a Pliocene-Pleistocene fluvial-lacustrine connection between Death Valley and the Colorado River? Quaternary Research 43, p. 286-296.

Brunzell, D. 2008. Plotting the Bradshaw route. CSUF 2008 Desert Symposium volume, p. 115-116.

Carreno, A. L. and J. T. Smith. 2007. Stratigraphy and correlation of the ancient Gulf of California and Maja California Peninsula, Mexico. Bulletin of American Paleontology, 372, p. 1-146.

Casebier, D. G. 1975. The Mojave Road. Norco, Tales of the Mojave Road Publishing Co.

Dibblee, T.W., Jr. 1954. Geology of the Imperial Valley Region, California in R. H. Jahns, ed, Geology of Southern California, Chapter 2, Geology of Natural Provinces. California Division of Mines, Bulletin 170, p. 21-28.

Dibblee, T.W., Jr. 2008. Geologic map of the Durmid 15 minute quadrangle, Riverside and Imperial counties, California. Dibblee Geology Center Map #DF-376. Santa Barbara Museum of Natural History.

Dohrenwend, J. C., L. D. McFadden, B. D. Turrin, and S. G. Wells. 1984. K-Ar dating of the Cima volcanic field, eastern Mojave Desert, California—Late Cenozoic volcanic history and landscape evolution. Geology, v. 12, p. 163–167.

Dorsey, R. J., B. A. Housen, S. U. Janecke, C. M. Fanning, and A. L. F. Spears. 2011. Stratigraphic record of basin development within the San Andreas fault system: Late Cenozoic Fish Creek-Vallecito basin, southern California. Geological Society of America Bulletin 123(5, 6), p. 771-793.

Dubois, R. L. and R. W. Brummett. 1968. Geology of the Eagle Mountain area, I Ore Deposits of the United States, 1933-1962. The Graton-Sales volume, New York, A.I.M.E. p. 1596-1606.

Eagle Mountain Railroad, 2013. http://en.wikipedia.org/wiki/Eagle_Mountain_Railroad, accessed 03-21-14.

Finney, S. C. 2011. Formal definition of the Quaternary System and redefinition of the Pleistocene Series by the International Commission on Stratigraphy. CSUF 2011 Desert Symposium volume, p. 127-129.

Fox, L. K., and D. M. Miller. 1990. Jurassic granitoids and related rocks of the southern Bristol Mountains, southern Providence Mountains, and Colton Hills, Mojave Desert, California, in The nature and origin of Cordilleran magmatism, J. L. Anderson, ed. Geological Society of America Memoir 174, p. 111-132.

Gardner, L. 2008. The vegetation of the Mojave and Colorado deserts, in Trough to trough, the Colorado River and the Salton Sea, R. E. Reynolds, ed. CSUF 2008 Desert Symposium volume, p. 31-38.

GeoPentech. 2003. Upper Chuckwalla groundwater basin storage, Draft Report. Produced for Metropolitan Water District of Southern California: http://www.waterboards.ca.gov/waterrights/water_issues/programs/water_quality_cert/docs/eagle_mountain_pumped_ferc13123/12_5_through_12_8.pdf, Accessed 3/3/2014.

Glazner, A. F., and J. M. Bartley. 1995. Early Miocene dome emplacement, eiking and limited tectonism in the northern Marble Mountains, eastern Mojave Desert, CA. SBCMA Quarterly 42(3), p. 29-34.

Gunther, J. D. 1984. Riverside County, California, place names: their origins and their stories. Self-published, Riverside CA.

Haenszel, A. M. and J. Reynolds. 1975. The historic San Bernardino Mission District: a self-guided driving tour. San Bernardino County Museum booklet.

Hazzard, J. C. 1928. Paleozoic and associated rocks of the Marble and Ship Mountains, San Bernardino County, California. University of California, M.A. thesis, 97 p.

Howard, K. A. 2002. Geologic map of the Sheep Hole Mountains 30' x 60' quadrangle, San Bernardino and Riverside Counties, California: U.S. Geological Survey map MF-2344, 2 sheets, http://pubs.usgs.gov/mf/2002/2344/, (1:100,000). Updated in 2004.

Howard, K. A., E. D. Horringa, D. M. Miller, and P. Stone. 1989. Geologic map of the eastern parts of the Cadiz Lake and Cadiz Valley 15-minute quadrangles, San Bernardino and Riverside Counties, California. U.S. Geological Survey Miscellaneous Field Studies Map MF-2086, scale 1:62,500.

Howard, K. A., and B. E. John. 1987. Crustal extension along a rooted system of imbricate low-angle faults: Colorado River extensional corridor, California and Arizona, in Continental extensional tectonics, M. P. Coward, J. F. Dewey, and P. L. Hancock, eds. Geological Society of London Special Publication No. 28, p. 299-311.

Howard, K. A., and D. M. Miller. 1992. Late Cenozoic faulting at the boundary between the Mojave and Sonoran blocks: Bristol Lake area, California, in Active faults in California, S. Richard., R. Dokka, and B. P. Luyendyk, eds., San Bernardino County Museum Special Publication, p. 37-47.

Howard, K. A., B. E. John, and C. F. Miller. 1987. Metamorphic core complexes, Mesozoic ductile thrusts, and Cenozoic detachments: Old Woman Mountains-Chemehuevi Mountains transect, California and Arizona, in Geologic diversity of Arizona and its margins: Excursions to choice areas, G. H. Davis and E. M. VandenDolder, eds., Arizona Bureau of Geology and Mineral Technology Geological Survey Branch Special Paper 5, p. 365-382.

James, W. C.; M. A. Knoll, and K. L. Mickus. 1993. Ship Mountains megabreccia: Implications for Miocene extensional tectonics, eastern Mojave Desert, California. Jour. of Geology, v. 101, p. 115-120.

Jefferson, G. T. and L. Lindsay. 2006. The Lake Cahuilla high shoreline and a stable overflow path elevation, southeastern California and northeastern Baja California, in Trough to trough: the Colorado River and the Salton Sea, R. E. Reynolds, ed. CSUF 2006 Desert Symposium volume, p. 107-109.

Jenkins, J. E. 1995. The Hope–New Method mine, San Bernardino County, California, in Ancient surfaces of the East Mojave Desert, R. E. Reynolds and J. Reynolds, eds. SBCMA Quarterly 42(3):27-28.

Jennings, C. W. 1967. Geologic map of California, Salton Sea sheet, scale 1:250,000.

Kenney Geoscience, 2012, Geologic structural evaluation of the Fenner Gap region located between the southern Marble Mountains and Ship Mountains, San Bernardino County, California; report available at: Appendix H1C: Cadiz Groundwater Modeling and Impact Analysis – Volume 3 (http://www.smwd.com/assets/downloads/cadiz/EIR/Appx%20H1c_Vol_3.pdf).

Kim, Joo-Hwan, Dong-Kap Kim, F. Forest, M. F. Fay, and M. W. Chase. 2010. Molecular phylogenetics of Ruscaceae sensu lato and related families (Asparagales) based on plastid and nuclear DNA sequences. Annals of Botany 106: 775–790.

Kirby, S. M., S. U. Janecke, R. J. Dorsey, B. A. Housen, V. E. Langenheim, K. A. McDougal, and A.N. Steely. 2007. Pleistocene Brawley and Ocotillo formations: Evidence for initial strike-slip deformation along the San Felipe and San Jacinto fault zones, south California. Journal of Geology, 115, p. 43-62.

Knoll, M. A., C. F. Miller, and W. C. James. 1986. Mid-Tertiary stratigraphic and structural evolution of the Piute Mountains basin and adjacent areas of the Old Woman Mountains region, southeastern California, in Cenozoic stratigraphy, structure, and mineralization in the Mojave Desert, J. E. Nielson and A. F. Glazner, eds. Geol. Soc. American Cordilleran Sect. Guidebook and Volume, 82nd Annual Meeting, p. 43-50.

Knoll, M. A. 1993. Stratigraphy of the "Southern" [sic] Ship Mountains and Little Piute Mountains, southeastern California. USGS Bull. 2053, p. 109-110.

Kupfer, D. H., F. C. Barstow, and A. M. Bassett. 1957. Core logs from Bristol Cadiz and Danby dry lakes, San Bernardino County California. United States Geological Survey Bulletin 1045-D.

LaFollette, P. I. 2012. Shell rubble beds of the mollusk Thylacodes (Gastropoda: Vermetidae) in the upper Miocene Imperial Formation near Whitewater, Riverside County, California, previously called the "worm tube bed" in Search for the Pliocene: the southern exposures, R. E. Reynolds, ed. CSUF 2012 Desert Symposium volume, p. 65-68.

Lancaster, N. 1995. Kelso Dunes, in Ancient surfaces of the East Mojave Desert, R. E. Reynolds and J. Reynolds, eds. SBCMA Quarterly, 42(3), p. 47-52.

Langenheim, V. E., and R. E. Powell. 2009. Basin geometry and cumulative offsets in the Eastern Transverse Ranges, southern California: Implications for transrotational deformation along the San Andreas fault system. Geosphere, v. 5, no. 1, p. 1-22.

Li, Hong-Chun. 2003. A 20-kyr climatic and hydrological history of Salton Basin, California, recorded by geochemical proxies in lacustrine deposits. CSU 2003 Desert Symposium volume, p. 57-60.

Lindsay, L. and W. G. Hample. 1998. Geology and geothermal resources of the Imperial and Mexicali valleys. San Diego Association of Geologists Annual Field Trip, L. Lindsay and W. G. Hample, eds.

Lowenstein, T. K. and F. Risacher. 2009. Closed basin brine evolution and the influence of Ca–Cl inflow waters: Death Valley and Bristol Dry Lake California, Qaidam Basin, China, and Salar de Atacama, Chile. Aquatic Geochemistry 15, p. 71-94.

Lynch, D. K., 2011. The Coming Land Bridge to Mullet Island, in Proceedings of the 2011 Desert Symposium, The Incredible Shrinking Pliocene, R. Reynolds (ed), 96-100

Lynch, D. K. and K. W. Hudnut. 2008. Geothermal structures southeast of the Salton Sea, in Trough to trough: the Colorado River and the Salton Sea, R. E. Reynolds, ed. CSUF, 2008 Desert Symposium volume, p. 96-101.

Lynch, D. K., K. W. Hudnut and P. M. Adams. 2013. Recently-Exposed Fumarole Fields near Mullet Island, Imperial Valley, California. Geomorphology 195, p. 27-44

McAuliffe, Joseph R., and E. V. McDonald, 1995. A Piedmont Landscape in the Eastern Mojave Desert: Examples of Linkages Between Biotic and physical Components. SBCMA Quarterly 42(3): p. 53-64.

McDonald, E. V., L. D. McFadden and S. G. Wells. 1995. The relative influences of climate change, desert dust, and lithologic control on soil-geomorphic processes on alluvial fans, Mojave Desert, CA: summary of results. SBCMA Quarterly 42(3), p. 35-42.

McDougall, K. 2008. Late Neogene marine incursions and the ancestral Gulf of California, in Geologic and biotic perspectives on Late Cenozoic drainage history of the southwestern Great Basin and lower Colorado River region, M. Reheis, R. Hershler, and D. M. Miller, D.M., eds. Geological Society of America Special Paper 439, p. 355-373.

McKibben, M. A., 2008. The Salton Sea geothermal brines. CSUF 2008 Desert Symposium volume, p. 102-105.

Mendenhall, W. 1909. Some desert watering places in southeastern California and southwestern Nevada. U.S. Geological Survey water-supply paper 224, 98 p.

Miller, D. M. 2012. Surficial geologic map of the Ivanpah 30' x 60' Quadrangle, San Bernardino County, California, and Clark County, Nevada. U.S. Geological Survey Scientific Investigations Map 3206, scale 1:100,000, 14 p.

Miller, D. M., and K. A. Howard. 1985. Bedrock geologic map of the Iron Mountains quadrangle, San Bernardino and Riverside Counties, California. U.S. Geological Survey Miscellaneous Field Studies MF-1736, scale 1:62,500.

Miller, D. M., S. R. Leslie, J. W. Hillhouse, J. L. Wooden, J. A. Vazquez, and R. E. Reynolds. 2010. Reconnaissance geochronology of tuffs in the Miocene Barstow Formation: implications for basin evolution and tectonics in the central Mojave Desert, in Overboard in the Mojave, R. E. Reynolds and D. M. Miller, eds. CSUF 2010 Desert Symposium volume, p. 70-84.

Morton, P. K. 1977. Geology and mineral resources of Imperial County, California. California Division of Mines and Geology, County Report 7, p. 18-19.

Mount, J. D. 1980. Characteristics of early Cambrian faunas from eastern San Bernardino County, California, in Paleontological tour of the Mojave Desert, California–Nevada, J. D. Mount, ed. Southern California Paleontological Society Special Publication 2:19-29.

Muffler, L. J. P. 1990. Salton Buttes lava domes, *in* Volcanoes of North America: United States and Canada, C. A. Wood and J. Kienle, eds. Cambridge University Press, p. 245.

Muffler, J. and D. White. 1969. Active metamorphism of the upper Cenozoic sediments in the Salton Sea geothermal field and the Salton trough, southern California. Geol. Soc. Am. Bull. 80, 157–182.

Murdoch, J. and R. W. Webb. 1966. Minerals of California, centennial volume (1866-1966). California Division Mines & Geology Bulletin 189.

Oglesby, L. C. 2005. The Salton Sea. Memoirs of the Southern California Academy of Sciences 10:1-240.

Ornish, Natalie, 1989, "Herman Ehrenberg," *Handbook of Texas Online* (http://www.tshaonline.org/handbook/online/articles/feh01), accessed March 18, 2014. Uploaded on June 12, 2010. Published by the Texas State Historical Association.

Pemberton, H. E. 1983. Minerals of California. Van Nostrand Reinholt Press.

Phillips, F.M. 2003. Cosmogenic 36Cl ages of Quaternary basalt flows in the Mojave Desert, California, USA. Geomorphology, v. 53, p. 199–208.

Powell, C. L. II. 1985. Bivalve molluscan paleoecology of northern exposures of the marine Neogene Imperial Formation in Riverside County, California. Western Society of Malacologists Annual Report, August 1985, volume 17 for 1984.

Powell, C. L. II. 1986. Stratigraphy and bivalve molluscan paleontology of the Neogene Imperial Formation in Riverside County, California. San Jose, California, M.S. thesis, San Jose State University, 325 p.

Powell, C. L. 1987. Correlation between sea level events and deposition of marine sediments in the proto-Gulf of California during the Neogene. Geological Society of America, Abstracts with program, 19(7): 809.

Powell, C. L. II, M. A. Roeder, and K. McDougall. 2011. A preliminary report on the paleontology of the Imperial Formation (ancestral Gulf of California: Pliocene) in the Indio Hills, Riverside County, Southern California. CalPaleo 2011 ab stracts with program, p. 22.

Presch, W. 2007. Notes on the fringe-toed lizard (Genus Uma) habitat in the east Mojave Desert, San Bernardino and Riverside Counties, in Wild, scenic and rapid, R. E. Reynolds, ed. CSUF 2007 Desert Symposium volume, p. 63-64.

Plotkin, H., R. S. Clarke, T. J. McCoy, and C. M. Corregan. 2012. The Old Woman, California, IIAB iron meteorite. Meteoritics and Planetary Science 47(5):929-946.

Reynolds, R. E. 2012. Searching for the Pliocene: field trip guide to southern exposures. CSU 2012 Desert Symposium volume, p. 5-18.

Reynolds, R. E., A. V. Buising, and K. K. Beratan. 1992. Old routes to the Colorado: the 1992 Mojave Desert Quaternary Research Center field trip, in Old routes to the Colorado, J. Reynolds, ed. SBCMA Special Publication 92-2: 5-27.

Reynolds, R. E., G. T. Jefferson, and D. K. Lynch. 2008. Trough to Trough: the 2008 Desert Symposium field trip. CSUF 2008 Desert Symposium volume, p. 5-30.

Reynolds, R. E. and M. A. Knoll. 1992. Miocene vertebrate faunas of the Little Piute Mountains, southeastern Mojave Desert, in Old Routes to the Colorado, J. Reynolds, ed. SBCMA Special Publication 92, p. 92-94.

Reynolds, R. E., D. M. Miller, and K. M. Bishop. 2003. Land of Lost Lakes: field trip guide. CSU 2003 Desert Symposium volume, p.3-26.

Reynolds, R. E., and R. L. Reynolds. 1992. Pleistocene faunas in the Bristol-Danby Trough. SBCMA Special Publication, 92-2, p. 83-86.

Roeder, M. A. 2005. Fossil fishes of the Anza-Borrego region, in Program and abstracts for Fossil Treasures of the Anza-Borrego Desert. Anza-Borrego Institute, California State Parks, and Sunbelt Publications, San Diego, p. 16-17.

Roeder, M. A. 2012. New records of fish from northern exposures of the Imperial Formation of Riverside County, California, in Search for the Pliocene: the southern exposures, R. E. Reynolds, ed. CSUF, 2012 Desert Symposium volume, p. 53-64.

Roeder, M. A. and R. W. Huddleston. 2011. First records of fossil fish remains from northern exposures of the marine Imperial Formation, Riverside County, California. Annual Meeting, Abstract No. 133, Bulletin of the Southern California Academy of Sciences, 110:115-116.

Rosen, M. R. 1991. Sedimentologic and geochemical constraints on the hydrologic evolution of Bristol Dry Lake, California, USA. Palaeogeography, Palaeoclimatology, Palaeoecology 84, p. 229-257.

Rosen, M. R. and J. K. Warren. 1990. The origin and significance of groundwater seepage gypsum from Bristol Dry Lake Ca., USA. Sedimentology 37, p. 983-996.

Ross, D. G. 1992. Gold road to La Paz, an interpretive guide to the Bradshaw Trail. Tales of the Mojave Road Pub. Co., 304 p.

Schmitt, A. K., A. Martin, D. Stockli, K. Farley, and O. Loveral. 2012. (U–Th)/He zircon and archaeological ages for a late prehistoric eruption in the Salton Trough (California, USA). http://geology.gsapubs.org/content/early/2012/10/12/G33634.1.abstract?sid=51228ff2-2f14-4bed-8fbb-484b270aacbd, first published Oct. 15, 2012, accessed March 22, 2014.

Skirvin, T. M. and S. G. Wells. 1990. Late Cenozoic structure, geomorphology, and landscape evolution of the Old Dad Mountain area, California, in At the end of the Mojave, Quaternary studies in the eastern Mojave Desert, R. E. Reynolds, S. G. Wells, and R. H. Brady III, eds. SBCMA Special Publication 90(1):73-88.

Smith, P.B. 1970. New evidence for Pliocene marine embayment along the lower Colorado River, California and Arizona. Geological Society of America Bulletin, v. 81, p. 1411-1420.

Spencer, J.E. 1984. Role of tectonic denudation in warping and uplift of low-angle normal faults. Geology, v. 12, p. 95–98.

Spencer, J. E., P. A. Pearthree, J. A. Roskowski, and P. J. Patchett. 2008. Extent and age of the Bouse Formation as indicated by strontium isotopes and tephrochronology in Blythe basin, in Trough to trough: the Colorado River and the Salton Sea, R. E. Reynolds, ed. CSUF 2008 Desert Symposium volume, p. 69-71.

Stevens, P. F. (2001 onwards). Angiosperm Phylogeny Website. Version 12, July 2012 [and more or less continuously updated since]. http://www.mobot.org/MOBOT/research/APweb/.

Stone, P., K. A. Howard, and W. Hamilton. 1983. Correlation of metamorphosed Paleozoic strata of the southern Mojave Desert region, California and Arizona. Geological Society of America Bulletin, v. 94, no. 10, p. 1135-1147.

Thompson, D. G. 1929. The Mojave Desert region, California. U.S. Geological Survey water-supply paper 578: 760 p.

Tong, B., and A. L. Regan. 2002. Human tradition in the American West, no. 10. Scholarly Resources, Inc., Wilmington, Delaware, 237 p.

Tratt, D. M., S. J. Young, D. K. Lynch, K. N. Buckland, P. D. Johnson, J. L. Hall, K. R. Westberg, M. L. Polak, B. P. Kasper, and J. Qian. 2011. Remotely-sensed ammonia emission from fumarolic vents associated with a hydrothermally active fault in the Salton Sea geothermal field, California. Journal of Geophysical Research, vol. 116, D21308, doi:10.1029/2011JD016282, 2011

Trexler, D. T. and W. N. Melhorn. 1986. Singing and booming land dunes of California and Nevada. California Geology 39(7):147-152.

Turner, W. G. and R. E. Reynolds. 1977. Dating the Salton Sea petroglyphs. Science News, 111 (February).

Wasson, J. T., and J. Willis. 1976. Discovery of a large IIAB iron meteorite in Southern California. Meteoritics 11, 386-387. Roy S. Clarke, Jr., Division of Meteorites, Smithsonian Institution, Washington, D.C. 20560, USA.

Wells, S.G., L. D. McFadden, J. Poths, and C. T. Olinger. 1995. Cosmogenic 3He surface-exposure dating of stone pavements—implications for landscape evolution in deserts. Geology, v. 23, p. 613–616.

Wells, S. G. and R. E. Reynolds. 1990. Desert wind, water, and brimstone: Quaternary landscape evolution in the eastern Mojave Desert, MDQRC field trip road log, Day 1, in At the End of the Mojave: Quaternary Studies in the Eastern Mojave Desert. SBCMA Special Publications 99-1, p. 117-118.

Wright, L. A., R. M. Stewart, T. E. Gay Jr., and G. C. Hazenbush. 1953. Mines and mineral deposits of San Bernardino County, California. California Journal of Mines and Geology, 49(1,2): 192 p.

Ozone transport into and across the Mojave: interpreting processes from long-term monitoring data

Richard (Tony) VanCuren

Air Quality Research Center, U.C. Davis, ravancuren@ucdavis.edu

ABSTRACT: The Mojave Desert in southern California and Nevada is highly valued for recreation, biologic conservation, and open space preservation. The Mojave lies downwind of the massive urbanization of the Southern California megalopolis (pop. 15M) as well as intensive farming and petroleum extraction region in California's San Joaquin Valley – two of the most polluted air basins in the United States. These upwind areas have been the subject of periodic large-scale intensive field studies and continuous routine air pollution monitoring since the 1960s, and these studies have consistently shown large pollutant fluxes into the Mojave. Despite wide interest in conserving the Mojave, there has been little systematic effort to characterize air pollution in the Mojave beyond documenting the upwind fluxes and localized monitoring by interested land managers (Department of Defense and National Park Service). Moreover, regulatory interest has historically focused on diagnosis of peak events, and the limited seasonal and annual exposure data in the literature are based on long-term statistics. No regionally integrated assessment of daily and seasonal air quality dynamics in the Mojave is available in the refereed literature. This paper draws on routine monitoring, reports from regulatory and land management agencies, focused studies in sub-regions of the Mojave (particularly the far western portion and the Las Vegas urban areas), and individual scientific reports spanning the past four decades to present a unified picture of ozone in the Mojave, with particular emphasis on recognizing the role of transport in elevated layers of the atmosphere. Based on this review, present understanding of air pollution impacts on the natural resources of the Mojave is summarized and new research challenges are identified.

Air quality in the Mojave region

Significance of air quality in the southwest U.S. and the Mojave region

Clear air and blue skies are a central part of the experience of the Southwestern Desert region of the U.S., both for it residents and for the large numbers of recreational visitors to the region. Clean air is has been a major Federal and State air quality management focus for the "Golden Triangle" of Grand Canyon, Zion, and Bryce Canyon National Parks on the Colorado Plateau and selected National Parks and Wilderness Areas throughout the west (GCVTC, 1996; WRAP, 2014), but good air quality is also a key amenity throughout the desert areas flanking the Colorado Plateau to the west and south. Although visibility protection activities have focused on National Parks and Wilderness Areas, all public lands in the Southwest derive much of their recreational appeal and wild lands value from the same landscape qualities of grand vistas, unbroken expanses of unique desert vegetation, and an overwhelming sense of remoteness.

Previous western regional assessment efforts, by the Western Regional Air Partnership (WRAP, 2014) and its predecessor, the Grand Canyon Visibility Transport Commission (GCVTC, 1996), have extensively studied the effects of air pollution on the scenic resources of the signature National Parks of the Colorado Plateau and other Federally designated Class I areas granted Federal visibility protection under the Clean Air Act (CAA, 1977).

Figure 1. Location map showing Mojave Desert (pale green), National Park Service lands, (dark green), and the pollution-sensitive U.S. Government flight test reservations (brown).

Formal Federal visibility-protection has only been extended to National Parks and Wildernesses in existence prior to 1977. The only such area in the Mojave is Joshua Tree National Park (Figure 1); none of the other National Park units (Figure 1) or other Federal lands administered by the Bureau of Land Management (BLM) and U.S. Forest Service (USFS) in the Mojave are afforded this protection.

In addition to the conservation values, the Mojave's clean air is also desired for flight test activities conducted by the U.S. military, the National Aeronautics and Space Agency (NASA), and private aerospace companies (Trijonis *et al.*, 1988) (Figure 1). These activities also do not have explicit protection under State or Federal regulations.

Scope of this report

This review focuses on understanding the processes that drive regional-scale distributions of anthropogenic pollutants across the Mojave bioregion, using ozone as a tracer of convenience to represent polluted air masses. This analysis is built on ozone data because it is monitored with hourly time resolution and thus has a much richer record, and because ozone transport (as opposed to local *in situ* formation) is qualitatively representative of most pollutant transport in the region.

The information presented here is drawn from routine monitoring data, reports from regulatory agencies, focused studies in sub-regions of the Mojave, research by the Department of Defense and the U.S. National

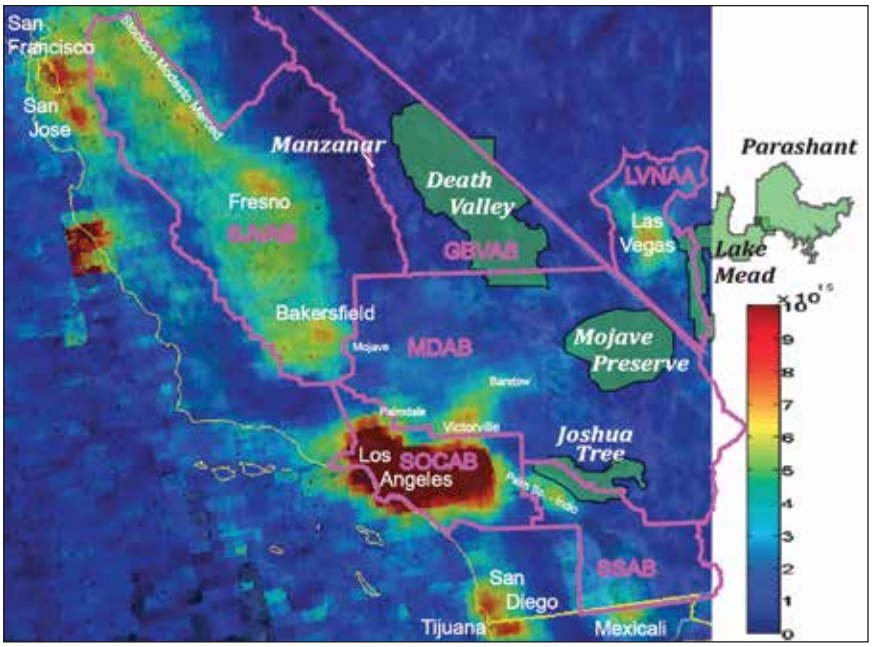

Figure 2. Regional pollution source areas characterized by aggregate NO2 column burden (molecules/cm2) observed by the OMI satellite, 2008 (Image base courtesy of Prof. Ron Cohen, U.C. Berkeley; see also: Russell et al., 2010). The major Federally recognized air quality planning units in the region are outlined and labeled: SJVAB - San Joaquin Valley Air Basin, GBVAB - Great Basin Valleys Air Basin; MDAB - Mojave Desert Air Basin; SOCAB - South Coast Air Basin; SSAB - Salton Sea Air Basin; LVNAA – Las Vegas Ozone Non-attainment Area. Note the lobes of emissions from urban expansion and heavy transport along the two largest transportation routes out of southern California, the I-15 corridor through Cajon Pass and Victorville toward Las Vegas, and the I-10 corridor through San Gorgonio Pass and the Palm Springs-Indio area toward Phoenix, and also the NO2 hot spot around Las Vegas.

Park Service, and individual scientific reports spanning the past four decades. This information base is sufficient to present a unified picture of air quality in the Mojave, but significant gaps in understanding remain, and further research is needed to clarify both atmospheric and biotic processes in the Mojave.

Air pollution sources affecting the Mojave region

Figure 2 provides a good regional perspective on the intensity of human activity in and around the Mojave. Satellite-mapped regional NO_2 emissions for 2008 (Russell *et al.*, 2010) make visible the major air pollution source areas and transport pathways in the region. NO_2 is a good surrogate for total anthropogenic emissions, as it is generated in almost all combustion processes, including motor vehicles, power production, industrial boilers, residential heating, and biomass burning, and it is both a precursor for ozone formation and a dominant source of anthropogenic nitrogen deposited to soil.

This report focuses on analysis of ozone, particularly the contributions from upwind areas. Anthropogenic ozone is predominantly due to combustion and vaporization of fossil fuels, thus it is strongly linked to urban and industrial activity. However, ozone is not the only air pollutant in the Mojave; the following section discusses Mojave pollution sources generally, in order to provide appropriate perspective.

Pollution sources internal to the Mojave

The major urban/industrial air pollution sources within the Mojave itself (Figure 1) are its two major population centers. The largest, located in the northeastern Mojave, is the city of Las Vegas, Nevada, which, with its surrounding communities, comprises the largest urban area in the region (pop. 1.9M (Nevada, 2012)). Along the southwestern boundary of the Mojave, groups of smaller cities and unincorporated communities, most clustered near the passes into the Southern California urbanized basins (Figures 1 and 2), constitute the other major population concentrations. These clusters include Antelope Valley (Palmdale, Lancaster and surroundings, approx. pop. 400,000) north of Soledad Pass, Victor Valley (Victorville, Adelanto, and surroundings, approx. pop. 300,000) north of Cajon Pass, and the cluster of communities northeast of San Gorgonio Pass and west of Joshua Tree N.P. (Morongo Valley, Yucca Valley, Joshua Tree, and Twentynine Palms – pop. about 70,000) (CDOF, 2012; US Census 2010).

Other, more remote communities in the Mojave are relatively small, the largest being Indian Wells Valley (Ridgecrest and Inyokern, serving China Lake NWC, about 40,000); Rosamond (18,000) and California City (14,000), north and west of Edwards AFB; Pahrump, Nevada (36,000), a retirement and bedroom community west of Las Vegas; and the rail and highway transportation hubs of Barstow (23,000) in the central Mojave and Mojave (4,300) in the far west (CDOF, 2012; US Census 2010) .

Anthropogenic pollution generated within the Mojave tends to be local in scale, with the exception of a few large combustion facilities (Figure 3). Only the Las Vegas area is large enough to drive significant urban pollution (Figures 2 and 3), affecting much of the area between the Spring Mts. and Lake Mead (Figure 1) with a distinct, visible particulate haze layer in winter and ozone in summer.

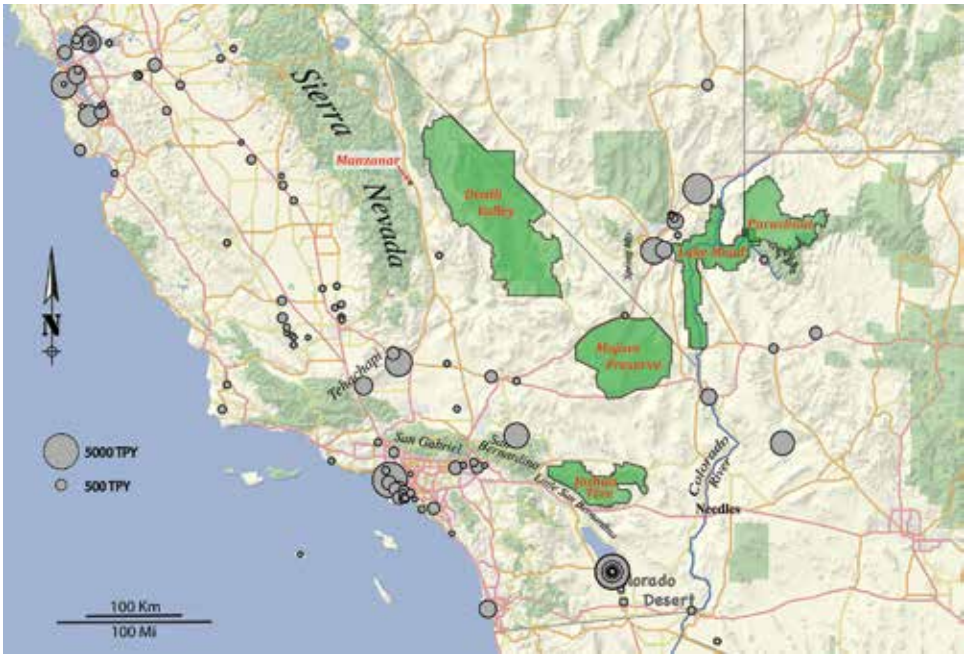

Figure 3. Map of major NO2 sources in and upwind of the Mojave. These very large NOx sources are primarily cement production and power generation facilities (USEPA, 2013)

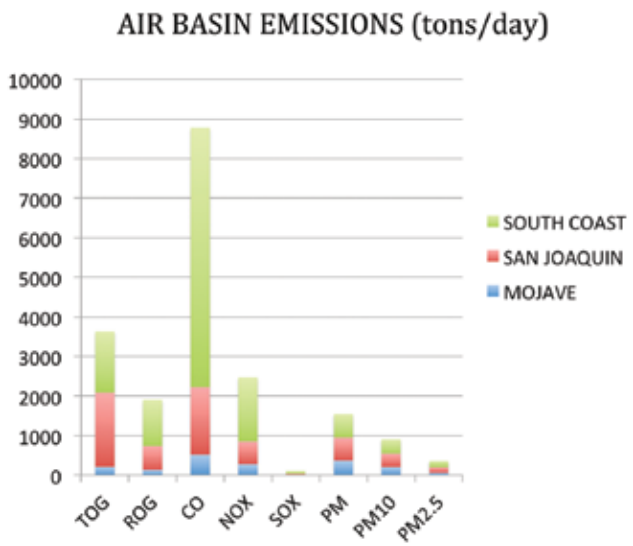

Figure 4. California Air Basin emission inventories, 2008. (Note: Nevada not included).

Figure 4 compares aggregate air pollutant (CARB, 2009a,b) for the San Joaquin Valley, South Coast, and Mojave Air Basins in California. Overall, and particularly for ozone precursors (reactive organic gases - ROG - and oxides of nitrogen - NO_x), the total source population is small in the Mojave, especially when compared to the upwind areas in California.

Pollution from the upwind areas in California

Although the Mojave is climatically isolated from the Pacific by mountains that effectively block most precipitation, there are low areas and gaps in the mountains that allow low-level air flow into the desert, carrying with it pollutants generated at ground level in the populated upwind areas (Figure 5). These are briefly described here.

Pollution from the San Joaquin Valley

The San Joaquin Valley (SJVAB in Figure 3) is a national hotspot of air pollution, with portions of it being rated by the EPA as severe or extreme for ozone, and the southern counties in the Valley also rated non-attainment for fine particles (PM2.5) (CARB, 2014).

On the far west boundary of the Mojave, the Sierra Nevada and Tehachapi Mts. block ground level air flow from the San Joaquin Valley into the desert. Two major passes connect the San Joaquin Valley and the Mojave (Figure 5).

Tehachapi Pass (1200m), which separates the southern Sierra Nevada from the Tehachapi Mts., provides a corridor for air flow into the western Mojave, allowing regular influx of a mixture of dust, biomass smoke, urban emissions, plus ozone and secondary particles into the area around the town of Mojave and spreading east toward Barstow and northward into the valleys east of the Sierra.

A secondary pathway from the Central Valley flows over the lower summits in the area north of Tehachapi Pass and through Walker Pass (1600m) into the Indian Wells Valley and areas to the east, including Panamint Valley, in the western portion of Death Valley National Park.

Figure 5. Major passes allowing low-altitude (800-1600m elevation) air flow into the Mojave (labeled arrows), and the approximate boundary between zones of San Joaquin Valley and South Coast influence (dashed line) (Trijonis, 1988).

Trijonis (1988) reports that both artificial chemical tracers and the chemistry of samples collected in the RESOLVE study show that air from the San Joaquin Valley tends to stay north of a line roughly parallel to Highway 58 as it runs from Mojave toward Barstow. This boundary zone is shown in Figure 5 as a dashed line. Modeling

studies also indicate that the San Joaquin Valley is a likely source region for transported ozone reaching the Las Vegas area. (Huys, 2013).

Pollution from the Southern California megalopolis

Sources of particulate and gaseous pollution in Southern California include surface and marine transportation, petroleum production and refining, manufacturing, and domestic emissions for a population around 15 million. The State of California and the South Coast Air Quality Management District have imposed strong emission controls throughout the megalopolis, and pollution levels have fallen significantly in recent decades, but the EPA continues to classify the South Coast Air Basin (SoCAB) as non-attainment for both PM2.5 and ozone (CARB, 2014).

Much of Southern California's economic activity and the associated emissions are concentrated in the northern portions of the region – Los Angeles, Orange, Riverside and San Bernardino Counties – which abut the mountains that separate the Mojave from the coastal lowlands. In the latter decades of the 20th century, significant population has also bled over the mountains into the western Mojave.

Both polluted air and a bit of the Southern California population spill into the western portion of the Mojave through three passes in the Transverse Ranges. The major passes are shown in Figure 5.

Near the southwest corner of the Mojave, Soledad Pass (980m) defines the western end of the San Gabriel Mts. Traversed by Highway 14, Soledad Pass provides a transportation corridor connecting the Southern California conurbation with the small cities of Palmdale and Lancaster and the other communities of this area known collectively as Antelope Valley (population about 400,000). Air from the urbanized coastal region also follows this corridor, driving poor air quality in this locale.

Cajon Pass (1170m), defines the break between the San Gabriel and San Bernardino Mts., about 100 km (62 mi) east of Soledad Pass. Traversed by Interstate 15, Cajon pass connects the inland areas of the Southern California urban region with the desert-margin communities of Victorville, Adelanto, Apple Valley and Hesperia – loosely gathered under the term Victor Valley (population about 300,000).

San Gorgonio Pass (790m), also known as Banning Pass, lies where the eastern Transverse Ranges are separated from the northern end of the Peninsular Ranges by the San Andreas Fault. Traversed by Interstate 10, it connects the coastal conurbation with the low desert cities of Palm Springs and Indio and the farming and resort communities of the Coachella Valley. This is the lowest of the three passes, distributing air into both the low deserts of the Salton Trough and into the south-central Mojave through flow around the east end of the San Bernardino Mts. into the small communities of Morongo Valley, Yucca Valley, Joshua Tree, and Twentynine Palms, and delivering strong pollution flow into JTNP as well.

Transport dynamics in Southern California

Low level transport

Figure 5 shows the common pathways for summer air flow through mountain passes to the deserts. This flow travels in daily pulses. Air moving eastward from Southern California travels with the daily rise and fall of the Pacific Ocean sea breeze, driven by the strong temperature gradients from the sea to the deserts. Air from the San Joaquin Valley is similarly driven by thermal gradients, with cooler marine air entering the northern end of the Valley through the Sacramento-San Joaquin Delta and flowing south to the warmer southern end, and then, assisted by afternoon heating, flowing over the mountain passes into the northwest Mojave.

As each daily pulse of air moves across the Los Angeles coastal plain or through the Central Valley, ozone precursors (NOx and VOCs) are added to the air and sunlight drives ozone production, resulting in progressively higher and later ozone peak concentrations as the air moves downwind.

The resulting daily ozone pattern is illustrated in Figure 6, which shows summertime ozone diurnal cycles for sites along a transect from the Pacific Ocean to the Colorado River. The transect follows a low altitude route, passing through San Gorgonio Pass (780m), then skirting the southern edge of the Mojave south of Joshua Tree National Park and reaching the Colorado River at Blythe.

At the bottom of Figure 6 are composite diurnal ozone cycles for sites along or near the low altitude route, based on all hours for June, July, and August, 2012 (CARB, 2014a). The progression of ozone

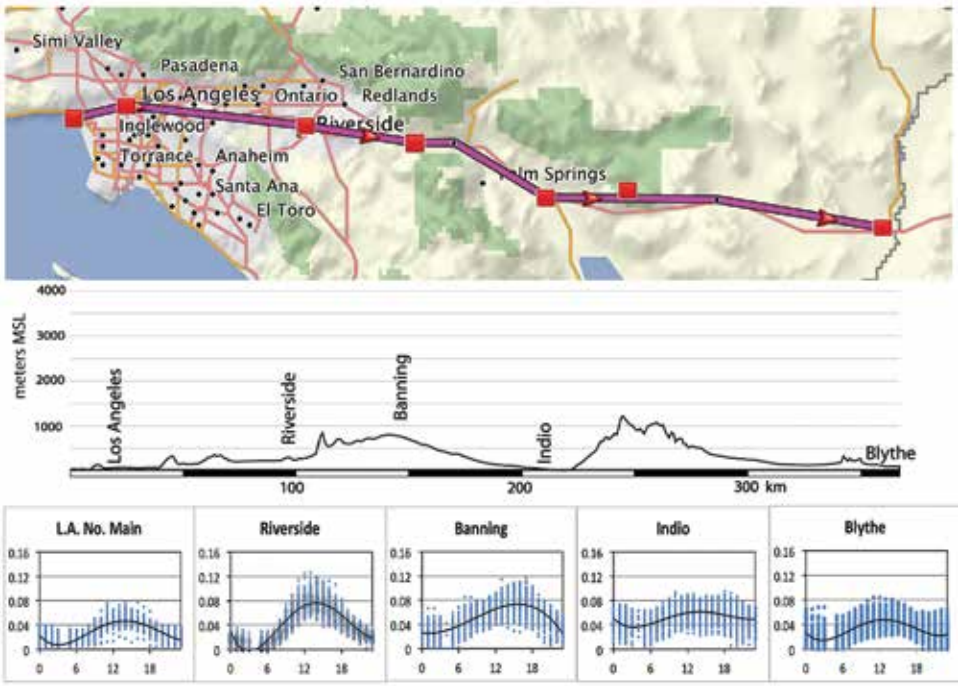

Figure 6. Ozone diurnal cycles along a transect from the Pacific Ocean to the Colorado River through San Gorgonio Pass. Top: map of transect. Middle: topographic profile along the transect. Bottom: Composite diurnal ozone cycles for selected sites along the transect, illustrating the evolution of the dally ozone "pulse" created by the sea breeze flowing from the Pacific Ocean into the desert.

production and its transport by the sea breeze are evident in the low, early ozone peak in downtown Los Angeles, the later and higher ozone peak at Riverside, due accumulated pollution in transit, then prolonged evening ozone as the coastal air streams over San Gorgonio Pass (Banning, 680m). As the air leaves the pass, it begins to spread out and mix vertically and horizontally, showing up at Indio (sea level) as sustained ozone long after dark, and eventually dissipating and having little impact at Blythe (82m). Common to all these sites is the early morning dip in ozone due to chemical destruction and overnight deposition of ozone, and fresh building of ozone each afternoon, generally interpreted as driven by daily pulses of fresh ozone from the upwind Air Basin.

This pattern is replicated near the other passes shown in Figure 5. Similar diurnal patterns were cited by CARB in designating the ozone violations in the Mojave Air Basin as due to transport from upwind areas (CARB, 2001, 2014B).

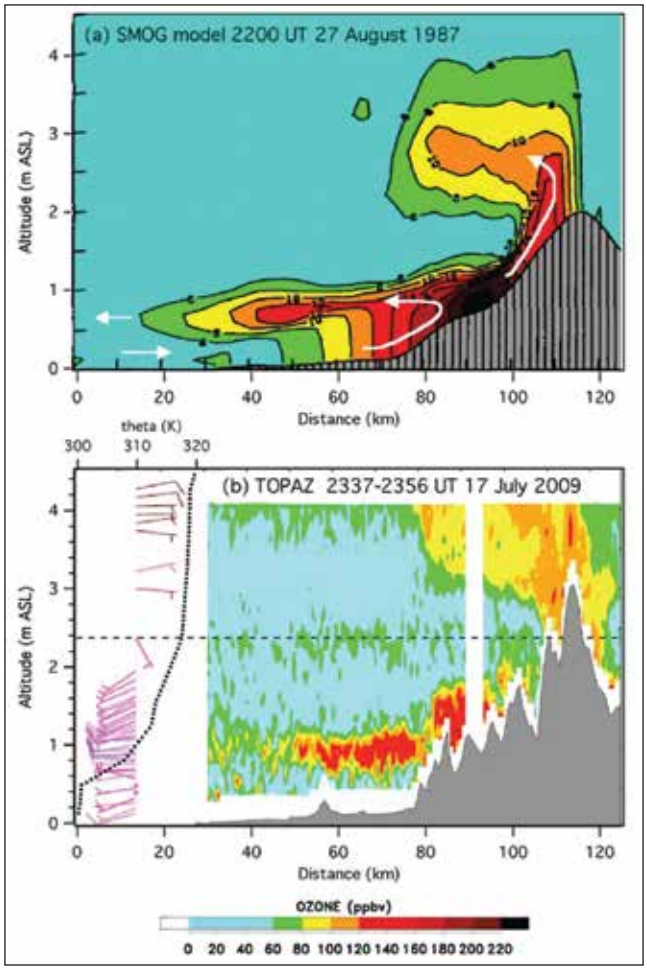

Figure 7. Ozone lofting by mountain slopes in the Transverse Ranges (from Langford et al, 2010). Solar heating of mountain slopes on the edge of the South Coast Air Basin causes a "chimney effect", driving polluted air above and over the mountains. Air aloft can be entrained in regional winds, or ride evening downslope winds to reach the desert areas on the lee side of the mountains.

Transport aloft

The dynamics illustrated in Figure 6 are well known. Although the venting of ozone to higher altitudes as the coastal air encounters the mountains has been known since the 1980s (Figure 8), literature review did not discover any information on its frequency or spatial extent, nor has its role in driving ozone concentrations across the Mojave been studied in detail. The evidence discussed here indicates it is widespread and frequent, but a quantitative assessment will require additional research.

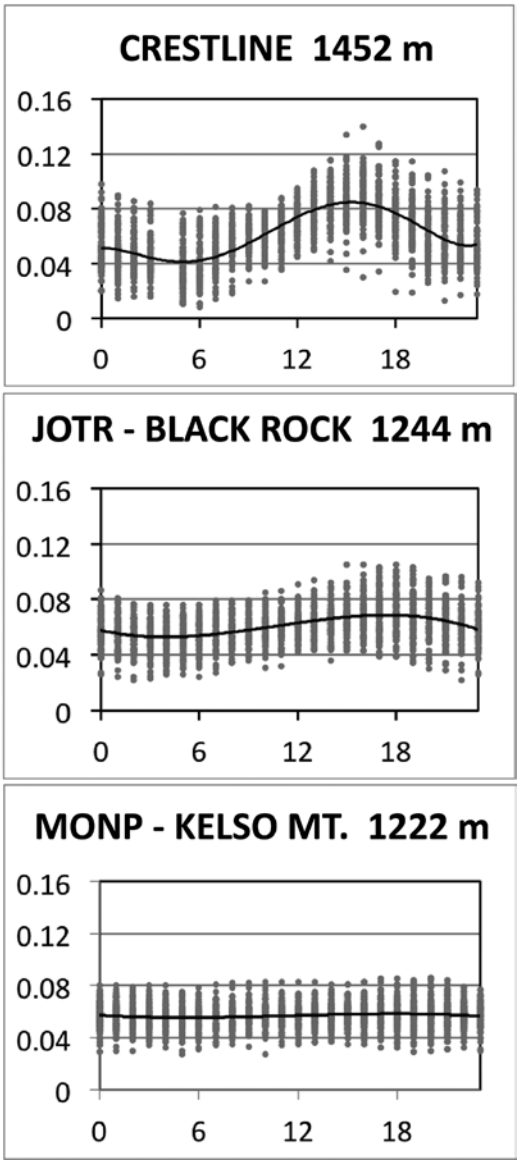

Figure 8. Diurnal cycles of ozone at elevated sites: Crestline (1390m), on the coastal side of the San Bernardino Mts., exhibits the expected diurnal cycle. Black Rock (Joshua Tree N.P.), is in the lee of the San Bernardino Mts., and Kelso Mt. (Mojave N.P.), a solitary peak, show suppressed diurnal cycles, consistent with elevated air masses having limited contact with the ground.

Direct evidence of transport aloft

The mountain barriers block low-level flow, but, under strong spring and summer sun, they create an additional pathway for pollutants to escape the upwind basins. Figure 7 shows two documented cases of ozone lofting by strong updrafts generated by solar heating of the San Gabriel mountain slopes. This "chimney effect" lofts polluted air from the basin floor to 4km altitude, more than a kilometer above the average height of the crest (Langford *et al.*, 2010). Air lofted above the crest can be entrained in regional flow, carrying Southern California pollutants long distances – in the case described by Langford, ozone transport was tentatively traced 1000 km east into southwestern Colorado.

While the frequency of such strong lofting events is uncertain, air from the South Coast regularly tops the Transverse Ranges in summer, as indicated by daily cycles of transported pollutants observed at Mt. Wilson (1730m) in the San Gabriel Mts. (Gorham *et al.*, 2010).

Figure 8 shows summer diurnal cycles for elevated sites. Crestline (1390m), in the San Bernardino Mts., experiences strong diurnal cycling as upslope flow delivers ozone in the afternoon and evening, then ozone drops as flow reverses over night. Unlike the low altitude transport, however, ozone at downwind elevated sites, represented in here by the diurnal plots for Black Rock (1215m) on the western edge of Joshua Tree National Park, and Kelso Mt. (1225m), an isolated high point in the Mojave National Preserve, experience sustained ozone concentrations that do not track with the sharp nocturnal drop in ozone observed at the lowland sites shown in Figure 6.

Unlike the pulsed-transport seen coming through the passes, air lofted over the mountain crests or traversing the passes at higher altitude appears to develop into a spatially broad elevated layer of ozone-rich air over the Mojave, with a base elevation a bit above 1000m above sea level, and persisting with little change through the day.

Two recent studies have also reported this phenomenon.

Burley *et al.* (2014) argues, based on extensive data from Joshua Tree National Park, that ozone exposure in the western portion of the Park must be due to flow over the crest of the San Bernardino Mts.

Much farther downwind, studies in the Las Vegas area (Huys, 2012), comparing ozone measured at an elevated site in the Spring Mts. paired with a site in Las Vegas Valley, indicate that a persistent ozone-rich layer was present over the valley (Figure 9, top). In this case, the low altitude site had the typical "local ozone" diurnal signature of a peak near noon on June 21, and began the next day (June 22, center of plot) following the same pattern, but late in the day, solar heating of the ground caused growth of the turbulent boundary layer to reach the ozone aloft, at which time the ground level concentration jumped as the aged ozone from above was rapidly mixed to

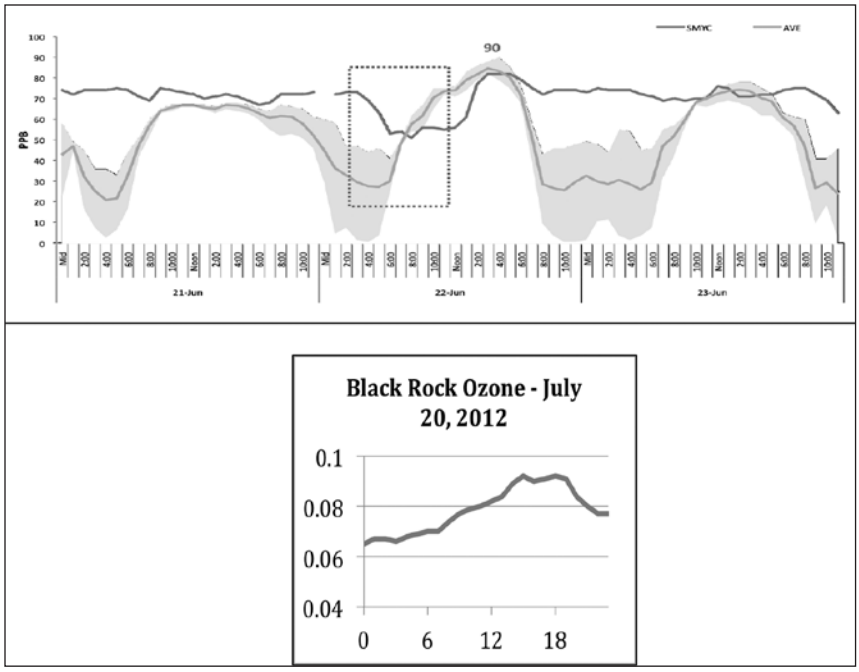

Figure 9. Ozone production from local biogenic precursors. a. Daily cycle of temperature and monoterpene emissions for creosote (Data from Jardine et al., 2010). b. Ozone at Death Valley, July 5-6, 2012 (no transport). c. Ozone all July 2012.

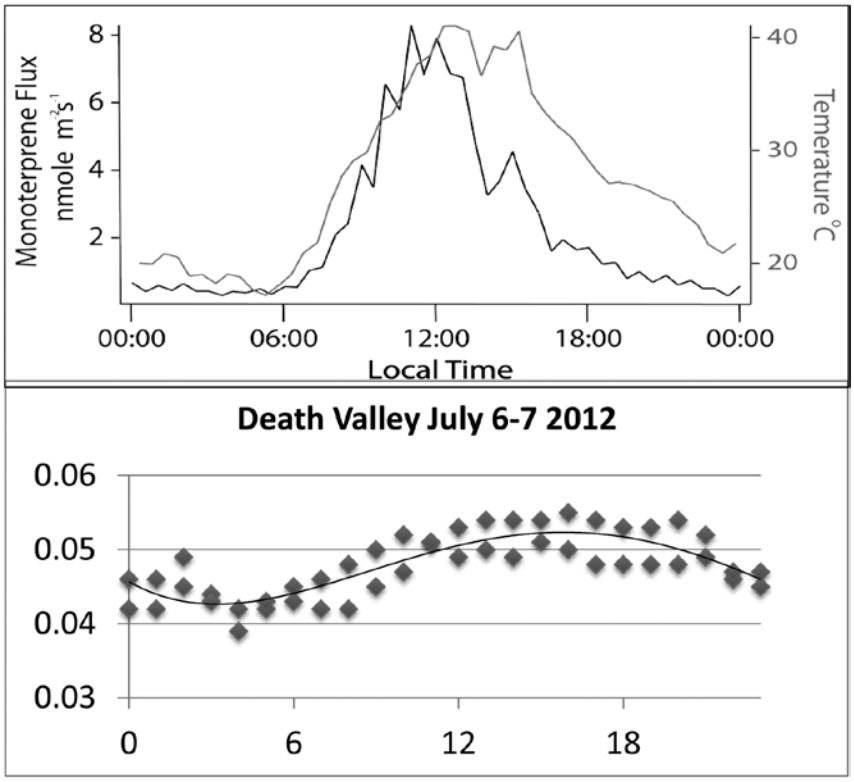

Figure 10. Diurnal structure of ozone fumigation from aloft: a. timelines of ozone at an elevated site in the Spring Mts. (SMYC) and an urban valley site in Las Vegas, summer 2011 (Huys, 2012). Afternoon heating mixes ozone from aloft to the surface, equalizing the concentrations each afternoon. b. transported ozone driving late ozone peak at Black Rock, JOTR.

the surface, causing a sustained afternoon – evening high ozone period. Finally, on June 23, the local ozone diurnal pattern returns with its midday peak. A similar diurnal profile, from Black Rock is shown as the lower plot in Figure 9 (discussed below).

The combination of the dynamics observed by Huys and the season-long persistence of ozone aloft shown by the monitoring data, particularly at Kelso Mt., suggest that transport aloft is a significant component of total ozone transport into and across the Mojave.

Indirect evidence for widespread ozone aloft

The limited number of elevated (above 1000m) ozone sampling sites in the Mojave makes direct observation of the spatial extent of the suspected regional layer impossible, but the afternoon mixing process observed by Huys (2013) can be used to detect ozone fumigation due to deep afternoon atmospheric mixing at other sites.

Efficient ozone production requires both strong sunlight and weak mixing, keeping both precursors and ozone confined and concentrated in a shallow boundary layer (Seinfeld and Pandis, 1998). The daily cycle of local ("natural") ozone production in the Mojave is tied to the availability of biogenic hydrocarbons released by plants, which tracks temperature and sunlight (Figure 10; Jardine *et al.*, 2010; Geron *et al.*, 2006; Martin *et al.*, 1999; La Franchi *et al.*, 2011). The diurnal ozone cycles for Death Valley for two days during a low-wind period (regional high pressure) in July 2012 Figure 10, bottom) illustrate

the resulting ozone diurnal cycle. Ozone on low wind days at Death Valley tracks the biogenic emissions from creosote, rising rapidly toward noon, then flattening as mixing begins to overpower ozone chemistry, driving a drop in ozone through the afternoon. It follows that diurnal cycles can be used to distinguish local ozone production from transported ozone, with local ozone must usually peaking near midday, while ozone derived from deep mixing, which cannot occur during cool morning hours, must be most more commonly observed as late afternoon or even evening peaks.

These considerations lead to the hypothesis that timing of ozone peaks can be read as an indicator of ozone sources—midday for local, later in the day for transported ozone—due to either the pulse model used to explain ozone downwind of the passes, or the aloft model explained as ozone delivered by deep mixing driven by solar heating. Unfortunately, individual days show large variations in ozone timing and concentrations, making it difficult to see such a pattern in a conventional time series. However, if the pattern is stronger than the day-to-day variation in numeric ozone concentrations, then analysis of many days can detect the pattern.

The results of testing this hypothesis are shown in Figure 10. Using all ozone data from the years 2007–2010, each plot presents the frequency of occurrence of daily peak ozone for each hour of the day (hours on the left baseline axis, with the day cycle shifted to run 04:00 – 03:00 to track with the daily ozone cycles, as seen in Figure 6), and summarized by month (right base axis).

Transformed in this way, it is easy to visualize the springtime transition from local ("natural") ozone production in the cool months (December to March) to the strong transport effects in the warm months (April to November).

The plots in Figure 10 show the overwhelming transport impacts at Black Rock and Kelso Mt., and pick up the subtler seasonal shifts at the far downwind sites of Pinto Wells and Mesquite, NV.

This analysis also helps explain why the onset of the afternoon peak does not migrate ever later in the day at the far downwind sites in the transect view (Figure 6, bottom), as would be expected if the daily pulses through the passes were the only significant ozone transport process in the Mojave.

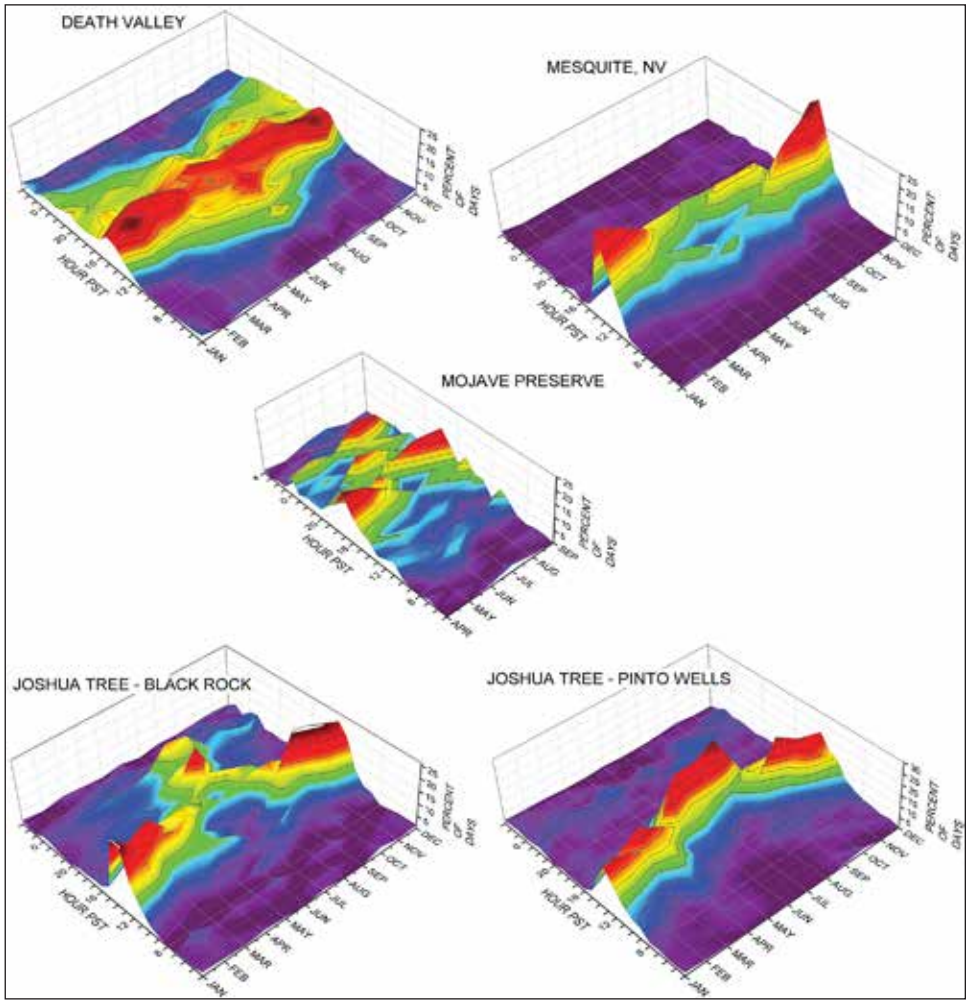

Figure 11. Frequency distributions by month for hour of peak ozone concentration based on hourly ozone data 2007-2010. Natural in situ ozone production peaks near noon due to dependence on solar uv flux. Elevated sites (Black Rock and Mojave Preserve) are regularly in contact with the deep layer of transported ozone in summer; low altitude sites in the path of the ozone cloud leaving southern California (Pinto Wells, Mesquite) show late afternoon peaks caused by thermally driven vertical transport of ozone from aloft.

Figure 12. Regional Fire impact on the Mojave, June 25, 2008. Left: MODIS satellite image showing smoke distribution from fires in northern California – note aged smoke along east side of Sierra Nevada, southern Central Valley, and in Mojave. Right: View looking north over Indian Wells Valley (northwest Mojave) with intense smoke haze causing red color shift and limited visual range.

Pollution from distant North American sources

Large wildfires are known to impact regional ozone pollution (Jaffe et al., 2008). Periodically, large wildfires in the Pacific Coastal Ranges or the Sierra-Cascade mountain belt can spread smoke plumes across the Mojave. Such an event occurred in June, 2008, when dry lightning started more than 1,000 fires in the northern Coast Ranges and northern Sierra Nevada mountains, covering much of California in smoke for several weeks, and causing widespread sustained high ozone. The impacts of this prolonged fire event were seen as exceptionally high ozone at Folsom June 23, June 27, and July 10, 2008, which led CARB and the local Air Pollution Districts in the Sacramento Valley Air Basin to prepare a detailed analysis of this wildfire ozone impact (CARB, 2011). This fire event caused widespread smoke haze in the Mojave (Figure 12), and no doubt increased ozone as well.

Although dramatic, fire impacts like that of June 2008 are sufficiently rare that they do not contribute significantly to long-term "average" air quality in the Mojave. No analysis of the impacts of fire on Mojave ozone is available, but Hand *et al.* (2012) report analyses of several years of IMPROVE particle data that indicate long term average biomass smoke is quite low in the Mojave region, suggesting that fires are an infrequent contributor to Mojave ozone.

Pollution sources In Asia

Most of North America, especially the interior West, is exposed to persistent low-concentration air pollution transported from Asia (VanCuren and Cahill, 2002; VanCuren 2003). This constitutes the single largest component of background aerosol in the free troposphere over North America. The Asian continental plume is a mixture of dust and combustion products (VanCuren 2003). Although the dust is a useful chemical tracer, long-term average fine particle chemical analysis shows that only 30% is mineral (dust, coal fly ash, etc.), while most of the rest is composed of combustion-related material.

Ozone is also a constituent of the Asian pollutant plume, as measurements in the Pacific Northwest have shown the Asian material to be accompanied by gaseous pollutants, including carbon monoxide,

ozone, and nitrogen oxides (Jaffe *et al*., 1999, 2001, 2004; Jaegle *et al.,* 2003; Fiore *et al*., 2002).

Direct observation of Asian ozone in the Mojave is a major research challenge, however a case study demonstrates how transport can occur. Huang *et al*., (2010) reported observing Asian ozone over the Pacific Ocean during aircraft sampling in June, 2008, and used those observations and a transport model to estimate Asian ozone impact in Southern California. The model showed that the cool marine air over the coastal areas prevented mixing to the ground, but the warm turbulent midday air over Joshua Tree NP drove strong mixing to the surface.

On a broad scale, Asian ozone is modeled to be of minor importance to surface ozone in the U.S. (Fiore *et al*., 2002; Reidmiller *et al*., 2009; Lin *et al*., 2010), however, the models used in these and similar studies lack the spatial resolution to properly deal with the sharp terrain gradients in the West US, and particularly in California (for example Reidmiller *et al*. use one station, Death Valley, to represent the entire region), leaving considerable uncertainty as to effects at particular locations.

Conclusions

A review of disparate lines of evidence, including long term ozone behavior at specific sites in the Mojave, limited case studies, and highly suggestive indirect inference, show ozone transported from upwind areas to be widespread in the Mojave, and that ozone exposure is not only modulated by distance from the source regions, but also by altitude. The data reviewed here suggest that ozone transport aloft (>1 km above sea level) into the Mojave is both regular and significant, and may be comparable in magnitude to surface flows, but quantitative analysis of total ozone flux cannot be made due to limited knowledge of the depth of the ozone layer(s).

These findings suggest two important conclusions: First, that ozone exposure to plants may be greater than previously estimated for high elevation lands in the Mojave, and second, that ozone concentrations as far downwind as Las Vegas and even southwestern Utah may be influenced by emissions in Southern California and the San Joaquin Valley.

These effects, however, also indicate that continued ozone control efforts in those source areas will produce widespread air quality benefits across the entire Mojave Desert.

Finally, it must be noted that the analysis presented here is largely qualitative. Additional research is needed to fully characterize the ozone transport pathways identified here, and to fully understand their ecological and public health implications.

References

Burley, J.D., A. Bytnerowicz, J.D. Ray, S. Schilling, E. B. Allen, 2014, Surface ozone in Joshua Tree National Park, *Atmospheric Environment* 87 (2014) 95-107.

Clean Air Act (CAA), 1977, *Title 1, Part C, Prevention of Significant Deterioration* (CAA § 160-169b; USC § 7470-7492). http://www.epa.gov/air/caa/index.html

California Air Resources Board (CARB), 2001, *Ozone Transport: 2001 Review*, Sacramento, CA. http://www.arb.ca.gov/aqd/transport/assessments/assessments.htm

California Air Resources Board (CARB), Almanac Emission Projection Data, Mojave Desert Air Basin. http://www.arb.ca.gov/app/emsinv/emssumcat_query.php? F_YR=2008&F_DIV=4&F_SEASON=A&SP=2009&F_AREA=AB&F_AB=MD

California Air Resources Board (CARB), Air Quality Almanac 2009, http://www.arb.ca.gov/aqd/almanac/almanac09/almanac09.htm

California Air Resources Board (CARB), Exceptional Events Demonstration for 1-Hour Ozone Exceedances in the Sacramento Regional Nonattainment Area Due to 2008 Wildfires, Updated Documentation, March 30, 2011. http://www.arb.ca.gov/desig/excevents/firemain.pdf

California Air Resources Board (CARB), 2012, Ocean-Going Vessels - Fuel Rule, "Fuel Sulfur and Other Operation Requirements for Ocean-Going Vessels within California Waters and 24 Nautical Miles of the California Baseline", http://www.arb.ca.gov/ports/marinevess/ogv.htm

CARB, 2014, Air Monitoring Site Information, http://www.arb.ca.gov/qaweb/siteinfo.php

California Air Resources Board (CARB), 2014, Air Quality Standards and Area Designations, http://www.arb.ca.gov/desig/desig.htm

State of California, Department of Finance (CDOF), 2012, *E-1 Population Estimates for Cities, Counties, and the State with Annual Percent Change — January 1, 2011 and 2012.* Sacramento, California. http://www.dof.ca.gov/research/demographic/reports/estimates/e-1/view.php

Fiore, Arlene M., Daniel J. Jacob, Isabelle Bey, Robert M. Yantosca, Brendan D. Field, Andrew C. Fusco, James G. Wilkinson, 2002, Background ozone over the United States in summer: Origin, trend, and contribution to pollution episodes, *J. Geophys. Res.* 107 (D15), 10.1029/2001JD000982.

GCVTC, 1996, *Report of the Grand Canyon Visibility Transport Commission to the United States Environmental Protection Agency*, June 1996

http://www.wrapair.org/WRAP/reports/GCVTCFinal.PDF

Geron, C. A. Guenther, J. Greenberg, T. Karl, R. Rasmussen, 2006, Biogenic volatile organic compound emissions from

desert vegetation of the southwestern US, *Atmospheric Environment* 40(9), 1645-1660. file://localhost/(http/::www.sciencedirect.com:science:article:pii:S1352231005010502)

Gorham, K.A., N.J. Blake, R.A. VanCuren, H.E. Fuelberg, S.Meinardi, and D.R. Blake, 2010, Seasonal and Diurnal Measurements of Carbon Monoxide and Nonmethane Hydrocarbons at Mt. Wilson, California: Indirect Evidence of Atomic Cl in the Los Angeles Basin, *Atmospheric Environment* 44, 2271-2279, doi:10.1016/j.atmosenv.2010.04.019. http://dx.doi.org/10.1016/j.atmosenv.2010.04.019

Hand, J.L., B. A. Schichtel, M. Pitchford, W. C. Malm, and N. H. Frank, 2012, Seasonal composition of remote and urban fine particulate matter in the United States, *J. Geophys. Res.* 117, D05209. doi:10.1029/2011JD017122.

Huang, M., G. R. Carmichael, B. Adhikary, S. N. Spak, S. Kulkarni, Y. F. Cheng, C. Wei, Y. Tang, D. D. Parrish, S. J. Oltmans, A. D'Allura, A. Kaduwela, C. Cai, A. J. Weinheimer, M.Wong, R. B. Pierce, J. A. Al-Saadi, D. G. Streets, and Q. Zhang, 2010, Impacts of transported background ozone on California air quality during the ARCTAS-CARB period – a multi-scale modeling study, *Atmos. Chem. Phys.*, 10, 6947–6968. www.atmos-chem-phys.net/10/6947/2010/ doi:10.5194/acp-10-6947-2010

Huys, J.P., 2012, Las Vegas ozone modeling and monitoring analysis, Westar, Western Ozone Transport Conference, Reno, NV, October, 2012. http://www.westar.org/12 Tech Conf/Presentations/Huys.pdf

Jaegle´, L., D. A. Jaffe, H. U. Price, P. Weiss-Penzias, P. I. Palmer, M. J. Evans, D. J. Jacob, and I. Bey, 2003, Sources and budgets for CO and O3 in the northeastern Pacific during the spring of 2001: Results from the PHOBEA-II Experiment, *J. Geophys. Res.*, 108(D20), 8802. doi:10.1029/2002JD003121

Jaffe D. A., T. Anderson, D. Covert, R. Kotchenruther, B. Trost, J. Danielson, W. Simpson, T. Berntsen, S. Karlsdottir, D. Blake, J. Harris, G. Carmichael, I. Uno, 1999, Transport of Asian air pollution to North America. *Geophysical Research Letters* 26, 711–714.

Jaffe DA, T. Anderson, D. Covert, B. Trost, J. Danielson, W. Simpson, D. Blake, J. Harris, D. Streets, 2001. Observations of ozone and related species in the northeast Pacific during the PHOBEA campaigns, 1: Ground based observations at Cheeka Peak. *Journal of Geophysical Research* 106, 7449–7461.

Jaffe, D., Isaac Bertschi, Lyatt Jaegle´, Paul Novelli, Jeffrey S. Reid, Hiroshi Tanimoto, Roxanne Vingarzan, and Douglas L. Westphal, 2004, Long-range transport of Siberian biomass burning emissions and impact on surface ozone in western North America, *Geophysical Research Letters* 31, L16106, doi:10.1029/2004GL020093.

Jaffe, D., D. Chand, W. Hafner, A. Westerling, and D. Spracklen (2008), Influence of fires on O3 concentrations in the western U.S., *Environ. Sci. Techol., 42*, 5885-5891.

Jardine, K., L. Abrell, S. A. Kurc, T. Huxman, J. Ortega, and A. Guenther, 2010, Volatile organic compound emissions from *Larrea tridentata* (creosotebush), *Atmos. Chem. Phys.*, 10, 12191–12206. www.atmos-chem-phys.net:10:12191:2010:doi/10.5194:acp-10-12191-2010

LaFranchi, B.W., A. H. Goldstein, and R. C. Cohen, 2011, Observations of the temperature dependent response of ozone to NOx reductions in the Sacramento, CA urban plume, *Atmos. Chem. Phys.*, 11, 6945–6960. www.atmos-chem-phys.net/11/6945/2011/doi:10.5194/acp-11-6945-2011

Langford, A.O., C. J. Senff, R. J. Alvarez II, R. M. Banta, and R. M. Hardesty, 2010, Long-range transport of ozone from the Los Angeles Basin: A case study, *Geophys. Res. Lett.* 37, L06807, doi:10.1029/2010GL042507.

Atmospheric Environment 22, 1229–1240.

Lin, Meiyun., Arlene M. Fiore, Larry W. Horowitz, Owen R. Cooper, Vaishali Naik, John Holloway, Bryan J. Johnson, Ann M. Middlebrook, Samuel J. Oltmans, Ilana B. Pollack, Tomas B. Ryerson, Juying X. Warner, Christine Wiedinmyer, John Wilson, and Bruce Wyman, 2012, Transport of Asian ozone pollution into surface air over the western United States in spring, J. Geophys. Res., 117, D00V07, doi:10.1029/2011JD016961

Martin, R., I. Villanueva, J. Zhang, C. Popp, 1999, Nonmethane Hydrocarbon, Monocarboxylic Acid, and Low Molecular Weight Aldehyde and Ketone Emissions from Vegetation in Central New Mexico, *Environmental Science & Technology 33* (13), 2186-2192. http://pubs.acs.org/doi/abs/10.1021/es980468q

Nevada State Demographer, 2012, Estimated Population 2011. http://nvdemography.org/data-and-publications/estimates/estimates-by-county-city-and-unincorporated-towns/

Reidmiller, D. R., A. M. Fiore, D. A. Jaffe, D. Bergmann, C. Cuvelier, F. J. Dentener, B. N. Duncan, G. Folberth, M. Gauss, S. Gong, P. Hess, J. E. Jonson, T. Keating, A. Lupu, E. Marmer, R. Park, M. G. Schultz, D. T. Shindell, S. Szopa, M. G. Vivanco, O. Wild, and A. Zuber, 2009, The influence of foreign vs. North American emissions on surface ozone in the US, *Atmos. Chem. Phys.*, 9, 5027-5042, 2009. file://localhost/www.atmos-chem-phys.net:9:5027:2009:doi/10.5194:acp-9-5027-2009

Russell, A., L. Valin, E. Bucsela, M. Wenig, R. Cohen, 2010, Space-Based Constraints On Spatial and Temporal Patterns of NOx Emissions In California, 2005-2008, *Environ. Sci. Technol.* 44, 3608–3615.

Seinfeld, J., and S. Pandis, 1998, A*tmospheric chemistry and physics: from air pollution to climate change*, Wiley, New York, 1326p.

Trijonis, J., M. McGown, M. Pitchford, D. Blumenthal, P. Roberts, W. White, E. Macias, R. Weiss, A. Waggoner, J. Watson, J. Chow, R. Flocchini, 1988, *RESOLVE Project Final Report: Visibility Conditions and Causes of Visibility Degradation In the Mojave Desert of California,* Report AD-A206322, Naval Weapons Center, China Lake, CA.

VanCuren, R., and T. Cahill, 2002, Asian aerosols in North America: Frequency and concentration of fine dust, *J. Geophys. Res.*, 107(D24), 4804, doi:10.1029/2002JD002204.

VanCuren, R. A., 2003, Asian aerosols in North America: Extracting the chemical composition and mass concentration of the Asian continental aerosol plume from long-term aerosol records in the western United States, *J. Geophys. Res.* 108(D20), 4623, doi:10.1029/2003JD003459.

Western Regional Air Partnership (WRAP), http://www.wrapair2.org

Stratigraphy and fauna of Proterozoic and Cambrian formations in the Marble Mountains, San Bernardino County, California

Bruce W. Bridenbecker

Professor of Earth Science, Copper Mountain College, PO Box 1398, Joshua Tree, CA 92252. bbridenbecker@cmccd.edu

ABSTRACT: Proterozoic and Cambrian rock formations outcropping in the Marble Mountains can be correlated with those of the Providence Mountains and formations from the base of the Grand Canyon Supergroup (Stone, et al., 1983). Fossil assemblages of brachiopods and trilobites have been correlated throughout southeastern California, western Nevada, and western Arizona suggesting an eastward transgression of a sea during Cambrian time (Stewart, 1970; Mount, 1980). The stratigraphy and fauna of the Wood Canyon Formation (Nolan, 1929), Zabriskie Quartzite (Hazzard, 1937) Latham Shale (Hazzard, 1954), Chambless Limestone (Hazzard, 1954), Cadiz Formation (Hazzard and Mason, 1936), and the Bonanza King Formation (Hazzard, 1937) are briefly discussed along with references for further investigation.

Introduction

The Marble Mountains are located in the eastern portion of the Mojave Desert Province approximately 22.5 km (14 miles) east of Amboy, California on Historic Route 66. They extend about 27 km (17 miles) in a northwesterly direction beginning in the vicinity of the Cadiz railroad station and culminating close to the junction of Interstate 40 and Kelbaker Road. As one travels northeast, they gradually increase in width from 1.6 km (1 mile) in the southeast to approximately 8 km (5 miles) in the northwest. Figure 1 shows the location of Paleozoic outcrops from Stone et al. (1983). The Providence and Marble Mountains are located in the northwest corner of Figure 1.

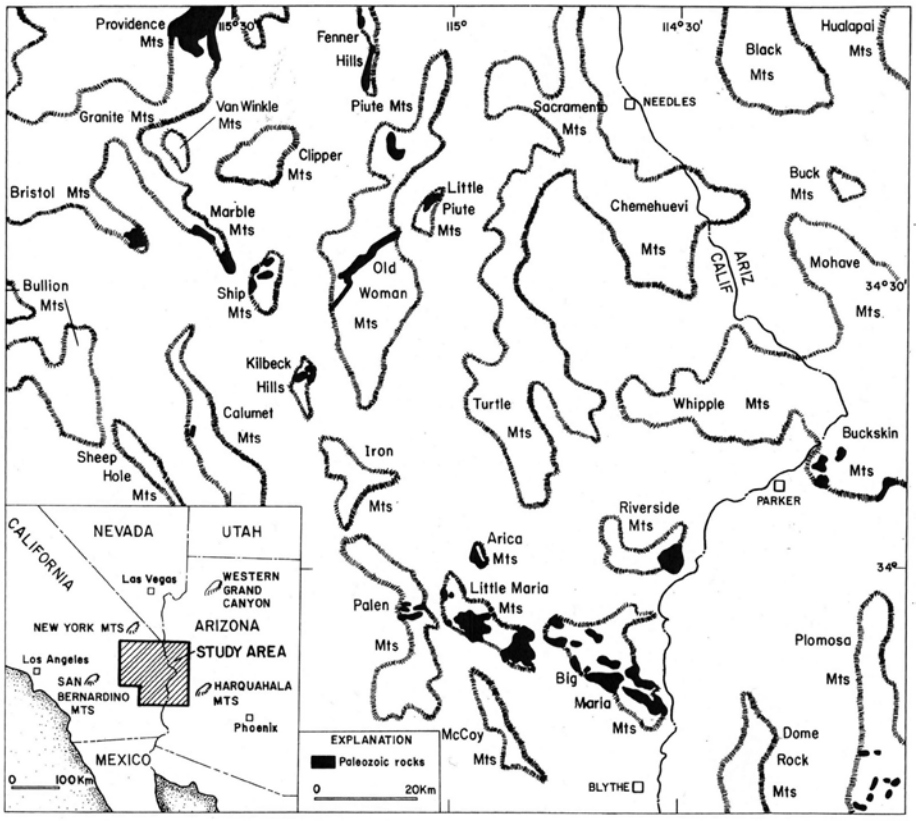

Figure 1. Index map showing Paleozoic outcrops in the southeastern Mojave Desert region, California and Arizona (from Stone, et al. 1983).

Figure 2. Marble Mountains north of Chambles (Photo by B. Bridenbecker).

Rising from the desert floor with elevations of 280 m (920 ft) to 1158 m (3800 ft) the Marble Mountains silhouette the horizon with a banded appearance resembling a layered cake (Figure 2). Marble outcrops are prominent throughout the range and that along with its appearance played a role in naming it (Kilian, 1964).

Proterozoic (Precambrian) igneous and metamorphic rocks lie unconformably below Paleozoic marine sedimentary rocks in many of the ranges located in the eastern Mojave Desert. Such is the case in the southeastern section of the Marble Mountains where granite and gneiss lie below rocks of Lower Cambrian to Devonian or younger age (Hazzard and Crickmay, 1933; Hazzard and Mason, 1936; Stewart, 1970; Stone, et.al. 1983; Hall, 1985). These sediments are primarily limestone and dolomite with lesser amounts of shale and quartzite. Except for faulting, this section of the Marble Mountains shows little structural activity.

In the south central Marble Mountains, the sedimentary section has been intruded by Middle Jurassic granitic rocks, and a series of felsic and mafic dike complexes. This is where marble formed and several episodes of ore emplacement occurred (Hall, 1985).

In the northern section of the Marble Mountains, volcanic rocks of Tertiary age dominate the landscape. These overlap older outcrops or occur as fault contacts with granite, marble, meta-igneous, and various clastic or detrital rocks (Hall, 1985). The Miocene Period of the Tertiary Epoch appears to be the time when volcanism was most prominent. Approximately 700 m (2000 ft) of basalts, dacites, and andesites were deposited along the northern and eastern portions of the area during this time (Kilian, 1964).

As this paper specifically addresses the stratigraphy and fauna of Proterozoic and Cambrian rocks in the Marble Mountains, a detailed discussion of Mesozoic and Cenozoic rock units is not included.

Proterozoic (Precambrian) Basement Rocks

Proterozoic (Precambrian) igneous and metamorphic rocks outcrop along the foot of the mountain range in the south and central portion of the Marble Mountains. Granite, granodiorite, diorite, and gneiss are the predominate rocks found in this area. Of these three, the diorite outcrops most frequently (Kilian, 1964). Metamorphism and dike emplacement lace the granitic rocks with chlorite replacing ferromagnesian minerals in many localities (Hall, 1985). Lanphere (1964) and Silver (1964) dated samples of the granite at 1400 to 1450 mybp using K-Ar, Rb-Sr, U-Pb methods on biotite, potassium feldspar, and zircon grains. Lanphere wrote that he dated one of the youngest intrusions in the area and that the age of the rocks is most likely much older.

Stratigraphy of late Proterozoic and Cambrian Rock Formations

Most of the Proterozoic (Precambrian) rocks appear to be the remnants of a paleohigh, which was covered as the Cambrian sea transgressed eastward throughout the region. The strata, have been correlated lithostratigraphically with the Providence Mountains, Marble Mountains, and the lower Grand Canyon Supergroup (Table 1). As a result, the lower Cambrian rocks consist of a conformable sequence of shallow marine, detrital and carbonate sediments in

Table 1. Correlation of Proterozoic and Cambrian formations in the southeastern Mojave Desert with the Grand Canyon Supergroup[1]

Age	Providence Mountains	Marble Mountains	Grand Canyon
Upper Cambrian	Nopah Fm Bonanza King Fm	Bonanza King Fm	Unnamed Dolomite Muav Limestone
Middle Cambrian	Cadiz Fm Chambless Limestone Latham Shale	Cadiz Fm Chambless Limestone Latham Shale	Bright Angel Shale
Lower Cambrian	Zabriskie Quartzite Upper Wood Canyon Fm	Zabriskie Quartzite Wood Canyon Fm (Tapeats Sandstone)	Tapeats Sandstone
Proterozoic	Lower Wood Canyon Fm Sterling Quartzite Johnie Formation Granite and Gneiss	Wood Canyon Fm Granite–Diorite Complex	Vishnu Schist

[1] compiled from; Stewart, 1970; Palmer and Halley, 1979; Mount, 1980; and Stone et al., 1983

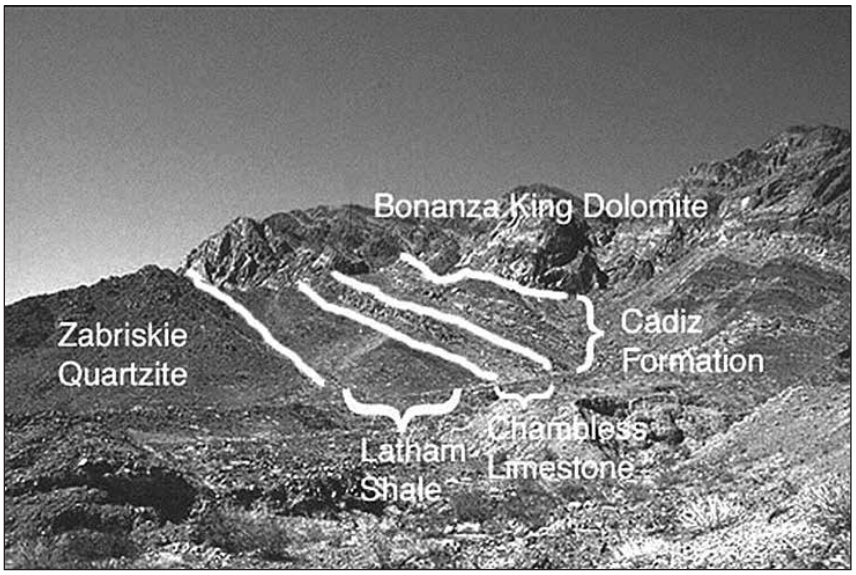

Figure 3. Labeled section of Cambrian formations in section 28 (From Waggoner, n.d.).

the region (McKee and Resser, 1945; Stewart, 1970; Palmer and Halley, 1979; Mount, 1980; Stone et al., 1983; Stewart, 1991).

The Tapeats Sandstone as identified by Stone et al. (1983) has been interpreted by Stewart (1970) to be the lithologic equivalent of the Wood Canyon Formation and the Zabriskie Quartzite (Table 1). According to Mount (1980) the division between the lower and upper members of the Wood Canyon Formation is based upon the presence of olenellid trilobites in the latter. Trace fossils are found in the Lower Wood Canyon Formation and may be tracks of trilobites suggesting a lower Cambrian age in some localities (Stewart, 1970). Nolan (1929) named the Wood Canyon Formation, which outcrops in many ranges throughout the southern Great Basin. In the Marble Mountains, the lower member outcrops as a slightly metamorphosed coarse to medium grained quartz-pebble conglomerate overlain by cross-bedded coarse-grained sandstone. There have been no fossils found in this formation in the Marble Mountains so they have been assigned an age of upper Proterozoic (Mount, 1980). The Upper Wood Canyon Formation described as siltstone and quartzite with trilobite tracks and trails was assigned a lower Cambrian age by Stewart (1970).

The Zabriskie Quartzite defined by Hazzard (1937) includes fine-grained quartzite and siltstones, which transition conformably from the Wood Canyon Formation (Stewart, 1970). In the Marble Mountains it displays horizontal bedding planes grading upward into small sets of high-angle cross-beds (Stewart, 1970). Mount (1980) reports finding a single specimen of olenellus in the Zabriskie Quartzite and the trace fossil skolithos in the area. Figure 3 shows a labeled section of Cambrian rocks in the southwest central part of the Marble Mountains.

Figure 4. *Olenellus clarki* from the Latham Shale section 28 (Photo by B. Bridenbecker).

Conformably above the Zabriskie Quartzite lies the Latham Shale of Hazzard (1954), which has been slightly metamorphosed in many localities. Consisting of grey-green and tan shale, micaceous siltstone, sandstone, and minor carbonate lenses the Latham Shale weathers to red thin fragments displaying an assemblage of fossils (Kilian, 1964; Stewart, 1970; Mount, 1980). The most notable are Early Cambrian olenellid trilobites (Figure 4). Many of the Latham Shale outcrops display a low-grade metamorphic texture with slaty cleavage.

The Western Trilobite Association (WTA) has compiled a list of trilobites found in the Providence and Marble Mountains. The author has included a list of Latham Shale trilobites from their website (Table 2); (Kurkewicz, n.d.).

Table 2. List of Latham Shale trilobites found in the Marble and Providence Mountains.

Bristolia anteros Palmer, 1979
Bristolia bristolensis (Resser, 1928)
Bristolia aff. *fragilis* A
Bristolia aff. *fragilis* B
Bristolia harringtoni
Bristolia insolens (Resser, 1928)
Bristolia new species (see Mount, 1980)
Mesonacis sp. A
Olenellus clarki (Resser, 1928)
Olenellus fremonti Walcott, 1910 ? = *Mesonacis fremonti*
Olenellus gilberti Meek in White, 1874
Olenellus aff. *gilberti* A
Olenellus aff. *gilberti* B
Olenellus mohavensis (Crickway, 1933)? = *Bristolia mohavensis*
Olenellus nevadensis (Walcott, 1910)
Olenellus aff. *terminatus*
Olenellus new species A (see Mount, 1980)
Onchocephalus new species (see Mount, 1980)
Peachella iddingsi (Walcott, 1884)

According to WTA, Lieberman (1999) described a new form of Bristolia bristolensis that he called Bristolia harringtoni from the Latham Shale. In the same paper he reassigned *Olenellus mohavensis* to *Bristolia*.

Above the shale is the light gray to dark gray cliff-forming Chambless Limestone described by Hazzard (1954). Composed mostly of fine-grained limestone muds, the most conspicuous feature in the rock unit is algal oncolites, of genus *Girvanella* found in the basal limestone (Figure 5); (Hazzard, 1937; Hazzard, 1954; Kilian, 1964; Stewart, 1970; Mount, 1980).

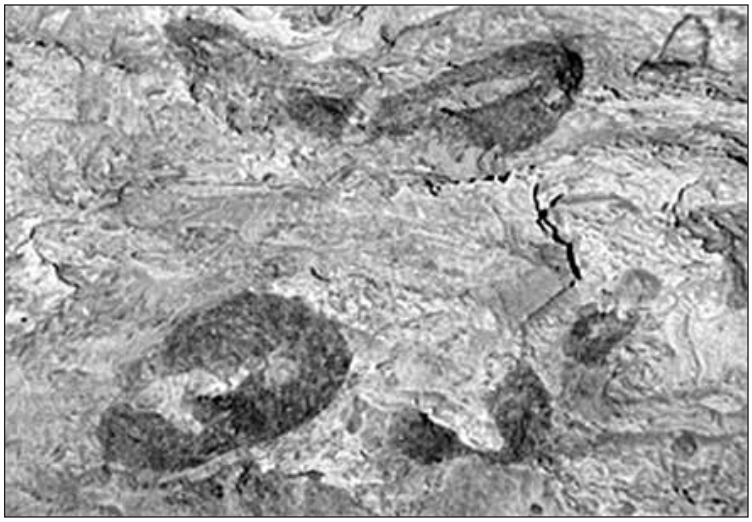

Figure 5. Oncolites from the Chambless Limestone (Photo by B. Bridenbecker).

The Cadiz Formation was originally proposed by Hazzard and Mason (1936), to describe the cliff forming upper rock units composed of quartzite, limestone, and shale in the Marble Mountains. It has been assigned a lower to middle Cambrian age based on fossil content and lies conformably above the Chambless Limestone (Hazzard, 1933; Hazzard, 1954; Kilian, 1964; Mount 1980). Fossils are uncommon and the distinguishing features of the Cadiz Formation are the red to brown colored shales and quartzites found at its base, grading upward into tan shales and limestones interlaced with green shales, and culminating in a bluish gray cliff-forming limestone in its upper regions (Kilian, 1964).

Conformably above the Cadiz Formation is the Bonanza King Formation named by Hazzard and Mason (1936) in the Providence and Marble Mountains. It is a cliff-forming tan to gray colored dolomite and limestone, which is the cap rock in much of the southern to central Marble Mountains (Kilian, 1964). It is correlated based on its stratigraphic position and lithology as described by Hazzard and Mason (1936) and redefined by Hazzard in 1954. Stone et al. (1983) correlated the upper dolomitic section of the Bonanza King Formation with the Undifferentiated Dolomites above the Muav Limestone in the Grand Canyon.

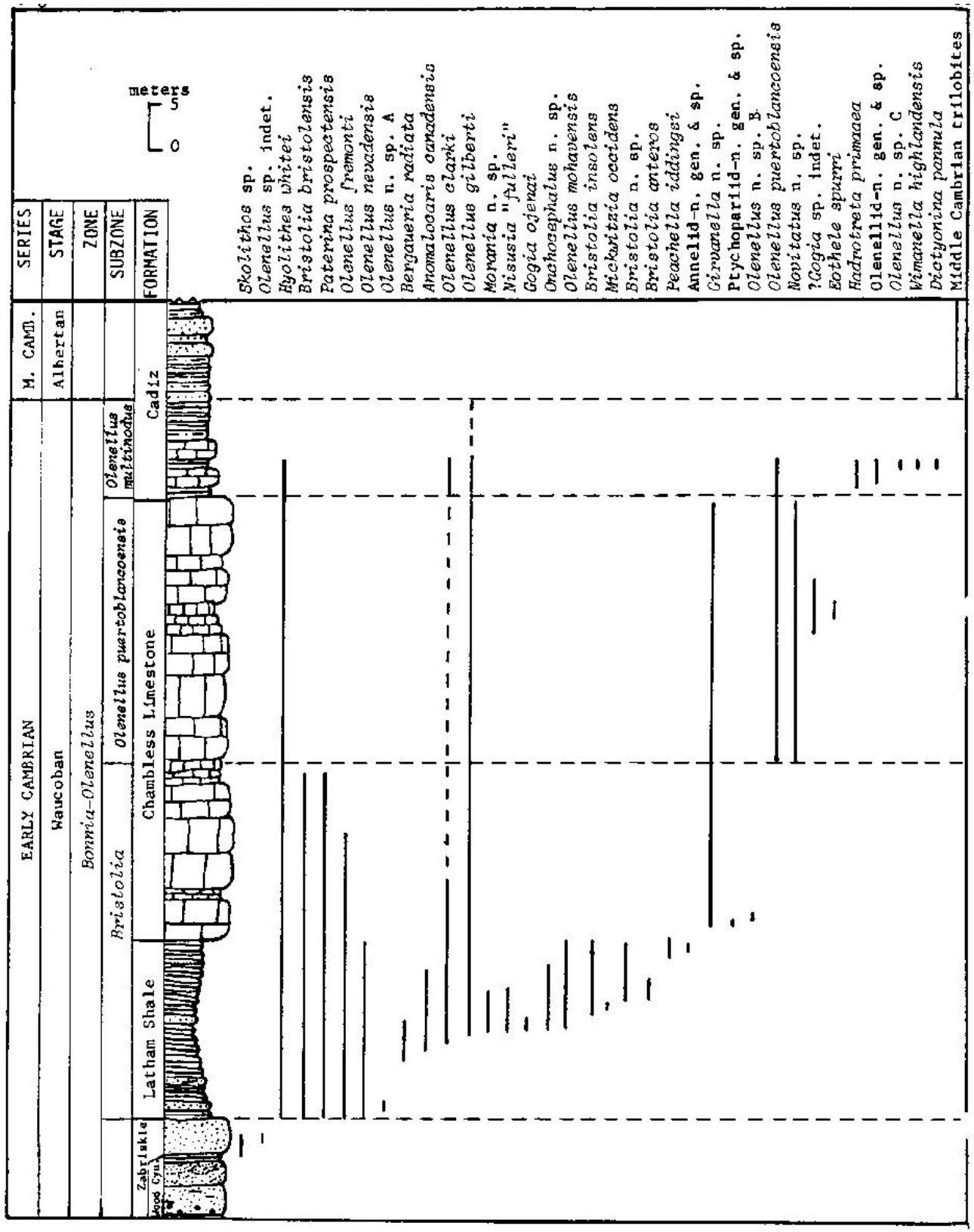

Figure 6. Stratigraphic distribution of Cambrian fossils from eastern San Bernardino County (From Mount, 1980).

The Providence and Marble Mountains are some of the best exposures of Cambrian rocks and fossil assemblages in the southeastern Mojave Desert. A literature search will reveal numerous field guides and papers by geoscientists describing them. Fossil assemblages compiled by Mount (1980) are shown in Figure 6. He has four pages of detailed drawings of fauna found in the Latham Shale, Chambless Limestone, and the Cadiz Formation in his paper which would serve as a starting point for one who wanted to do further research of fauna in the area.

References cited

Hall, D. L., (1985). Contact Metamorphism, Hydrothermal Alteration, and Iron-Ore Deposition in the South-Central Marble Mountains, San Bernardino County, California. Unpub. M. S. Thesis, Univ. of Calif., Riverside, 212 p.

Hazzard, J. C., (1937). Paleozoic section in the Nopah and Resting Springs Mountains, Inyo County, California: Calif. Journ. Mines and Geology, v. 33, no. 4, pp 273-339.

Hazzard, J. C., (1954). Rocks and structure of the Northern Providence Mountains, San Bernardino County, California: Calif. Div. Mines Bull. 170, Chapter IV, Contr. 4, pp. 27-35.

Hazzard, J. C., and Crickmay, C. H., (1933). Notes on the Cambrian rocks of the Eastern Mojave Desert: Univ. Calif. Publ. Geol. Sci., v.23, pp. 57-78.

Hazzard, J. C., and Mason, J. F., (1936). Middle Cambrian formations of the Providence and Marble Mountains: Geol. Soc. Am. Bull., v.47, pp. 229-240.

Kilian, H. M., (1964). Geology of the Marble Mountains, San Bernardino County, California: Unpub. M.A. thesis, Univ. of So. Cal., 109p.

Kurkewitz, R., Communications Director, (n.d.). Western Trilobite Association, retrieved from: http://www.westerntrilobites.com/index.html on December 29, 2013.

Lanphere, M. A., (1964). Geochronologic studies in the Eastern Mojave Desert, California: Jour. Geol., v. 72, pp. 381-399.

Liberman, B. S. (1979). Systematic Revision of the Olenelloidea (Trilobita, Cambrian). Bulletin 45, Peabody Museum of Natural History, Yale University.

McKee, E. D. and Resser, C. E., (1945). Cambrian History of the Grand Canyon Region. Carnegie Institution of Washington, Pub. 563, 232 p.

Mount, J. D., (1980). Characteristics of early Cambrian faunas from Eastern San Bernardino County, California: So. California Paleo. Soc. Sp. Pub., no 2, pp. 19-29.

Nolan, T. B., (1929). Notes on the stratigraphy and structure of the northwest portion of Spring Mountain, Nevada. Amerian Jour. Sci. v. 17, pp. 461-472.

Palmer, A. R. and Halley, R. B., (1979). Physical Stratigraphy and Trilobite Biostratigraphy of the Carrara Formation (Lower and Middle Cambrian) in the Southern Great Basin: U.S. Geological Survey Professional Paper 1041, 160 p.

Silver, L. T., (1964). U/Pb radiometric date quoted on Geologic Maps of California, Needles Sheet.

Stone, P., Howard, K., and Hamilton, W., (1983). Correlation of metamorphosed Paleozoic strata in the southwestern Mojave Desert Region, California and Arizona. Geol. Soc. Am. Bull. v 94, pp 1135-1147.

Stewart, J. H., (1970). Upper Precambrian and Lower Cambrian Strata in the southern Great Basin, California and Nevada. U.S. Geological Survey Professional Paper 620, 206 p.

Stewart, J. H., (1991). Latest Protterozoic and Cambrian rocks of the Western United States – an overview, in Cooper, J. D. and Stevens, C.H., eds., (1991). Paleozoic Paleography of the Western United States: Vols I & II, Pacific Section SEPM, v 67, pp 13-38.

Waggoner, B., (n.d.). Localities of the Cambrian: The Marble Mountains, Retreived from http://www.ucmp.berkeley.edu/cambrian/marblemts/marbleslabeled.jpg on 1/15/08.

Tertiary basin evolution in the Ship Mountains of southeastern California

Martin Knoll

Professor of Geology and Hydrology, Dept of Forestry and Geology, University of the South, Sewanee, TN 37383, mknoll@sewanee.edu

The Ship Mountains are located in the eastern Mojave Desert of southern California (Figure 1). In the NE part of the range Miocene-aged strata reach a thickness of more than 1700 m and lie unconformably above a basement complex of Precambrian gneisses, Mesozoic granite, and Paleozoic metasedimentary rocks (Figure 2). The Miocene sequence records syntectonic sedimentation and volcanism associated with a major episode of extensional tectonism in the SW U.S. (Howard and John 1987; Knoll et al. 1986; Nielson 1986; Hileman et al. 1987; Hileman et al. 1990; James et al. 1993). The Ship Mountains structural block moved down to the west along a large-scale, low-angle listric normal fault (Figure 3). This detachment fault is exposed on the western flank of the Old Woman Mountains and extends westward beneath the Ship Mountains (Ship Mountains Fault of Figure 1) (Hileman et al. 1990). Its presence between the two ranges has been corroborated by gravity studies (James et al. 1993). Provenance studies of clasts along with paleocurrent measurements in the Ship Mountains Miocene sedimentary sequence indicate that the Old Woman Mountains to the east acted as a structural horst and primary source for sediment (Knoll 1988).

Miocene Sequence

The Miocene strata in the Ship Mountains can be divided into a lower clastic sedimentary sequence, a volcanic sequence and an upper clastic sedimentary sequence (Figure 3). The lower sequence is separated from younger units by a megabreccia layer (Figure 3). The only age control is provided by the Peach Springs Tuff at the top of the volcanic sequence (Figure 3), originally dated at 18.5 +/- 0.2 Ma (Young and Brennan 1974; Glazner et al. 1986; Nielson et al. 1990) and then later dated at 18.78 +/- 0.02 Ma (Ferguson et al. 2013). Although an older age constraint is lacking in the Ship Mountains, similar Miocene strata in adjacent ranges suggest basal age dates between 18-23 Ma (Howard et al. 1982; Glazner and Nielson 1986).

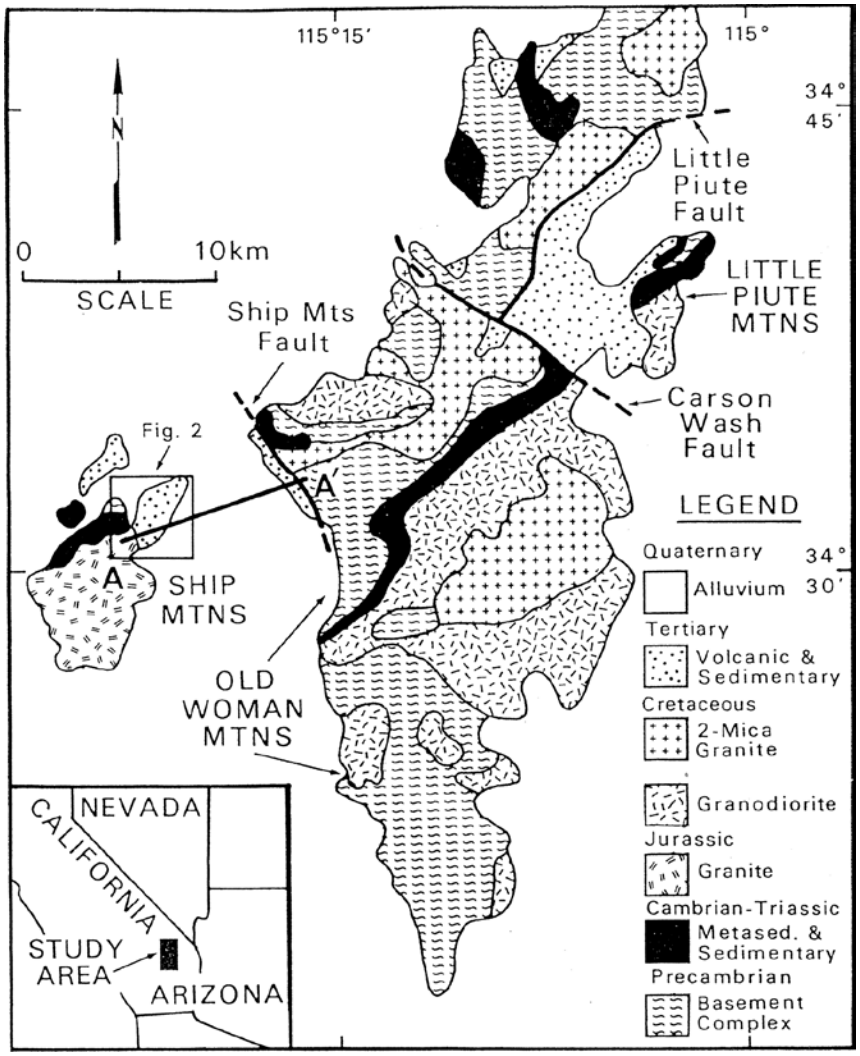

Figure 1: Generalized geologic map of Ship Mountains-Old Woman Mountains area. Note location of figure 2 and cross section A-A'. Adapted from Hileman et al. (1990)

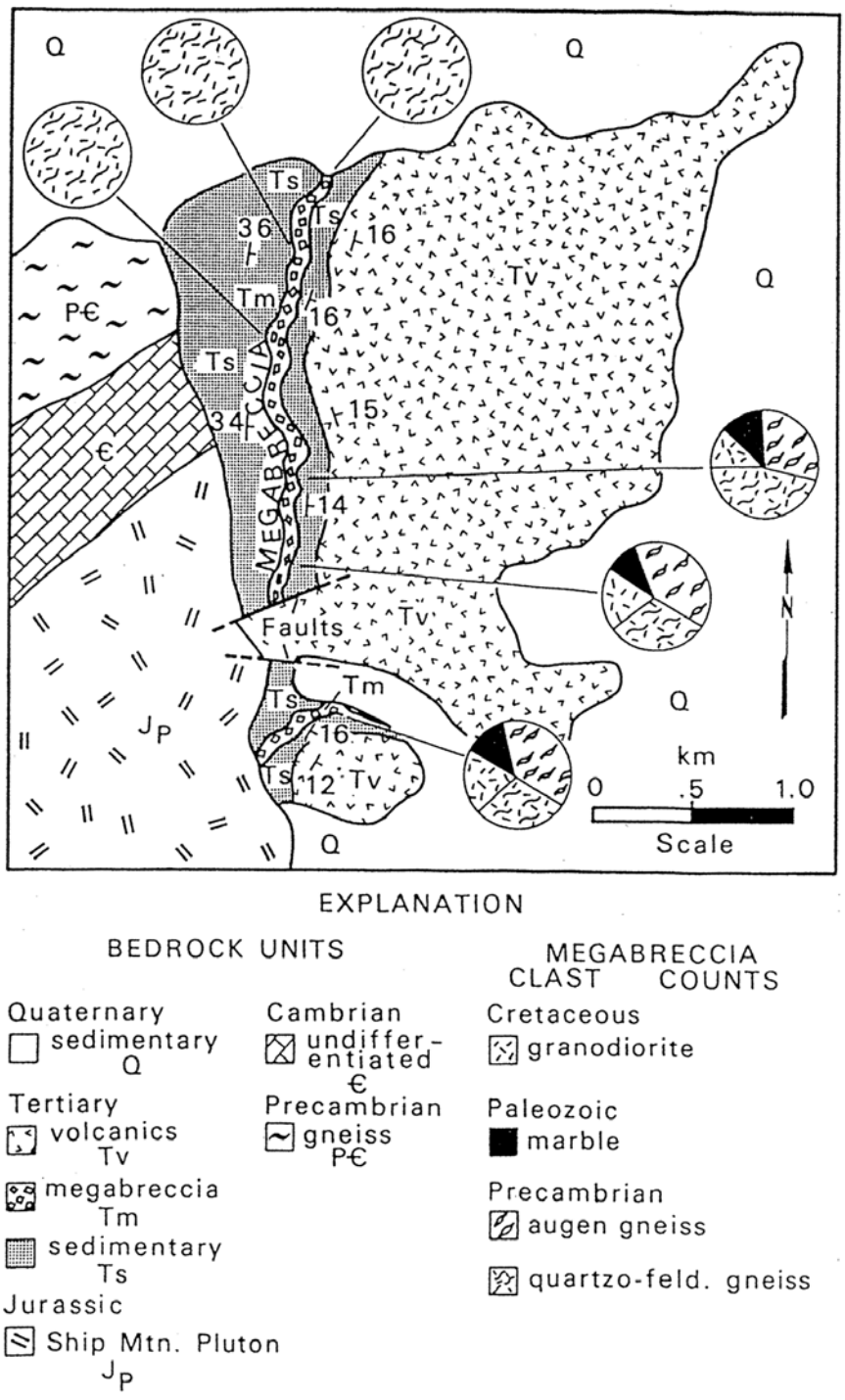

Figure 2: Geologic map of northeastern Ship Mountains. Pie diagrams record 200 grain clast composition counts of megabreccia. From James et al. (1993)

Lower Sedimentary Sequence

The lower sequence (approximately 400 m) is composed of sandstones and conglomerates with gravel-sized clasts and sand-sized lithic fragments dominated by plutonic and metamorphic lithologies. Local basement clasts of Jurassic granite appear in the basal strata above the depositional surface. Volcanic rock fragments first appear in the upper one-third of this lower sequence. These are initially silicic to intermediate in composition, but there is a change to more mafic lithologies upward through the section.

With the exception of the Jurassic granite and volcanic clasts, most other rock fragments are correlative with basement lithologies exposed to the east in the Old Woman Mountains. Paleocurrent direction indicators measured from clast imbrication and cross bedding reaffirm transport of sediment westward from the Old Woman Mountains into the Ship Mountains paleobasin.

An extensive facies analysis of the sedimentary rocks by Knoll (1988) indicates deposition on coalescing alluvial sheets, or braidplains, which emanated from the highlands of the Old Woman Mountains to the east. These sheets filled a narrow, laterally restricted basin now exposed in the Tertiary section of the Ship Mountains.

Megabreccia

Separating the lower clastic sequence from the overlying volcanic sequence is a megabreccia unit that is exposed in outcrop for about 3 km (Figure 2). It ranges in thickness from 65 m in its northern exposure to 33 m to the south. The unit is composed of clast-supported boulders and cobbles. Many clasts are 10 -20 m in diameter and are intricately fractured. Clasts are composed of Proterozoic leucocratic, quartzo-feldspathic gneiss and Proterozoic quartzo-feldspathic augen gneiss, with subordinate Cretaceous granodiorite and Paleozoic marble. Clasts are correlative with basement lithologies now exposed to the east in the Old Woman Mountains. The top of the megabreccia is covered with a 25 cm thick, siltstone to fine sandstone layer with local

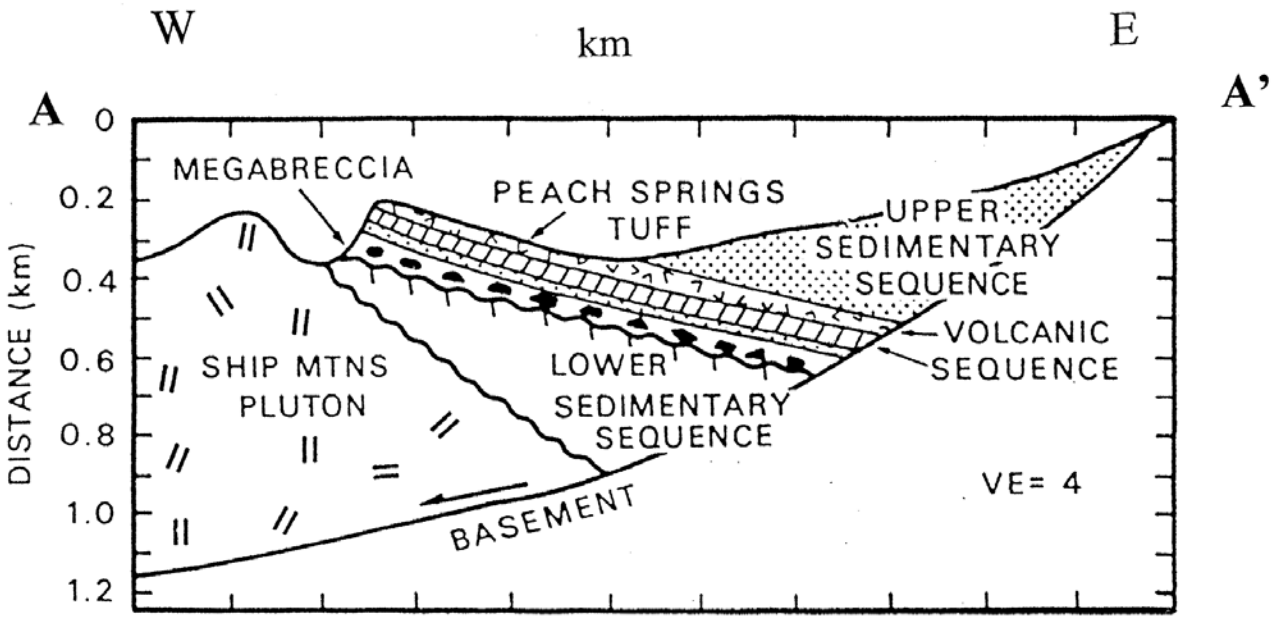

Figure 3: Reconstructed cross section (A-A') depicted in Figure 1 from western flank of Old Woman Mountains through northeastern Ship Mountains, showing west dipping normal fault and east tilted Miocene strata.

normal grading. The northernmost 0.7 km of megabreccia is characterized by a localized actinolite-magnetite mineralization that, like the clasts, is heavily fractured. Mineralization does not extend past the upper contact into overlying layers. The megabreccia is in places dissected by vertical sandstone dikes that were emplaced from below and that are not fractured. The megabreccia has been interpreted as a catastrophic landslide deposit, with large clasts fracturing upon impact with each other and the ground as the slide came to its final resting place (James et al. 1993; Knoll 1988). This is corroborated by the sandstone dikes that were injected from below, and by the clast lithologies, which correlate with units now exposed to the east in the Old Woman Mountains. Furthermore, the megabreccia dips to the east at between 12-16 degrees, while the sequence below dips eastward at 34-36 degrees. This implies multiple phases of fault block rotation along the listric detachment surface. Initial fault block rotation down to the west moved the lower sequence westward and exposed a steep fault scarp to the east in the Old Woman

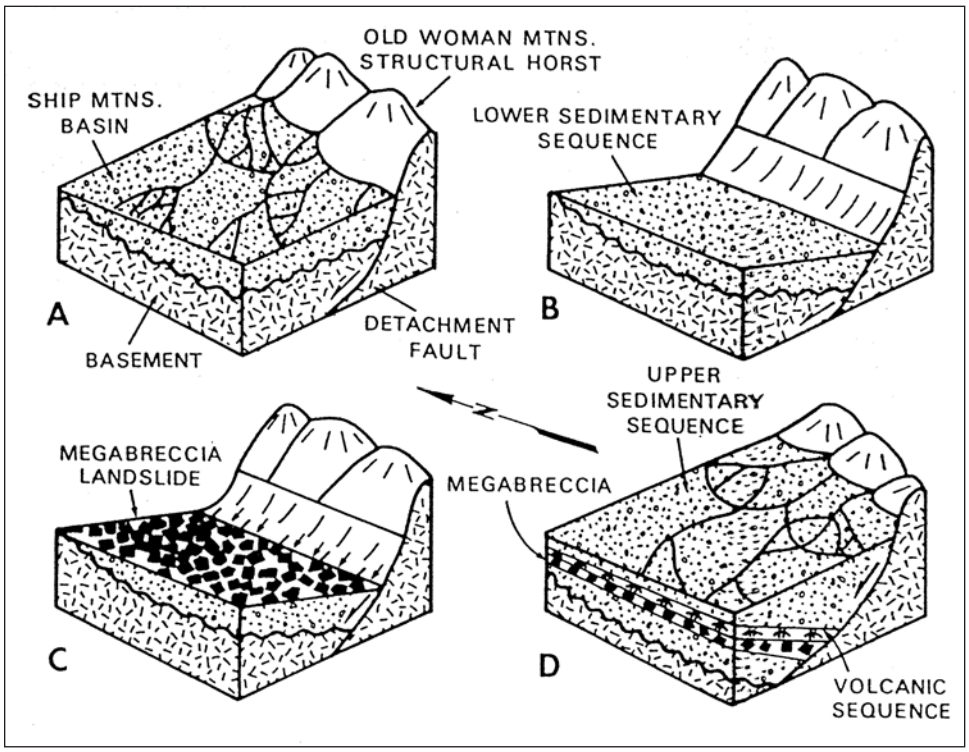

Figure 4: Basin evolution and megabreccia genesis, west of the Old Woman Mountains structural horst. (*A*) Deposition of lower sedimentary sequence; (*B*) Contemporaneous and subsequent rotation of strata along detachment surface producing exposed fault scarp; (*C*) Formation of megabreccia unit as landslide from the Old Woman Mountains; (*D*) Subsequent block movement along detachment fault, rotation of strata, and deposition of volcanic sequence and upper sedimentary sequences. From James et al. (1993).

Mountains from which the landslide originated (Figure 4).

Volcanic and Upper Sedimentary Sequences

The multiple basalt flows of the volcanic sequence indicate an important phase of mafic local volcanism that persisted until deposition of the Peach Springs Tuff (Figure 3). Numerous mafic volcanic rock fragments in the upper clastic sedimentary sequence indicate continued volcanic activity in the Ship Mountains area in post-Peach Springs Tuff time. However, the last major volcanic phase in the Ship Mountains is represented by the uppermost basalt flows of the volcanic sequence. The Peach Springs Tuff cannot be considered as the final major volcanic pulse in the range because its source, the Silver Creek Caldera near Oatman, Arizona, is far removed from the Old Woman Mountains area (Ferguson et al. 2012). Sub-Peach Springs Tuff conglomerates which directly overlie the last mafic flows in the Ship Mountains are composed of clasts of Old Woman Mountains basement lithologies and record a return to denudation of the Old Woman Mountains source block. The lack of Peach Springs Tuff clasts in the upper sedimentary sequence of the Ship Mountains indicates rapid burial of the tuff after deposition.

Conclusion

The Miocene strata of the Ship Mountains record syntectonic sedimentation and volcanism within a laterally restricted basin. Clastic sediments were deposited within the framework of a coalescing alluvial fan complex and were derived primarily from basement lithologies to the east in the Old Woman Mountains. Volcanic rock fragments and basaltic flows indicate a change from initial silicic to intermediate volcanism to mafic volcanism. The most important unit in the Miocene sequence is the megabreccia, which is interpreted as an avalanche deposit originating from a steep fault headwall to the east in the Old Woman Mountains. Decreasing dip of strata upward through the section indicates periodic movement along the west-dipping, underlying listric detachment surface.

References cited

Ferguson, C. A.; McIntosh, W. C.; and Miller, C. F., 2013, Silver Creek caldera- The tectonically dismembered source of the Peach Spring Tuff: Geology, v. 41, p. 3-6.

Glazner, A. F.; Nielson, J. E.; Howard, K. A.; and Miller, C. F., 1986, Correlation of the Peach Springs Tuff, a large-volume Miocene ignimbrite sheet in California and Arizona: Geology, v. 14, p. 840-843.

Glazner, A. F., and Nielson, J. E., 1986, Introduction and road log, *in* Nielson, J. E., and Glazner, A. F., eds., Cenozoic stratigraphy, structure, and minerlization in the Mojave Desert: Geol. Soc. America Cordilleran Sect. Guidebook and Volume, 82nd Annual Meeting, p. 1-6.

Hileman, G. E.; Miller, C. F.; and Knoll, M. A., 1987, Middle Tertiary structure of the Old Woman Mountains region, southeastern California: Geol. Soc. America Abs. with Prog., v. 19, p. 389.

Hileman, G. E.; Miller, C. F.; and Knoll, M. A., 1990, Mid-Tertiary structural evolution Of the Old Woman Mountains area: implications for crustal extension across Southeastern California: Jour. Geophys. Res., v. 95, p. 581-597.

Howard, K. A., and John, B. E., 1983, Extensional faulting through the upper crust, California-Arizona border: Geol. Soc. America Abs. with Prog. V. 15, p. 309.

Howard, K. A.; Stone, P.; Pernokas, M. A.; and Marvin, R. F., 1982, Geologic and Geochronologic reconnaissance of the Turtle Mountains area, California: western Border of the Whipple Mountains Detachment Terrane, *in* Frost, E. G., and Martin, D. L., eds., Mesozoic-Cenozoic Tectonic Evolution of the Colorado River Region, California, Arizona, and Nevada: San Diego, California: Cordilleran Pub., p. 341-355.

James, W. C.; Knoll, M. A.; and Mickus, K. L., 1993, Ship Mountains megabreccia: Implications for Miocene extensional tectonics, eastern Mojave Desert, California: Jour. of Geology, v. 101, p. 115-120.

Knoll, M. A.; Miller, C. F.; and James, W. C., 1986, Mid-Tertiary stratigraphic and Structural evolution of the Piute Mountains basin and adjacent areas of the Old Woman Mountains region, southeastern California, *in* Nielson, J. E., and Glazner, A. F., eds., Cenozoic stratigraphy, structure, and mineralization in the Mojave Desert: Geol. Soc. American Cordilleran Sect. Guidebook and Volume, 82nd Annual Meeting, p. 43-50.

Knoll, M. A., 1988, Tertiary basin evolution, eastern Mojave Desert: PhD Dissertation, University of Texas, El Paso, 189 p.

Nielson, J. E., 1986, Miocene stratigraphy of the Mojave Mountains, Arizona, and correlation with adjacent ranges: *in* Nielson, J. E., and Glazner, A. F., eds., Cenozoic stratigraphy, structure, and mineralization in the Mojave Desert: Geol. Soc. America Cordilleran Sect. Guidebook and Volume, 82nd Annual Meeting, p. 15-24.

Nielson, J. E.; Lux, D. R.; Dalrymple, G. B.; and Glazner, A. F., 1990, Age of the Peach Springs Tuff, southeastern California and western Arizona: Jour. Geophys. Res., v. 95, p. 571-580.

Young, R. A., and Brennan, W. J., 1974, Peach Springs Tuff: its bearing on structural Evolution of the Colorado Plateau and development of Cenozoic drainage in Mojave County, Arizona: Geol. Soc. America Bull., v. 85, p. 83-90.

Ship Mountains mines

Larry M. Vredenburgh

Bureau of Land Management, 3801 Pegasus Dr., Bakersfield, CA 93308

The first published report of mining activity in the Ship Mountains did not appear until 1901. In September of that year, the Los Angeles Mining Review noted that Walter L. Hastings, owner of the Vulcania, Black Warrior, Copper Carbonate, Ventura, Little Ida, and Imperial mining claims had sunk a 40 foot shaft on the Vulcania which assayed up to 1.5 ounces of gold across a 16 inch pay streak. J. A. McCarty leased the Little Ida claim and was sinking a shallow shaft that showed rich values of copper and gold.

One month later, Hastings sold his claims to a Mr. Delane, who immediately began working a "force of men" mining and "sacking ore." In February 1902, a strike was reported from the Vulcania which reportedly yielded $174 to the ton (nearly 9 ounces) across an 18 foot ledge. About this same time McCarty employed four men to drive an adit on the Iron Cap mine that assayed high values of gold.

In July 1902 a contract was let to Huff and Wolacott to sink a 100 foot shaft with drifts 100 feet each way along the vein on the Vulcania.

P. H. McDermot, president and general manager of the Siam Mining Company, in June 1906 shipped 25 tons of gold ore to the Needles smelter that yielded $43 per ton in gold (gold was $20 per ounce at that time). The mine by now had about 1,000 feet of underground workings. A July 1907 report by mining engineer D. L. Vandervoort extolled the virtues of the property as follows:

> The sight which greets the visitor upon arrival at the Siam property is most pleasing. In plain view are the necessary mine buildings, engine house,

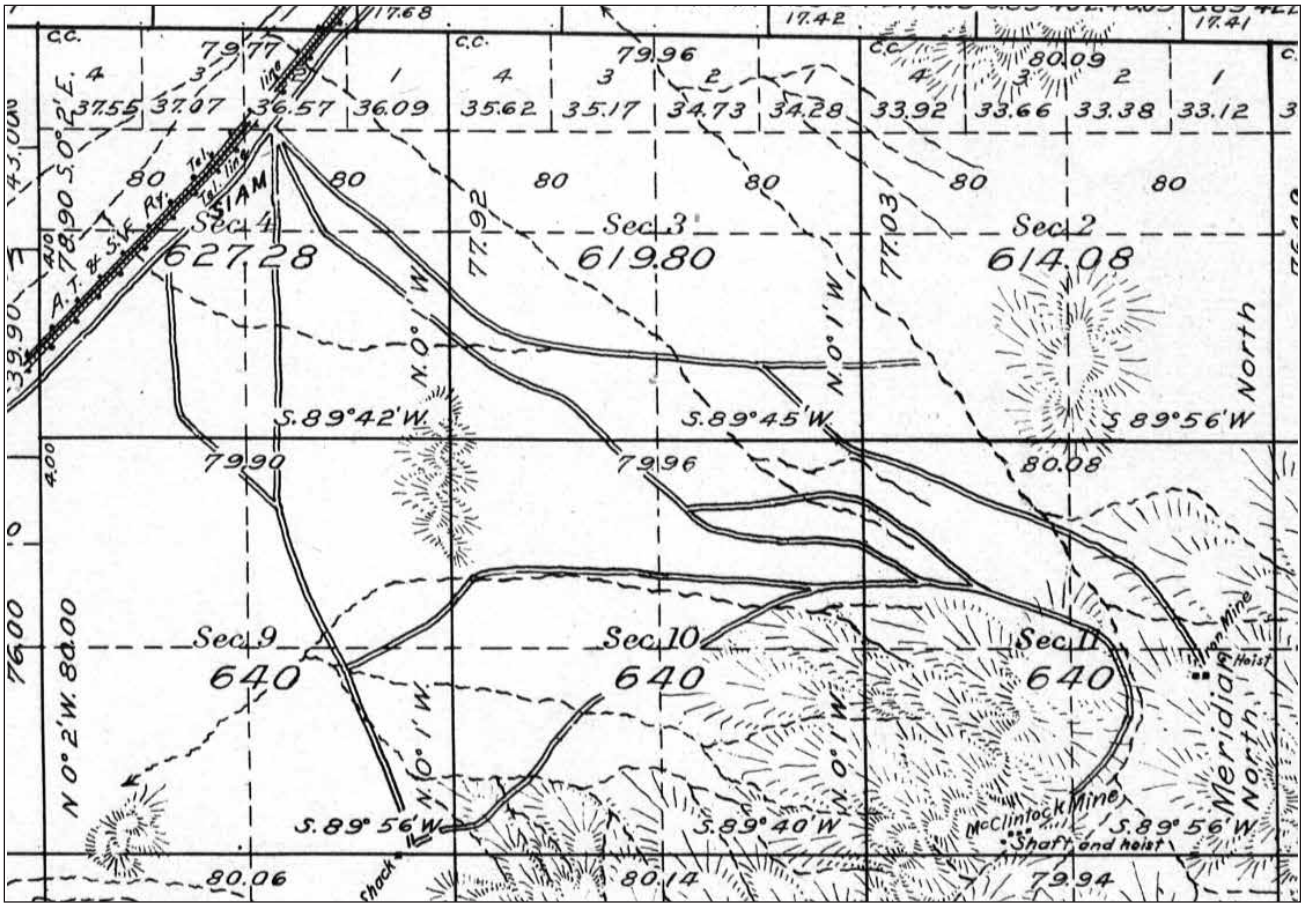

1923 General Land Office Survey of Northern Ship Mountain

> machine shops, assay office, cook house, bunk houses and offices. Most impressive perhaps is the stately gallows frame which rests upon the collar of a perfectly constructed and timbered shaft 400 feet in depth.

When the General Land Office cadastral surveyors visited the site around 1920, the Vulcan mine is shown on their survey plat as "McClintock Mine." I can't help but think McClintock is really McDermot, but more research is obviously needed to straighten this out.

W. B. Tucker in 1943 wrote:

> Located in 1898 by McClintock, the property has been worked off and on to date. From 1935 to 1937, it was under lease to Funk Brothers and H. J. Jackson, Ludlow, California. During this period the production was $50,000 in gold, the ore being mined from the 100-foot level to surface. Ore shipped is reported to have averaged $40 per ton in gold. From February 1941 to February 1942, the property was under lease to Rashly, Inc., William W. Dowsing, president, R. C. Aurand, secretary, Santa Monica, California. They shipped 1500 tons of ore to American Smelting & Refining Company's smelter, Hayden, Arizona.

The Ship Mountains iron deposit, located about a quarter mile northeast of the Vulcan mine, was first described by James Crossman in 1890. The property was examined in the early 1943 as part of a thorough examination of the iron deposits of California. At that time the mine was operated by Earl Paul of Upland California. It was developed by four short adits and a 365 foot incline shaft with 830 feet of underground workings. Total reserves were estimated as 80,000 long tons.

On October 6, 1936 the United States issued a patent for 160 acres to Ira J. Coe for the Siam No. 1 Placer Mining claim. This property, also known as the Twin Buttes, is located in the southwest quarter of Section 9. T5N, R15E. The deposit was estimated to contain 8 million tons of dolomite. In 1947 the property was under lease to Charles I. Chubbuck.

References

Crossman, James H. "San Bernardino County It Mineral and Other Resources – Number V" *Mining and Scientific Press,* 9 Aug 1890, p. 85.

De Kehoe, Joe, 2007, *The Silence and the Sun* (Trails End Publishing Company: Bakersfield, CA) p. 74 – 88.

Engineering and Mining Journal: 29 Mar 1902, 26 Jul 1902, 28 Jun 1906 p.645, 17 Nov 1906 p. 945.

Lamey, Carl A., 1948, "Ship Mountains Iron-Ore Deposit, San Bernardino County," *California, Iron Resources of California*, California Division of Mines, Bulletin 129 p. 113 – 116.

Logan, C. A. , 1947, "Limestone in California", *California Journal of Mines and Geology*, Vol. 43, No. 3, p. 296.

Los Angeles Mining Review: 21 Sep 1901, 26 Oct 1901, 16 Nov 1901, 8 Mar 1902, 5 Jul 1902.

Los Angeles *Herald*: 1 March 1902, 1 July 1906, 3 Jan 1907, 22 July 1907, 4 Nov 1907, 9 Dec 1907 p. 10.

Mining World: 28 Jul 1906, p. 10.

Redlands *Citrograph:* 15 Mar 1902.

San Bernardino *Sun* 5 Jan 1907, page 12.

Siam No. 1 Placer Mining Claim. Patent No. 052395, CALA 0052395, 6 Oct 1936.

Tucker, W. B. and Sampson, R. J., 1943, "San Bernardino County" *California Division of Mines*, Report Vol. 39, pp 137.

Weight, Harold O., "Gem 'Harbors' in the Ship Mountains," Desert Magazine, Vo. 19, No. 8, Aug. 1956, p. 6–10.

Wright, L. A., et. al. 1953, "Mines and Mineral Deposits of San Bernardino County, California," *California Division of Mines* Report Vol. 49, p. 62.

History of mining in the Old Woman Mountains

Larry M. Vredenburgh
Bureau of Land Management, 3801 Pegasus Dr., Bakersfield, CA 93308

Beginning in February 1889, articles began appearing in newspapers describing the immense deposits that had been discovered in the Old Woman Mountains. Captain Bethune, who had just returned from a prospecting trip to the range, stated confidently,

> I candidly believe this to be the largest body of mineral in the world." Another prospector was quoted saying, "The ore on the surface is so abundant that it would keep smelting works such as those at Argo, Colorado, busy for fifty years.

The Scanlon Mining District that sprang up here was named after a prospector, Peter Scanlon, who had prospected the range for years. In the summer of 1889, Captain Bethune arrived in Redlands to escape the hot weather and pronounced, "Our mining prospects are grand and… we must have a smelter at Needles." Despite these optimistic predictions, just a year later, in 1890, the Scanlon District was described as being "so little developed as hardly to merit... mention."

Based on numerous not-so-reliable reports, small stringers of high grade silver and gold ore were found throughout the range. Portions of the Old Woman Mountains have so many mine symbols on the 7 ½ minute topographical maps that the area resembles a pin-cushion. However, production from the Scanlon District was modest at best. A contribution to the low production may be that most of the values appear to have been tied up in sulfide minerals and were not free milling. Silver caused the 1889 excitement, but gold and tungsten were also produced.

On the northwest side of the range about 6 miles from Danby, the Wheel of Fortune Mine was discovered about 1897. Later, in March 1911, Walter G. Pinkett, a Danby saloon owner, owned the mine and had a "force of men" working on a 60 foot shaft on the property. In December 1913, a bunkhouse and a blacksmith shop were on the property.

The Warwick mine, owned by Mr. A. W. Warwick of Martinez, Arizona, was located near the Wheel of Fortune. In January 1900 an article stated a 10-stamp mill had been erected, but a year and a half later it was reported that "the company will start up the mill… soon." Lack of water was the cause of the delay. By December 1902 it was stated that "the owners of Camp Warwick… are doing assessment work."

The Silver Wave Mine, high on the west side of the range in Scanlon Canyon, was first worked prior to 1890, but was inactive until late 1899. At that time Milo James Smith, a native of West Virginia, purchased the property for $150. After making a strike of rich ore, Mr. D. Jackson secured a bond on the property for $35,000. Between the purchase and March 1902, $12,000 had been expended in development. By July the adit was 650 feet long. A five-stamp, steam-powered mill was erected and running about July 1902, and 20 men were employed on the property. In 1909 the mine camp, which was

Headframe on the east side of the range in the early 1970s. Photo by the author.

near a spring, was in ruins, and the mill had been dismantled.

The Stemwinder Mine was "doing well" in January, 1900, but it was not until 1905 that this mine, located 20 miles south of Danby (perhaps in Carbonate Gulch), began to draw attention. During that year, the Stemwinder Mining and Development Company, capitalized for a quarter of a million dollars, was developing the mine. In September, 1911, a brief note indicated that the owners were waiting for cooler weather before mining.

On the southwest end of the range, the Black Metal Mine was first located before 1896. It was relocated in 1902 by M. J. Smith and George B. Parks of Barstow. In 1910 they had hoped to lease it to C. H. Scheu, a Los Angeles mining man, for $30,000. In September Scheu and Parks visited the property, but the deal apparently fell through.

Smith and Parks, in February 1911, dissolved their partnership in the Black Metal and other property they owned. Parks became owner of the Black Metal and the Desert Butte Group near Kilbeck Siding. In March 1911, he purchased a span of mules to haul ore from the Black Metal and Desert Butte Group. That April, George Parks and his wife left for the mines with a "carload of goods and supplies." Parks was busy mining during the next two months; his first rail car-load (20 tons) of ore grossed $27 a ton. In August he was ready to ship another 20 tons of ore. That November (1911) Parks and his wife left the Black Metal, and he pursued general contracting.

The Grass Roots Mine, which was adjacent to the Black Metal, was discovered about 1889 by A. E. S. "Scott" Price. After the Parker branch of the Santa Fe was built, Price, in partnership with A. Bert Day, began working the mine, and they were richly rewarded. In November 1910 they brought specimens to Parker, Arizona which assayed 300 ounces in silver, 12 percent copper, a large percentage of lead, and some gold. As soon as news was out and, prospectors and mining men from all directions are began to arrive there. Day and Price located a townsite and predicted "that a camp will be started."

In March, 1911, the shaft was down to 60 feet. In April, they shipped a car load of ore. In June the Garner brothers of San Bernardino purchased the interest of Day. Sinking of the shaft was resumed

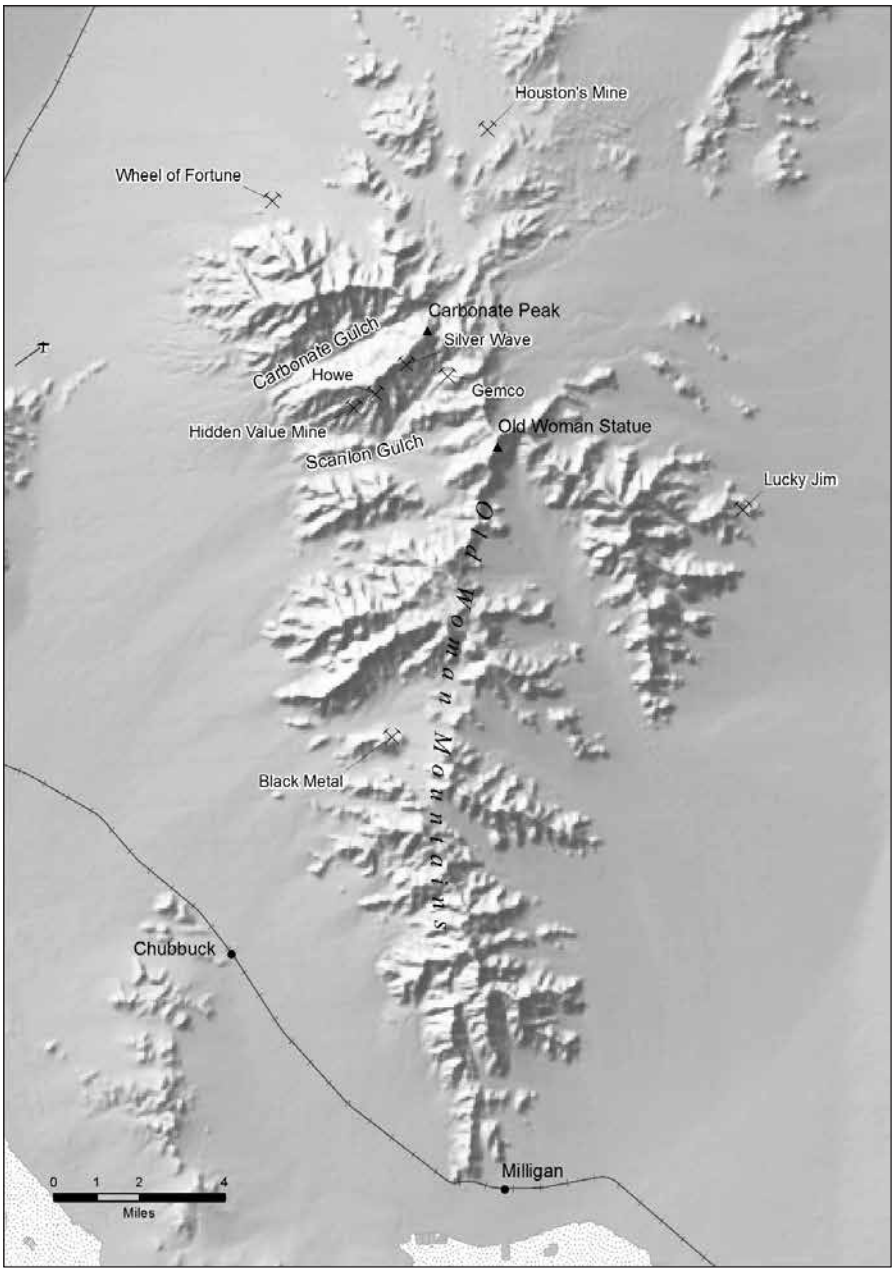

Map of the Old Woman Mountains showing location of mines and shafts.

that August, but was halted in October after Harry Nelson, who was employed sinking a 25 foot shaft, was killed in a cave in. Operations were idle until September 1912, when Scott Price and Fred Schmickle resumed operations. There was plenty of water nearby and they expected, by February 1913, to put in a large mill, but nothing further is heard about the mine.

Poker Flat was located in the northern most portion of the range, at what is now named Weaver's Well. Sam Houston was overhauling his stamp mill here in February 1911, and on the Consolidated Mining Company claims, owned by Walter G. Hopkins, a new strike was made in March 1911. Houston's mine is shown on the 1910 General Land Office survey of this township.

The Lucky Jim silver mine, situated on the southeast side of the range, was located by P. W. Dayton in 1911. The property was purchased by the Maricopa Queen Oil Company, and by June 1913 a camp was established here, with water piped from a spring about 3 miles to the southwest (Sec 33 T5N, R18W). In 1914, the camp consisted of bunkhouses, a boarding house, and a barn. The property was active at least until 1916; at that time ten men were employed and silver ore was hauled to the railroad siding of Milligan. During this period of operation the mine is variously referred to as the Dayton or the Maricopa Queen.

In November 1917, David G. Thompson with the U. S. Geological Services visited the mine camp which he referred to as Wilhelm Camp. However, the General Land Office survey of the township, which was underway when Thompson visited, depicts Morath's Mine and shows a house and adit just to the north. This survey also shows the pipeline from "Wilhelm Spring" ending at Morath's mine.

As early as 1921 the mine was owned by Eugene G. Morath of Long Beach; in 1930 it was under lease to F. A. Crampton. Three men were employed at the mine and the camp consisted of three cabins and a blacksmith shop. One former miner who was employed here between the late 1920s and early 1930s noted that the main adit was engineered (in the period 1913–1916) with a slight slope, so that a full ore car could be pushed out with very little effort. Between 1911 and 1930, about $35,000 worth of silver, gold, copper, and lead were produced.

During World War II, Hidden Value and the Howe produced tungsten ore. These mines are located on the west side of the range southwest of Carbonate Peak. Ore from the Hidden Value was treated in a small mill located in Danby. The workings from both mines were connected with aerial trams. At the Howe a small mill was erected in 1952.

References

Barstow Printer, 15 Mar 1902, 22 Jul 1910, 10 Mar 1911, 10 Feb 1911, 10 Mar 1911, 24 Mar 1911, 7 Apr 1911, 8 Aug 1911, 22 Sep 1911, 31 Jan 1913.

Battye, Charles, "Old Woman Mountains," *Desert,* December, 1940, p. 36.

Blythe *Palo Verde Valley Herald 16* Mar 1911, 6 Apr 1911, 26 Jun 1911, 10 Aug 1911, 19 Oct 1911, 19 Sep 1912, 1 Feb 1913.

Cooper, Thomas, "The Tunnel-Driving Wilhelms", *Desert Magazine*, Feb. 1980, p. 55.

Crossman, James H., "San Bernardino County, Its Mineral and Other Resources," *Mining and Scientific Press*, January 10, 1891.

DeGroot, H, 1890, "San Bernardino County: Its Mountains, Plains and Valleys," California Mining Bureau Report 10, 1890, p. 533.

Engineering and Mining Journal: 20 Jan 1900, 6 Apr 1901, 25 may 1901, 12 Apr 1902 26 Jul 1902, 22 Nov, 1902, 6 Dec 1902, 12 Dec 1902.

Los Angeles *Herald*: 17 Apr 1892, 11 May 1892, 11 Dec 1896, 28 Oct 1902, 29 Dec 1902, 28 May 1905, 23 Jun 1907, 23 Nov 1910.

Los Angeles *Mining Review*: 11 Mar 1899, 20 Jul 1901, 21 Sep 1901, 28 Sep 1901, 12 Oct 1901, 26 Oct 1901, 16 Nov 1901, 11 Jan 1902, 8 Mar 1902, 2 Aug 1902, 29 Dec 1902.

Mining and Scientific Press: 10 Jan 1891, 1 May 1891, 2 Apr 1898, 11 Feb 1899, 11 Mar 1899, 8 Sep 1899.

Needles *Booth's Bazoo*: 16 Mar 1889, 30 Mar 1889, 27 Apr 1889, 4 May 1889, 3 Aug 1889, 17 Aug 1889.

Parker *Post*: 14 Oct 1911, 25 Jan 1912, 14 Jun 1913, 9 Oct 1915, 22 Jan 1916, 17 Jun 1916.

Redlands *Citrograph*: 27 Apr 1889, 10 Aug 1889, 20, Mar 1897, March 15, 1902, June 3, 1905.

Thompson, David G, 1921, "Routes to Desert Watering Places in the Mohave Desert Region," *U. S. Geological Survey Water Supply Paper 490-B*, p. 221.

Tucker W. B. and R. J. Sampson, 1931, "Los Angeles Field Division, San Bernardino County," *California Division of Mines Report 27,* p. 274.

Vredenburgh, Larry M., Shumway, Gary L., Hartill, Russell D., 1981, Desert Fever (Living West Press: Canoga Park) pp. 127–133.

Wright, L. A. et. al., 1953, "Mines and Mineral Deposits of San Bernardino County, California," *California Journal of Mines and Geology, Vol. 49,* p. 148, 149.

Chubbuck, California

Larry M. Vredenburgh

Bureau of Land Management, 3801 Pegasus Dr., Bakersfield, CA 93561s

A short time prior to the San Francisco 1906 earthquake and fire, Charles Inglis Chubbuck moved to the city from Ottawa, Canada, and with a Mr. Harris founded a building materials business, "Chubbuck and Harris." After the earthquake, demand for construction materials proved a windfall for these men.

Around 1921 Chubbuck formed his own business that included plants in Los Angeles and San Francisco adjacent to Union Carbide plants that produced acetylene gas from calcium carbide. The calcium carbide was produced in New York, and shipped by rail. A lime slurry was produced as a byproduct, which Chubbuck processed and sold as hydrated lime.

However, the lime had bluish flecks of carbide which made it less than desirable; so in 1921 Chubbuck purchased mining claims along the Parker branch of the Santa Fe Railroad to secure a source of limestone as a whitening agent. The limestone was also to be marketed as crushed limestone and as quick-lime. Between 1922 and 1923 a mining railroad and processing facilities were built; full scale production did not begin until 1925.

A one-mile long, 30-inch gauge railroad connected the limestone quarries and the processing facilities. Motive power for the railroad operations came from two small gasoline "dinkies." One of the locomotives, a Milwaukee gasoline engine, and most of the ore cars and rail came from a winery at Cucamonga. The other locomotive, a Plymouth gasoline engine, and a few side-dump cars came from the construction of the Panama Canal. The Plymouth transported the ore approximately 600 feet from the quarries to a crushing and screening plant just below the quarry, one mile from Chubbuck. The crushed products were taken by the Milwaukee engine to the lime kiln, or to limestone products plant, at Chubbuck siding. The lime kiln produced processed lime and pebble lime. The limestone products plant yielded 40 mesh limestone, 200 mesh for whiting, chicken grits, and foundry rock in 1.5 to 2.5 inch sizes. Most of Chubbuck's equipment for the production of lime and limestone, including the two vertical kilns,

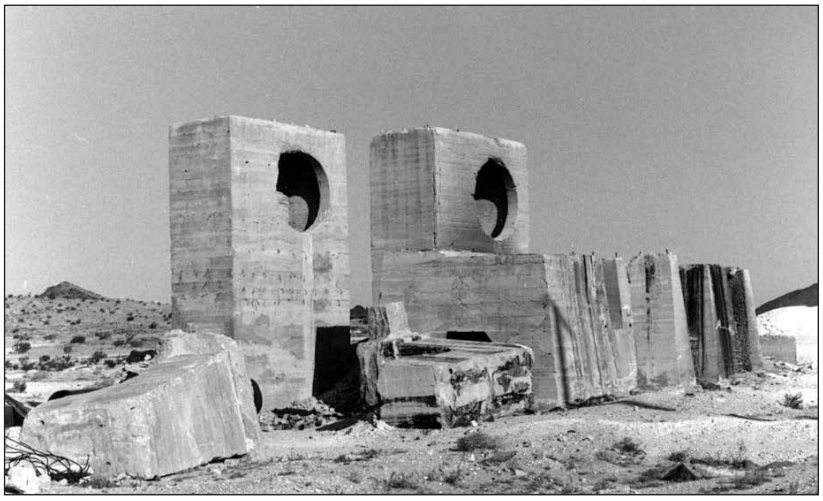

The Chubbuck cement plant. Early 1970s – photo by the author.

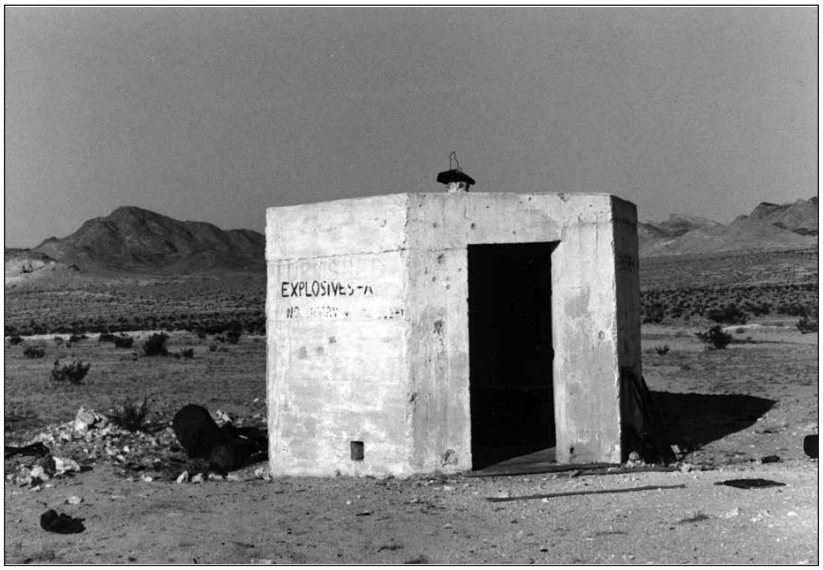

The explosives storage building early 1970s

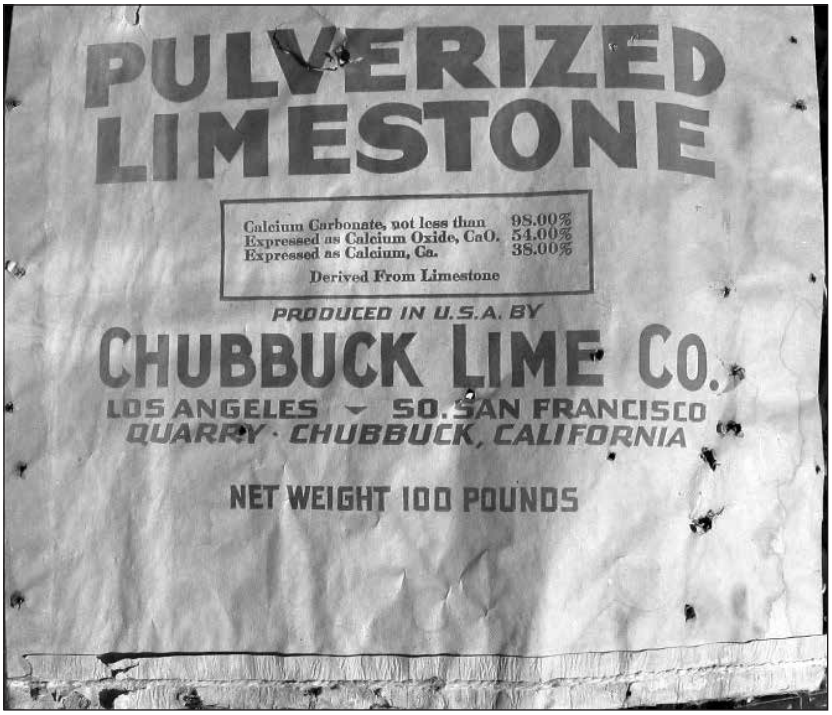

came from limestone quarries at Baxter, in Afton Canyon, on the Union Pacific Railroad.

A horizontal rotary kiln was built, as a stock promotion, by Texas-based company adjacent to Chubbuck's vertical kilns. After it failed to work out, it was given to Chubbuck Lime Company.

Chubbuck consisted of a company store, post office, and school. There were residences for the some 25 workers and their families. A one-room school on the west side of "town" opened by 1932, housing grades one through eight. The school's yearly enrollment ranged from 13 to 40 pupils. A post office was established in May 1938, which was housed in the company store. Water was hauled in by the Santa Fe in tank cars from wells at Cadiz. The workers, who were largely Mexican, earned 25 to 30 cents an hour. The workers were supplied with water and electricity.

Between 1937 and 1938, Chubbuck lime products were used in the construction of the Colorado River Aqueduct by producing a white reflective coating. Concrete was poured for the aqueduct, then covered with asphalt to seal in the moisture for better curing, then a coating of Chubbuck's "Metropolitan White" was sprayed on to reflect the heat. After the contract with the Metropolitan Water District, "Metropolitan White," later named "Snow Coat," was marketed to home owners living in hot areas to reflect the heat off their roofs. After World War II nearly ninety percent of the houses in Palm Springs had roofs coated with this product. It was still being manufactured in the 1970s. The Chubbuck Company also purchased dried calcium-chloride from operations at Bristol Lake and made a product called "Cal" which was used to accelerate the setting of cement. It was also used in the "Snow Coat" and in stucco.

In the late 1940s the Carson Lime Company of Virginia developed a slick, plastic lime that was easier to work. The U.S. Lime Products, division of Flint Kote, was the only company on the West Coast to get the patent rights to the product, called "Miracle Lime." This new product hurt other lime producers. Also during this period Union Carbide stopped shipping its carbide west and ceased their west coast operations. These combined events forced Chubbuck out of business. Production from the Chubbuck quarries was continuous from 1925 through 1948, then intermittent until 1951.

By that time about 500,000 tons of limestone had been produced; two-thirds of this was used for approximately 165,000 tons of lime products; the other third was used directly for limestone products.

In 1951 the Harms Brothers Construction Company of Sacramento purchased the property and equipment from the Reconstruction Finance Company (RFC), since the Chubbuck Limestone Company had stopped payment on a $100,000 loan taken out with the RFC in the 1930s. The Harms Brothers Company intended to mine the limestone and produce lime, but too much silica was present in the limestone. They also had hoped to sell limestone as ballast, but the market never materialized. In its operations the Harms Brothers trucked crushed rock to the kilns.

In 1950 the school, post office, and company store closed. After August of that year the mail was sent to nearby Cadiz. For a few years afterward the population consisted of a few workers employed by the Harms Brothers.

Representatives of several companies were present when the equipment was finally auctioned off by the Harms Brothers. This auction probably took place

in 1954. The kilns were sold for scrap. Chubbuck siding was removed when Santa Fe re-laid the Parker Branch during the winter of 1975-1976.

The sites of the limestone products plant and the company have been bulldozed. Only a heap of rubble remains. The foundations of the other buildings are visible. Some even have the dying remains of trees that were originally planted around the buildings. The scars of Chubbuck's mining railroad are still evident, and most of the ties are there. The crushed limestone roadbed is still prominent although slowly eroding.

References

De Kehoe, Joe, 2007, *The Silence and the Sun* (Trails End Publishing Company: Bakersfield, CA) pp. 108 – 174.

Dixon Chubbuck interviewed July 31, 1977 in his home;

Orrin E. Dunlap, "The first Calcic Carbide Plant" *Mining and Scientific Press*, February 1, 1896 p. 87.

Tucker, W. B. and Sampson, R. J., 1943, "San Bernardino County" *California Division of Mines*, Report Vol. 39, pp 518-520.

Vredenburgh, Larry M., Shumway, Gary L., Hartill, Russell D., 1981, Desert Fever (Living West Press: Canoga Park) p. 132 -134.

Wright, L. A., et. al. 1953, "Mines and Mineral Deposits of San Bernardino County, California," *California Divison of Mines* Report Vol. 49, p. 173.

Danby Dry Lake salt operations

Larry M. Vredenburgh

Bureau of Land Management, 3801 Pegasus Dr., Bakersfield, CA 93561

Danby Dry Lake, situated in the Ward Valley some 30 miles south of the railroad siding of Danby, has been the site of sporadic salt production since the early 1880s. As early as 1882, J. B. Cook, who was associated with the discovery of Bonanza King silver mine, sank a 35 foot shaft in solid rock salt on the north end of Danby Lake. During the 1880s salt from Danby Lake was hauled by freight team to the Santa Fe railroad and shipped to the Waterman, Waterloo, and Bonanza King Mines, as well as to mines in Arizona. Salt was an essential ingredient used in processing silver ore. In 1891 it was reported that W. H. Drew owned the property and that salt from here was being "shipped to Arizona and Mexico for curing beef, salting stock, and for culinary purposes."

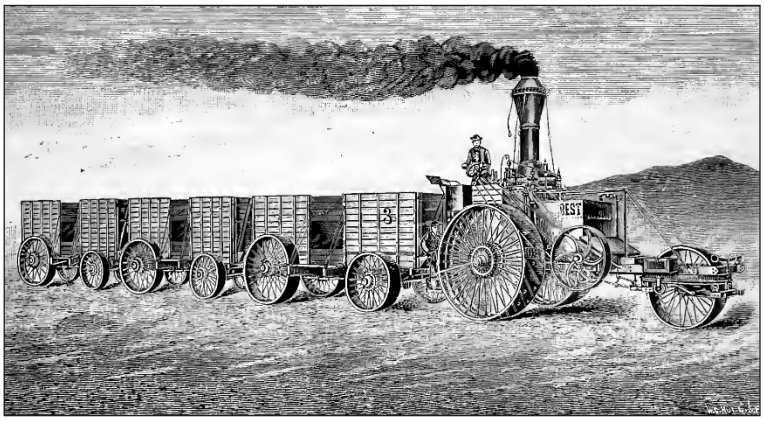

Sketch of Osborne's "self-propelling wagon train"

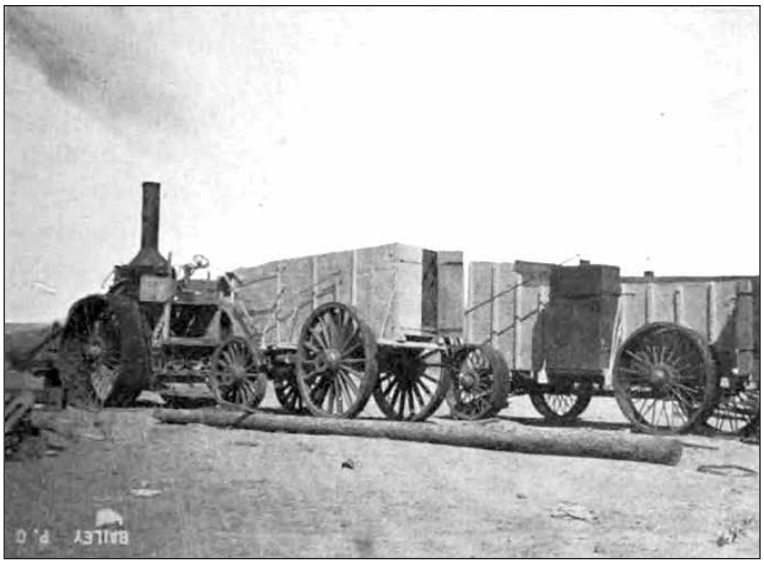

Right: Osborne's "self-propelling wagon-train" sitting at Danby. Photo Bailey (1902, p. 129).

But Jonas B. Osborne, a wealthy Daggett mine owner, envisioned an easier way to haul the product to the railhead. On August 15, 1893, Osborne, Meyer Lewis of Alameda, W. E. Steadman of San Francisco, J. W. Sullivan of Seligman, Arizona, and E. E. Lewis of Los Angeles incorporated the Crystal Salt Company to work the deposit at Danby Lake. Osborn, constructed a road from Danby to Danby Lake that he paved with volcanic cinder and other rock for use by his steam traction engine powered "wagon train." This "self-propelling wagon-train" was his own design, and he received a patent for it.

The steam tractor and wagons were constructed by Daniel Best of San Leandro. The engine developed 50 horsepower, and hauled an average 40 tons of salt per trip. Including time for loading and unloading the 60-mile round trip took a day and a half.

The Mining and Scientific Press in 1898 described the failure of this expensive experiment:

> Danby is the shipping point for the Los Angeles companies now developing salt mines thirty miles south of here. Here is the field for operating traction engines, and here lies the remains of Osborn's Leviathan—the huge monster that wouldn't pull. It is said that this experiment cost a good man an even $100,000.

Osborne's "wagon-train" was parked near the rail siding at Danby where it sat rusting at least until 1905.

When the Crystal Salt Company was active, a building was constructed of blocks of salt on the north end of Danby Lake. This curiosity, which measured about 16 x 25 feet, stood for some 50 years

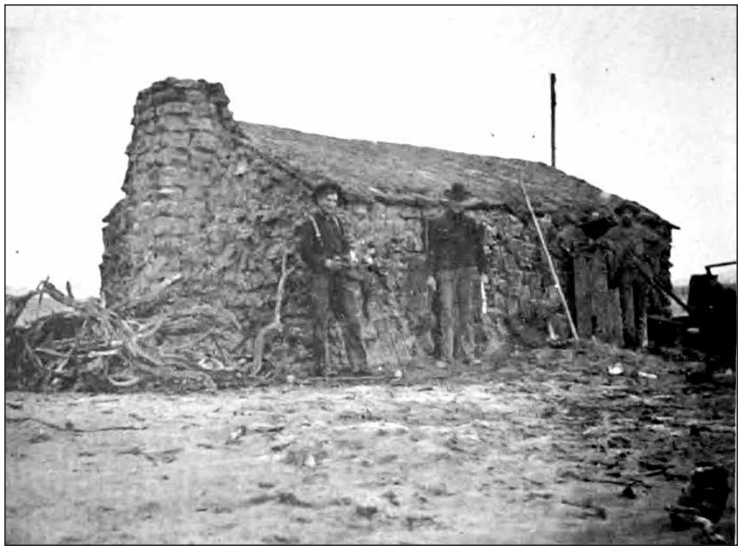

The Danby Dry Lake salt house. Photo Bailey (1902, p. 104).

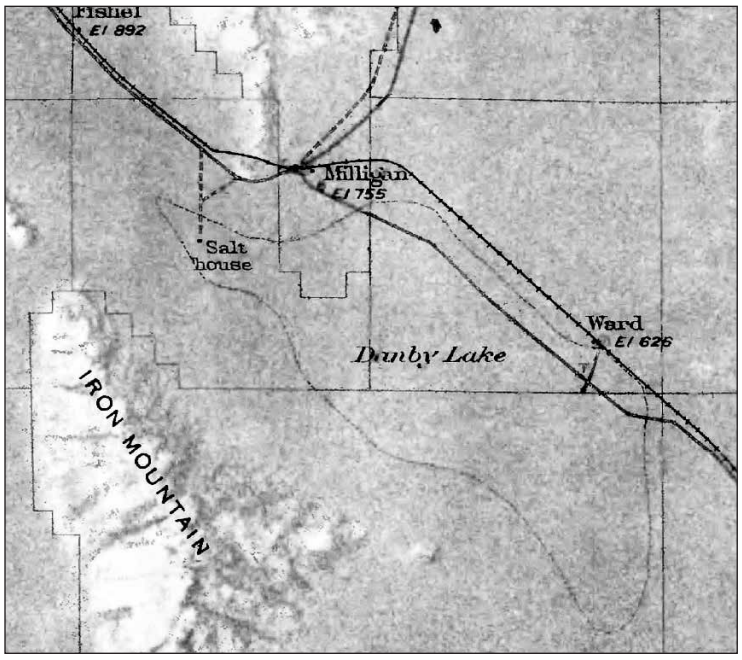

Map showing the Salt House location based on Thompson's 1917-1918 field work.

before it apparently melted into the ground. Photographs of it appeared in newspapers and the Mining Bureau's 1902 Bulletin on salines early in the 1900s.

On July 1, 1910, the Arizona and California Railway was completed from Phoenix, Arizona to the Santa Fe railroad at Cadiz. The railroad provided new opportunities to develop the Danby Lake salt resources. A few years later, Fred D. Milligan, manager of the Milligan Salt Company, was producing high grade table salt from the site of the Crystal Salt Company's earlier operations. Undoubtedly Milligan's name was inspiration for railroad siding of the same name.

David G. Thompson, who conducted field work for the U. S. Geological Survey during 1917–1918, indicated that water was available at Milligan, a railroad section headquarters, and at Ward (later Saltmarsh), which was located about 2 miles down the tracks on the southeast side of Danby Lake. The railroad had sunk a well at Ward but at that time Milligan only had a cistern. Thompson also noted that there "was no store at either place where supplies could be obtained."

Operations of the Crystal Salt Company, and others that followed, in part were located on Section 16 T2N, R17E—a square mile of land deeded to the State of California in 1857, and subsequently sold. In 1912 F. Lee Fuller obtained mineral patent for 20 acres adjoining this parcel on the south. Following enactment of the Mineral Leasing Act of 1920, salt could only be obtained under lease from the U. S. government. Since then there have been numerous sodium leases issued by the General Land Office, and since 1946, the Bureau of Land Management.

In 1977 the Standard Salt & Chemical and the Danby Salt companies were extracting salt here. On September 13, 2010, Salt Products Company, with headquarters in Indio, California, was granted a lease for 960 acres from the Bureau of Land Management.

References

Bailey, Gilbert E., 1902, Saline Deposits of California, California State Mining Bureau Bulletin No. 24, pp. 104,128-129.

BLM Lease CACA 050576 approved 13 Sep 2010.

Cloudman, H. C., Huguenin, Emile, Merrill, F. J. H., 1919, "San Bernardino County," California Mining Bureau Report 15, p. 893-894.

De Kehoe, Joe, 2007, *The Silence and the Sun* (Trails End Publishing Company: Bakersfield, CA) p. 175-181

Engineering and Mining Journal: 30 Mar 1901, p. 410.

Los Angeles *Herald:* 10 June 1905, p. 4.

Los Angeles *Mining Review:* 17 Jun 1905, p. 6, 28 Sep 1901.

McLane, Dave, "Growing Salt at Danby Lake" http://www.actual-life.com/?p=784 Accessed 31 Jan 2014.

Mining and Scientific Press: 16 Aug 1890, p. 105, 10 Jan 1891, p. 18, 28 Jan 1898, 2 Apr 1898, p. 373, 11 Feb 1899, p. 155.

Myrick, David F., 2001, *Santa Fe to Phoenix, Railroads of Arizona, Volume 5* (Signature Press: Wilton, CA), p. 224.

Sacramento *Daily Union*, Volume 85, Number 150, 15 August 1893.

San Francisco *Call* 15 Aug 1893.

"Self-propelling wagon-train" http://www.google.com/patents/US352346 Accessed 31 Jan 2014.

Strong, Mary Frances, "Three Salty Sisters," Desert Magazine December 1977, p. 46.

Thompson, David G., 1929, "The Mohave Desert Region, California," U. S. Geological Survey Water-Supply Paper 578, p. 709.

"Traction Engine and Train for Steam Freighting," Mining and Scientific Press, Vol. 70, No. 10.

Tucker, W. B., 1921, "Los Angeles Field Division, San Bernardino County," California Mining Bureau Report 17, p. 357.

Tucker W. B. and R. J. Sampson, 1931, "Los Angeles Field Division, San Bernardino County," *California Division of Mines Report 27, p. 396.*

Tucker, W. B. and Sampson, R. J., 1943, "San Bernardino County" *California Division of Mines*, Report Vol. 39, p. 5339-540.

Wright, L. A., et. al. 1953, "Mines and Mineral Deposits of San Bernardino County, California," *California Divison of Mines* Report Vol. 49, p. 180, 218, 240.

Danby Playa: ringed with salty questions

Robert E. Reynolds[1] and Thomas A. Schweich[2]

[1]Redlands CA 92373, rreynolds220@verizon.net; [2]University of California, Berkeley and Jepson Herbaria, tomas@schweich.com

ABSTRACT: Danby Playa, at the southern end of the Bristol-Cadiz-Danby trough in the southern Mojave Desert, is a dry lake whose surface is distinguished by large rings of resistant gypsum crystals along with a flora of salt-tolerant plants typical of playas in the Mojave Desert. We speculate that the rings result from interactions between saline water and plants. One higher set of rings apparently formed in the late Pleistocene; a second set of large circular rings and small polygons is more recent and may be actively forming. If deep-rooted phreatophytic plants, such as mesquite, played a major role in the formation of large Pleistocene and Holocene rings, they are not currently present to continue that process. Continued formation of the small polygonal rings suggests that, at least during the recent period, phreatophytes have not been involved in ring formation.

Introduction

The Bristol-Cadiz-Danby Trough is located in the southern Mojave Desert of San Bernardino County, CA. The trough is southeast of Route 66 and Amboy and Cadiz, and north of SR 62 running to Rice, Vidal Junction and Earp. From the private road to the Iron Mountain Pumping Plant to the southeast tip of Danby Playa, the current playa surface contains a band of resistant gypsum outcrops (Howard, 2002) remaining after wind erosion. The Danby depression has apparently not contained perennial fresh water for the last 3 Ma (Rosen, 1991; Brown and Rosen, 1995); however, the presence of Pleistocene mammal fossils suggests that fresh water may have been available seasonally. Pleistocene tan to brown sediments were deposited when available moisture allowed capture of aeolian silts and fine grained sediments transported along the Bristol though from the west, from the Old Woman piedmont (north), the Turtle piedmont (northeast), and the Iron Mountain piedmont (south).

Danby Playa contains saline minerals at depth and as surface efflorescences and crystals. These may have precipitated and crystallized from brines during the Pliocene and during Pleistocene interpluvial periods. Crystallization of chloride minerals (halite, NaCl) and sulfates (gypsum, $CaSO_4.2H_20$; and celestine, $SrSO_4$) increased during the dry Holocene.

On Danby Playa surface, rings of crystallized gypsum are exposed in a seven mile long, approximately half-mile wide belt oriented roughly along the northwest trending axis of the playa. Excellent examples of gypsum rings are seen south of the

Figure 1. Resistant rings of late Pleistocene gypsum stand at least 8 ft higher than the currently active Danby playa surface at 610 feet. Vegetation becomes relatively thick in silt with low saline content, but vegetation is absent in silt and sand with halite and gypsum. Reynolds photo.

Figure 2. Google Earth imagery 6/27/2011 of ring structures on Danby Playa one mile south of Saltmarsh Siding.

railroad siding of Saltmarsh. The rings are evenly distributed over the surface, and there appear to be no concentrations at the termination of major lateral watercourses.

Stratigraphy and age

Silts and sands with saline efflorescences exposed along Cadiz Road are at or above the 630 ft elevation. Silts are at higher elevations (640 ft) at the deltaic mouth of the Ward Valley drainage. Sands and silts may have been directly derived from bajada drainages west and east of the Old Woman Mountains, and from the south along the eastern Iron Mountains. However, with the drying of the climate in the Holocene, there was probably an increased influx of eolian silt and sand from Bristol and Cadiz playas to the northwest. Vertebrate fossils (*Equus* sp., *Camelops* sp.; Reynolds and Reynolds, 1992) recovered from the Danby sediments during excavation along Cadiz Road reinforce a Pleistocene age for these sediments near the highest elevation, and the presence of fossil mammalian herbivores infers at least intermittently available water and vegetation.

Topography

With reduced moisture in the Holocene, wind erosion began to excavate the playa surface from a high elevation at playa margins (along Cadiz Road) of 630+ ft to its present surface elevation around 610 ft., with channels cutting to a depth of 606 ft. Rain water and runoff from late winter storms and summer monsoons continue to recycle playa silts and salts from higher to lower elevations.

Wind erosion has removed silt, leaving lag deposits containing clasts and, rarely, fossils, and exposed resistant structures of gypsum crystals in a matrix of halite. The pronounced gypsum structures are concentric rings that stand 6 to 8 feet above the 610 ft elevation surface (Figs 1, 2) suggesting that they crystallized in the late Pleistocene, prior to wind reduction of the playa surface. The rings are highly visible in aerial imagery (Fig. 2). At the current 610 ft elevation surface, relict and

Figure 3. Degraded late Pleistocene gypsum core surrounded by white efflorescent halite.

recent gypsum ring structures appear in silt that has been subjected to recent ponding (Figs 4, 5).

Figure 4. Young gypsum and halite rings on active playa surface have central silt core.

Figure 5. Young ring of white efflorescent halite around silt and gypsum core.

Description of rings

Gypsum/halite rings can be divided into three categories:

Older Rings, High Elevation: occur at high elevations 8 - 10 ft above the current playa surface (610 ft). These rings are concentric circles, with upper surfaces somewhat concave, suggesting that silt is concentrated in the centers. They reach 40 to 55 feet in diameter. Exposures (Fig. 1) suggest that they have a vertical (tubular) component. Broad "caps" of gypsum (Fig. 1) suggest that gypsum growth was greatest in each sandy Pleistocene horizon.

Old Rings, Low Elevations: large, evenly and regularly spaced round but indistinct rings to 30 ft diameter appear on the active playa surface (610 ft). Because they are less distinct and have slightly smaller diameter than the large rings at higher elevation, they might be relict structures of the older rings, suggesting a tubular structure that, downward, decreased in diameter as well as decreasing in the amount of crystallized gypsum.

Young Small Rings: small, dark, polygonal rings form between the large rings exposed on the current playa active surface (610 ft.) Most small structures are rectangular or polygonal, and only a few are circular. These small structures vary in diameter from 6 to 20 feet, and often "surround" larger rings. Several of the small structures have decayed roots centrally. The relationship of the small dark polygonal rings surrounding the large, degraded circular rings suggests that the process of gypsum ring formation is continuing concurrent with the cycle of playa wetting, drying, and wind erosion.

Vegetation

Saline tolerant plants are associated with the rings of halite, gypsum, and silt at playa surface (610 ft). Their position indicates their tolerance of sediment with a high saline content. Certain plants (*Atriplex* sp.) may be an indicator of silts with low salinity.

Sesuvium verrucosum Raf. -- sea purslane, in the ice plant family and native to California. (Figs 6, 7). The low growing, fleshy, broad leafed plant is the most common plant found on the playa surface. It grows in the center of the silt core of the rings, but occurs in greater numbers outside the rings.

Allenrolfea occidentalis (S. Watson) Kuntze -- iodine bush or pickleweed, California native; (Fig. 8) The upright "string of beads" plant is found centrally

Figure 6. Sea purslane (*Sesuvium verrucosum*) rarely grows within the silty core of the ring, but is more plentiful around the exterior of the gypsum rings.

Figure 7. Sea purslane (*Sesuvium verrucosum*) in the silty core of a gypsum ring.

Figure 8. Iodine bush or pickleweed (*Allenrolfea occidentalis*) grows within the silty core and around the silty margin of the gypsum rings.

Figure 9. Black or Mojave sea-blite (*Suaeda nigra*), a gray, slender leafed bush, is the tallest but rarest on the gypsiferous playa surface.

Figure 10. (right) Cattle spinach (*Atriplex polycarpa*), here within a faint gypsum ring formed in silt with no apparent white halite efflorescence. *A. polycarpa* is common around playa margins since it is not really an alkali playa plant. This suggests that it has low tolerance for saline silts and that it is an indicator of silts with low salinity.

in the silt core of the rings, and is moderately common around the exterior.

Suaeda nigra (Raf.) J. F. Macbr. -- black or Mojave sea-blite, also called seepweed, California native, (Fig. 9). The tall, gray-leafed bush is the rarest plant locally.

Atriplex polycarpa (Torr.) S. Watson -- cattle spinach, California native, (Fig. 10). This tall bush is rarely associated with the gypsum rings and more common around the edges of the playa.

The plants now found at this site do not reach sufficient biomass to explain the size of the rings. Therefore, other, larger taxa, such as mesquite, need to be invoked to support a plant-based explanation.

Models

Following are speculative models for the formation of halite and gypsum var. selenite rings around a core of low salinity silt:

Artesian Model

Although the rings might form in response to "artesian" groundwater discharge, there are no apparent geographic concentrations on the playa near sources of possible stream flow from the Kilbeck Hills to the northwest, from Ward Valley to the north, or from the Iron Mountains to the south. Although groundwater discharge could occur at a change in surface slope, at a (buried) fault, or at the low point in a basin, that doesn't seem to be the case in Danby playa, since the zone of gypsum rings is half a mile wide and seven miles long.

Phreatophyte Model

Phreatophytes, such as mesquite, have deep roots that reach acceptably "fresh" water. The intake of water by phreatophitic plants might leave a halo of concentrated brine, from which gypsum and halite would precipitate in periods with reduced influx of fresh water. Since the roots reach great depth, this might produce a tubular gypsum structure with a silty interior and resistant ribs where dense concentrations of gypsum crystallized in horizontal strata of porous sand. As mentioned above, several of the rings contain centrally located, woody, root-like material.

Contemporary analogs to this site may be found in the Cronese Basin or the west side of Death Valley using mesquite (*Prosopis* sp.) as a model, or in the Devil's Cornfield of Death Valley using arrowweed (*Pluchea sericea* (Nutt.) Coville) as a model.

Concretion Model

If the gypsum rings are concentric spheres, and not tubular structures, they might have formed like concretions, with gypsum crystallizing in outward expanding concentric layers around a central core. A test would involve scraping a vertical surface to see if these were stacked concentric hemispheres or tubular structures.

Daily Percolation Model

Since the seven mile long zone of ringed structures is located centrally along Danby Playa, perhaps the hygroscopic halite and gypsum draw available fresh water centrally, and create a "wicking" effect that is evenly distributed over the central saline core. The movement of uniformly distributed water to the playa surface by daily percolation and evaporation might create the uniform "honeycomb" packing effect that appears on the playa surface.

Several of these models may also work in tandem, or one may enable another. The authors currently favor the phreatophyte model of gypsum/halite ring formation. It is the simplest of the models, and can be compared to current analogs.

Acknowledgment

We thank M. R. Rosen for reviewing this manuscript.

References cited

Brown, W. J., & M. R. Rosen, 1995, Was there a Pliocene-Pleistocene fluvial–lacustrine connection between Death Valley and the Colorado River? Quaternary Research 43:286-296.

Howard, K. A., 2002, Geologic map of the Sheep Hole Mountains 30' x 60' quadrangle, San Bernardino and Riverside Counties, California: U.S. Geological Survey map MF-2344, 2 sheets, http://pubs.usgs.gov/mf/2002/2344/, (1:100,000). Updated in 2004.

Reynolds, R. E., and R. L. Reynolds, 1992, Pleistocene faunas in the Bristol–Danby Trough: San Bernardino County Museum Association Special Publication, 92-2:83-86.

Rosen, M. R., 1991, Sedimentologic and geochemical constraints on the hydrologic evolution of Bristol Dry Lake, California, USA: Palaeogeography, palaeoclimatology, palaeoecology 84: 229-257.

Vertebrate fossils from Desert Center, Chuckwalla Valley, California

Joey Raum[1], Geraldine L. Aron[1] and Robert E. Reynolds[2]

[1]Paleo Solutions Inc., 911 S. Primrose Ave., Unit J., Monrovia, CA 91024, geraldine@paleosolutions.com; [2]Redlands, CA 92373, rreynolds220@verizon.net

Paleontological monitoring for the Desert Sunlight Solar Farm project (project) (Paleo Solutions, 2013) in Desert Center, Chuckwalla Valley, California resulted in the discovery of several new fossil localities, adding to existing paleontological data and helping better document and reconstruct Pleistocene history of the valley. Well-preserved remains of snakes, lizards, desert tortoise, birds, deer, fox and llama, camel, saber-tooth cat (Table 1), the latter three confirming a Pleistocene age, were recovered from alluvial sediments in the valley. Locality 20130515MO.01 was discovered approximately 2.4 km (1.5 miles) east of Kaiser Road on Bureau of Land Management administered lands. The saber-tooth cat fossils from this site are of special interest because they represent the first large predatory mammal documented in Pleistocene-age sediments in the region.

Four bone fragments of *Smilodon* were recovered from Locality 20130515MO.01 (Figure 1). The specimens are orange-brown to beige in color and, aside from being fragmented, are well preserved. They include three fragments that measure less than 2 cm wide and between 3.25 cm and 4.75 cm in length and one proximal left metacarpal II that is 5.25 cm in length and 2.25 cm wide. The proximal left metacarpal II is also fragmented but retains enough structure to be confidently identified as *Smilodon*.

The sediments in Chuckwalla Valley consist of recent/Holocene age surficial deposits, mapped by Jennings (1967) as Quaternary alluvium (Qa), and Pleistocene non-marine older alluvium and fanglomerate deposits (Qc). Younger alluvium is distributed throughout the flood plains and basins of the Desert Center area. The authors have observed these sediments in the field and describe them as tan-brown in color, poorly indurated, poorly sorted fine-grained sands with subangular igneous (both plutonic and volcanic) and metamorphic clasts ranging from small pebbles to cobbles. Older alluvium and fanglomerate deposits, derived from the igneous and metamorphic rocks of the adjacent mountains, are mapped (Jennings, 1967) in the northwestern half, the south-central, and the southeastern portions of the Desert Sunlight Solar Farm site. Field observations by the authors indicate that these older, moderately indurated sediments are red-brown in color, suggestive of paleosols.

Figure 1. *Smilodon sp.* proximal left metacarpal II and (3) fragments comprising Locality 20130305MO.01 in Desert Sunlight Solar Farm in Desert Center, CA. Paleo Solutions photo.

Figure 2. *Smilodon fatalis* proximal left metacarpal II. R. E. Reynolds photo.

Table 1. Vertebrate Biota from Desert Sunlight Solar Farm

Scientific Name	Common Name
Anaxyrus boreas	Western or California toad
Colubrid	Snake
Dipsosaurus sp.	Desert iguana
Gopherus agassizii	Desert tortoise
Lacertilia	Lizard
Phrynosoma sp.	Horned lizard
Sceloporus sp.	Spiny lizard
Aves	Bird
Fringillidae	Finch
Perognathus or *Chaetodipus* sp.	Pocket mouse
Reithrodontomys sp.	Harvest mouse
Spermophilus sp. cf. *tereticaudus*	Round-tailed squirrel
Camelidae, cf. *hemiauchenia*	Llama
Camelops sp.	Camel
Cervidae	Deer
Dipodomys sp.	Kangaroo rat
Smilodon sp.	Saber-tooth cat
Spermophilus sp.	Ground squirrel
Thomomys sp.	Gopher
Vulpes macrotis	Kit fox

They are similar in clast composition to younger Qa but are located under well developed, imbricated and varnished desert pavement. Pleistocene older alluvium also underlies the younger alluvium (Qa) and has been found at varying depths across the project site. The contact between these units fluctuates between several cm below to several m below the surface. Paleosols observed throughout the project have produced significant rodent and reptile fossils (Table 1). The *Smilodon* remains were discovered at (or just below) the surface of Qa.

Existing paleontological data for Chuckwalla Valley is minimal and is mostly come from ground disturbing construction projects. Prior to construction of the Desert Sunlight Solar Farm, no fossil localities had been recorded in the vicinity. However, Pinto Basin, which is located several km north of the site and is connected by a valley to Chuckwalla Valley, has yielded numerous Pleistocene fossils including mammoth, wolf-sized canids, horses, llamas, and camels (Jefferson, 1973, 1991; Scott, 2009). Examples of Pleistocene fossils from Chuckwalla Valley compared with the bones of modern species are shown in figures 3 and 4.

Paleosols similar to those observed at project site are reported in alluvial sediments to the southeast, near Blythe. These produced Pleistocene vertebrates including tortoise, rabbit, eggshells, horse, mammoth

Figure 3. Comparison of the anterior/dorsal surfaces of the Desert Center fossil Bighorn Sheep (*Ovis canadensis*, left) with a recent deer (*Odocoileus hemionus*, center) and recent Pronghorn (*Antilocapra americana*, right). The *Ovis* sp. is robust, and there is no "step" on the proximal articulatory surface. R. E. Reynolds photo.

Figure 4. Comparison of the posterior/ventral surfaces of the Desert Center fossil Bighorn Sheep (*Ovis canadensis*, left) with a recent deer (*Odocoileus hemionus*, center) and recent Pronghorn (*Antilocapra americana*, right). The *Ovis* sp. is robust, and there is a pit on the proximal posterior surface. R. E. Reynolds photo.

or mastodon (Proboscidea), and microvertebrates including rodents (Stewart and Williams, 2012). The preservation of fossils in paleosols is generally good, especially compared to fossils found in higher energy alluvial sediments. Although the *Smilodon* remains from the project were surface discoveries and not *in situ*, the well-preserved condition of these fossils

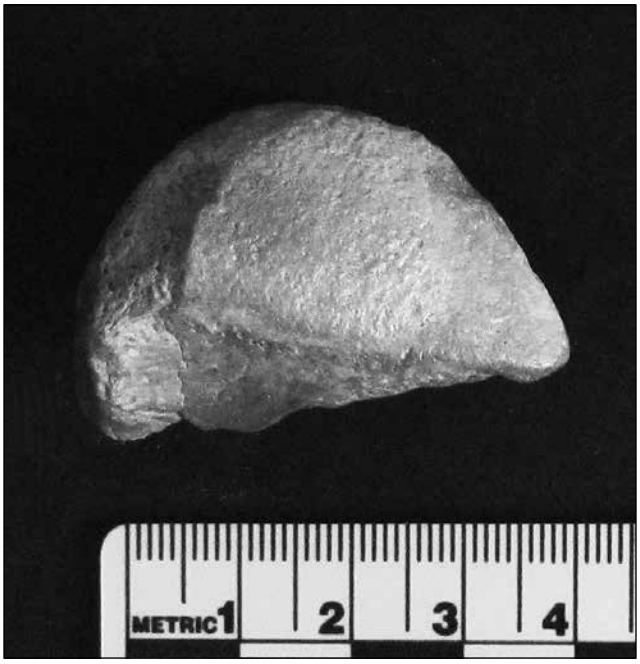

Figure 5. Hemiauchenia sp. occipital condyle fragment. R. E. Reynolds photo.

suggests they may have come from paleosols and not Quaternary alluvium deposits. Quaternary alluvium, both younger (Qa) and older (Qc), generally does not yield pristine fossils.

The addition of *Smilodon* to the Chuckwalla Valley assemblage provides critical information adding to our understanding of the individual taxa in the assemblage as well as the paleoecology, paleoenvironment, and paleogeography of Chuckwalla Valley during the Pleistocene.

Acknowledgements

The authors gratefully acknowledge assistance with specimen identification provided by G. T. Jefferson, L. Murray, and G. Takeuchi. This article benefited by in-depth review by G. Jefferson, ABDSP. The fossils collected will be curated into the Western Science Center in Hemet, Riverside County, California.

References

Jefferson, G.T., 1973, A re-examination of the Pinto Basin site, Joshua Tree National Monument, California. Society for American Archaeology, Abstracts of Papers Submitted for the Meetings, San Francisco.

Jefferson, G.T., 1991, A catalog of late Quaternary vertebrates from California: Natural History Museum of Los Angeles County, Technical Reports 7:1-129.

Jennings, C.W., 1967, Geologic Map of California, Salton Sea Sheet, Scale 1:250,000. California Division of Mines and Geology.

Paleo Solutions: Aron, Geraldine L., and Jennifer Kelly. Addendum to the Paleontological Resource Mitigation and Monitoring Plan: Desert Sunlight Solar Farm, Desert Center, Riverside County, California. Prepared for BLM. 27 June 2013.

Scott, E., 2009, Paleontological resources records check for the proposed Desert Sunlight Solar Farm Project, Riverside County, Project area: San Bernardino County Museum, 5 p.

Stewart, J.D., Williams, M., Hakel, M., and Musick, S., 2012. Was it washed in? New evidence for the genesis of Pleistocene fossil vertebrate remains in the Mojave Desert of southern California. In: The 2012 Desert Symposium Field Guide and Proceedings, R. Reynolds, ed: 140-143.

Population dynamics of the Joshua tree (*Yucca brevifolia*): twenty-three-year analysis, Lost Horse Valley, Joshua Tree National Park

James W. Cornett

JWC Ecological Consultants, P.O. Box 846, Palm Springs, California 92263, jwcornett@aol.com

ABSTRACT: From 1990 through 2013, Joshua tree (*Yucca brevifolia*) numbers declined within a one-hectare study site in Lost Horse Valley, Joshua Tree National Park. This decline along with declines at two additional sites and projected long-term increases in temperature and drought frequency indicate this species may be extirpated from the Park as early as the 22nd century.

Introduction

One of the most distinctive plants in the southwest is the Joshua tree, *Yucca brevifolia*. Large size, dagger-like leaves and endlessly varying form give it a distinctive appearance and have made it a symbol of the Mojave Desert (Bakker, 1971; Foster, 1987; Jaeger, 1950). The Joshua tree is the only native tree found on Mojave Desert flatlands and provides important habitat for many animals, particularly birds (Miller and Stebbins, 1964). In three units of the national park system—Joshua Tree, Mojave, and Death Valley—the trees are locally common and form what have been referred to as woodlands (Munz, 1974) or forests (Jaeger, 1957). As a subject of research, the Joshua tree's large size and distinctive appearance provide a unique opportunity to accurately assess population dynamics and evaluate them in terms of long-term environmental changes. This paper describes the results of twenty-three years of monitoring a one-hectare Joshua tree study site in Lost Horse Valley, Joshua Tree National Park, California.

Study site

Lost Horse Valley is located near the geographical center of Joshua tree distribution in Joshua Tree National Park (Figure 2). In November 1990 a one-hectare study site was established within an area of relatively high *Yucca brevifolia* density where both mature and immature trees were present. The site lies on an alluvial plain at an elevation of 1,330 meters above sea level (33°58.403′N, 116°10.049′W). Low hills and mountains surround Lost Horse Valley with drainage to the north through Quail Wash.

Within site boundaries soil is a mix of sand and silt. Perennial plant species, listed in decreasing order of ground cover, were *Hilaria rigida, Stipa speciosa*, *Yucca brevifolia, Ephedra aspera, Coleogyne ramosissima, Eriogonum fasciculatum, Ambrosia salsola, Sporobolus contractus, Lycium cooperi, Atriplex canescens, Tetradymia stenolepis*, *Senna armata, Cylindropuntia echinocarpa, Echi-*

Joshua trees in Lost Horse Valley, Joshua Tree National Park.

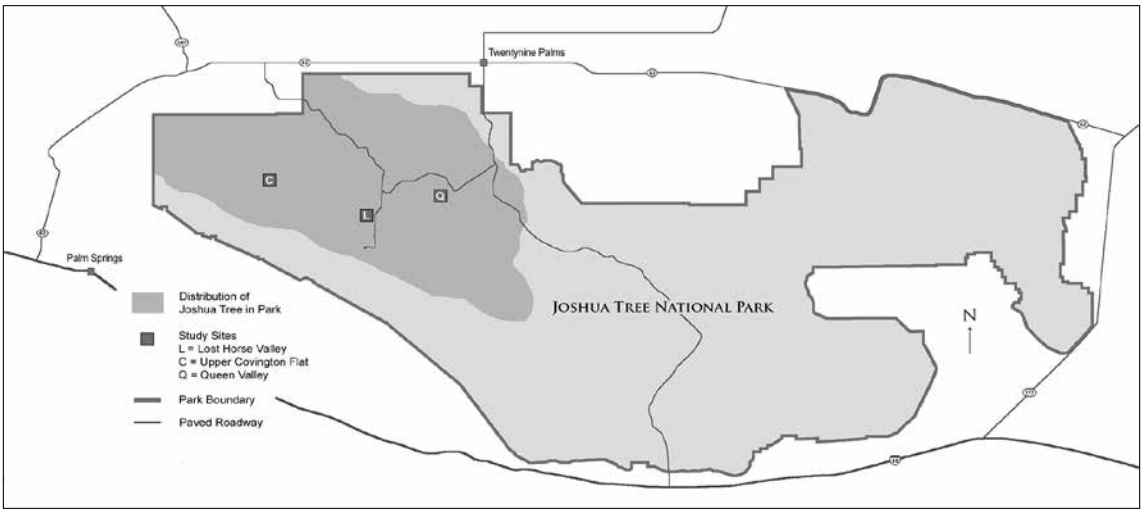

Figure 2. Location of Lost Horse Valley, Queen Valley and Upper Covington Flat study sites in Joshua Tree National Park.

nocereus mojavensis, Cylindropuntia ramosissima and *Opuntia basilaris*. Taxonomic nomenclature is taken from *The Jepson Manual* (Baldwin et al., 2012).

Reliable air temperature data was available for Lost Horse Valley beginning in 1993 (Western Regional Climate Center, 2014). From 1993 through 2013, December was the coldest month with a mean minimum temperature of -0.3°C. Temperature often dropped below freezing in December and January. The coldest temperature recorded was -12.2°C on 17 January 1997. July was the hottest month with an average daily maximum temperature of 33.7°C. The highest temperature recorded was 41.7°C on 18 July 2005. Reliable precipitation data was available from 1995 through 2013 (Western Regional Climate Center, 2014). Average annual precipitation during this period was 12.93 cm. The least amount of precipitation fell in 2002 when only 2.26 cm was recorded for the entire year. The highest annual precipitation, 38.38 cm, was recorded in 2005.

Cattle were introduced into Lost Horse Valley in the mid-1870s (Greene, 1983). Commercial grazing continued intermittently through World War II, but by 1950 all grazing permits were inactive or had been rescinded. Grazing cattle have been absent from Lost Horse Valley and Joshua Tree National Park since that time.

Methods

From 1990 through 2013, individual Joshua trees within the Lost Horse Valley study site were monitored annually with regard to dimensions, vigor and reproductive status. Individual trees were identified with numbered aluminum tags loosely wired around trunks at the inception of the study. Site visits occurred in late winter and spring when Joshua tree would be blooming. Mature trees were defined as those in bloom during the annual site visit or which possessed an expired inflorescence from a previous year's bloom. (All or part of an expired inflorescence typically remains attached to a tree for a decade or more.) Immature trees were those which had not yet blossomed. A tree with one or more green terminal leaf rosettes was considered a living tree. An erect tree with no green leaf rosettes was considered dead unless it possessed one or more crown or rhizome clonal sprouts which possessed a green leaf rosette.

Results

Seventy living trees were present in 1990, representing 44 mature (approximately 63% of total) and 26 immature individuals (37%). By 2013 *Y. brevifolia* numbers had declined to 47 individuals, an approximately 33% decrease. Of the 46 remaining trees, 43 were mature trees (approximately 93% of total) and 3 were immature trees (7%). No new, young Joshua trees appeared during the study period.

This data indicates the number of *Yucca brevifolia* within the Lost Horse Valley study site had declined in numbers from 1990 through 2013. The decline was greatest among immature trees (93%). Immature were inevitably smaller and with less extensive roots systems and less moisture and nutrient reserves than mature trees.

Discussion

The results in Lost Horse Valley parallel those found at two other study sites in Joshua Tree National Park (Figure 2). A second site at Upper Covington Flat showed a 16% decline in Joshua tree numbers from 1988 through 2008 (Cornett, 2009). A third site in Queen Valley showed a wildfire-assisted 73% decrease from 1990 through 2013 (Cornett, 2013). Taken together the three sites represent a broad geographical sampling within Joshua Tree National Park. The declines at all three sites, along with mortality of selected large trees (Cornett, 2006) would seem to indicate *Yucca brevifolia* numbers are declining throughout the Park.

The high percentage of immature tree death, lack of seedling establishment and absence of other detectable causes suggest recurring droughts combined with warmer temperatures over the past twenty-three years are the most likely causes of declining Joshua tree numbers. From 1988 through 2012 the desert regions of southeastern California experienced a 16% decrease in precipitation compared with the previous twenty-five year period (1963 through 1987). Perhaps more importantly, severe drought years, when annual precipitation was less than half the long-term average, occurred only twice in the previous twenty-five years but six times between 1988 through 2012 (National Climatic Data Center, 2013). The severity of drought was exacerbated by a rise in annual temperature of approximately 2 degrees C beginning in the late 1970s. Long-term climatic predictions indicate these conditions are likely to continue (Seager et al. 2007; Solomon et al. 2007) and, if the present rate of decline continues, the extinction of *Yucca brevifolia* in Joshua Tree National Park could occur as early as the twenty-second century.

Acknowledgments

The Garden Club of the Desert and Joshua Tree National Park Association provided financial support for this research. Cameron Barrows reviewed the entire manuscript and made many helpful suggestions. Joe Zarki provided information on the history of cattle grazing in Joshua Tree National Park. Terry Cornett reviewed the manuscript for clarity and consistency and made many helpful suggestions. I thank each of these organizations and individuals for their assistance and support.

Literature cited

Bakker, E. S. 1971. *An island called California.* University of California Press, Berkeley, California.

Baldwin, G. G., D. H. Goldman, D. J. Keil, R. Patterson, T. J. Rosatti and D. H. Wilken, editors. 2012. *The Jepson manual: vascular plants of California, second edition*. University of California Press, Berkeley.

Cole, K.L., K. Ironside, J. Eischeid, G. Garfin, P. B. Duffy and C. Toney. 2011. Past and ongoing shifts in Joshua tree distribution support future modeled range contraction. *Ecological Adaptations* 21(1):137-149.

Cornett, J. W. 2006. Rapid demise of giant Joshua trees. California State University, DesertStudies Consortium. Abstracts from 2006 Desert Symposium, pages 72-73.

Cornett, J. W. 2009. Population dynamics of the Joshua tree (*Yucca brevifolia*): twenty-year analysis, Upper Covington Flat, Joshua Tree National Park. California State University, Desert Studies Consortium, Abstracts 2009 Desert Symposium.

Cornett, J. W. 2013. Population dynamics of the Joshua tree (*Yucca brevifolia*): twenty-three-year analysis, Queen Valley, Joshua Tree National Park. *Raising questions in the central Mojave Desert,* R. Reynolds, editor. California State University Desert Studies Center, 2013 Desert Symposium.

Foster, L. 1987. *Adventuring in the California desert.* Sierra Club Books, San Francisco, California.

Greene, L. W. 1983. *Historic resource study, a history of land use in Joshua Tree National Monument*. Branch of Cultural Resources, Alaska/Pacific Northwest/Western Team, U.S. Department of the Interior, National Park Service, Denver Service Center.

Jaeger, E. C. 1957. *The North American deserts.* Stanford University Press, Stanford, California.

Jaeger, E. C. 1961. *Desert wildlife.* Stanford University Press, Stanford, California.

Miller, A. H. and R. C. Stebbins. 1964. *The lives of desert animals in Joshua Tree National Monument.* University of California Press, Berkeley, California.

Munz, P. A. 1974. *A flora of Southern California.* University of California Press, Berkeley, California.

National Climatic Data Center. 2014. Retrieved data available at http://www.ncdc.noaa.gov/cag/time-series/us.

Seager, R., M. Ting, I. Held, Y. Kushnir, J. Lu, G. Vecchi, H. Huang, N. Harnik, A Leetmaa, N. Lau, C. Li, J. Velez and N. Naik. 2007. Model projections of an imminent transition to a more arid climate in southwestern North America. Science 316:1181–1184.

Solomon, S., D. Qin, M. Manning, Z. Chen, M. Marquis, K. B. Averyt, M. Tignor, and H. L. Miller, editors. 2007. Climate change 2007: the physical science basis. Contribution of Working Group I to the Fourth Assessment Report of the Intergovernmental Panel on Climate Change. Cambridge University Press, Cambridge, UK.

Western Regional Climate Center (2014). RAWS USA Climate Archive, Lost Horse California. Retrieved from http://www.wrcc.dri.edu/.

A notable fossil plant assemblage from the Indio Hills Formation, Indio Hills, Riverside County, California

Joey Raum[1], Geraldine L. Aron[1], and Robert E. Reynolds[2]

[1]Paleo Solutions Inc., 911 S. Primrose Ave., Unit J., Monrovia, CA 91024, geraldine@paleosolutions.com; [2]Redlands, CA., 92373

Paleontological monitoring for the Devers Paleo Verde No. 2 Project (Paleo Solutions, 2013) resulted in the discovery of a new, unique fossil locality in a previously barren area. The site produced a scientifically important assemblage of vertebrate, invertebrate and most notably plant fossils (Tables 1, 2, 3 and 4). Locality 20120703JR.01 was discovered in the Indio Hills, located northwest of Dillon Road on Bureau of Land Management administered lands. The elevation of the locality is between 186 feet to 191 feet. The locality was discovered in the Plio-Pleistocene Indio Hills Formation (Buwalda and Stanton, 1930), in a grayish-green, fine-grained mudstone. The mudstone is sandwiched between two coarser, lighter colored sandstone beds that are underlain and overlain by conglomerates. Following the initial discovery, approximately 1,500 kg (3,000 pounds) of bulk matrix and a sample of mudstone containing numerous leaf impressions in a leaf mat were collected and processed for further analysis. Dry and wet screening of matrix through1/8 inch and 1/16 inch mesh and subsequent hand picking under microscopes yielded numerous vertebrate, invertebrate and plant specimens. Palynological analysis of matrix and paleobotanical analysis of leaf impressions resulted in the identification of numerous plant species (Tables 3 and 4). These taxa are used to infer paleoclimate and paleoenvironment, as well as better constrain age of the deposit.

The plant fossil assemblage, identified from the leaf impressions in the leaf mat sediments, is moderately diverse and includes willow, elder, and poplar leaves, and cattail reeds (Figures 1, 2, 3, 4 and 5). Four (4) samples of matrix from the leaf mat layer and from stratigraphically just above this layer were prepared on slides and examined for palynomorphs such as for pollen, spores, algal cysts, and dinoflagellates. All four samples produced identifiable palynomorphs. The assemblage consists of twenty-two (22) taxa. Ferns and their allies are represented by a single fern spore and spores of *Equisetum* (horsetail) and *Juncus* (rush). Conifers are represented by pollen of *Pinus* (pine), *Picea* (spruce), *Pseudotsuga* (Douglas

Table 1. Vertebrate Biota from Locality 20120703JR.01

Name	Element (number)	Common name
cf. *Dipsosaurus* sp	Distal femur frag (recent?) (1)	Desert iguana
Iguanidae? lizard	Prox. femur frag. (1)	Desert iguana
Lacertilia undet.	Limb frag (1)	Lizard
Neotoma sp. cf. *N. lepida*	Lt /m3 (2), Rt /m3 (1)	Desert woodrat
Sylvilagus sp.	Molariform frag (2)	Cottontail rabbit
Xerospermophilus sp. cf. *X. mohavensis*	Lt /I1(1), Rt /I1(1)	Mohave ground squirrel
Neotoma sp.	Rt /I1(1)	Packrat/woodrat
Rodentia	Tibia frag. (1), Caudal vert. frag (1), Metapodial frag (1), 2nd phalange (2)	Unidentified rodent
Sylvilagus sp.	Terminal digit frag (1)	Cottontail rabbit
Mammalia	Limb frag (1), Bone frags (10)	Unidentified mammal

Table 2. Invertebrate fossils from Locality 20120703JR.01.

Name	Element (number)	Common name
Deroceras sp.	Slug internal test (1)	Slug

Table 3. Plant fossils from Locality 20120703JR.01

Name	Element (number)	Common name
Silicified wood	5 frags	Wood
Concretions around reeds	6 frags	Reeds
Leaf Impression: *Populus* sp.	4 specimens	Poplar
Leaf Impression: *Sambucus* sp.	4 specimens	Elder
Leaf Impression: *Salix* sp.	4 specimens	Willow
Leaf Impression: *Typha*	4 specimens	Cattail

Table 4. Pollens and microfossils found during palynological examination of the sediments from locality 20120703JR.01

Scientific Name	Common Name
Spiniferites sp.	Fresh-water dinoflagellates
Various	Algal cysts
Various	Fungal spores
Various	Ferns
Equisetum sp.	Horsetail, scouring rush
Juncus sp.	Rush
Pinus spp.	Pines
Picea sp.	Spruce
TCT (Taxaceae-Cupressaceae-Taxodiaceae)	(most probably juniper)
Pseudotsuga sp.	Douglas fir
Monosulcites sp.	Palm
Typha	Cattails
Graminae/Poaceae	Grasses
Pterocarya sp.	Wingnut
Ulmus sp	Elm
Alnus sp.	Alders
Salix sp.	Willows
Populus sp.	Poplars and cottonwoods
Quercus sp.	Oaks
Shepherdia sp.	Buffalo berry
Chenopodiaceae & Amaranthaceae families	Chenopods
Compositae/Asteraceae	Sunflower/aster family

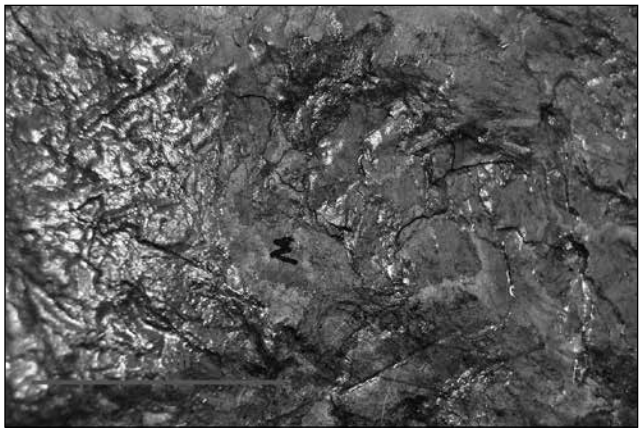

Figure 1. Macroscopic sample of leaf mat sample from Locality 20120703JR.01 in the Devers Paleo Verde No. 2 Project in Indio, CA. Paleo Solutions photo.

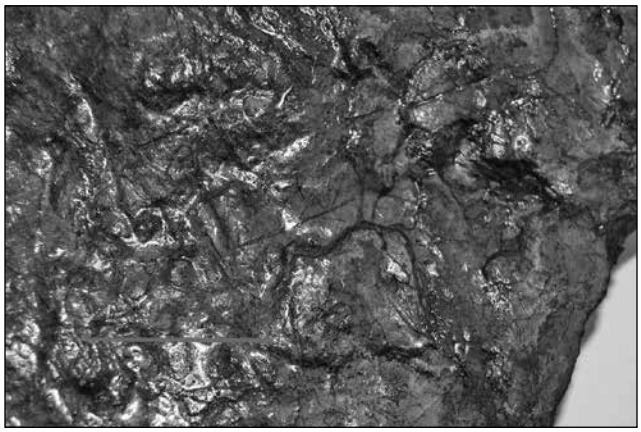

Figure 2. Macroscopic sample of leaf mat sample from Locality 20120703JR.01 in the Devers Paleo Verde No. 2 Project in Indio, CA. Paleo Solutions photo.

fir), and Cupressaceae (most probably *Juniperus* [juniper]). Flowering plants are represented by pollen of *Typha* (cattail), Poaceae (grasses), *Quercus* (oak), *Alnus* (alder), *Ulmus* (elm), Palmae (palm), *Salix* (willow), *Shepherdia* (buffalo berry), Asteraceae (sunflower family), and Chenopodiaceae and Amaranthaceae (chenopod family). Also present are a single fungal spore and abundant freshwater algal cysts and dinoflagellates (Fisk and Maloney, 2013).

The paleobotanical and palynological taxa are consistent with the live oak, juniper, and pinyon pine plant community and climate found today at elevations above approximately 310 m (1,000 feet) in the San Bernardino Mountains. The presence of willow, poplar, and cattails is indicative of a riparian environment. This is further supported by the abundance of algal cysts, freshwater dinoflagellates, cattail pollen (*Typha*), and rush spores (*Equisetum* and *Juncus*). All of these taxa are typically found growing in shallow water or on margins of wetlands. Elm and *Pterocarya* (wingnut), species that require summer rain, suggest wetter and cooler conditions than present day. Additionally, wingnut was extirpated from southwestern North America by late Pleistocene (Tidwell, 1932). The presence of *Planorbula* (aquatic gastropod) and *Deroceras* (slug) suggests a pond or slow moving stream environment. A relatively dry environment surrounding the wetlands is suggested by the abundance of chenopod pollen. Excellent preservation of the leaf mat, pollens, the slug, and the overall low abundance of palynomorphs, combined with the sediment characteristics, suggest an anaerobic

Figure 3. Macroscopic sample of leaf mat sample from Locality 20120703JR.01 in the Devers Paleo Verde No. 2 Project in Indio, CA. Paleo Solutions photo.

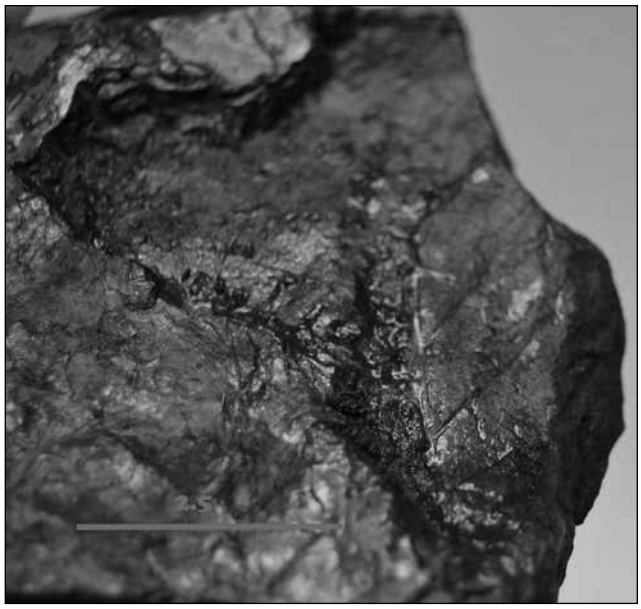

Figure 4. Macroscopic sample of leaf mat sample from Locality 20120703JR.01 in the Devers Paleo Verde No. 2 Project in Indio, CA. Paleo Solutions photo.

depositional environment that underwent rapid burial. The inference of a milder and wetter environment than that which exists today is consistent with interpretations by Axelrod of the Pleistocene Soboba flora (1966) and Mount Eden flora (1937). The mixed conifer forest community of the Soboba, located near San Jacinto, suggests an approximate doubling of the areas current precipitation during the Pleistocene. The Pine-oak woodland and big-cone spruce forest of the Mount Eden flora, located south of Beaumont and north of Palm springs, also suggest in increase in rainfall during the late Miocene (early Pliocene).

Although limited paleo-chronological data were provided by the recovered specimens, which are all currently extant (Tables 1, 2, 3 and 4), palynological analysis provides a potentially narrower depositional age for the samples. In particular, the presence of Tertiary exotic taxa such as *Ulmus* (elm) and *Pterocarya* (wingnut) are useful. These taxa were gone from southern California by middle Pleistocene time, suggesting that the sediments are not younger than early Pleistocene. Furthermore, the absence of typical middle Pliocene palynomorphs suggests that the age of the sampled sediments is younger than middle Pliocene. These data are consistent with the previously suggested age for the Indio Hills Formation of late Pliocene to early Pleistocene (Buwalda and Stanton, 1930).

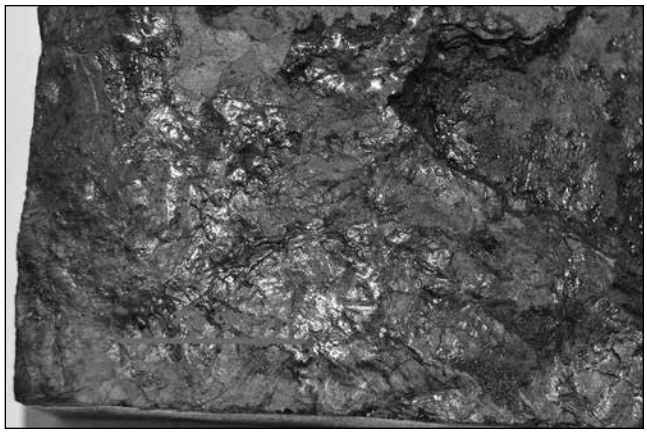

Figure 5. Macroscopic sample of leaf mat sample from Locality 20120703JR.01 in the Devers Paleo Verde No. 2 Project in Indio, CA. Paleo Solutions photo.

The Indio Hills Formation has produced six (6) species of Plio-Pleistocene fossil vertebrates (Stotts, 1965; Jefferson, 2007) and is of particular importance. Irvingtonian-Blancan paleo-faunas from this unit provide critical information for our understanding of the evolution and diversification of Pliocene and Pleistocene paleo-communities (Cassilliano, 2002). However, Plio-Pleistocene sedimentary rocks in the southern California deserts rarely yield fossil plant remains, and there are few previous reports of fossil palynomorphs. Fleming (1993, 1994) and Remeika and Fleming (1995) reported on fossil palynomorphs from the Palm Spring Formation in Anza Borrego Desert State Park. However, the emphasis of their work was on Cretaceous palynomorphs reworked into the Palm Spring Formation from the Colorado Plateau as in indication of the age of erosion of the Grand Canyon. To date, no detailed description of the palynoflora from the Indio Hills Formation, or correlative age units elsewhere in the Salton Trough, e.g. Arroyo Diablo, Ocotillo, or Hueso Formations, have been published. Thus, any identifiable plant microfossils recovered from this formation are highly significant and the recovered specimens have high scientific importance. They contribute to our understanding of the paleoclimate in which the vegetation grew, and the depositional environment in which they were buried and preserved (Fisk and Maloney, 2013).

Additionally, with many recent scientific studies focusing on climate and environment, new paleontological data pertaining to environmental change in climatically sensitive habitats such as the deserts of southwestern United States is increasingly important.

Acknowledgements

The authors give a special thanks to Audry Williams, Senior Archaeologist, and the Natural & Cultural Resources Division at Southern California Edison, without whom this would not be possible. We also gratefully acknowledges the assistance and in depth review of this article by George Jefferson.

References

Axelrod, D. I. 1937. A Pliocene flora from the Mount Eden beds, southern California.

Contributions to Palaeontology, Carnegie Institute of Washington Publication 476:125-183.

Axelrod, D. I. 1966. The Pleistocene Soboba flora of Southern California. University of California Publications in Geological Sciences 60:1-79.

Buwalda, J.P., and Stanton, W.L, 1930. Geological Events in the History of the Indio Hills and Salton Basin, Southern California. Science 24 January 1930: vol. 71 no. 1830. pp 104-106.

Cassiliano, M. L., 2002 .Revision of the stratigraphic nomenclature of the Plio-Pleistocene Palm Spring Group (new rank), Anza Borrego Desert, Southern California: Proceedings of the San Diego Society of Natural History, v. 38, p. 1-30.

Fisk, L.H., and Maloney, D.F., 2013. Palynology of Sediment Samples Collected from the Plio-Pleistocene Palm Spring Formation in the Indio Hills, Riverside County, California. Manuscript on file with Paleo Solutions.

Fleming, R. F., 1993, Palynological data from the Imperial and Palm Spring Formation, Anza Borrego Desert State Park, California: U. S. Geological Survey Open-File Report 93-678, p. 129.

Fleming, R. F., 1994, Cretaceous pollen in Pliocene rocks: implications for Pliocene climate in the southwestern United States: Geology, vol. 22, no. 9, p. 787-790.

Jefferson, G.T., 2007. Salton Sea SRA 623 paleontologic resources inventory and management recommendations. Document on File, California Department of Parks and Recreation, Colorado District Stout Research Center, 6 p.

Paleo Solutions: Aron, Geraldine L., and Jennifer Kelly. Paleontological Monitoring Report: Southern California Edison Devers-Palo Verde No. 2 Project, Riverside County, California. Prepared for BLM. Ed. Collin Lawson and Joseph Raum. 27 Aug. 2013.

Remeika, P., and Fleming, R. F., 1995, Cretaceous palynoflora and Neogene angiosperm woods from Anza-Borrego Desert State Park, California—implications for Pliocene climate of the

Colorado Plateau and age of the Grand Canyon: p. 64-81 in Remeika, P., and Sturz, A. A. (editors), Paleontology and geology of the western Salton Trough Detachment, Anza-Borrego Desert State Park, California, San Diego Association of Geologists, San Diego, CA, 220 p.

Remeika, P., 2006. Ancestral woodlands of the Colorado River delta plain. In The Fossil Treasures of the Anza-Borrego Desert, edited by G.T. Jefferson and L. Lindsay, Sunbelt Publications, San Diego, California p. 75-87.

Stotts, J.L., 1965. Stratigraphy and structure of the northwest Indio Hills, Riverside County, California. Master of Arts Thesis, Department of Geological Sciences, University of California, Riverside ** p

Tidwell, W. D. 1932. Common fossil plants of western North America. Brigham Young University Press, Provo. 197 p.

Dos Palmas Preserve: an expanding oasis

James W. Cornett

JWC Ecological Consultants, P.O. Box 846, Palm Springs, California 92263, jwcornett@aol.com

Located five kilometers east of Southern California's Salton Sea, Dos Palmas Preserve is a desert paradox. In spite of hyperarid climate aggravated by recent winter droughts, I found the Preserve to contain the most rapidly expanding palm oasis and wetlands anywhere in the California deserts.

History of Dos Palmas

Native Americans knew of natural springs at Dos Palmas for hundreds, if not thousands, of years. Ancient foot trails (now the Bradshaw Trail) indicate Dos Palmas was an important and reliable waterhole along an Indian trade route linking central Arizona cultures with the Cahuilla and other tribes of Southern California (George Kline, personal communication). Archaeological sites discovered in the area reveal both temporary and seasonal camps as well as fish traps (actually weirs) found less than a kilometer to the northeast.

It is said that Mexican prospectors encountered the springs in the mid nineteenth century and, finding two palms there, named the site Dos Palmas (Henderson, 1947). In the 1860s the springs' existence became widely known when placer gold deposits were discovered along the Colorado River near La Paz, Arizona. Persons of European ancestry, traveling east from the Los Angeles Basin, regularly stopped at Dos Palmas oasis as it was one of the few reliable waterholes on the way to the Colorado River. Dos Palmas was located approximately halfway between San Bernardino to the west and distant Las Paz to the east. Eventually, Dos Palmas became a regular stop along a stage route. An adobe-walled station was constructed to house a caretaker (Henderson, 1947).

Hard rock mining was the focus of activity at Dos Palmas in the 1890s. The Orocopia Mining Company pumped water from the spring to mines 20 kilometers north in the Orocopia Mountains (Mendenhall,

1909). It is said the mine was not profitable and Randall Henderson, the late editor and publisher of the now defunct Desert Magazine, found no trace of the mining company's operation on his last visit to the site in 1946.

In 1906 naturalist George Wharton James and artist Carl Eytel stopped at Dos Palmas with their pack burros while on an exploratory trip through the Colorado Desert. James wrote about their experiences including a visit to the spring in his two-volume book Wonders of the Colorado Desert.

> Our canteens hang empty on our shoulders. There is no more danger of thirst, for in the morning, only a few miles farther on, are palms rising out of the desert, telling of the presence of an oasis where there is an abundance of water. It is Dos Palmas, well-loved spot of desert teamsters and prospectors; the old stagestation, where two springs supply an abundance of good water so that animals and men can drink all they desire without fear. . . . A small shack . . . stands close by the spring, which is surrounded by beautiful trees, carrizo, grass and flowers to which it gives life.

Sometime in the 1920s prospector Frank Coffey built a cabin at Dos Palmas. So far as is known, Coffey was the first person to introduce an exotic species to the springs. He placed fish, possibly carp, in one of the pools. Coffey died in 1938 and shortly thereafter his cabin was set afire. According to Henderson (1947), the fish were gone from the springs by 1946.

The idea of Dos Palmas becoming a natural preserve was first advanced by Raymond Morgan who purchased land near the springs in 1944 (Henderson, 1947). Morgan had several residential structures built on his property and used the complex as a desert retreat for his friends and family. By 1947 he had increased his holdings to 1,400 acres including the springs at Dos Palmas. In 1989 the Nature Conservancy began acquiring land in the area including Morgan's holdings (Center for Natural Lands Management, 2013). On October 28, 1990, I attended a ceremony in which the "Rancho Dos Palmas Preserve" was formerly dedicated and opened to the public for the first time. A few years later the Nature Conservancy transferred management of the Preserve to the Bureau of Land Management which has incorporated it into the approximately 20,000-acre Salt Creek Area of Critical Environmental Concern (Bureau of Land Management, 2011).

Physical setting

Dos Palmas Preserve lies within a geological province known as the Salton Trough, an area stretching 226 kilometers from the Gulf of California to the San Gorgonio Pass in Southern California (Sharp, 1994). Between the Imperial and Coachella valleys there are more than 3,200 square kilometers of landscape below sea level making it the largest such area in the Western Hemisphere. Although Badwater in Death Valley is lower, -86 meters compared with the Salton Trough's -83, the area below sea level is much smaller.

The Salton Trough is a graben created by downwarping along the San Andreas Fault. The fault is the meeting place of two plates of the earth's crust known as the North American (east side of fault) and Pacific (west side of fault). Movements of these plates over the past twenty million years have crushed alluvial materials at the plate boundary creating sediments known collectively as fault gouge. So small and tightly packed are the particles in fault gouge that they form a subsurface layer impervious to water. Springs form when flows of underground water from higher ground are dammed by the impervious layer at the fault. At specific locations the dammed waters reach, or nearly reach, the surface where they are tapped by palms and other plants (Cornett, 2010). This is the process by which the springs at Dos Palmas were initially created.

During the late Miocene epoch, approximately six million years before present, the springs at Dos Palmas (if they existed) were beneath the waters of the Gulf of California. It was not until the early Pliocene epoch, four million years before present, that ocean water was pushed south by sediment deposition at the mouth of the Colorado River (Bergen et al., 1997). From four million years ago onward depositions in the Imperial and Coachella valleys are non-marine sediments.

Fossils of aquatic organisms, tufa deposits and ancient shorelines indicate that several times during the Pleistocene, and even into the Holocene, freshwater lakes covered much of the Imperial and Coachella valleys. Collectively known as Ancient Lake

Cahuilla in acknowledgement of the Native Americans who used weirs to capture fish along its shoreline, the last lake evaporated away sometime between A.D. 900 and 1400 (Norris and Webb, 1990). The origin of the freshwater that filled the U.S. portion of the Salton Trough was the heavily sediment-laden Colorado River. Several times during the past two million years sediment build up at the mouth of the river was so great the path of least resistance became the below-sea-level Imperial and Coachella valleys rather than the Gulf of California. Enormous lakes resulted, some more than 300 feet deep, with ten times the surface area of today's Salton Sea. After many centuries sediment buildup changed the course of the Colorado River again and it flowed back into the gulf. Without a large supply of freshwater, each successive Lake Cahuilla evaporated away leaving a salt-covered dry lakebed in its place (Cornett, 2008). As Dos Palmas Preserve lies at an average elevation of approximately -34 meters, the oasis was deep beneath the surface of Lake Cahuilla during major inundations from the Colorado River. Thus, I estimate its most recent appearance as a desert spring occurred within the past thousand years. The arrival of palms would have occurred sometime after the appearance of the spring.

Dos Palmas lies within the Colorado Desert subdivision of the Sonoran Desert. The region is hot and arid due to low elevation and the rain shadow effect of the Peninsular and Transverse ranges that lie to the west and north. These mountains usually prevent cool eastward-moving Pacific air from ameliorating interior temperatures and block all but the largest winter cyclonic storms originating in the Gulf of Alaska. The aridity is intensified by the cold California Current that runs down the Pacific Coast. The current both reduces the moisture content of the air and assists in the establishment of a dominant high pressure system that pushes eastward traveling storm systems farther to the north.

These climate-related phenomena result in Dos Palmas Preserve experiencing hot summer temperatures. In fact, it is the second hottest region in the California deserts. The average daily maximum temperature in July, the hottest month, is 43°C as recorded at the weather station at Mecca, California (National Climatic Data Center, 2014). The record high temperature at that same locality is 52°C. In addition to the region having very hot summers, it is also the second most arid place in North America. Average annual precipitation in the heart of the trough is just 8.5 cm categorizing it as a hyperarid desert similar to Death Valley.

The hyperaridity of the region has been exacerbated by recent and severe recurring droughts. From 1988 through 2012, the desert regions of southeastern California experienced a 16% decrease in precipitation compared with the previous twenty-five year period (1963 through 1987). Perhaps more importantly, severe drought years, when annual precipitation was less than half the long-term average, occurred only twice in the previous twenty-five years but seven times from 1988 through 2013 (National Climatic Data Center, 2013). The severity of drought was exacerbated by a rise in annual temperature of approximately 2 degrees C beginning in the late 1970s. Long-term climatic predictions indicate these conditions are likely to continue (Seager et al. 2007; Solomon et al. 2007).

Animal life

As one might expect, an oasis in the hyperarid Colorado Desert attracts many wildlife species. Mule deer (*Odocoileus hemionus*) visit the ponds to drink, muskrats (*Ondatra zibethicus*) have reached the Preserve presumably from the Coachella Canal and I routinely find coyote (*Canis latrans*) scat heavily laden with desert fan palm seeds on most trails. Waterfowl occupy all the large ponds and in January of 2014 we observed many winter visiting birds including ruby-crowned kinglets (*Regulus calendula*), yellow-rumped warblers (*Dendroica coronata*) and white-crowned sparrows (*Zonotrichia leucophrys*). Several years ago I encountered a large checkered garter (*Thamnophis marcianus*) at Dos Palmas, a species typically associated with aquatic environments in the desert Southwest (Stebbins, 2003).

One of the primary purposes of both the Preserve and ACEC is the protection of several sensitive, threatened or endangered species (Bureau of Land Management, 2011). The Yuma clapper rail (*Rallus longrostris yumanensis*) can be observed along marsh edges. It was declared endangered by the U.S. Fish & Wildlife Service in 1966. There are probably not more than 600 individuals remaining. Another officially endangered species found at the Preserve is the desert pupfish (*Cyprinodon macularis*) which abounds in several ponds. The California black rail (*Laterallus*

jamaicensis coturniculus), a State of California threatened species, can occasionally be seen in dense vegetation along pond margins.

Plant life

Due to an abundance of water at or near the surface, vegetation is unexpectedly dense and diverse for a location in the Colorado Desert. The desert fan palm, *Washingtonia filifera*, is easily the most distinctive plant species at Dos Palmas, though many other perennial species are abundant as well. On a visit to the oasis portion of the Preserve, in January of 2014, I found arrow-weed (*Pluchea sericea*) to be exceedingly abundant along with iodine bush (*Allenrolfea occidentalis*), alkali goldenbush (*Isocoma acradenia*), cattle spinach (*Atriplex polycarpa*), giant reed (*Phragmites australis*) and salt grass (*Distichlis spicata*). Each of these species is tolerant of the high soil salinity indicated by white, alkaline deposits covering much of the Preserve's landscape. As mentioned previously, the Preserve is located in the Salton Trough, a desert sink, where alkaline deposits have been accumulating for tens of thousands of years.

I found both native California species of mesquite at Dos Palmas: honey mesquite (*Prosopis glandulosa*) and screw bean (*P. pubescens*). I have visited every known location where desert fan palms occur in Mexico and the American Southwest and this is the only palm oasis where the two species are sympatric.

In or near ponds, most of which have been artificially created, I found cattail (*Typha domingensis*), bulrush (*Scirpus microcarpus*), willow (*Salix* sp.) and Fremont cottonwood (*Populus fremontii*).

In addition to *Washingtonia filifera*, two exotic palm species have made their way into the Preserve. Both the Mexican fan palm (*Washingtonia robusta*) and date palm (*Phoenix dactilyfera*) are found, albeit in very small numbers. Neither of these species was recorded at Dos Palmas on my first visit in 1984.

Although I recorded abundant tamarisk (*Tamarix ramosissima*) presence at Dos Palmas in 1984, I did not encounter a single individual on either of my two visits in January of 2014.

Tracking fan palm numbers

As stated previously, the desert fan palm (*Washingtonia filifera*), is easily the most distinctive plant species at Dos Palmas Preserve. It requires perpetually moist soil to survive (Cornett, 2010). Yet in spite of long-term hyperaridity and severe recent droughts, desert fan palm numbers have been steadily increasing. Over the past century, albeit through both natural and human-facilitated actions, it has become the most rapidly expanding desert fan palm oasis in North America.

As the name indicates, only two desert fan palms presumably occurred at the springs in the mid-nineteenth century when it was named (Henderson, 1947). The number of palms had not changed when Mendenhall visited the springs in 1909. However, the first time Randall Henderson arrived at Dos Palmas in 1920 the number of palms had increased to "three or four grown palms at the springs . . . , and several smaller trees" (Henderson, 1947). Henderson returned to Dos Palmas in 1946 and by that time palms numbered 27 (Henderson, 1947).

A large increase in groundwater at Dos Palmas began in 1949 when water from the Colorado River was diverted to the region via the earthen-bottom Coachella Canal (Coachella Valley Water District, 2014). The canal is located approximately 800 meters northeast and 40 meters upslope from Dos Palmas. Seepage from the canal flowed downhill and underground to the nearby San Andreas Fault where the springs at Dos Palmas were located. In 2006, the portion of the canal adjacent to Dos Palmas was concrete lined and seepage was effectively halted. However, to maintain the Dos Palmas Preserve as an important wildlife sanctuary, and through a cooperative agreement between the Coachella Valley Water District and several other agencies, a preserve management plan was adopted. The agreement required the CVWD to mitigate the loss of water due to the cessation of canal seepage by enhancing existing artesian wells as well as creating new ones. More recently, percolation ponds have been added using canal water (Cameron Barrows, personal communication).

When I censused palm numbers at Dos Palmas in 1984, I counted 340 mature palms (flower producing) over 4 meters in height, 20 immature palms (not yet flower producing) between 2 and 4 meters, 29 between 1 and 2 meters and 118 less than 1 meter in height excluding seedlings. When I visited the oasis 30 years later, in January of 2014, the number of adult palms at Dos Palmas had increased to more than 1,000 mature individuals.

It is reasonable to assume that seepage from the Coachella Canal, beginning in 1949, made significantly more water available to the palms and was at least partially responsible for the dramatic increase in numbers. However, as previously shown, palm numbers were increasing prior to canal construction. The pre-canal increase in palm numbers is similar to increases I have recorded in most other desert fan palm oases in the twentieth century, a phenomenon which has been associated with global warming (Cornett, 1989).

Today, Dos Palmas is open to the public every day of the year. The Preserve may be reached from Highway 111 south of Indio, California. Travel on Highway 111 through the towns of Coachella and Mecca. Approximately 16 kilometers (10 miles) southeast of Mecca, look for the Park Headquarters of the Salton Sea State Recreation Area on the right. Turn left opposite park headquarters onto Parkside Drive. Take Parkside to the end (3.2 kilometers; 2 miles) and turn right onto Desert Aire Drive. Take Desert Aire Drive to Powerline Road. Turn left onto Powerline Road and drive 1 kilometer (0.6 miles). Turn left onto Sea Breeze Drive. Drive nearly 3 kilometers (1.9 miles) until the gate is encountered. Park in the parking lot on the right and walk into Dos Palmas Preserve down Sea Breeze Road.

Acknowledgments

The Garden Club of the Desert and Joshua Tree National Park Association provided financial support for this research. Cameron Barrows reviewed the entire manuscript and corrected several of my errors. Terry Cornett checked the manuscript for clarity and consistency and made many helpful suggestions. I thank each of these organizations and individuals for their assistance and support.

Literature cited

Baldwin, G. G., D. H. Goldman, D. J. Keil, R. Patterson, T. J. Rosatti and D. H. Wilken, editors. 2012. *The Jepson manual: vascular plants of California, second edition*. University of California Press, Berkeley.

Bergen, F. W., H. J. Clifford and S. G. Spear. 1997. *Geology of San Diego County.* Sunbelt Publications, San Diego, California.

Bureau of Land Management. 2011. Dos Palmas Preserve. Available at http://www.blm.gov/ca/st/en/prog/wildlife/watchable/areas/dospalmas.html.

Center for Natural Lands Management. 2013. Preserve – Dos Palmas. Available at http://www.cnlm.org/cms/index.php?Itemid=183&id=42&option=com_content&task=view.

Cornett, J. W. 1989. The desert fan palm: not a relict. San Bernardino County Museum Quarterly 36(2):56-58.

Cornett, J. W. 2008. *Wonders of the Coachella Valley.* Nature Trails Press, Palm Springs, California.

Cornett, J. W. 2010. *Desert palm oasis.* Nature Trails Press, Palm Springs, California.

Henderson, R. 1947. Waterhole on the Old Bradshaw Trail. Desert Magazine 10(3):4-7.

James, G. W. 1906. The wonders of the Colorado Desert (Volume II). Little, Brown, and Company, Boston, Massachusetts.

Mendenhall, W. C. 1909. Some desert watering places in southeastern California and southwestern Nevada. Water-supply paper 224, Department of the Interior, United States Geological Survey, Washington D. C.

Norris, R. M. and R. W. Webb. 1990. *Geology of California.* John Wiley and Sons, New York, New York.

Sharp, R. P. 1994. *A field guide to Southern California.* Kendall-Hunt Publishing Company, Dubuque, Iowa.

Seager, R., M. Ting, I. Held, Y. Kushnir, J. Lu, G. Vecchi, H. Huang, N. Harnik, A Leetmaa, N. Lau, C. Li, J. Velez and N. Naik. 2007. Model projections of an imminent transition to a more arid climate in southwestern North America. Science 316:1181–1184.

Solomon, S., D. Qin, M. Manning, Z. Chen, M. Marquis, K. B. Averyt, M. Tignor, and H. L. Miller, editors. 2007. Climate change 2007: the physical science basis. Contribution of Working Group I to the Fourth Assessment Report of the Intergovernmental Panel on Climate Change. Cambridge University Press, Cambridge, UK.

Stebbins, R. C. 2003. *Western reptiles and amphibians.* Houghton Mifflin Company, Boston, Massachusetts.

Width and dip of the southern San Andreas Fault at Salt Creek from modeling of geophysical data

Victoria Langenheim[1], Noah Athens[2], Daniel Scheirer[1], Gary Fuis[1], Michael Rymer[1], and Mark Goldman[1]

[1]U. S. Geological Survey (USGS), Menlo Park, California; [2]U. S. Geological Survey, Portland, Oregon

ABSTRACT: We investigate the geometry and width of the southernmost stretch of the San Andreas Fault zone using new gravity and magnetic data along line 7 of the Salton Seismic Imaging Project. In the Salt Creek area of Durmid Hill, the San Andreas Fault coincides with a complex magnetic signature, with high-amplitude, short-wavelength magnetic anomalies superposed on a broader magnetic anomaly that is at least 5 km wide centered 2–3 km northeast of the fault. Marine magnetic data show that high-frequency magnetic anomalies extend more than 1 km west of the mapped trace of the San Andreas Fault. Modeling of magnetic data is consistent with a moderate to steep (> 50 degrees) northeast dip of the San Andreas Fault, but also suggests that the sedimentary sequence is folded west of the fault, causing the short wavelength of the anomalies west of the fault. Gravity anomalies are consistent with the previously modeled seismic velocity structure across the San Andreas Fault. Modeling of gravity data indicates a steep dip for the San Andreas Fault, but does not resolve unequivocally the direction of dip. Gravity data define a deeper basin, bounded by the Powerline and Hot Springs Faults, than imaged by the seismic experiment. This basin extends southeast of Line 7 for nearly 20 km, with linear margins parallel to the San Andreas Fault. These data suggest that the San Andreas Fault zone is wider than indicated by its mapped surface trace.

Introduction

The southern San Andreas Fault has not produced a major earthquake since the late 17th century (Sieh, 1986; Sieh and Williams, 1990; Weldon and others, 2004; Philibosian and others, 2011). A well-known simulation of a southern San Andreas rupture (Jones and others, 2008; Perry and others, 2008) initiates the earthquake at Bombay Beach (BB in Fig. 1), rupturing northwestward and breaking through not only the small transpressional uplifts along the fault at Durmid Hill, Mecca Hills, and Indio Hills, but also the pronounced left bend of the fault at in the San Gorgonio Pass area. Such an earthquake is predicted to produce significant ground shaking in Coachella Valley as well as in the Los Angeles Basin some 150 km to the west. The simulation assumes that the San Andreas Fault is vertical, except between Indio and San Gorgonio Pass. Fuis and others (2012b) presented evidence that the San Andreas Fault is not vertical along most of its stretch in the rupture scenario, the significance being that a dipping fault produces asymmetric ground shaking, with the strongest shaking in the hanging wall of the fault.

The Durmid Hill stretch of the fault is the southernmost part of the San Andreas Fault before it curves south into the Brawley Seismic Zone at Bombay Beach. Double-difference relocated microseismicity is parallel to and northeast of the fault (Lin and others, 2007). Projection of the microseismicity to the surface is nearly coincident with the surface trace of the San Andreas Fault, suggesting a northeast dip (Lin and others, 2007; Fuis and others, 2012b). Alternate interpretations are possible, however, such as the microseismicity is not produced by the San Andreas Fault, but by a subsidiary fault (Nicholson and others, 2009), or, less likely, the microearthquakes, although precisely located with respect to their neighbors, may be systematically mislocated because of an inaccurate seismic velocity model. Here we investigate the dip and width of the San Andreas Fault using potential-field data and

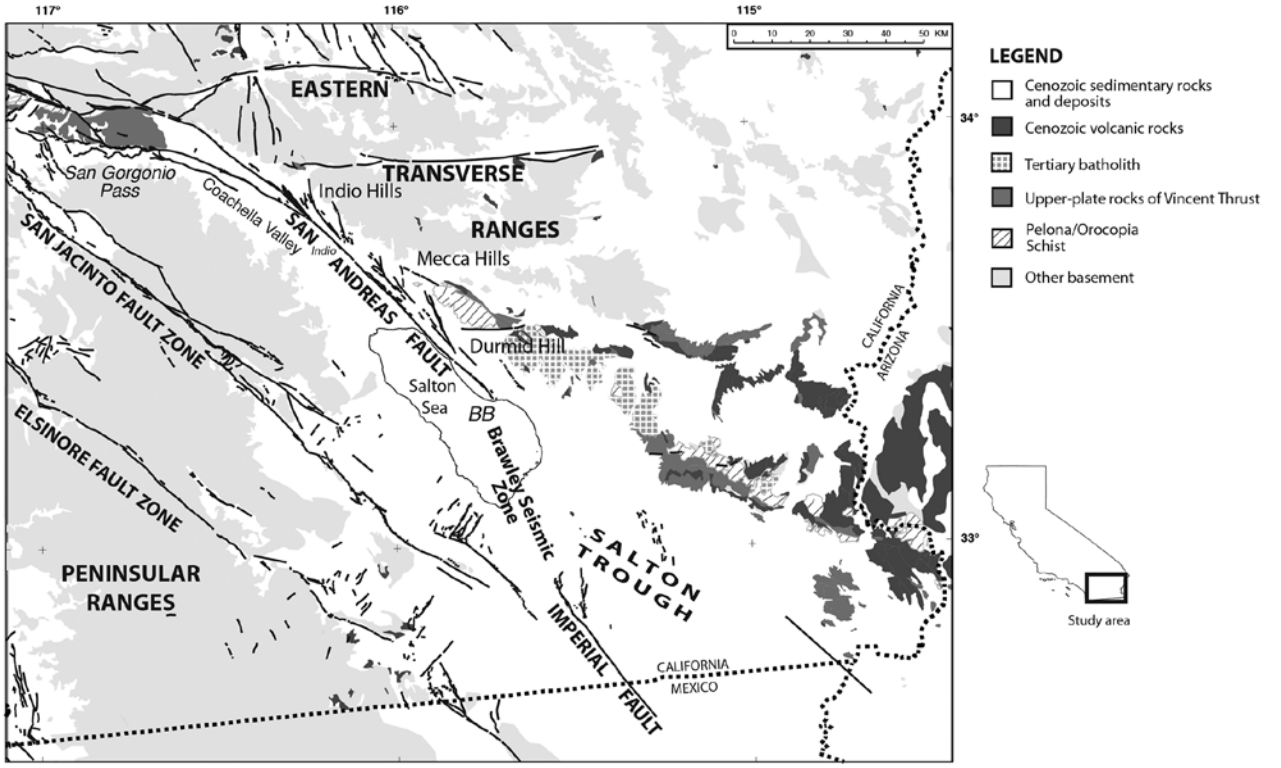

Figure 1. Simplified regional geologic map of the southern San Andreas Fault modified from Jennings and others (1977). BB, Bombay Beach.

present a model along Line 7 of the Salton Seismic Imaging Project (SSIP) that integrates new detailed magnetic, gravity and seismic–velocity data.

Durmid Hill and its geologic setting

Durmid Hill is the southernmost of three topographic highs where Plio–Pleistocene sedimentary rocks are uplifted and folded along the southern San Andreas Fault. Durmid Hill is approximately 20 km long with its highest point at Bat Caves Buttes, about 100 m above the Salton Sea. At Bat Cave Buttes, the oldest rocks are exposed, consisting of Pliocene and Pleistocene arkosic conglomerate, sandstone and siltstone of the Shavers Well Formation (Babcock, 1974; identified as Palm Spring Formation by Dibblee, 1954 and Dibblee and Minch, 2008). The clasts appear to be locally derived from the Orocopia and Chocolate Mountains to the east (Babcock, 1974). Immediately east of the San Andreas Fault, laminated, poorly indurated siltstone and sandstone, most likely lacustrine, are exposed. To the southwest these rocks are truncated by the San Andreas Fault and juxtaposed against the lacustrine siltstone and claystone of the Pleistocene Borrego Formation. Northeast of the fault the Shavers Wells Formation is overlain with an angular discordance of about 18° by the Borrego Formation (Babcock, 1974). Durmid Hill and surrounding lowlands are mantled by deposits of Lake Cahuilla, an intermittent Holocene–Late Pleistocene lake fed primarily by inflow from the Colorado River. Bat Caves Buttes were islands during the last high stand of Lake Cahuilla about 300 years ago and have wave-cut planar surfaces that are tilted 2.3° to the northeast (Sylvester and others, 1993).

The Shavers Well Formation dips consistently and moderately to the northeast, in contrast to the folded Borrego Formation. The Shavers Well Formation is apparently more competent than the Borrego Formation (Babcock, 1974). Southwest of the San Andreas Fault, the Borrego Formation is folded into the Durmid anticline, which forms the southern 4 km of Durmid Hill. Superposed on the anticline are smaller, en echelon folds with wavelengths and amplitudes ranging from centimeters to hundreds of meters (Babcock, 1974; Bürgmann, 1991). A white ash layer identified as the Bishop Ash by Merriam and Bishoff (1975) and Sarna-Wojcicki and others (1984) forms a distinctive marker bed used by Bürgmann to estimate significant extension parallel to the fold axes. Both Babcock (1974) and Bürgmann (1991) documented significant shortening perpendicular to

the fold axes as well as uplift of 1–2 mm/yr based on exposed stratigraphy and incision of the antecedent stream at Salt Creek. Uplift continues today, as revealed by leveling (Bilham and Williams, 1985; Sylvester and others, 1993). This stretch also experienced creep triggered by earthquakes, most recently by the 2010 El Mayor–Cucapah earthquake (Rymer and others, 2010; Wei and others, 2011).

The deformation in the Indio Hills, Mecca Hills, and Durmid Hill has been attributed to oblique-slip transpression (Sylvester and Smith, 1976). In these areas, the fault appears to strike slightly more westerly than the inferred local azimuth of plate motion (Bilham and Williams, 1985). Bürgmann (1991) estimated that 9-14% of the total San Andreas Fault displacement is accommodated by transpression forming Durmid Hill. Geologic complications in this area include (1) termination of the San Andreas Fault at Bombay Beach and its stepover to the Imperial Fault through the Brawley Seismic Zone, (2) intersection of the San Andreas Fault and the left-lateral Salton Creek fault, and (3) the presence of subsidiary faults, such as the Hidden Spring and Hot Springs faults. The Brawley Seismic Zone is located within a releasing step between the San Andreas and Imperial Faults and has been interpreted as a buried spreading center based on its high heat flow, young volcanism, and geophysical signature (Elders and others, 1972; Fuis and others, 1984). Brothers and others (2009) mapped normal faults beneath the Salton Sea that they interpret as having formed when the right step between the San Andreas and Imperial Faults formed sometime after 500 ka.

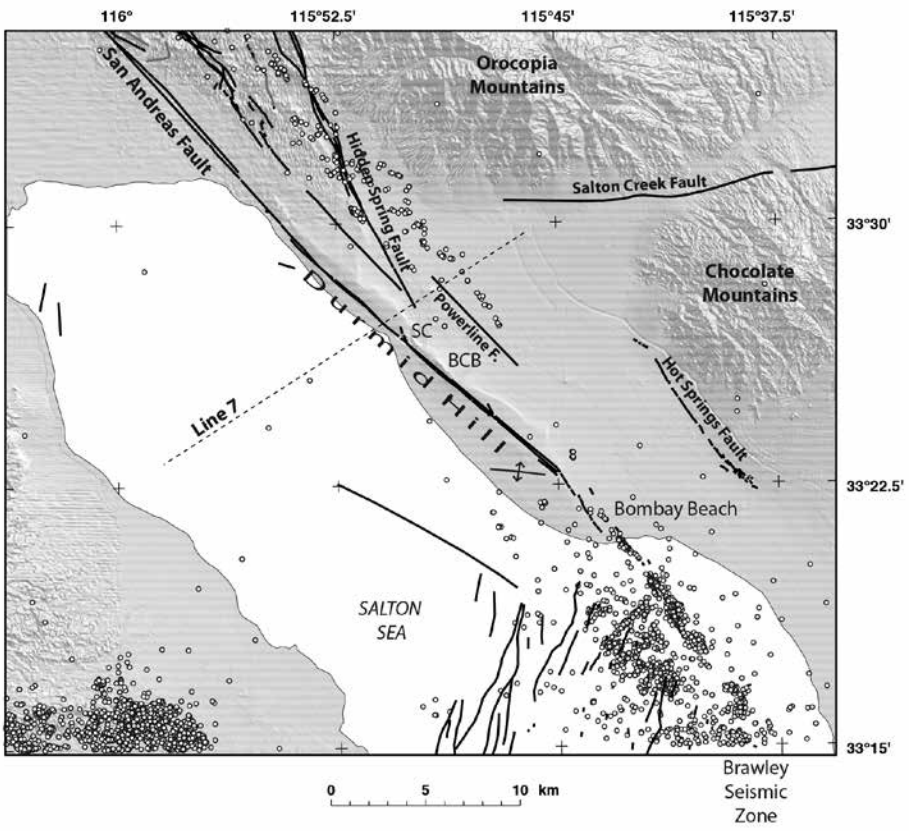

Figure 2. Index map of Durmid Hill and vicinity. Black lines, Quaternary faults from U.S. Geological Survey and California Geological Survey (2012) and Brothers and others (2009). White circles, seismicity from Lin and others (2007). BCB, Bat Caves Buttes, SC, Salt Creek.

Gravity and magnetic data

New gravity data were collected to augment existing data (Mariano and others, 1986), which include transects by Babcock (1969) in the Durmid Hill area. Data collection focused on the area of SSIP high-resolution line 7 near Salt Creek (Fig. 2), adding a 400-m-spaced grid of gravity measurements north of Salt Creek, transects crossing the San Andreas Fault to the north and south of Salt Creek, and supplemental data to fill in gaps (Fig. 3a). Gravity data were reduced to isostatic anomalies using a reduction density of 2,670 kg/m^3 and included earth–tide, instrument drift, free-air, Bouguer, latitude, curvature, and terrain corrections (e.g. Blakely, 1996). An isostatic correction using a sea-level crustal thickness of 25 km and a mantle–crust density contrast of 400 kg/m^3 was applied to the gravity data to remove the long-wavelength gravitational effect of isostatic compensation of the crust due to topographic loading. The data were gridded at a spacing of 200 m using a minimum curvature algorithm (Briggs, 1974). The resulting gravity field is termed the isostatic residual gravity anomaly and reflects density variations in the upper and middle crust (Fig. 3).

Aeromagnetic data from a merged data set compiled by Roberts and Jachens (1999) provide

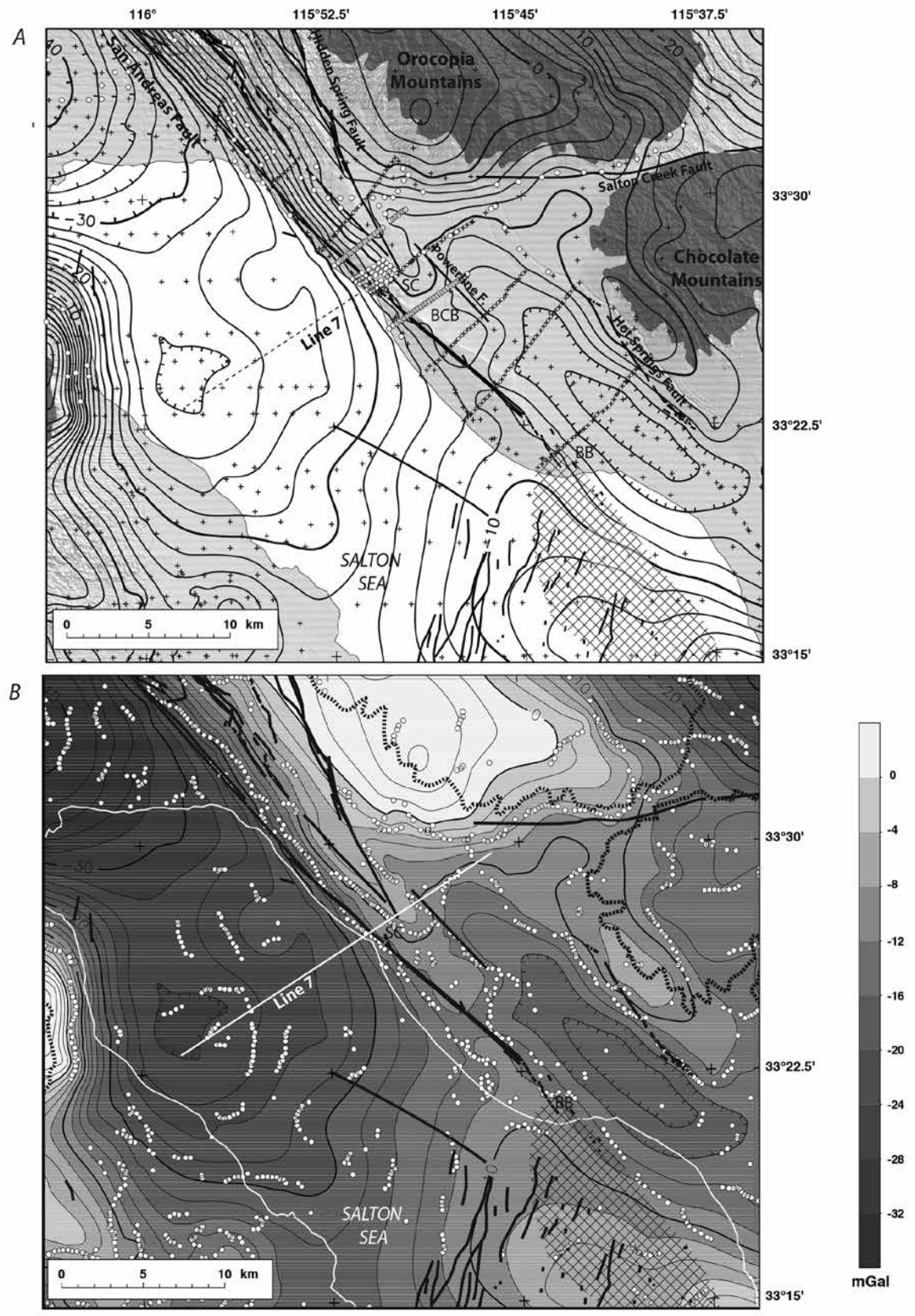

Figure 3. A) Isostatic gravity contours on top of shaded-relief topography. Small crosses, preexisting gravity data; white circles, new gravity data. Dark polygons, extent of exposed crystalline basement. BB, Bombay Beach; BCB, Bat Caves Buttes; SC, Salt Creek. B) Gray-shade isostatic gravity map of Durmid Hill and vicinity. White circles, density boundaries based on maximum horizontal gradient. White line, Salton Sea; heavy black dotted line, extent of exposed crystalline basement. Cross-hatched area, Brawley Seismic Zone.

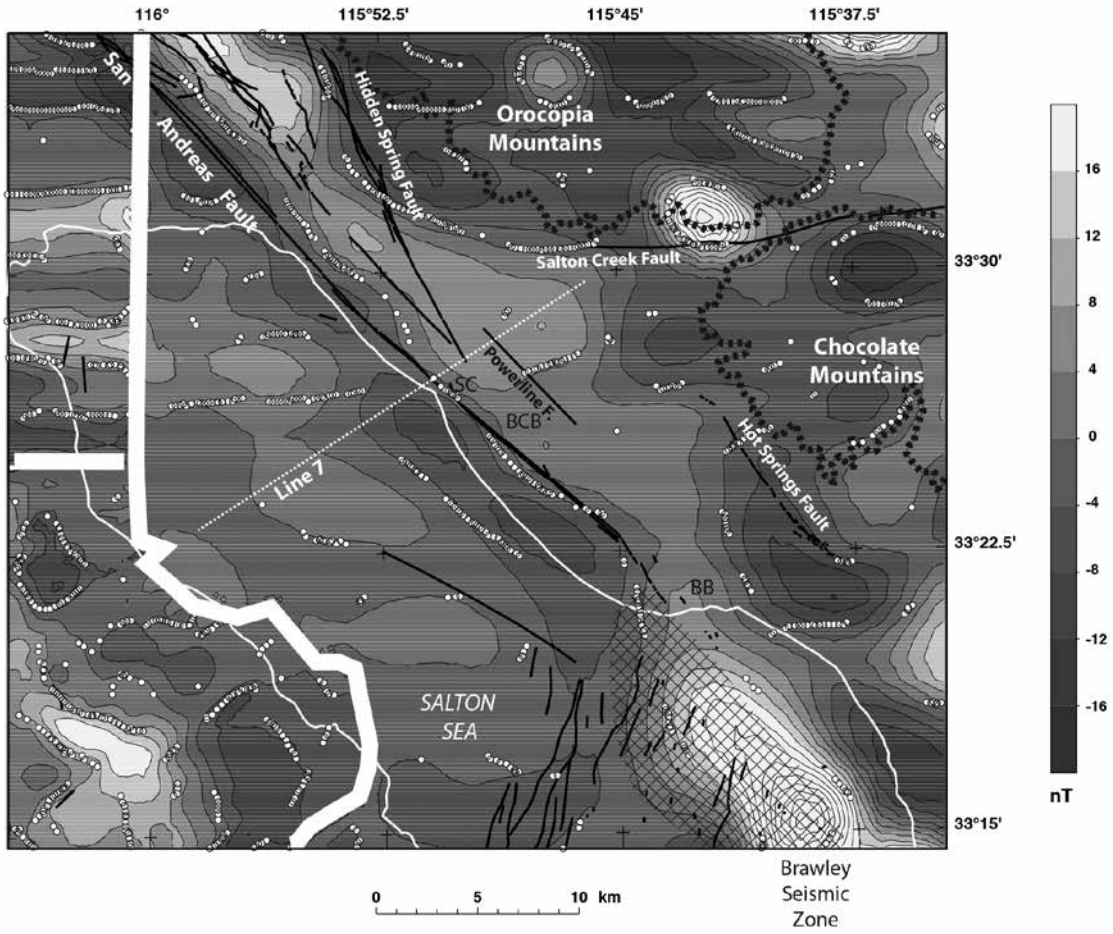

Figure 4. Residual aeromagnetic anomaly map of Durmid Hill and vicinity. Cross-hatched area, Brawley Seismic Zone. White circles, magnetization boundaries based on maximum horizontal gradient. Heavy white lines, boundaries between aeromagnetic surveys.

regional coverage of the study area. To reveal the magnetic anomalies produced by near-surface sources, we removed a regional field derived by upward continuation. By transforming the magnetic field measured on one surface to another field that would be measured on a surface 1 km higher (farther from the source), upward continuation smooths the field by attenuating short-wavelength anomalies (Dobrin and Savit, 1988). This smoothed, upward continued field is then subtracted from the observed field to produce a residual field (Fig. 4) that reflects sources in the upper 10 km. Because the flight lines were not flown perpendicular to the strike of the San Andreas Fault or at a spacing conducive to modeling fault dip, this map can be used only for broad-scale interpretation of fault geometry.

To supplement the aeromagnetic coverage, ground and marine magnetic data were collected with a Geometrics G-858 cesium magnetometer. For onshore measurements, the total field magnetometer was mounted in a backpack system with the magnetic sensor about 2.5 m above the ground. Measurements were collected at a sample rate of 1 Hz while walking at typical speeds of 5 km/hour (3 miles/hour), which yields a sample spacing of about 1.5 m. In total, nearly 40 km of ground magnetic data were collected. For offshore measurements, the magnetometer was mounted on a boom projecting off of the bow of the boat (Boston Whaler) and the GPS antenna was mounted on a pole about 1.2 m vertically above the boat. More than 60 km of marine magnetic data were collected at 10 Hz. The navigation of both onshore and offshore measurements was collected using a non-magnetic Trimble Ag-GPS132 system that utilizes differential GPS corrections broadcast from a satellite, with a specified horizontal precision of <1 m. Diurnal variations recorded by a base station magnetometer were removed from the dataset. For the marine data, a heading correction was applied to improve crossing errors and a 50-m

low-pass filter was applied to smooth high-frequency noise due to wave action. The resulting magnetic map is shown in Figure 5.

To help delineate structural trends and gradients expressed in the gravity and magnetic fields (Fig. 3, 4), a computer algorithm was used to locate the maximum horizontal gradient (Cordell and Grauch, 1985; Blakely and Simpson, 1986). We used the magnetic potential ("pseudogravity") field to calculate the maximum horizontal gradient. Gradient maxima occur approximately over steeply dipping contacts that separate rocks of contrasting densities or magnetizations. For moderate to steep dips (45° to vertical), the horizontal displacement of a gradient maximum from the top edge of an offset horizontal layer is always less than or equal to the depth to the top of the source (Grauch and Cordell, 1987).

Gravity and magnetic anomalies

Gravity and magnetic anomalies provide information on the structural setting of the southern San Andreas Fault. The highest gravity values coincide with exposures of the Orocopia Schist on the east side of the Salton Sea and with batholithic rocks of the Peninsular Ranges on the west side of the Sea (Fig. 3). The lowest gravity values (-40 mGal) are in the northwest corner of the study area and are the southernmost expression of a prominent, narrow northwest-trending gravity low in Coachella Valley. The gravity low diminishes gradually across the Salton Sea to form a relative gravity high in the southeast corner of the study area. Southeast of the study area, these gravity values continue to increase in amplitude to their highest values near the southern shore of the Salton Sea and have been attributed to young sedimentary rocks affected by metamorphism and hydrothermal alteration at shallow depth, to mafic sills, dikes, and flows that intrude these rocks (Biehler and others, 1964; Kasameyer and Hearst, 1988) and to mafic intrusions in the middle to lower crust (Fuis and others, 1984).

The northeast margin of the gravity low discussed above is marked by a linear gradient that decreases in amplitude to the southeast. The San Andreas Fault is located near the base of this steep southwest-facing gravity gradient, suggesting a steep northeast dip of the basement contact, with higher-density rocks northeast of the fault. About 5 km south of Salt Creek, the fault changes its position relative to the gravity field and is located at the top of a northeast-facing gravity gradient. This reversal in gradient coincides with the northwesternmost extent of the Durmid anticline. The northeast-facing gradient indicates high-density material on the southwest side juxtaposed against low-density rocks on the northeast side of the fault. The gradient appears to continue to the southeast, rather than follow the Brawley Seismic Zone, and is approximately aligned with mud pot lineaments attributed to a southeastern extension or an abandoned strand of the San Andreas Fault (Lynch and Hudnut, 2008).

The residual aeromagnetic data show a gradient along the San Andreas Fault, with magnetic rocks concealed northeast of the fault (Fig. 4). The detailed magnetic data, although noisy, show that the magnetic high is double-peaked, with a narrow (500 to 1,000 m) high bounded on the southwest by the San Andreas Fault that is seen on all the ground magnetic profiles and a broader magnetic high to the northeast imaged on those profiles north of Salt Creek (Fig. 5)[1]. At Bombay Beach, the magnetic gradient associated with the fault curves to the south around a southeast-elongated magnetic body (Fig. 4). The northeast margin of the magnetic body coincides with the gravity gradient, indicating a dense, magnetic body interpreted to be a mafic pluton or dike swarm, whose top is estimated to be about 2 km deep (Griscom and Muffler, 1971).

Northeast of the San Andreas Fault are other Quaternary faults that coincide with gravity gradients (Fig. 3b), notably the Powerline and Hot Springs Faults (Babcock, 1969) and the Salton Creek Fault. The Powerline Fault marks the northeast margin of the gravity high interpreted by Babcock (1969) as a horst; the horst is bounded by the San Andreas Fault to the southwest and is about 4 km wide. Based on the gravity gradients shown in Fig. 3b, the horst does not appear to extend more than 7 km southeast of Salt Creek. Babcock also suggested that the Hidden Spring Fault formed part of the northeast margin

1 Babcock (1969) also measured ground magnetic data at a 300-m interval in the Durmid Hill area, but only along his detailed gravity traverses (that are spaced 4-7 km apart). The data were too noisy and dissimilar from profile to profile to image the magnetic high north of the San Andreas Fault; he attributed the irregularity of the surface magnetic profiles to "localized concentrations of magnetite in the surficial Lake Cahuilla sediments and to scattered magnetite rich boulders." Our data show that ground magnetic methods can work in this area if the spacing of the profiles is not too great.

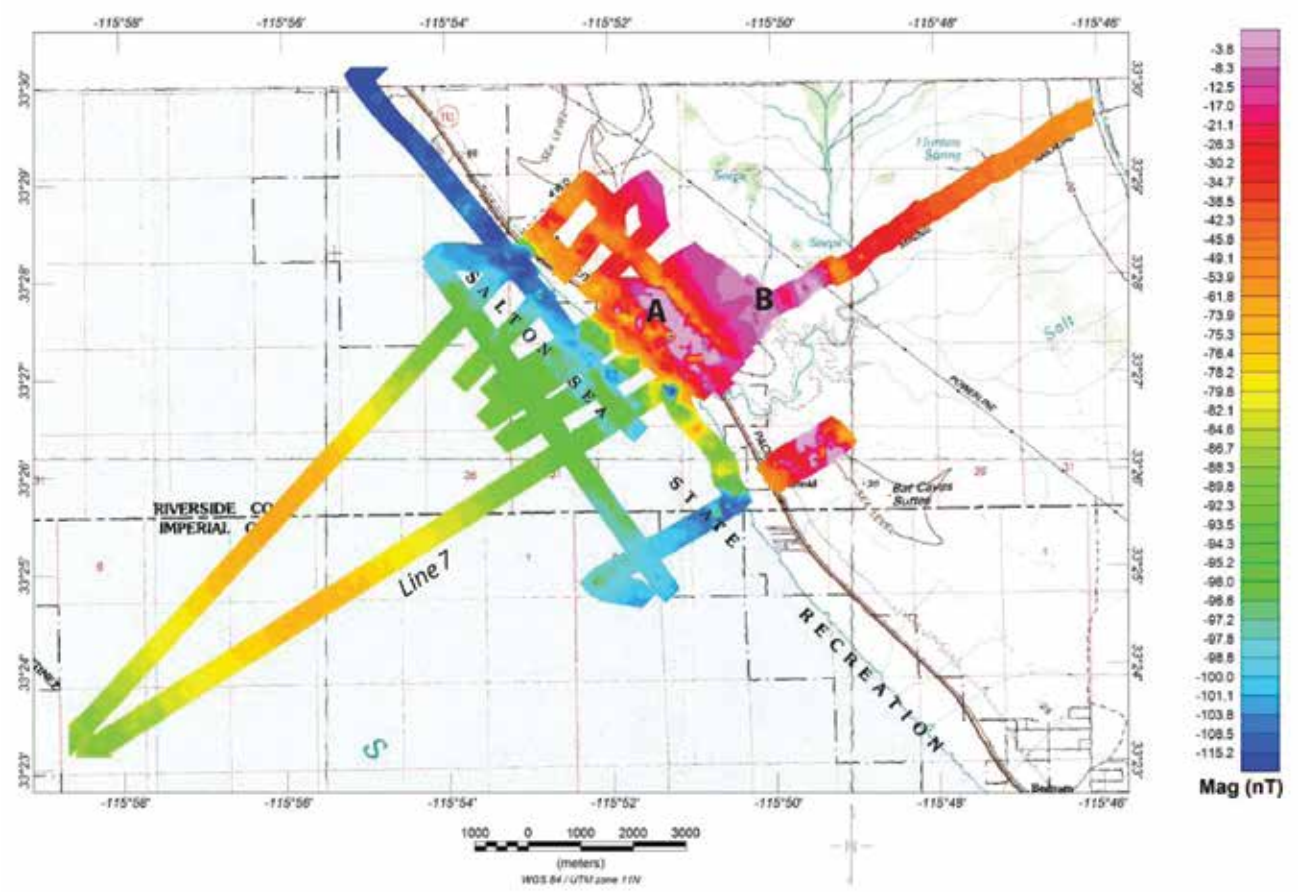

Figure 5. Detailed magnetic anomaly map based on ground and marine data. Note the prominent magnetic high along the San Andreas Fault and a broader magnetic high 2 km northeast of the fault.

of the horst; the Hidden Spring Fault, however, trends more northerly than the Powerline Fault and its corresponding gravity gradient and cuts across the center of the gravity high at its southernmost mapped extent. This suggests that the Hidden Spring Fault does not have significant (> 1 km) vertical or horizontal displacement resulting from its being only recently active, a slow slip rate, or both.

Northeast of the interpreted horst is an elongate gravity low that reflects a basin that is estimated to be about 2 km deep (Biehler and others, 1964; Babcock, 1969). The Hot Springs Fault, marked by geothermal springs and wells, coincides with a steep gravity gradient marking the northeast margin of the basin. The gravity gradient extends another 10 km to the northwest of the Hot Springs Fault, suggesting the continuation of this fault, albeit concealed, to the Salton Creek Fault. The Powerline and San Andreas Faults form the stepped, southwest margin of the basin. The basin, approximately 20 km long, could speculatively reflect a basin formed by a right step between the San Andreas and the Hot Springs Faults. Alternatively, the basin could be related to transrotation of the Eastern Transverse Ranges and left slip on the Salton Creek Fault. A triangular basin is predicted at the intersection of the San Andreas and Salton Creek Faults if the blocks are assumed to be rigid; perhaps the deviation from this basin geometry reflects partly non-rigid behavior.

Geophysical model across Line 7 (Salt Creek line)

Model setup

We modeled the gravity and detailed magnetic data along SSIP Line 7 (Fig. 6) guided by the modeled seismic velocity variations of Fuis and others (2012a). See Rose and others (2013) for a description of the SSIP seismic survey. Density and seismic velocity are related properties. In general, velocities greater than 5–6 km/s are typical of crystalline basement, although fracturing and cracks (particularly in the upper 1 km) can reduce these velocities by half. For velocities equal to or less than 5 km/s, we used the relationship of Gardner and others (1974) that was empirically derived from sedimentary rocks

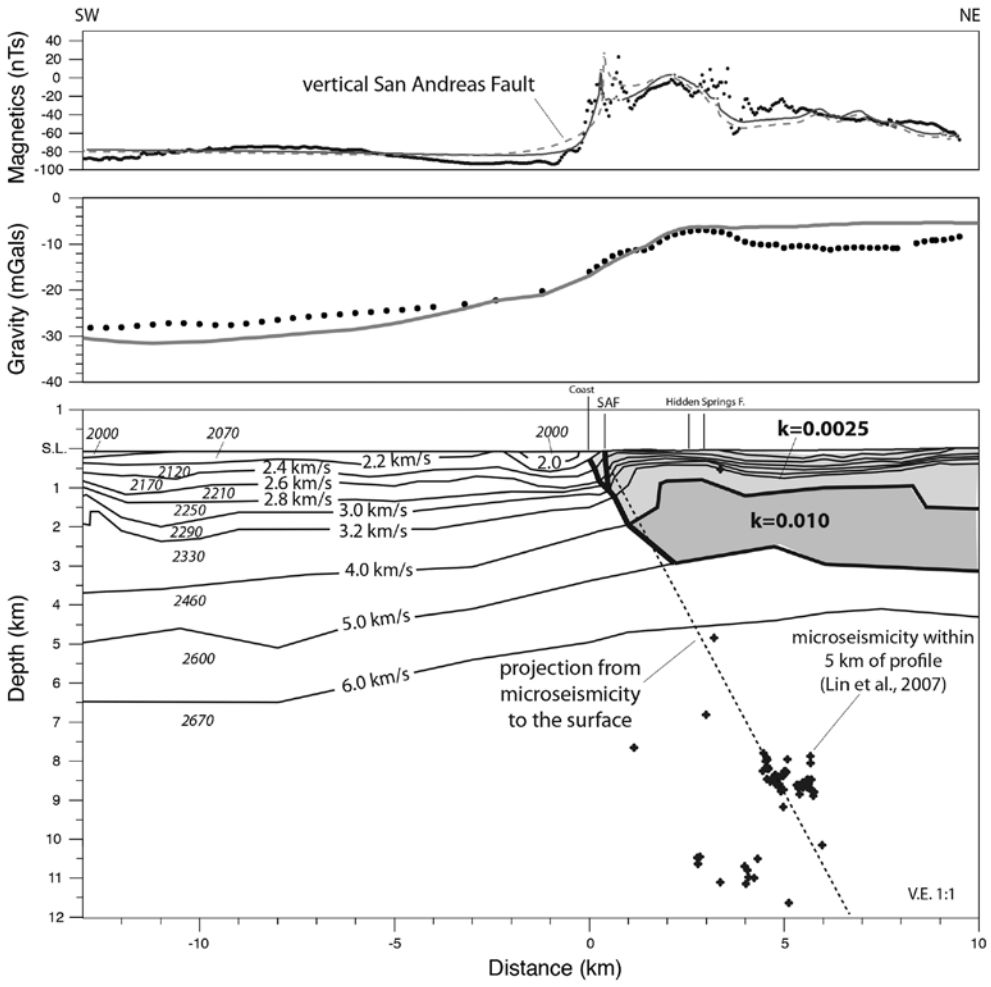

Figure 6. Gravity and magnetic model along Line 7. Numbers in italics are densities in kg/m^3. Shaded regions are magnetic bodies; k, magnetic susceptibility (SI unit).

to convert velocity to density. Although velocities greater than 6 km/s were modeled along Line 7 at depths of 6 to 7.5 km near the center of the profile, these depths are near the margins of the ray-path coverage. We did not model any velocity greater than 6 km/s and thus used a maximum density of 2,670 kg/m^3.

For the magnetic model, we assign magnetization only to bodies northeast and within the San Andreas Fault zone. Limited data on the magnetic properties of the sedimentary rocks west of the San Andreas Fault imply that rocks within the Salton Sea are at most weakly magnetic (Griscom and Muffler, 1971). We therefore did not model the basin fill as magnetic southwest of the San Andreas Fault. Northeast of the fault, the frequency content of the magnetic high suggests two sources: a shallow source to account for the sharp and narrow magnetic highs at the fault and east of the Hidden Spring Fault and a deeper source to produce the broad magnetic high. Babcock (1969) surmised that the high-frequency magnetic anomalies he measured along widely-spaced traverses were caused by surficial deposits. We, however, measured magnetic susceptibilities from the Shavers Well and Borrego Formations and found that these sedimentary rocks are weakly to moderately magnetic (0.5–5.5 x10^{-3} SI). Based on these measurements, we assigned a susceptibility of 2.5 x 10^{-3} SI to the sedimentary deposits northeast of the San Andreas Fault. We assume that the source of the broader magnetic high is basement and use the 4 km/s contour to define the top of basement. Basement rocks of San Gabriel Mountains type are exposed nearby in the Orocopia and Chocolate Mountains; the Orocopia Schist is not magnetic, but the rocks that reside in the upper plate of the Vincent Thrust above the Schist are (Langenheim and Powell, 2009). We assign a susceptibility of 1 x10^{-2} SI to these upper-plate rocks, which leads to a thickness of ~ 2 km of these rocks to account for the amplitude of the broad magnetic high.

Results

The gravity variation predicted by simple conversion of velocity to density compares favorably with the observed gravity variation along Line 7 (Fig. 6). To first order, the modeled location and amplitude of the gravity gradient match the location and amplitude of the observed gravity gradient. The seismic velocity model, however, does not predict the broad gravity low observed northeast of the Hidden Spring

Fault nor the step in the gravity gradient that is observed at km 1.5 on Line 7. The seismic velocity model likely does not have sufficient resolution to image these details within the upper kilometer of the surface. Unfortunately, the existing coverage of gravity measurements does not have the resolution to verify the pocket of low velocities just southwest of the Salton Sea coast. Because the San Andreas Fault does not juxtapose sedimentary rocks against basement at the surface along Line 7, it is not possible at this time to resolve unequivocally the direction of dip on the San Andreas Fault.

The magnetic data are consistent with a steep northeast dip of the San Andreas Fault with a sliver of magnetic rocks that extend southwest of the fault in the upper 1 km; the predicted magnetic variation (solid line in Fig. 6) matches the steepness of the observed gradient. A vertical San Andreas Fault produces a gentler magnetic gradient (dotted line in Fig. 6) than observed. The dipping fault is slightly better at matching the southwest gradient of the broader magnetic high, although the model is less sensitive to the configuration of the magnetic basement layer. Upward projection of the microseismicity (Lin and others, 2007) within 5 km of the profile is approximately aligned with the dip of the San Andreas Fault as modeled from the magnetic data.

Discussion and conclusions

To first order, the gravity and seismic velocity data are consistent with each other across the San Andreas Fault at Salt Creek and suggest a moderate to steep dip for the San Andreas Fault in the upper 1–2 km. Further refinement of the gravity model is warranted to match the gravity low northeast of the Hidden Spring Fault and the step in the gravity gradient associated with the San Andreas Fault and to account for reduction in velocity near the San Andreas Fault. Modeling of the magnetic data suggests that the San Andreas Fault has a northeast dip that is greater than 50° and that a sliver of magnetic basin fill in the upper 1 km lies southwest of the fault. This could reflect folding west of the fault due to transpression, similar to what is mapped in the Durmid anticline, and indicates that deformation associated with the fault zone is wider than just the mapped surface trace. Babcock (1974) was unable to map structure west of Salt Creek in the area of Line 7 because of poor exposure. A more recent geologic map by Dibblee and Minch (2008) shows an anticline mapped in Borrego Formation immediately to the south of Salt Creek southwest of the fault; the magnetic data suggest that folding may extend southwest of the coastline.

A northeast dip of the San Andreas Fault is supported by microseismicity (Lin and others, 2007). Although the microseismicity can conceivably also be projected up to the Hidden Spring Fault, the microseismicity to the northwest of Salt Creek forms a band that is parallel to the San Andreas Fault rather than the more northerly trending Hidden Spring Fault (Fig. 2). A northeast-dipping San Andreas Fault also accounts for the asymmetry in geodetically measured strain rates across the southern San Andreas Fault (Lindsey and Fialko, 2013).

The gravity data highlight the width of deformation associated with the San Andreas Fault northeast of Durmid Hill. A similarly wide zone of deformation is exposed in the Mecca Hills (Sylvester and Smith, 1976) to the northwest and likely continues in some fashion into the study area, but is concealed, likely because of the interactions between the Salton Creek and San Andreas Faults during rotation of the eastern Transverse Ranges. The width of deformation as defined by the basin between the San Andreas and Hot Springs Faults may also reflect the encroachment of transtension northwards from the Gulf of California as manifested by the Brawley Seismic Zone, high heat flow, and intrusion of mafic material into the crust.

Acknowledgements

Thanks to Tom Anderson, Megan Creegan, and Erik Duerkop of the Sonny Bono Salton Sea National Wildlife Refuge for their help in the boat survey. We gratefully acknowledge reviews by Bob Jachens and Bob Powell.

References

Babcock, E.A., 1969, Structural geology and geophysics of the Durmid area, Imperial Valley, California [Ph.D. dissertation]: Riverside, University of California, 149 p.

Babcock, E.A., 1974, Geology of the northeast margin of the Salton Trough, Salton Sea, California: Geological Society of America Bulletin, v. 85, p. 321-332.

Biehler, S., Kovach, R.L., and Allen, C.R., 1964, Geophysical framework of northern end of the Gulf of California structural province: American Association of Petroleum Geologists Memoir 3, p. 126-143.

Blakely, R.J., 1996, Potential theory in gravity and magnetic applications: Cambridge University Press, 441 p.

Bilham, R., and Williams, P., 1985, Sawtooth segmentation and deformation processes of the southern San Andreas Fault, California: Geophysical Research Letters, v. 12, p. 557-560.

Blakely, R.J., and Simpson, R.W., 1986, Approximating edges of source bodies from magnetic or gravity anomalies: Geophysics, v. 51, p. 1494–1498.

Briggs, I.C., 1974, Machine contouring using minimum curvature: Geophysics, v. 39, p. 39-48.

Brothers, D.S., Driscoll, N.W., Kent, G.M., Harding, A.J., Babcock, J.M., and Baskin, R.L., 2009, Tectonic evolution of the Salton Sea inferred from seismic reflection data: Nature Geoscience, v. 2, p. 581-584.

Bürgmann, R., 1991, Tranpression along the southern San Andreas Fault, Durmid Hill, California: Tectonics, v. 10, p. 1152-1163.

Cordell, Lindrith, and Grauch, V.J.S., 1985, Mapping basement magnetization zones from aeromagnetic data in the San Juan Basin, New Mexico, *in* Hinze, W.J., ed., The utility of regional gravity and magnetic anomaly maps: Society of Exploration Geophysicists, p. 181–192.

Dibblee, T.W., Jr., 1954, Geology of the Imperial Valley region, California, *in* Jahns, R.H., ed., Geology of Southern California: California Division of Mines and Geology Bulletin 170, p. 21-28.

Dibblee, T.W., Jr., and Minch, J.A., 2008, Geologic map of the Durmid 15' quadrangle, Riverside and Imperial counties, California: Dibblee Foundation Map DF-376, scale 1:62,500.

Dobrin, M.B., and Savit, C.H., 1988, Introduction to Geophysical Prospecting: New York, McGraw-Hill, Inc., 867 p.

Elders, W.A., Rex, R.W., Media, T., Robinson, P.T. and Biehler. S., 1972. Crustal spreading in Southern California: Science, v. 178, p. 15-24

Fuis, G.S., Hole, J.A., Stock, J.M., Driscoll, N.W., Kent, G.U., Harding, A.J., Kell, A.M., Goldman, M.R., Rose, E.J., Catchings, R.D., Rymer, M.J., Langenheim, V.E., Scheirer, D.S., Athens, N.D., and Tarnowski, J.M., 2012a, Investigating earthquake hazards in the northern Salton Trough, southern California, using data from the Salton Seismic Imaging Project (SSIP): Abstract T44A-06 presented at 2012 Fall Meeting, American Geophysical Union, San Francisco, Calif.

Fuis, G.S., Mooney, W.D., Healy, J.H., McMechan, G.A., and Lutter, W.J., 1984, A seismic refraction survey of the Imperial Valley Region, California: Journal of Geophysical Research, v. 89, p. 1165-1189.

Fuis, G.S., Scheirer, D.S., Langenheim, V.E., and Kohler, M., 2012b, A new perspective on the geometry of the San Andreas Fault in southern California and its relationship to lithospheric structure: Bulletin of the Seismological Society of America, v. 102, p. 236-251.

Gardner, G.H., Gardner, L.W., and Gregory, A.R., 1974, Formation velocity and density: the diagnostic basis for stratigraphic traps: Geophysics, v. 39, p. 770-780.

Grauch, V.J.S., and Cordell, Lindrith, 1987, Limitations of determining density or magnetic boundaries from the horizontal gradient of gravity or pseudogravity data: Geophysics, v. 52, no. 1, p. 118–121.

Griscom, A., and Muffler, L.J.P., 1971, Aeromagnetic map and interpretation of the Salton Sea geothermal area, California: U.S. Geological Survey Geophysical Investigations Map GP-754, 5 p., scale 1:62,500.

Jennings, C.W., Strand, R.G., and Rogers, T.H., 1977, Geologic map of California: California Division of Mines and Geology, scale 1:750,000.

Jones, L.M., Bernknopf, R., Cox, D., Goltz, J., Hudnut, K., Mileti, D., Perry, S., Ponti, D., Porter, K., Reichle, M., Seligson, H., Shoaf, K., Treiman, J., and Wein, A., 2008, The ShakeOut Scenario: U.S. Geological Survey Open-File Report 2008-1150 and California Geological Survey Preliminary Report 25, 312 p. [http:pubs.usgs.gov/of/2008/1150].

Kasameyer , P.W. and Hearst, J.R., 1988, Borehole gravity measurements in the Salton Sea Scientific Drilling Project well State 2-14: Journal of Geophysical Research, v. 93, p. 13,037-13,045.

Langenheim, V.E., and Powell, R.E., 2009, Basin geometry and cumulative offsets in the Eastern Transverse Ranges, southern California: Implications for transrotational deformation along the San Andreas fault system: Geosphere, v. 5, no. 1, p. 1-22.

Lin, G., Shearer, P.M., and Hauksson, E., 2007, Applying a three-dimensional velocity model, waveform cross correlation, and cluster analysis to locate southern California seismicity from 1981-2005: Journal of Geophysical Research, v. 112, B12309, doi:10.0129/2007JB004986, 14 p.

Lindsey, E.O., and Fialko, Y., 2013, Geodetic slip rates in the southern San Andreas Fault system: Effects of elastic heterogeneity and fault geometry: Journal of Geophysical Research, v. 118, p. 689-697.

Lynch, D.K., and Hudnut, K.W., 2008, Wister mud pot lineament: southeastward extension or abandoned strand of the San Andreas Fault?: Bulletin of the Seismological Society of America, v. 98, p. 1720-1729.

Mariano, J., Helferty, M.G., and Gage, T.B., 1986, Bouguer and isostatic residual gravity maps of the Colorado River region, including the Kingman, Needles, Salton Sea, and El Centro quadrangles: U.S. Geological Survey Open-File Report 86-374, 7 plates, scale 1:250,000.

Merriam, R., and Bischoff, J.L., 1975, Bishop Ash: a widespread volcanic ash extended to Southern California: Journal of Sedimentarty Petrology, v. 45, p. 207-211.

Nicholson, C., Hauksson, E., Plesch, A., and Shearer, P.M., 2009, Revised 3D fault models for CFM along the southern San Andreas and Elsinore-Earthquake Valley fault systems: 2009 Southern California Earthquake Center Annual Meeting Proceedings and Abstracts, vol. XIX, p. 265. (accessed 9 Jan 2014 at http://www.scec.org/ meetings/2009am/2009SCECAnnualMeetingVolume.pdf).

Perry, S., Cox, D., Jones, L., Bernknopf, R., Goltz, J., Hudnut, K., Mileti, D., Ponti, D., Porter, K., Reichle, M., Seligson, H., Shoaf, K., Treiman, J., and Wein, A., 2008, The ShakeOut Earthquake Scenario; a story that southern Californians are writing: U.S. Geological Survey Circular 1324 and California Geological Survey Special Report 207, 16 p. [http://pubs.usgs.gov/circ/1324/].

Philibosian, B., Fumal, T., and Weldon, R., 2011, San Andreas fault earthquake chronology and Lake Cahuilla history at Coachella, California: Bulletin of the Seismological Society of America, v. 101, p. 13-38.

Roberts, C.W., and Jachens, R.C., 1999, Preliminary aeromagnetic anomaly map of California: U.S. Geological Survey Open-File Report 99-440, 14 p.

Rose, E.J., Fuis, G.S., Stock, J.M., Hole, J.A., Kell, A.M., Kent, G., Driscoll, N.W., Crum, S., Goldman, M., Reusch, A.M., Han, L., Sickler, R.R., Catchings, R.D., Rymer, M.J., Criley, C.J., Scheirer, D.S., Skinner, S.M., Slayday-Criley, C.J., Murphy, J.M., Jensen, E.G., McClearn, R., Ferguson, A.J., Butcher, L.A., Gardner, M.A., Emmons, I., Loughran, C.L., Svitek, J.R., Bastien, P.C., Cotton, J.A., Croker, D.S., Harding, A.J., Babcock, J.M., Harder, S.H., and C.M. Rosa, 2013, Borehole-explosion and air-gun data acquired in the 2011 Salton Seismic Imaging Project (SSIP), southern California: Description of the survey: U.S. Geological Survey Open-File Report 2013-1172, 84. [http://pubs.usgs.gov/of/2013/1172].

Rymer, M.J., Treiman, J.A., Kendrick, K.J., Lienkaemper, J.J., Weldon, R.J., Bilham, R., Wei, M., Fielding, E.J., Hernandez, J.L., Olson, B.P.E., Irvine, P.J., Knepprath, N., Sickler, R.R., Tong, X., and Siem, M.E., 2010, Triggered surface slips in southern California associated with the 2010 El Mayor-Cucapah, Baja California, Mexico, earthquake: U.S. Geological Survey Open-File Report 2010-1033 and California Geological Survey Special Report 221, 62 p.

Sarna-Wojcicki, A.M., Bowman, H.W., Meyer, C.E., Russell, P.C., Woodward, M.J., McCoy, G., Rowe, J.J., and Baedecker, P.A., 1984, Chemical analyses, correlations, and ages of upper Pliocene and Pleistocene ash layers of east-central and southern California: U.S. Geological Survey Professional Paper 1293, 40 p.

Sieh, K., 1986, Slip rate across the San Andreas Fault and prehistoric earthquakes at Indio, California: Eos, Transactions, American Geophysical Union, v. 67, p. 1200.

Sieh, K.E., and Williams, P.L., 1990, Behavior of the southernmost San Andreas fault during the past 300 years: Journal of Geophysical Research, v. 95, p. 6629-6645.

Sylvester, A.G., and Smith, R.R., 1976, Tectonic transpression and basement-controlled deformation in San Andreas Fault zone, Salton Trough, California: American Association of Petroleum Geologists Bulletin, v. 60, p. 2081-2102.

Sylvester, A.G., Bilham, R., Jackson, M., and Barrientos, S., 1993, Aseismic growth of Durmid Hill, southeasternmost San Andreas Fault, California, Journal of Geophysical Research, v. 98, p. 14,233-14,243.

U.S. Geological Survey and California Geological Survey, 2012, Quaternary fault and fold database for the United States, accessed Feb 22, 2012 at http//earthquake.usgs.gov/hazards/qfaults/.

Wei, M., Sandwell, D., Fialko, Y., and Bilham, R., 2011, Slip on faults in the Imperial Valley triggered by the 4 April 2010 Mw 7.2 El Mayor-Cucapah earthquake revealed by InSAR: Geophysical Research Letters, v. 38, L01308, doi:10.1029/2010GL045235.

Weldon, R., Scharer, K., Fumal, T., and Biasi, G., 2004, Wrightwood and the earthquake cycle: What a long recurrence record tells us about how faults work: GSA Today, v. 14, no. 9, p. 4-10.

Records of freshwater bony fish from the latest Pleistocene to Holocene Lake Cahuilla beds of western Imperial County, California

Mark A. Roeder and Gino Calvano

Department of Paleontology, San Diego Natural History Museum

Introduction

From September 17, 2010 through April 3, 2012, paleontologists from the Department of Paleontology of the San Diego Natural History Museum (SDNHM) monitored ground disturbing activities during construction of San Diego Gas and Electric Company's Sunrise Powerlink Transmission Line (SRPL) for paleontological resources. The SRPL was built along a 118 mile-long (191 km) corridor extending from south of Poway, San Diego County to southwest of Seeley, Imperial County. The project consisted of construction of 500 kV transmission towers, installation of underground utility lines, construction of new substations, and improvements to existing substations and other attendant facilities. Much of the paleontological resource monitoring was conducted on the auguring for transmission tower supports. During the auguring of Transmission Tower EP 353 (Link 1) located about 8 miles (13 km) southwest of the community of Seeley, fossil-bearing fine-grained sediments were brought up from a depth of 30 feet (9 m). These sediments were originally mapped as Brawley Formation (Deméré and Siren, 2012). But Jefferson (pers. com. 2014) suggests that they should be assigned to the Lake Cahuilla beds (Blake, 1907). One of us (GC) collected and processed a 250 kg (500 lb) sample (SDNHM locality 6531) from a planar-laminated siltstone with interbeded claystone interpreted as lacustrine (lake) deposits. From this sample, the remains of at least four kinds of freshwater fish were recovered (Table 1).

Table 1. Fish remains recovered from SDNHM locality 6531 in the Lake Cahuilla beds, at San Diego Gas Electric Company Sunrise Powerlink Project at Transmission Tower EP 353, southwest of Seeley, Imperial County, California.

Species	Common Name	Element	Comments
Gila	chub	pharyngeal	
Xyrauchen texanus	razorback sucker	pharyngeal	
Gasterosteus aculeatus	threespine stickleback	pelvic? spine	first record
Osteichthyes	very small fish	vertebra	not identified

Stratigraphy

The west side of Imperial Valley is underlain by Lake Cahuilla beds, which consist of interbedded lenticular and tabular silt, sand, and clay that are 60 to 100 meters thick (Van de Kamp, 2006). Although modern in age at the surface, these lake/playa sediments increase in age with depth and where dated (Li and others, 2008) are latest Pleistocene and Holocene in age (Van de Kamp, 2006). According to Van de Kamp (2006), the Lake Cahuilla beds sediments came from two sources. The first source was the Colorado River which intermittently flowed into the southern portion of the Salton Trough, and deposited sand and mud in deltaic, fluvial and lacustrine environments. The second source was the sediments derived from the basin margin. A recent study by Li and others (2008) dating various layers of calcareous oncoids tufa (a carbonate coral-like rock deposited by algae that encrusts boulders in freshwater lakes and streams) at Travertine Rock on the Riverside-Imperial County Line, near Salton City, found evidence of at least 30 basin filling lakes in the Salton Trough in the last 20,000 years. Evidence of these inundations and subsequent desiccations are chronicled in the sediments of the Lake Cahuilla beds. Only the last 5 to 10 lake phases of the Lake Cahuilla sediments (from the 400 to 5900 years before present) have been studied in any detail (Bowersox 1972; Waters 1980, 1983; Reynolds 1989; Whistler, and others 1995; Wagner 2007; Crull and others, 2008; Li and others, 2008). In surficial exposures, Lake Cahuilla beds are usually horizontal where Brawley Formation strata are usually dipping (Jefferson 2014).

Systematic Accounts

Modern environmental/ecological information, geographic ranges and other data used in systematic accounts are

from Eschmeyer and Herald (1983), La Rivers (1962), McGinnus (2006), Moyle (1976), Miller and Lea (1972), and Swift and others (1993).

Gasterosteus aculeatus–threespine stickleback (Figure 1)

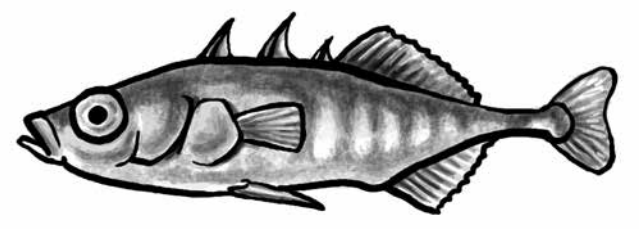

Figure 1. Modern threespine stickleback (*Gasterosteus aculeatus*), average size 5 cm. Illustration by Katura Reynolds.

Today, threespine sticklebacks are found in coastal waters throughout the Holoactic region from the Mediterranean and Europe north to Russia, and across Japan and Korea into North America. On the east coast of North America, these fish are found south to Chesapeake Bay. Marine populations on the west coast of North America are found as far south as Monterey Bay, California. Populations inhabit coastal drainages as far south as Rio Rosario, northern Baja California, Mexico. In California, freshwater forms can be found in coastal streams up to major barriers such as falls or rapids. Freshwater sticklebacks, which rarely exceed three inches in length, usually frequent the quiet waters of streams. Often they are observed in weedy ponds and backwaters, among emergent plants along stream banks and sandy bottoms.

Sticklebacks have three stout dorsal spines anterior to the dorsal fin and a spine anterior to each pelvic fin. Fossil stickleback spines that probably represent *Gasterosteus* have been reported from the middle Miocene Barstow Formation at Argonaut Site, and Toomey Hills near Yermo in San Bernardino County (Bell and Reynolds, 2010). The Barstow Formation in this area is early Barstovian NALMA in age approximately 16 Ma (Bell and Reynolds, 2010).

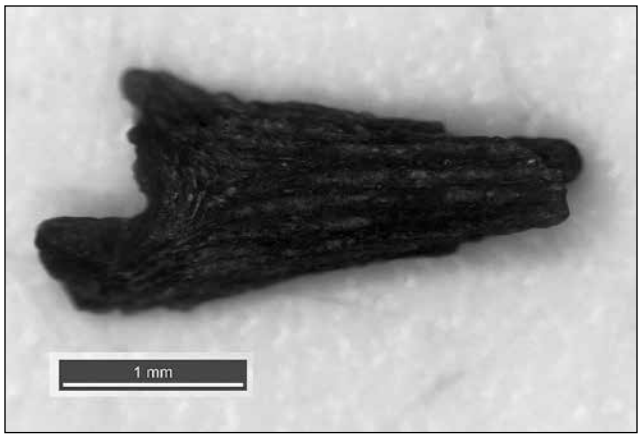

Figure 2. Partial fossil *Gasterosteus aculeatus* (threespine stickleback), left? pelvic spine SDNHM 6531/134473, bar scale is 1 mm.

Material: a single left? pelvic spine fragment was recovered SDNHM 6531/134473. (Figure 2).

Gila elegans–bonytail (Figure 3)

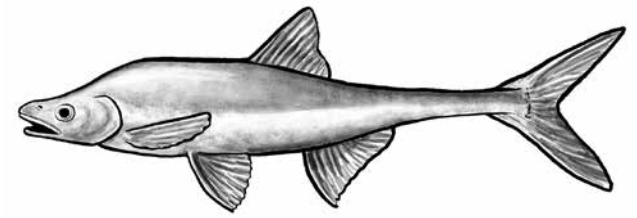

Figure 3. Modern chub–bonytail (*Gila elegans*), size 60 cm. Illustration by Katura Reynolds.

There are three species in the genus *Gila* (chubs) known in the Colorado River drainage (Smith and others, 1979). The bonytail (*Gila elegans*) is the largest of the three, attaining lengths up to 62 cm (24.5 inches) (Figure 3). This is the most common chub and has a streamlined body with an extremely thin or "bonytail" and a smaller hump between the head and the dorsal fin. Bonytails are usually found in eddies and pools along streams. Bonytail bones are the most abundant fish remains recovered from archaeological sites around the old shorelines of Lake Cahuilla (Gobalet, 1992).

In the summer of 1905, flashflood conditions along the Colorado River drainage resulted in the breaching of artificial levees on the delta and the catastrophic diversion of the entire flow of the Colorado River to the north and into the Salton Trough. This formed the largest inland body of water in California and is today called the Salton Sea. The river continued flowing until February of 1907, when it was finally diverted back into its former channel, allowing the river to again flow south into the Gulf of California. The fish fauna of the early Salton Sea consisted entirely of freshwater species including the bonytail, humpback sucker, rainbow trout, striped mullet, desert pupfish, and carp (Evermann, 1916). However, because of the high salt content of irrigation water draining into the Salton Sea and rapid

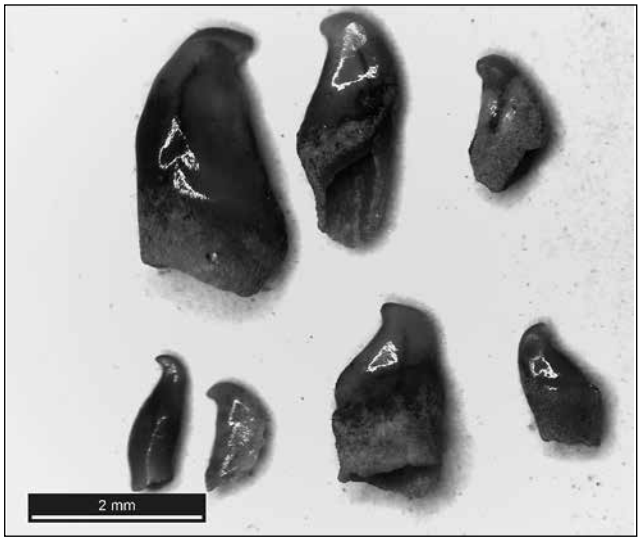

Figure 4. Fossil *Gila* isolated pharyngeal teeth SDNHM 6531/134468, bar scale is 2 mm.

evaporation rates on the Sea itself, rising salinities caused changes in the fish fauna. By 1916, the bonytail were uncommon (Evermann 1916) and in 1929 this fish could not be found at all (Coleman, 1929). Although locally extinct in California, the bonytail still exists in the upper reaches of the Colorado River drainage.

The humpback chub (*Gila cypha*) is streamlined like the bonytail, but has an extremely pronounced dorsal hump. Slightly smaller than the bonytail, this fish reaches lengths up to 50 cm (20 inches). The humpback chub was not recognized scientifically until 1946. This species lives exclusively in deep canyon stretches along the main Colorado River drainage.

The roundtail chub (*Gila robusta*) is smaller than the other two chubs only attaining lengths up to 43 cm (17 inches). From the early 1900s there are a few records of this fish in the lower Colorado River, but today roundtail chubs only occur farther upstream in larger tributaries. Their elongated body and streamlined fin make the roundtail chub well adapted for swift moving water. Fossil remains of roundtail chubs have been reported from the upper Miocene Bidihochi Formation of northeastern Arizona (Uyeno and Miller, 1965).

Based on isolated pharyngeal (throat) teeth, *Gila* (chub) has been identified from sediments of the Plio-Pleistocene Palm Spring Group in Anza-Borrego Desert State Park that date about 1 Ma (Gensler and others, 2006; Roeder, 2006).

Material: a single *Gila* partial pharyngeal arch SDNHM 6531/133470, and 20 *Gila* isolated pharyngeal teeth SDNHM 6531/13472 were recovered (Figure 4).

Xyrauchen texanus–razorback sucker (Figure 5)

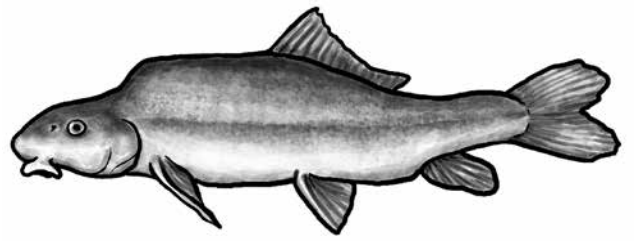

Figure 5. Modern razorback sucker (*Xyrauchen texanus*), size up to 1 m. Illustration by Katura Reynolds.

Razorback suckers can be distinguished from all other suckers by the sharp-edged keel on the back immediately anterior of the dorsal fin. This anatomical feature appears to be an adaptation for living in swift muddy waters of large rivers. However, recent studies indicate that this feature may prevent this fish from being swallowed by predators. Razorback suckers reach lengths of up to one meter (39 inches) and weights up to 7.3 kg. (16 lbs.). In the past, this fish was widely distributed in the Colorado River system, but the construction of dams, destruction of habitat, and the introduction of exotic game fishes have greatly reduced both the range and numbers of

Figure 6. Fossil *Xyrauchen texanus* (razorback sucker) isolated pharyngeal teeth. SDNHM 6531/134468, bar scale is 2 mm.

this fish. Where present, the razorback sucker prefers the slower moving parts of large streams and their backwaters.

To Native Americans living along the lower Colorado River and the shore of Lake Cahuilla, this fish was an important food item (Gobalet, 1992; McGinnus, 2006). Like the roundtail chub, the razorback sucker has a relatively long fossil record. A nearly complete skeleton was found in a sandstone concretion from the Pliocene Arroyo Diablo Formation in the northern portion of the San Felipe Hills of Imperial County (Stewart and Roeder, 1993; Hoetker and Gobalet, 1999). The Arroyo Diablo Formation is 4.25 to approximately 3.7 Ma old (Dorsey and others, 2011), and represents ancient Colorado River delta environments.

Material: twelve isolated pharyngeal teeth SDNHM 6531/134467 (Figure 4), 10 isolated pharyngeal teeth SDNHM 6531/134468, and one fin spine SDNHM 6531/134469 were recovered.

Osteichthyes–bony fish

A small vertebra was recovered, but because of a lack of comparative material from very small freshwater fish such as desert pupfish (*Cyprinodon maculatus*) precludes identification.

Material: a single vertebra SDNHM 6531/134481.

Discussion

A 250 kg (500 pound) sample of Lake Cahuilla beds sediment collected during paleontological monitoring of construction activities at SRPL Transmission Tower EP 393 was water screened through 24 mesh metal sieves. The concentrate was sorted for fossil remains with the aid of a binocular microscope (Deméré and Siren, 2012).

Today, in southern California, the freshwater threespine stickleback is only known from coastal drainages. They are not found in the Salton Trough nor the Colorado River system (Moyle, 1976; McGinnis, 2006; Swift and others, 1993), which makes their presence in the Brawley Formation very interesting. Today, they are found in coastal drainages on Pacific Coast as far south as Rio Rosario, Baja California Norte, Mexico which is about 400 km (250 miles) south of the U. S. border, and in marine waters from Monterey Bay northward. One explanation for the presence of fossil stickleback in the Lake Cahuilla beds is that during glacial periods, cooler marine waters (the California current) extended south of El Rosario possibly down to the tip of Baja California, allowing sticklebacks to enter the Gulf of California and into the Salton Trough. Presently, there are at least 19 species of marine fish that have disjunction ranges with the main populations along southern California and Baja California, Mexico Pacific coasts and isolated populations in the northern Gulf of California (Buckhorn, 2012). These isolated fish species are absent in the southern region of the Gulf. The current thought is that these disjunct distributions were caused by the southward shift in marine temperature regimes during Pleistocene glacial episodes (Horn and Stephens, 2006).

There are three biogeographic marine provinces along the southern California and Baja California Pacific coasts. These provinces are primarily based on water temperature. The warm temperate province ranges from Point Conception, southern California to Punta Eugenia, Bahia Vizcaino, central Baja California, Mexico. The second province, subtropical, ranges from Punta Eugenia to the western tip of Baja California. The third province, tropical, is the entire Gulf of California and south. With colder oceanic temperatures during glacial cycles, the northeastern biogeographic marine provinces in the East Pacific Ocean shifted to the south allowing some fish species to disperse around the tip of Baja California into the Gulf of California. During the warmer interglacial periods, these provinces shifted north, and tropical waters moved north, isolating several fish species in the northern Gulf of California.

The presence of *Xyrauchen texanus* in the Lake Cahuilla beds is not surprising since remains of this species occur in the Plio-Pleistocene Palm Spring Group as exposed in Anza-Borrego Desert State Park (Stewart and Roeder, 1993; Hoetker and Gobalet, 1999; Gensler and others, 2006; Roeder 2006) and from Lake Cahuilla beds (Whistler and others, 1995).

As with *Xyrauchen*, isolated *Gila* teeth are known from sediments of the Plio-Pleistocene Palm Spring Group (Gensler and others, 2006; Roeder,2006). When compared with osteological material from the three known species of *Gila* (*elegans, cypha, robusta*) in the Colorado River drainage, these isolated pharyngeal teeth from the Lake Cahuilla beds maybe identified.

Acknowledgements

We would like to thank Tom Deméré, curator, and Kesler Randell, collections manager, of the Paleontology Department of the San Diego Natural History Museum for bringing to our attention the fossil bonyfish from the Lake Cahuilla beds from the San Diego Gas and Electric Company Sunrise Powerlink Project. Also, we would like to thank George T. Jefferson (Paleontologist Emeritus) and Lyn Murray (District Paleontologist) at the Stout Research Center, Anza-Borrego Desert State Park. San Diego Gas and Electric Company funded the paleontological monitoring and recovery of paleontological resources during construction of the Sunrise Powerlink Project by Paleontological Services, Inc. of the San Diego Natural History Museum.

References

Bell, M.A. and R.E. Reynolds, 2010. Miocene and Late Pleistocene stickleback spines from the Mojave Desert, California. In Overboard in the Mojave, 20 Million Years of Lakes and Wetlands, edited by R.E. Reynolds and D.M. Miller, Desert Studies Consortium, California State University, Fullerton, pp. 162-168.

Blake, W.P.,1907. Lake Cahuilla, the ancient lake of the Colorado Desert. National Geographic Magazine 18:830.

Buckhorn, M.L., 2012. Guide to the marine fishes of the Gulf of California. American Fisheries Society, Betheseda, Maryland, p. 5.

Coleman, G.A., 1929. A biological survey of Salton Sea. California Fish and Game, 15(3):218-227.

Crull, S., A.H. Hoover,, and H.M., 2008. An archaeological and paleontological mitigation monitoring report for Tract 31714, the Coachella 150 Project, City of Coachella, Riverside County, California prepared for Khovanian/Forecast Homes by L & L Environmental, Inc., Corona, 19 p.

Deméré T.A., and S.A. Siren, 2012. Paleontological monitoring report, Sunrise Powerlink Transmission Line, San Diego and Imperial Counties, California. Prepared for: Sunrise Powerlink, San Diego Gas and Electric Company, San Diego. Prepared by: Department of PaleoServices, San Diego Natural History Museum, San Diego, 71 p.

Dorsey, R.J., B.A. Housen, S.U. Janecke, C.M. Fanning, and A.L.F. Spears, 2011. Stratigraphic record of basin development within the San Andreas fault system: Late Cenozoic Fish Creek-Vallecito basin, southern California. Geological Society of America Bulletin 123(5,6):771-793.

Eschmeyer, W.N. and E.S. Herald, 1983, A field guide to Pacific Coast fishes of North America. The Peterson Field Guide Series Houghton Mifflin Company, Boston, 336 p.

Evermann, B.W., 1916. Fishes of the Salton Sea. Copeia 1916 (34):61-63.

Gensler, P., M.A. Roeder, and G.T. Jefferson, 2007. The fossil lower vertebrates: fish, amphibians, and reptiles. In Fossil Treasures of the Anza-Borrego Desert, edited by G.T. Jefferson, and L. Lindsay, Sunbelt Publications, San Diego, Chapter 8, pp. 139-149.

Gobalet, K.W., 1992. Colorado River fishes of Lake Cahuilla, Salton Basin, Southern California: A Cautionary Tale for Zooarchaeologists. Bulletin of the Southern California Academy of Sciences, 91(2), 1992, 70-83.

Hoetker, G.M. and K.W. Gobalet, 1999. Fossil razorback sucker (Pisces: Catostomidae, *Xyrauchen texanus*) from southeastern California. Copeia (3):755-759.

Horn, M.H. and J.S. Stephens, 2006. Climate change and overexploitation. In. The Ecology of Marine Fishes, California and adjacent waters, edited by L.G. Allen, D.J. Pondella, II and M.H. Horn, University of California Press, Berkeley, Chapter 25, p. 623.

Jefferson, G.T., 2014 (March 10). Sunrise Powerlink-Imperial Valley Substation. email from George T. Jefferson, Anza-Borrego Desert State Park to Mark A. Roeder, Paleo Environmental Associates.

Landers, E.B., 2009. Paleontologic resource impact mitigation program, final technical report of results and findings prepared in support of Miles Avenue Bridge Construction Project, Indio, Riverside County, California submitted to ASM Affliates, Inc., Carlsbad on behalf of County of Riverside Transportation and Land Management Agency, Transportation Department, Riverside, submitted by Paleo Environmental Associates, Inc., Altadena, 12 p.

La Rivers, I., 1962. Fishes and fisheries of Nevada. Nevada State Fish and Game Commission, 782 p.

Li, C.-L., C.F. You, , T.-L. Ku,, X.-M. Xu,, H.P. Buchheim,, N.-J. Wau, R.-W. Wang, and M.-L. Shen, 2007. Isotope and geochemical evidence of palaeoclimate changes in the Salton Basin, California during the past 20 yrk: 2 $^{87}SR/^{86}$ ratio in lake tufa as an indicator of connection between the Colorado River and Salton Basin. In Lake Systems, Sedimentary archives climate change and tectonics, EGU General Assembly. Palaeography, Palaeoclimatology, Palaeoecology, 259(2-3):198-212.

McGinnus, S.M., 2006. Field guide to freshwater fishes of California. California Natural History Guides. University of California Press, Berkeley 539 p.

Miller, D.J. and R.N. Lea, 1972. Guide to the coastal marine fishes of California. State of California, Fish Bulletin 157, Department of Fish and Game, Sacramento.

Moyle, P., 1976. Inland fishes of California. University of California Press, Berkeley, 405 p.

Reynolds, R.E., 1989. Paleontologic monitoring and salvage, Imperial Irrigation District Transmission Line, Riverside and Imperial Counties, California: Final Report. Prepared by the San Bernardino County Museum, Redlands for Mission Power Engineering Company, Irvine, California 258 p.

Roeder, M.A., 2006. Fossil fishes of the Anza-Borrego region. In Program and Abstracts for Fossil Treasures of the Anza-Borrego Desert. Anza-Borrego Institute, California State Parks, and Sunbelt Publications, San Diego, pp. 16-17.

Stewart, J.D, and Roeder, M.A., 1993. Razorback sucker (*Xyrauchen texanus*) from the Anza-Borrego Desert and the ancestral Colorado River. San Bernardino County Museum Association Special Publication, 93(1):94-96.

Swift, C.C., T.R. Haglund,, M. Ruiz, and R.N. Fisher, 1993. The status and distribution of the freshwater fishes of southern Californina. Bulletin of the Southern California Academy of Sciences, 92(3):101-167.

Uyeno, T. and R.R. Miller, 1965. Middle Pliocene cyprinid fishes from the Bidahochi Formation, Arizona. Copeia, 1965(1):28-41.

Van de Camp, P.C., 2006. Holocene Continental Sedimentation in the Salton Basin, California: A Reconnaisance. Bulletin of the Seismological Society of America. 96(6): 2304-2328.

Wagner, H.M., 2007. Final Report Coachella 150, prepared for KHovanian/Forecast Homes by L & L Environmental, Inc., Corona, 9 p.

Waters, M.R., 1980. Lake Cahuilla: late Quaternary lacustrine history of the Salton Trough, California. Master of Science Thesis, Department of Geosciences, University of Arizona, College of Earth Sciences, Department of Geosciences, Research Reports, 1979-1980.

Waters, M. R., 1983, Late Holocene lacustrine chronology and archaeology of ancient Lake Cahuilla, California. Quaternary Research, 19:373-387.

Whistler, D.P., E.B. Lander, and M.A. Roeder, 1995. Diverse record of microfossils and fossil plants, invertebrates, and small vertebrates from the Late Holocene Lake Cahuilla Beds, Riverside County, California. In Paleontology and Geology of the Western Salton Trough Detachment, Anza-Borrego Desert State Park, California. Field Trip Guidebook and Volume for the 1995 San Diego Association of Geologists Field Trip to Anza-Borrego Desert State Park, edited by P. Remeika and A. Sturz, 1:109-118.

A mineralogical inventory of geothermal features southeast of the Salton Sea, Imperial County, California

Paul M. Adams and David K. Lynch

The Aerospace Corporation, P. O. Box 92957, Los Angeles, CA 90009

Introduction

The Salton Trough is a topographic low in southern California and northern Baja and Sonora Mexico that represents the transition between the San Andreas Fault system and rifting centers in the Gulf of California. The area is seismically active and has a high geothermal gradient that supports a number of commercial geothermal electricity generating plants. The heat from the geothermal field is the result of a shallow magma body from one or more spreading centers. The Salton Sea occupies the lowest part of the Salton trough in Imperial County, CA.

The purpose of this paper is to document the surface mineralogy of the Salton Sea geothermal features, with particular attention to those minerals not included in Pembertons' Mineralogy of California (1983). The three areas to be described range from 1) a high temperature very active ammonia-emitting and sulfate-rich fumarole area which has an unusual assemblage of ammonium sulfate minerals, 2) a moderately active geothermal fumarole area with minor ammonia-free sulfate mineralization, and 3) a carbonate-rich sulfate-poor cold mound spring system.

The high temperature fumarole area has been studied by long wavelength infrared (LWIR) hyperspectral remote sensing using the SEBASS and Mako sensors (Hackwell, et al., 1996, Warren, et al., 2010) which have identified ammonia emissions (Tratt, et al., 2011). Mineral identifications reported in this paper will be used in ongoing remote sensing efforts to map mineral distributions associated with these geothermal features.

Mineral identifications were made using powder X-ray diffraction (XRD), coupled with energy dispersive X-ray spectroscopy in the scanning electron microscope (SEM). Fourier transform infrared (FTIR) spectroscopy was performed in the field with an Agilent/A2 Exoscan portable spectrometer for comparison with remote sensing measurements.

F1–F2 Fumarole Field mineralogy

The F1 and F2 fumarole fields are located on a sand spit east of what was Mullet Island (see this volume), 5 miles SW of Niland, and have been described in detail by Lynch, et al. (2013). During their initial survey several unusual ammonium sulfates were identified, including boussingaultite and lecontite. More detailed follow on field studies were conducted during October 2013–January 2014. F1, the westernmost fumarole field, is elliptical, about 25 m x 50 m, and has abundant small clear boiling pools, sulfur vents and associated sulfate crusts and accumulations (Figure 1). The subsurface generally consists of dark gray to black mud, sand and locally has hard deposits of cemented small pelecypod shells. Living plants are in close proximity to the fumaroles and dead plant material is common and often mixed in with the mud and ammonium salts. Water and mud temperatures range from ambient to boiling. The F2 field is roughly 120 m x 400 m and irregular in shape. It is subdivided into the F2 north complex (F2NC), a small outlier to the northwest and the F2 base complex (F2BC). The fluids at F2 are more viscous than at F1 which has allowed the development of mud pots and mud volcanoes/gryphons to 1–2 m high (Figure 2), though the height varies with time and seasonal ground water levels.

The mineralogies of F1 and F2 are similar and ammonium sulfates are present at both fields. Sulfur vents and living and dead vegetation are more common at F1, compared with F2. The fumaroles at F1 are less extensive and more approachable than F2. Plumes of ammonia gas have been observed emerging from the F1 and F2 fields (Tratt, et al. 2011) and are thought to produce the ammonium sulfates. The source of the ammonia has been assumed to be from thermal decomposition

of fertilizer residues from agricultural runoff or decomposing plant matter. However, it is noted that elevated levels of dissolved ammonia have been measured in the deep seated hypersaline brines beneath the region (McKibben, 2008). Ammonium sulfates have been found at other fumarole fields where irrigation and agricultural runoff are not a potential source of ammonia. This includes ammonioalunite, ammoniojarosite, boussingaultite, letovicite, mascagnite, and tschermigite from the Geysers in Sonoma County, CA (Dunning and Cooper, 1993; Koenig, 1969) and boussingaultite from Coso Hot Springs Inyo Countv CA (Anthony, et al., 2003; Ross and Yates, 1942).

The pH of the water in the bubbling and boiling pools (measured with colorpHast pH strips) is nominally neutral (6.5–7.5) and the total dissolved solids in 4 clear to milky pools range from 0.3 to 8.7 wt %. Residues remaining after evaporation consist primarily of halite though gypsum was the main constituent of two pools (Table 1). Minor to trace amounts of ammonium salts, such as sal ammoniac, lecontite and boussingaultite occur in some residues. As a result, it is clear that the extensive ammonium sulfate salts do not form from the simple evaporation of the water from the bubbling and boiling pools. Instead it is conjectured that ammonia and SO_2/H_2S percolating through the wet sand and mud near gas vents react to form ammonium sulfate solutions that are concentrated and then brought to the surface by capillary action to form the efflorescent growths (Figure 3).

As a result of this study four new minerals (lecontite, koktaite, tamarugite and konyaite) have been identified that previously had not been reported from California (Pemberton, 1983). Based on preliminary remote sensing

Figure 1. Clear boiling pool (20 cm) with mascagnite, gypsum, lecontite and boussingaultite salt crusts. F1 fumarole field.

Figure 2. Small gryphon (1 m) "Sulfur Hill" with nitratine, mascagnite, boussingaultite efflorescence. F2 fumarole field.

Figure 3. Ammonium sulfate mineralization (2 m x 3 m) around a small bubbling pool and vent. Southeast F2 fumarole field. White areas contain mascagnite, with thin (1 ft) outer rim of boussingaultite. Dark brown outer ring contains nitratine.

Table 1. Total dissolved solids (TDS, wt%) from water sources and mineralogy of solid residues after evaporation. XXXX = Major, Xxxx = Minor, xxxx = trace constituent.

Location	Sample	TDS (wt%)	Residue Determined by XRD
F1	A	0.3	GYPSUM, Halite, Sal ammoniac, lecontite, boussingaultite
F1	B	0.3	HALITE, Gypsum, lecontite, boussingaultite, sal ammoniac
F2	WP303	0.3	HALITE, Sal ammoniac, Gypsum, lecontite
F2	WP450	0.3	GYPSUM, Mascagnite, boussingaultite, lecontite
F2	WP451	3.4	HALITE, gypsum, sal ammoniac, sylvine, calcite?
F2	N Pool	8.7	HALITE, gypsum, unknown?
F2	SE Pool	0.3	HALITE, Gypsum, Sal ammoniac, boussingaultite
Rt 111	S1	2.0	HALITE, dolomite, magnesite
Rt 111	S2	1.9	HALITE, sylvine, dolomite, magnesite
Rt 111	S6	2.0	HALITE, dolomite, magnesite, sylvine
Salton Sea		4.8	HALITE, gypsum, bloedite, hexahydrite

studies the F1 fumarole field appears to have much more extensive nitratine deposits and less gypsum–bloedite–thenardite than F2, though locally the mineralogies are very similar.

Sulfur S

Dry hissing thermal vents up to 3 cm in diameter commonly have intergrowths of yellow bladed sulfur crystals associated with them (Figure 4). Dendritic growths of sulfur crystals have also been seen growing on dead vegetation. These vents are at ground level at F1 but at F2 they may also be near the summits, or on the flanks, of gryphons. The individual crystals range up to 3 mm in length and have a skeletal appearance (Figure 5). Beneath the surface, close to the vents, cavities (to 8 cm) in wet black mud often have a thin lining of sulfur. Crude bladed gypsum crystals (to 0.5 mm) are often associated with, or in close proximity, to the sulfur crystals. Sulfur crystals associated with these fumarole vents had been documented by Hanks (1882) as early as the late 1800's.

Gypsum $CaSO_4 \cdot 2H_2O$

Mats of white to cream-colored crude bladed gypsum crystals (to 1 mm) are often associated with sulfur vents and mascagnite (Figure 6). Gypsum may also occur as fibrous aggregates and clear thin fibers found underneath other sulfate crusts. Other associated species include boussingaulite, tschermigite and koktaite.

Mascagnite $(NH_4)_2SO_4$

White, cream or light gray botryoidal crusts of mascagnite (to 10 cm) are relatively common and are often found close to sulfur vents and boiling pools at both F1 and F2. The mascagnite is typically very

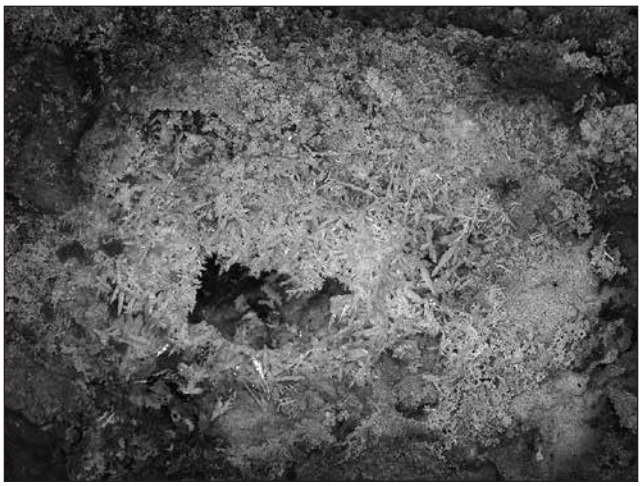

Figure 4. Dendritic sulfur crystals surrounding a gas vent (1 x 1.5 cm opening). F1 fumarole field.

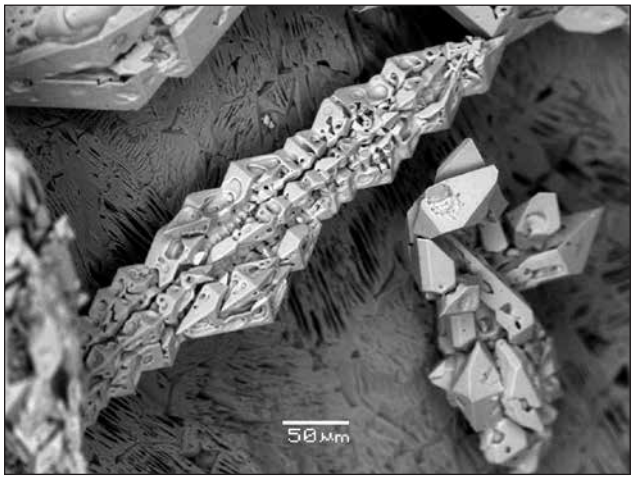

Figure 5. Cavernous sulfur crystals in parallel growth from F1 fumarole field. SEM image.

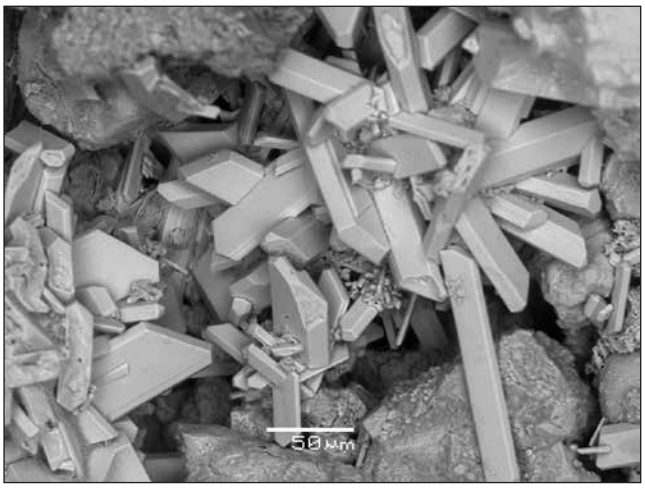

Figure 6. Gypsum crystals from F1 fumarole field. SEM image.

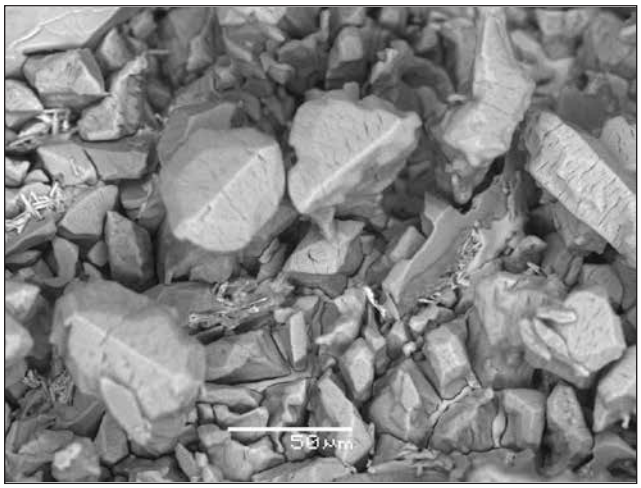

Figure 8. Lecontite crystals from F2 fumarole field. SEM image.

fine grained but bladed crystals to 0.2 mm have been observed. Mascagnite may also be associated with lecontite, boussingaultite, koktaite or sal ammoniac (Figure 7).

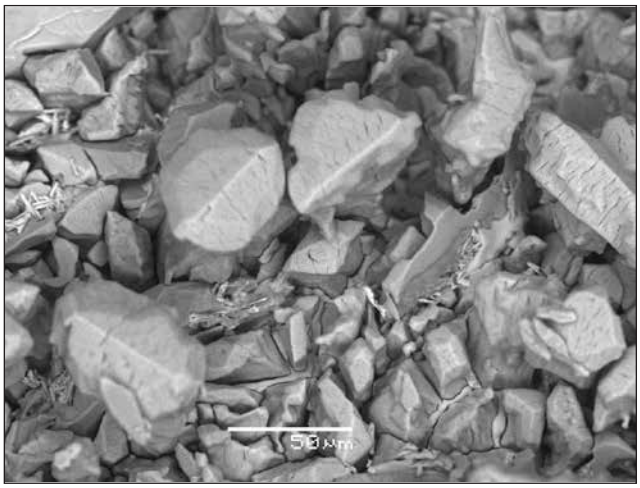

Figure 9. Equant boussingaultite crystals with tabular gypsum. SEM image.

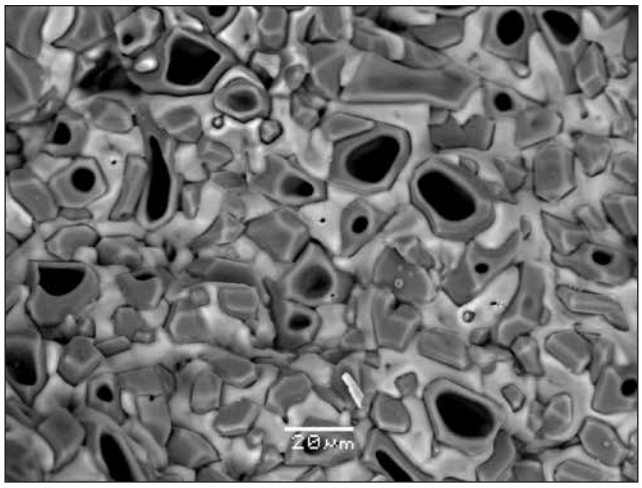

Figure 7. Sal ammoniac (light gray) between cavernous mascagnite crystals. SEM image.

Lecontite $(NH_4,K)Na(SO_4)\cdot 2H_2O$

Botryoidal mascagnite crusts from F1 and F2 occasionally contain minor amounts of lecontite. It also occurs with boussingaultite at F2. Euhedral lecontite crystals (to 0.1 mm) have only been recognized in a few specimens of more pure lecontite from F1 (Figure 8).

Koktaite $(NH_4)_2Ca(SO_4)\cdot 2H_2O$

Minor amounts of koktaite have been identified with boussingaultite and mascagnite by XRD in samples from F1 and F2. It has not been recognized in hand specimens.

Boussingaultite $(NH_4)_2Mg(SO_4)_2\cdot 6H_2O$

Boussingaultite is often a constituent of botryoidal crusts associated with vents. It commonly occurs with mascagnite, lecontite, tschermigite, koktaite and bloedite. Crystals are typically only a few tenths of a mm long but larger corroded bladed crystals (to

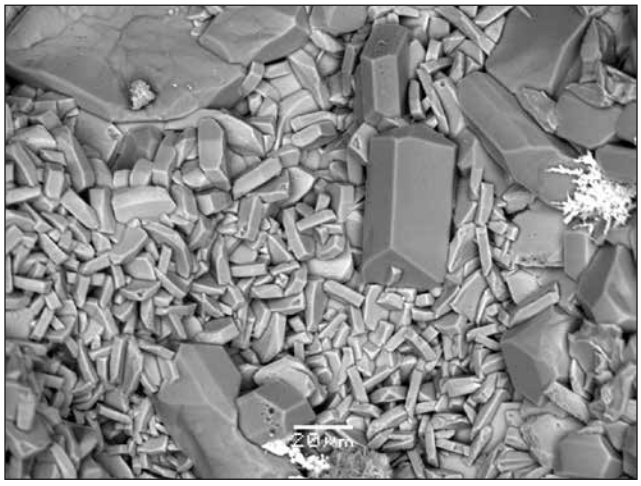

Figure 10. Boussingaultite (larger medium gray) with bloedite (small light gray) crystals. SEM image.

4 mm) have been found in unconsolidated material below other crusts at F1 (Figures 9, 10).

Tschermigite $(NH_4)Al(SO_4)_2 \cdot 12H_2O$

XRD analyses have indicated that minor amounts of tschermigite occur with boussingaultite and gypsum in samples from F1 and F2. It has not been recognized in hand specimens.

Sal ammoniac NH_4Cl

Minor amounts of sal ammoniac have been identified with mascagnite by EDS from F2 (Figure 7). It also occurs in evaporation residues of water collected from hot milky pools at F2. It has not been recognized in hand specimens. Sal ammoniac specimens from the fumaroles were identified as early as 1850, by the less than scientific method of "the sharpness of their taste" (Leconte, 1855).

Epsomite $MgSO_4 \cdot 7H_2O$

Epsomite was a major constituent of a small light gray ring around a 1 m orange patch of boussingaultite at F1.

Tamarugite $NaAl(SO_4)_2 \cdot 6H_2O$

Tamarugite was identified by XRD from one specimen with alum-(Na) in a sulfate patch at the SE end of F2 that also contained lecontite, mascagnite and boussingaultite. It has not been recognized in hand samples.

Bloedite $Na_2Mg(SO_4)_2.4H_2O$

An FTIR survey of a small gryphon dubbed "Sulfur Hill" on the southwest side of F2 indicated the presence of bloedite. It was found in localized areas of two roughly circular (2–3 m dia.) white sulfate deposits associated with small vents at ground level. It also has been identified by XRD from several areas at F2 where it is associated with boussingaultite (Figure 10). In January 2014 extensive regions of halite at the perimeter F1 were found to contain minor amounts of thenardite and bloedite.

Konyaite $Na_2Mg(SO_4)_2 \cdot 5H_20$

On November 28, 2013 botryoidal efflorescent konyaite occurred in growths collected from several inch-deep boot prints following a heavy rain that occurred 5 days earlier. On a later trip it formed more extensive deposits at the base of a small gryphon (Sulfur Hill at F2). Konyaite is relatively unstable and under low humidity conditions alters to bloedite (van Doesburg, et al., 1982).

Thenardite $NaSO_4$

The presence of thenardite appears to be ephemeral. Crystalline growths of thenardite up 1.5 cm have been observed with mirabilite scattered on mud flats near the brush line southeast of the F2 fumarole field. Isolated patches of thenardite have also been identified from the outer portions of the F2 north complex. About a month after a heavy rain (0.94") on November 23, 2013 extensive crusts of thenardite, often with or after mirabilite (Figure 11) were observed on the west side of F2 complex and the F2 SE brush line mud flats. These crusts were not present on previous visits. In January 2014 extensive regions of halite around F1 were identified as containing minor amounts of thenardite and bloedite.

Mirabilite $NaSO_4 \cdot 10H_2O$

The existence of mirabilite is also ephemeral and extensive crusts altering to thenardite were observed in late December 2013 on the west side of the F2 field and along the brush line SE of F2. Bladed crystals of mirabilite, to 4 mm x 20 mm, altering to thenardite were found in deep boot prints and tire tracks at F2. At some point after the visit on November 29, 2013 these depressions evidently partially filled with saturated fluids from which the mirabilite crystallized. The thenardite forms pseudomorphic hollow casts after the mirabilite crystals.

Figure 11. Thenardite casts after mirabilite crystals. F2 fumarole field.

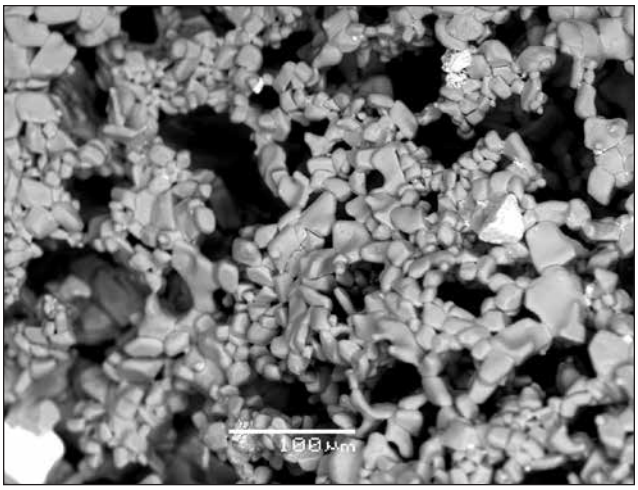

Figure 12. Lattice work of minute nitratine crystals. Sulfur Hill gryphon – F2 fumarole field. SEM image.

Nitratine $NaNO_3$

Nitratine was originally identified during an FTIR field survey of a small gryphon dubbed "Sulfur Hill" on the southwest side of F2. It occurs as delicate branching intergrowths of white to clear 0.05 mm crystals (Figure 12). In January 2014 an FTIR survey of sulfate patches in the SE corner of F2 revealed the presence of nitratine. It was inconspicuous and found in black and brown areas just outside of the ammonium sulfate growths around small bubbling pools and vents. On the same trip areas several meters across at F1 were found by FTIR to contain nitratine. Many of these areas were also black to brown in color like at F2, however, thin white crystalline crusts of nitratine were also common. Nitratine had been identified as early as 1902 from along the old beach lines of the Salton Sea east of the "Mud Volcanoes" in T.10S., R.14E. (Bailey, 1902).

Halite NaCl

Halite is ubiquitous as thin white surface films and crystalline crusts away from the gryphons and fumaroles. The extent of the halite efflorescence varies depending how recently it rained and the amount of time to draw saline solutions to the surface from capillary action. Cubic crystals of halite to 3 mm have been observed in boot prints and tire tracks after heavy rains.

Lynch, et al (2013) identified 9 sulfate minerals occurring at the fumarole fields, which have continued to change with time since they emerged from the Salton Sea in about 2007 as a result of falling sea/lake levels. This study has increased the number of identified sulfate and evaporite minerals to 15 which should greatly aid in making more accurate remote sensing mineral distribution maps. A number of LWIR remote sensing data collects have been made since 2009, in addition to those reported by Tratt, et al. (2011). This affords the possibility of plotting the development and evolution of the sulfate deposits as a function of time since emergence of the fumaroles and various rainfall conditions.

Davis–Schrimpf Fumarole Field mineralogy

The Davis–Schrimpf (D–S) fumarole field is located at the northeast corner of Davis (now Wister) and Schrimpf roads 4 miles SW of Niland. It is on property leased to Energy Source from whom permission to enter must be obtained. It has been studied in detail by Onderdonk et al., (2011). It differs from the F1–F2 fields in that the temperatures are lower (to 69C) and the mud somewhat cooler and thicker. Many mud pots are present and the gryphons are typically taller (to 2 m) than at F2 and are often hollow. Bursting mud bubbles can be heard reverberating in the gryphons even though no activity is visible on the outside. Other than thin halite crusts at ground level, "salt" accumulations are uncommon at D–S. The only interesting sulfate occurrences

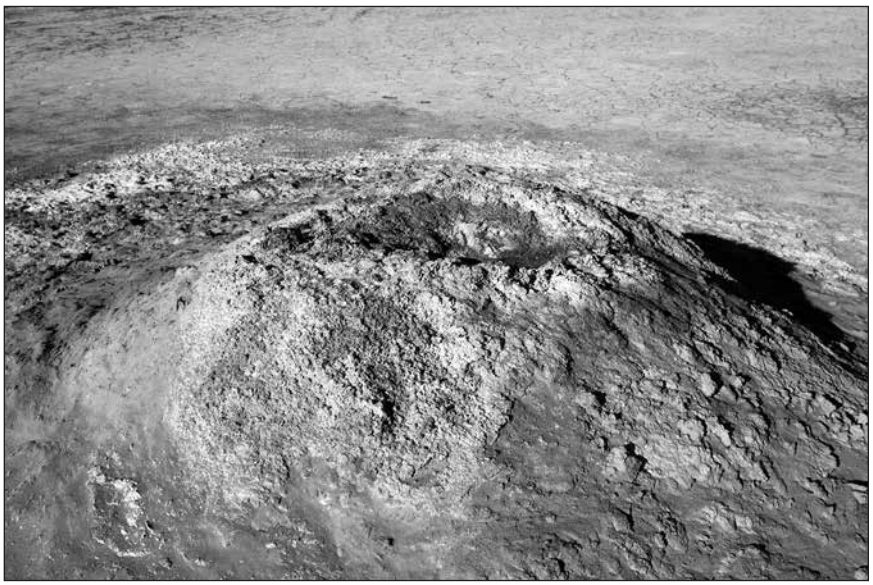

Figure 13 . Sulfate mineralization is concentrated at the summit of gryphon S3 (FOV ~ 2 m). Davis-Schrimpf fumarole field.

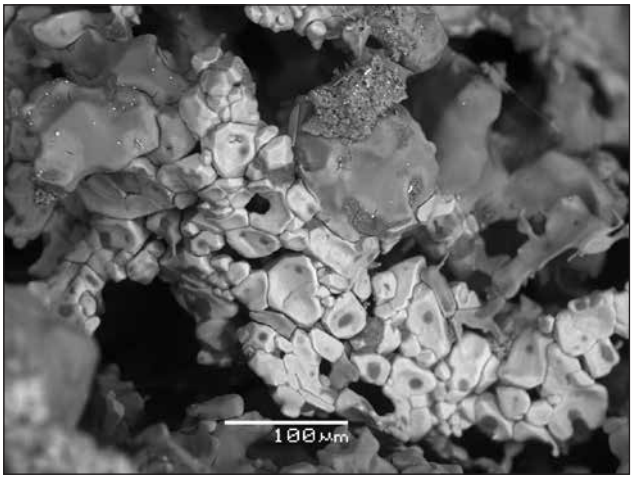

Figure 14. Alum-(K) (medium gray) and Fe sulfate (light gray) from Davis-Schrimpf S3 gryphon. SEM image.

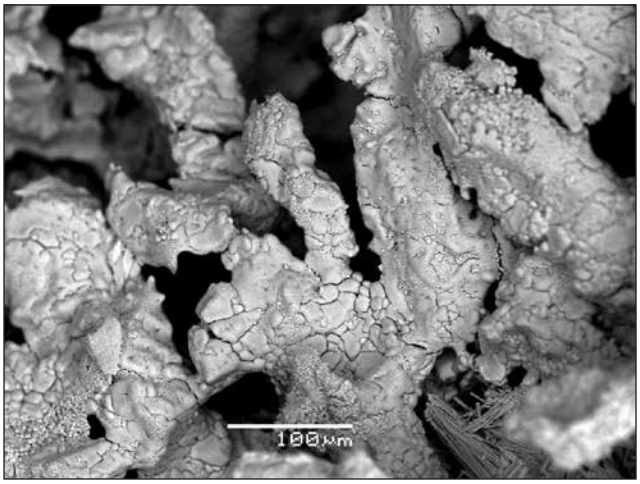

Figure 15. Hexahydrite from Davis-Schrimpf S3 gryphon. SEM image.

are located at the south end of the field (Mazzini, et al., 2011). They consist of two white to light yellow patches (S1: 1 x 1.5 m and S2: 3 x 3 m) at ground level and two small episodic gryphons (S3, S4) approximately 1 m high. S2 and S4 are the eastern most features. The S1 and S2 sulfate patches are nominally at ambient temperature while the gryphons S3 and S4 have elevated temperatures (to 37C) at their summit vents. During visits in November and December 2013 the vent on S4 was dry and could be heard hissing. Subsequent to December 21, 2013 and before January 17, 2014 a mud eruption(s?) occurred producing several flows to 2 meters in length. During the January 2014 visit S4 could be heard loudly gurgling. The majority of the sulfates are concentrated at S2 and S3. Only S3 was sampled during our first two visits. At those times the sulfates at S3 were located at the top of the gryphon, in an area approximately 35 cm in diameter that surrounded the central vent (Figure 13). They consisted of delicate white to yellow lattice works consisting of hexahydrite and tamarugite. Following a heavy rain on November 23, 2013 the sulfates had been dispersed down the sides of the gryphon. By January 2014 the delicate sulfate crusts at the top of S3 had regrown. Tamarugite, bloedite, gypsum and K-ferrite had been reported previously from D–S (Mazzini, et al, 2011).

Alum-(K) $KAI(SO_4)_2{\cdot}12H_2O$

Alum-(K) is a relatively common constituent with bloedite and gypsum at S2 and gypsum at S3. It occurs as crude minute (0.1 mm) octahedral crystals with Fe-sulfates (Figure 14).

Bloedite $Na_2Mg(SO_4)_2{\cdot}4H_2O$

Bloedite was identified by XRD and EDS with thenardite and gypsum in chalky white patches from S1 and S2 and in minor amounts near the vent on S4.

Epsomite $MgSO_4{\cdot}7H_2O$
Hexahydrite $MgSO_4{\cdot}6H_2O$
Starkeyite $MgSO_4{\cdot}4H_2O$

Very fine grained (<0.03 mm) hexahydrite is relatively common at S3 and S2 where it occurs with tamarugite and gypsum (Figure 15). Epsomite and starkeyite have been identified by XRD from isolated samples from S3. It would not be surprising to also find pentahydrite ($MgSO_4{\cdot}5H_2O$) present at some point in time.

Gypsum $CaSO_4{\cdot}2H_2O$
Anhydrite $CaSO_4$

Gypsum has been identified in material beneath many of the delicate sulfate growths at the top of S3 and at S1, S2 and S4. It was also identified in the subsurface soil at S1–S2 (Mazzini,et al., 2011).

Halotrichite $Fe^{2+}Al_2(SO_4)_4{\cdot}22H_2O$
Pickeringite $MgAl_2(SO_4)_4{\cdot}22H_2O$

Silky white fibrous pickeringite-halotrichite has been found at S3 associated with tamarugite, voltaite, hexahydrite, starkeyite and gypsum (Figure 16). Visually it is indistinguishable from tamarugite.

Natrojarosite $NaFe_3(SO_4)_2(OH)_6$

Thin yellow crusts of minute (0.010 mm) pseudo-hexagonal crystals on S3 have a composition, determined by semiquantitative EDS, to be similar to natrojarosite. It is associated with hexahydrite and Fe-pickeringite

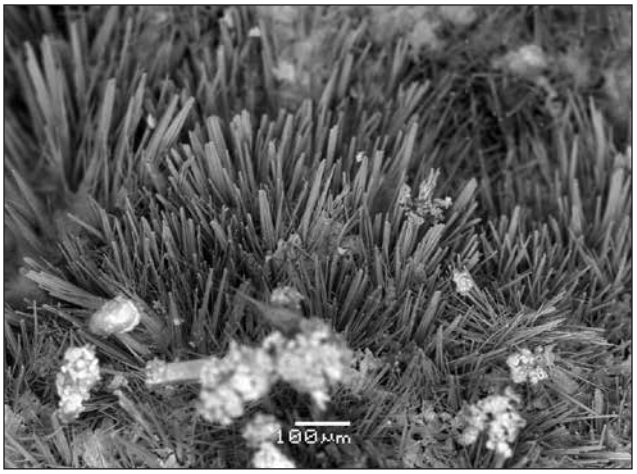

Figure 16. Acicular Fe-pickeringite from Davis-Schrimpf S3 gryphon. SEM image.

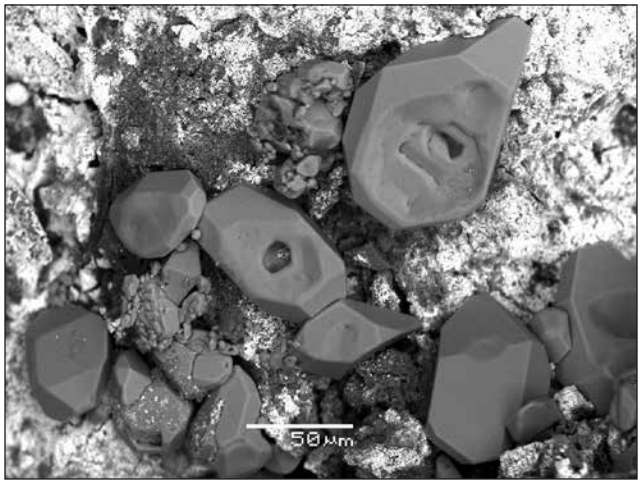

Figure 17 . Cavernous sulfur crystals and cinnabar (white) from Davis-Schrimpf gryphon S3. SEM image.

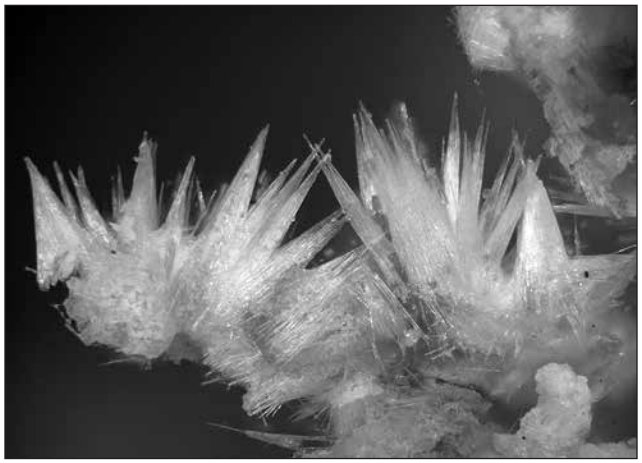

Figure 18. Fibrous tamarugite crystals (FOV = 3 mm). Davis-Schrimpf gryphon S3.

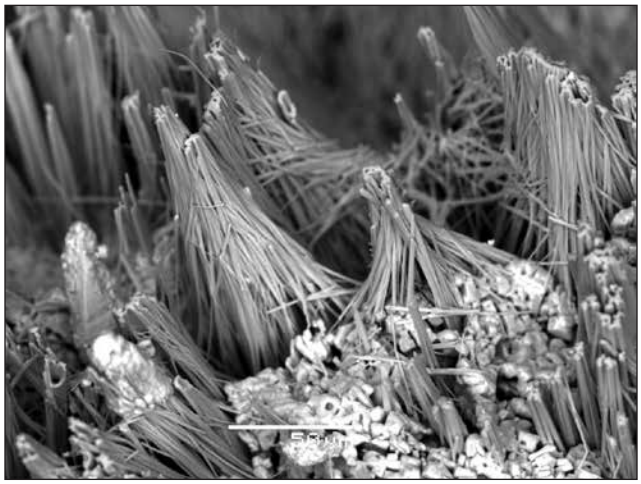

Figure 19. Fibrous tamarugite crystals – SEM image. Davis-Schrimpf gryphon S3.

Sulfur S

Sparse minute (0.05 mm) light yellow equant sulfur crystals were observed near the vent of S4 prior to the mud eruption. Similar sulfur crystals have been found at S3 associated with submicron cinnabar crystals (Figure 17).

Tamarugite $NaAl(SO_4)_2 \cdot 6H_2O$

Tamarugite was found as white to cream-colored, often twisted and tapered, silky fibrous growths to 2 mm in length associated with hexahydrite on S3 (Figures 18, 19).

Thenardite $NaSO_4$

Thenardite was identified by XRD and EDS with bloedite in chalky white patches from S1 and S2. It has also been found in minor amounts of the flank and base of S3 after a heavy rain.

Voltaite $K_2Fe_5^{2+}Fe_3^{3+}Al(SO_4)_{12} \cdot 18H_2O$

Microcrystalline crusts of voltaite have been found on S3 associated with Fe-pickeringite and tamarugite (Figure 20).

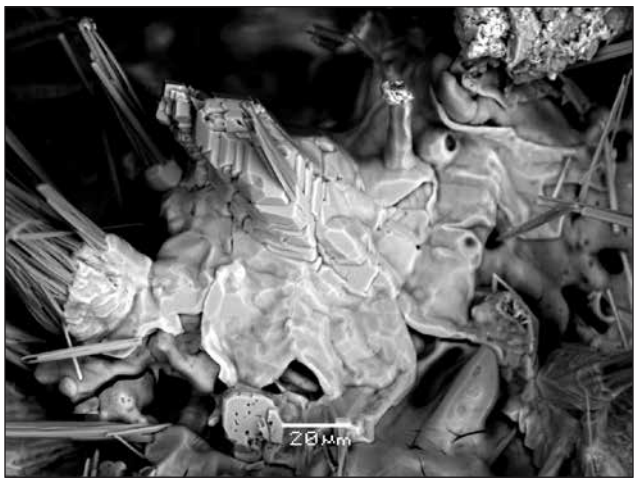

Figure 20. Voltaite on acicular Fe-pickeringite from Davis-Schrimpf S3 gryphon. SEM image.

Figure 21. Magnesium carbonate mineralization around a salse. Large salse is ~3 m wide. Rt 111 cold mound springs. Note smaller salses and cracked pressure ridges.

From a remote sensing standpoint, the sulfate deposits at the Davis–Schrimpf fumarole field are near, or below, the spatial resolution (1m x 1 m) of the SEBASS/Mako sensor. This combined with the fact that they are mixtures implies that individual mineral identifications may not be possible. A LWIR remote sensing study of the D–S field has been published (Reath and Ramsey, 2013). They mapped the small sulfate bodies described above as containing quartz with minor amounts of anhydrite but did map extensive areas of a tentative unidentified Mg-sulfate mineral and anhydrite around the fumarole area. Reath and Ramsey performed very limited and inconclusive ground truth sampling and analyses to support their conclusions and their maps have gross georeferencing errors (N arrow is actually W and figures are mirror images). The work of Mazzini et al.(2011) and this work failed to identify any significant anhydrite or Mg-sulfate minerals away from the very localized areas described above.

CA Route 111 Mound Springs Mineralogy

A field of low mound springs is located on private property just east of California Route 111 at Wister Road, 5 miles NW of Niland. These springs were noted (W9 and W10) by Lynch and Hudnut (2008) in their study of the nearby Wister mud pot lineaments, but they are outliers and have a significantly different structure. Mound springs are cold gryphons with central pools (salses). At these mound springs the fluid is very watery with only minor carbon dioxide bubbling and turbulence. As a result, the springs form volcanoes that are of "shield" type, up to 25 m in diameter, with very low relief. Central pools range from 15 cm to 4 m and the pH is nominally neutral

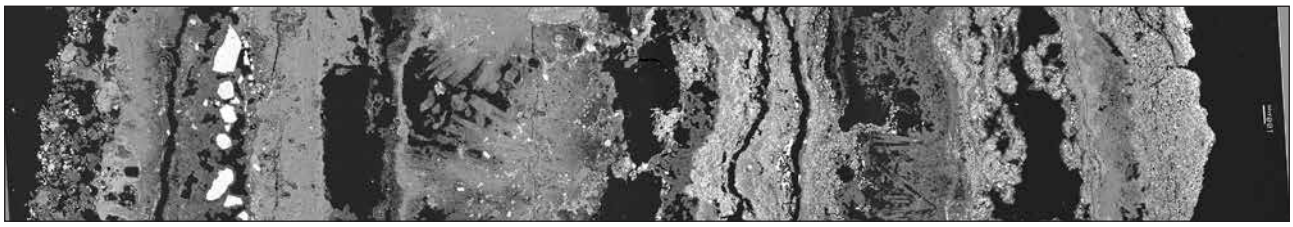

Figure 22 (above). SEM image of polished cross section through a magnesium carbonate deposit from Rt 111 cold mound spring. Scale bar at right is 100 µm; total FOV = 6.2 mm. Outside surface is at left. Black areas are voids and bright white spots are clastic quartz and feldspar grains. Medium gray bands are predominantly magnesium carbonates, while light gray bands contain some fine grained aragonite. At left of center and middle right are voids with fine grained magnesium carbonates replacing bladed crystals of an unknown mineral.

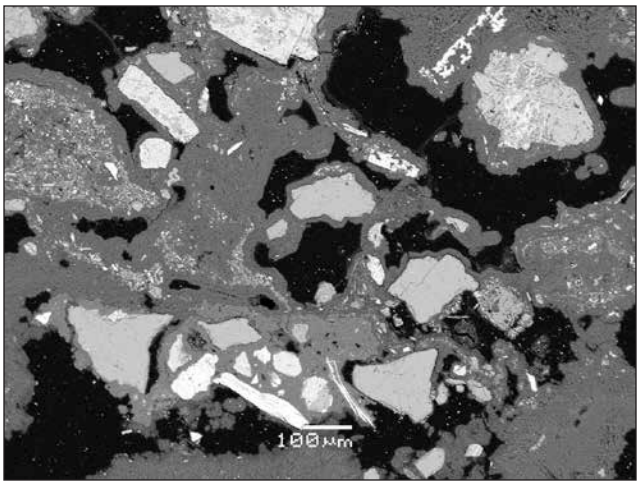

Figure 23 (right). SEM image of polished cross section through a magnesium carbonate deposit from Rt 111 cold mound spring. Large angular grains are clastic quartz and feldspar (white elongate grains near scale bar are mica). Areas with minute light grains (top left) contain aragonite.

(6.5–7.5). The total dissolved solids content of three pools is 2.0 % with the dominant residue after evaporation being halite with trace amounts of carbonates such as dolomite and magnesite also being present. White crusts of magnesium carbonates (magnesite, hyromagnesite and nesquehonite), in addition to aragonite, dolomite and northupite, are associated with some of the salses in the northeast corner of the field (Figure 21). The carbonate deposits are bedded with significant porosity or gaps between relatively solid layers (Figures 22, 23). Individual layers may be 1) relatively pure fine grained magnesium carbonates, 2) magnesium carbonates mixed with fine grained (< 10 μm) acicular aragonite, or 3) contain significant amounts of clastic grains (quartz, plagioclase, potassium feldspar, mica (to 150 μm) in a matrix of magnesium carbonates (Figure 23). The clastic grains may represent windblown sand that was subsequently cemented by carbonates. The presence of halite with the magnesium carbonate deposits is ephemeral. At some times it is nearly absent, while at others it may form a near continuous layer to about 2–3 mm thick. This ephemeral halite may be responsible for the large gaps between the carbonate layers. Conceivably a layer of the carbonate may form on halite, which subsequently dissolves to form the large gaps.

Aragonite $CaCO_3$
Strontianite $SrCO_3$

Aragonite occurs as minute acicular crystals (to 0.01 mm) that tend to be concentrated in specific layers in the magnesium carbonate deposits (Figure 24). Calcium-rich strontianite is uncommon and has been found with strontian-barite in coarse grained (to 0.07 mm) aragonite, dolomite and magnesite veins in fine grained banded dolomite–aragonite nodules.

Dolomite $CaMg(CO_3)_2$

Dolomite is a major constituent of some surface crusts near a salse in the NE corner of the field and in some layered nodular growths.

Halite NaCl

Extensive halite efflorescence is common in the southwest corner of the field and in other areas is ephemeral. In some areas along the northern margin of the field twisted filiform growths consisting of stacked halite crystals were observed (Figures 25, 26). This type of halite growth is uncommon but has been observed in some caves where air flow has been considered critical to their formation (Filippi, et al., 2011).

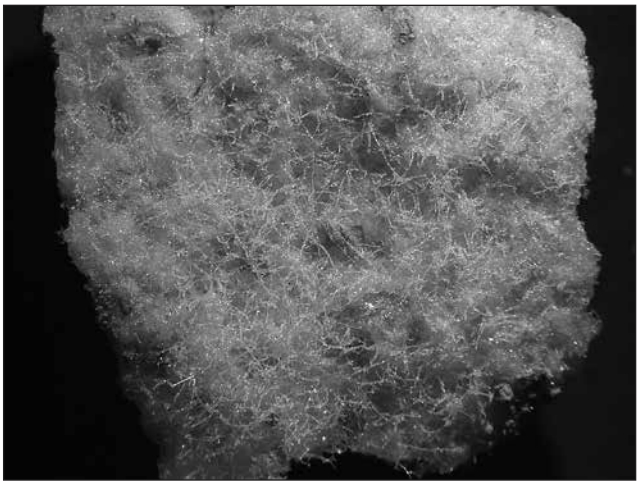

Figure 25. Filiform halite crystal growth (3 cm x 3 cm). Rt 111 mound springs.

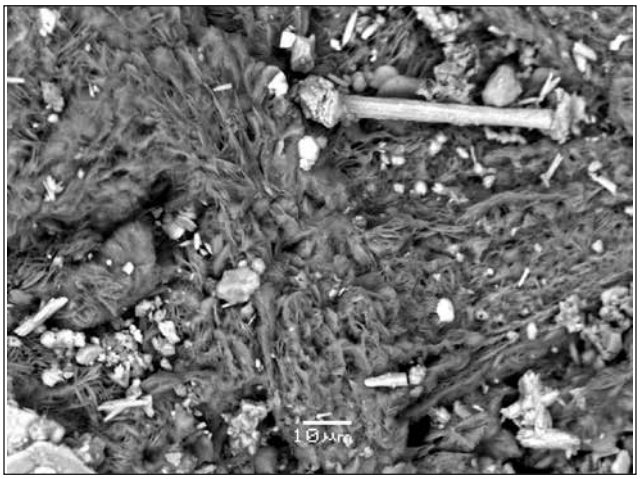

Figure 24. Platy hydromagnesite crystals (gray) with acicular aragonite (white). Rt 111 mound springs. SEM image.

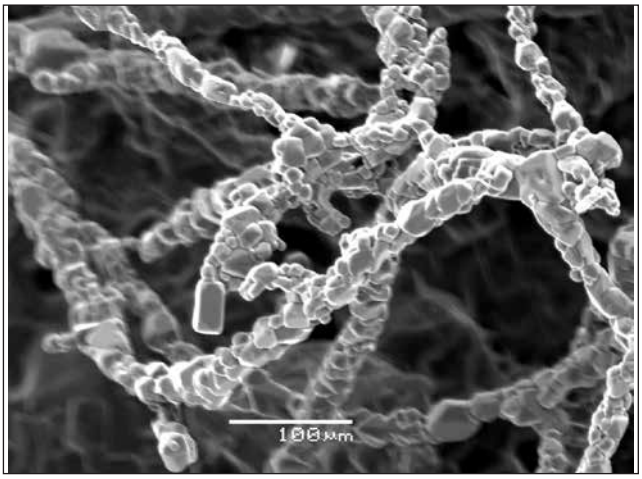

Figure 26. Filiform halite crystal growth. Rt 111 mound springs. SEM image.

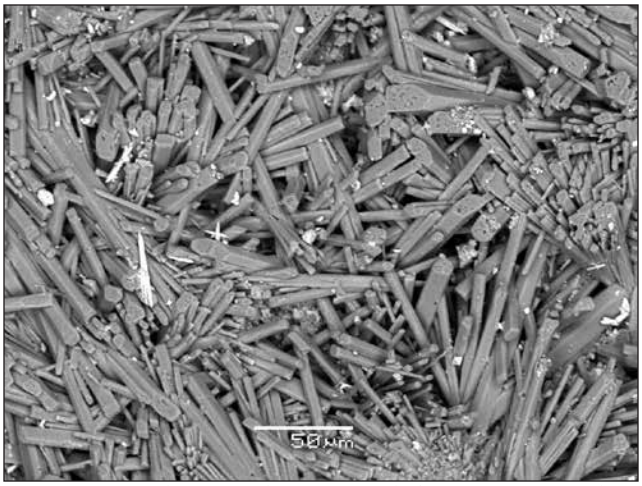

Figure 27. Acicular nesquehonite crystals from Rt 111 mound springs. SEM image.

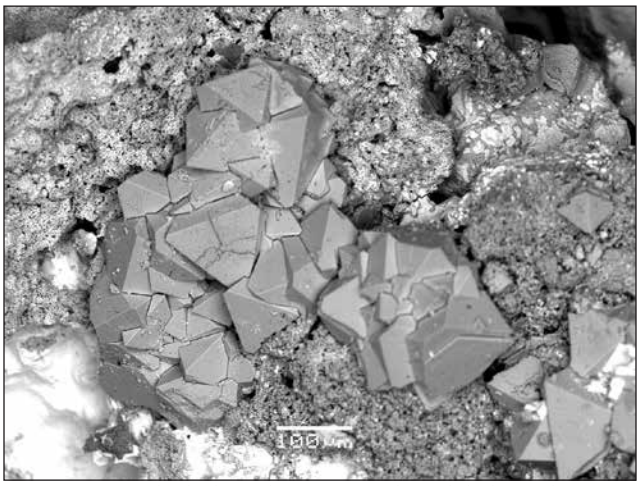

Figure 28. Octahedral northupite crystals with halite (white). Rt 111 mound springs. SEM image.

Hydromagnesite $Mg_5(CO_3)_4(OH)_2 . 4H_2O$
Hydromagnesite forms dense aggregates of tiny (0.01 x 0.001 mm) platelets, often associated with aragonite (Figure 24) in crusts with other magnesium carbonates.

Magnesite $MgCO_3$
Fine grained white to light gray magnesite is common as surface crusts and bulk deposits in the northeast corner of the field.

Nesquehonite $Mg(HCO_3)(OH)\cdot 2H_2O$
Nesquehonite is found as small (0.1 x 0.01 mm) acicular crystals forming white mats on the surface surrounding some salses (Figure 27).

Northupite $Na_3Mg(CO_3)_2Cl$
Minute (0.10 mm) octrahedra of northupite form white crusts with other magnesium carbonates around some salses in the northeast corner of the field (Figure 28).

Polyhalite $K_2Ca_2Mg(SO_4)_4\cdot 2H_2O$
Polyhalite and another potassium sulfate were identified by XRD and EDS as occurring with hydromagnesite, halite and aragonite near some small active gryphons.

Thenardite $NaSO_4$
Thenardite is uncommon and with the exception of rare barite the only sulfate found at the RT 111 deposit. It was found as clusters of minute (0.01 mm) tabular crystals associated with halite, aragonite and hydromagnesite near a small active gryphon.

The Rt 111 mound spring deposits are unusual in that many magnesium carbonate deposits are associated with the weathering of ultramafic rocks (Braithwaite and Zedef, 1996; Renaut and Stead, 1991). The source of the magnesium in the Rt 111 deposits is uncertain. From our SEM studies of the RT 111 magnesium carbonate deposits we have shown that some minerals (northupite, nesquehonite) occur as crystals in excess of 10s of microns which should produce strong LWIR reflectance spectra, which has been confirmed with our field FTIR (Exoscan) measurements. Hydromagnesite and to a lesser extent aragonite are found as crystals < 10 microns which produce very weak and low contrast LWIR reflectance signatures. In fact, in the field, the Exoscan did not have sufficient signal from hydromagnesite samples to acquire spectra. This could only be accomplished in the laboratory with a high sensitivity mercury cadmium telluride detector.

White Rock is a feature on Mars that gathered a significant amount of attention during the 1990s (Russell et al., 1999) and was suspected of containing magnesium carbonates, which would have confirmed the presence of water, making White Rock a possible target for the search of past life on Mars. On earth some magnesium carbonate spring and lake deposits have been linked to biologic activity (Braithwaite, et al., 1996; Russell et al., 1999; Power, et al., 2007). LWIR remote sensing using TES on the Mars Global Surveyor spacecraft failed to confirm the presence of carbonates and albedo measurements argued against their existence (Ruff, et al., 2001). In fact, TES failed to produce any LWIR spectra signature from White Rock so the presence of carbonates cannot be completely ruled out. Our studies have shown that

very fine grained hydromagnesite can produce very weak, near featureless LWIR reflectance spectra, potentially analogous to what has been seen on Mars for White Rock. This situation is similar to what we have observed for calcium carbonate rocks with very fine scale weathering surfaces (Kirkland, et al., 2002 and 2003). The RT 111 magnesium carbonate deposit is an easily accessible site that could be used to study the role of carbonate mineral particle size on detectability by various remote sensing platforms, which might be used to better understand the limitations of LWIR studies on Mars and on earth.

Acknowledgements

This research was supported in part by The Aerospace Corporation's Independent Research and Development program. The authors would like to thank Dr. R. Housley for reviewing the manuscript.

References

Anthony, J. W., Bideaux, R. A., Bladh, K. W. and Nichols, M. C. (2003) Handbook of Mineralogy, Volume V, Borates, Carbonates, Sulfates, p82.

Bailey. G. E. (1902) The saline deposits of California, Calif. State Min. Bur. Rpt. 24, pp. 178, 180.

Braithwaite C. J. R. and Zedef, V. (1996) Hydromagnesite stromatolites in an alkaline lake, Salda Golu, Turkey, J. Sediment. Res., 66, 991-1002.

Dunning, G. E. and Cooper, J. F., Jr. (1993) History and minerals of the Geysers, Sonoma County, California, Mineralogical Record, 24, 339-354.

Filippi, M., Bruthans, J., Palatinus, L., Zare, M. and Asadi, N. (2011) Secondary halite deposits in the Iranian salt karst: general description and origin, Int. J. Speleology, 40, 141-162.

Hackwell, J. A., D. W. Warren, R.P. Bongiovi, S. J. Hansel, T. L. Hayhurst, D. J. Mabry, M. G. Sivjee, and J. W. Skinner (1996), "LWIR/MWIR imaging hyperspectral sensor for airborne and ground-based remote sensing," Proceedings of SPIE, 2819, 102-107, doi:10.1117/12.258057.

Hanks, H.G., (1882). Mud volcanoes and the Colorado Desert. Second Report of the State Mineralogist of California; From December 1, 1880 to October 1, 1882, Calif. Min. Bur. Rept., 2, 227-240.

Kirkland, L., Herr, K., Keim, E., Adams, P., Salisbury, J., Hackwell, J. and Treiman, A. (2002), First use of an airborne thermal infrared hyperspectral scanner for compositional mapping, Remote Sens. Environ., 80, 447-459.

Koenig, J. B., (1969) The Geysers geothermal field, Mineral Information Service, 22, 123-128.

Leconte, (1855) Account of some volcanic springs in the desert of the Colorado, Southern California, Am. J. Sci. 2nd ed., 19, 1-6.

Lynch, D. K and Hudnut, K. W. (2008) The Wister mud pot lineament: Southeastward extension or abandoned strand of the San Andreas fault, Bull. Seismol. Soc. Amer., 98, 1720-1729.

Lynch, D. K., Hudnut, K. W. and Adams, P. M. (2013) Development and growth of recently-exposed fumarole fields near Mullet Island, Imperial County, California, Geomorphology, 195, 27-44.

Mazzini, A., Svenson, H., Etiope, G., Onderdonk, N. and Banks, D. (2011) Fluid origin, gas fluxes and plumbing system in the sediment-hosted Salton Sea geothermal system (California, USA), J. Volcano. Geotherm. Res., 205, 67-83.

McKibben, M. A. (2008) The Salton Sea geothermal brines, 2008 Desert Symposium Field Guide and Proceedings, Cal. State Univ., Fullerton Desert Studies Consortium, 102-106.

Onderdonk, N., Shafer, L, Mazzini, A. and Svenson, H. (2011) Controls on the expression and evolution of gryphons, mud pots, and caldera features at hydrothermal seeps in the Salton Sea Geothermal Field, Southern California, Geomorphology, 130, 327-342.

Pemberton, H. E (1983) Minerals of California, Van Nostrand Reinhold, New York, 591pp.

Ross, C. P. and Yates, R. G. (1942) The Coso quicksilver district Inyo County, California, U.S.G.S. Bull. 936-Q, 394-415.

Power, I. M., Wilson, S. A., Thom, J. M., Dipple, G. M. and Southam, G. (2007) Biologically induced mineralization of dypingite by cyanobacteria from an alkaline wetland near Atlin, British Columbia, Canada, Geochemical Transactions, 8:13, doi:10.1186/1467-4866-8-13.

Reath, K. A. and Ramsey, M. S. (2013) Exploration of geothermal systems using hyperspectral thermal infrared remote sensing, J. Volcan. Geotherm. Res., 265, 27-38.

Renaut, R. W. and Stead, D. (1991) Recent magnesite-hydromagnesite sedimentation in playa basins of the Cariboo plateau, British Columbia, British Columbia Geol. Soc. Geol. Fieldwork 1990, Paper 1991-1.

Ruff, S. W., Christensen, P. R., Clark, R. H., Kieffer, H. H., Malin, M. C., Bandfield, J. C., Jackosky, B. M., Lane, M. D., Mellon, M. T. and Presley, M. M. (2001) Mars' "White Rock" feature lacks evidence of an aqueous origin: Results from Mars Global Surveyor, J. Geophys. Res., 106, 23921-23927.

Russell, M. J., Ingham, K., Zedef, V., Maktav, D., Sunar, F., Hall, A. J. and Fallick (1999) Search for signs of ancient life on Mars: expectations from hydromagnesite microbalites, Salda Lake, Turkey, J. Geol. Soc., London, 156, 869-888.

Tratt, D. M., Young, S. J., Lynch, D. K., Buckland, K. N., Johnson, P. D., Hall, J. L., Westberg, K. R., Polak, M. L., Kasper, B. P. and J. Qian (2011), "Remotely-sensed ammonia emission from fumarolic vents associated with a hydrothermally active fault in the Salton Sea Geothermal Field, California," J. Geophys. Res., 116(D21), D21308, doi:10.1029/2011JD016282.

Warren, D. W., Boucher, R. H., Gutierrez, D. J., Keim, E. R. and M. G. Sivjee (2010), "MAKO: A high-performance, airborne imaging spectrometer for the long-wave infrared," Proceedings of SPIE, 7812, 78120N, doi:10.1117/12.861374.

Van Doesburg, J. D. J., Vergouen, L. and van der Plas, L. (1982) Konyaite $Na_2Mg(SO_4)_2{\cdot}5H_2O$, a new mineral from the Great Konya Basin, Turkey, Am. Mineral., 67, 1035-1038.

Salton Sea carbon dioxide field

Larry M. Vredenburgh

Bureau of Land Management, 3801 Pegasus Dr., Bakersfield, CA 93308

Naturally occurring carbon dioxide is trapped in Quaternary sedimentary rocks that underlie the southeast end of the Salton Sea. Thermal springs emit brine, steam, and carbon dioxide into clay-rich soil forming ponds of mud from which large bubbles of carbon dioxide and steam evolve. Around the most active springs, accumulations of mud form small cones which resemble small volcanos.

Carbon dioxide plant near Wister (above) and bubbling carbon dioxide well. Both photos by Jennifer Reynolds, December 2006.

In 1927, the Pioneer Development Company drilled the first three exploratory holes in the area to test potential for geothermal steam. Steam was encountered in a hole on Mullet Island, but the low pressures and flow volume discouraged further attempts. However, the presence of large volumes of carbon dioxide with the steam drew commercial interest. In September 1932, a hole was drilled for carbon dioxide by the Salton Sea Chemical Products Corporation. It was the first such well drilled in California. Carbon dioxide was encountered at 310 feet, but the hole was abandoned at 1,054 feet due to drilling difficulties.

A second well was drilled in October 1932 to a depth of 750 feet. It yielded a large volume of carbon dioxide, but there was no commercial production. A third nearby hole produced enough carbon dioxide to operate a small dry ice plant, which was completed in August 1934.

Gas was produced from a northeast-trending area 3 miles long and 1 mile wide. More than 160 wells were drilled. However, the life of a well was only about 2 years, and fewer than 20 wells were producing at any one time. Total production has been estimated to be more than 3.5 billion cubic feet.

Carbon dioxide for use as dry ice was produced from the field until 1954 when production was discontinued. Factors contributing to the shut-down were the rise of the level of the Salton Sea, widespread use of modern refrigeration systems, distance to marketing centers, short well life, and competition from artificially produced gases.

References

Morton, Paul K ,1977, Geology and Mineral Resources of Imperial County, California, California Division of Mines and Geology, County Report 7, p. 33.

Laflin, P., 1995. The Salton Sea: California's overlooked treasure. The Periscope, Coachella Valley Historical Society, Indio, California. 61 pp. (Reprinted in 1999) Accessed February 18, 2014. http://www.sci.sdsu.edu/salton/PeriscopeSaltonSeaCh7-9.html

Mullet Island has become a peninsula

David K. Lynch[1], Paul M. Adams[2] and David M. Tratt[2]

[1] U.S. Geological Survey; [2] The Aerospace Corporation

ABSTRACT: Sometime between 28 Aug and 24 Sept 2013, a land bridge formed between Mullet Island and the adjacent mainland. This occurred when the Salton Sea level dropped to an elevation of -232.4 ft., the lowest since the 1950's. As expected, predators reached the island, presumably coyotes. They have raided the cormorant nesting sites, leaving the now-peninsula essentially barren of bird life.

Figure 1. Aerial photographs showing the emergence of the land bridge. Left: 28 August 2013, altitude 6000 ft. AGL. Right: 24 Sept 2013, altitude 12,000 ft. AGL.

Figure 2. Panoramic view of the land bridge from Mullet Island looking southeast, 12 Oct 2013. The authors walked to the island on firm but moist mud across the land bridge.

1. The land bridge

With the legally mandated lowering of the Salton Sea (Quantification Settlement Agreement 2003), formation of a land bridge was inevitable. In a previous paper (Lynch 2011), we predicted that the bridge would form when the sea level reached -232.4 ft (USGS Westmoreland Gauge). This event took place sometime during a 27-day period between 28 Aug 2013 and 24 Sept 2013 (Figures 1, 2 & 3).

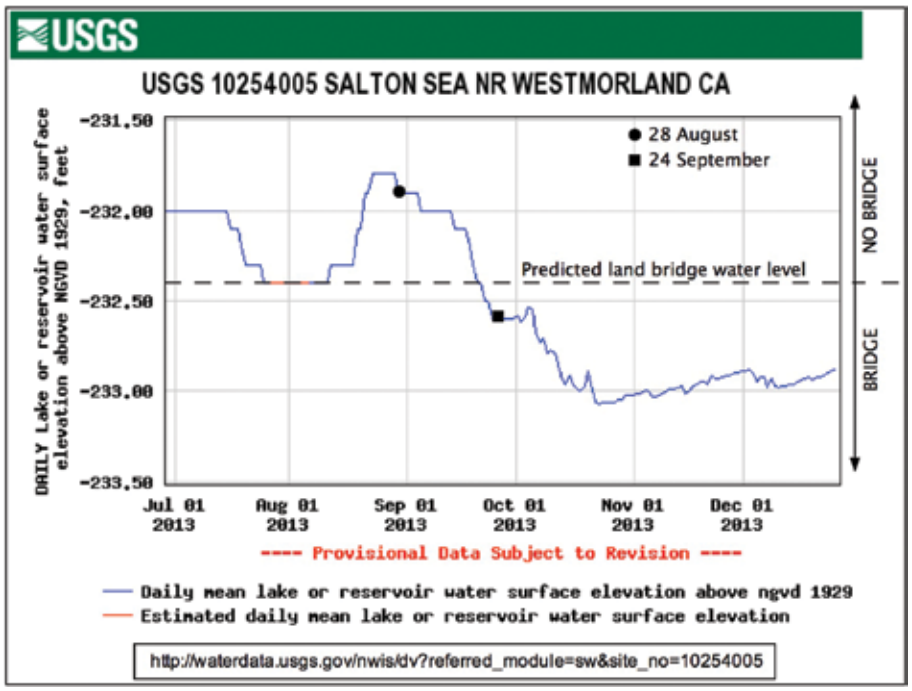

Figure 3. Water level of the Salton Sea showing the predicted land bridge formation water level (Lynch 2011) and the times of the aerial images shown in Figure 1. The bridge could have formed as early as late July 2013.

The land bridge is a broad, flat sand bar that was formerly the Salton Sea level bottom. It is composed primarily of quartz, gypsum, and various amounts of alkali sulfate evaporites, and halite.

2. Impact on cormorant mesting

Double Crested Cormorants have been nesting on the island since the 1960's, although their general abundance was recognized as far back as the 1920's when it was known as Cormorant Island (Rogers 1926, Weight 1948). Owing to the island's isolation and inaccessibility, the nests were densely located on the ground (Figure 4, 25 Jan 2011). Figure 5 shows a photograph of the same scene on 12 Oct 2013. The differences were dramatic, as not a single cormorant was found and there was no evidence of bird occupancy at all. A few empty nests remained intact. While we did not witness predation by coyotes, we presume that they were the principal cause of the elimination or dispersal of the cormorant population. Indeed we saw many *canid* tracks leading from the mainland brush directly to the island (Figure 6).

A close examination of Figure 1 (Aug 28 2013) reveals no cormorants. Although individual birds would be too small to be seen, the flock of black cormorants was easily seen in previous years from great distances as a dark mass against the white island (e.g., Riesz 2011). Therefore, it seems that the predators reached the island before the land bridge formed, perhaps by wading through shallow water.

During a visit to the site on Dec 21, 2013, it was clear that the land bridge had been flooded since our October visit. While the water had receded somewhat and it was still possible to walk to the island, fluctuations in the water level evidently produced transient land bridges that the *canids* may have used. During this time we observed a flock of cormorants on the far western part of the island, though we do not know if they were nesting. This seems unlikely

Figure 4. View of cormorants and nests on 25 Jan 2011. Figure 5. Same view as shown in Figure 4, but taken on 12 Oct 2013.

Figure 6. Fresh canid tracks on the land bridge (12 Oct 2013).

Figure 7. Top: Tire tracks leading across the land bridge to Mullet Island. Bottom: Tire tracks leading to the summit.

because we also observed tire tracks crossing the land bridge and up to the summit of the island, indications of human visits that were not present in October 2013 (Figure 7).

3. Discussion

Like all animals, cormorants adapt to their environment. In finding a safe new place to roost, the birds settled on Mullet Island in the 1960's. But it wasn't always an island. In 1937 it was in the middle of agricultural fields, the Salton Sea shore lying 3 km away (Figure 8). Before that, transient Lake Cahuilla episodically submerged and exposed the small volcanic neck in response to shifting sediments of the Colorado River delta. The sediments altered the river's course, causing it to alternately flow into the Salton Trough and the Sea of Cortez.

With fewer and fewer southern California wetlands, the Salton Sea is one of the only remaining places on the Pacific Flyway for migrating birds to find respite (and nonmigrating birds such as the cormorants). Over 400 bird species have been recorded in and around the Salton Sea.

Much of the area east of Mullet Island is under the control of the California Dept. of Fish and Game. F&G is caught in a perverse political dichotomy. They seasonally flood levee-bounded fields so that migrating ducks have places to rest, and so that hunters can shoot them. Birders and hunters have

Figure 8. Aerial photo of the Mullet Island area from 1937. Mullet Island is outlined.

legitimate and long-standing recreational interests in the area.

Acknowledgements

The authors would like to thank Christian Schoneman of the US Fish and Wildlife Service for logistic support on numerous occasions. This research was partially supported by The Aerospace Corporation's Independent Research and Development program. Mullet Island is owned by the Imperial Irrigation District.

References

Lynch, David K., 2011. The Coming Land Bridge to Mullet Island, in Proceedings of the 2011 Desert Symposium, *The Incredible Shrinking Pliocene*, R. Reynolds (ed), 96-100

Quantification Settlement Agreement, 2003 http://www.sdcwa.org/quantification-settlement-agreement

Riesz, Karen, 2011. Double-crested Cormorants on Mullet Island [image], *Flickr*. http://www.flickr.com/photos/californiadfg/7421150680

Rogers, Austin F., 1926. Geology of Cormorant Island, Salton Sea, Imperial County, California [abstract], Bulletin of the Geological Society of America, 37(1), p.219.

USGS Westmoreland Gauge. http://waterdata.usgs.gov/nwis/dv?referred_module=sw&site_no=10254005

Weight, Harold O., 1948. Nature's Freaks on Salton Shore, The Desert Magazine, 11(6), 5-8.

Hot volcanic vents on Red Island, Imperial County, California

David K. Lynch[1] and Paul M. Adams[2]

[1] U. S. Geological Survey; [2] Thule Scientific

ABSTRACT: A survey of Red Island's northern volcanic neck using a thermal imaging camera and infrared thermometer revealed five hot vents. Rock temperatures 1–2 m into the vents were 35°–38°C (95°–100°F). The vents were found on the south-facing slope at the summit, and were spaced along a ~80 m long line trending N65E. Photos, calibrated thermal images, vent locations and IR imagery of all the Salton Buttes are shown.

1. Introduction

The Salton Buttes are five rhyolitic necks in the Salton Sea Geothermal Field (SSGF) of Imperial County, CA. They lie along a slightly curving, NNE trending line and span a distance of about 7 km. One of them—Red Island—consists of two conjoined volcanoes with related though distinctly different geology. Red Island (also called Red Hill, dating back to before the Salton Sea formed in 1905) is roughly 2.4 km SSW of the Mullet Island fumaroles (Lynch, Hudnut and Adams 2013). The SSGF lies in a tectonic step over region and spreading center between the San Andreas and Imperial faults. The high geothermal gradient results from a shallow magma body and provides the source for geothermal energy plants (Hulen et al. 2002).

Until recently, the Salton Buttes were thought to have formed in the late Pleistocene (~16,000 bp, Muffler and White 1969). More recent work (Lynch et al. 2011, Schmidt et al. 2013) suggests that they could be much younger, with Holocene eruptions as recently 2000 bp. As such, the buttes have come under the purview of the USGS California Volcano Observatory and are now the subject of the CGS mandate to study geologic threats to California.

During the 2008 Desert Symposium field trip (Reynolds, Jefferson & Lynch 2008), Michael McKibben mentioned a volcanic "hotspot" on the southwestern flank of the northern volcano at Red Island (personal communication). A brief search of the area during the field trip did not reveal its location, so we later undertook a systematic search of the buttes. In this paper we report the discovery of five hot vents during a partial survey of Red Island North on November 6, 7 & 29, 2013.

2. Methods

As part of a larger effort to identify the surface thermal morphology of the buttes, we began by searching the southern flank of Red Island's northern volcano, in Red Hill Park, Imperial County. Three search tactics were employed, both during early morning before sunrise when it was coolest and thermal contrast between cold and hot rocks were highest. 1) Using an Agema Thermo-Vision 570 infrared camera (wavelengths ~8–13 micrometers), we looked for areas that were warmer than the background, 2) we stuck our hands into holes and crevasses to see if they felt warm, and 3) we remotely measured temperatures of rocks using a Martin P. Jones & Associates, Inc., Model 9910 TE Infrared Thermometer. Owing to systematic effects with the IR camera, absolute temperatures could be off by 3–4°C, although the relative temperatures between different parts of the scene are preserved. IR thermometer temperatures were usually higher than those recorded by the IR camera because the thermometer was smaller and could be placed deeper into the vent.

Once the vents were identified, we inserted a type K thermocouple (with an Omega HH-52 digital thermocouple reader) into the opening—sometimes horizontally as the geometry of the vent dictated—and measured the temperature as a function of depth. Typical insertion distances were about two

Figure 1. Google Earth image of the vent area with locations marked. The line of vegetation is the result of water flushed from the tank.

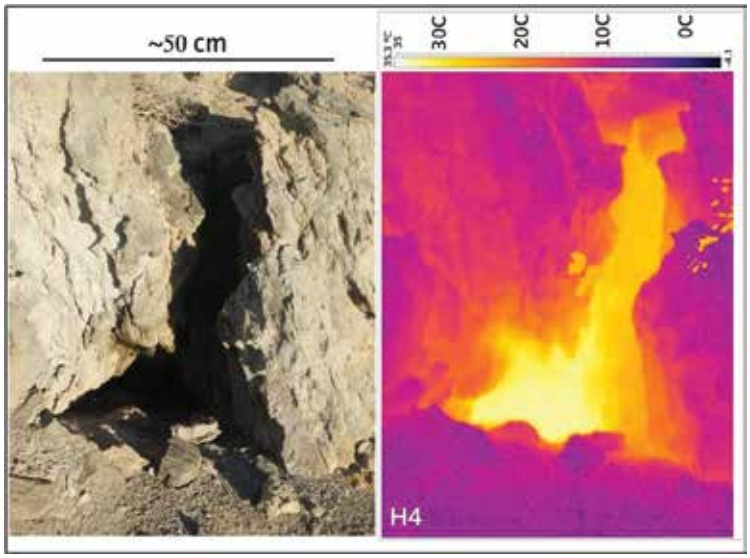

Figure 2. H4. Left: visible, Right: thermal infrared. Bad pixels in the IR camera are obvious as sharp yellow patches at center and center right.

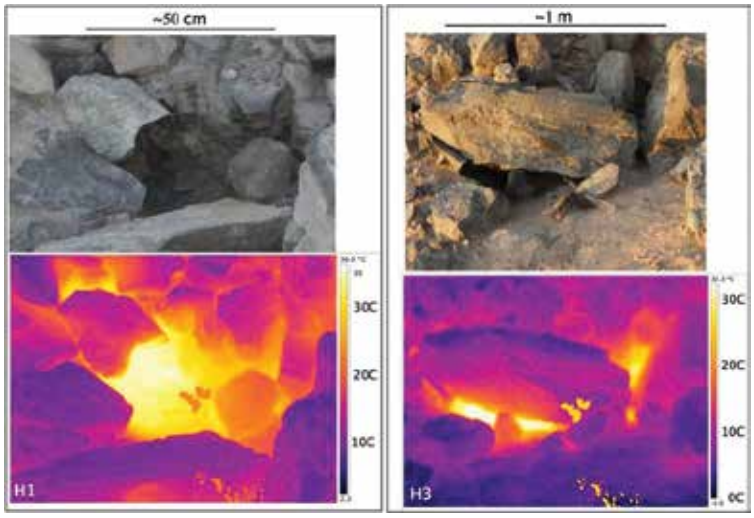

Figure 3. Top: visible, Bottom: thermal infrared.

meters before resistance prevented deeper penetration. In all cases the temperature rose quickly with depth and leveled out around 38°C, often only a half meter into the vent. Thus we were unable to determine the local geothermal gradient.

3. Results on Red Island North

Figure 1 shows a Google Earth image with the locations of the hot vents on Nov 29, 2013. Table 1 lists their locations. Thermal IR (TIR) images and corresponding visible photographs for vent H4 are shown in Figures 2. Figure 3 shows visible and TIR pairs for H1 and H3. All vents were emitting hot moist air that condensed to form a cloud, and the surrounding rocks were wet due to condensation of emitted water vapor. Except for water and greenish algae, no other surface deposits (e.g. sulfur) were seen. Bees were seen flying in and out of several vents. The vents were found on a south-facing slope at the summit. They were distributed along a ~80 m long line trending N65E, a possible fault. Within this and the area extending 225 m to the south and west, we are reasonably confident that there are no additional hot vents.

Table 1

Name	WGS84 Latitude	WGS84 Longitude
H1	33.19977	-115.61249
H2	33.19986	-115.61206
H3	33.20004	-115.61172
H4	33.19981	-115.61211
H5	33.19985	-115.61222

Even from relatively nearby—a few meters—the vents appeared unremarkable among the uneven field of loose, jutting volcanic rocks. One was found by feeling hot air coming from it, two were located with the IR camera, one was identified by noticing wet rock, and one was found by seeing a small cloud emanating from it. The clouds form when warm humid air coming

Figure 4. Single frame from a video showing the emerging cloud from H1.

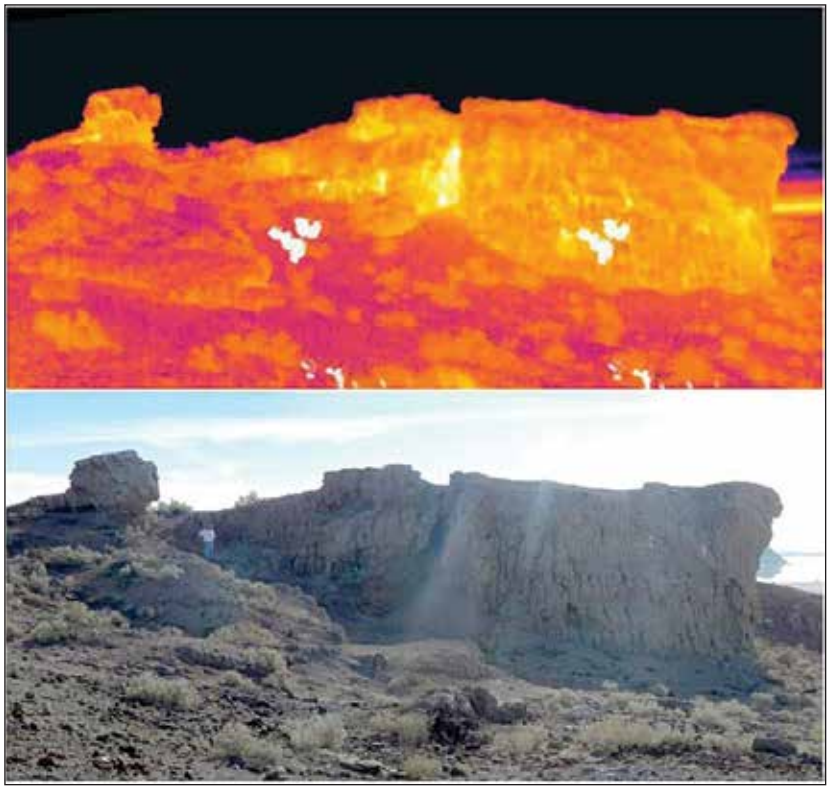

Figure 5. Thermal infrared panorama (top) and visible panorama (bottom) from the thermal survey. Shown here is a north-facing wall on Red Island South. Note bright (warm) crevasses near the center of the upper TIR image. White areas are bad pixels in the TIR camera. There is man standing in the lower image for scale.

from the vent mixes with cold ambient air and condenses. After locating the vents and viewing them in the direction of the low sun, the location of each was found to be readily visible by forward scattering of sunlight from their cloud's water droplets (Fig. 4).

On Jan 18–19, 2014, we did a complete imaging survey of all the five buttes. During the day we took visible images in groups at many points, and marked each location using a hand-held GPS receiver. After midnight we obtained thermal IR imagery from the same locations as the daytime photos. Images were digitally stitched together (Figure 5) and the images were registered using image-warping software. Hundreds of "warm spots" were found, that upon closer examination on foot with better spatial resolution might turn out to be volcanic vents. The approach is to use the TIR images to guide us to hot spot locations, using the visible images as references. This is an ongoing project.

5. Comments

In view of McKibben's information (Section 1), it seems that at least one of these vents was known to local people and perhaps to visitors to Red Hill Park. While the vents were not marked, one of them (H3) looked as though someone may have piled rocks around it.

The Red Island hotspots could represent heat from the original volcanism, or recent magma intrusions that have not reached the surface. All are at the summit of Red Island (north volcano), where one might in general expect magma to appear at the surface (as opposed to a flank).

We believe that the source of the heat in the hot vents is volcanic in origin. We further speculate that the vents are only the surface manifestation of much deeper openings into the volcano. Although we found many openings that were superficially similar to those of the hot spots, none were hot and none had water vapor emission. The origin of the water vapor that is being emitted is unknown, but is almost certainly water from the Salton Sea, which lies 95 ft. lower.

Whether this water is found higher in the volcano – a water table of sorts – is not known.

It is worth noting that there is a water tank very close to the vents. One might worry that perhaps water is leaking from it and providing the source of water. We view this as improbable, and in any event does not explain the heat source.

With air temperatures around 8°C (46°F) during our study, it seems unlikely that warm air coming from the vents could have been felt on a hot and/or windy day. It also seems unlikely that TIR images would reveal the vents on hot days; so working on cold nights seems to be the optimum approach. Indeed, daytime TIR images were dominated by warm, sunlit surfaces.

Much of the surface of Red Island North and Obsidian Butte have been bulldozed, quarried or otherwise man-modified. Such activity would fill in vents and heat diffusion to the surface, thereby suppressing thermal signals. Deeper cuts might expose warmer interior temperatures.

Many "warm" spots were also found on the largely undisturbed, southwest flank Red Island's northern volcano. These were places that the IR camera found to be roughly 5°–10°C (9 – 18° F) warmer than ambient. Such warm spots may represent weak signals from the warm interior of the volcano. We believe, however, that most of them were due to emissivity variations in the rocks layers, or normal temperature distributions that occur in crevasses where the rock is not able to radiate its heat to the cold night sky. None of these "warm" spots was associated with a vent or outgassing.

Acknowledgements: The authors are grateful to Chris Schoneman and Mark Stewart of the US Fish & Wildlife service for hospitality and logistic assistance. David Tratt of The Aerospace Corporation kindly made Mako's airborne hyperspectral imagery of the buttes available to us.

References

Hulen, Jeffrey, Dennis Kaspereit, Denis Norton, William Osborn and Fred S. Pulka 2002 "Refined Conceptual Modeling and a New Resource Estimate For the Salton Sea Geothermal Field, Imperial Valley, California", Geothermal Resources Council Transactions, Vol. 26, September 22–25, 2002

Lynch, David K., Axel K. Schmitt, Dylan Rood, Sinan Akciz, 2011 Radiometric Dating of the Salton Buttes, Proposal to the Southern California Earthquake Center (not funded).

Lynch, David K., Kenneth W. Hudnut and Paul M. Adams 2013 "Recently-Exposed Fumarole Fields near Mullet Island, Imperial Valley, California", Geomorphology 195, 27–44 (2013)

Muffler, L. J. P and D. E. White (1969) "Active Metamorphism of Upper Cenozoic Sediments in the Salton Sea Geothermal Field and the Salton Trough, Southeastern California", Bul. Geo. Soc. Am. 80, p. 157–182

Reynolds, Robert E., George T. Jefferson, and David K. Lynch 2008 Trough to Trough: The Colorado River and the Salton Sea, Proceedings of the 2008 Desert Symposium, Robert E. Reynolds, editor, California State University, Desert Studies Consortium and LSA Associates, Inc.

Schmitt, A.K., Arturo Martín, Daniel F. Stockli, Kenneth A. Farley, and Oscar M. Lovera, 2013 (U–Th)/He zircon and archaeological ages for a late prehistoric eruption in the Salton Trough (California, USA) Geology, January 2013, v. 41, p. 7–10 doi:10.1130/G33634.1

The first fossil record of *Gila elegans* (bonytail) from the Ocotillo Formation (late Pleistocene), Borrego Badlands of Anza -Borrego Desert State Park, San Diego County, California

Mark A. Roeder[1] and Jeanne Johnstone[2]

[1]*Department of Paleontology, San Diego Natural History Museum, P.O. Box 131290, San Diego, California 92112*
[2]*Department of Parks and Recreation, Colorado Desert District Stout Research Center, Borrego Springs, California 92004*

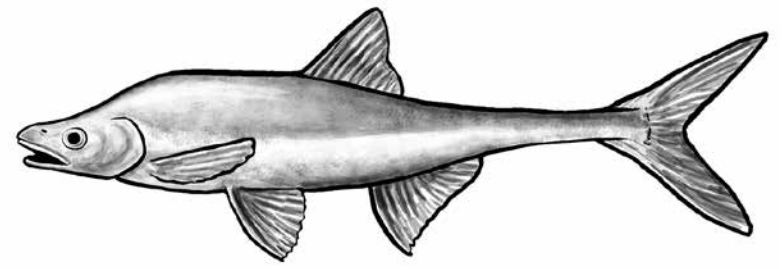

Figure 1. Modern Bonytail Chub (*Gila elegans*). Illustration by Katura Reynolds.

Over the last 60 years, fossil collecting within Anza-Borrego Desert State Park (ABDSP) by volunteers and staff of ABDSP, Imperial Valley College Museum, and the Natural History Museum of Los Angeles County has yielded a small number of freshwater bony fish remains from the late Pleistocene Ocotillo Formation. This material largely consists of disarticulated skeletons: skull bones, vertebrae, and teeth. The fossil fishes from the Ocotillo Formation were described by Gensler and others (2006), and three species were identified: *Ptychocheilus lucius*–pike minnow, *Xyrauchen texanus*–razorback sucker, and *Gila*–chub. These fish are all native to the Colorado River.

Recently, one of us, Jeanne Johnstone of ABDSP, has been surveying the Borrego Badlands within the Park for fossils as part of the Park's on-going paleontological resources inventory. In this area,

Figure 2. Mesial views of right pharyngeal arches of species of *Gila*.

Upper left: *Gila robusta* (roundtail chub), El Fuerte, Rio del Fuerte, Sinoloa, Mexico. Robert R. Miller and others, February 20, 1957, 228 mm standard length, University of Michigan, Museum of Zoology 178285.

Upper right: *Gila cypha* (humpback chub), below Hide-Out Forest Camp, Green River, Daggett County, Utah, United States. Gerald R. Smith and others, July 25, 1957, 292 mm standard length, University of Michigan, Museum of Zoology 180682-S.

Lower left: *Gila elegans* (bonytail), Base of Flaming Gorge Dam, Daggett County, Utah, United States. Robert R. Miller and others, September 1-2, 1962, 283 mm standard length, male, University of Michigan, Museum of Paleontology 182476-S.

Lower right: Fossil. *Gila elegans* (bonytail) ABDSP 3572/V9283, Qo 12 facies of the Ocotillo Formation (Lutz and Dorsey, 2003), Borrego Badlands, Anza-Borrego Desert State Park, San Diego County, California, collected by Jeanne Johnston on 29 March 2011.

she recovered the fairly complete skeletons of fossil freshwater fish from ABDSP 3572 and other localities within the Ocotillo Formation.

The Ocotillo Formation exposed in the Borrego Badlands is a locally-derived fluvial lateral facies of the lacustrine Brawley Formation (Dibblee, 1954) and is found throughout the Borrego/San Felipe basin (Ocotillo Formation of Lutz and Dorsey 2003 formerly Ocotillo Conglomerate of Dibblee 1954). South of the Borrego Badlands in the San Felipe Hills, recent magnetostratigraphic work by Kirby and others (2007) date the Brawley Formation at about 1.1 to 0.5–0.6 Ma. ABDSP 3572 is in the Qo 12 facies of the Ocotillo Formation (Lutz and Dorsey, 2003) about 150 meters stratigraphically below the Bishop Ash which has been dated at .758 Ma (Reimeka, 2006). The estimated age of the locality is approximately 1 Ma.

One the bony fish skeletons recovered from the ABDSP 3572 was identified as partial skeleton of *Gila*–chub. One of the bones exposed during preparation of this specimen was a complete right pharyngeal arch with teeth. Cyprinids (minnows) have no teeth on the premaxilla and dentary bones, but the use pharyngeal (throat) teeth to process food. The pharyngeal apparatus consists of a modified thick fifth pharyngeal arch that bears teeth and a masticatory (chewing) pad that is located in the roof of the pharynx. Comparative skeletons of the three species of *Gila* (*G. elegans*–bonytail, *Gila cypha*–humpback chub, *Gila robusta*–roundtail chub) that inhabit the Colorado River system (Smith and others, 1979) were obtained from the University of Michigan Museum of Zoology. Through direct comparison of the fossil pharyngeal ABDSP 3572/V9283 with pharyngeals of the three modern species of *Gila*, we were able to identify the specimen as *Gila elegans*–bonytail (Figure 1). This determination is based primarily on the shape of the outer margin of the arch (Figure 2). Visually, *Gila elegans* can be separated from the two other species of *Gila, G. robusta* (roundtail chub) and *G. cypha* (humpback chub), by its long caudal peduncle and deeply forked tail (Figure 1).

This note is preliminary because several additional partial fish skeletons and isolated bones representing *Gila* and other species were collected at ABDSP 3572 and at other sites in the vicinity which are currently being prepared and analyzed.

References

Dibblee, T.W., Jr. 1954. Geology of the Imperial Valley region, California. In Geology of Southern California, edited by R.H. Jahns, California Division of Mines and Geology Bulletin 170(2,2):21-81.

Gensler, P., Roeder, M.A., and G.T. Jefferson, 2007. The fossil lower vertebrates: fish, amphibians, and reptiles. In Fossil Treasures of the Anza-Borrego Desert, edited by G.T. Jefferson, and L. Lindsay, Sunbelt Publications, San Diego, Chapter 8, pp. 139-149.

Kirby, S.M., Janecke, S.U., Dorsey, R.J., Housen, B.A., Langenheim, V.E., McDougall, K.A., and A.N. Steely 2007. Pleistocene Brawley and Ocotillo Formations: evidence for initial strike-slip deformation along the San Felipe and San Jacinto Fault Zone, southern California, The Journal of Geology, 115:43-62.

Lutz, A.T. and R.J. Dorsey 2003. Stratigraphy of the Ocotillo Conglomerate, Borrego Badlands, southern California. Geological Society of America Abstracts with Program 35(6):248.

Smith G.R., Miller, R.R. and W.D. Sable 1979. Species relationships among fishes of the genus *Gila* in the upper Colorado River drainage. In Proceedings of the First Conference on Scientific Research in the National Parks, edited by R.M. Linn, U.S. ,Department of the Interior, National Park Service, Transactions and Proceedings, 5:613-623

A preliminary report on new records of fossils from the Brawley Formation (Middle to Late Pleistocene), northern Superstition Hills, Imperial County, California

Mark A. Roeder [1] and Paul Remeika[2]

[1]*Department of Paleontology, San Diego Natural History Museum, P.O. Box 121390, San Diego, CA 92112; maroeder1731@aol.com*

[2]*Anza-Borrego Foundation, P.O. Box 2001, Borrego Springs, CA 92004; premeika@cableusa.com*

The late Pleistocene Brawley Formation (Dibblee, 1954) is exposed at the surface in several large areas in the Salton Trough. This unit crops out as badlands in the Durmid, San Felipe, and Superstition Hills. Magnetostratigraphic work by Kirby and others (2007) in the San Felipe Hills date the Brawley Formation at about 1.1 to 0.5-0.6 million years before present. This sedimentary rock unit consists of fluvial, lacustrine, and deltaic deposits associated with the ancient Colorado River delta and to a lesser extent basin sediments such as aeolian, playa (dry lake), and alluvial. The Brawley Formation in the San Felipe Hills contains evidence of several marine incursions based on fossil foraminifera, ostracods, minute mollusks, and echinoids (Kirby and others, 2007). For the most part, the paleontology of the Brawley Formation is poorly known.

Shell beds consisting almost entirely of the extinct clam, *Rangia lecontei* are exposed in badlands of the Brawley Formation at the northern end of the Superstition Hills on Naval Reservation lands. Two test samples of sediment from one of these shell beds (MAR1226-2012-01) were water screened through fine screens and the remaining concentrate sorted with the aid of a binocular microscope. The samples yielded vertebrate fossils not previously known from the Brawley Formation. The identifications were made by Robert E. Reynolds and Mark A. Roeder.

The fossil assemblage consists of shortfin corvina (*Cynoscion parvipinnus*), corvina (*Cynoscion*), and chub (*Gila).* Freshwater chub inhabits major rivers like the Colorado River, while shortfin corvina (Figure 1) is usually found in shallow inshore marine waters. In the screened samples were a large number of very small corvina otoliths that may be from shortfin corvina and/or another species of *Cynoscion.*

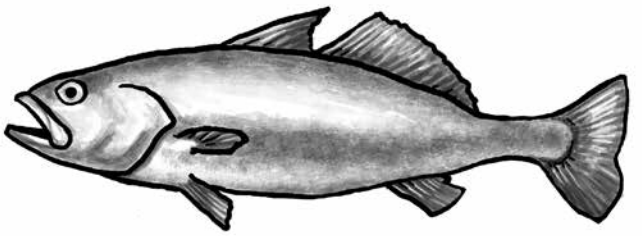

Figure 1. Modern shortfin corvina, size 50 cm. Illustration by Katura Reynolds.

This suggests that this area may have been a "nursery" for these fish until they reached a size large enough to survive in more open marine waters. Modern species of *Rangia* are found in brackish waters of bays, and estuaries. The *Rangia lecontei* shell bed was probably deposited in a delta front lagoon within the Colorado River delta system. This paleoecological setting is consistent with the habitat requirements of *Gila* and *Cynoscion*.

Land mammals associated with the marine fauna include vole? (*Microtus*), pocket mouse (*Perognathus*), spiny pocket mouse? (*Perognathus spinatus*), desert pocket mouse (*Perognathus* sp. cf. *P. penicillatus*), deer mouse? (peromyscine), and kangaroo rat (*Dipodomys*). *Perognathus* and *Dipodomys* inhabit the desert area today, but deer mice presently are found in grasslands, in brushy areas, and in woodlands and forests.

References cited

Dibblee, T.W., Jr. 1954. Geology of the Imperial Valley region, California. In Geology of Southern California, edited by R.H. Jahns, California Division of Mines and Geology Bulletin 170(2,2):21-81.

Kirby, S.M., Janecke, S.U., Dorsey, R.J., Housen, B.A., Langenheim, V.E., McDougall, K.A., and A.N. Steely, 2007. Pleistocene Brawley and Ocotillo Formations: Evidence for Initial Strike-Slip Deformation along the San Felipe and San Jacinto Fault Zone, Southern California. The Journal of Geology, Volume 115, pp. 43-62.

Mullet added to El Golfo De Santa Clara Paleofauna, Irvingtonian (Early to Middle Pleistocene), northwestern Sonora, Mexico

Mark A. Roeder
Department of Paleontology, San Diego Natural History Museum, P.O. Box 121390, San Diego, CA, maroeder1731@aol.com

The El Golfo de Santa Clara badlands are located in the northwestern part of Sonora, Mexico. Although the El Golfo was collected for fossils as early as 1938 by Chester Stock of California Institute of Technology there are small and large collections housed in at least 8 institutions. However, over the last 19 years, by the far the largest and most extensive collections, as well as recorded information in this area, have been made by the staff and volunteers from Reserva de la Biosfera–Alto Golfo de California y Delta del Rio Colorado, Arizona Western College (AWC), and George C. Page Museum. These institutions have made a concerted effort to survey exposures of Pleistocene-age Colorado River delta sediments for paleontological resources. This work was under the direction of Fred W. Croxen III (AWC) and Christopher A. Shaw (Page Museum).

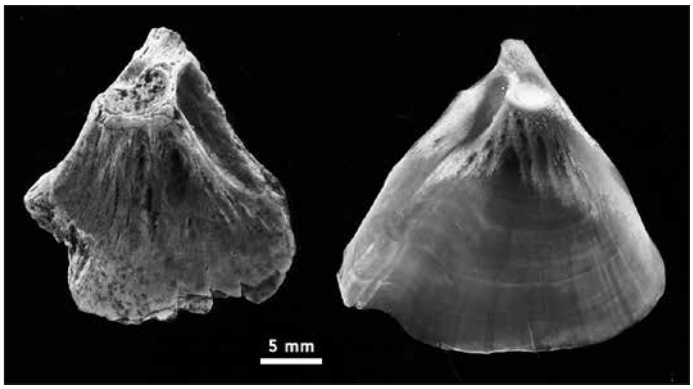

Figure 1. (Left) Fossil left opercle (skull bone) of a mullet (Mugilidae), Arizona Western College Specimen Number 11945 collected by Phillip Gensler in Forbidden Canyon at El Golfo de Santa Clara, Sonora, Mexico, March 12, 2002. (Right) Left opercle of a modern stripped mullet San Diego Natural History Museum F-0035, 189 mm standard length, Lanier Basin, Glynn County, Georgia, collector Jim Music, June 6, 1980. Photograph by Pat I. LaFollette.

Although the age of the El Golfo deposits is not well known, the fossil mammalian fauna correlates with the Irvingtonian-age section of the Anza Borrego Desert State Park stratigraphic sequence and has been dated early to middle Pleistocene. At El Golfo, more than 3500 mapped fossil vertebrate localities have yielded over 66 genera (Croxen and others, 2007). In addition to the larger vertebrate fossils, several new microvertebrate localities have been identified. A small number of bony fish remains also have been recovered. These remains consist primarily of isolated bones, teeth and vertebrae. Previously, Roeder (2007) reported three species of freshwater fish that currently inhabit the Colorado River from the El Golfo deposits: razorback sucker (*Xyrauchen texanus*), pike minnow (*Ptychocheilus lucius*), and chub (*Gila*). Recently, a fourth fish was identified, a mullet of the genus, either *Mugil* or *Chaenomugil,* from a single opercle fragment (Figure 1). Today, there are four species of mullet present in the Gulf of California (Buckhorn, 2012): *Chaenomugil proboscideus*-snouted mullet, *Mugil cephalus*-striped mullet, *Mugil curema*-white mullet, and *Mugil hospes*-Hospe mullet. The striped and white mullets occupy freshwater, brackish, and marine habitats (Eschmeyer and others, 1983; Robins and others, 1986). Until comparative material is available for all of the Gulf of California mullet, the striped mullet is a likely candidate for the fossil recovered.

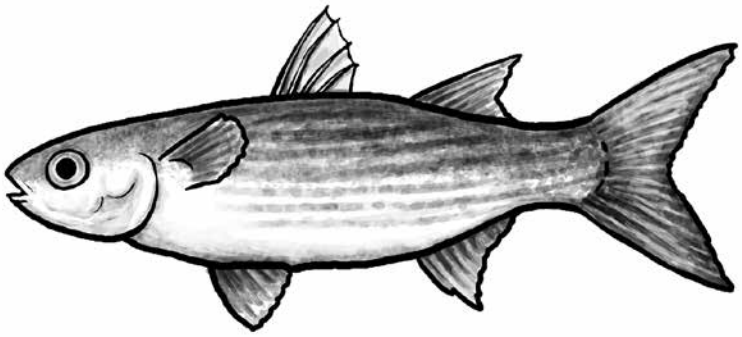

Figure 2. Striped mullet, size 35 to 50 cm. Illustration by Katura Reynolds..

The striped mullet is found worldwide (Figure 1, 2). It is present in the Gulf of California, the lower Colorado River, in southern California coastal, bay, and lagoonal marine waters and coastal freshwater streams. This species is catadromous, part of the year inhabiting freshwater environments and later in the year, returning to marine waters to spawn as adults (McGinnis, 2006). In the years 1915 to 1921 and 1943 to 1953, there was a thriving gillnet fishery for the striped mullet in the Salton Sea. These fish had entered the Salton Sea via irrigation canals connected to the Colorado River. But in the 1950s, with an important and flourishing sport fishery of introduced marine species, commercial netting came to an end. With no new mullet recruitment through irrigation canals from the Colorado River, the mullet population eventually died out (McGinnis, 2006). Striped mullet remains also have been found in a number of archaeological sites around the edge of the former late Holocene Lake Cahuilla (Gobalet, 1992).

References cited

Buckhorn, M.L., 2012. Guide to the Marine Fishes of the Gulf of California. American Fisheries Society, Betheseda, Maryland.

Croxen, F.W., Shaw, C.A. and D.R. Sussman, 2007. Pleistocene geology and paleontology of the Colorado River Delta at Golfo de Santa Clara, Sonora, Mexico in Robert E. Reynolds, editor, Wild, scenic and rapid: Symposium field guide and abstracts from the 2007 California, State University, Fullerton, Desert Studies Consortium and LSA Associates, 84-89.

Eschmeyer, W.N., 1983. A Field Guide to Pacific Coast Fishes, North America. Peterson Field Guide Number 32, Houghton Mifflin Company, Boston.

Gobalet, K.W., 1992. Colorado River Fishes of Lake Cahuilla, Salton Basin, Southern California: A Cautionary Tale for Zooarchaeologists. Bulletin of the Southern California Academy of Sciences, 91(2) 70-83.

McGinnis, S.M., 2006. Field Guide to Freshwater Fishes of California. California Natural Guides, Number 77. University of California Press, Berkeley, California.

Robbins, C.R., 1986. A Field Guide to Atlantic Coast Fishes, North America. Peterson Field Guide Number 28, Houghton Mifflin Company, Boston.

Roeder, M.A., 2007. A preliminary report of fossil bony fish remains recovered from early Pleistocene Colorado River delta deposits exposed in northwestern Sonora, Mexico in Robert E. Reynolds, editor, Wild, scenic and rapid: Symposium field guide and abstracts from the 2007 California, State University, Fullerton, Desert Studies Consortium and LSA Associates, 90.

The first record of Rancholabrean age fossils from the Anza-Borrego Desert

Lyndon K. Murray, George T. Jefferson, Sandra Keeley, Robert Keeley, and Arnold Mroz
Colorado Desert District Stout Research Center, Borrego Springs CA 92004; lyndon.murray@parks.ca.gov

Introduction

The Anza-Borrego Desert (ABD) has produced a prolific array of fossils from erosional surfaces of uplifted, deep paleo basins of the Salton Trough, formed and filled throughout the co-evolution of several regional geologic features: Western Salton Detachment Fault; Southern San Andreas Fault; Gulf of California; Colorado River Delta; and the Peninsular Range. The sediments filling these basins have been dated using radiometric and magnetic polarity stratigraphic methods. The absolute ages thus obtained range from Miocene through mid-Pleistocene. The oldest dates, based on volcanic rocks, are estimated at 22-15 million years (Ma = megaannus) and the youngest, based on volcanic ash, are less than about 760 thousand years (ka = kiloannus). The uplifted sedimentary units often are blanketed with a thin layer of horizontal lying, undated, but very young conglomerate. Current valley floors consist of mostly un-eroded, actively accreting surfaces of Holocene age (less than 10 ka) sediments, concealing sub-layers of unknown thickness and age. Most of the Holocene dates are based on radiocarbon analyses of archaeological sites. Until recently, there were no recognized fossil-bearing sedimentary units within the ABD that were measurably older than Holocene and younger than about 760 ka.

Well over 20,000 fossil specimens have been collected from the ABD and most have been identified and catalogued. Currently, over 550 fossil taxa have been recognized, including marine and terrestrial invertebrates, marine and terrestrial vertebrates, plants, other life forms, and traces. The terrestrial portion of the Fish Creek-Vallecito Creek section has produced a continuum of vertebrate assemblages, each morphing through time, due to appearance and disappearance of stratigraphically associated taxa. Biostratigraphic co-occurrence of certain taxonomic groups led to recognition of faunal associations of several NALMAs (North American Land Mammal Age), including late Hemphillian through early Irvingtonian. These were identified as local faunas (Downs and White, 1965, 1968), Layer Cake (Blancan), Arroyo Seco (late Blancan), and Vallecito Creek (early Irvingtonian). Whereas some taxa may persist through more than one NALMA, associations of taxa during a given geological –chronological interval are used, generally, to characterize a given NALMA.

Herein we report the discovery of the first recognized Rancholabrean NALMA (< 210 ka, Bell et al. 2004) vertebrate fossil assemblage from the Anza-Borrego Desert

Geologic setting

The new Rancholabrean NALMA fossil vertebrate assemblage was recovered from the Bow Willow beds in the Carrizo Badlands of the southern part of Anza-Borrego Desert State Park (ABDSP). This largely flat lying informal stratigraphic unit (in part, Carrizo Wash Lake beds of Downs, 1960; Jefferson, 1994; Dorsey et al., 2011) crops out in the western Vallecito Badlands and the northern Carrizo Badlands. The unit consists of fluvial channel sediments (coarse-grained sands and conglomerates) and overbank sediments (silty fine-grained sands and silty claystones). It is approximately 38 m-thick. The Bow Willow beds conformably overly the Hueso Formation northwest of Vallecito Creek, where the top of the Hueso Formation is marked by a weak calcic paleosol. To the south, along the Vallecito Creek and Carrizo Creek drainages, they unconformably overlie the west dipping Hueso Formation. To the northwest of Vallecito Creek, the Bow Willow beds dip to the west. The southern-most Bow Willow beds appear to have been deposited from west to east in an east-west trending paleo-valley that occupies the present Carrizo Creek drainage west of state highway S2. The top of the Bow Willow beds is marked by a deeply weathered calcic paleosol. The Bow Willow beds are locally nonconformably

Table 1. Bow Willow Beds vertebrate assemblage list

Taxon	Catalogue number	Element
? *Cathartes*	ABDSP 4055/V9258 (Fig. 1)	humerus, right, distal end
Neotoma	ABDSP 4062/V9251	dentary, right, anterior portion, with teeth i/1, m/1, m/2
Canis dirus	ABDSP 3710/V9085 (Fig. 2)	dentary, right, ascending ramus with mandibular condyle
Mammuthus columbi	ABDSP 3676/V9195 ABDSP 3734/V9259 (see Keeley et al., this volume)	incisor (tusk) partial skeleton with skull and mandible
Equus	multiple records	various fragmentary elements
Capromeryx	ABDSP(LACM) 1499/V8772	humerus, left, distal shaft
Camelops	multiple records	various fragmentary elements
Hemiauchenia	ABDSP 4064/V9255	phalanx first
Ovis canadensis	ABDSP 3667/V9194 ABDSP 3730/V9051.1 (Fig. 3)	horn core, portion of outer shaft; vertebra cervical third, anterior centrum; tibia
Bison	ABDSP 3904/V9260 (Fig. 4)	vertebra cervical sixth

overlain by a 1-2 m-thick layer of cobble to boulder conglomerate (in part, the Mesa Conglomerate of Woodard, 1963).

New taxonomic discoveries

Over 56 fossil vertebrate specimens have been recovered from 36 sites in the Bow Willow beds. Six or seven of the localities were recovered by survey parties of the Los Angeles County Museum in the 1950-60s, and later by parties from the Imperial Valley College Museum, in the 1970-80s. No taxa were recognized among those fossils that differ significantly from the Vallecito local fauna (early Irvingtonian NALMA), from the Hueso Formation. The remaining fossil localities were recently discovered by Park Paleontology staff and volunteers during intensive survey efforts in the previously lightly surveyed beds. The remains consist largely of extinct horses and camels, with lesser numbers of birds, rodents, mammoths, a wolf, an antilocaprid, big horn sheep, and a bison (Table 1).

The following fossil descriptions represent the first report of new taxa from Park sediments: A fossil bird humerus (ABDSP 4055/V9258, Figure 1) compares closely in size and morphology to a modern vulture (*Cathartes*) specimen from the Park, although the fossil has not yet been compared with other raptor-size birds; a wolf specimen (ABDSP 3710/V9085, Figure 2) consists of an ascending ramus of a dentary and is comparable in size and morphology to a cast of a dire wolf (*Canis dirus*) mandible from Rancho La Brea; several bighorn sheep elements (horn core ABDSP 3667/V9194, three vertebrae and tibia ABDSP 3730/V9051.1; Figure 3) are all comparable in size and morphology to modern *Ovis canadensis* specimens

Figure 1. ? *Cathartes*, distal right humerus, palmar aspect (ABDSP 4055/V9258); scale bar 2 cm

Figure 2. *Canis dirus*, ascending ramus with mandibular condyle of right dentary, medial aspect (ABDSP 3710/V9085); scale bar 5 cm

Figure 3. *Ovis canadensis*, anterior centrum of third cervical vertebra, anterior-ventral aspect (ABDSP 3730/V9051.1); scale bar 5 cm.

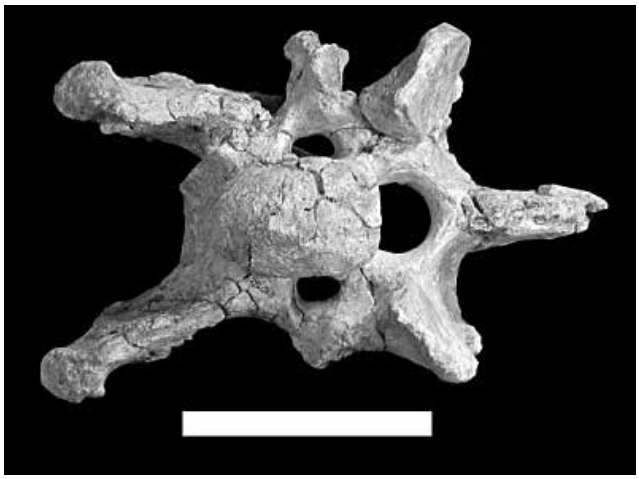

Figure 4. *Bison*, sixth cervical vertebra, anterior aspect (ABDSP 3904/V9260); scale bar 10 cm

from the Park; and a bison specimen (ABDSP 3904/V9260, Figure 4). The nearly complete 6th cervical vertebra, missing some of the neural spine, has a unique morphology in the cervical series and is readily identifiable as *Bison*. The size is very large in comparison to modern *Bison* and may represent *Bison latifrons*, although direct comparison with *Bison latifrons* or another often recorded southern California late Pleistocene taxon, *Bison antiquus*, has not been done.

Conclusions and significance

Prior age estimates of the lowest (<0.99 Ma, Dorsey et al. 2011) and highest (<300 ka, Jefferson, pers. comm.) portions of the Bow Willow beds fall within the age range of the mid- to late Irvingtonian NALMA. The presence of *Mammuthus* (see Keeley et al., this volume) places the Bow-Willow local fauna within the Pleistocene epoch. The oldest well-dated records of North American *Mammuthus* are around 1.4 Ma, and represent the beginning of the Irvingtonian NALMA (Bell et al., 2004). *Canis dirus* evolved from the slightly smaller *Canis armbrusteri* in North America during late Irvingtonian NALMA (Tedford et al., 2009). The earliest North American records of *Ovis canadensis* are from mid-Irvingtonian NALMA localities (Mead and Taylor, 2004). *Cathartes*, *Neotoma*, *Mammuthus columbi*, *Canis dirus*, *Equus, Capromeryx*, *Camelops*, *Hemiauchenia*, and *Ovis canadensis*, although known from the Irvingtonian NALMA, also are present through the end of the Pleistocene, are common members of Rancholabrean NALMA paleofaunas, and as a group or as individual taxa are not decisive indicators of a particular NALMA.

Refinement of Savage's (1951) original definition of the lower boundary of the Rancholabrean NALMA (the first appearance of *Bison* in North America) was made by Bell et al. (2004). The newly defined beginning of the Rancholabrean NALMA is predicated on the first appearance of *Bison* in North America below 55 degrees north latitude, thus eliminating the complications caused by inclusion of eastern Beringia faunas. Based on the earliest well-associated dates for *Bison* localities, they determined the boundary date to be between 210 and 160 ka. The presence of multiple taxa that went extinct in North America at the end of the Pleistocene and end of the Rancholabrean NALMA (*Mammuthus columbi*, *Canis dirus*, *Equus*, *Camelops*, *Hemiauchenia*, *Capromeryx*) in addition to the presence of *Bison* clearly places the new ABDSP assemblage in the Rancholabrean NALMA.

Acknowledgements

We wish to thank L. Gilbert for database and map research and P. Ache and J. Ingwall for specimen identifications.

References

Bell, C.J., E.L. Lundelius Jr., A.D. Barnosky, R.W. Graham, E.H. Lindsay, D.R. Ruez Jr., H.A. Semken Jr., S.D. Webb, and R.J. Zakrzewski 2004. The Blancan, Irvingtonian, and Rancholabrean Mammal Ages. In Late Cretaceous and Cenozoic Mammals of North America, edited by M.O. Woodburne, Columbia University Press, pp. 232-314.

Dorsey, R.J., B.A. Housen, S.U. Janecke, C.M. Fanning, and A.L.F. Spears 2011. Stratigraphic record of basin development within the San Andreas Fault system: Late Cenozoic Fish Creek-Vallecito basin, southern California. Geological Society of America Bulletin 123(5,6):771-793.

Downs, T. 1960. Unpublished field notes. On File Stout Research Center Library Archives, dated 19 April 1960, Book 7, pp. 12-14.

Downs, T., and J.A. White 1965. Late Cenozoic vertebrates of the Anza-Borrego Desert area, southern California. American Association for the Advancement of Science Meeting 1965:10-11.

— 1968. A vertebrate faunal succession in superposed sediments from late Pliocene to middle Pleistocene in California. In Tertiary/Quaternary Boundary, edited by J. Tajkal, 23rd International Geological Congress, Prague 10:41-47.

Jefferson, G.T. 1994. Unpublished field notes. On File Stout Research Center Library Archives, (first use of the nomen Bow Willow beds) Book 4, dated 29 December 1994.

Mead, J.I., and L.H. Taylor 2004. Pleistocene (Irvingtonian) Artiodactyla from Porcupine Cave. In Biodiversity Response to Climate Change in the Middle Pleistocene, The Porcupine Cave Fauna from Colorado, edited by A.D. Barnosky, University of California Press, Berkeley, pp. 280-292.

Savage, D.E. 1951. Late Cenozoic vertebrates of the San Francisco Bay region. University of California Publications, Bulletin of the Department of Geological Sciences 28:215-314.

Tedford, T.G., X. Wang, and B.E. Taylor. 2009. Phylogenetic Systematics of the North American Fossil Caninae (Carnivora: Canidae). Bulletin of the American Museum of Natural History 325, 218 pp.

Woodard, G.D. 1963. The Cenozoic Succession of the West Colorado Desert, San Diego and Imperial Counties, Southern California. PhD Dissertation, University of California, Berkeley, 165 p.

Imperial Group invertebrate fossils Part 1: The science of the proto-gulf

N. Scott Rugh

Colorado Desert District Stout Research Center, Borrego Springs CA 92004

Introduction

The region of the Colorado Desert from which Imperial Group fossil invertebrates are observed and collected (where legal) is a place of spectacular beauty. Weathered mountains, hills and badlands, seemingly barren, come into a life of their own in the play of light under all kinds of conditions – stormy to sunny days. The pastel purples and golden tan of the Santa Rosa range in the morning hours are often transformed by the day's end to a fiery orange glow in the light of the setting sun and coming of dusk. A unique character is carved into the landforms of this region in steep canyon walls and wrinkled bluffs. In some places the buried fossils have contributed to this shaping of the landscape. Hardened beds of abundant oysters, sometimes several feet thick, resist erosion, and leave behind unique structures. Buried in this desert, the fossil invertebrates reveal the existence of the northern end of an ancient inland sea: the prehistoric Gulf of California (often called the proto-Gulf). These buried and exposed fossil invertebrate communities have recorded the environment of this ancient sea.

An understanding of the prehistoric proto-Gulf may be had by exploring the modern Gulf of California. Here are many environments, from long sandy stretches of shore, to boulder beaches, coves, hidden bays, and estuaries, including salt marshes in the north end of the gulf gradually replaced by mangroves to the south. There are corals in the gulf, but nowhere forming true reefs, except at El Pulmo, near the southernmost end of Baja California.

History of Gulf of California explorations

It is worthwhile to examine the history of exploration in the present day Gulf of California to understand our present state of knowledge about the organisms living there. Studies of the fossil invertebrate species of the Imperial Group are based on historical research of the same or closely related living species in the Gulf of California, as well as the Caribbean Sea. For centuries, ships have sailed the oceans of the world, but prior to the last century, relatively little scientific attention was paid to marine organisms. The Galapagos Islands were an exception. In 1826, the pioneer conchologist Hugh Cuming set out from Valparaiso, Chile on the yacht *Discoverer*. Five of the Galapagos Islands were on the itinerary, according to the *Report of the British Association for the Advancement of Science* for 1856. Cuming's collections of crustaceans and mollusks were extensive and contained a high proportion of species new to science. From the point of view of scientific exploration, the year 1835 stands out by itself. In that year the Beagle sailed northward along the coast of Chile and Peru and west to the Galapagos, with Charles Darwin on board. Although his observations were primarily on terrestrial species, with the birds taking much of his attention, marine shells from the beaches and fish from the sea comprise his contribution to marine zoology (Fraser, 1943).

In the last century, more attention was given to the Gulf of California as numerous scientific expeditions were sent there to explore the islands, marine depths and shores. Every kind of marine and land organism was collected. Each expedition tended to have a different study purpose or collecting scheme. For example, dredging was prevalent in some, whereas shore exploration or studies of terrestrial life were emphasized during others. Some expeditions studied and collected more land life, and other expeditions specialized in marine organisms.

One of the earliest expeditions of the past century into the Gulf of California was the 1921 California Academy of Sciences expedition aboard the 22-ton gasoline schooner *Silver Gate* (Williams, 2007). The ship carried a crew of four and the captain, John Ross. Also on board were eight scientists from the California Academy of Sciences and other California academic institutions, as well as the Museo Nacional de Mexico. Among the scientists was Dr. Fred Baker of Point Loma, California, Department

of Paleontology. The purpose of the expedition was to make as comprehensive and thorough study of the fauna and flora of the islands in the Gulf, and of localities on the adjacent mainland, as time, funds, and weather conditions permitted (Slevin, 1923). Fraser (1943) noted that a good map of the Gulf of California was published in Slevin (1923), but erroneously stated the collecting was entirely terrestrial. Steinbeck and Ricketts (1941:170) referred to the 1921 California Academy of Sciences expedition as a "well known scientific expedition into the Gulf, about thirty years ago." They noted that the expedition collected 31 shallow water species of echinoderms from inside the Gulf and after only nine days of collecting in the Gulf, they had taken nearly double this total number of species.

From December, 1931 to March, 1941, a series of ten expeditions aboard the *Velero III* was funded through the Allan Hancock Foundation of the University of Southern California. These expeditions explored the eastern subtropical Pacific (southern California and northern Baja California) and tropical Pacific (southern outer coast of Baja California through the Gulf of California, to the west coast of Mexico and Central America). The paleontologist Leo H. Grant, of the California Academy of Sciences, was on the first expedition. Scientific reports followed these studies, published by the University of Southern California Press. The introduction by Fraser (1943) provides a good history of exploration of the tropical Pacific, from the nineteenth century to the time of the Allan Hancock Pacific Expeditions, but provides little detail about these later expeditions. At the time, Steinbeck and Ricketts (1941) valued this information, but lamented the cost and lack of availability of the reports. The motor cruiser *Velero III* was presented to the University of Southern California as floating research laboratory in January, 1939 (Fraser, 1943).

The Scripps Institution of Oceanography and the U.S. Geological Survey jointly sponsored another study. From October 5 to December 22, 1940, the auxiliary research schooner *E. W. Scripps* made a scientific cruise to the Gulf of California. The paleontologist J. Wyatt Durham joined the expedition in Guaymas, Mexico. Fossil invertebrates from the late Pliocene to early Pleistocene were collected from about 100 localities,between San Carlos Bay on the south and Angel de la Guarda Island on the north. All localities, except three on Tiburón Island, were collected along the eastern edge of Baja California, on the west side of the Gulf. The invertebrate species collected included pelecypods, gastropods, echinoids, corals, and barnacles (Durham, 1950).

One of the best known expeditions into the Gulf of California was not sponsored by a scientific institution, but rather was the idea of marine biologist Edward F. Ricketts and fiction writer John Steinbeck. Their adventure was driven by a shared desire to learn about the tide pools and marine organisms to be found along the shores of the Gulf. They left Monterey harbor on March 11, 1940 on the 75 foot long purse seiner *Western Flyer*, returning on April 13, after observing and collecting marine organisms along the western side of the Gulf of California. Their work is recorded in the book *The Sea of Cortez* (Steinbeck and Ricketts, 1941); including photographs and drawings, as well as a few color plates of marine life they collected and studied. Copies of this work are not easily obtained. The narrative portion of the book, the *Log from the Sea of Cortez* was later published without the figures and appendix of the original, and stands alone as an enjoyable account of exploration of marine life in the gulf (Steinbeck, 1951). The marine organisms collected by Steinbeck and Ricketts include newly described species, and the collections are currently stored and maintained by the California Academy of Sciences, where the collections of the 1921 *Silver Gate* expedition are also maintained.

An expedition sponsored by the San Diego Natural History Museum and the Belvedere Scientific Fund began from Bahía de los Angeles, Baja California on March 15, 1962 and concluded at La Paz, Baja California on April 21, 1962. On board the expedition's ship *San Agustín II* was William K. Emerson, chairman of the Department of Living Invertebrates, of the American Museum of Natural History. Fossil invertebrates; mostly mollusks, echinoids and corals, were collected (Emerson and Hertlein, 1964).

All of this exploration resulted in an increased knowledge of living and fossil invertebrates of the Gulf of California. Scientific journal articles provided the foundation that specialists eventually could build on. Two excellent references to marine invertebrates of the gulf are *Seashells of Tropical West America,* 2nd edition (Keen, 1971), and *Common Intertidal Invertebrates of the Gulf of California,* 2nd

edition (Brusca, 1980). Marine invertebrates of the tropical Pacific are very closely related to species of the Caribbean Sea because they share ancestors from only a few million years ago when the ocean on both sides of Central America was connected (see discussion below, Caribbean connections). References on western Atlantic invertebrates are essential for comparison of some of the fossil ancestors in the Imperial Group of the Colorado Desert region. *American Seashells*, 2nd ed., by R. Tucker Abbott (1974), is highly recommended. This book covers North American mollusks and is an excellent reference to species from the Caribbean region.

History of paleontological research

At the beginning of the last century, relatively few scientific collections of modern invertebrates from the Gulf of California could be used for comparison with the related fossil species of the Imperial Group. Good collections of very similar modern tropical Atlantic invertebrates were available at this time, and might have been used for comparison and identification of the fossil species in the relative absence of modern examples from the tropical Pacific. However, the Atlantic species are generally not as closely related to the Imperial Group fossil species as are those from the Gulf of California.

Paleontologists realized that the invertebrate fauna needed for critical comparison was only to be obtained in the Gulf of California. G. Dallas Hanna, curator of the California Academy of Sciences, withheld his publication on the Imperial Group fossil species until the Academy sent its expedition there in 1921 (Hanna, 1926). This prevented a considerable number of inaccuracies which would have been inevitable had the report been published in 1921 and identifications were made more from Atlantic species than Pacific species.

Hanna's publication remains a good reference to Imperial Group invertebrate fossils; with 10 plates that illustrate mostly mollusks (one echinoderm test and one shark tooth are pictured). Descriptions of additional species of corals and echinoderms known from the time are given in the text. He described new species of mollusks, including Cassis subtuberosa, *Turritella imperialis*, and *Pecten* (*Chlamys*) *mediacostatus*. Hanna proposed the name "Imperial Formation" for the fossil coral reef beds around the Coyote Mountains. The designation "Imperial Group" is now used as a collective term for these tropical marine late Miocene to mid Pliocene fossil beds of the Salton Trough (Winker and Kidwell, 1996). Hanna also referred to the mollusk-rich sandstones of the region, derived from clear ocean waters of the proto-Gulf, as the "Latrania Sands." Today we refer to this deposit as the Latrania Formation. Hanna's contemporaries contributed significantly to our knowledge of the invertebrate fossils of the region of Anza-Borrego Desert State Park and the Coyote Mountains, including work on pectens by Ralph Arnold (1906), echinoderms by Kew (1914), and on corals by T.W. Vaughan (1917). Hanna's paper gives a very good historical account of these and other paleontologists who studied the Imperial Group fossils. We are indebted to this early research for our present day understanding of the marine deposits and invertebrate fossils of the region of the Salton Trough, throughout the Gulf of California, and north to the San Gorgonio Pass, where deposits from the northernmost extension of the proto-Gulf crop out. A few examples of more recent research include; a study of tropical marine fossil species from Miocene deposits in Baja California related to species of the Imperial Group (Smith, 1984), a study of giant pecten species from the California and the Tertiary Caribbean province (Smith, 1991a.), and Pliocene invertebrates from Travertine Point, Imperial County, California, just west of the Salton Sea (Powell, 2008).

Caribbean connections

During the time the Imperial Group invertebrate fossils were deposited, the eastern Pacific Ocean was connected with the Caribbean Sea through openings in the Central American land bridge. The fossil record indicates that the maximum extent of this Tertiary Caribbean fauna occurred during the Miocene. The distribution of fossil assemblages and radiometric data also show that an early gulf, similar in extent to the present one, existed as early as 13 million years ago. By the late middle Miocene the Gulf of California extended as far north as the Salton Trough, as indicated by Imperial Group invertebrate fossils at San Gorgonio Pass, California. Evidence from foraminifera, vertebrate, and sedimentology studies suggest that the connections between the Caribbean Sea and the eastern Pacific remained open until the middle Pliocene, 3.5 to 3.1 million years ago (Smith, 1991b.)

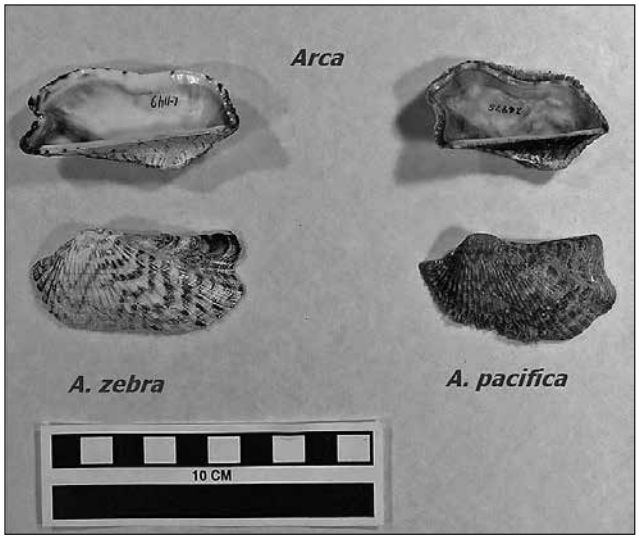

Figure 1-1. Ark clams; *Arca zebra* from the tropical west Atlantic (left), and *A. pacifica* from the Gulf of California (right). Photo by Lollo Enstad.

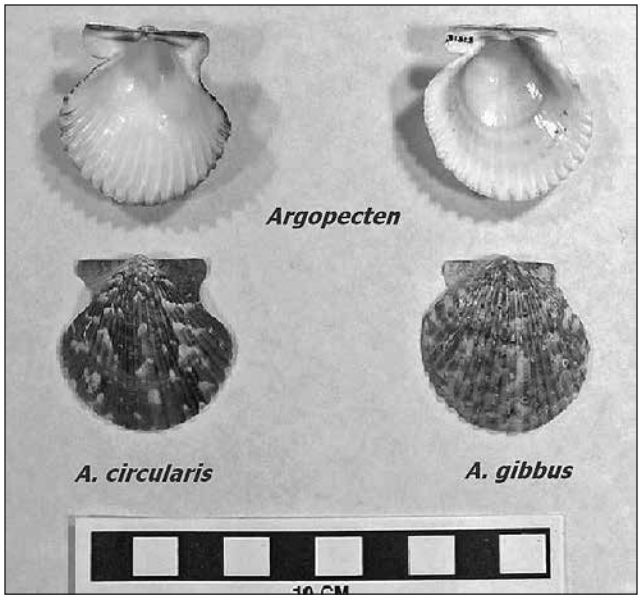

Figure 1-2. Bay scallops; *Argopecten circularis* from the Gulf of California (left), and *A. gibbus* from the tropical west Atlantic (right). Photo by Lollo Enstad.

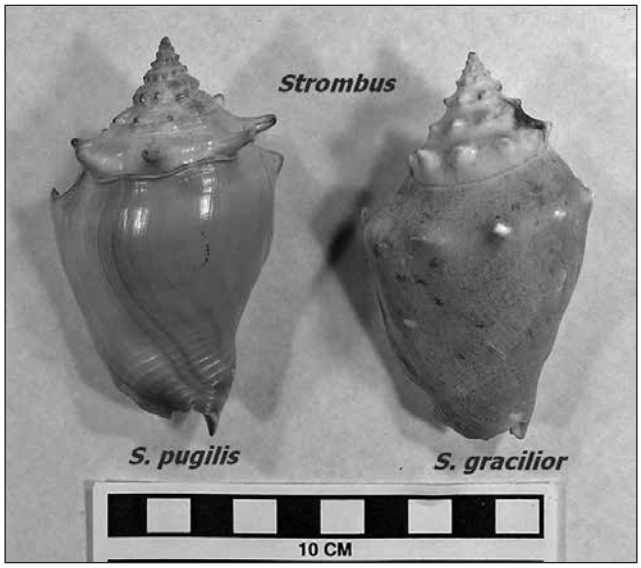

Figure 1-3. Fighting conches; *Strombus pugilis* from the tropical west Atlantic (left), and *S. gracilior* from the Gulf of California (right). Photo by Lollo Enstad.

In *The Sea of Cortez* (Steinbeck and Ricketts, 1941), the writers found a small statue of a Virgin Mary figure, "Our Lady of Loreto," in a church. They spoke of her with a scientific reverence, and observed that the Lady of Loreto was a very important factor to the community of the city, and that "not to know her and her strength is to fail to know Loreto." This observation was followed by a remarkable analogy to the Virgin figure:

> One could not ignore a granite monolith in the path of the waves. Such a rock, breaking the rushing waters, would have an effect on animal distribution radiating in circles like a dropped stone in a pool.

This passage is like a metaphor for the closing of the Central American seaway during the middle Pliocene. The closing of the openings between the Pacific and Atlantic oceans—a relatively recent event—resulted in a large scale evolution of descendent species pairs of invertebrates, fish, etc. through the process of allopatric speciation. Today we observe the existence of species "twins", with one species in the tropical eastern Pacific, and the other species in the western Atlantic. For example the most common large sea biscuit (Family Clypeasteridae) of the tropical Atlantic, *Clypeaster rosaceus*, closely resembles the Imperial Group fossil *Clypeaster bowersi*, though the later species tends to be more rotund than the former. The Imperial Group coral *Solenastrea fairbanksi* is very similar to the modern coral *Solenastrea bournoni* from the Caribbean. Three examples of mollusk species pairs are figured; ark clams (Family Arcidae, Figure 1-1), bay scallops (Family Pectinidae, Figure 1-2, and conches (Family Strombidae Figure 1-3)

While the majority of fossil species from the Imperial Group clearly are most closely related to the fauna of the modern Gulf of California, there are notable examples of species that seem to have a closer affinity to modern Caribbean species. All fossil

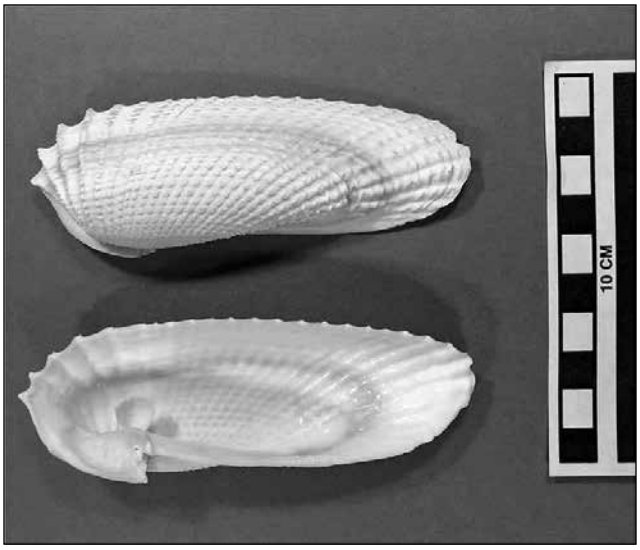

Figure 1-4. A modern angel wing, *Cyrtopleura costata*. This species is extinct in the east Pacific, but internal mold fossils of this bivalve are common in the Deguynos Formation. Photo by Lollo Enstad.

specimens figured are from the Kidwell Collection, discussed in Part II:

> *Cyrtopleura costata* is common in the Deguynos Formation. This species is not present in the gulf today but lives deeply buried in the muds of mangrove estuaries in Florida and the Caribbean. (modern specimen, Figure 1-4).
>
> The only helmet species (Family Cassidae) in the Gulf today are the small forms *Cypraecassis (Cypraecassis) tenuis* and *Cypraecassis (Levenia) coarctata*. Today, there are no species of *Cassis* in the tropical eastern Pacific, but there are three species in the Caribbean. Hanna considered the Imperial Group species *Cassis subtuberosa* to be most closely related to the Atlantic species *Cassis tuberosa*. However, *C. subtuberosa* was a relatively small species, not often exceeding 10 cm, and compares well with the smallest Atlantic species *C. flammea* (Figure 1-5).
>
> The pecten *Euvola keepi* of the Imperial Group more closely resembles the Caribbean species *Euvola ziczac* than any living Gulf of California species.
>
> The Imperial Group fossil pecten *Lindapecten corteziana* closely resembles the southeast Atlantic pecten *Aequipecten muscosus*, with about 18 scaly ribs, and a noticeably long anterior ear on the right valve.
>
> The presence of the common large cockle cf. *Dinocardium* sp. in the Imperial Group collections is surprising. This genus occurs today on the Atlantic coast, not the Pacific Coast. Fossils match well with the modern *Dinocardium robustum* (Figure 1-6). This bivalve genus does not appear to have been described from the Imperial Group. There are many examples in the collection ranging from juveniles a few centimeters long to a very large steinkern valve over 10 cm long.

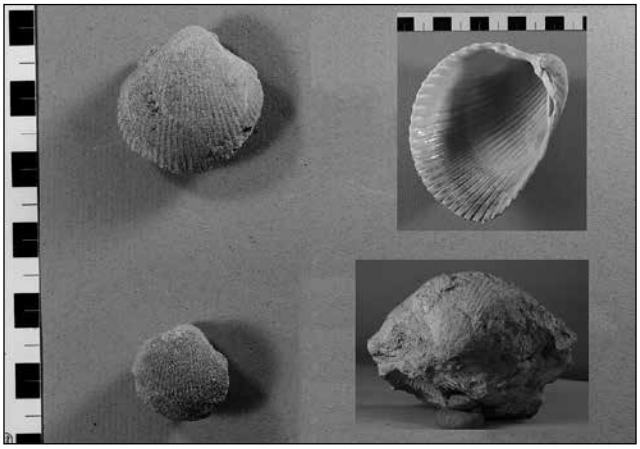

Figure 1-6. Juvenile internal molds of cf. *Dinocardium* sp (left) and a large (over 10 cm long) right valve internal mold (insert, lower right). A modern *Dinocardium robustum* right valve from the west tropical Atlantic is shown for comparison (insert, upper right). Photo by Hugh Vance.

Figure 1-5. An internal mold of the fossil helmet snail species *Cassis subtuberosus* (left) with a similar sized modern shell of the Caribbean *Cassis flammea* (right). Photo by Hugh Vance

Figure 1-7. The rare extinct auger, *Terebra gauspata*, preserved with original calcitic shell. Note the clearly defined spiral groove. Photo by Hugh Vance.

Hanna (1926) observed the auger species *Terebra gauspata* more closely resembles *T. dislocata* of the Atlantic coast than its contemporary, *T. martini*, of the Pliocene of coastal southern California (Figure 1-7). *Terebra gauspata*, like *T. dislocata* has a deep groove high on the whorls that is not present in *T. martini*.

The gastropod *Architectonica nobilis* is present on both the Atlantic and Pacific coasts, and occurs as a fossil in the Imperial Group.

Living species give clues about the fossil environment

Different species may tell us about differences in the marine environment. The bay scallop, *Argopecten deserti* (Figure 1-8) resembles the modern species *A. circularis,* which is most common in eelgrass beds in calm bays. The fossil species *A. deserti* is very common in the Deguynos Formation, along with *Dendostrea*? *vespertina* and *Anomia subcostata*. These species lived on the flats of a vast estuary. *Argopecten deserti* closely resembles the Pliocene species *A. invalida* of the San Diego Formation (see Hertlein and Grant, 1972). The giant bittersweet, *Glycymeris gigantea* (Figure 1-9) is a thick-shelled, heavy clam that lives buried only a few cm in sand. The ark clam, *Arca pacifica* (Figure 1-10), lives in rocky areas, and attaches to the undersides of rocks with byssus threads. Another bivalve that lives in rocky areas but in deeper water, often attached to gorgonian corals, is the winged pearly oyster *Pteria sterna* (Figure 1-11). This bivalve is a tropical species that may be found as

Figure 1-8. Fossil bay scallop *Argopecten deserti* with the common oyster *Dendostrea? vespertina* attached, from the Deguynos Formation. Both species are preserved as original calicitic shell. The closely related modern *A. circularis* (right) from the Gulf of California is shown for comparison. Photo by Hugh Vance.

Figure 1-9. A modern giant bittersweet, *Glycymeris gigantea* from the Gulf of California, with a paired internal mold fossil (left). Notice the fragment of calcitic shell on the right side of the fossil pair. Photo by Hugh Vance.

Figure 1-10. A modern *Arca pacifica* pair (top), and two internal mold fossils (bottom). The specimen on the lower left shows the hinge side. Photo by Hugh Vance.

Figure 1-11. Fossil left valve of the winged pearly oyster, *Pteria sterna*, on a block of matrix. The valve is eroded and difficult to discern from the matrix, so it has been outlined in the photo. The tropical west Atlantic *Pteria colymbus* from Eleuthera, Bahamas (right) is shown for comparison. Photo by Hugh Vance.

Figure 12. A modern young specimen of the spiny jewel box, *Arcinella californica*, collected from off Cedros Island (southern Baja) next to an internal mold fossil adult pair (right). Photo by Hugh Vance.

far north as the southern coast of California, where stormy weather occasionally tosses one ashore with the red gorgonian corals they live on. The fossil valve of *Pteria sterna* is shown next to its Caribbean counterpart, *P. colymbus* (Figure 1-11). This is the only specimen in the Kidwell collection and may be the only example from the Imperial Group. Steinkerns of the spiny jewel box *Arcinella californica* look very different from the modern shell (Figure 1-12). This is because the internal mold only shows the form of the inner cavity of the shell and not the spiny outer surface. This species glues its lower valve firmly to subtidal rocks.

Conclusions

Fossil invertebrates are a common feature in the Colorado Desert. The presence of corals and large tropical gastropods and bivalves, among other kinds of invertebrates, are evidence that this region was once a prehistoric northern extension of the Gulf of California, often referred to as the proto-Gulf. The sediments in which these fossil invertebrates occur range in age from the late Miocene, when the environment was predominately a clear water tropical sea rich in marine species, to the mid Pliocene, when this sea was replaced by a vast shallow-water estuary with few species and abundant individuals. These deposits are collectively referred to as the Imperial Group. The similarity of living invertebrate species between the Gulf of California and the Caribbean, and the information from the fossil record from this region has provided evidence that these seas were connected in the late Miocene through the mid Pliocene through openings in the Central American land bridge. The present state of knowledge about the geological history of this desert region draws on the scientific history of exploration of the modern biology and paleontology of the Gulf of California. Continued research, such as that of Dr. Susan Kidwell, her colleagues, and other researchers described in Part II will further add to our knowledge of this fascinating region.

References

Abbott, R.T. 1974. American seashells, the marine Mollusca of the Atlantic and Pacific coasts of North America. Van Nostrand Reinhold Company, New York, 663 p.

Arnold, R. 1906. The Tertiary and Quaternary pectens of California. U.S. Geological Survey Professional Paper, 47:1–264.

Brusca, R.C. 1980. Common intertidal invertebrates of the Gulf of California, Revised and Expanded Second Edition. University of Arizona Press. 513 p.

Durham, J.W. 1950. 1940 E.W. Scripps cruise to the Gulf of California; part II, Megascopic paleontology and marine stratigraphy. Memoir Geological Society of America, 43:1–216.

Emerson, W.K., and L.G. Hertlein 1964. Invertebrate megafossils of the Belvedere Expedition to the Gulf of California. Transactions San Diego Society of Natural History, 13:333–368.

Fraser, C.M. 1943. Allan Hancock Expeditions. general account of the scientific work of the *Velero III* in the Eastern Pacific, 1931-41. Part I. Historical Introduction, *Velero III,* Personnel. University of Southern California Press, 1(1):1-45.

Hanna, G.D., 1926. Paleontology of Coyote Mountains, Imperial County, California. Proceedings California Academy of Sciences, Fourth Series, v. 14, p. 427–503.

Hertlein, L.G., and U.S. Grant IV. 1972. The geology and paleontology of the marine Pliocene of San Diego, California (Paleontology: Pelecypoda). Memoir San Diego Society of Natural History, 2:1–409.

Keen, A.M. 1971. Sea shells of tropical west America; marine mollusks from Baja California to Peru. Stanford University Press, California, 1064 p.

Kew. Wm S.W. 1914. Tertiary Echinoids of the Carrizo Creek Region in the Colorado Desert. Univ. Calif. Publ. Bull. Dept. Geol. Vol. 8 pp. 39-60.

Powell, C.L. II 2008. Pliocene invertebrates from the Travertine Point outcrop of the Imperial Formation, Imperial County, California. U.S. Geological Survey Scientific Investigations Report 2008-5155, 25 p., http://pubs.usgs.gov/sir/2008/5155/sir2008-5155.pdf.

Slevin, J.R. 1923. Expedition of the California Academy of Sciences to the Gulf of California in 1921: General Account. Proceedings of the California Academy of Sciences, Fourth Series, 12(6):55–72.

Smith, J.T. 1984. Miocene and Pliocene marine molluscs and preliminary correlations, Vizcaino peninsula to Arroyo la Purisma, northwestern Baja California Sur, Mexico, in V.A. Frizzell, Jr., ed., Geology of the Baja California peninsula: Pacific Section, SEPM, v. 39, p. 197-217.

Smith, J.T. 1991a. Cenozoic giant pectinids from California and the Tertiary Caribbean province: *Lyropecten*, "*Macrochlamis*", *Vertipecten*, and *Nodipecten* species. U.S. Geological Survey Professional Paper 1391, 155 p.

Smith, J.T. 1991b. Cenozoic marine mollusks and the paleogeography of the Gulf of California. *In* The Gulf and Peninsular Province of the Californias, edited by J.P. Dauphin, and B.R.T. Simoneit, American Association of Petroleum Geologists Memoir 47: 637-666.

Steinbeck, J. 1951. The log from the Sea of Cortez. Viking Press. 288 p.

Steinbeck, J., and E.F. Ricketts 1941. The Sea of Cortez: a leisurely journal of travel and research. Viking Press, 598 p.

Vaughn 1917. The Reef-coral Fauna of Carrizo Creek, Imperial County, California, and its Significance. U.S. Geological Survey Professional Paper 98, pt. 5. 355-386 pp., pls. 94-102.

Williams, G.C 2007. History of invertebrate zoology at the California Academy of Sciences. Proceedings of the California Academy of Sciences, Fourth Series, 58(12):197–239.

Winker, Charles D., and Susan M. Kidwell. 1996. Stratigraphy of a Marine Rift Basin: Neogene of the Western Salton Trough, California *in* Abbott, Patrick L., and John D. Cooper (eds.) Field Conference Guide and Volume for the American Association of Petroleum Geologists Annual Convention , San Diego, May 1996: 295-336.

Imperial Group invertebrate fossils Part 2: The Kidwell collection

N. Scott Rugh

Colorado Desert District Stout Research Center, Borrego Springs CA 92004

Dr. Susan Kidwell's extensive work on processes of fossil deposition have provided us with a greater understanding of the fossil record, including how accurate an interpretation of the paleoenvironment can be obtained from these fossil deposits. The majority of her work is done with sea floor bottom environments, both modern and fossil. From this setting, Dr. Kidwell collects vast amounts of data on the nature of shell deposits, including the interaction of live and dead animal communities, shell density, state of preservation, and many other factors that provide information about how these shell beds are preserved. This is precisely what she was doing in the Colorado (Sonoran) Desert, from the Anza-Borrego Desert State Park (ABDSP) to the Coyote Mountains during the mid-1980s to the early 1990s. Along with her graduate students, Dr. Kidwell collected a great number of invertebrate fossils from the desert region. These fossils constitute the most complete and largest stratigraphic collection of marine fossils from the ancestral Gulf of California. The data obtained from this research contributed to a study comparing fossil deposition in a recently rifted continental margin (Miocene/Pliocene Imperial Group, southeastern California) with a mature passive margin (Miocene Calvert and Choptank Formations, Maryland coastal plain) (Kidwell, 1987) in which low sedimentation rates were shown to be important for fossil accumulation.

The collection itself was not a primary objective during fieldwork in the 1980s. The fossils were collected in the field as sections were measured to provide specimen vouchers for stratigraphy and paleogeography. However, with good field data available to the level of fossil beds, and with the fossils identified to species, the collections will prove valuable to many workers in the field of paleobiology. Data from this field collection has provided material for research for more than two decades. Dr. Kidwell and her students were very concerned about the preservation and care of this great research collection. Through the tireless effort and dedication of volunteer members of the ABDSP Paleontology Society at the Stout Research Center (SRC), the collection was soon on its way home to ABDSP. Volunteers Jimmy and Judy Smith, Bob and Sandra Keeley, and Norbert Sanders went to Chicago in November 2009 to pack and prepare the fossils for shipment to the SRC (Bahar, 2009).

From 16 November 2012 to 21 March 2013, I identified the invertebrate fossil specimens of the Kidwell Collection, working together on bivalves with researcher Dr. Astrid Montiel Boehringer. Astrid is a post-doctoral fellow under Dr. Richard Norris, professor of Paleobiology at Scripps Institution of Oceanography. The objective of our research is to create an accurate and complete catalogue of the bivalve species of the Imperial Group. Astrid's research interests include the biogeography of the Salton Trough and the origin of bivalve families from the Gulf of California during the Miocene. The 9,643 specimens in the Kidwell Collection occupy a dozen standard-size museum cases in the SRC. The collection contains fossil material from the base of the Latrania Formation to the top of the Deguynos Formation (collectively known as the Imperial Group, Dorsey et al. 2011). This sequence represents changing paleo-ecosystems through time, from about 6 to 4.5 million years ago, late Miocene and early Pliocene. During this period, the marine environment went from a shallow-water inland sea to a vast estuary as the water became shallower. The older marine environments supported tropical marine bottom communities, including common corals not quite dense enough to be considered reefs. Later, in the shallower water of the estuary environment the corals and large tropical invertebrates eventually were replaced by dense beds of oysters, scallops and jingle shells (*Anomia* sp.). The Kidwell Collection invertebrates are characterized by high species diversity. Our work resulted in the identification of 175 taxa. Most of these are mollusks,

including 94 bivalves and 56 gastropods. Other invertebrate species include 9 cnidarians (corals), 8 echinoderms, 5 arthropods, 1 sponge, 1 annelid, and 1 bryozoan (Table 1).

Because the specimens in the Kidwell Collection were recovered as voucher specimens for stratigraphic and paleo-geographic study and not selected as the best examples of the species present in the field, many of the specimens are not well preserved. In fact, this poor preservation of specimens contributed to the reasoning for the collection of voucher specimens – since they could not easily be identified in the field, relatively large numbers of these could be collected during field work to be identified later in the laboratory. Despite the prevalent poor state of preservation of these fossils, most internal mold specimens had enough of the form present that identification, usually to species, was possible. Where original shell material was preserved, especially common in collections from the Deguynos Formation, even fragments could be identified.

Fossils of most Imperial Group invertebrate species are preserved as steinkerns, or internal molds – the sediment trapped in the original clam or sea snail preserves the internal form of the shell, which was previously dissolved away. This is especially true of the late Miocene Latrania Formation. These internal molds are often preserved in a brown to reddish-brown fine to coarse pebbly sandstone. While mollusks are preserved as steinkerns in the Latrania formation, the sand dollars, sea biscuits, corals and arthropods, including barnacles, and crab parts, are preserved as a mineralized version of the original shell material (usually calcite). The more common internal molds of mollusks in the Latrania Formation are typically of fairly large tropical clam and gastropod species. In fossil material from the early Pliocene Deguynos Formation, where oyster and scallop species predominate, most of the mollusks have been preserved as original shell. These shells often have a yellowish tint to them, derived from the estuarine muds prevalent during the time of deposition.

Several very large species of tropical marine snails and clams stand out, measuring upwards from 10 cm. These include the gastropods *Pleuroploca princeps, Melongena patula, Strombus galeatus, Malea ringens*, and *Cassis subtuberosa*. and the bivalves *Pinna latrania, Spondylus bostrychites, Panopea globosa*, and *Pycnodonte heermanni*. The largest species of mollusks are impressive. The conch *Strombus galeatus* could reach an adult size of 20 cm. The juvenile of *S. galeatus* is conical, and was often mistaken by students for a very large *Conus* species, which would be nothing like any species present in the gulf today. The biggest bivalve species, *Pinna latrania*, grew even larger. Though not often found as complete fossils, adult valves of this species easily could reach 30 cm in size.

Identification issues

Often, the identification of internal mold fossils of the many mollusk species from the Latrania Formation is not difficult. This is because the shape of the mold follows the shape of the original shell in which it was formed. Some species however, resemble others. Juveniles of the large conch, *Strombus galeatus*, are conical and resemble large *Conus*, but are not as tightly coiled. Internal molds of *Cassis* are also often mistaken for *Conus* fossils. The disk shaped venerid clam *Dosinia* sp. looks like the lucinid clams *Codakia* and *Miltha*. A mold pair of *Miltha* is usually distinguished from the others by its much flatter profile. The mold of a Codakia pair is more inflated, with a central beak or hinge area. *Dosinia* has its hinge more to the anterior side and the beaks turn in that direction. However, if a mold pair of one of these species is badly worn, it can be impossible to discern it from one of the other species.

One species of tellinid clam in the Kidwell Collection had to be re-identified twice because of confusion with other taxa (Figure 2-1). The internal molds of this bivalve were first identified as *Tellina ochracea*, a common gulf species. But in time, it became apparent that this species may more closely match *Macoma secta*, common today on the outer coast of California and Baja, but not in the Gulf of California. The specimens had a small shelf-like extension of the mold pair on the posterior end that seemed a perfect match for modern valves of *Macoma secta*. However, a more likely species, *Psammotreta vidriotincta*, also could produce a shelf-like extension on the posterior portion of the pair, where the valves compress inward along a groove. The outline of *Psammotreta* was a better match for the fossil than that of *Macoma*. It is important that the identification of fossil species be accurate. If *Macoma secta* was the correct identification, this species, which lives along the exposed

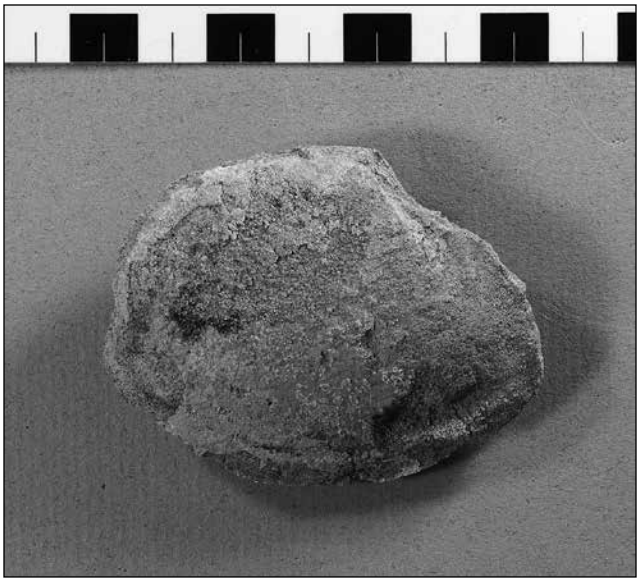

Figure 2-1. An internal mold pair of *Psammotreta viridotincta*, a species common today in the Gulf of California. In size and shape it is similar to *Tellina ochracea*, which is a bit more rounded and inflated, and *Macoma secta*, which lives outside the Gulf. Photo by Hugh Vance.

ocean today, could falsely support a hypothesis that there was a channel that went through the Baja peninsula, connecting the Gulf to the Pacific Ocean. Such a channel may have existed, but if correctly identified as *Psammotreta vidriotincta*, this tellinid fossil does not provide evidence to support this hypothesis.

Though it may be fairly easy to identify an internal mold fossil of a gastropod or bivalve from its distinctive form, it may be far more difficult to identify similar species within a genus. One very good example of this is the bivalve genus *Dosinia*. In the Gulf of California, there are at least three large (several cm in length) living species of *Dosinia*, including; *D. ponderosa*, *D. semiobliterata*, and *D. dunkeri*. There are small differences in surface sculpture of the valves between these species, but the overall shape of each species is very similar. Very few of the *Dosinia* specimens in the Kidwell Collection have any original shell material with some surface pattern. Thus, identification of *Dosinia* species may not be made with confidence. Specimens in the collection previously named *D. semiobliterata* and *D. delicatissima* (a fossil species) have been left as genus *Dosinia* sp. only. In the future, the few specimens with surface sculpture may be studied to determine the correct species present in the collection.

Some other genera in the collection consist of species that are very similar. Time did not permit the careful study of these genera. Several species of *Argopecten* are described for the Imperial Group, but it was decided that the smaller, generally convex *A. deserti* and the larger, generally flatter *A. mendenhalli* best described the material. Perhaps future research will reveal other species or subspecies of *Argopecten*. Species of oysters are even more difficult to distinguish. There are two ostreids present, *Dendostrea*? *vespertina*, and *Myrakeena angelica*, and the giant gryphaeid oyster *Pycnodonte heermanni*. All of these species may be confused with one another. It may be possible that among the *Dendostrea*? *vespertina* specimens, there is another very similar species, *Dendostrea frons*.

Uncommon species and others possibly new for the Imperial Group

There are too many invertebrate fossil species in the Kidwell Collection to describe more than a few in this paper. Several interesting bivalve and gastropod species are mentioned and figured in Part I. In addition to the prevalent mollusk fossils in the collection are beautiful examples of various coral species, and interesting arthropods, including a number of barnacle species (one of which burrows into coral). The full list of species is provided in Table 1.

In the collection are some species that are rare, and others that may be new records for the Imperial Group. The winged pearly oyster specimen, *Pteria perna*, described in Part I may be a new record. The rare fossil *Terebra gauspata* (See Part I) in the

Figure 2-2. A species of *Cantharus* resembling *Gemophos ringens*; could be a new fossil species. Hanna (1926) figured a similar specimen as *Solenosteira anomala*. The pictured specimen is original calcitic shell.Photo by Hugh Vance

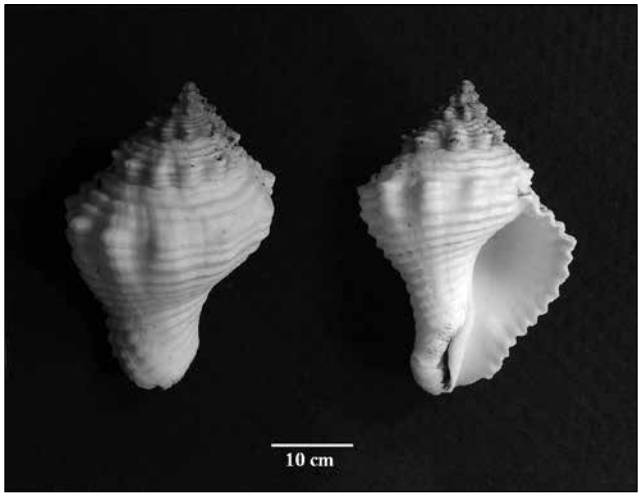

Figure 2-3. A modern specimen of *Solenosteira anomala* from Tumbes, Peru, for comparison with the fossil specimen in Figure 2. Note the fossil has a shorter siphonal canal, a more rounded shape, and differences in sculpture. Photo by Hugh Vance

collection was figured by Hanna (1926:Plate 22), who noted very few examples were available. A few specimens of another gastropod species from the collection are similar to that identified by Hanna as *Solenosteira anomala* in Plate 20 (Figure 2-2). However, the figured specimen, and those in the collection, more closely resemble *Gemophos ringens*, which has a lower spire, broader and more closely placed knobs on the whorls, equal sized spiral cords, and a short siphonal canal, compared to *S. anomala*. The specimen pictured in Hanna has a higher spire than those in the Kidwell Collection but looks closer to *Gemophos* with respect to all other characters. A modern specimen of *Solenosteira anomala* is shown for contrast with the specimen figured in Hanna (1926) and those in the collection (Figure 2-3).

Conclusions

Fossil material from the Kidwell Collection has already captured the interest of invertebrate paleontologists. Judith Smith, a research associate of the Smithsonian Institution, has examined the large pectens and *Spondylus* from the collection. A large cowry, *Muracypraea* collected by Charles Winker (a research associate of Dr. Kidwell) is the only specimen in a study of this genus to have precise locality data; from a specific shell bed in the Jackson Fork Member of the Deguynos Formation, in the North Fork of Fish Creek, Imperial County (Arnold, 1998). Many corals in the collection were accurately identified by Ann Budd (Professor of Invertebrate Paleontology of the University of Iowa), whose research includes previous work with the corals of the Imperial Group (Foster, 1979).

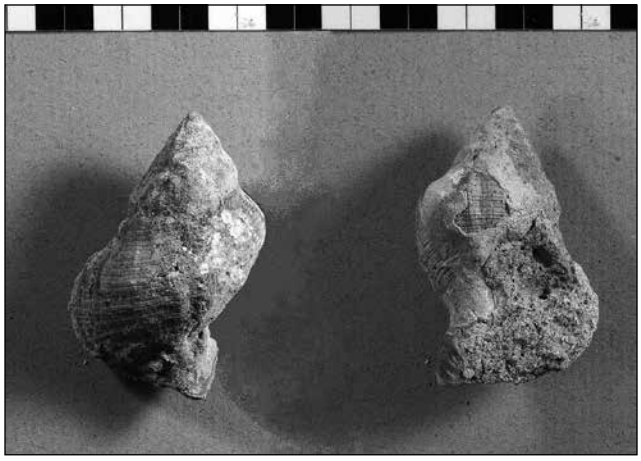

Figure 2-4. A possible new species of whelk, Family Buccinidae. The specimen figured is partly encrusted by a colony of the bryozoan *Biflustra commensale*. Photo by Hugh Vance.

Kidwell and Gyllenhaal (1998) described the paleobiology of bryozoan masses (bryoliths) of *Biflustra commensale* in Pliocene tidal channel deposits of the Deguynos Formation. These thick masses of bryozoans cover the valves of bivalves and a common undescribed buccinid whelk (Figure 2-4). This whelk has previously been tentatively named a

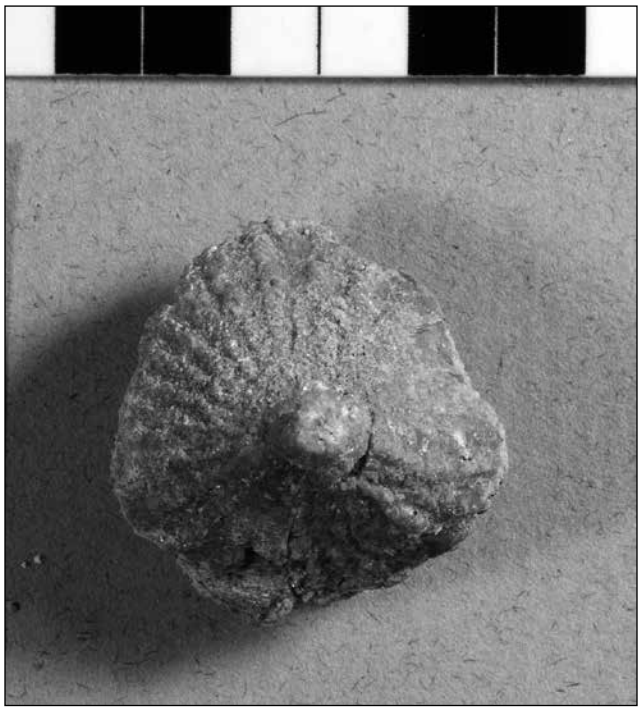

Figure 2-5. The cup-and-saucer snail, *Crucibulum* cf. *scutellatum*. This species is often found with the new buccinid (Figure 2-4) and commonly attached to other mollusk shells. Photo by Hugh Vance.

Table 1. Systematic list of fossil invertebrates in the Kidwell collection

Phylum Porifera
Class Demospongiae
Order Hadromerida
Family Clionaidae
Phylum Annelida
Class Polychaeta
Order Sabellida
Family Serpulidae
Phylum Bryozoa
Order Cheilostomata
Family Membraniporidae
Biflustra commensale
Phylum Cnidaria
Class Anthozoa
Order Scleractinia
Family Faviidae
Solenastrea fairbanksi
Family Meandrinidae
Dichocoenia eminens
Dichocoenia merriami
Eusmilia carrizensis
Meandrina bowersi
Family Pocilloporidae
Madracis sp
Family Poritidae
Porites carrizensis
Family Rhizangiidae
Astrangia haimei
Family Siderastreidae
Siderastrea mendenhalli
Phylum Mollusca
Class Bivalvia
Order Nuculoida
Family Nuculanidae
Nuculana sp
Family Nuculidae
Nucula sp
Order Arcoida
Family Arcidae
Anadara cf. *adamsi*
Anadara carrizoensis
Anadara concinna
Anadara formosa
Anadara cf. *multicostata*
Arca pacifica
Barbatia gradata
Barbatia reeveana
Family Glycymerididae
Glycymeris gigantea
Glycymeris multicostata
Order Mytiloida
Family Mytilidae
Lithophaga sp
Mytilus sp
Order Pterioida
Family Isognomonidae
Isognomon cf. *alatus*
Isognomon janus
Family Pinnidae
Atrina stephensi
Pinna latrania
Family Pteridae
Pteria sterna
Order Ostreoida
Family Gryphaeidae
Pycnodonte heermanni
Family Ostreidae
Dendostrea? *vespertina*
Myrakeena angelica
Family Pectinidae
Argopecten cf. *abietis abietis*
Argopecten bramkampi
Argopecten circularis
Argopecten deserti
Argopecten mendenhalli
Argopecten sverdrupi
Chlamys mediacostata
Euvola keepi
Flabellipecten carrizoensis
Leptopecten palmeri
Leptopecten tumbezensis
Lyropecten tiburonensis
Lindapecten corteziana
Order Pectinoida
Family Anomiidae
Anomia subcostata
Family Plicatulidae
Plicatula sp
Family Propeamussiidae
Amusium cf. *lompocensis*
Family Spondylidae
Spondylus bostrychites
Spondylus princeps
Order Carditoida
Family Carditidae
Carditamera affinis
Cardites laticostata
Cardites megastropha
Order Lucinoida
Family Lucinidae
Codakia distinguenda
cf. *Ctena* sp
Divalinga eburnea
Lucina undatoides
Lucinisca fenestrata
Miltha xantusi
Pegophysema edentuloides
Pegophysema species A
Pleurolucina leucocymoides
Order Myoida
Family Corbulidae
*Corbul*a sp
Family Hiatellidae
Panopea generosa
Panopea globosa
Family Pholadidae
Cyrtopleura costata
Family Teredinidae
Order Veneroida
Family Cardiidae
Americardia cf. *bianglulata*
cf. *Dinocardium* sp
Laevicardium sp
Papyridea sp
cf. *Trachycardium consors*
Family Chamidae
Arcinella californica
Chama sp
Pseudochama sp
Family Crassatellidae
Eucrassatella antillarum
Eucrassatella subgibbosa
Family Mactridae
*Raeta undulat*a
Rangia sp
Spisula cf. *dolabriformis*
Family Psammobidae
Gari sp
Family Semelidae
Semele cf. *rosea*
Family Solecurtidae
Tagelus affinis
Family Tellinidae
Macoma elytrum
cf. *Macoma grandis*
Psammotreta viridotincta
Psammotreta cognata
Psammotreta dombei
Tellina cumingii
Tellina ochracea
Tellina simulans
Family Veneridae
Callpita frizzelli
Chione cf. *mariae*
Chione cf. *subrugosa*
Dosinia sp
Globivenus isocardia
Megapitaria squalida
Periglypta multicostata
Pitar catharius
Pitar mexicanus
Pitar cf. *pollicaris*
Protothaca grata
Order Anomalodesmata
Family Pandoridae
Pandora sp
Family Thraciidae
Cyathodonta undulata
Class Gastropoda
Order Vestigastropoda
Family Trochidae
Family Turbinidae
cf. *Turbo* sp
Order Cycloneritimorpha
Family Nertidae
Nerita scabricosta
Order Neotaenioglossa
Family Bursidae
Bursa aff. *calcipicta*
Family Calyptraeidae
Crucibulum cf. *scutellatum*
Family Cassidae
Cassis subtuberosus
Family Cerithiidae
Family Cypraeidae
Muracypraea sp
Macrocypraea cervinetta
Family Ficidae
Ficus ventricosa
Family Hipponicidae
Hipponix sp
Family Naticidae
Polinices bifasciatus
Polinices uber
Polinices unifasciata
Sinum debile
Family Potamididae
Cerithidea sp
Family Strombidae
Strombus galeatus
Strombus gracilior
Strombus obliteratus
Family Tonnidae
Malea ringens
Family Triviidae
Trivia sanguinea
Family Turritellidae
Turritella imperialis.
Vermicularia sp
Family Vermetidae
Family Xenophoridae
Xenophora sp
Order Neogastropoda
Family Buccinidae
Antillophos sp
Cantharus sp
Gemophos aff. *ringens*
cf. *Northia* sp
new buccinid species
Family Cancellariidae
Cancellaria cf. *gemmulata*
Cancellaria obesa
Family Columbellidae
cf. *Anachis* sp
Mitrella sp
Family Conidae
Conus sp
Family Fasciolariidae
Fusinus dupetitthouarsii
cf. *Latirus* sp
Pleuroploca princeps
Family Melongenidae
Melongena patula
Family Mitridae
Mitra sp
Family Muricidae
cf. *Aspella cunninghami*
Ceratostoma sp
Eupleura muriciformis
Hexaplex sp
Thais sp
Family Nassariidae
Nassarius sp
Family Olividae
Agaronia testacea
Oliva incrassata
Oliva porphyria
Oliva cf. spicata
Family Pseudolividae
cf. *Macron* sp
Family Terebridae
Terebra gauspata
Family Turbinellidae
Vasum pufferi
Family Turridae
cf. *Knefastia* sp
Order Heterostropha
Family Architectonicidae
Architectonica nobilis
Order Cephalaspidea
Family Bullidae
Bulla cf. *gouldiana*
Bulla striata
Phylum Arthropoda
Class Malacostraca
Order Decapoda
Family Paguridae
Class Maxillopoda
Order Sessilia
Family Balanidae
Balanus sp
Megabalanus sp
Family Tetraclitidae
cf. *Tetraclita* sp
Family Pyrgomatidae
Ceratoconcha sp
Phylum Echinodermata
Class Echinoidea
Order Camarodonta
Family Toxopneustidae
Tripneustes californicus
Order Cidaroida
Family Cidaridae
Eucidaris thourarsii
Order Clypeasteroida
Family Clypeasteridae
cf. *Clypeaster bowersi*
Clypeaster cf. *deserti*
Family Echinoneidae
Family Mellitidae
Encope tenuis
Order Spatangoida
Family Brissidae
cf. *Meoma* sp
Family Loveniidae
aff. *Lovenia* sp
Family Schizasteridae
Schizaster morlini

species of *Solenosteira*, and is referred to here as "new buccinid species" (Table 1). It superficially resembles in form the fossil and modern genus *Searlesia*. It also resembles *Cymia heimi* in form and surface sculpture (see Smith, 1984), except it does not bear the strong knobs of this species. The whelk and encrusting bryozoan are associated in the collections with the ever familiar *Argopecten deserti*, *Anomia subcostata*, and *Dendostrea*? *vespertina*. Also common in these collections are the barnacle *Megabalanus*, the coral *Astrangia haimei*, and the cup-and-saucer snail, *Crucibulum* cf. *scutellatum* (Figure 2-5).

The Kidwell Collection has already provided material for research for the last two decades, and there is great promise that this diverse collection of invertebrates will continue to serve the scientific community as a valuable resource in the future.

Acknowledgements

I would like to first thank Dr. Susan Kidwell for returning the Imperial Group fossil invertebrates from her research at the University of Chicago back to the Colorado Desert from where they came so they may be cared for by the dedicated volunteers and staff of the SRC. I am very thankful to George Jefferson and Lyndon Murray for reviewing this manuscript and for their support and guidance during the identification work. Linda Gilbert and Lou Bahar's tireless work overseeing the entering of the species names into the collection database is greatly appreciated by me and many others. I am also very grateful to Hugh Vance for the excellent photography. I appreciate Astrid Boehringer's enthusiasm and confidence in my work. I am especially grateful to Myrl Beck and Ann Nourse for sharing their homes while I stayed in the desert. I greatly appreciate Mark Roeder encouraging me to write this paper. I want to give a heartfelt thanks to the Stout Foundation, and the ABDSP Society who funded my work on the Kidwell Collection. And I can't forget the many volunteers who helped me move trays and shared their enthusiasm for the project. Thank you all.

References

Arnold, T.S. 1998. *Muracypraea* Woodring, 1957 (Gastropoda: Cypraeidae) in the upper Miocene and lower Pliocene Latrania Formation (Imperial Group) of Imperial County, southern California. The Festivus. Vol. XXX(8) p. 89 - 93

Bahar, L. 2009. Volunteers bring invertebrate fossils home Tracks, Colorado Desert District Newsletter, November p. 14.

Dorsey, R.J., Housen, B.A., Janecke, S.U., Fanning, C.M., and Spears, A.L.F., 2011, Stratigraphic record of basin development within the San Andreas fault system: Late Cenozoic Fish Creek-Vallecito basin, southern California. Geol. Soc. America Bulletin, v. 123, p. 771-793.

Foster, A.B. 1979. Environmental variation in a fossil scleractinian coral. Lethaia. 12: 245-264

Hanna, G.D., 1926. Paleontology of Coyote Mountains, Imperial County, California. Proceedings California Academy of Sciences, Fourth Series, v. 14, p. 427–503.

Kidwell, S.M., and E.D. Gyllenhaal. 1998. Symbiosis, competition, and physical disturbance in the growth histories of Pliocene cheilostome bryoliths. Lethaia, Vol. 31 pp. 221-239.

Smith, J.T. 1984. Miocene and Pliocene marine molluscs and preliminary correlations, Vizcaino peninsula to Arroyo la Purisma, northwestern Baja California Sur, Mexico, in V.A. Frizzell, Jr., ed., Geology of the Baja California peninsula: Pacific Section, SEPM, v. 39, p. 197-217.

Digitizing ichnotypes from the Cenozoic of the southwestern United States at the Raymond M. Alf Museum of Paleontology

Tristan T. Duque,[1] Stephanie J. Rapoport,[1] and Andrew A. Farke[2]

[1]The Webb Schools, 1175 West Baseline Road, Claremont, CA 91711; [2]Raymond M. Alf Museum of Paleontology, 1175 West Baseline Road, Claremont, CA 91711

Introduction

Illustration is a challenging yet essential aspect of any paleontological description. Distortion, color variation, damage, matrix, and specimen mounts all present obstacles in clearly communicating morphology. Visual depictions of fossil footprints have additional complications. The complex interaction between the foot of the trackmaker and the substrate means that the boundaries between what is the "print" portion of a specimen and the "matrix" are fuzzy indeed. This introduces complications when trying to address ichnotaxonomy, compare specimens, and evaluate track-making processes.

Traditional methods of illustrating footprints include photographs, line drawings, or more complex drawings (e.g., stippling, shading). Photographs can best show the specimen itself, but color variation across a slab makes interpretation of morphology difficult. Additionally, the importance of three-dimensional morphology means that inconsistencies in lighting during photography can make it difficult to interpret the morphology. Line drawings are easy to produce and not subject to the problems of lighting, but require a heavy degree of subjectivity, particularly when the boundaries of an individual print are unclear. Other modes of illustration, such as stippled drawings, overcome many of the disadvantages of other imaging methods, but are time-consuming to produce and require specialized skill.

Three-dimensional (3D) digital imaging techniques afford another tool to quickly, cheaply, and accurately illustrate complex ichnological specimens. Photogrammetry, which reconstructs 3D objects from two-dimensional images, and laser scanning, which directly produces a 3D model using a specialized scanner, are both increasingly used to image footprints. Both can produce accurate shaded renderings, combining the best characteristics of photography and drawing. Features that are poorly visible in photographs (or even the original specimen) are often clearly defined on the digital model, when color information is excluded.

Here, we apply 3D digital imaging techniques to selected ichnotypes from the Raymond M. Alf Museum of Paleontology. Many of these specimens have been illustrated previously with photographs and line-drawings, but are here re-illustrated using recently developed techniques. This paper is intended as an in-progress atlas to supplement previous descriptions.

The Alf Museum collection

Unlike any other museum in the world, The Raymond M. Alf Museum of Paleontology (RAM, Claremont, California) involves high school students in all aspects of professional paleontological research. In fact, 95 percent of the museum's nearly 150,000 specimens were discovered by students, teachers, and alumni from The Webb Schools. Since the start of a fossil collection by Webb biology teacher Raymond M. Alf in 1936, the museum has enjoyed a vigorous research program.

Ichnofossils, including over 800 specimens from the Coconino, Moenkopi, Moenave, Wasatch, Barstow, Avawatz, Tecopa, and Muddy Creek formations, among others, form an important component of the Alf Museum collection (Lofgren et al., 2006.) Twenty-two holotype, syntype or paratype specimens representing 14 ichnotaxa, including invertebrates, vertebrates, mammals, and reptiles are housed at RAM (Lofgren et al., 2006.) They have formed the core of a number of ichnological studies

(e.g., Lucas and Hunt, 2007; Sarjeant et al., 2002; Sarjeant and Reynolds, 1999, 2001).

After renovation of the museum's exhibit halls in 2011, a new project was launched, using photogrammetry and laser scanning to create three-dimensional, digital models of many of the ichnofossils within the museum collection. This ongoing work will allow scientists and the public better access to the museum's collection and create a duplicate for long-term conservation.

Methods

Using a Nikon D90 camera with a Tamron AF PROMASTER 62 mm lens, each specimen was photographed from various angles. The number of photographs varied depending upon the specimen. Point clouds were reconstructed using photogrammetry, implemented in BundlerTools (https://server.topoi.hu-berlin.de/groups/bundlertools/), a software package incorporating Bundler, CMVS, and PNVS2. After point clouds were imported into MeshLab, a surface reconstruction was created using a poisson algorithm, with an octree depth of 9 and a solver divide of 8. In order to image the surface meshes, the render mode was changed to smooth and digital lighting was set to illuminate the specimen from the upper left.

Imaged ichnotypes

Alaripeda bristolia (Reynolds, 2012)

Figure 1

Ichnotype.—RAM 14740, slab with three pedal prints in relief.

Locality.—RAM V201208, San Bernardino County, California

Age and Horizon. Early Pliocene, Bouse Formation.

Presumed track maker.—Neornithes (bird); similar to tracks produced by least sandpipers (Reynolds, 2012).

Anatipeda alfi (Sarjeant and Reynolds, 2001)

Figure 2

Ichnotype.—RAM 111, slab with three pedal prints in relief.

Locality.—RAM V94135, San Bernardino County, California

Age and Horizon.—Clarendonian, Miocene, Avawatz Formation.

Presumed track maker.—Neornithes (bird); potentially an anseriform, phoenicopteriform, or pelecaniform (Sarjeant and Reynolds, 2001).

Anatipeda californica (Sarjeant and Reynolds, 2001)

Figure 3

Ichnotype.—RAM 115, slab with one track in relief.

Locality.—RAM V94135, San Bernardino County, California

Age and Horizon.—Clarendonian, Miocene, Avawatz Formation.

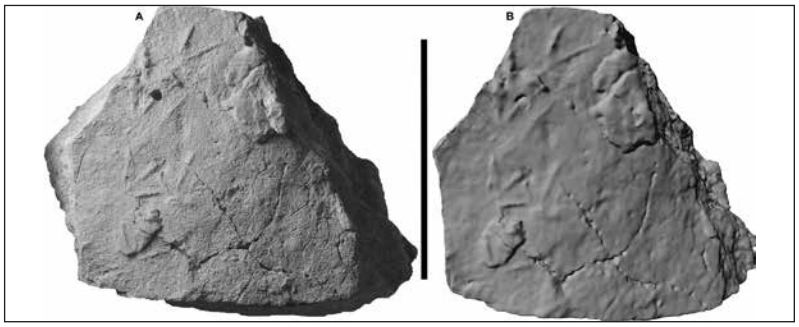

Figure 1. Photograph (A) and digital surface reconstruction (B) of RAM 14740, the ichnotype for *Aleripeda bristolia*. Scale bar = 10 cm.

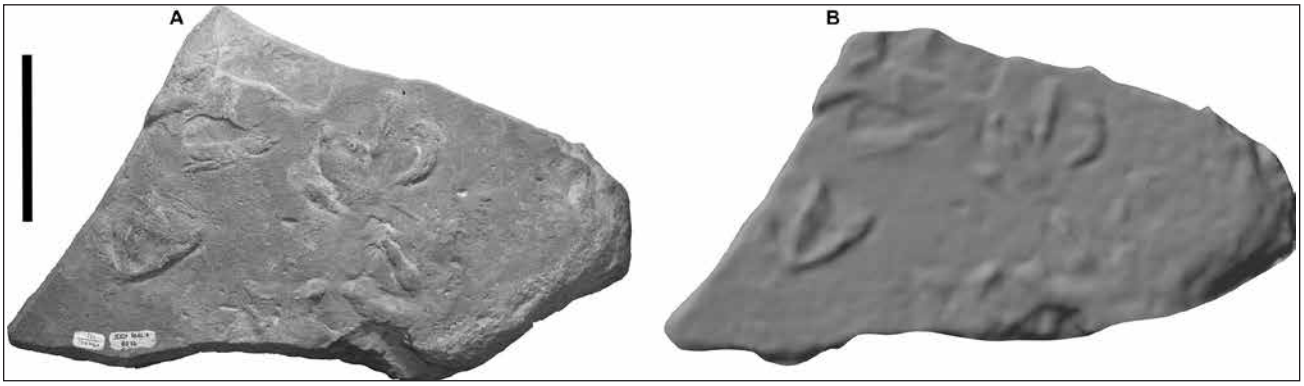

Figure 2. Photograph (A) and digital surface reconstruction (B) of RAM 111, the ichnotype for *Anatipeda alfi*. Scale bar = 10 cm.

Presumed track maker.—Neornithes (bird); potentially an anseriform, phoenicopteriform, or pelecaniform (Sarjeant and Reynolds, 2001).

Avipeda gryponyx (Sarjeant and Reynolds, 2001)

Figure 4

Ichnotype.—RAM 110, slab with at least seven pedal prints in relief.

Locality.—RAM V94021, San Bernardino County, California

Age and Horizon.—Clarendonian, Miocene, Avawatz Formation.

Presumed track maker.—Neornithes (bird), perhaps "small wading birds" (Sarjeant and Reynolds, 2001:25).

Dizygopodium dorydium (Sarjeant, 1999)

Figure 5

Ichnotype.—RAM 209, slab with two tracks. The better preserved of the two was designated as the lectotype (Lucas and Hunt, 2007).

Locality.— RAM V94021, San Bernardino County, California.

Age and Horizon.—Clarendonian, Miocene, Avawatz Formation.

Presumed track maker.—Camelidae.

Comments.—Sarjeant and Reynolds (1999) designated RAM 197 and 209 as syntypes, and Lucas and Hunt (2007) assigned a single print from RAM 209 as the lectotype. *Dizygopodium dorydium* was considered a junior synonym of *Lamaichnum guanicoe* by Lucas and Hunt (2007).

Dizygopodium quadracordatum (Sarjeant and Reynolds, 1999)

Figure 6

Ichnotype.—RAM 216, track (impression).

Locality.—RAM V94134, San Bernardino County, California

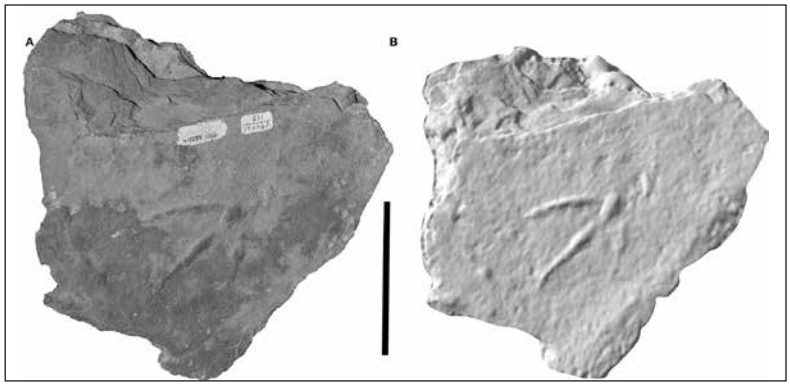

Figure 3 Photograph (A) and digital surface reconstruction (B) of RAM 115, the ichnotype for *Anatipeda californica*. Scale bar = 10 cm.

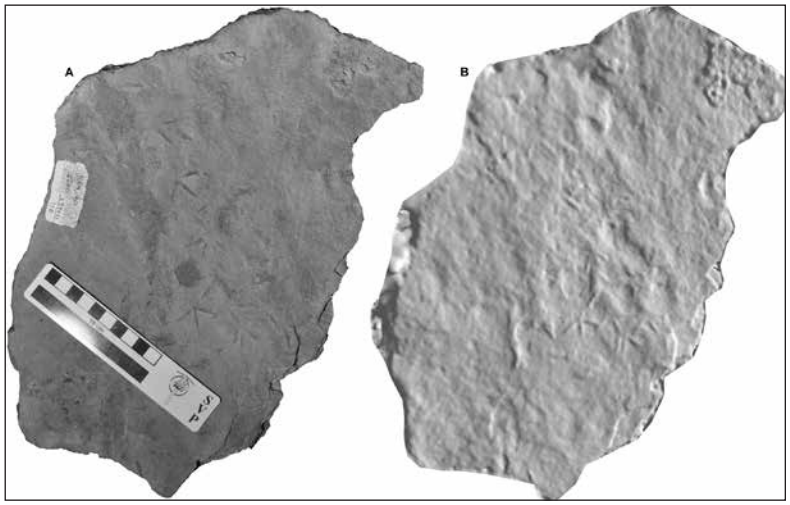

Figure 4. Photograph (A) and digital surface reconstruction (B) of RAM 110, the ichnotype for *Avipeda gryponyx*. Scale bar = 10 cm.

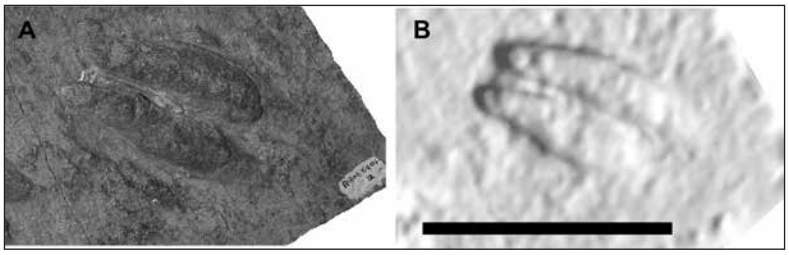

Figure 5. Photograph (A) and digital surface reconstruction (B) of RAM 209, the lectotype for *Dizygopodium dorydium*. Scale bar = 10 cm.

Age and Horizon.—Clarendonian, Miocene, Avawatz Formation.

Presumed track maker.—Camelidae

Comments.—Sarjeant and Reynolds (1999) designated a slab containing multiple prints, RAM 185, as the syntype for *D. quadracordatum*. Based on the figures from that paper, this is in fact RAM 216. A single print from the specimen was later designated as the lectotype, and the taxon synonymized with *Lamaichnum guanicoe* (Lucas and Hunt, 2007).

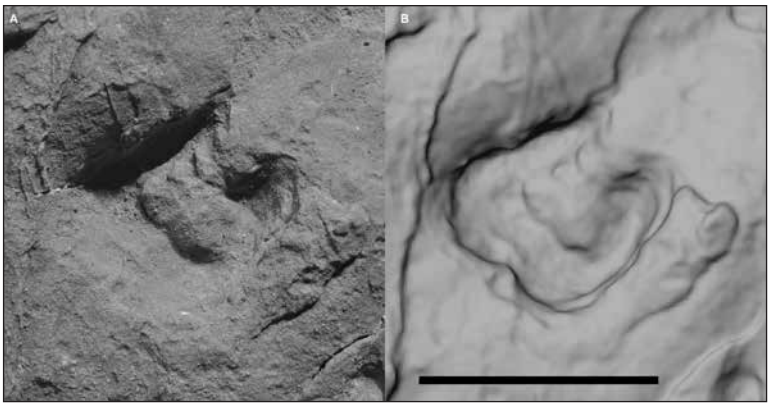

Figure 6. Photograph (A) and digital surface reconstruction (B) of RAM 216, the lectotype for *Dizygopodium quadracordatum*. Scale bar = 10 cm.

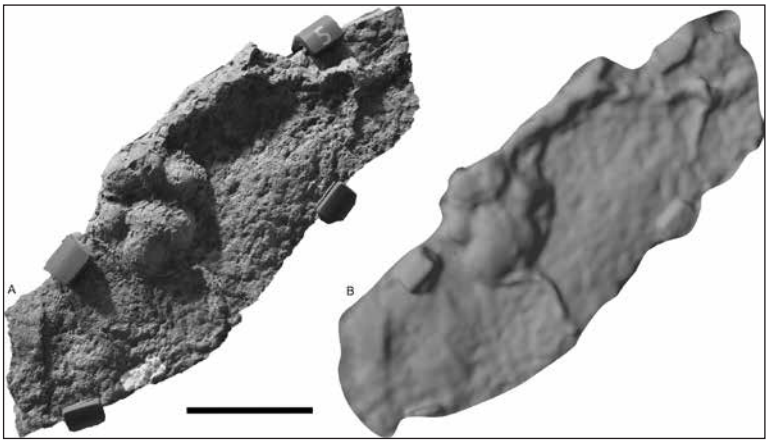

Figure 7. Photograph (A) and digital surface reconstruction (B) of RAM 103, the ichnotype for *Felipeda bottjeri*. Scale bar = 10 cm.

Felipeda bottjeri (Sarjeant et al., 2002)

Figure 7

Ichnotype.—RAM 103, slab with one track.

Locality.—RAM V201103, San Bernardino County, California

Age and Horizon.—Barstovian, Miocene, Barstow Formation.

Presumed track maker.—Felidae.

Hirpexipes alfi (Sarjeant, 2002)

Figure 8

Ichnotype.—RAM 100, slab with trackway of a single animal.

Locality.—RAM V94272, San Bernardino County, California

Age and Horizon.—Barstovian, Miocene, Barstow Formation.

Presumed track maker.—Amphicyonidae (bear-dog).

Comments.—Due to the difficulty of digitizing the entire trackway for this specimen, only a single pair of tracks are figured here (one pedal and one manual track).

Lamaichnum alfi (Sarjeant and Reynolds, 1999)

Figure 9

Ichnotype.—RAM 159, slab with one track (cast of right pedal print).

Locality.—RAM V94276, Barstow, San Bernardino County, California

Age and Horizon.—Miocene, Barstow Formation.

Presumed track maker.—Camelidae.

Comments.—Sarjeant and Reynolds (1999) designated RAM 159 and 182 as syntypes, and Lucas and Hunt (2007) assigned RAM 159 as the lectotype. *Lamaichnum alfi* was considered a junior synonym of *L. guanicoe* by Lucas and Hunt (2007).

Lamaichnum macropodum (Sarjeant and Reynolds, 1999)

Figure 10

Ichnotype.—RAM 165, slab with one track (natural cast of right pes).

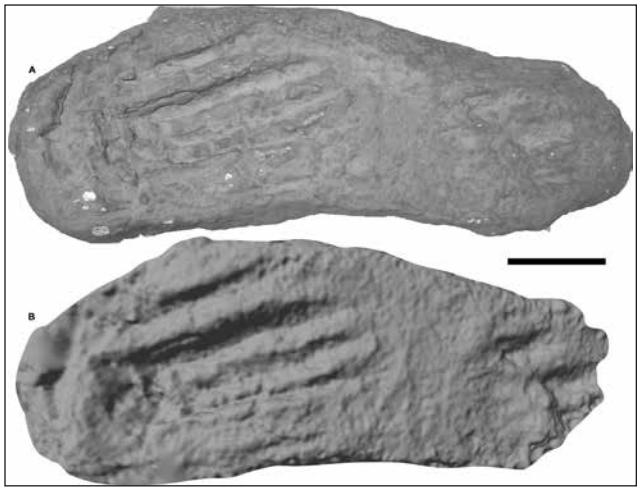

Figure 8. Photograph (A) and digital surface reconstruction (B) of RAM 100, one pair of tracks from the ichnotype for *Hirpexipes alfi*. Scale bar = 10 cm.

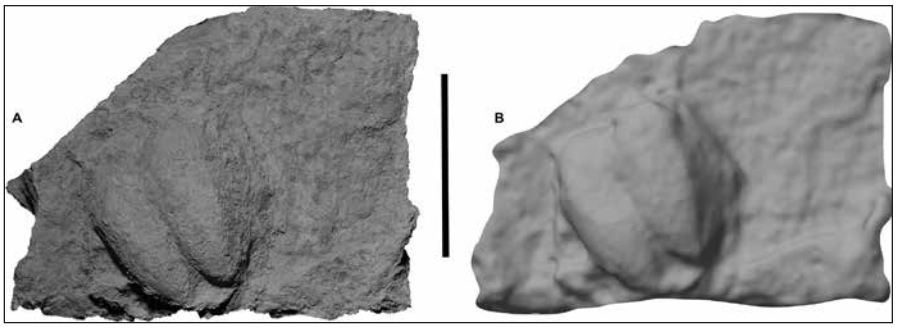

Figure 9. Photograph (A) and digital surface reconstruction (B) of RAM 159, the lectotype for *Lamaichnum alfi*. Scale bar = 10 cm.

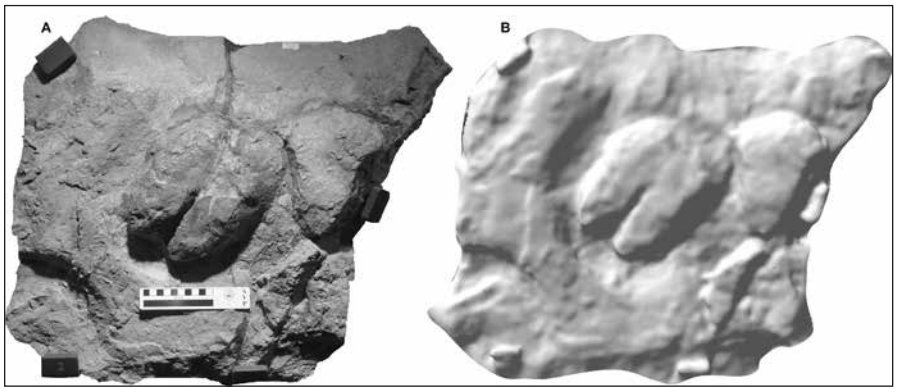

Figure 10. Photograph (A) and digital surface reconstruction (B) of RAM 165, the lectotype for *Lamaichnum macropodum*. Scale bar =10 cm.

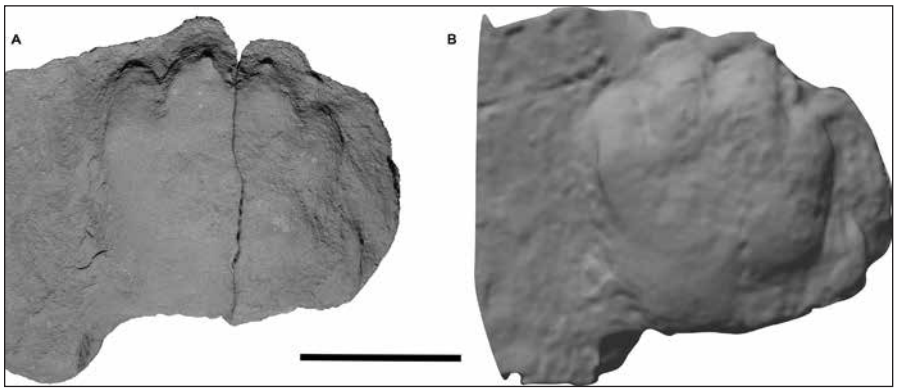

Figure 11. Photograph (A) and digital surface reconstruction (B) of RAM 277, the lectotype for *Platykopus ilyacalcator*. Scale bar = 10 cm.

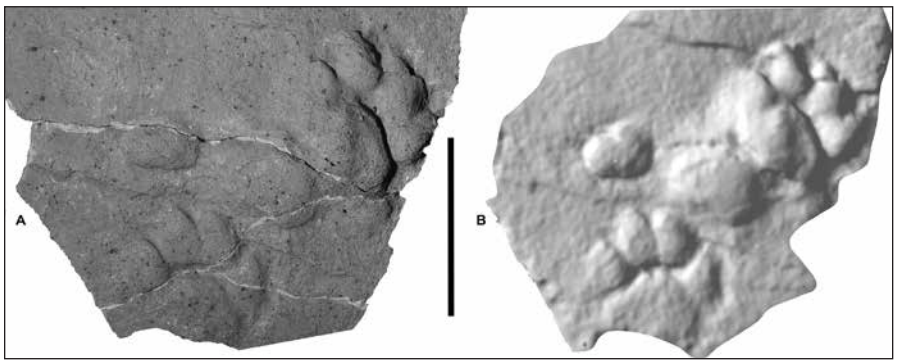

Figure 12. Photograph (A) and digital surface reconstruction (B) of RAM 205, the lectotype for *Pycnodactylopus achras*. Scale bar = 10 cm.

Locality.—RAM V94215, Sperry Wash, San Bernardino County, California.

Age and Horizon.—Miocene, Tecopa Formation

Presumed track maker.—Camelidae.

Comments.—Sarjeant and Reynolds (1999) designated syntypes for *L. macropodum* (RAM 146 and 167). Based on the published figures, Lucas and Hunt (2007) noted that the RAM 167 is in fact numbered as RAM 165 in the official museum collection. This specimen was thus identified as the lectotype, a decision that is followed here.

Platykopus ilyacalcator (Sarjeant et al., 2002)

Figure 11

Ichnotype.—RAM 277, slab with one track (natural cast of manual track).

Locality.—RAM V94163, Clark County, Nevada

Age and Horizon.—Hemphillian, Miocene, Muddy Creek Formation

Presumed track maker.—Ursidae (bear).

Pycnodactylopus achras (Sarjeant et al., 2002)

Figure 12

Ichnotype.—RAM 205, slab with two tracks in relief (presumably one pedal and one manual).

Locality.—RAM V94134, San Bernardino County, California

Age and Horizon.—Clarendonian, Miocene, Avawatz Formation.

Presumed track maker.—Felidae (cat).

Acknowledgments

Student research at the Alf Museum is supported by the Mary Stuart Rogers Foundation and the David B. Jones Foundation. The fossils figured here originated on federal lands over decades of collecting, and the United States Bureau of Land Management–California is gratefully acknowledged for assistance with permitting and logistics.

References cited

Lofgren, D.L., J.A. Greening, C.F. Johnson, S.J. Lewis, and M.A. Torres. 2006. Fossil tracks at the Raymond Alf Museum of Paleontology and management of tracks on public lands. New Mexico Museum of Natural History and Science Bulletin 34:109–118.

Lucas S.G., and A.P. Hunt. 2007. Ichnotaxonomy of camel footprints. Bulletin of the New Mexico Museum of Natural History and Science 42:155–168.

Reynolds, R.E. 2012. Ichnites in the Bouse Formation, Amboy, San Bernardino County, California, in Reynolds, R.E. (ed.), Search for the Pliocene: The Southern Exposures. Fullerton, California: California State University Desert Studies Consortium. p. 136–139.

Sadler, J.C. 1993. Arthropod trace fossils from the Permian De Chelly Sandstone, northeastern Arizona. Journal of Paleontology. 67:240–249.

Sarjeant, W.A.S., and R.E. Reynolds. 1999. Camel and horse footprints from the Miocene of California. San Bernadino County Museum Association Quarterly 46(2):3–19.

Sarjeant,W.A.S., and R.E. Reynolds. 2001. Bird footprints from the Miocene of California, in Reynolds, R.E. (ed.),. The Changing Face of the East Mojave Desert. California. Fullerton, California: California State University Desert Studies Consortium. p. 21–40.

Sarjeant, W.A.S., R.E. Reynolds, and M.M. Kissell-Jones. 2002. Fossil creodont and carnivore footprints from California, Nevada, and Wyoming, in Reynolds, R.E. (ed.), Between the Basins: Exploring the Western Mojave and Southern Basin and Range Province. Fullerton, California: California State University Desert Studies Consortium. p. 37–50.

Tortoises from the Middle Miocene Barstow Formation of California

Don Lofgren[1] and Rachel Choi[2]

[1]*Raymond M. Alf Museum of Paleontology, Claremont, CA 91711;* [2]*The Webb Schools, Claremont, CA 91711*

Introduction

Fossil tortoises from the Barstow Formation contribute to our understanding of North American tortoise evolution during the Miocene. The first tortoise described from the Barstow Formation was designated the new species, *Testudo mohavense* (holotype UCMP 21575) (Merriam, 1919). Later, *Testudo mohavense* was referred to *Gopherus mohavense* and a specimen of *Testudo mohavense* (UCMP 21574) was designated as the holotype of *Testudo milleri* (Brattstrom, 1961). Des Lauriers (1965) provided a summary of Barstovian aged tortoises of Southern California including *Testudo milleri* and *Gopherus mohavense* and also noted that the name *mohavense* does not agree grammatically with *Gopherus* and changed *Gopherus mohavense* to *Gopherus* "*mohavetus*" without further discussion (Des Lauriers, 1965: 8).

Bramble (1982) proposed a new genus, *Scaptochelys* (a junior synonym of *Xerobates*) for some gopher tortoises, including *Gopherus mohavense*, and synonymized *Testudo milleri* with *Gopherus mohavense* (*G. mohavense* having priority). Bramble (1982) did not follow the suggestion of Des Lauriers (1965) to change *Gopherus mohavense* to *Gopherus* "*mohavetus.*" Crumly (1992) examined phylogenetic relationships among North American gopher tortoises and determined that many characters Bramble (1982) used in establishing *Xerobates* ("*Scaptochelys*") were plesiomorphies and that DNA analysis of gopher tortoises did not support a monophyletic *Xerobates*, indicating gopher tortoises should be recognized as G*opherus*. The phylogenetic analysis of Reynoso and Montellano-Ballesteros (2004) indicated that *Gopherus* is monophyletic and that *G.* "*mohavetus*" falls outside the clade *Gopherus*. A more recent phylogenetic analysis of gopher tortoises indicates that *Gopherus* and *Xerobates* are sister taxa and that *Gopherus* "*mohavetus*" is likely to be within *Xerobates* based on cervical vertebrae (Jones, 2008).

The tortoise collection from the Barstow Formation housed at Raymond M. Alf Museum of Paleontology consists of the remains of fourteen individuals that range from complete shells with post-cranial elements, to an isolated carapace or plastron fragment. These specimens are briefly described here and include the only well-preserved postcranial remains known of Barstow Formation tortoises. Also, a complete list of all reported tortoise specimens from the Barstow Formation is provided. All of these fossils are considered to represent *Gopherus mohavense* until a consensus is reached concerning the taxonomy of Barstow Formation tortoises.

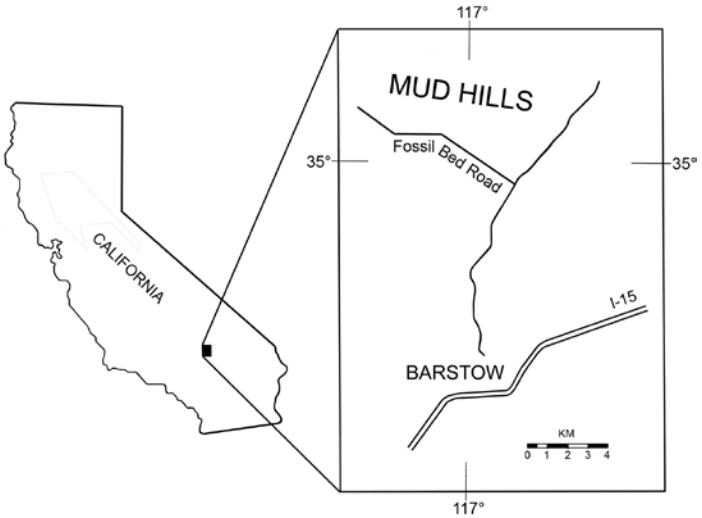

Figure 1. Location of the Barstow Formation within the Mud Hills, Mojave Desert, California (adapted from Steinen, 1966).

Institutional Abbreviations—AMNH, American Museum of Natural History, New York, New York; **CIT**, California Institute of Technology, Pasadena, California (specimens now housed at the LACM); **LACM**, Los Angeles County Museum, Los Angeles, California; **RAM**, Raymond M. Alf Museum of Paleontology, Claremont, California; **UCMP**, University of California Museum of Paleontology, Berkeley, California; **USGS**, United States

Geological Survey, Menlo Park, California; **Other Abbreviations**— **Ba1**, Barstovian Biochron 1; **Ba2**, Barstovian Biochron 2; **NALMA**, North American Land Mammal Age.

Stratigraphic setting

The Barstow Formation crops out in the Mud Hills, about 15 km north of Barstow, California (Figure 1), and consists of about 1,000 m of fluvial and lacustrine sediments, and air-fall tuffs, deposited in an inlan non-marine basin during the middle Miocene (Woodburne et al., 1990). Detailed lithostratigraphic and biostratigraphic treatments of the Barstow Formation are provided by Woodburne et al. (1990), and Pagnac (2005, 2009).

RAM crews, initially led by museum founder Raymond Alf, began collecting in the Barstow Formation in 1936 (Lofgren and Anand, 2010) and still do today. Surprisingly, tortoises in the RAM collections were all collected after 1990. These remains are from two localities in the Middle Member and three in the unnamed upper member of the formation. Middle Member sites, V94177 and V94138, are located above the Oreodont Tuff, but far below the Skyline Tuff (Figure 2). Upper member sites, V98004, V200025, and V200047 are below the *Hemicyon* Tuff, but only V98004 can be precisely correlated to this distinct marker bed. Strata that contain V98004 are stratigraphically equivalent to those of Easter Quarry (Frick AMNH site), and both sites are about 30 m below the *Hemicyon* Tuff (Lofgren et al. 2012). The majority of the tortoise remains in the RAM collections are from V98004, a site that also yielded the holotype of *Megahippus mckennai* (a partial skull, RAM 910) described by Tedford and Alf (1962), and an upper molar of *Gomphotherium* (RAM 10362), which represents the oldest record of Gomphotheridae from the Barstow Formation (Lofgren et al., 2012). Also, at V98004 is a 5 cm thick lens of siltstone (whose lateral extent is about 2 m) that contains a concentration of well-preserved and mostly isolated elements of small mammals and birds. Preliminary excavation of this lens indicates that it preserves a rich microvertebrate fauna with a high percentage of avian elements. Excavation of this fossil rich lens has yet to be initiated.

RAM locality V200025 is a few meters below the "Lake Bed" (UCMP locality V5253) of Lindsay (1972), in an area he termed Bird Canyon. As correlated

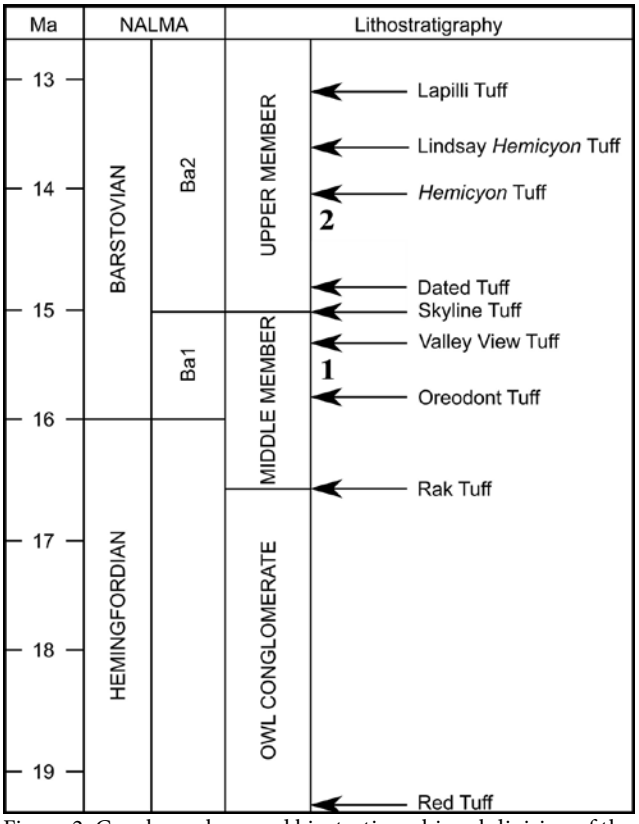

Figure 2. Geochronology and biostratigraphic subdivision of the Barstow Formation (adapted from Pagnac, 2009). Approximate stratigraphic position of RAM sites yielding tortoises in the Middle Member (1) and unnamed upper member (2) denoted by numbers.

by Lindsay (1972; figure 2), UCMP locality V5253 is about 35 meters below the *Hemicyon* Tuff. Thus, RAM locality V200025 would be slightly older. RAM locality V200047 is also located in Bird Canyon and is a few meters below V200025.

The two RAM sites that yield tortoise remains from the Middle Member are early Barstovian (Ba1) or about 15-16 myo and those from the unnamed upper member are late Barstovian (Ba2) or 14-15 myo based on the biostratigraphic and geochronologic correlations of Woodburne et al. (1990), Tedford et al. (2004), and Pagnac (2009).

Tortoises in the RAM collections

Middle Member

Tortoise remains are rarely found in the Middle Member of the Barstow Formation. Only two are present in the RAM collections after years of intensive prospecting. RAM 15447 is a carapace or plastron fragment found in 2012 from RAM locality V94177 (equals Frick AMNH site Sunder Ridge Quarry). RAM 7608 is a partial shell with much of its

Figure 3. Shell of RAM 7148 from locality V98004. A) dorsal view showing carapace ; B) ventral view showing plastron. Scale in cm.

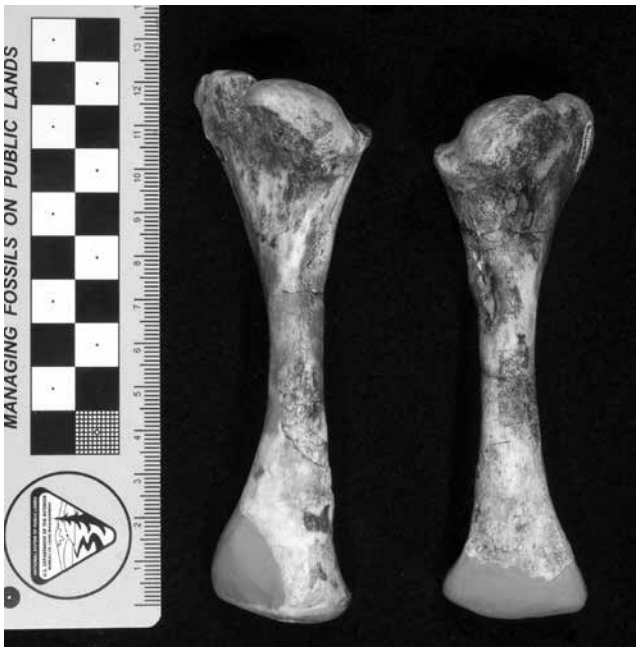

Figure 4. Left and right humerus of RAM 7148. Scale in cm.

Figure 5. Left and right pubis of RAM 7148. Scale in cm.

carapace missing, found in a conglomeratic sandstone exposed on the bank of a narrow wash (RAM locality V94138). The plastron of RAM 7608 is still partially encased in rock, but appears to be mostly intact. RAM 7608 is approximately 37 cm in width and has a minimum length of 38 cm.

Unnamed Upper Member

In comparison to the Middle Member, tortoise remains are more common in the unnamed upper member and are relatively abundant at V98004. Nine of ten specimens from this site are fragmentary; peripheral II fragment (RAM 203), four shell fragments (RAM 204), a carapace fragment (RAM 7622), a xiphiplastron? fragment (RAM 7623), a peripheral fragment (RAM 16167), a carapace fragment (RAM 16168), sixty-seven carapace fragments and a broken scapula (RAM 16169), a limb and shell fragment (RAM 16170), and twenty carapace fragments

Figure 6. Shell of RAM 7624 from locality V200025. A) dorsal view showing carapace ; B) ventral view showing plastron. Scale in cm.

(RAM 16189). The other specimen, RAM 7148, is a uncrushed shell (figures 3A and 3B) that is 45 cm in length and 39 cm in width, with associated pectoral girdle with left and right scapula and coracoid, left and right humerus (figure 4), right ulna, left and right pubis (figure 5) and ilium, three cervical vertebrae, six unidentified fragmentary limb or girdle elements, two phalanges, and nine phalange/podial elements. RAM 7148 is the only tortoise from the Barstow Formation that includes well preserved postcranial remains in addition to the carapace and plastron.

RAM 7624 is a nearly complete but slightly crushed shell (figures 6A and 6B), about 32 cm in length and 23 cm in width (carapace/plastron distorted from crushing), with a few limb fragments from RAM locality V200025. RAM 16190 is a small isolated neural from RAM locality V200047.

Barstow Formation tortoises housed at other institutions

These specimens are listed by institution. Merriam (1919) described the UCMP specimens and Brattstrom (1961) the CIT, LACM and USGS specimens (if an illustration was published, the source is noted). A digital search of the AMNH collections indicates that no cataloged tortoise remains are present even though crews hired by Childs Frick collected extensively throughout the Barstow Formation during the first half of the twentieth century.

LACM and CIT (CIT specimens now housed at the LACM)

CIT 494/5131: fragments of plastron, carapace and pectoral girdle

CIT 303/5132: anterior and posterior parts of a plastron

CIT 494/5129: anterior half of shell (Brattstrom, 1961; figures 5 and 6)

CIT 495/5130: complete shell with crushed carapace missing its central portion

LACM A1420: mold of shell with bones of plastron

USGS

USGS 473: shell fragments with endoplastron

UCMP

UCMP 21575: nearly complete plastron and carapace (Merriam, 1919; figures 4a and 4b); holotype of *Gopherus mohavense*.

UCMP 21573: partial plastron with epiplastron and entoplastron (Merriam, 1919; figures 6a and 6b)

UCMP 21574: carapace and plastron (Merriam, 1919; figures 5a and 5b)

Note: the sample of *Testudo mohavense* described by Merriam (1919) consisted of the holotype (UCMP 21575) and two other specimens (UCMP 21574 and UCMP 21573). Later, Brattstrom (1961) referred *Testudo mohavense* to *Gopherus mohavense* and UCMP 21574 was designated as the holotype of

Testudo milleri. Additional specimens referred to *Gopherus mohavense* were CIT 494/5131, USGS 473, and LACM A1420 (Brattstrom, 1961). Additional specimens referred to "*Testudo milleri*" were CIT 494/5129 and CIT 495/5130, with UCMP 21573 being too fragmentary to identify to genus (Brattstrom, 1961).

Conclusions

Tortoise specimens are not abundant in the Barstow Formation but are often found in the unnamed upper member. The first report of Barstow tortoises was by Merriam (1919) and a few decades later Brattstrom (1961) described six additional specimens. Tortoises housed at the RAM were all collected since 1990, with most remains recovered from a single site (V98004) in the unnamed upper member, about 30 m below the *Hemicyon* Tuff. Specimens from V98004 include the only well-preserved postcranial remains of tortoises reported from the Barstow Formation. Tortoises from the Barstow Formation have been referred to *Testudo*, *Gopherus, Scaptochelys*, and *Xerobates* (Merriam, 1919; Brattstrom, 1961; Bramble,1982; Crumly, 1992; Jones, 2008). Until a consensus on their taxonomy has been reached, we refer all Barstow Formation to *Gopherus mohavense*.

Acknowledgements

We thank J. Shearer of the California BLM for assistance with permits, J. H. Hutchison for helpful discussions, L. Gluckstein for photos, P. Kloess for assistance with figures, and the Mary Stuart Rogers Foundation and the David B. Jones Foundation for financial support.

References

Bramble, D.M., 1982. *Scaptochelys*: Generic Revision and Evolution of Gopher Tortoises. Copeia 1982:852-867.

Brattstrom, B.H., 1961. Some New Fossil Tortoises from Western North America with Remarks on the Zoogeography and Paleoecology of Tortoises. Journal of Paleontology 35:543-560.

Crumly, C.R., 1992. Phylogenetic Systematics of North American Tortoises (genus *Gopherus*): Evidence For Their Classification. US Department of the Interior, National Biological Survey, Washington D.C., Fish and Wildlife Research 13:7-32.

Des Lauriers, J.R., 1965. A New Miocene Tortoise from Southern California. Bulletin of the Southern California Academy of Sciences 64:1-10.

Jones, C.B., 2008. Systematic Review of Gopher Tortoises. Master's Thesis, San Diego State University 1-103.

Lindsay, E. H., 1972. Small mammal fossils from the Barstow Formation, California. University of California Publications in Geological Sciences 93:1-104.

Lofgren, D. L., and R. S. Anand, 2010. 75 years of fieldwork in the Barstow Formation by the Raymond Alf Museum of Paleontology. Pp. 169-176, in Reynolds, R. E. and D. M. Miller (eds.), Overboard in the Mojave, 20 million years of lakes and wetlands. Desert Studies Consortium.

Lofgren, D. L., Pagnac D., Hess, A., Liskanich, P. and D. Silver, 2012. Review of proboscideans from the Middle Miocene Barstow Formation of California. Pp. 125-134, in Reynolds, R. E. (ed.), Search for the Pliocene: the southern exposures. California State University Desert Studies Consortium.

Merriam, J. C., 1919. Tertiary mammalian faunas of the Mohave Desert. University of California Publications in Geological Sciences 11:437a-437e, 438-585.

Pagnac, D. C., 2005. A systematic review of the mammalian megafauna of the middle Miocene Barstow Formation, Mojave Desert, California (PhD dissertation). University of California-Riverside. 384 pp.

Pagnac, D. C., 2009. Revised large mammal biostratigraphy and biochronology of the Barstow Formation (Middle Miocene), California. Paleobios 29:48-59.

Reynoso, V.H., M. Montellano-Ballesteros, 2004. A New Giant Turtle of the Genus *Gopherus* (Chelonia: Testudinidae) from the Pleistocene of Tamaulipas, Mexico, and a Review of the Phylogeny and Biogeography of Gopher Tortoises. Journal of Vertebrate Paleontology 24:822-837

Steinen, R. P., 1966. Stratigraphy of the middle and upper Miocene, Barstow Formation, California. (m.s. thesis): University of California-Riverside, 150 pp.

Tedford, R. H., and R. M. Alf, 1962. A new *Megahippus* from the Barstow Formation San Bernardino County, California. Bulletin of the Southern California Academy of Sciences 61:113-122.

Tedford, R. H., Albright III, L. B., Barnosky, A. D., Ferrusquia-Villafranca, I., Hunt Jr., R. M., Storer, J. S., Swisher III, C. C., Voorhies, M. R., Webb S. D., and D. P. Whistler, 2004. Mammalian biochronology of the Arikareean through Hemphillian interval (late Oligocene through early Pliocene epochs). Pp. 169-231, in M. O Woodburne (ed.), Late Cretaceous and Cenozoic mammals of North America. Columbia University Press, New York.

Woodburne, M. O., Tedford, R. H. and C. C. Swisher III, 1990. Lithostratigraphy, biostratigraphy, and geochronology of the Barstow Formation, Mojave Desert, southern California. Geological Society of America Bulletin 102:459-477.

Preliminary analysis of an important vertebrate-bearing horizon with abundant avian material from the upper member of the Barstow Formation of California

Donald Lofgren[1], Christopher Kwon[2], Jake Todd[2], Skyler Marquez[2], Adam Holliday[2], Robert Stoddard[2], and Peter Kloess[1, 3]

[1]Raymond M. Alf Museum of Paleontology, Claremont, California; [2]The Webb Schools, Claremont, California; [3]California State University-Fullerton, Fullerton, California.

Introduction

The Middle Miocene Barstow Formation is well exposed throughout the Mud Hills, about 12 km north of Barstow, California (Figure 1). Miocene vertebrate fossils were first reported from the area by Merriam (1911) from the University of California based on fossils brought to him by one of his students. Shortly thereafter, University of California crews were sent to the Mud Hills to make further collections and these fossils were described a few years later (Merriam, 1919). Frick Laboratory crews, financed by Childs Frick, collected extensively in the Barstow Formation from 1923 through 1939, and then in the early 1950s; these fossils are now housed at the American Museum of Natural History (AMNH) in New York. Other than the AMNH, museums that currently house significant collections from the Barstow Formation include the University of California Museum of Paleontology, Natural History Museum of Los Angeles County, San Bernardino County Museum, and the Raymond M. Alf Museum of Paleontology (RAM).

Raymond Alf, founder of the RAM, began collecting fossils in the Barstow Formation with students of The Webb Schools in the mid-1930s (RAM is located on the Webb campus). In 1936, a peccary skull was found by Alf and his student Bill Webb that was described as the new genus and species, *Dyseohyus fricki*, by Stock (1937). This discovery inspired Alf to continue his collecting efforts in the Barstow Formation until his retirement in the 1970s. Alf and his students recovered many important specimens including well-preserved trackways of camels, proboscideans, and amphicyonids, as well as partial skulls of rare mammals such as *Zygolophodon* and *Megahippus* (Tedford and Alf, 1962; Lofgren and Anand, 2010, 2011), fossils now housed at the RAM.

Some of Alf's early collecting sites in the Barstow Formation were not well documented, but most of these localities were relocated during field surveys in the 1990s using slides and prints stored in the RAM archives. On one of these trips in 1998, D.

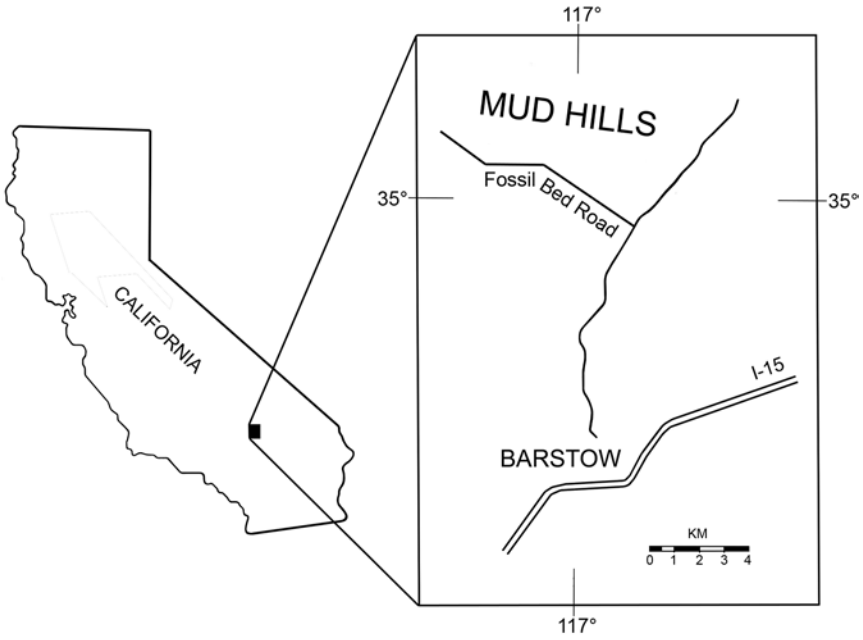

Figure 1. Location of the Barstow Formation within the Mud Hills, Mojave Desert, California (adapted from Steinen 1966).

Lofgren and student J. King surveyed several canyons east of Fossil Canyon and located the type locality of *Megahippus mckennai* (RAM 910) using a photo of the site taken in 1957. Lofgren and King noted that the stratigraphic interval yielding RAM 910 could be traced for a few hundred meters laterally and they collected many well-preserved skeletal elements, mainly of horses and camels. The productive stratigraphic interval was 10 meters thick and was designated as RAM locality V98004. On a return trip to V98004 the following year, student L. Kong found the terminal phalange of an avian raptor as float and showed Lofgren its source, a 10 cm thick siltstone lens that contained a high concentration of disarticulated skeletal elements of small-bodied vertebrates only 10 meters from the spot that yielded the holotype of *Megahippus mckennai*. The bone-bearing lens was not excavated, although a few partially eroded chunks of the lens were broken off and stored in the RAM collections. Recently, a few of these were partially prepared and more than 50% of the skeletal elements recovered were avian. Concentrations of avian remains are rarely reported from Miocene nonmarine strata so the lens represents an unusual taphonomic setting. A preliminary description of the site and its vertebrate fauna is presented.

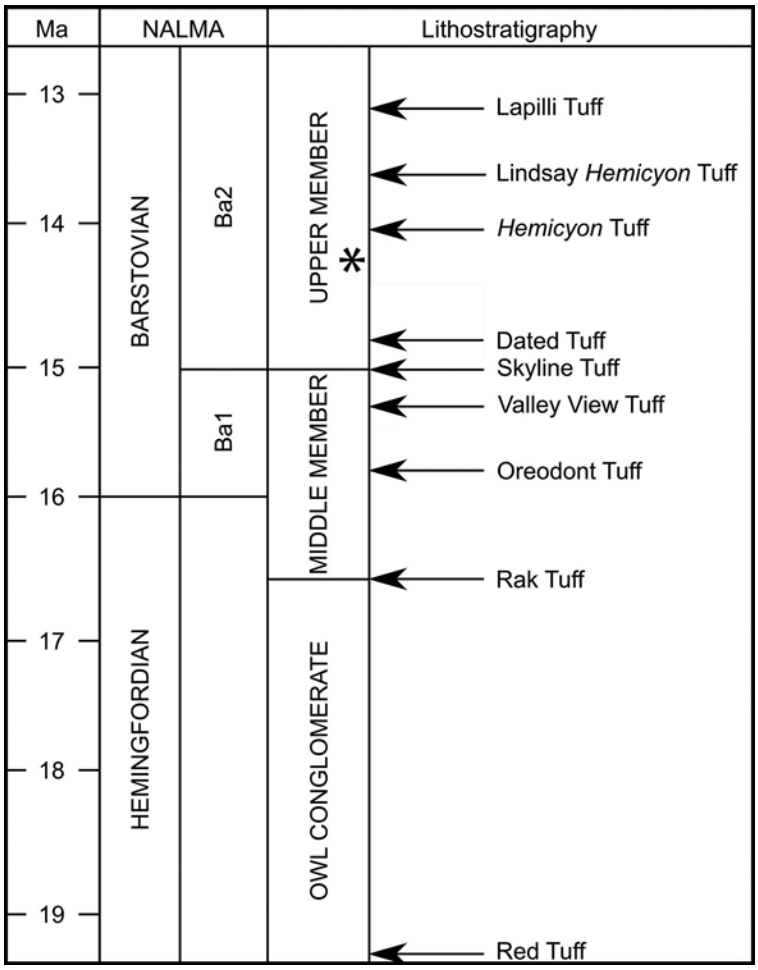

Figure 2. Geochronology and biostratigraphic subdivision of the Barstow Formation (adapted from Pagnac, 2009). Stratigraphic position of the V98004 and V94067 noted by *

Geologic and biostratigraphic setting

The Barstow Formation in the Mud Hills consists of about 1,000 meters of nonmarine strata subdivided into three members that, in ascending stratigraphic order, are the Owl Conglomerate Member, the middle member, and the upper member (Woodburne, et al., 1990). The Barstow Formation contains many tuffs and a few were used to define the lithostratigraphic boundaries between members; the Rak Tuff separates the Owl Conglomerate and middle members and the Skyline Tuff separates the middle and upper members. Isotopic dating of selected tuffs indicates that the formation was deposited between 19.3 to 13.4 Ma (Woodburne et al., 1990) (Figure 2). Although the mammal fauna of the Barstow Formation is the name bearer for the Barstovian North American Land Mammal Age (NALMA) (Wood et al., 1941), it yields both Hemingfordian and Barstovian aged mammals, with the Barstovian part of the section subdivided into the Ba1 and Ba2 biochrons (Woodburne et al., 1990; Tedford et al., 2004, Pagnac, 2009).

When King and Lofgren discovered RAM locality V98004 in 1998, they did not realize this stratigraphic interval was equivalent to that of RAM locality V94067, located about one kilometer to the southeast. Discovered in 1994, RAM locality V94067 was later determined to encompass outcrops that included the Frick Lab/AMNH Easter Quarry based on the work of B. Evander. In the late 1990s, Evander visited the Mud Hills to GPS and photograph sites worked by Frick Laboratory crews decades earlier and he was kind enough to show King where most of the Frick quarries were located. King photographed each quarry and deposited these photos in the RAM archives. Evander's map and King's photographs indicated that Easter Quarry was part of RAM

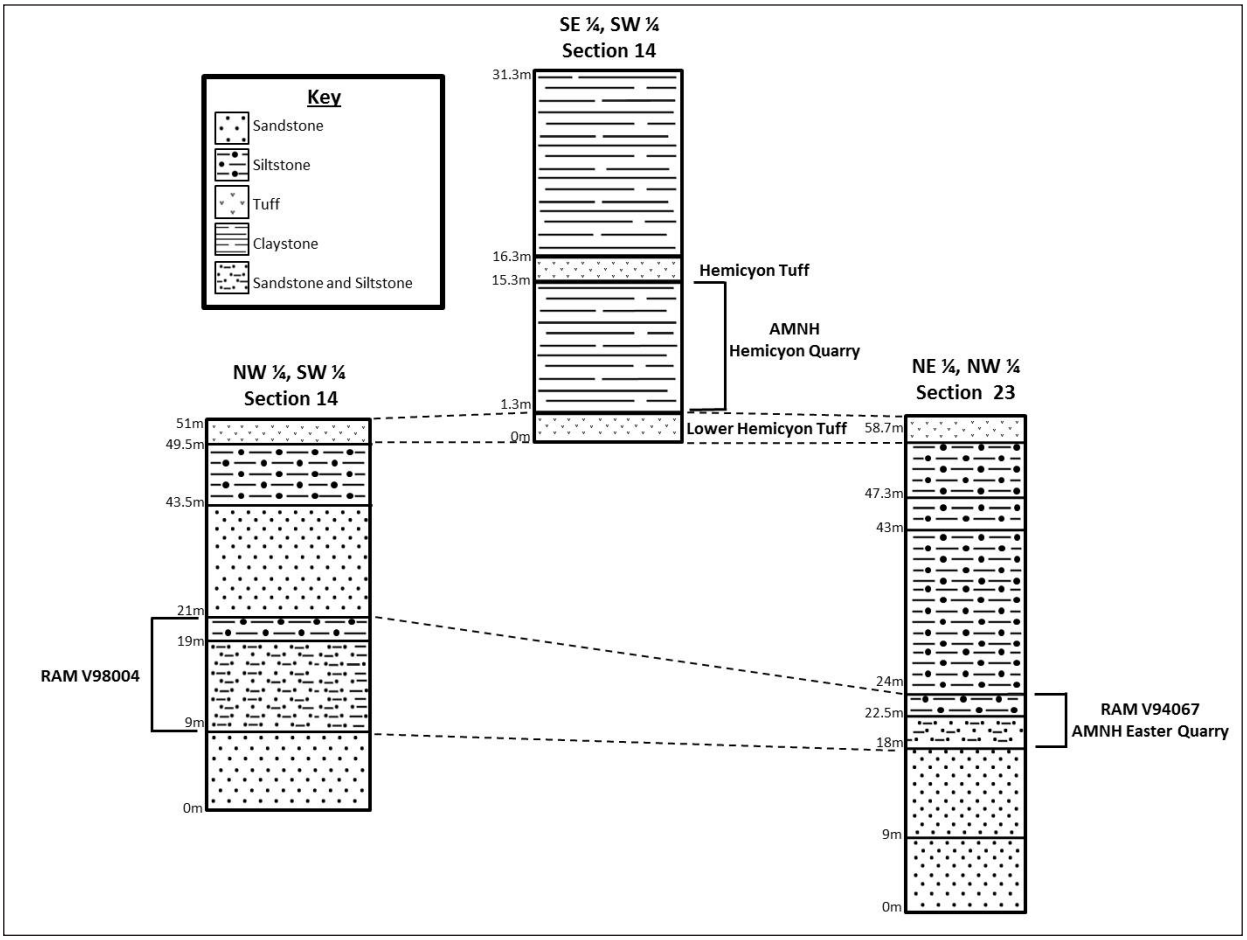

Figure 3. Measured sections showing stratigraphic correlation of Easter Quarry/V94067, *Hemicyon* Quarry, and V98004 in relation to the Lower *Hemicyon* and *Hemicyon* tuffs.

locality V94067, and a subsequent visit confirmed that the old quarry scar at V94067 was indeed Easter Quarry.

A series of three measured sections indicate that both V98004 and V94067 are from the same stratigraphic interval and are about 30 meters below a one meter thick tuff that underlies the Frick Lab/AMNH *Hemicyon* Stratum (or Quarry) (Figure 3). We refer to this tuff as the Lower *Hemicyon* Tuff. The tuff that overlies the *Hemicyon* Stratum is usually called the *Hemicyon* Tuff and is dated at 14.0 Ma (Woodburne et al., 1990). Thus, RAM localities V98004 and V94067 are in the upper member of the formation and their fossil assemblages are late Barstovian (Ba2 biochron), slightly older than 14.0 Ma and the vertebrate assemblage from the *Hemicyon* Stratum (Figure 2).

Figure 4. The bone-bearing lens (outlined in box) within strata designated as RAM locality V98004; Jacob staff 1.5 m in length.

Figure 5. Partially prepared block of bone-bearing lens showing the proximal humerus of a bird on right.

Fossil-yielding strata at V98004 consist of 10 meters of interbedded buff colored sandstone and siltstone capped by a two-meter thick gray tuffaceous siltstone that has a faint purple hue. At V94067 this same gray tuffaceous siltstone is the same thickness, but the buff colored sandstone–siltstone interval is only about half as thick (4.5 meters) (Figure 3). The 10 cm thick siltstone lens at V98004 occurs within the buff colored sandstone and siltstone interval, about two meters above its base, but its lateral extent is very limited, about two meters (Figure 4). Avian material in this lens is abundant and usually well preserved (Figure 5).

Abbreviations

AMNH, American Museum of Natural History, New York, New York; **Ba1**, Barstovian Biochron 1; **Ba2**, Barstovian Biochron 2; **CIT**, California Institute of Technology, Pasadena, California (collections now at the LACM); **CM**, Carnegie Museum of Natural History, Pittsburgh, Pennsylvania; **LACM**, Los Angeles County Museum, Los Angeles, California; **NALMA**, North American Land Mammal Age; **RAM**, Raymond M. Alf Museum of Paleontology, Claremont, California; **RV**, University of California Riverside, Riverside, California (specimens now housed at the UCMP); **SBCM**, San Bernardino County Museum, Redlands, California; **UCLA**, University of California Los Angeles, Los Angeles, California; **UCMP**, University of California Museum of Paleontology, Berkeley, California.

Macrovertebrates from V98004 and V94067

The first and only comprehensive study of the medium and large-bodied mammals from the Barstow Formation in the 20th century was by Merriam (1919). By the 1990s, a massive number of macrovertebrate fossils from the Barstow Formation had been collected, most housed at the AMNH. Nearly 100 years after Merriam (1919), D. Pagnac completed a systematic review of the mammalian megafauna from the Barstow Formation (2005a). Descriptions of new camels and a new equid appeared (Pagnac, 2005b, 2006), as well as a revision of the biostratigraphy and biochronology of the formation (Pagnac, 2009). Detailed description of the macrofauna from V98004 and V94067 will be an important addition to the biostratigraphy of the upper member of the formation. For example, V98004 has yielded the oldest known record of *Gomphotherium* from the Barstow Formation (Lofgren et al., 2012).

Table 1. Totals of identified specimens from V98004 and V94067, and microvertebrate specimens from the siltstone lens at V98004.

Macrofauna Taxa	V98004	V94067	Microfauna Taxa	V98004
Gopherus mohavense	9	0	Bird	125
Megahippus mckennai	2	0	Mammal	46
Scaphohippus sp.	17	3	Amphibian or Lizard	4
Gomphotherium sp.	1	0	Unknown	52
Merycodus necatus	1	0	Total	227
Paratomarctus temerarius	3	0		
Aepycamelus alexandrae	1	0		
Antilocapridae	5	0		
Proboscidea	1	0		
Camelidae	38	13		
Equidae	136	57		
Carnivora	4	1		
Total	218	74		

Figure 6. Occlusal view of RAM 910, holotype of *Megahippus mckennai,* maxilla with left and right P1-M3 and left I1-I2 from RAM locality V98004.

There are 218 macrovertebrate specimens from V98004 and 74 from V94067 housed at the RAM, not including fossils from the bone-bearing siltstone lens at V98004. The vertebrate assemblage from V98004 & V94067 consists of horses, camels, antelopes, proboscideans, turtles, and carnivores, all medium and large-bodied animals (Table 1). The faunal list for V98004 will expand significantly once specimens of small-bodied vertebrates from the bone-bearing lens are added. In the meantime, a preliminary description of the vertebrate fauna from V98004 and V94067 is provided.

Gopherus mohavense is the only tortoise species currently recognized from the Barstow Formation (Lofgren and Choi, this volume). Although tortoises are not common in the Barstow Formation, ten specimens are known from V98004 (none from V94067). The most complete is RAM 7148, an uncrushed shell with many postcranial elements (Lofgren and Choi, this volume, figs. 3–5). RAM 7148 is the only tortoise from the Barstow Formation that preserves part of the postcranial skeleton. Most of the tortoises known from the Barstow Formation were recovered from the upper member and they appear to be most abundant in the stratigraphic interval represented by V98004.

Megahippus mckennai is very rarely found in the Barstow Formation and is restricted to the upper member (Pagnac, 2009), except for a single occurrence at Skyline Quarry in the uppermost part of the middle member (Gonzalez and Lofgren, 2013). The holotype of *Megahippus mckennai*, RAM 910, a partial maxilla (Figure 6), was collected in 1957 (Tedford and Alf, 1962) from strata that were later included in V98004. A second partial maxilla (RAM 7454) from V98004 with heavily weathered and worn teeth probably represents *Megahippus*, although *Hypohippus affinis* is another possibility (Gonzalez and Lofgren, 2013).

Scaphohippus is the most common taxon recovered from V98004 and V94067 (Table 1). Two species are known from the upper member, *S. intermontanus* and *S. sumani* (Pagnac, 2006, 2009). Partial dentaries and maxillae of *Scaphohippus* are common at V98004 but are difficult to identify to species. Most of the equid postcranial elements from V98004 and V94067 are of the size that would correspond to *Scaphohippus*.

Gomphotherium is rarely found in the Barstow Formation and only two specimens, both from the upper member, are known: SBCM A489-200 (a damaged dp4?) and RAM 10362 (a right M2) (Lofgren et al., 2012, fig. 10). RAM 10362 was collected in 2007 from V98004 and represents the oldest well-documented occurrence of *Gomphotherium* from the Barstow Formation (Lofgren et al., 2012).

Merycodus necatus is the only antilocaprid species identified from V98004 or V94067 and it is represented by RAM 7619, a horn core.

Aepycamelus alexandrae is known from V98004 based on a single specimen, RAM 7585, which preserves a damaged axis and cervical vertebrae 3–5 (Figure 7). The holotype of *Aepycamelus alexandrae* (*"Alticamelus" alexandrae*) from the Barstow Formation included a skull, dentary, and part of the postcranial skeleton (UCMP 26015), including the cervical vertebrae (Davidson, 1923). The length of the centrum of the axis, 3rd cervical, and 4th cervical vertebrae of the holotype are 172 mm, 174 mm, and

Figure 7. Dorsal view of RAM 7585, cervical vertebrae of Aepycamelus alexandrae (partial 3rd and complete 4th and 5th cervical vertebrae) from RAM locality V98004.

162.5 mm (Davidson, 1923), and the corresponding length of the axis, 3rd cervical, and 4th cervical vertebrae of RAM 7585 is 180 mm, 225 mm, and 230 mm. Thus, RAM 7585 represents a very large individual of the species.

Paratomarctus temerius is known from three partial dentaries from V98004. This canid is widely reported from Miocene strata throughout the western United States (Wang et al., 1999). It is found at a number of localities in the upper member of the Barstow Formation (Pagnac, 2009) in addition to V98004.

More than 200 specimens of postcranial elements from V98004 and V94067 represent Antilocapridae, Equidae, Camelidae, and Carnivora. Equids are most common, followed by camels (Table 1).

Microvertebrates from V98004

Elements of small-bodied vertebrates can be common in some units in the upper member of the Barstow Formation and to recover these often tiny specimens, screen washing techniques can be employed. Initial systematic sampling and detailed description of Barstow Formation microvertebrates was completed by Lindsay (1972), with later contributions by Reynolds (1991) and Lindsay and Reynolds (2008). Recently, I. Browne screen-washed selected sites from the Barstow Formation and presented some preliminary results (Browne et al., 2010; Browne and Smith, 2013).

The bone-bearing lens at V98004 is an important addition to the microvertebrate record of the Barstow Formation because the site has a high concentration of specimens. The weathered top of this 10 cm thick lens exhibits well-preserved elements of both birds and mammals (Figure 8). When viewed in cross section, the lens contains a high concentration of small bones (Figure 9). A combination of acid and mechanical preparation techniques is necessary to recover specimens from the lens as it is composed of well-indurated calcareous siltstone. Preliminary identifications of the 227 skeletal elements recovered thus far indicate that avian remains dominate (Table 1) as 55% are avian, 20% mammalian, 2% amphibian or lizard, and 23% could not be identified to taxon.

Figure 8. Block of the bone bearing lens at V98004 showing a mammal calcaneum (circled on right) and tibia fragment (lower left), and an avian phalange (upper left) exposed by erosion.

Figure 9. Cross section of the bone-bearing lens showing concentration of small elements (black) of mammals and birds.

The high percentage of avian remains indicates that the bone-bearing lens preserves a very unusual depositional and taphonomic setting, one rarely sampled in the Miocene nonmarine record.

Birds are usually underrepresented in museum collections from Miocene strata compared to mammals. Previously, the avian record from the Barstow Formation was no exception as specimens were rare and no new records of avian fossils were reported since the early 1950s. The first avian remains found in the Barstow Formation were three specimens referred to falconiformes by Merriam (1919). They were a tarsometatarsus (UCMP 30438) of a buteonid hawk larger than *Buteo borealis* from UCMP locality 2056, a tibiotarsus (UCMP 21517) of *Buteo* between the size of *B. borealis* and *B. swainsoni* from UCMP locality 2061, and a fragmentary femur from UCMP locality 2061 (Merriam, 1919). Later, Miller (1952) described fifteen specimens collected by R. Tedford and R. Shultz in the late 1940s and early 1950s. Six of the specimens described by Miller (1952) were cataloged by UCLA (UCLA 2303, 2303A, 2303B, 2346, 2346C, 2346D) and one by the UCMP (UCMP 42223). The remaining specimens were listed by Miller (1952) using the field numbers of Tedford and Schultz (V471, V492, V493, V498). Five avian orders are represented: Falconiformes, Ciconiiformes, Anseriformes, Galliformes, and Charadriiformes. These specimens, listed below, are grouped by locality. Site information, identifications, and descriptions are from Miller (1952) and S. McLeod (pers. comm., 2014). The four sites listed below appear to be in the upper member.

***Hemicyon* Stratum**: the field number used (V471) corresponds to CIT locality 489. Tibial condyles (LACM 2862) belonging to a species of Anseriformes about the size of a female Mallard, and specimens too fragmented to be identified to genus were recovered.

Lake Bed Horizon: the field number used (V492) corresponds to CIT locality 493, LACM locality 1090, and apparently UCMP locality V5253. Nine specimens were recovered. A coracoid (UCLA 2346), distal condyles of a tibiotarsus (UCLA 2303), distal end of an ulna (UCLA 2303A), and distal end of a phalange (UCLA 2303B) were identified as *Megapaloelodus connectens*, a flamingo-like member of the Ciconiiformes. A coracoid about the size of a female baldpate (LACM 2859) and the head of a coracoid (LACM 2861) the size of a ruddy duck were also recovered from this site. Two other specimens collected represent gull-like birds (Charadriiformes), tibial condyles (UCLA 2346C) close to the size of the California gull and an ungual phalanx (UCLA 2346D) that was assigned to the gull family with uncertainty. A carpometacarpus (UCMP 42223) is the final specimen from this site and it is the holotype of *Cyrtonyx tedfordi*, a quail-like member of Galliformes.

Beds of tuff/sandstone: the field number used (V493) corresponds to CIT locality 494 and LACM locality 1091.Two specimens were recovered: distal condyles of a femur (LACM 2864) about the size of a mallard and the head of a coracoid (LACM 2863) from a duck about the size of a female green-winged teal.

Beds of orange-brown tuff: the field number used (V498) corresponds to CIT locality 495. Three specimens were recovered: distal condyles of the humerus (LACM 2856) of a small duck, the head of a coracoid (LACM 2858) similar to that of a ruddy duck, and the ungual phalanx) (LACM 2857) of what appears to be a small species of *Buteo* (Falconiformes).

As noted above, avian skeletal elements are abundant at V98004. One representative specimen selected for description is the terminal phalange or talon (RAM 16253) found as float by L. Kong in 1999 that led to the discovery of the bone-bearing lens. RAM 16253 (Figure 10) is a talon representative of the family Accipitridae, diurnal birds of prey that include hawks, eagles, and harriers (amongst others). Extant accipitrids whose talons most closely resemble RAM 16253 are the Cooper's hawk and red-tailed hawk. A Miocene representative of *Buteo* was previously reported from the upper member of the Barstow Formation (Merriam, 1919; Miller, 1952) and

Figure 10. Lateral view of RAM 16253, an accipitrid talon that probably represents a hawk. RAM 16253 is about 2 cm in length.

Figure 11. Occlusal view of RAM 16254, a right maxilla fragment with P3-4 of Miomustela; P4 is 5.16 mm in labial length.

RAM 16253 may represent this taxon. However, until avian material from V98004 is thoroughly analyzed, this remains uncertain.

We also describe an example of a mammalian specimen in this preliminary report. RAM 16254, a right maxilla fragment with P3–4 (Figure 11) appears to represent *Miomustela*, a small mustelid reported from late Arikareean to late Barstovian strata in the United States (Florida, Wyoming, Nebraska, and Montana) and Canada (Saskatchewan) (Baskin, 1998). However, because of the lack of a detailed systematic treatment, *Miomustela* is poorly known and some of these records are questionable (e.g. Tedford and Frailey, 1976). *Miomustela* is based on CM 848, a dentary fragment with canine, p3–4 and m1, which was originally described as *Martes*? *minor* (Douglass, 1904), and later referred to *Martes*? *madisonae*, as *Martes minor* had been occupied previously (Douglass, 1929). A year later, Hall (1930) erected the genus *Miomustela* and designated CM 848 as the genotype of *Miomustela madisonae*. The only description of the upper dentition of *Miomustela* is that the carnassial notch (metastyle notch) is absent on the metastyle blade of P4 (Baskin, 1998).

Miomustela was reported from the Barstow Formation by Pagnac (2005a), but description of these specimens, housed at the UCMP, was beyond the scope of his study. UCMP 320005, a right maxilla fragment with P3–4 from RV locality 5101 from the upper member, apparently represents part of the upper dentition. Measurements of RAM 16254 are: P3 length 2.78 mm and width 1.38 mm, P4 lingual length 4.82 mm, labial length 5.16 mm, and width 2.53 mm. Measurements of UCMP 320005 are: P3 length 5.32 mm and width 2.06 mm, P4 lingual length 7.95 mm, labial length 6.97 mm, and width 4.10 mm; P4 cusp terminology follows Flynn and Galliano (1982, fig. 1), and orientation of P4 measurements follow MacIntyre (1966, fig. 3).

The P4 of both UCMP 320005 and RAM 16254 lack a metastyle or carnassial notch and thus have the character noted by Baskin (1998) as representative of *Miomustela*, but the dentition of UCMP 320005 is significantly larger than that of RAM 16254. UCMP 320005 has a relatively narrower P3 compared to the P3 of RAM 16254 and the P4 protocone of UCMP 320005 is much larger than the P4 protocone of RAM 16254. Also, the protocone and parastyle of the P4 of RAM 16254 are subequal in size and transversely parallel, whereas the protocone of the P4 of UCMP 320005 is much larger and extends much farther anteriorly in comparison to the parastyle. These significant differences suggest that if these specimens do indeed represent *Miomustela*, there are two species present in the upper member of the Barstow Formation. Based on size, if either represent *Miomustela madisonae*, it is more likely to be RAM 16254 because the average length of the m1 of *M. madisonae* is 5.1 mm (Baskin, 1998), more similar to the maximum length of the P4 of RAM 16254 (5.16 mm), than the P4 of UCMP 320005 (7.95 mm).

Discussion

The importance of RAM locality V98004 is twofold. It has already yielded a number of important specimens of larger-bodied vertebrates, including the oldest known occurrence of *Gomphotherium* from

the Barstow Formation, the holotype of *Megahippus mckennai*, and the only tortoise shell with associated postcrania known from the Barstow Formation. In addition, preparation of only a few small blocks of the bone-bearing lens indicates that well-preserved skeletal elements are abundant, of which a high percentage are avian. Based on the currently visible exposure of the lens, it is estimated that about 1% of the number of fossils the lens could potentially yield have been recovered. Since 227 specimens have already been collected, the lens has the potential to yield thousands of specimens of small-bodied vertebrates. The partial maxilla (RAM 16254) that probably represents the rare mustelid *Miomustela*, is an example of the significance of its mammalian sample. Also, the high number of avian elements the lens can yield will provide a unique opportunity to expand knowledge of middle Miocene birds from southern California. In short, V98004 will likely become one of the most significant microvertebrate sites from the Barstow Formation and perhaps from middle Miocene strata in western North America. The RAM is requesting an excavation permit from the California Bureau of Land Management so a RAM crew can remove the remainder of the bone-bearing lens to preserve its unique fossil resource.

The bone-bearing lens at V98004 is also interesting from a taphonomic standpoint. The high concentration of disarticulated whole and broken elements of both birds and mammals in a 10 cm thick siltstone lens that is only two meters in lateral extent, suggests the lens records the activity of predators at a single roost or nest. Formulating any conclusions concerning the taphonomy of the bone-bearing lens is speculative at this point, but an intriguing hypothesis is that the concentration of bones in the lens records the feeding activities of predators. The high percentage of avian bones in the assemblage suggests an avian raptor, specifically a diurnal raptor as owls are nocturnal and thus feed almost exclusively on mammals. Diurnal raptors often select both mammals and birds as prey, but some extant diurnal raptors have an abundance of disarticulated skeletal elements of birds in their pellets and peregrines are known to be highly selective for birds (Andrews, 1990). Presence of the accipitrid talon (RAM 16253) at the site lends support for the diurnal raptor hypothesis.

Microvertebrate skeletal elements from V980004 are usually complete or are broken with one end intact. Bones consumed by diurnal raptors and deposited in pellets are extensively broken and are rarely fully intact (Hoffman, 1988; Andrews, 1990). However, the nest area of a diurnal raptor may be littered with the discarded remains of its prey and nests of the common buzzard (*Buteo buteo*) are known to contain disarticulated wings and limbs of birds (Andrews, 1990). Thus, it appears that at this particular nesting site or roost, only part of the prey skeleton was ingested, the remainder being discarded in the immediate area.

Acknowledgements

We thank P. Liskanich, J. King, L. Kong, other students of The Webb Schools, and A. Farke for field assistance, R. Choi for help with figure 2, M. Stokes for fossil preparation, J. Shearer of the California Bureau of Land Management for permits, P. Holroyd of the UCMP for access to and loan of specimens, S. McLeod and V. Rhue of the LACM for information on avian fossils from the Barstow Formation in the LACM collections, D. Pagnac for identification of specimens, and the Mary Stuart Rogers Foundation, Augustyn Family Fund, and the David B. Jones Foundation for financial support.

References cited

Andrews, P., 1990. Owls, caves, and fossils. University of Chicago Press, Chicago, Illinois. 231 pages.

Baskin, J. A., 1998. Mustelidae. pp. 152-173, in C. M. Janis, K. S. Scott and L. L. Jacobs (eds.), Evolution of Tertiary Mammals of North America, Volume 1: Terrestrial carnivores, ungulates, and ungulatelike mammals. Cambridge University Press, United Kingdom.

Brattstrom, B.H., 1961. Some new fossil tortoises from Western North America with remarks on the zoogeography and paleoecology of tortoises. Journal of Paleontology 35:543-560.

Browne, I., K. Smith, and N. Czaplewski. 2010. New collections of late Hemingfordian and early Barstovian small mammals from the Barstow Formation, Mojave Desert, California. Journal of Vertebrate Paleontology, Program and Abstracts 2010, p. 66A.

Browne, I., and K. Smith. 2013. Species relationships of Copemys (Rodentia, Cricetidae) specimens recovered from the middle Miocene Barstow Formation. Journal of Vertebrate Paleontology, Program and Abstracts 2013, p. 96.

Davidson, P., 1923. Alticamelus alexandrae, a new camel from the Barstow upper Miocene of the Mohave Desert. University of California Publications Geological Sciences 14:397-408.

Douglass, E., 1904. New vertebrates from the Montana Tertiary. Annuals of the Carnegie Museum 2:145-199.

Douglass, E., 1929. General notes. Journal of Mammology 10:167-171.

Flynn J. J., and H. Galiano. 1982. Phylogeny of early Tertiary Carnivora, with a description of a new species of Protictis from the middle Eocene of northwestern Wyoming. American Museum Novitates 2725:1-64.

Gonzalez, B., and D. L. Lofgren. 2013. Review of Megahippus and Hypohippus from the middle Miocene Barstow Formation of California. Pp. 78-89, in Reynolds, R. E. (ed.), Raising questions in the central Mojave Desert. California State University-Fullerton Desert Studies Consortium.

Hall, E. R., 1930. Three new genera of Mustelidae from the later Tertiary of North America. Journal of Mammology 11:146-155.

Hoffman, R., 1988. The contribution of raptorial birds to patterning in small mammal assemblages. Paleobiology 14:81-90.

Lindsay, E. H., 1972. Small mammal fossils from the Barstow Formation, California. University of California Publications in Geological Sciences 93:1-104.

Lindsay, E. H., and R. E. Reynolds. 2008. Heteromyid rodents from Miocene faunas of the Mojave Desert, California. Natural History Museum of Los Angeles County, Science Series 41:213-236.

Lofgren, D. L., and R. S. Anand. 2010. 75 years of fieldwork in the Barstow Formation by the Raymond Alf Museum of Paleontology. Pp. 169-176, in Reynolds, R. E. and D. M. Miller (eds.), Overboard in the Mojave, 20 million years of lakes and wetlands. California State University-Fullerton Desert Studies Consortium.

Lofgren, D. L., and R. S. Anand. 2011. Partial skull of Zygolophodon (Mammalia, Proboscidea) from the Barstow Formation of California. Journal of Vertebrate Paleontology 31:1392-1396.

Lofgren, D. L., and H. Choi. this volume. Tortoises from the middle Miocene Barstow Formation of California. California State University-Fullerton Desert Studies Consortium.

Lofgren, D. L., D. Pagnac, A. Hess, P. Liskanich, and D. Silver. 2012. Review of proboscideans from the Middle Miocene Barstow Formation of California. Pp. 125-134, in Reynolds, R. E. (ed.), Search for the Pliocene: the southern exposures. California State University-Fullerton Desert Studies Consortium.

MacIntyre, G. T., 1966. The Miacidae (Mammalia, Carnivora). Part 1. The systematics of Ictidopappus and Protictis. Bulletin of the American Museum of Natural History 131:115-210.

Merriam, J. C., 1911. A collection of mammalian remains from Tertiary beds on the Mohave Desert. California University Publications in Geological Sciences 6:167-169.

Merriam, J. C., 1919. Tertiary mammalian faunas of the Mohave Desert. University of California Publications in Geological Sciences 11:437a-437e, 438-585.

Miller, L., 1952. The avifauna of the Barstow Miocene of California. The Condor 54: 296-301.

Pagnac, D. C., 2005a. A systematic review of the mammalian megafauna of the middle Miocene Barstow Formation, Mojave Desert, California (PhD dissertation). University of California-Riverside. 384 pp.

Pagnac, D., 2005b. New camels (Mammalia, Artiodactyla) from the Barstow Formation (middle Miocene), San Bernardino County, California. Paleobios 25:19-31.

Pagnac, D., 2006. Scaphohippus, a new genus of horse (Mammalia, Equidae) from the Barstow Formation of California. Journal of Mammalian Evolution 13: 3761.

Pagnac, D. C., 2009. Revised large mammal biostratigraphy and biochronology of the Barstow Formation (Middle Miocene), California. Paleobios 29:48-59.

Reynolds, R.E., 1991. Hemingfordian/Barstovian Land Mammal Age faunas in the central Mojave Desert, exclusive of the Barstow Fossil Beds, in Inland Southern California: the last 70 million years, M.O. Woodburne, R.E. Reynolds, and D.P. Whistler, eds. Redlands, San Bernardino County Museum Association Quarterly 38(3, 4):88-90.

Steinen, R. P., 1966. Stratigraphy of the middle and upper Miocene, Barstow Formation, California. (m.s. thesis): University of California-Riverside, 150 pp.

Stock, C. A., 1937. A peccary skull from the Barstow Miocene, California. National Academy of Sciences Proceedings 23:398-404.

Tedford, R. H., and R. M. Alf. 1962. A new Megahippus from the Barstow Formation, San Bernardino County, California. Bulletin of the Southern California Academy of Sciences 61:113-122.

Tedford, R. H., and D. Frailey. 1976. Review of some Carnivora (Mammalia) from the Thomas Farm Local Fauna (Hemingfordian, Gilchrist County, Florida). American Museum Novitates 2610:1-9.

Tedford, R. H., Albright III, L. B., Barnosky, A. D., Ferrusquia-Villafranca, I., Hunt Jr., R. M., Storer, J. S., Swisher II, C. C., Voorhies, M. R., Webb S. D., and D. P. Whistler. 2004. Mammalian biochronology of the Arikareean through Hemphillian interval (late Oligocene through early Pliocene epochs). Pp. 169-231, in M. O Woodburne (ed.), Late Cretaceous and Cenozoic mammals of North America. Columbia University Press, New York.

Wang, X., R. H. Tedford, and B. E. Taylor. 1999. Phylogenetic systematics of the Borophaginae (Carnivora, Canidae). Bulletin of the American Museum of Natural History 243:1-391.

Wood, H. E., R. W. Chaney, J. Clark, E. H. Colbert, G. L. Jepsen, J. B. Reeside Jr., and C. Stock. 1941. Nomenclature and correlation of the North American continental Tertiary. Geological Society of America Bulletin 52:1-48.

Woodburne, M. O., Tedford, R. H. and C. C. Swisher III. 1990. Lithostratigraphy, biostratigraphy, and geochronology of the Barstow Formation, Mojave Desert, southern California. Geological Society of America Bulletin 102:459-477.

Mojaveite and bluebellite, two new minerals from the central Mojave Desert

Stuart J. Mills[1]*, Anthony R. Kampf[2], Andrew G. Christy[3], Robert M. Housley[4], George R. Rossman[4], Robert E. Reynolds[5], and Joe Marty[6]

*[1]Geosciences, Museum Victoria, GPO Box 666, Melbourne 3001, Victoria, Australia; [2]Mineral Sciences Department, Natural History Museum of Los Angeles County, 900 Exposition Blvd, Los Angeles, CA 90007, USA; [3]Centre for Advanced Microscopy, Australian National University, Canberra, ACT 0200, Australia; [4]Division of Geological and Planetary Sciences, California Institute of Technology, Pasadena, CA 91125, USA; [5]220 South Buena Vista St, Redlands, CA 92373, USA; [6]5199 E. Silver Oak Rd, Salt Lake City, UT 84108, USA; *E-mail: smills@museum.vic.gov.au*

The Mojave Desert in the U.S. Southwest contains thousands of old mines and prospects, the vast majority of which were never economically profitable. However, a few deposits, though they produced little ore, have yielded a noteworthy variety of rare and unusual minerals. One of these deposits is the Blue Bell claims in the Soda Mountains, about 11 km west of Baker, San Bernardino County, California, which has been a prolific producer of micro-crystals of rare species for six decades (Crowley 1977; Maynard et al. 1984; Kampf et al. 2009; Mills et al. 2010; Housley et al. 2011). Importantly, the Blue Bell claims are the type locality for the new minerals fluorphosphohedyphane (Kampf and Housley 2011), plumbophyllite (Kampf et al. 2009) and reynoldsite (Kampf et al. 2012b). A little farther east, another world-class mineral locality is found at Otto Mountain, 1.5 km northwest of Baker. Twelve new secondary minerals (Table 1) have been described from this remarkable mineral assemblage. Here we announce two new minerals, bluebellite and mojaveite, which have recently been approved by the International Mineralogical Association Commission on New Minerals, Nomenclature and Classification.

Table 1. New minerals previously described from Otto Mountain.

Mineral	Ideal Formula	Reference
Ottoite	$Pb_2Te^{6+}O_5$	Kampf et al. (2010a)
Housleyite	$Pb_6Cu^{2+}Te^{6+}{}_4O_{18}(OH)_2$	Kampf et al. (2010b)
Thorneite	$Pb_6(Te^{6+}{}_2O_{10})(CO_3)Cl_2(H_2O)$	Kampf et al. (2010c)
Markcooperite	$Pb_2(UO_2)Te^{4+}O_6$	Kampf et al. (2010d)
Timroseite	$Pb_2Cu^{2+}{}_5(Te^{6+}O_6)_2(OH)_2$	Kampf et al. (2010e)
Paratimroseite	$Pb_2Cu^{2+}{}_4(Te^{6+}O_6)_2(H_2O)_2$	Kampf et al. (2010e)
Telluroperite	$Pb_3Te^{4+}O_4Cl_2$	Kampf et al. (2010f)
Chromschieffelinite	$Pb_{10}Te^{6+}{}_6O_{20}(CrO_4)(H_2O)_5$	Kampf et al. (2012a)
Fuettererite	$Pb_3Cu^{2+}{}_6Te^{6+}O_6(OH)_7Cl_5$	Kampf et al. (2013a)
Agaite	$Pb_3Cu^{2+}Te^{6+}O_5(OH)_2(CO_3)$	Kampf et al. (2013b)
Bairdite	$Pb_2Cu^{2+}{}_4Te^{6+}{}_2O_{10}(OH)_2(SO_4)(H_2O)$	Kampf et al. (2013c)
Eckhardite	$(Ca,Pb)Cu^{2+}Te^{6+}O_5(H_2O)$	Kampf et al. (2013d)

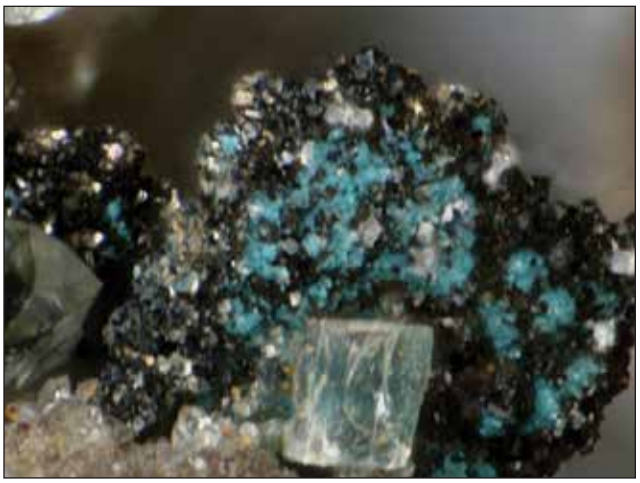

Fig. 1. Bluebellite with fluorite on murdochite pseudo-morphous after wulfenite (2 mm FOV) from the Blue Bell claims.

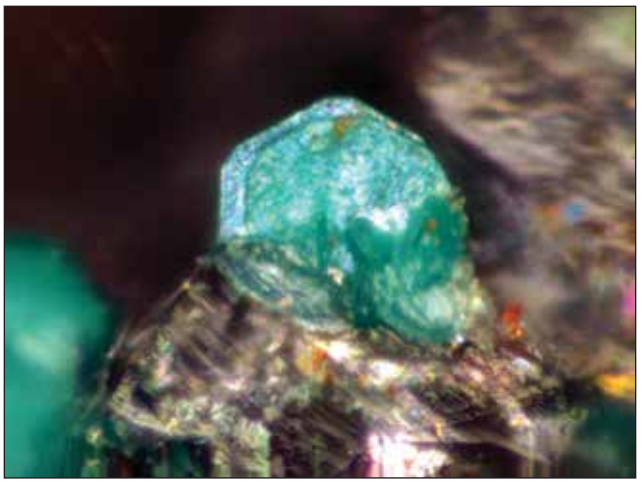

Fig. 2. Crystals of mojaveite on quartz (1 mm FOV) from Otto Mountain.

Bluebellite

Bluebellite, $Cu_6[IO_3](OH)_{10}Cl$, was discovered by the late John Jenkins of Redlands, California in 1983 at the shallow D shaft, Blue Bell claims, where world-class specimens of quetzalcoatlite were also found. Bluebellite occurs as bright bluish-green plates or flakes up to about 20 x 20 x 5 μm in size. Plates are generally curved and are intergrown in irregular aggregates. Bluebellite occurs in direct association with murdochite (often as pseudomorphs after wulfenite; Figure 1), calcite, fluorite, and hemimorphite in a highly siliceous hornfels. Rarely, dioptase is also found in association with bluebellite.

Bluebellite crystallizes in the trigonal system, with the space group *R*3 and unit cell parameters a = 8.3017(5), c = 13.259(1) Å, V = 791.4(1) Å^3 and Z = 3. The cotype specimens are housed in the collections of the Natural History Museum of Los Angeles County and Museum Victoria (Australia).

Mojaveite

Mojaveite, $Cu_6[TeO_4(OH)_2](OH)_7Cl$, was discovered by one of the authors (JM) in 2005 on Otto Mountain at the Aga mine and Bird Nest drift and in 2011 in the small E pit at Blue Bell. Mojaveite is the tellurate analogue of bluebellite, with $Te^{6+}O$ replacing $I^{5+}OH$ in the crystal structure. Mojaveite occurs as greenish-blue plates, which rarely show a hexagonal outline (Figure 2). The plates are generally curved and are intergrown in irregular aggregates. Mojaveite also occurs as compact balls, varying in colour from sky blue to medium greenish blue. Both individual plates and compact balls reach 0.5 mm in maximum dimension. At the Blue Bell claims, mojaveite occurs in direct association with andradite, cerussite, chlorargyrite, chrysocolla, hemimorphite, kettnerite, perite, quartz and wulfenite. At the Aga mine mojaveite is associated with cerussite, chrysocolla, khinite, perite and quartz. At the Bird Nest drift, it is associated with andradite, chrysocolla, cerussite, burckhardtite, galena, goethite, khinite, mcalpineite, thorneite, timroseite, paratimroseite, quartz and wulfenite.

Mojaveite crystallizes in the trigonal system, with the space group *R*3 and unit cell parameters a = 8.316(2), c = 13.202(6) Å, V = 790.7(1) Å^3 and Z = 3. The cotype specimens are also housed in the collections of the Natural History Museum of Los Angeles County and Museum Victoria (Australia).

Conclusions

Seventeen minerals new to science have been discovered from the Blue Bell claims and at Otto Mountain in the past five years, but while the majority of unidentified species have been named, there are still many unknowns from these two deposits, which may yet yield new mineral species. These sites are truly remarkable occurrences, not only in California and the USA, but world-wide!

References

Crowley, J. A. (1977) Minerals of the Blue Bell mine, San Bernardino County, California. Mineralogical Record, 8, 494–496, 518.

Housley, R.M., Kampf, A.R., Mills, S.J., Marty, J., and Thorne, B. (2011) The remarkable occurrence of rare secondary tellurium minerals at Otto Mountain near Baker, California —including seven new species. Rocks and Minerals, 86, 132–142.

Kampf, A.R. and Housley, R.M. (2011) Fluorphosphohedyphane, $Ca_2Pb_3(PO_4)_3F$, the first apatite supergroup mineral with essential Pb and F. American Mineralogist, 96, 423–429.

Kampf, A.R., Housley, R.M., Mills, S.J., Marty, J. and Thorne, B. (2010a) Lead–tellurium oxysalts from Otto Mountain near Baker, California: I. Ottoite, Pb_2TeO_5, a new mineral with chains of tellurate octahedra. American Mineralogist, 95, 1329–1336.

Kampf, A.R., Marty, J. and Thorne, B. (2010b) Lead–tellurium oxysalts from Otto Mountain near Baker, California: II. Housleyite, $Pb_6CuTe_4TeO_{18}(OH)_2$, a new mineral with Cu–Te octahedral sheets. American Mineralogist, 95, 1337–1342.

Kampf, A.R., Housley, R.M. and Marty, J. (2010c) Lead–tellurium oxysalts from Otto Mountain near Baker, California: III. Thorneite, $Pb_6(Te_2O_{10})(CO_3)Cl_2(H_2O)$, the first mineral with edge-sharing octahedral dimers. American Mineralogist, 95, 1548–1553.

Kampf, A.R., Mills, S.J., Housley, R.M., Marty, J. and Thorne, B. (2010d) Lead–tellurium oxysalts from Otto Mountain near Baker, California: IV. Markcooperite, $Pb_2(UO_2)Te^{6+}O_6$, the first natural uranyl tellurate. American Mineralogist, 95, 1554–1559.

Kampf, A.R., Mills, S.J., Housley, R M., Marty, J. and Thorne, B. (2010e) Lead–tellurium oxysalts from Otto Mountain near Baker, California: V. Timroseite, $Pb_2Cu^{2+}{}_5(Te^{6+}O_6)_2(OH)_2$, and paratimroseite, $Pb_2Cu^{2+}{}_4(Te^{6+}O_6)_2(H_2O)_2$, new minerals with edge-sharing Cu–Te octahedral chains. American Mineralogist, 95, 1560–1568.

Kampf, A.R., Mills, S.J., Housley, R.M., Marty, J. and Thorne, B. (2010f) Lead–tellurium oxysalts from Otto Mountain near Baker, California: VI. Telluroperite, $Pb_3Te^{4+}O_4Cl_2$, the Te analogue of perite and nadorite. American Mineralogist, 95, 1569–1573.

Kampf, A.R., Mills, S.J., Housley, R.M., Rumsey, M.S., and Spratt, J. (2012a) Lead–tellurium oxysalts from Otto Mountain near Baker, California: VII. Chromschieffelinite,

$Pb_{10}Te_6O_{20}(CrO_4)(H_2O)_5$, the chromate analogue of schieffelinite. American Mineralogist, 97, 212–219.

Kampf, A.R., Mills, S.J., Housley, R.M., Bottrill, R.S. and Kolitsch, U. (2012b) Reynoldsite, $Pb_2Mn^{4+}{}_2O_5(CrO_4)$, a new phyllomanganate-chromate from the Blue Bell claims, California and the Red Lead mine, Tasmania. American Mineralogist, 97, 1187–1192.

Kampf, A.R., Mills, S.J., Housley, R.M., and Marty, J. (2013a) Lead–tellurium oxysalts from Otto Mountain near Baker, California: VIII. Fuettererite, $Pb_3Cu^{2+}{}_6Te^{6+}O_6(OH)_7Cl_5$, a new mineral with double spangolite–type sheets. American Mineralogist, 97, 506–511.

Kampf, A.R., Mills, S.J., Housley, R.M., and Marty, J. (2013b) Lead-tellurium oxysalts from Otto Mountain near Baker, California: IX. Agaite, $Pb_3Cu^{2+}Te^{6+}O_5(OH)_2(CO_3)$, a new mineral with CuO_5–TeO_6 polyhedral sheets. American Mineralogist, 97, 512–517.

Kampf, A.R., Mills, S.J., Housley, R.M., Rossman, G.R., Marty, J., and Thorne, B. (2013c) Lead–tellurium oxysalts from Otto Mountain near Baker, California: X. Bairdite, $Pb_2Cu^{2+}{}_4Te^{6+}{}_2O_{10}(OH)_2(SO_4)\cdot H_2O$, a new mineral with thick HCP layers. American Mineralogist, 97, 1315–1321.

Kampf, A.R., Mills, S.J., Housley, R.M., Rossman, G.R., Marty, J. and Thorne, B. (2013d) Lead–tellurium oxysalts from Otto Mountain near Baker, California: XI. Eckhardite, (Ca,Pb) $Cu^{2+}Te^{6+}O_5(H_2O)$, a new mineral with HCP stair-step layers. American Mineralogist, 98, 1617–1623.

Kampf, A.R., Rossman, G.R. and Housley, R.M. (2009) Plumbophyllite, a new species from the Blue Bell claims near Baker, San Bernardino County, California. American Mineralogist, 94, 1198–1204.

Maynard, M.F., Valenti, A., Jenkins, J., Jenkins, F., Hall, D., Hall, J., White, B., White, S., Mansfield, M. and Mansfield, E. (1984) *The Blue Bell Claims*. San Bernardino County Museum Special Publication, San Bernardino County Museum, San Bernardino.

Mills, S.J., Kampf, A.R., Kolitsch, U., Housley, R.M., and Raudsepp, M. (2010) The crystal chemistry and crystal structure of kuksite, $Pb_3Zn_3Te^{6+}P_2O_{14}$, and a note on the crystal structure of yafsoanite, $(Ca,Pb)_3Zn(TeO_6)_2$. American Mineralogist, 95, 933–938.

Geologic history, ore mineralization, and paragenetic sequence of Lead Mountain, Barstow, CA

Taylor van Hoorebeke

Department of Geological Sciences, California State Polytechnic University, Pomona

ABSTRACT: Lead Mountain is located on the southeastern end of the Mitchel Range, approximately four air miles NE of Barstow, CA. It is host to several NW-striking, vein-hosted epithermal barite-Pb-Zn deposits. The deposits are rich in prismatic barite and secondary ore minerals. Mineralization occurs as open-space filling along faults and fractures related to Miocene detachment faulting. Mineralization has been documented in four distinct rock units within Lead Mountain, from the late Paleozoic Waterman Gneiss to the middle Miocene Barstow Formation. Unlike the nearby Calico Mining District, Lead Mountain does not contain economical silver reserves. The limited extent of mining operations within Lead Mountain suggests historical silver grades were low as well.

The evolution of the barite deposits of the central Mojave Desert, and especially Lead Mountain, is of importance to this study. A hypothetical model is presented which seeks to explain where the barite originated and attempts to define the mechanism by which it was transported and emplaced within Lead Mountain. In essence, the barite originated from a hydrothermal vent on a boundary of the Farallon Plate. Some time after the Farallon subducted beneath the North American Plate the barite would have been heated to the point where it partially solubilized and subsequently rose through conduits in the crust. The most likely conduits for ore emplacement are listric faults related to detachment faulting in the central Mojave. Geothermometric analysis suggests barite emplacement 1-1.5 km below the surface.

One of the most important features of the Lead Mountain deposits is their mineral paragenesis. The order in which the oxide and sulfide minerals formed is anomalous for an epithermal deposit. An original hypothesis seeks to explain the paragenesis. The hypothesis proposes that the Eh (reduction potential) of the ore fluid was increased by H_2S gas, allowing sulfide minerals to form from oxide minerals. The H_2S gas is of volcanic origin and may be related to volcanism due to Miocene-extension. The origin of the primary mineral assemblage is proposed as an exhalative marine deposit, such as a volcanogenic massive sulfide. The regional geologic setting and similarities in mineral assemblage between Lead Mountain and the proposed VMS deposit support this claim. The source of the sulfur and metal ions is an important consideration for understanding the atypical nature of Lead Mountain's mineral paragenesis.

Introduction

Since the first prospectors arrived in Barstow, CA in 1881, mining in the central Mojave Desert, especially in the Calico Mountains, has produced over fifteen million ounces of silver. Within ten years of the initial silver discovery over fifty mines began operations in the region, including a small prospect on Lead Mountain. More than ten separate adits, mines, and pits have been excavated in Lead Mountain, despite the fact that silver grades never contended with those of the nearby Calico District. Barite was mined from the prospect in the first half

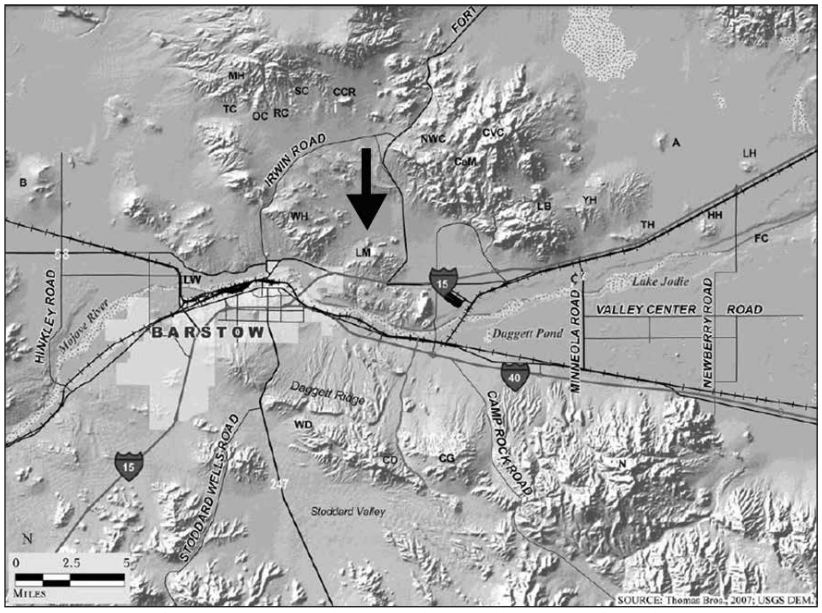

Figure 1: Map of Barstow, CA with arrow showing location of Lead Mountain (LM). Borrowed with permission and edited from Reynolds, et al. (2010)

of the twentieth century. The mining of barite from hydrothermal veins quickly became uneconomical when the immense barite deposits of Missouri and Nevada were heavily exploited between 1930-1970. No documented mining activity has occurred at Lead Mountain since the 1970's.

Geologic history of Lead Mountain

The Waterman Gneiss, the oldest of the basement rocks underlying Lead Mountain, is considered to be late Paleozoic to early Mesozoic in age. It is comprised of mylonitized metasedimentary and metaigneous rocks. The gneiss is overlain by middle to late Mesozoic granitic masses ranging in composition from diorite to granodiorite and quartz monzonite. The contact between the basement rocks and the overlying Miocene-aged volcanic and sedimentary rocks is unconformable and is interpreted as a regional detachment fault.

An important structural feature of the central Mojave silver-barite deposit systems is the Waterman Hills detachment fault (WHDF). The NW-trending normal fault formed near the Oligocene-Miocene boundary. Glazner et al. (2002) claims the WHDF may be a result of dextral shear movement between the North American and Pacific plates. Total displacement along the WHDF is a controversial topic and has been projected from at most 10 km by Fletcher (1986) and Singleton and Gans (2008) to as much as 65 km by Dokka (1989) and Glazner et al. (1989). Extension in the central Mojave triggered by the WHDF resulted in the formation of NW-trending listric faults. At least two of these listric faults cut through Lead Mountain. Volcanism related to shear movement along the North American-Pacific plate boundary and extension along the WHDF led to the development of the Pickhandle Formation.

The Pickhandle Formation is comprised of early to middle Miocene volcaniclastic sediments and felsic volcanic rocks. Jessey (2010) reported similar-aged massive dacitic and rhyolitic flows in the Calico Mountains, but these do not extend into Lead Mountain. The Pickhandle volcanics are associated with extension in the central Mojave. The formation is of economic importance because the largest and most easily accessible vein-hosted ores occur within the Pickhandle. Jessey (2010) notes volcanism relating to the Pickhandle continued after the cessation of detachment faulting in the central Mojave approximately 18 Ma.

The volcanic rocks comprising the bulk of Lead Mountain are rhyo-dacitic tuffs and tuff breccias, collectively called ignimbrites. The felsic composition and estimated timing of these ignimbrites are the only relations to the Pickhandle volcanic flows of the Calico Mountains. The age of the Lead Mountain volcanics is unknown but studies by Nielson et al. (1990) and Reynolds et al. (2010) suggest that the ignimbrites may belong to the immense Peach Springs Tuff and not simply the localized Pickhandle Formation.

The middle Miocene Barstow Formation lies above the Pickhandle in the sequence. It is primarily composed of interbeds of fluvial sandstones and siltstones, shale, and alluvial conglomerate. A 70-foot sandy limestone unit of lacustrine origin also lies within the formation. Dibblee (1967) refers to this limestone as MSL (massive stromatolitic limestone). Several small tuff beds that outcrop in the Barstow Formation suggest early Miocene volcanism overlapped into the middle Miocene sediment deposition. The contact between the Pickhandle and Barstow Formations is unconformable.

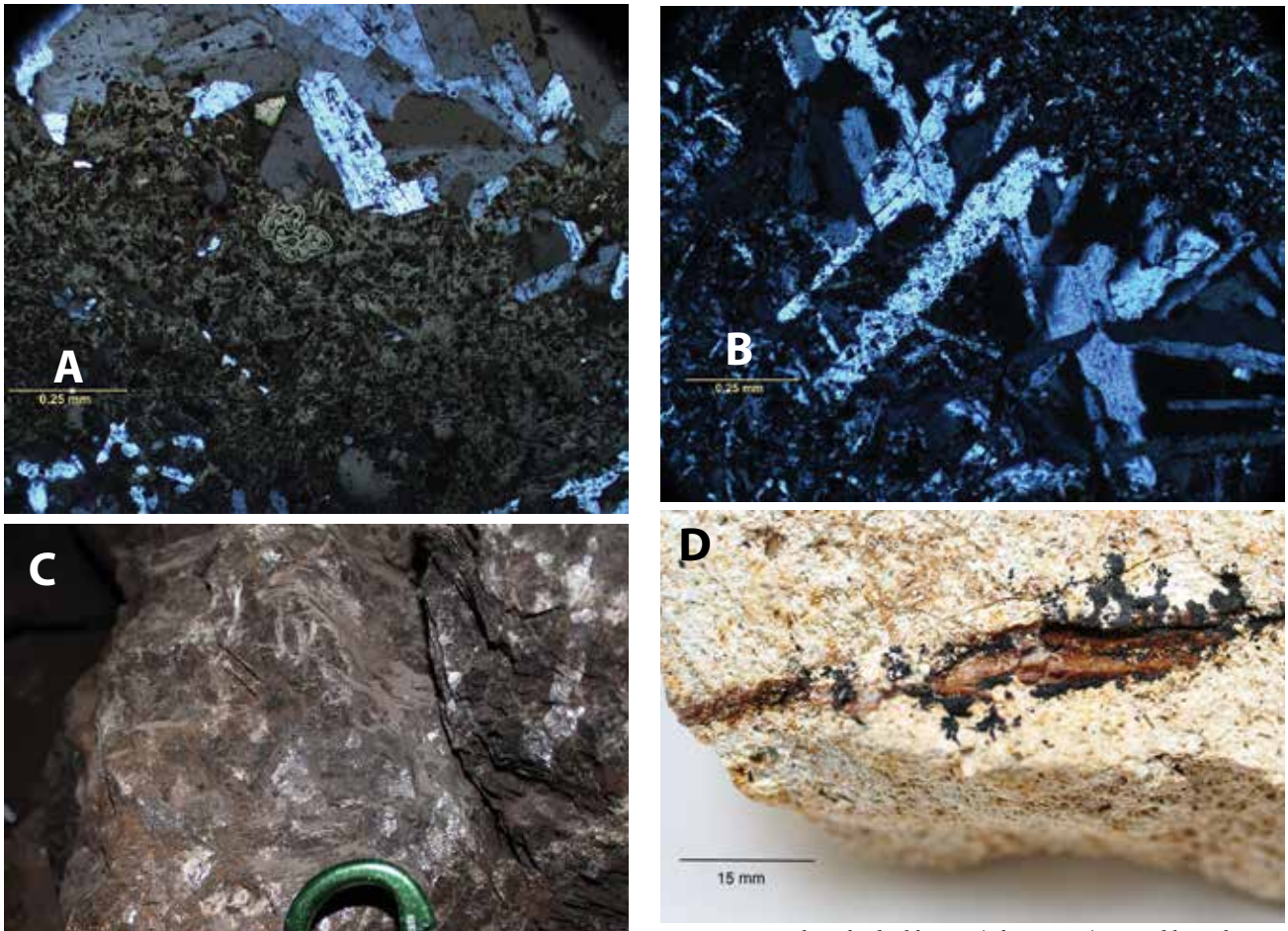

Figure 2A: Early euhedral barite (white, gray) coated by galena (brown) and sphalerite (dark gray). Scale reads 0.25mm. B: Subhedral barite exhibiting typical open-space filling mineralization. Matrix is comprised of ash, disseminated quartz and feldspar. Scale reads 0.25mm. C: Example of massive barite stained by iron and manganese oxides and/or sulfides. Photo taken in main mine. D: Sample of rhyolite with a dendritic Mn-oxide (not pyrolusite) leached from vein. Field of view is 6.5cm

Durrell (1954) suggests that before the rhyolitic ignimbrites and overlying sedimentary layers silicified iron oxide stained the rocks red. Most of the tuffs and breccias and all of the various sedimentary beds were either silicified by chalcedony and fine- to medium-grained quartz or cemented by carbonate minerals. The exact origin of the silica cement is unknown. Most ground waters are low in dissolved silica and the subsurface of Lead Mountain was probably no exception. The silica may have been derived from hot springs, where unusually high amounts of dissolved silica are common. It is possible the silica originated with the barite and ore minerals at the proposed VMS deposit. Clarke (1924) notes that in the case of hot springs, groundwater is likely not the solvent, therefore the silica may have been of a deep-seated, hydrothermal origin.

Hydrothermal fluid deposited the ore minerals in the listric faults and fractures of Lead Mountain. The primary mineral assemblage consists of barite, Fe- and Mn-oxides, galena, quartz/chalcedony, and calcite. Jessey (2010) suggests these fault-controlled deposits formed 19 Ma. Geochronological studies on altered barite from the Calico Mountains yielded alteration ages of 18 Ma, further supporting Jessey's claim. The minerals occur as open-space filling vein deposits and comb structures, as is depicted in Figures 2B and 3. Durrell (1954), Jessey and Tarman (1994), and Jessey (2010) have noted barite veins in the Waterman Gneiss. Barite mineralization has been observed in the Pickhandle and Barstow Formations and the Peach Springs Tuff by the author. Figure 5 depicts a detailed paragenetic sequence.

Figure 3: Comb structure depicting alternating layers of barite and oxide minerals. Thin section analysis revealed minute amounts of sulfide minerals, suggesting this vein is from early barite and oxide mineralization phase. Straight edge of protractor is 6 inches long.

Figure 4: Limited argillic alteration located 10 meters from the main vein outcrop. The white mineral is kaolinite, red minerals are hematite and unknown iron oxy-hydroxides. Clasts are brecciated andesite, dacite, and rhyolite. Sericite and chlorite are visible with a hand lens. Field of view is 4 feet.

Limited mineralization was noted in the sedimentary layers of the Barstow Formation; minerals present were predominantly disseminated silicates and carbonates and fine-grained barite in permeable siltstones and porous sandstones. Durrell (1954) noted anhydrite and barite occurrences in a twenty-foot sandstone bed on the SE portion of the mountain.

The Lead Mountain vein deposits are fault-controlled. Jessey (oral communication) states the Waterman Hills detachment fault is not responsible for ore emplacement in the central Mojave. Listric faults related to the WHDF are the most likely conduits through which hydrothermally circulating fluid deposited the ore minerals. Two NW-trending, high angle normal faults within Lead Mountain have been noted by Durrell (1954), Dibblee (1967) and the author. Macroscopic barite crystals were found along one of these faults within the mine. The second fault was found outside the mine, therefore any substantial barite crystals present had eroded away. Thin-section analyses of samples collected from both fault planes yielded small tablets of fully formed, prismatic barite and interstices filled by galena and cerussite (Figure 2A).

At the time of formation many calcite and quartz crystals contained inclusions of iron and manganese oxides that stained the veins reddish-brown or black. This oxide staining was also observed in barite crystals that formed after the initiation of the first mineralization phase (Figure 2C). The oxide minerals within the barite may have originated along with the barite at the proposed marine hydrothermal vent. Sulfide minerals were oxidized upon precipitation, which suggests either emplacement at shallow depths or a presence of aqueous oxygen gas at the time of formation.

It is important to note that the author did not find silver-bearing minerals in his study of the mine. Housley (unpublished) reported microscopic acanthite and various silver halides in samples collected from adits within Lead Mountain. The lack of development of the Lead Mountain mine workings suggests that silver grades were historically low. It is unlikely that galena from the mine is argentiferous.

Upon oxidization, the Pickhandle ignimbrites and most of the aforementioned minerals underwent standard supergene alteration processes. Many barite crystals were stained red by Fe-oxides such as hematite and brownish-black by Mn-oxides. Primary sulfide minerals were altered to secondary carbonate and silicate minerals. Galena altered to cerussite and Pb-jarosite, while sphalerite altered to hemimorphite and smithsonite. Some hematite and magnetite altered to limonite and other iron oxy-hydroxides. An unidentified manganese oxide, likely pyrolusite, was observed along the ore-bearing veinlets and in the altered zones of the rhyolite breccia (Figure 2D).

Although the author did not find them, past research by Durrell (1954) and Dibblee (1967) notes the presence of syenitic and diabasic sills that intrude

Lead Mountain's tuffaceous and sedimentary rocks. The ages of these intrusions are estimated between 10-13.5 Ma.

Sometime after the end of barite mineralization the Harper Lake and Calico Faults formed. Both faults exhibit dextral shear motion and a NW-strike, suggesting they are part of a large system of lateral-faults that accommodate slip between the North American and Pacific plates (Jessey 2010). Total displacement along each of these faults is estimated at five and three kilometers, respectively. At some point in the Pliocene dacite and andesite were intruded into the Pickhandle and Barstow formations of the Waterman Hills and Calico District. The intrusions arched the rock sequences. No evidence has been found that proves the andesite and dacite intruded into Lead Mountain.

Small faults developed in Lead Mountain during the Quaternary Period. The fractures have random orientations and are responsible for brecciating the vein deposits. The fractures, acting as conduits, have allowed water to alter the outer fringes of the main vein, turning most of the original ignimbrite wall rock into clay (Figure 4).

Silicification is the most extensive type of alteration in Lead Mountain. The silicified tuff and breccia are predominantly dark red due to staining by iron oxide. Although Durrell (1954) claims the rhyolites were highly altered hydrothermally, the author only observed limited intermediate argillic alteration in the localized Pickhandle Formation of Lead Mountain. Evidence for the alteration was observed at two separate locations within the mine, both of which were at least ten meters from the main vein (Figure 4). The observed mineral assemblage included quartz, kaolinite-montmorillonite, sericite, chlorite, unidentified clays (illite ± smectite), and minor biotite. Almost all plagioclase had been altered to kaolinite in these two zones. The general lack of wall rock alteration in the mine may have been due to a water deficiency associated with the Miocene ore emplacement.

The barite deposits

Several questions arise when considering the significant barite deposits within Lead Mountain and throughout the central Mojave. How did so much barite become localized in the region? Where did all of the barite come from? How did barite veins form in the Waterman Gneiss, the basement rock beneath Lead Mountain? Why is a substantial amount of the barite stained by Fe- and Mn-oxides? A hypothetical model may be able to answer these questions.

Assume that a substantial amount of barite precipitated from a hydrothermal venting system on the Farallon Plate. The hydrothermal barite could have deposited as part of a volcanogenic massive sulfide, where barite occurrences are quite common.. Preservation of the barite would not be difficult considering the wealth of dissolved sulfates in the deep ocean (Guilbert 1986). A model devised by Atwater (2009) shows the Farallon Plate subducted beneath North America in a generally east-northeast strike. As the western edge of the Farallon disappeared beneath the North American Plate some 25 Ma, the eastern edge of the Pacific Plate caught North America and eventually formed the San Andreas Fault. Dextral shear motion along the San Andreas extended the crust of southwestern North America, forming the central Mojave's Waterman Hills detachment fault in the process. Movement along the WHDF created a series of NW-striking listric faults that cut from the Pickhandle Formation to unknown depths, at least through the Waterman Gneiss. As the Farallon Plate subducted deeper beneath North America the geothermal gradient rose. Once the temperature was high enough the barite would have been partially solubilized and transported into the overriding continental crust. The partially melted barite would then travel upwards through the crust, which had been thinned out from the early Miocene extension event. Eventually the barite reached the listric faults embedded deep beneath Lead Mountain.

One would expect some amount of mixing to occur after the barite and associated mineral assemblage partially melted. Such mixing was observed in several locations within the main mine. Red-brown and black barite was likely stained by iron and manganese oxides/sulfides as the ore fluid was rising through the continental crust. Figure 2C shows an example of the black barite from the main mine.

Geothermometric analyses on barite from the central Mojave were examined by Rosso et al. (1992) and Jessey and Tarman (1994). Jessey and Tarman (1994) published fluid inclusion analyses on hydrothermally emplaced barite in the Pickhandle Formation. Their data yielded homogenization temperatures ranging from 250-310° C. This fluid inclusion analysis supports the hypothesis that the

barite deposits of Lead Mountain formed at depths of 1-1.5 km. These temperature and depth of formation values are quite substantial compared to typical epithermal vein deposits.

Mineral paragenesis

The most unique feature of the Lead Mountain ore deposits is their mineral paragenesis. Three distinct mineralization phases dominate the system, although the third is predominantly an alteration phase. Each of these phases correlates to specific temperature ranges and depths and are thus governed, at least in part, by structural parameters (Guilbert 1986).

The early phase resulted in the deposition of sulfate and oxide minerals, primarily barite, magnetite, and unidentified Mn-oxides. Precipitation of quartz and chalcedony began in this phase. Depth of formation is approximated between 1-1.5 km. The middle phase saw the deposition of sulfide minerals, mostly galena and sphalerite, and fine-grained barite. A later alteration phase induced by supergene processes led to the development of cerussite, jarosite, hemimorphite, calcite/smithsonite, and various iron and manganese oxide minerals, namely hematite and pyrolusite. Precipitation of quartz and chalcedony occurred during this phase as well.

The order in which the oxide and sulfide minerals formed is anomalous. Ordinarily, reducing conditions precede oxidizing conditions as the minerals precipitate at depth and the deposit is subsequently uplifted towards the surface. However, something different occurred at Lead Mountain. The best hypothesis relies upon a single hydrothermal event with a gradually changing chemistry and suggests the origin of the ore minerals is a hydrothermal marine deposit. The hypothesis states that an intrusion of H_2S gas provided a fluctuation in the chemistry of the ore fluid, allowing sulfide minerals to form from reduced oxide minerals.

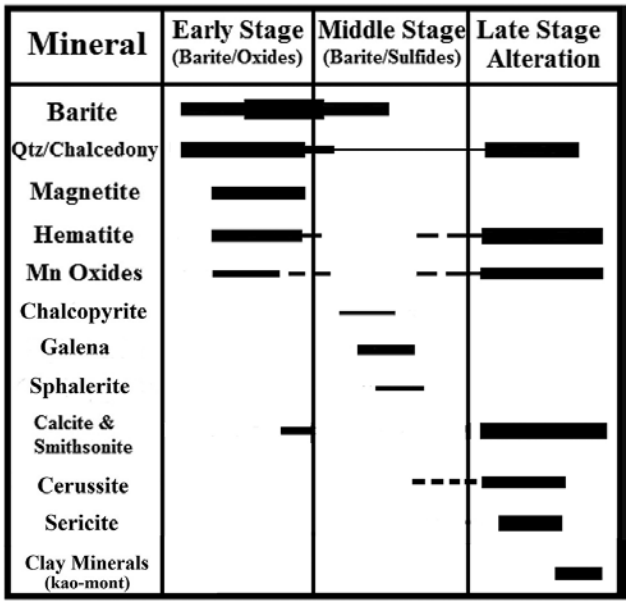

Figure 5: Detailed paragenetic sequence of Lead Mountain epithermal vein-hosted deposits. Relationships discerned with thin section analyses.

As previously stated, the hypothesis requires the chemistry of the fluid to evolve over time. Jessey (2010) concluded that the atypical paragenetic sequence of oxides preceding sulfides was likely due to a drop in Eh. In order for sulfides to form from oxides the Eh of the fluid would need to increase. H_2S is both an extremely common volcanic gas and an acid that is capable of inducing such a change in Eh. Therefore H_2S could be the reducing agent needed to convert oxide minerals such as magnetite and litharge into sulfides such as pyrite and galena. It is highly likely the gas was released in conjunction with the early Miocene Pickhandle volcanism. Consider the following reactions:

$$PbO + H_2S \rightarrow PbS + H_2O$$
$$2PbO_2 + 2H_2S \rightarrow 2PbS + 2H_2O + O_2$$
$$Fe_3O_4 + 6H_2S \rightarrow 3FeS_2 + 4H_2O + 2H_2$$

According to Kuhn and Försterling (2000), H_2S is very acidic and has an acid dissociation constant, or K_a, of $10^{(-7)}$. Therefore the pK_a of H_2S is 7, which is considered a low pK_a value (Kuhn and Försterling 2000). Natural systems favor low energy states. As an acidic solution nears neutrality it enters a low energy state. Therefore reactions that will take a system from high acidity (low pK_a) to low acidity (high pK_a), such as the three listed above, will occur spontaneously. In an anoxic environment oxide minerals will already be unstable. The addition of hot, aqueous H_2S to the system could provide the acidity needed to extract the metal ions. Once the metals have been extracted H_2S would provide the sulfur anion needed to create sulfide minerals. These reactions would occur *after* the completion of the early mineralization phase and not while the original ore fluid is being transported to Lead Mountain.

Note the above reactions would create steam. Any residual water would be able to induce wall rock alteration. The O_2 gas byproduct could be partially responsible for the early oxidation of the galena. The additional presence of a strong acid or base can

potentially alter the productivity of these reactions, driving the required temperature conditions up or dropping them considerably. Detailed geochemical analyses beyond the scope of this research paper are required to fine-tune the details of these sulfide-forming reactions.

From where did the elemental constituents of the barite, oxides, and sulfides come? Assuming they all originated from the same setting, a simple explanation is some type of submarine exhalative deposit. Perhaps the most well known example of an exhalative deposit is a volcanogenic massive sulfide. These vents are found along active plate boundaries, such as a spreading center, or hot spots. The VMS model is used to define the original source for the *cations* and *anions*, not the minerals themselves.

In the center of a typical VMS deposit one would expect to find a stockwork structure consisting of iron sulfides. Different types of ores grade into separate facies, basically in a halo shape that surrounds the stockwork. According to Guilbert (1986), typical VMS ore facies, from stockwork outwards, consist of pyrite-chalcopyrite, pyrite-sphalerite, sphalerite-galena, then galena-manganese, and finally chert-hematite-manganese. Other various oxide minerals such as magnetite and plattnerite sporadically occur in the outer halos. What is particularly interesting about this list of facies is the trend in chemical composition of the ore as one looks out from the stockwork. The outermost halos of a typical VMS are compositionally identical to the vein deposits found in Lead Mountain.

In the ideal model the minerals exhaled from the hydrothermal vent would need to accumulate in a sedimentary basin. Downslope of the vent, the basin would be laterally extensive in scope. Over time the basin would be buried in pelagic sediment. At some point during the Eocene or Oligocene epochs the buried basin would be subducted beneath North America. From here, the model follows the one initially discussed in the barite section of this paper.

Summary and discussion

Defining the origin of the ions that eventually formed the ore in Lead Mountain's vein deposits provides an appreciation for how geographically distinct geologic settings can be interrelated with one other. It also provides an understanding of how ions and chemical compounds can be recycled in natural inorganic processes.

The model for original barite, sulfide, and oxide deposition in a VMS-type setting is satisfactory. The VMS model accounts for the observed mineral assemblage in Lead Mountain. Early Miocene subduction of the Farallon Plate accounts for emplacement of the VMS deposit beneath the newly extended crust below the central Mojave. Volcanism related to early Miocene crustal extension provides the convective currents and heat flow required to transport the barite and various metal ions from the subducted oceanic crust to the listric faults. Upon the initial mineralization phase a release of H_2S gas into the recently precipitated vein deposits increased the Eh of the ore fluid, resulting in the formation of sulfides from oxides.

Though satisfactory, the model concerning the barite deposits and atypical paragenetic sequence leaves critical questions unanswered. At what temperature and pressure would barite partially solubilize, and are these values congruent with near-boundary plate subduction? At what temperatures and pressures would oxide minerals such as litharge and magnetite reduce to galena and pyrite, respectively? It is highly unlikely the listric faults breach the continental crust. What other conduits were responsible for transporting the barite from the subducted oceanic plate to the listric faults? How far would the Farallon Plate have to laterally subduct before the temperature was hot enough to partially melt the VMS deposits? Would the presence of a particular acid, such as sulfuric or nitric acid, influence the suggested reactions in a way so that higher temperatures are not required? If the minerals originated in a VMS deposit, why was a very small amount of pyrite observed in vein samples? A detailed study into each of these questions would lead to a better understanding of the evolution of Lead Mountain and its vein deposits.

Acknowledgments

My greatest appreciation goes to my undergraduate thesis advisor Dave Jessey. Without his endorsement this project wouldn't have been possible. I give special thanks to Bob Housley of Cal Tech for access to his exploration log at Lead Mountain, Bob Hilburn of the Mojave River Valley Museum for aiding in my research, Bob Reynolds for his patience and his assistance with editing, Ken Craig of Cal Poly Pomona for

helping construct models for ore emplacement, and Marc Montana of Cal State Fullerton for his peer-review of this research paper.

References

Alpers, Charles N., Jambore, J.L., Nordstrom, D.K., 2000, Sulfate minerals: crystallography, geochemistry, and environmental significance, Paul H. Ribbe, ed. Washington, DC: Mineralogical Society of America.

Atwater, Tanya, 2007, N.E. Pacific and W. North America plate history, 38 Ma to Present (animation). Educational Multimedia Visualization Center, Department of Earth Science, U.C.S.B.

Bowen, Oliver E., 1954, Geology and mineral deposits of Barstow Quadrangle, San Bernardino County, California: California Division of Mines Bulletin 165.

Clarke, F. W., 1924, Data of geochemistry: *U. S. Geol. Survey*, Bulletin 770.

Dibblee Jr., Thomas W., 1967, Areal geology of the Western Mojave Desert, California. Geological Survey Professional Paper no. 522. United States Government Printing Office, Washington D. C.

Dokka. R.K., 1989, The Mojave extensional belt of southern California: Tectonics, v. 8, p. 363-390.

Dorn, Ronald, 2006, Geomorphology of Desert Environments. *Desert Rock Coatings*, A. J. Parsons and A. Abrahams, ed. 2007.

Durrell, Cordell, 1954, Barite deposits near Barstow, San Bernardino County, California: California Division of Mines Special Report 39.

Fletcher, D. I., 1986, Geology and genesis of the Waterloo and Langtry silver-barite deposits, California: Unpublished Ph.D. Dissertation, Stanford University, 158 p.

Glazner, A. F., Bartley, J. M., and Walker, J. D., 1989, Magnitude and significance of Miocene crustal extension in the central Mojave Desert, California: Geology, v. 17, p. 50-53.

Glazner, A.F., Walker, J.D., Bartley, J.M., and Fletcher, J.M., 2002, Cenozoic evolution of the Mojave block of southern California, in Geological evolution of the Mojave Desert and southwestern Basin and Range, A.F. Glazner et al., eds: Geological Society of America Memoir 195, p. 19-41

Guilbert, John M., and Charles Frederick Park, Jr., 1986, Deposition of the Ores, in The geology of ore deposits, p. 126-48.

Hanor, Jeffery S., 2000, Barite-Celestine geochemistry and environments of formation." *Reviews in Mineralogy and Geochemistry* v. 40, p. 193-275.

Housley, R., Unpublished log of explorations at Lead Mountain, accessed Nov. 8, 2013.

Jessey, D. R., and Tarman, Donald W., 1994, Implications of fluid inclusion P/T data from Miocene hydrothermal barite deposits, central Mojave Desert, San Bernardino County, California: San Bernardino County Museum Association Quarterly, v. 41 n. 3, p. 22-23.

Jessey, David R., 2010, Geology and ore genesis of the Calico Mining District, in Overboard in the Mojave: 20 million years of lakes and wetlands, Robert E. Reynolds, ed. California Desert Studies Symposium 2010, Zzyzx, pp. 213-223

Jones, Craig H., et al., 2011, Hydrodynamic mechanism for the Laramide Orogeny: *Geosphere*, v. 7, p. 183-201.

Kamradt, Andreas, 2008, Ore petrography, geochemistry and SWIR-reflectance spectroscopy of the Chichaklou Zn-Pb Deposit, Takab Province, NW Iran. Published Thesis: Martin-Luther-Universität Halle-Wittenberg, 2008. Halle, DE: Economic Geology & Petrology

Koski, Randolph A., Hein, James R., 2003, Stratiform barite deposits in the Roberts Mountains allochton, Nevada: a review of potential analogs in modern sea-floor environments. Contributions to Industrial Minerals Research. USGS Bulletin 2209. p. 6-13.

Kuhn, H., Försterling, H.D., 2000, Principles of physical chemistry: understanding atoms, molecules and supramolecular machines, Wiley-Interscience, Ed. 1

Misra, Kula C., 2000, Interpretation of mineral deposits, in Understanding mineral deposits. Dordrecht: Springer Netherlands. 116-24.

Mojave River Valley Museum, November 2013; miscellaneous posters, brochures, displays, and conversation with Bob Hilburn.

Nielson, J.E., Lux, D.R., Dalrymple, G.B., and Glazner, A.F., 1990, Age of the Peach Springs Tuff, Southeastern California and Western Arizona: Journal of Geophysical Research, vol. 95, no. B1, pp. 571-580.

Reynolds, R.E., Miller, D.M., Woodburne, M.O., and Albright, L.B., 2010, Extending the boundaries of the Barstow Formation in the central Mojave Desert, in Overboard in the Mojave: 20 million years of lakes and wetlands, Robert E. Reynolds ed., Desert Studies Symposium 2010, Zzyzx, pp. 148-158.

Rosso, K. M., Jessey, D. R., and Tarman, D. W., 1992, Fluid inclusion geothermometry and geochemistry of silver-barite mineralization in the Pickhandle Formation, Calico Mountains, San Bernardino County, California: Geological Society of America Abstracts with Programs, Annual Meeting, p. 79.

Singleton, J.S. and Gans, P.B., 2008, Structural and stratigraphic evolution of the Calico Mountains: implications for early Miocene extension and Neogene transpression in the central Mojave Desert, California: *Geosphere*, v. 4, p. 459-479.

Tijskens, E., 1988, Ore Mineralogy of the Tatestown Prospect, Ireland, in Base metal sulfide deposits in sedimentary and volcanic environments: proceedings of the DMG-GDMB-SGA-meeting, Aachen, 1985, by Günther Friedrich and Peter M. Herzig. Berlin: Springer-Verlag.

Vaughan, David J., and James R. Craig., 1978, Replacement and alteration textures, in Mineral chemistry of metal sulfides. Cambridge: Cambridge UP. p. 210-11.

Vaughan, David J., and James R. Craig., 1978, Sulfide Equilibria in Aqueous Systems, in Mineral chemistry of metal sulfides. Cambridge: Cambridge UP. p. 315.

Vredenburgh, Larry M., 2013, Calico—a brief overview of mining history, in Raising Questions in the central Mojave Desert, Robert E Reynolds., ed. Desert Studies Symposium 2013, Zzyzx, pp. 90-94.

A regional-scale landslide model for the origin of west-vergent, low-angle faults in the Silurian Hills, Old Dad Mountain, Soda Mountains, and other areas, Eastern Mojave Desert, California

Kim M. Bishop

Dept. of Geosciences and Environment, California State University, Los Angeles

ABSTRACT: Several mountain ranges in the Baker area of eastern California contain exposures of allochthonous carbonate emplaced above Mesozoic and older rock. The Silurian Hills, Soda Mountains, and Old Dad Mountain areas provide evidence for the nature of the low-angle faulting responsible for allochthon emplacement. Observations from these ranges indicate the faulting was west-vergent and locally involved extensional deformation of the allochthon. Carbonate rock comprising the allochthon is Paleozoic. It is interpreted that the best explanation for the faulting and allochthon emplacement in the various ranges is related to a single deformational episode that occurred in the late Cretaceous, coeval with west-directed thrust faulting of the Sevier orogeny. Faulting in the Baker area occurred in an area of arc magmatism in the hinterland of the active Sevier thrust belt. Evidence suggests the low-angle fault responsible for allochthon emplacement dipped westward at a maximum of about 5 to 7 degrees during the time it was active. Nowhere has a location been identified where the fault turns downward to root into the crust. In other words, all of the allochthon outcrops are klippe. Given the lack of a root, it is proposed that the carbonate allochthon is a regional-scale landslide. The size of the landslide is similar to the Eocene Heart Mountain landslide in Wyoming.

Introduction

Scattered exposures of poorly understood low-angle faults that juxtapose allochthonous carbonate with various autochthonous Mesozoic and older rocks are present across an area of roughly 4000 km^2 (1500 mi^2) centered roughly on the city of Baker, California are. The region of the faults is bounded by the Valjean Hills on the north, Cima Dome on the east, Old Dad Mountain and the Cow Hole Mountains on the south, and the Soda and Avawatz Mountains on the west (Fig. 1).

Of the various fault outcrop areas, three locations present the best and most abundant evidence for interpreting the kinematics and history of the low-angle faulting. These areas are the Silurian Hills, which were studied by Kupfer (1960), Old Dad Mountain studied by Dunne (1977), and the Soda Mountains studied by Grose (1959) and Walker and Wardlaw (1989) (Fig. 1). In each of these areas low-angle faults separate Paleozoic carbonate in the hanging wall from Proterozoic gneissic, late Proterozoic and Paleozoic metasedimentary, and/or Mesozoic volcanic and sedimentary rock in the footwall. Because these three outcrop areas provide the best evidence for the low-angle faulting in the region, this study focuses on them. As will be shown, the age of the low-angle faulting is mid to late Mesozoic.

Despite detailed geologic studies of each of the three ranges, the tectonic origin of the low-angle faulting in the ranges remains enigmatic. The area of the low-angle faulting discussed in this report is located between two major Mesozoic orogenic belts, the Sevier thrust zone to the east and the Eastern Sierra Thrust System (ESTS) to the west (Fig. 2).

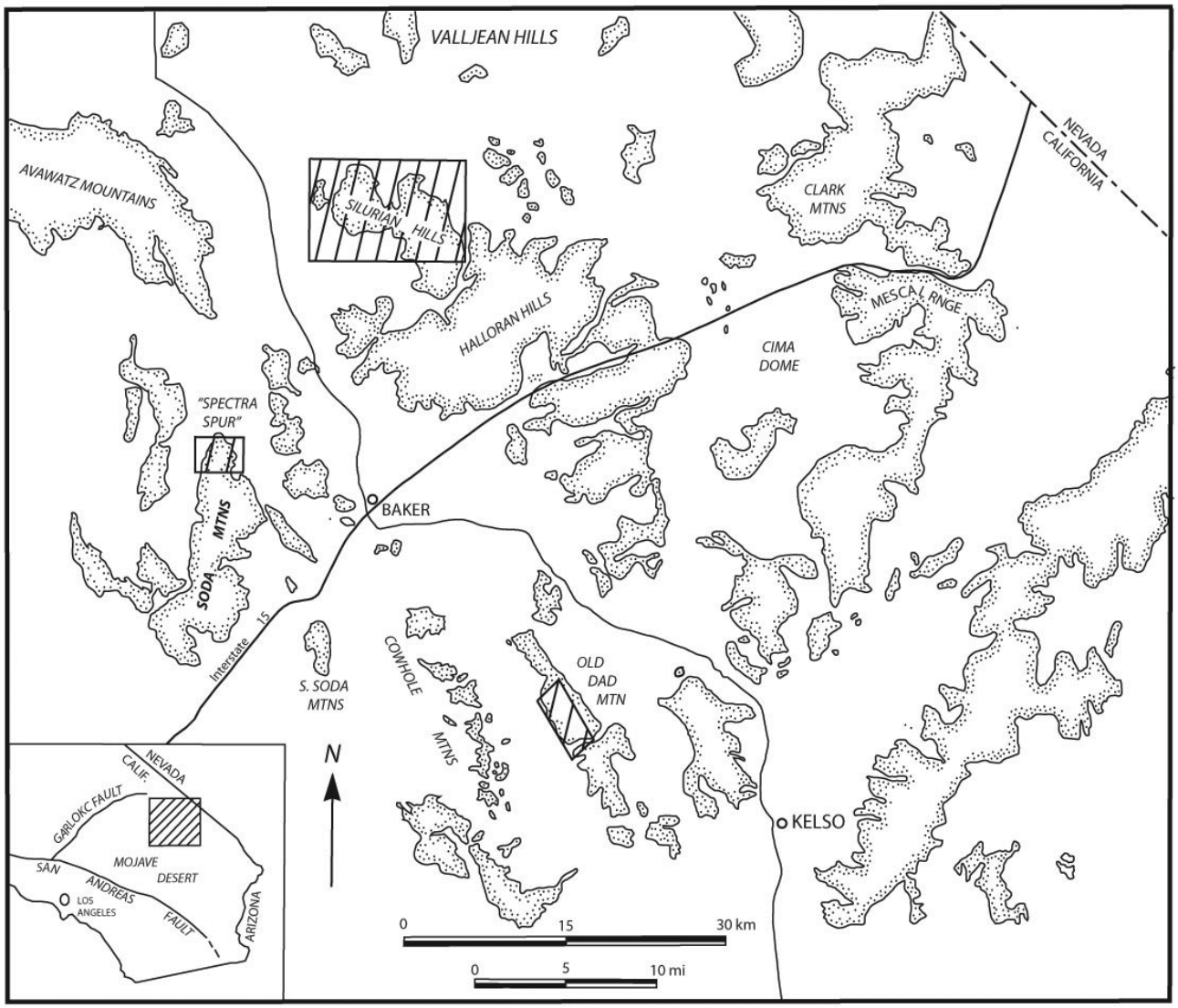

Figure 1: Location Map. Cross-hatched areas show locations of maps presented in Figures 3, 6, and 8.

No clear ties have been proposed for the low-angle faulting in the Baker area and these reasonably well-understood orogenic belts. Furthermore, distances of 10 to 30 km between outcrops of the low-angle faults in the Baker area renders interpretation of the structural relationships between the outcrops uncertain.

The purpose of this paper is to propose a model whereby the Mesozoic low-angle faulting in the Silurian Hills, Old Dad Mountain, and Soda Mountains is related to a single tectonic origin. Before presenting the model, important aspects of the Mesozoic low-angle faults in the three areas will be described. The reasons why the low-angle faulting in each of the three ranges is likely related is then discussed. Finally, a tectonic model that explains the origin of faulting and how the faulting fits into the regional tectonic evolution will be presented.

Silurian Hills

A major low-angle fault, the Riggs fault, is well-exposed throughout the 50 km^2 (20 mi^2) Silurian Hills (Kupfer, 1960) (Fig. 3). The fault places carbonate sedimentary sequence at least several hundred meters thick atop Proterozoic and Paleozoic siliciclastic strata.

An east-west cross-section of the Silurian Hills shows the low-angle geometry of the Riggs fault (Fig. 4). Although the Riggs fault is cut by a series of Miocene high-angle faults that uplift and down-drop the fault in various fault blocks and the fault is locally warped gently, the overall geometry of the fault across the range is horizontal.

The hanging wall block of the Riggs fault consists of recrystallized carbonate that in most places cannot be readily correlated with regional formations

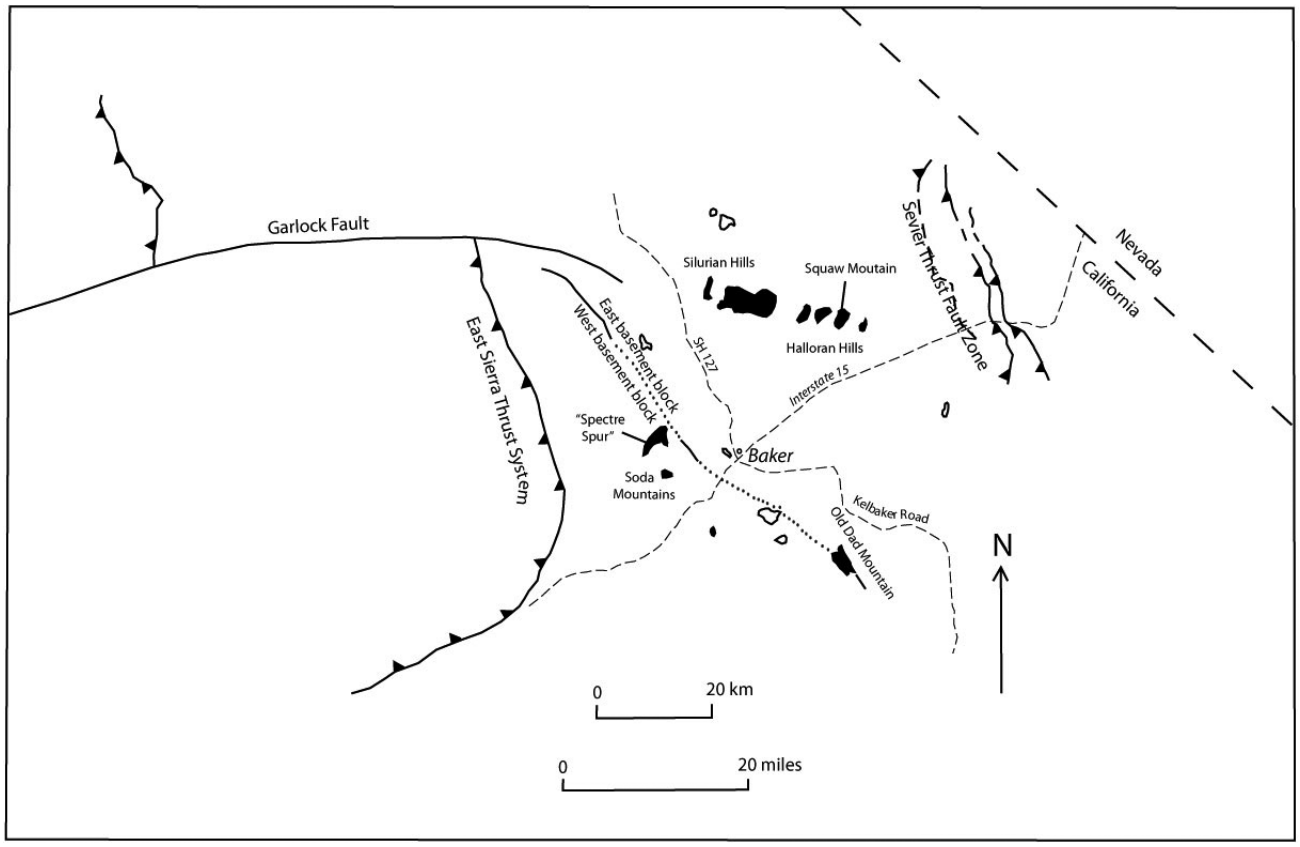

Figure 2: Regional Map showing the outcrop areas of allochthonous carbonate discussed in this paper relative to the Mesozoic East Sierra Thrust System and Sevier thrust zone. Areas of solid black show locations of carbonate considered definitely related to the subject of this article. Note solid shaded areas are outcrops of carbonate possibly related to this article. Footwall rocks below the allochthonous carbonate can be divided into east and west blocks as shown on the map. The east block exposes Proterozoic to Paleozoic units and the west block exposes Mesozoic volcanic and sedimentary strata.

because of its strong recrystallization. Kupfer (1960) makes a strong argument on the basis of thickness and lithologic characteristics that the carbonate is Paleozoic. Confirmation of this interpretation was made by Walker and Wardlaw (1989), who identified the Cambrian Bonanza King through Mississippian Monte Cristo Formations in the eastern Silurian Hills where the carbonate is not as strongly recrystallized as other parts of the range. An important aspect of the upper plate rock is that it is folded annd the folds are cut by the Riggs fault.

Exposed footwall rock consists of Proterozoic cratonal basement, upper Proterozoic Pahrump Group strata, and upper Proterozoic to lower Paleozoic siliciclastic miogeoclinal deposits of the Johnny, Stirling, Wood Canyon, Zabriskie, and Carrara Formations (Kupfer, 1960; Basse, 1978). The geometry of these units defines a horizontal, west-northwest trending anticline that extends the 5 km width of the Silurian Hills. This lower plate fold is cut by and, thus, older than the Riggs fault. Similarly, large scale folds in the upper plate carbonate are also cut by the fault.

A "chaos structure" is developed in the footwall of the fault in a zone up to a few hundred meters thick just below the fault (Kupfer, 1960). The chaos zone contains a series of fault blocks bounded by anastomosing low-angle faults that are sub-parallel to the Riggs fault. Kupfer called the zone "chaos structure" because of its structural similarities to what Noble (1941) named chaos structure in the Death Valley area. An important aspect of chaos structure in both areas is that the chaos blocks are stacked in a younger-on-older arrangement. This geometry is most easily explained by normal faulting. Indeed, for the Death Valley area, the chaos structure is attributed to movement along the Amargosa "thrust fault" (Hunt and Mabey, 1966), a fault now recognized as a regional-scale low angle normal fault (Wright and Troxel, 1987).

It is clear the chaos structure in the Silurian Hills developed at the time of Riggs fault activity. Critical

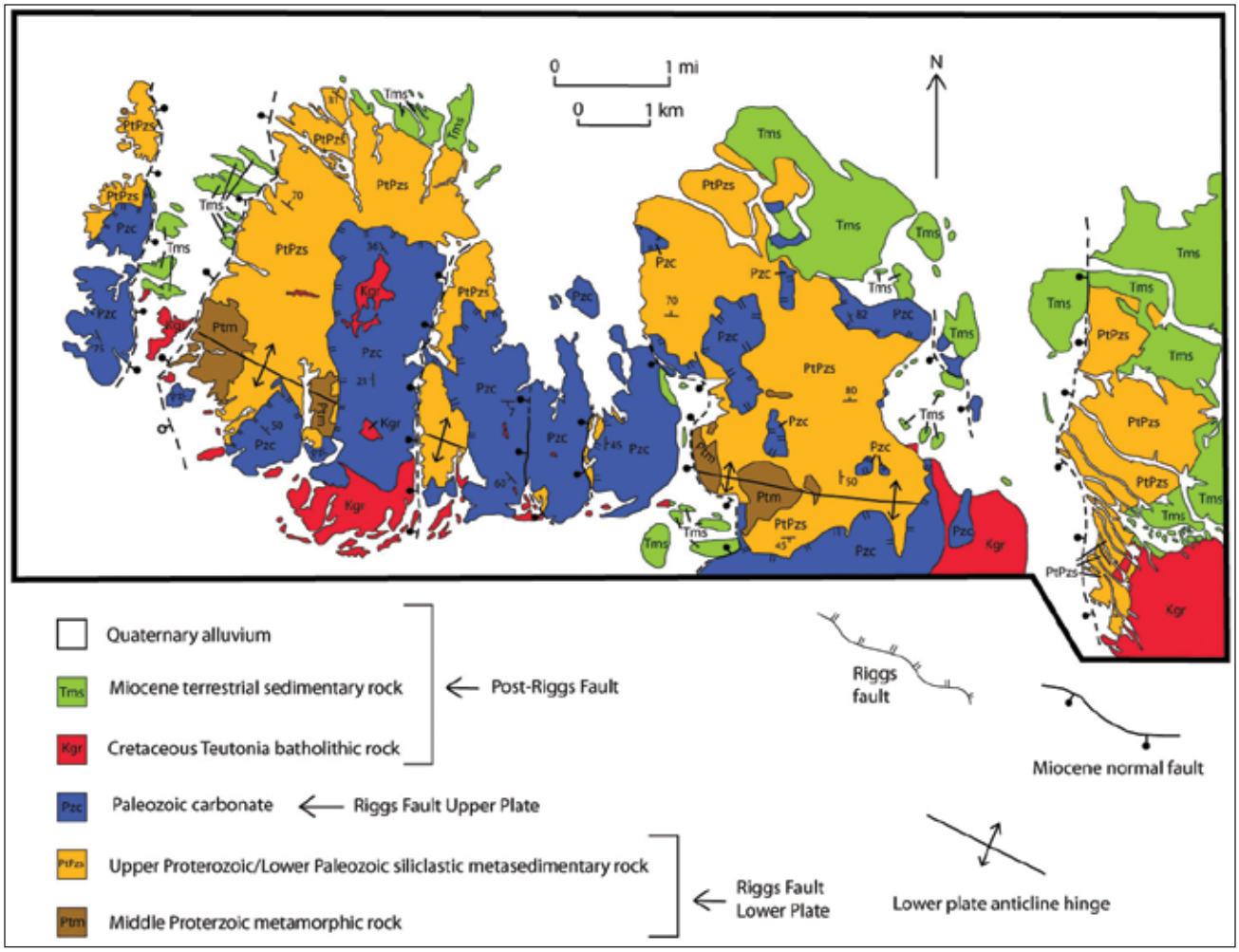

Figure 3: Geologic map of Silurian Hills. Modified from Kupfer (1960).

evidence supporting this notion is the observation that the chaos structure is locally developed in the Riggs fault hanging wall. At these locations, one or more lenses of siliciclastic lower plate rocks are structurally encased within the Riggs upper-plate carbonate.

The development of the chaos structure in the Silurian Hills is interpreted to be the result of drag stresses caused by the movement of the Riggs carbonate allochthon across the footwall. The thickest part of the chaos structure is developed in the hinge zone of the footwall's large anticlinal fold.

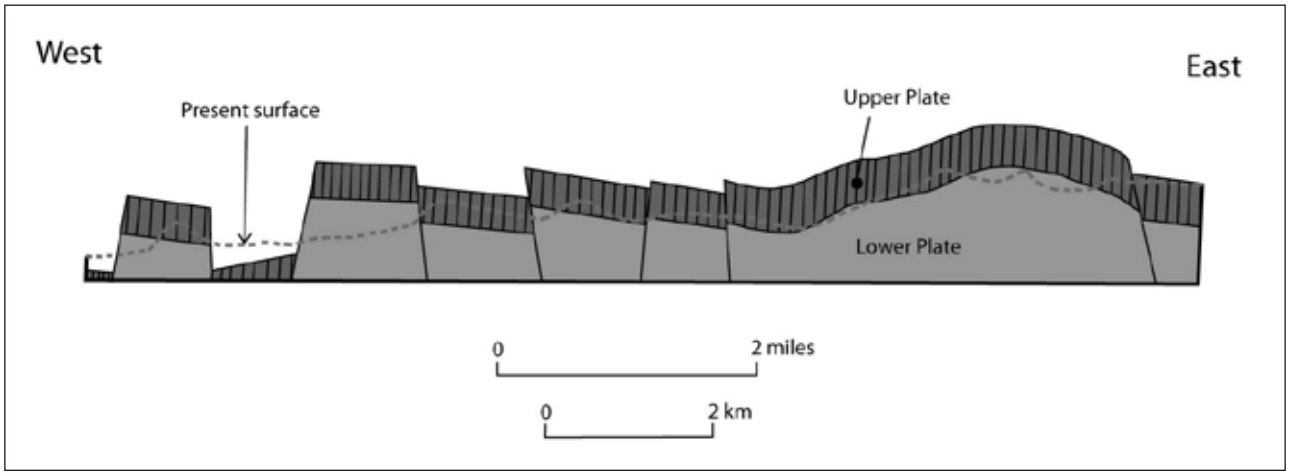

Figure 4: Diagrammatic east-west cross-section of the Silurian Hills. Modified from Kupfer (1960).

Figure 5: Photo of chaos faults in the western Silurian Hills. View towards north. Notice each fault displaces east-dipping strata westward.

In the hinge zone, the weak bedding planes in the footwall strata are parallel to the Riggs fault plane and, therefore, favorably oriented for slippage caused by shear stresses present when the Riggs allochthon slipped across the footwall rocks (Bishop, 1994). Locally, the sense of displacement of chaos faults can be discerned from matching offset beds across faults. An excellent example is shown in Figure 5, where upper plate strata of each fault are displaced westward relative to footwall strata. Given the evidence that the chaos faults are coeval with the Riggs fault, the Riggs allochthon is interpreted to have been west-directed.

Sutter (1968) interpreted the timing of Riggs fault activity to be 85-95 m.y.a. based on K-Ar dates from granitic intrusions that pre- and post-date Riggs fault movement. Walker and Wardlaw (1989) used uranium-lead geochronology on zircon obtained from a granitic intrusion that cuts the fault and determined an age of 104 +/- 30 m.y. The 90-100 Ma Teutonia batholith (De Witt et al., 1984) intrudes the fault (Bishop, 1994). Collectively, these ages support a Cretaceous age for the fault.

Within the Riggs allochthon are numerous normal faults that were active coevally with the Riggs fault. The contemporaneous relation of the faults is demonstrated by the observation that the normal faults root into either the Riggs fault or secondary low-angle faults associated with the Riggs fault. Stereographic plots of fault and slickenline orientations (Fig. 6) indicate the extension direction accommodated by the normal faulting is nearly due east-west. Assuming extension was parallel to the direction of upper plate transport, then this observation in conjunction with offset directions of chaos faults indicates the Riggs allochthon moved essentially due west.

East of the Silurian Hills in the Halloran Hills are outcrops of rocks correlative to both the footwall and hanging wall rocks of the Riggs fault. Four outcrop areas of Paleozoic carbonate in the Halloran Hills are isolated remnants of the Riggs allochthon (Fig. 2) (Bishop, 1994). An important observation is that the hanging wall rocks at Squaw Mountain contain not only carbonate, but also stratigraphically older siliciclastic strata including Cambrian Wood Canyon,

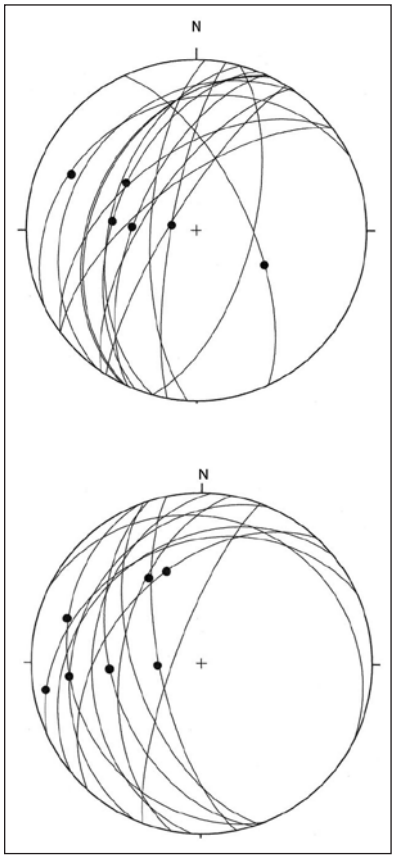

Figure 6: Equal area, upper hemisphere stereogram for synkinematic normal faults in the Riggs fault upper plate, Silurian Hills. The upper diagram shows data from the western Silurian Hills and the lower diagram shows data from the eastern part of the range. Great circles represent fault planes and dots represent slickenlines.

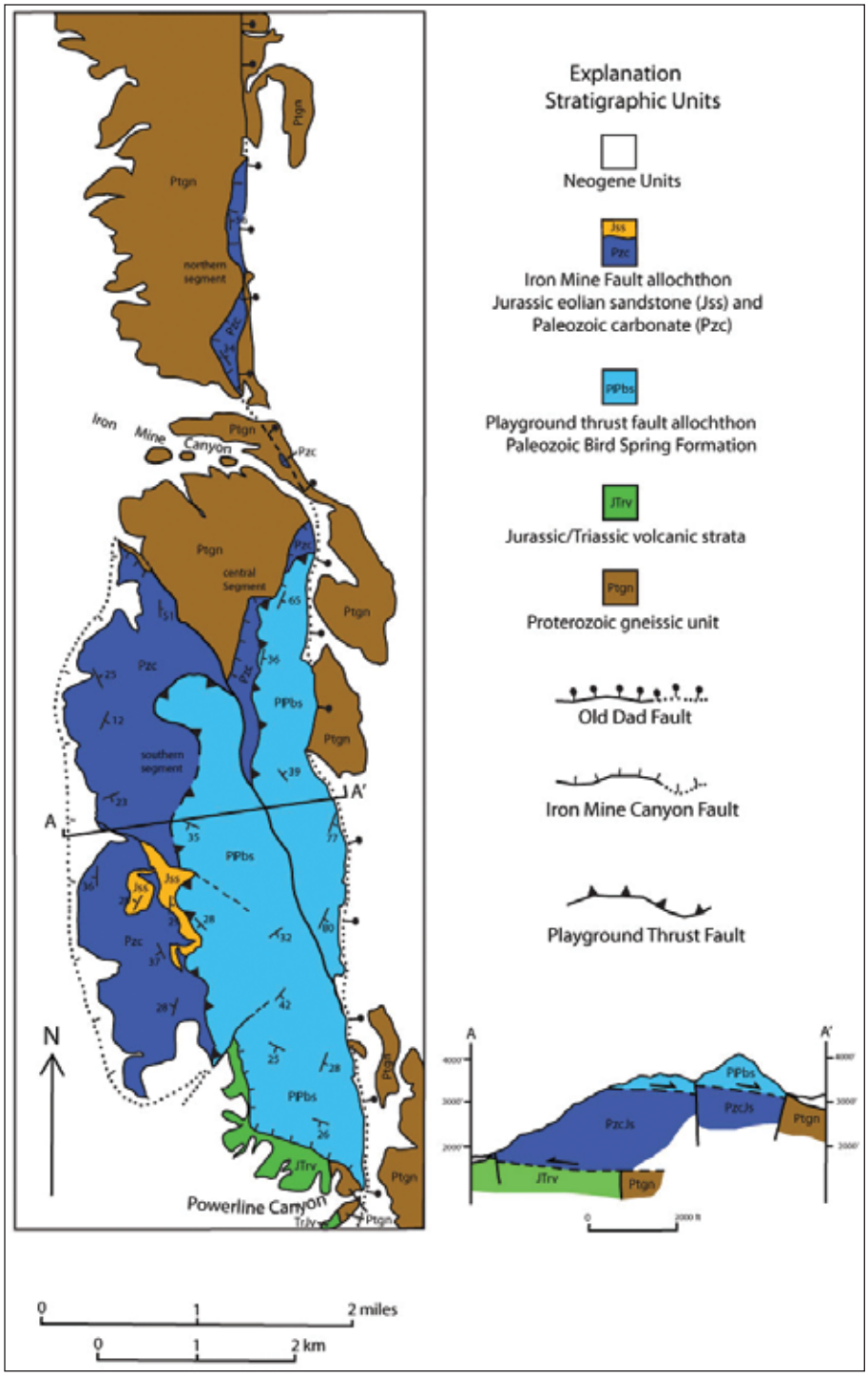

Figure 7: Geologic map of Old Dad Mountain area. Modified from Dunne (1977).

Zabriskie, and Carrara Formations. Thus, the Riggs allochthon is not entirely Paleozoic carbonate. Another important observation from the western Halloran Hills is that footwall rocks include Bonanza King Formation, which indicates the autochthonous rocks locally includes strata correlative to the allochthon strata. Clearly, the Riggs fault cuts across stratigraphic horizons. This agrees with the observation that upper and lower plate folds are cut by the Riggs fault. The overall conclusion is that the Riggs fault is developed primarily in Paleozoic miogeoclinal carbonate, but not entirely.

Old Dad Mountain

Old Dad Mountain exposes low- to moderately- east dipping fault segments divided by Dunne (1977) into southern, central, and northern segments (Fig. 7). When corrected for Cenozoic tilting based on restoring nearby Miocene sedimentary rock to horizontal, the faults are nearly horizontal. The three segments are exposed in a north-trending outcrop belt and are separated from one another by younger high angle faults. Dunne (1977) interpreted the three segments as likely related to one another and named the system the Playground thrust fault.

Kinematic evidence documented by Dunne (1977), mainly from the geometry of asymmetric folds developed in the hanging wall just above the Playground thrust, indicates southeast transport of the allochthon. Dunne indicates his data was collected along the central segment.

More recent kinematic data collected from the northern segment, however, contradicts the evidence cited by Dunne from the central segment. Upper plate carbonate rock within a zone 1 to 2 meters above the northern fault segment contains a ductile fabric with asymmetric folds and mineral lineations. Overturned asymmetric folds consistently indicate southwestward vergence (Fig. 8). Ductile mineral lineations trend approximately

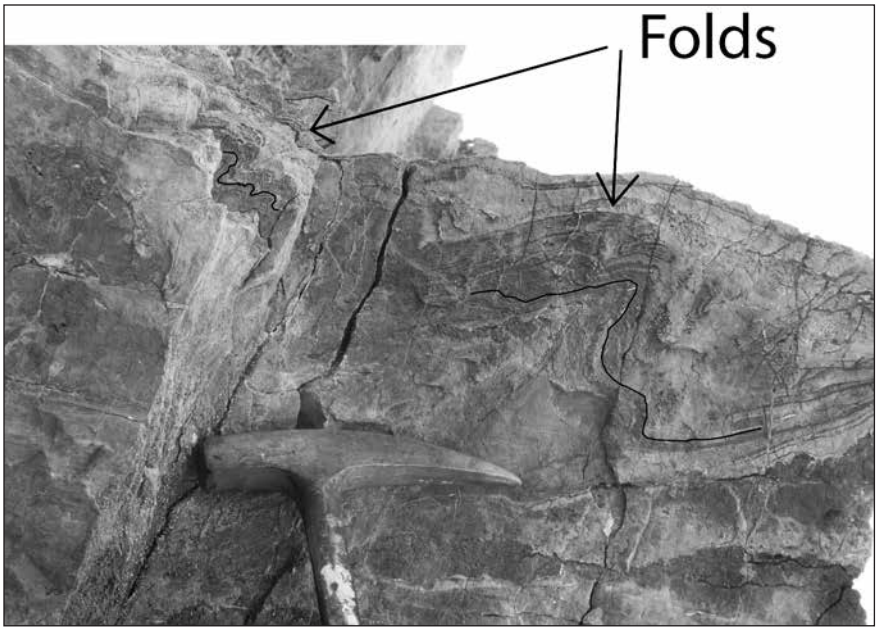

Figure 8: Asymmetric folds in ductile carbonate along the Iron Canyon fault. View is toward the south. Dark line outlining folds is drawn on photo to clarify folds.

S45W (Bishop and Cole, 1996) (Fig. 9). The divergence of transport directions for the central and northern segments indicates the two segments are not part of the same deformation episode. The northern segment is herein named the Iron Mine Canyon fault and the term Playground thrust fault reserved for the portions of the central and southern segments where the Bird Springs Formation is placed on either Jurassic sandstone or Bird Spring Formation. The Playground thrust designation thus applies to the majority of the central and southern segments, but is not considered to apply to the portions where the Iron Canyon fault and Playground thrust fault merge. Support for this interpretation comes from the fact that the Iron Mine Canyon fault contains lower Paleozoic carbonate in its hanging wall, whereas the Playground thrust fault has upper Paleozoic Bird Springs Formation in its hanging wall.

The two faults are interpreted to merge in two areas at Old Dad Mountain. One area is just south of Iron Mine Canyon, where the faults merge and are coincident for a distance of approximately 300 m (Fig. 7). The second area is just north of Powerline Canyon where the two faults merge at the northernmost point where Bird Spring Formation overlies volcanic strata and are coincident for a distance of 2 km (Fig. 7). Where the two faults are merged, one fault must cut or overprint the other, but it has not yet been determined directly from structural evidence along the fault which deformational episode is younger.

Regional considerations, however, provide evidence that the Playground thrust fault is older than and thus is cut or overprinted by the Iron Mine Canyon fault. The Playground thrust fault cuts Jurassic eolian sandstone deposits in the footwall that rest unconformably on Bird Spring Formation. The Jurassic unconformity below the Playground thrust, which does not contain the volcanic strata, is stratigraphically similar to the Jurassic unconformity (referred to as the J-0 unconformity) present in the Mescal Range northeast of Old Dad Mountain (Marzolf, 1990). As described by Marzolf (1990) this J-0 unconformity with Jurassic eolian sandstone on Bird Spring Formation forms a north-trending belt to the north of the Mescal Range. Marzolf noted that the unconformity located at Old Dad Mountain is misaligned from that of the belt to the north. Further

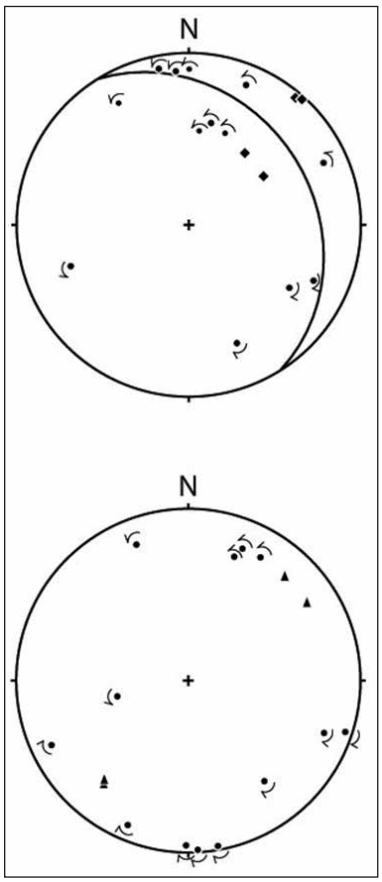

Figure 9: Equal area lower hemisphere stereogram of data from Iron Mine Canyon fault at Old Dad Mountain showing orientation of asymmetric folds and ductile mineral lineations in hanging wall along Iron Mine Canyon fault. The great circle represents the strike and dip of the fault plane, dots represent fold hinges and diamonds represent mineral lineations. Top diagram shows data as measured in field. Bottom diagram shows rotated data assuming fault plane is horizontal. The arrows along fold hinges show sense-of-shear indicated by fold asymmetry when viewed down-plunge of the fold hinge.

noting that the Playground thrust fault occupies the same structural position as the Mollusk Mine thrust in the Mescal Range, he suggests that the Playground thrust fault and the underlying footwall with the sandstone/Bird Spring Formation J-0 unconformity have been displaced westward from a position originally south of the Mescal Range. The Iron Mine Canyon fault, with its southwestward upper plate displacement direction would be the logical candidate to have moved the Playground thrust fault westward, but obviously only if the Iron Mine Canyon fault is younger than the Playground thrust fault.

Assuming the Iron Mine Canyon fault is younger than the Playground fault, then the Iron Canyon Mine fault must be younger than the eolian sandstone beds, which are cut by the Playground fault. The sandstone beds are correlated to the Middle Jurassic Carmel or Entrada Formations (Busby-Spera, 1988) or with the Early (to Middle?) Jurassic Aztec Sandstone (Marzolf, 1990). As an upper constraint, the Iron Mine Canyon fault is older than the Miocene Old Dad fault that cuts it (Dunne, 1977). If the Iron Mine Canyon fault correlates with the Cretaceous Mollusk Mine fault in the Mescal Range (Fig. 1) as suggested by Marzolf (1990), then it, too, must be Cretaceous.

Soda Mountains

Geological mapping of the Soda Mountains was performed by Grose (1959). Walker and Wardlaw (1989) later published a detailed map of an area in the northern Soda Mountains informally referred to by Grose as "Spectre Spur" (Figs. 1 and 8). Within the Soda Mountains, including at Spectre Spur, are several erosional remnants of a Paleozoic carbonate allochthon resting on top of a lithologically varied autochthon (Grose, 1959).

The autochthonous rocks are divided into two lithologically distinctive blocks by the high-angle, north-striking Soda Mountains fault zone that cuts through the center of the Soda Mountains. East of the fault, exposed autochthonous rocks consist of Middle Proterozoic gneiss and Upper Proterozoic to Cambrian siliciclastic metasedimentary units. West of the fault, exposed autochthonous rocks consist of Mesozoic volcanic and sedimentary rock. The autochthonous rock structure in the Soda Mountains is strongly reminiscent of the autochthon structure at Old Dad Mountain. According to Grose's (1959) mapping, the Soda Mountains fault zone aligns with the active Southern Death Valley fault zone and is a segment of it. In this region south of the Avawatz Mountains (Fig. 1), evidence suggests no more than a few kilometers offset along the Southern Death Valley fault zone (Davis, 1977).

In the area east of the Soda Mountains fault zone, the fault contact between allochthonous Paleozoic carbonate and autochthonous older units are sparse and cryptic (Grose, 1959). West of the fault zone, the low-angle contact is locally moderately well-exposed. The carbonate on volcanic rocks relationship is particularly well-displayed in the southern Soda Mountains south of Interstate 15 where a klippe of carbonate occurs high on the crest of the range surrounded by topographically and structurally lower volcanic rock. Chert blebs and stringers in the carbonate suggest the carbonate correlates to the Mississippian Monte Cristo Formation. A few smaller outcrops of recrystallized carbonate at the foot of the mountains east of ZZYZX Desert Studies Center also clearly overlie Mesozoic volcanic and sedimentary rock.

The Spectre Spur area in the northern Soda Mountains provides evidence for the sense of displacement of the low-angle faulting. At this location the largest exposure of allochthonous carbonate within the Soda Mountains is exposed (Grose, 1959) (Fig. 10). Although the basal detachment surface is not exposed, within the carbonate allochthon are seven stacked low-angle faults that are well-exposed and interpreted as related to the large displacement low-angle fault separating the carbonate from structurally underlying volcanic rock throughout the range (Grose, 1959). The hanging wall strata in each fault block dip moderately to steeply eastward and are cut discordantly by the underlying low-angle fault. The strata dip is attributed to a deformational event prior to development of the low-angle faults. An east-west cross-section constructed using Walker and Wardlaw's (1989) map is presented in Figure 10. Because displacements along the low-angle faults are not large, offset stratigraphic contacts can be matched across many of the faults. The displaced contacts indicate top-to-the-west separation.

The volcanic and sedimentary strata underlying the carbonate allochthon provide a lower age constraint for the age low-angle faulting. Within the Mesozoic volcanic and sedimentary sequence

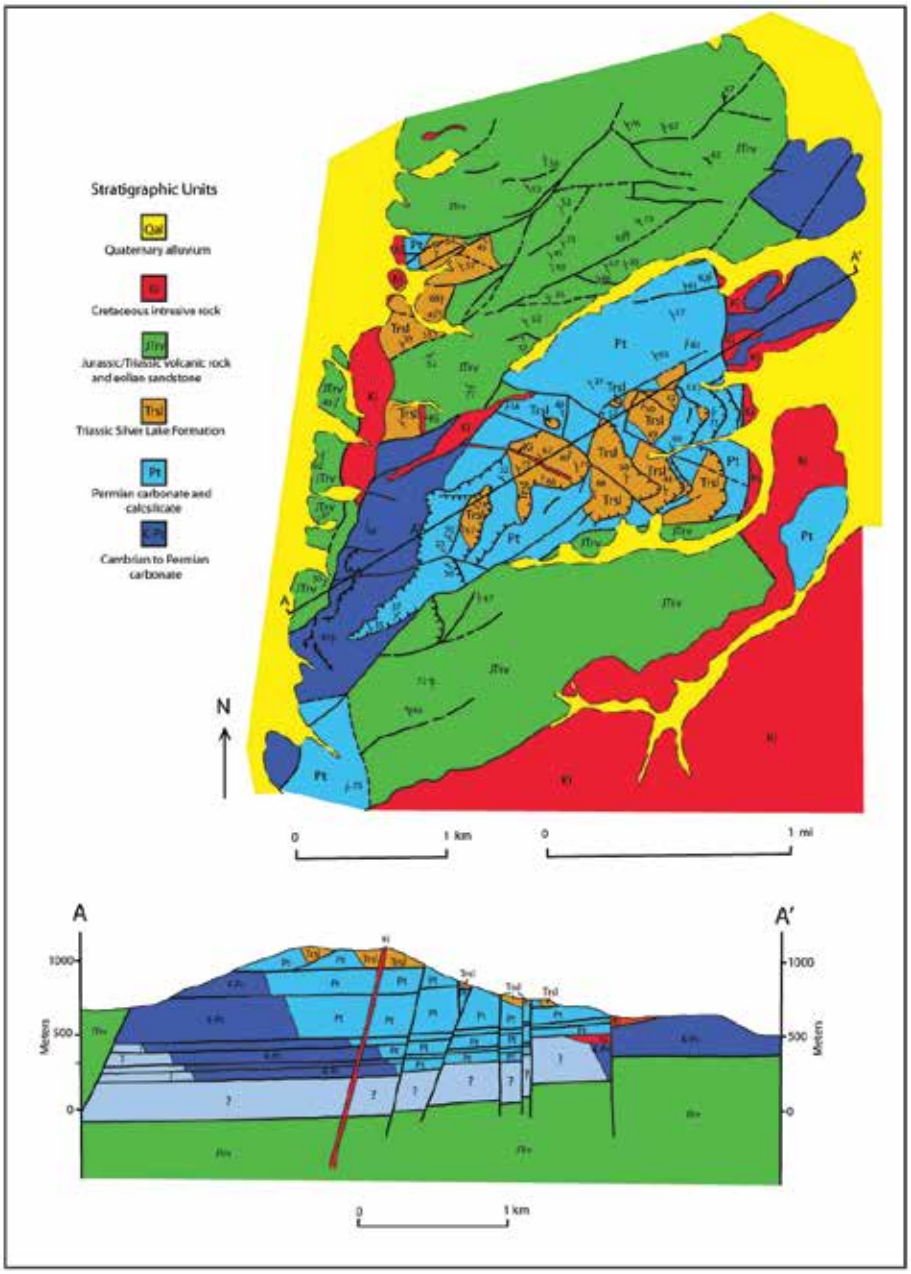

Figure 10: Geologic map and cross-section of "Spectre Spur" in the northern Soda Mountains. Modified from Walker and Wardlaw (1989).

are sandstone beds with large-scale eolian cross-bedding (Grose, 1959; Walker and Wardlaw, 1989). These sandstones are interpreted to correlate with the Middle Jurassic Carmel or Entrada Formations (Busby-Spera, 1988) or with the Early (to Middle?) Jurassic Aztec Sandstone (Marzolf, 1990). Another age constraint for the faulting is provided by Cretaceous intrusive rocks that cross-cut the low-angle faults at Spectre Spur (Walker and Wardlaw, 1989). Thus, the age of low-angle faulting in the Soda Mountains is constrained by cross-cutting relationships to have occurred between the Middle Jurassic and Cretaceous.

Exposure of the Mesozoic volcanic and sedimentary rock sequence exposed in the northern Soda Mountains continues northward into the western Avawatz Mountains. Exposed just east of these outcrops in the southern Avawatz Mountais are tilted and erosionally beveled Miocene sedimentary strata. Intercalated within the sedimentary strata are several megabreccia beds interpreted to be rock avalanche deposits (Spencer, 1990) that were derived from the area of the Mesozoic rock (Bishop and Brady, 2006). Most of the megabreccia deposits consist of Paleozoic carbonate. A few of the megabreccia masses contain lenses of Mesozoic volcanic rock below the carbonate. This relationship is interpreted to indicate that the landslides were derived from the volcanic rocks at a time when an allochthon of Paleozoic carbonate was present above the Mesozoic volcanic rocks (Bishop and Brady, 2006). The carbonate allochthon is now completely erosionally removed from the area of the Mesozoic outcrops. The cryptic allochthon is interpreted to have been the northern extension of the carbonate allochthon present in the Soda Mountains and gives evidence to its regional extent.

Discussion

The following summary observations and interpretations from the Silurian Hills, Soda Mountains, and Old Dad Mountain are considered key to understanding low-angle faulting in the region of these mountains.

1. Structural evidence from the Silurian Hills indicates the Riggs carbonate allochthon was transported approximately due west.
2. Evidence of synkinematic upper plate extension and the presence of "younger-on-older" chaos structures throughout the Silurian Hills is evidence that the low-angle faulting does not represent regional scale thrust faulting (i.e., horizontal compressional deformation).
3. Offset strata in the Soda Mountains indicate westward displacement for the allochthons exposed in the range.
4. Structural evidence from Old Dad Mountain indicates the upper plate of the Iron Mine Canyon fault, a low-angle structure below the Playground thrust fault, was transported approximately S45W.
5. In each of the three ranges, allochthonous carbonate underwent significant deformation prior to the low-angle faulting.

A fundamental question in understanding the tectonic origin of faulting in the Silurian Hills, Soda Mountains, and Old Dad Mountain is whether or not the faulting in the three ranges is related to a single deformational event. The salient evidence in attempting to answer this question is the following. At each location, the upper plate consists primarily of Paleozoic carbonate that was transported westward or southwestward, which is anomalous to the east-directed thrusting in the ESTS to the west and the Sevier thrust belt to the east. Radiometric and cross-cutting relationships indicate faulting occurred in the Jurassic and/or Cretaceous in each case (Walker et al., 1995; Walker et al. 1990). Where most tightly constrained, the age of faulting is indicated to be Cretaceous. Finally, both the autochthonous and allochthonous rocks were deformed prior to low angle faulting. Autochothonous rocks consist of Proterozoic and lower Paleozoic rocks in eastern areas and Mesozoic volcanic and sedimentary rock in the west (Fig. 2). This configuration of autochthonous rocks is interpreted to reflect the presence of a northwest-striking fault that divides the area into east and west fault blocks. The fault is exposed in the southern Old Dad Mountain area (Fig. 7) and corresponds to the Soda Mountains fault in the Soda Mountains. Because of the similarities in vergence, age, and the rock involved, it is interpreted here that the low-angle faults have a common geologic origin and their present limited distribution represents erosional remnants of a once continuous allochthon.

If the low-angle west-directed faulting in the three ranges is not related, then one must assume there were three separate tectonic events that created the structural similarities between the ranges. The likelihood that unrelated low-angle faults involving similar rock with similar transport direction active at similar or identical time seems low. The simplest, and seemingly best interpretation, is that there is common origin for the low-angle faults exposed in the various ranges.

Model

Because Baker, California is more or less centered between the Silurian Hills, Soda Mountains, and Old Dad Mountain, the low-angle faulting in these ranges collectively will be referred to as the "Baker area low-angle faulting". The Middle and/or Late Mesozoic Baker area low-angle faulting was contemporaneous with horizontal shortening associated with plate tectonic convergence along the Cordillera margin. The East Sierra thrust system in the central Mojave Desert has been interpreted to have been active in the late Middle or early Late Jurassic (Walker et al., 1990) and the Sevier thrust system in the eastern Mojave to have been active from the Late Jurassic through the Cretaceous (Walker et al., 1995). The evidence for the age of the Baker area low-angle faulting indicates it was likely contemporaneous with Sevier thrusting. If so, the Baker area faulting occurred in the hinterland of the active Sevier thrust belt.

Crustal extension in the Sevier hinterland during thrust activity has been proposed for many areas of the southern Cordillera (Hodges and Walker, 1992), including the region of the Baker area low-angle faulting. In many of the hinterland areas structural evidence indicates the extension involved west-directed upper plate movement. Hodges and Walker (1992) presented a model whereby the extension is hypothesized to have resulted from gravitational unloading of the hinterland crust thickened by Sevier thrusting. In their model extension occurred at mid to deep crustal levels along buried ductile detachment faults that did not reach upper crustal levels. Wells and Hoisch (2008) describe Cretaceous extension along west-vergent low-angle normal faults

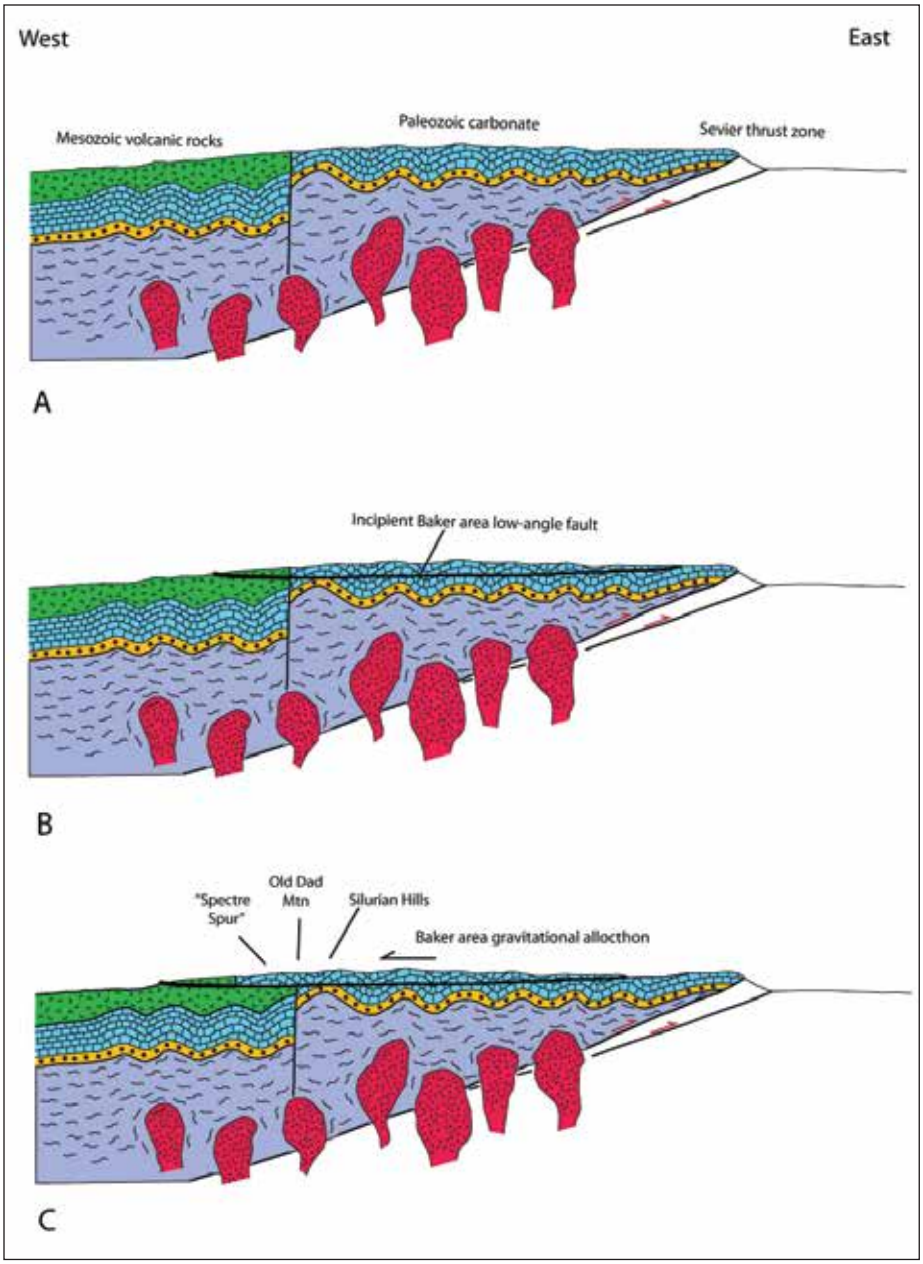

Figure 11 A-C: Conceptual model for the origin of Mesozoic Baker area low-angle faulting. Diagram A shows the region just prior to development of the faulting. Regional deformation and uplift is associated with Sevier thrust faulting and/or arc plutonic activity. B shows incipient low-angle fault surface, which represents the base of a regional scale landslide. C shows landslide allochthon after displacement. Note carbonate has moved across the high angle fault and is emplaced above Mesozoic volcanic rocks.

coeval with Sevier thrust faulting, but attribute the extension to mantle delamination. In their model, the hinterland extension was accommodated by low angle normal faults that reached from upper crustal levels and rooted into the lower crust. In their model, the upper plates of these low-angle detachment faults were extended by high-angle normal faulting.

Because of the evidence for upper plate extensional deformation in the Silurian Hills and because the Baker area low-angle faulting was west-vergent, it is attractive to attempt to tie the Baker area faulting to either the Hodges and Walker (1992) or Wells and Hoisch (2008) model. In trying to discriminate which model might better apply, it needs to be noted that nowhere in the Baker area low-angle faulting is mylonite present in the footwall, which indicates that the exposed faults were active at brittle upper crustal levels. Thus, the Hodges and Walker (1992) model does not appear applicable to the Baker area faulting. The model proposed by Wells and Hoisch (2008), which allows for upper crust faulting, seems more compatible. However, is no evidence that the Baker area low-angle faulting roots into the lower crust as in the model of Wells and Hoisch (2008).

In the direction of upper plate transport, east to west, the exposures of the Baker area low-angle faults occur in a belt 40 km (25 miles) wide. Across the belt, there is no indication the basal fault cuts significantly downward into the crust. If it is assumed the Mesozoic volcanic and sedimentary rocks in the area have a stratigraphic thickness of about 5 km, which is the maximum thickness identified in the East-southern and -central California region (e.g., Stevens et al., 1998; Dibblee, 1994), then the depth of the basal Baker area low-angle faulting can be no more than 5 km because the Mesozoic rocks occur in the footwall.

Assuming a breakaway in the eastern Halloran Hills area, the furthest east area with carbonate that is confidently interpreted as part of the allochthon, and a depth of 5 km in the Soda Mountains, where

the footwall Mesozoic rock occur, then the dip angle for the basal fault averaged 7 degrees when it was active. It is important to note that this is a maximum average dip angle based on the least possible horizontal distance. Assuming a breakaway in the Cima Dome area, where an outcrop of carbonate (Fig. 2) rests structurally on Proterozoic gneissic rock, and a horizontal distance that extends to the westernmost Mesozoic rock exposure (just east of the ESTS), the horizontal distance is 60 km. This geometry leads to the basal fault having an average dip of 5 degrees. A dip of 5 to 7 degrees for a tectonic fault that was active within a few km of the surface across a horizontal distance of more than 40 km seems unlikely. The best known potential tectonic analogue known to this author for such low-angle, crustal-scale fault dips are the "detachment" normal faults that formed in many western North America locations during Oligocene/Miocene continental extension (Burchfiel et al., 1992; Wernicke, 1985). The Miocene low-angle faults cut through upper crustal levels for many kilometers, but the dip of these faults at the time of activity was 10 to 15 degrees, approximately twice as steep as the dip indicated for the Baker area low-angle normal faulting. Another difference between the Miocene detachment faults and the Baker area low-angle faults, which is related to the dip differences of the faults, is that most of the more widely exposed Miocene faults display mylonitized footwall rock. No mylonitic footwall rocks are exposed below the Baker area low-angle faults.

A more significant problem to attributing the Baker area low-angle faulting to crustal extension is that nowhere west of the Soda Mountains has a west-directed low-angle fault been mapped, much less a low-angle fault that cuts downward into the crust, in other words, the lack of a crustal rooting fault. All known outcrops of the Baker area allochthon are klippe. If the Baker area faulting is represents tectonic faulting produced by crustal extension, then somewhere a basal fault must cut downward into the lower crust. The lack of any such fault suggests the Baker area fault zone is not the result of crustal-scale extension.

Based on the lack of evidence for a crustal rooting basal fault and a shallow depth of faulting across more than 40 km minimum, the model that emerges to explain the Baker area low-angle faulting is one of a large-scale west-vergent landslide. A conceptual model for the faulting is presented in Figure 11. In the model, gravitational potential for landslide movement is provided by uplift of the hinterland during Sevier thrust faulting and/or thermal regional uplift from arc intrusive activity. An attractive aspect of this model is that it is consistent with the Baker area low-angle faulting having been coeval with thrusting in the Sevier belt.

The majority of the allochthon consists of Paleozoic carbonate that was deposited as a several kilometer thick sequence along the passive margin of Western North America (Burchfiel et al., 1992). Stratigraphically below the carbonate, the passive margin sequence consists of latest Proterozoic to earliest Paleozoic siliclastic units. These siliclastic units were involved in the landsliding to only a minor extent. A couple explanations might account for the mainly exclusive involvement of carbonate. First, the carbonate forms the upper part of the several thick passive margin sequence in the region. Landsliding requires a downhill gradient of the slip surface in order to move under gravitational influence. It may have been that geometrically only a slip surface developed in the carbonate could have had the required gradient. In other words, the siliclastic units may have been too deep to be involved in landsliding. Another possibility is that only the carbonate rocks had sufficient shear weakness to move down the low-angle slip surface. Frictional and cohesive resistance to sliding of the siliclastic units may have been sufficient that an extensive slip surface could not develop in these units.

A remarkable aspect of the landslide is the low angle of the fault plane. The mechanics for movement across such a low gradient surface are not clear. However, a regional scale landsliding across a slide plane dipping only a few degrees has precedent. The Eocene Heart Mountain allochthon, a landslide that covered at least 3400 km^2 (Hauge, 1985), a size comparable to the 4000 km^2 or more Baker area allochthon, slid on a surface that dipped at less than 2 degrees (Hague, 1985).

A major controversy regarding the Heart Mountain allochthon is the rate of movement. Evidence has been presented for slow rates of movement (Hague, 1985) and for catastrophic rates (Craddock et al., 2009). The evidence of ductile deformation in the hanging wall block along the fault in the Old Dad Mountains suggests slow displacement. Perhaps

carbonate flowage rather than frictional sliding accounts for the mechanics of slippage along the low gradient of the Baker area low-angle fault.

A few questions arise regarding the Baker area allochthon. First, how much displacement occurred? In order to place Paleozoic carbonate on top of the Mesozoic rocks exposed in the west part of the allochthon area, a minimum of about 6 km (4 miles) is required. Second, where is the toe of the landslide allochthon? Presumably, the west part of the allochthon consisted of Mesozoic strata as shown in Figure 11. Allochthonous Mesozoic strata have not been identified, but this could be because the strata have been erosionally removed since emplacement of the allochthon. In the model presented here, the toe area is to the west of the Spectre Spur area, but need not be further west than approximately 6 km, the minimum displacement distance of the allochthon.

Despite uncertainties in the gravitational allochthon model for the Baker area low-angle faulting, the model seems to best explain all of the available evidence. Furthermore, the model provides a unified explanation for the low-angle faulting and eliminates the need for a model in which the deformation in the various ranges serendipitously involves structurally and temporally similar, but unconnected, faulting.

Acknowledgements

The author thanks Nate Onderdonk and Andre Ellis for helpful reviews of the article.

References

Basse, R. A., 1978, Stratigraphy, sedimentology, and depositional setting of the Late Precambrian Pahrump Group, Silurian Hills, California (M.S. thesis): Palo Alto, California, Stanford University, 79 p.

Bishop, K. M., 2009, The Riggs fault, southeastern California: a brittle, west-vergent, Mesozoic low-angle normal fault: Geological Society of America Abstracts with Programs, v. 41, no. 7, p. 129.

Bishop, K. M., 1994, Mesozoic and Cenozoic extensional tectonics of the Halloran and Silurian Hills area, eastern San Bernardino County, California (Ph.D. dissertation): University of Southern California, 252 p.

Bishop, K. M. and Brady, M., 2006, Stratigraphic evidence from Miocene megabreccia deposits for a regional-scale Mesozoic allochthon in the western Soda and Avawatz Mountains, eastern Mojave Desert, California; in Girty, G.H. and Cooper, J.D., Using Stratigraphy, Sedimentology, and Geochemistry to Unravel the Geologic History of the Southwestern Cordillera, Pacific Section SEPM Society for Sedimentary Geology, p. 337-254.

Bishop, K. M. and Cole, D., 1996, Evidence for a southwest-vergent Mesozoic low-angle fault in the Old Dad Mountains, southeastern California: Geological Society of America Abstracts with Programs, v. 28, no. 7, p. A-115.

Burchfiel, B. C., Cowan, D. S., and Davis, G. A., 1992, Tectonic overview of the Cordilleran orogen in the western U. S., in Burchfiel, B. C., Lipman, P. W., and Zoback, M. L., eds., The Cordilleran Orogen: conterminous U. S.: The Geology of North America, Volume G-3, Decade of North American Geology, Geological Society of America, Boulder, p. 407-480.

Busby-Spera, C. J., 1988, Speculative tectonic model for the early Mesozoic arc of the southwest Cordilleran United States: Geology, v. 16, p. 1121-1125.

Craddock, J. P., Malone, D. H., Magloughlin, J., Cook, A. L., Rieser, M. E., and Doyle, J. R., 2009, Dynamics of the emplacement of the Heart Mountain allochthon at White Mountain: Constraints from calcite twinning strains, anisotropy of magnetic susceptibility, and thermodynamic calculations: Geological Society of America Bulletin, v. 121 no. 5-6 **p. 919-938.**

Davis, G. A., 1977, Limitations on displacement and southeastward extent of the Death Valley fault zone, California: California Division of Mines and Geology Special Report 129, p. 27-33.

De Witt, E., Armstrong, R. L., Sutter, J. F., and Zartman, R. E., 1984, U-Th-Pb, Rb-Sr, and Ar-Ar mineral and whole-rock isotopic systematics in a metamorphosed granitic terrane, southeastern California: Geological Society of America Bulletin, v. 95, p. 723-739.

Dibblee, T. W., Jr., 1994, Pre-Cenozoic rock units of the Mojave Desert; in, Murbach, D. and Baldwin, J., eds., Mojave Desert Annual Field Trip Guidebook #22, South Coast Geological Society, Santa Ana, CA, p. 100-127.

Dunne, G. C., 1977, Geology and structural evolution of Old Dad Mountain, Mojave Desert, California: Geological Society of America Bulletin, v. 88, p. 737-748.

Grose, L. T., 1959, Structure and petrology of the northeast part of the Soda Mountains, San Bernardino County, California: Geological Society of America Bulletin, v. 70, p. 1509-1547.

Hauge, T. A., 1985, Gravity-spreading origin of the Heart Mountain allochthon, northwestern Wyoming: Geological Society of America Bulletin, v. 96, p. 1440-1456.

Hodges, K. V. and Walker, J. D., 1992, Extension in the Cretaceous Sevier orogen, North American craton: Geological Society of America Bulletin, v. 104, p. 560-569.

Hunt, C. B., and Mabey, D. R. (1966). Stratigraphy and structure Death Valley, California. U.S. Geological Survey Professional Paper 494-A.

Kupfer, D. H., 1960, Thrust faulting and chaos structures in the Silurian Hills, San Bernardino County, California: Geological Society of America Bulletin, v. 71, p. 181-214.

Marzolf, J. E., 1990, Reconstruction of extensionally dismembered early Mesozoic sedimentary basins; southwestern Colorado Plateau to the eastern Mojave Desert, in Wernicke, B.P., ed., Basin and Range extensional tectonics of Las Vegas, Nevada: Boulder, Colarado, Geological Society of America Memoir 176, p. 477-500.

Noble, L. F., 1941, Structural features of the Virgin Spring area, Death Valley, California: Geological Society of America Bulletin, v. 52, p. 941-1000.

Spencer, J. E., 1990, Late Cenozoic extensional and compressional tectonism in the southern and western Avawatz Mountains, southeastern California: in Wernicke, B. P., ed., Basin and Range Extensional tectonics near the latitude of Las Vegas, Nevada, Geological Society of America Memoir 176, p. 317-333.

Stevens, C. H., Stone, P., Dunne, G. C., Greene, D. C., Walker, J. D., and Swanson, B. J., 1998, Paleozoic and Mesozoic evolution of east-central California; in, Ernst, W. G. and Nelson, C. A., eds., Integrated Earth and Environmental Evolution of the Southwestern United States: The Clarence A. Hall, Jr., Volume, Bellwether Publishing, Ltd., Columbia, MD, p. 119-160.

Sutter, J. F., 1968, Geochronology of major thrusts, southern Great Basin, California (M.A. thesis): Houston, Texas, Rice University, 32 p.

Troxel, B. W. and Wright, L. A., 1987, Tertiary extensional features, Death Valley region, eastern California, in Hill, M. L., ed., Decade of North America Geology, Centennial Field Guide, v. 1, p. 121-132.

Walker, J. D., Burchfiel, B. C., and Davis, G. A., 1995, New age controls on initiation and timing of foreland belt thrusting in the Clark Mountains, southern California: Geological Society of America Bulletin, v. 107, p. 742-750.

Walker, J. D., Martin, M. W., Bartley, J. M., and Coleman, D. S., 1990, Timing and kinematics of deformation in the Cronese Hills, California, and implications for Mesozoic structure of the southwestern Cordillera: Geology, v. 18, p. 554-557.

Walker, J. D., and Wardlaw, B. R., 1989, Implications of Paleozoic and Mesozoic rocks in the Soda Mountains, northeastern Mojave Desert, California, for late Paleozoic and Mesozoic Cordilleran orogenesis: Geological Society of America Bulletin, v. 101, p. 1574-1583.

Wells, M. L. and Hoisch, T. D., 2008, The role of mantle delamination in widespread Late Cretaceous extension and magmatism in the Cordilleran orogen, western United States: Geological Society of America Bulletin, v. 120, p. 515-530.

Wernicke, B., 1985, Uniforma-sense normal simple shear of the continental lithosphere: Canadian Journal of Earth Sciences, v. 22, p. 108-125.

Interstratified arkosic and volcanic rocks of the Miocene Spanish Canyon Formation, Alvord Mountain area, California—descriptions and interpretations

David Buesch

Geology, Minerals, Energy, and Geophysics Science Center, U.S. Geological Survey, 345 Middlefield Road, MS 973, Menlo Park, CA 94025; dbuesch@usgs.gov

ABSTRACT: The Spanish Canyon Formation in the Alvord Mountain area, California, varies from about 50 to 120 m thick and records the interstratification of arkosic sandstone and conglomerate with tuffaceous deposits and lava flows. In the lower third of the formation, arkosic sandstone and conglomerate are interstratified with tuffaceous deposits. Some tuffs might have been deposited as primary, nonwelded to partially welded ignimbrites or fallout tephra. Many of the tuffaceous deposits represent redeposited material that formed tuffaceous sandstone, and many of these deposits contain arkosic grains that represent mixing of different source materials. Arkosic sandstone, and especially conglomerate (some with maximum clast lengths up to 1 m), represent intermittent incursions of coarser plutoniclastic fan deposits into otherwise finer grained and mostly volcaniclastic basin deposits. After deposition of the 18.78 Ma Peach Spring Tuff, the amount of tuffaceous material decreased. The upper two-thirds of the formation has arkosic sandstone and conglomerate interstratified with two olivine basalt lava flows. Locally, conglomerate clasts in this part of the section have maximum lengths up to 1 m. Many tuffaceous and arkosic sandstone beds of the Spanish Canyon Formation have tabular to broad (low-relief) lenticular geometry, and locally, some arkosic conglomerate fills channels as much as 1.5 m deep. These bedforms are consistent with deposition in medial to distal alluvial-fan or fluvial environments; some finer-grained deposits might have formed in lacustrine environments.

Introduction

The Spanish Canyon Formation exposed in the Alvord Mountain area, southern California, contains arkosic sandstone and conglomerate that are interstratified with primary and redeposited tuffs and two olivine basalt lava flows (Byers, 1960; Buesch and others, 2013; Figure 1). The formation represents incursions of alluvial fans into a depocenter dominated by tuffaceous rocks in the lower part of the section and two incursions of olivine basalt lava flows near the top of the section.

Arkosic sandstone and conglomerate also forms most of the Clews Formation, which underlies the Spanish Canyon Formation in many locations, and most of the Barstow Formation, which overlies the Spanish Canyon Formation (Byers, 1960; Fillmore, 1993). Many plutonic and metamorphic clasts in the Clews, Spanish Canyon, and Barstow Formations were derived from rocks exposed in the nearby Alvord Mountain and Cronese Hills, and some clasts were derived from rocks exposed in the Paradise Range to the northwest of the Alvord Mountain area (Byers, 1960; Fillmore, 1993). The Clews Formation locally includes minor amounts of tuffaceous beds near the bottom, middle, and top of the formation, and the Barstow Formation locally includes tuffaceous deposits and a three basalt flows (Byers, 1960). In the east-central Alvord Mountain area along the western limb of the Spanish Canyon anticline, the Alvord Peak basalt is a thick accumulation of

basaltic andesite that overlies the Clews Formation and underlies the Spanish Canyon Formation (Byers, 1960). Byers (1960) described two other locations where the stratigraphic relations of what was mapped as possible Alvord Peak basalt are not well exposed, and he speculated that these exposures might be interstratified with the Barstow Formation. Fillmore (1993), citing unpublished mapping, also describes the possible interstratification Alvord Peak basalt and Barstow Formation. These potentially anomalous relations of Alvord Peak basalt remain unresolved and do not influence any of the stratigraphic relations described in this paper.

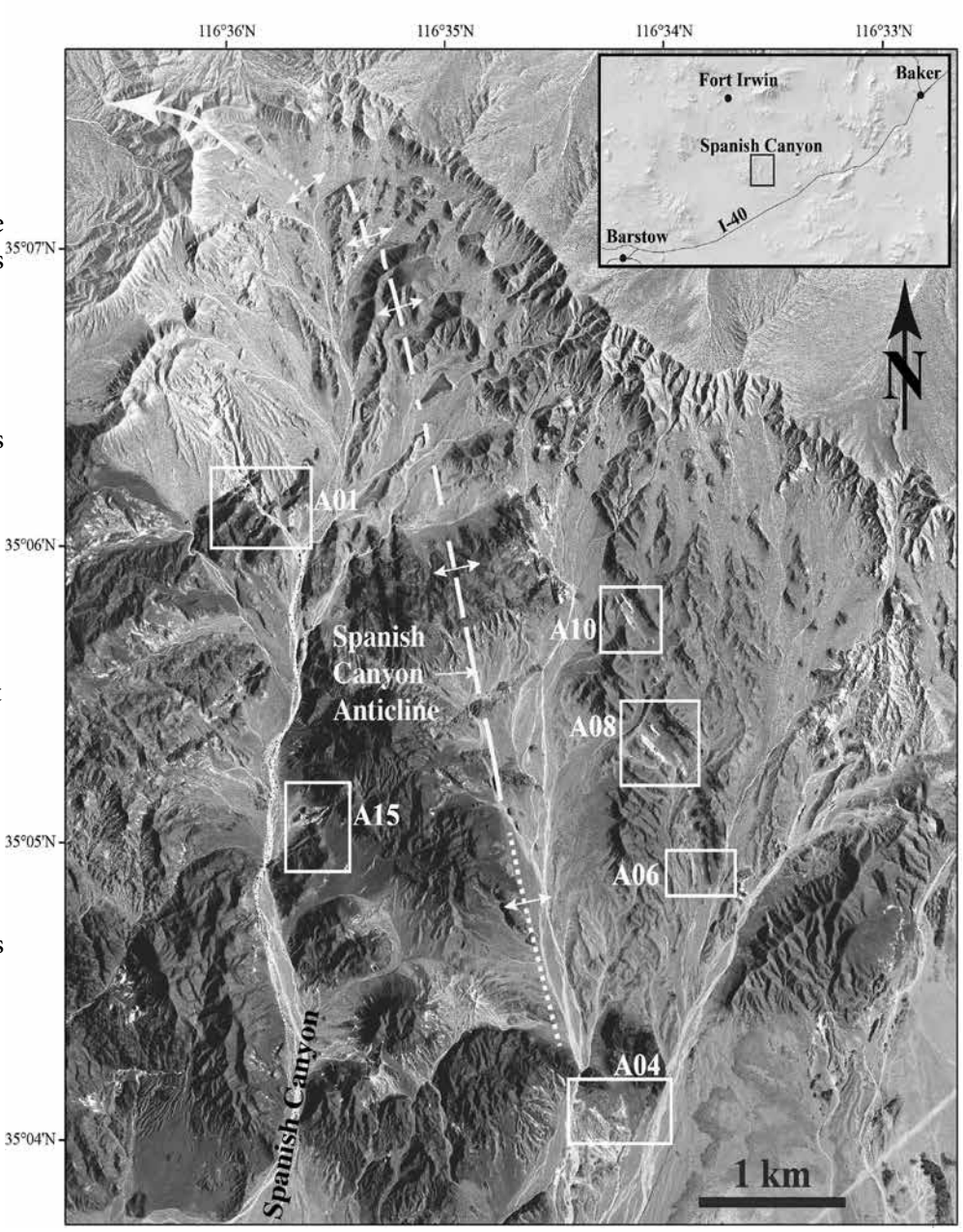

Figure 1. Areas of measured sections around the Spanish Canyon Anticline, Alvord Mountain area, California. Inset map shows location of the Spanish Canyon area in the east-central Mojave Desert.

The age of the Spanish Canyon Formation ranges from about 19.6 ± 0.2 Ma to between 18.5 and 18.0 Ma (Hillhouse and Miller, 2011; Buesch and others, 2013). The older age is based on paleomagnetic polarity zones and zircon U-Pb geochronologic data from the "gray tuff" that occurs near the base of the formation (Buesch and others, 2013). The younger age is more poorly constrained by the paleomagnetic polarity of two olivine basalt flows near the top of the formation. The lower basalt is reversely polarized and correlated to the lower part of chron C5E that ranges in age from 18.524 to 18.748 Ma, and the upper basalt is normally polarized and correlated to the upper part of chron C5E that ranges in age from 18.056 to 18.524 Ma (Hillhouse and Miller, 2011). In addition to these upper and lower age constraints, the Peach Spring Tuff (18.78 ± 0.02 Ma from Ferguson and others, 2013) occurs as a key marker bed within the formation (Fillmore, 1993; Hillhouse and Miller, 2011; Buesch, 2012; Buesch and others, 2013).

The Spanish Canyon Formation is discontinuously exposed for a distance of about 11 km along the limbs of the Spanish Canyon anticline (Figure 1). Byers (1960) initially named and described the formation as consisting of interstratified arkosic sandstone and conglomerate, tuff, and olivine basalt flows where tuffaceous deposits are at the base of the formation

Table 1. Lithostratigraphic sequences in the Spanish Canyon Formation, Alvord Mountain area, California

Symbol	Name
bs	olivine basalt and arkosic sandstone sequence
ub	upper basalt subsequence
as	arkosic sandstone subsequence
lb	lower basalt subsequence
us	upper sandstone sequence
ut	upper tuffaceous sequence (primarily formed by the Peach Spring Tuff)
ls	lower sandstone and tuffaceous sequence
lt	lower tuffaceous sequence

and the upper of two olivine basalts is at the top. Descriptions by Byers (1960) form the framework for the more detailed present study in which five lithostratigraphic sequences are distinguished: (1) the lower tuffaceous sequence, (2) the lower sandstone and tuffaceous sequence, (3) the upper tuffaceous sequence, (4) the upper sandstone sequence, and (5) the olivine basalt and arkosic sandstone sequence (Buesch and others, 2013; Table 1). The uppermost sequence is subdivided into three distinctly different units including the (A) lower basalt subsequence, (B) arkosic sandstone subsequence, and (C) upper basalt subsequence. Two sequences (the lower sandstone and tuffaceous sequence and upper sandstone sequence) and the arkosic sandstone subsequence contain various amounts of arkosic sandstone and conglomerate.

Throughout the Spanish Canyon Formation, several dip-slope ridges provide good exposures along the anti-dip slopes. Many tuffaceous deposits in the lower and upper tuffaceous sequences and the lava flows in the basalt and sandstone sequence are erosionally resistant and form dip-slope ridges. Typically, arkosic sandstone is not erosionally resistant, and in many places the beds are covered by alluvium or colluvium, so they only crop out locally. Some conglomerate beds form small ridges because large clasts mantle the beds and protect them from erosion. Many of the best exposures of arkosic sandstone and conglomerate are along anti-dip slopes.

Nine measured sections in six areas around the Spanish Canyon anticline, two on the west limb (areas A01 and A15) and four on the east limb (A10, A08, A06, and A04), demonstrate variations in thickness of the five sequences and the stratigraphic positions of notable amounts of coarse-grained arkosic sandstone and conglomerate (Figures 1 and 2; Table 2). All measured sections begin at the base of the Spanish Canyon Formation where it is overlies either the Alvord Peak basalt or the Clews Formation. In the following descriptions, the stratigraphic position is referenced to the height above the base of the measured section. Stratigraphic positions of (1) almost entirely arkosic sandstone and/or conglomerate bedsets, and (2) almost entirely tuffaceous bedsets are symbolically depicted in Figure 2. In the following descriptions, the areas are discussed from north to south, first along the west limb of the Spanish Canyon anticline, and then along the east limb.

Descriptions of arkosic sandstone and conglomerate

The amount of arkosic sandstone and conglomerate varies by area and lithostratigraphic sequence (Figure 2). The lower sandstone and tuffaceous sequence typically contains mostly redeposited (and possibly some primary) tuffs interspersed with arkosic sandstone and conglomerate. The upper sandstone sequence is primarily arkosic sandstone and conglomerate that locally contain a tuffaceous matrix in the lower part of the sequence giving way to a more arkosic matrix up section. The arkosic sandstone subsequence (within the olivine basalt lava and sandstone sequence) is arkosic sandstone and conglomerate. In both the upper sandstone sequence and the arkosic sandstone subsequence, the upper 1 to 2 m are progressively more reddish yellow to light red (Figure 3). Although this reddening might be attributed to thermal effects of the overlying basalt flow, it also could be due to oxidation associated with a relatively stable geomorphic surface developed on the sandstone prior to deposition of the lava flow.

Many coarse-grained arkosic sandstone and conglomerate bedsets can be traced for about 5 to 100 m (with some local cover by alluvium), and in areas 08 and 10, conglomeratic bedsets can be traced for about 220 and 170 m, respectively. Although individual bedsets have limited lateral extents, exposures are consistent with several bedsets at effectively the same stratigraphic position. Correlations of some stratigraphically equivalent conglomeratic bedsets between areas are supported by intermittent exposures.

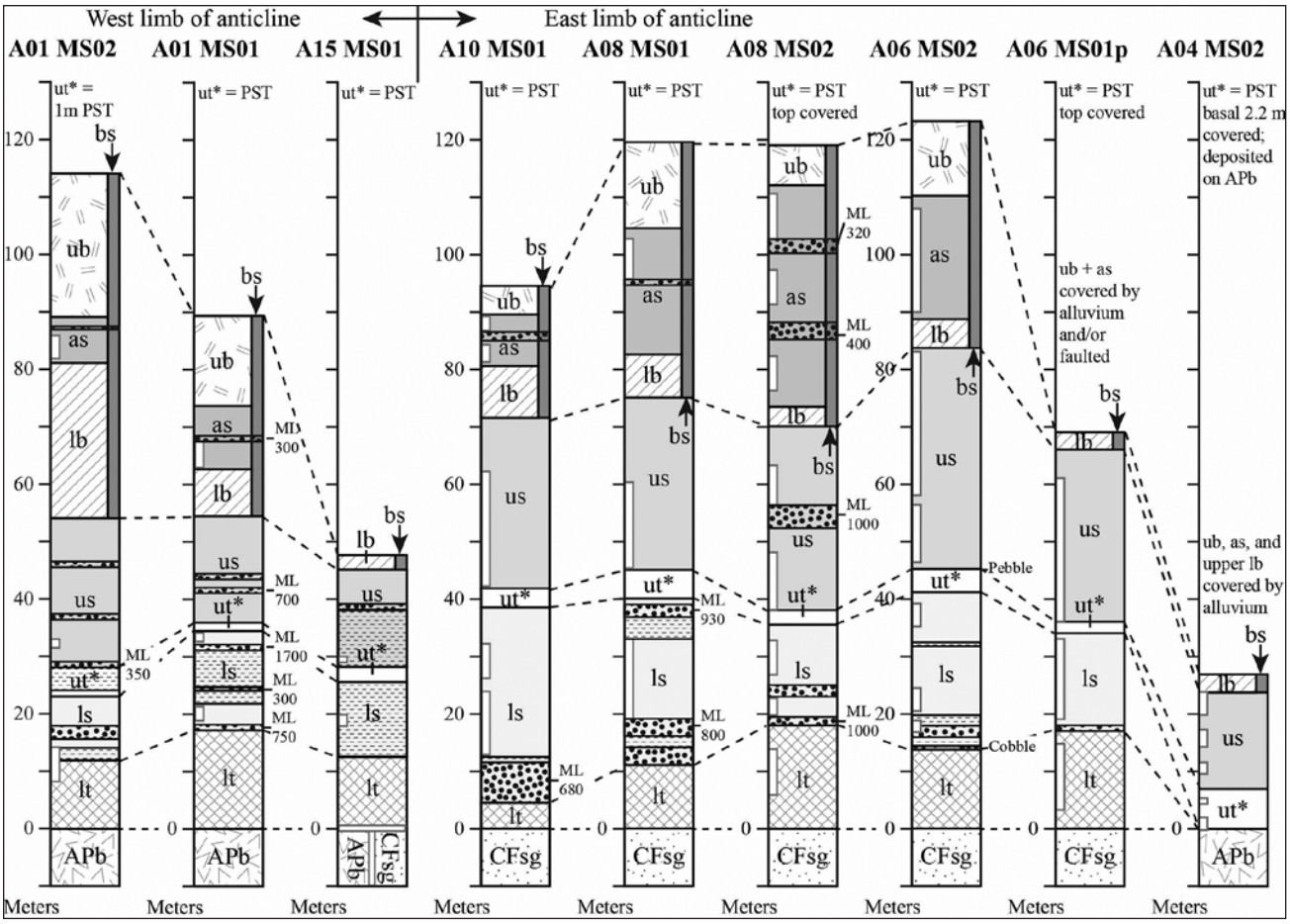

Figure 2. Measured sections in the Spanish Canyon Formation, Alvord Mountain area, California. Large dot overlays are mostly coarse-grained arkosic sandstone and conglomerate bedsets. Short horizontal dash overlays are mostly tuffaceous bedsets. See Tables 1 and 2 for definitions of stratigraphic sequences and symbols.

Area 01

Area 01 contains the type section of the Spanish Canyon Formation defined by Byers (1960), and measured section A01-MS01 closely approximates the type section. Section A01-MS02 is only about 250 m to the northwest of A01-MS01; however, there are two faults between these measured sections. One fault, which is concealed beneath alluvium, has about 25-30 m of right-slip separation across a 345° striking and an apparently steeply dipping fault. The other fault strikes ~035° with moderate to steep dips to the southeast, and has mostly normal dip-slip separation with an unconfirmed amount of strike-slip separation. Between the two measured sections, exposures of some of the more distinctive bedsets support correlations of these units. Even though the five lithostratigraphic sequences can be correlated between the two measured sections, combinations of the two faults and local depositional facies decrease the ability to correlate individual beds or even bedsets.

In measured section A01-MS01, the lower sandstone and tuffaceous sequence consists of more tuffaceous rocks than arkosic sandstone and conglomerate. There are three arkosic conglomerate bedsets in this sequence (Figure 2). At 17.1 m is the base of a 1-m thick, arkosic cobble conglomerate containing mostly granitoid clasts, but also some diorite clasts. This bedset is discontinuously traced about 45 m eastward to a poorly exposed, 1-m to 2-m thick boulder conglomerate where the largest (maximum diameter) granitoid clast is 750 mm and the largest diorite clast is 220 mm (Table 3). At 25.5 m is a 30-cm thick arkosic cobble-to-boulder conglomerate in which the largest granitoid clast is 300 mm and the largest diorite clast is 100 mm (Table 3). At 31.9 m is a locally exposed (possibly a channel filling), 1-m thick arkosic boulder conglomerate in

Table 2. Thickness of lithostratigraphic sequences in measured sections in six areas of the Spanish Canyon Formation, Alvord Mountain area, California.
APb = Alvord Peak basalt; CFm = Clews Formation; PST = Peach Spring Tuff.

Cumulative thickness (top of unit)

Spanish Canyon sequences	Symbol	A01 MS01	A01 MS02	A15 MS01	A04 MS02	A06 MS01p	A06 MS02	A08 MS01	A08 MS02	A10 MS01
Basalt and sandstone sequence	bs									
upper olivine basalt lava	ub	89.3	114.0				123.2	119.5	119.0	94.5
arkosic sandstone-conglomerate	as	73.6	89.0				110.2	104.5	112.0	89.5
lower olivine basalt lava	lb	62.6	81.0	47.5		69.0	88.7	82.5	73.4	80.5
Upper arkosic sandstone sequence	us	54.4	54.0	45.0	23.8	66.0	83.7	75.0	70.0	71.5
Upper tuffaceous sequence (mostly PST)	ut	35.9	**28.0**	28.1	**7.0**	36.0	45.2	45.0	38.0	41.8
Lower arkosic sandstone and tuff sequence	ls	34.4	23.0	25.5	**ND**	**34.0**	41.2	40.0	35.5	38.5
Lower tuffaceous sequence	lt	17.1	12.0	12.5	**ND**	**17.0**	13.7	11.0	18.0	4.5
Substrate to Spanish Canyon Formation		APb	APb	APb or CFm	APb	CFm	CFm	CFm	CFm	CFm

PST is 1 m

Maximum thickness
ND - not deposited

Poorly exposed

Separate thickness

Spanish Canyon sequences	Symbol	A01 MS01	A01 MS02	A15 MS01	A04 MS02	A06 MS01	A06 MS02	A08 MS01	A08 MS02	A10 MS01
Basalt and sandstone sequence	bs									
upper olivine basalt lava	ub	15.7	25.0				13.0	15.0	7.0	5.0
arkosic sandstone-conglomerate	as	11.0	8.0				21.5	22.0	38.6	9.0
lower olivine basalt lava	lb	8.2	27.0	2.5		3.0	5.0	7.5	3.4	9.0
Upper arkosic sandstone sequence	us	18.5	26.0	16.9	16.8	30.0	38.5	30.0	32.0	29.7
Upper tuffaceous sequence (mostly PST)	ut	1.5	**5.0**	2.6	**7.0**	2.0	4.0	5.0	2.5	3.3
Lower arkosic sandstone and tuff sequence	ls	17.3	11.0	13.0	**ND**	**17.0**	27.5	29.0	17.5	34.0
Lower tuffaceous sequence	lt	17.1	12.0	12.5	**ND**	**17.0**	13.7	11.0	18.0	4.5

PST is 1 m

Maximum thickness
ND - not deposited

Poorly exposed

which the largest granitoid clast is 1700 mm and the largest diorite clast is 1030 mm (Table 3).

In the lower sandstone and tuffaceous sequence in section A01-MS01, most of the medium- to light-gray tuffaceous beds range in thickness from 5 cm to 1 m, are nonwelded, and have textures consistent with deposition from pyroclastic or debris flows and as redeposited tuffaceous sandstone. At 22.0 m is a 2.2-m thick, medium gray, nonwelded to partially welded tuff (ignimbrite) that is the thickest tuff in the sequence (Figure 4). The deposit contains pumice clasts (some with phenocrysts) and crystal fragments, but it also contains various amounts and sizes of rounded to subangular, stained quartz, feldspar, and

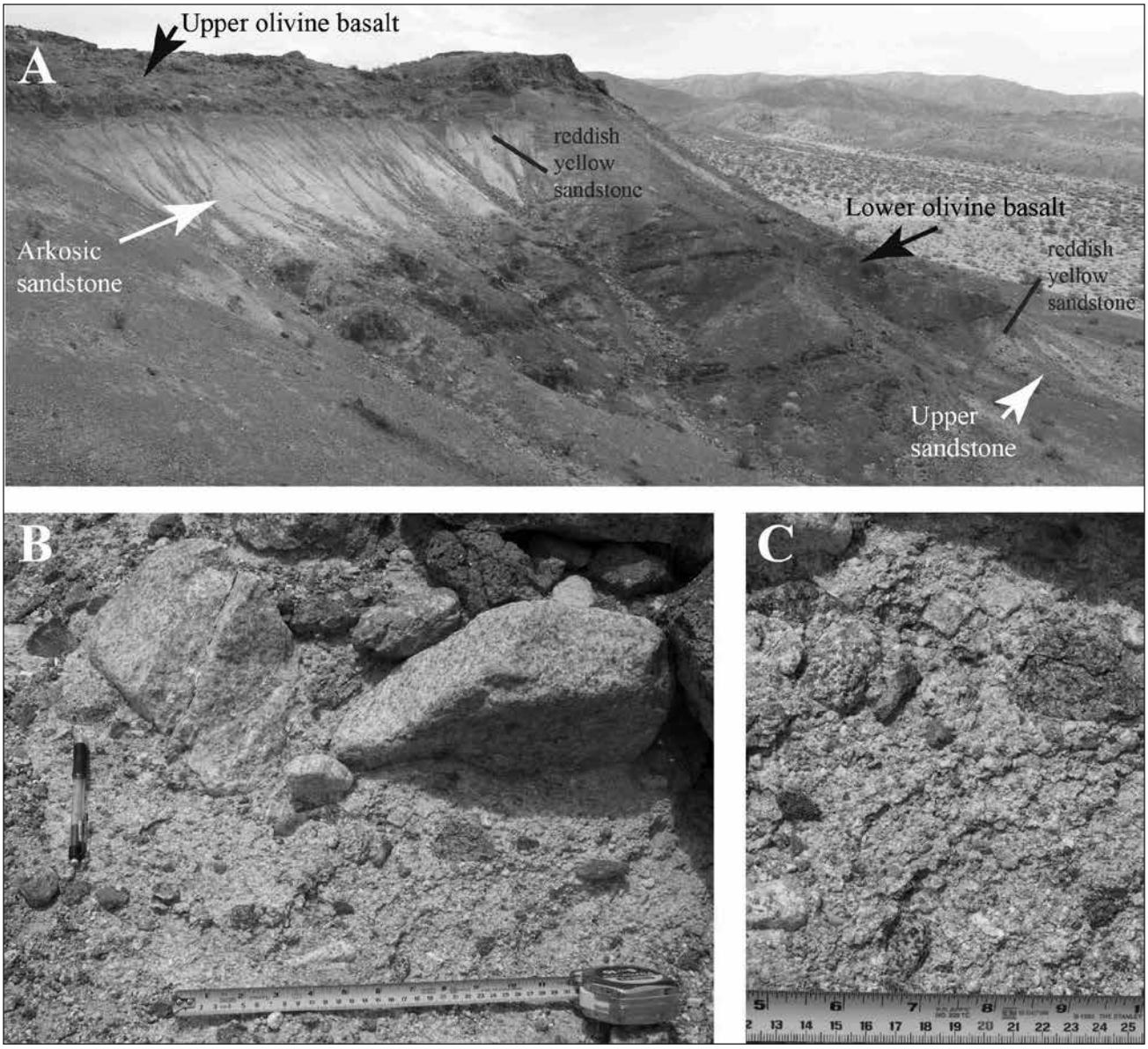

Figure 3. Photographs of the olivine basalt and arkosic sandstone sequence in measured section A01 MS01. (A) Overview of the sequence with reddish yellow (oxidized?) sandstone beneath the lava flows. (B) Detailed view of an arkosic conglomerate at 67.5 m in the section. (C) Detailed view of matrix in arkosic conglomerate.

plutonic clasts. This bed has a poorly developed basal layer that is 5 to 15 cm thick with a slight concentration of plutonic clasts and a few volcanic clasts that are less than 15 mm in size, and the upper contact of this basal layer is gradational with the main overlying bed. In addition, there is a large (maximum diameter of 320 mm) plutonic lithic clast at the base. The slightly lithic-rich basal layer and large clast are consistent with incorporation of substrate clasts into the base of a flow that had significant velocity (or high enough effective viscosity). In the middle of the bed, the aspect ratios of 16 pumice clasts (that is, the long axis divided by the short axis) range from 2 to 6 with an average of 3.7. These values for aspect ratios of pumice clasts are consistent with tuffs that are at least partially welded (Peterson, 1979). Based on similarities of crystal and pumice fragments, and the position just beneath the arkosic conglomerate, it is possible that this deposit also occurs in other measured sections (in particular, about 36 m in A08-MS01).

In both the upper sandstone sequence and the arkosic sandstone subsequence of measured section A01-MS01, the amount of arkosic material increases up section. The lowermost few meters of the upper sandstone sequence consist of sandstone with

Table 3. Maximum long axis of clasts in measured sections in six areas of the Spanish Canyon Formation, Alvord Mountain area, California.

Area	Way Point	Strat position (m)	Lithologic unit	Clast type	Descriptive term	Maximum long axis (ML, mm)	Comments
A01 ~MS01	3	~5	ls	volcanic		20	Base of "gray" tuff of Hillhouse and Miller (2011)
A01 ~MS01	3	~6.3	ls	volcanic		15	Upper part of "gray" tuff
A01 MS01	775	18	ls	granitoid		750	Projected ~45 m to MS01
A01 MS01	775	18	ls	diorite		220	Projected ~45 m to MS01
A01 ~MS01	~5	~25.5	ls	plutonic		80	
A01 MS01	~777	25.5	ls	granitoid		300	
A01 MS01	~777	25.5	ls	diorite		100	
A01 MS01	779	31.9	ls	granitoid		1700	
A01 MS01	779	31.9	ls	diorite		1030	
A01 ~MS01	8	42	us	granitic		700	
A01 MS01		67.5	as	granitoid and hbl diorite		300	
A01	771	~31.9	ls	granitoid	coarse conglomerate		Equivalent to MS01 31.9 m
A01	985	~31.9	ls	granitoid		500	Equivalent to MS01 31.9 m
A01	985	~31.9	ls	diorite		240	
A01 MS02	593	28	us	granitic/plutonic		350	
A01 MS02	599	86	as	granitoid	pebbly		
A04	146	7	us	volcanic and plutonic	sandstone		Deposited on the PST
A04	147	13.2	us	plutonic (and metamorphic?)	pebbles, cobbles		Possibly terrace deposit
A06 MS02	1017	13.7	ls	plutonic	coarse conglomerate		First arkosic conglomerate at base of "ls"
A06 ~MS02	1005	~14.4	ls	plutonic	sandstone		
A06 MS02	1006	19.7	ls	plutonic	sandstone		Tuffaceous sandstone
A06 MS02	1007	33.3	ls	pumiceous and plutonic	sandstone		Pumiceous tuff interstratified with arkosic sandstone
A06	26	~15	lt	pumice		30	Tuffaceous sandstone
A06	29	~42.5	us	???	pebbly ss		Bed deposited on top of PST

Table 3 continues

plutonic (granitoid and a few diorite) clasts with various amounts of tuffaceous matrix. In these exposures, the amount of arkosic material leads to the classification of these beds as part of the upper sandstone sequence rather than a redeposited tuff in the upper tuffaceous sequence. At about 42 m in section A01-MS01 (in the upper sandstone sequence), there are several conglomerate bedsets, one of which has a maximum clast diameter of 700 mm (Figure 2; Table 3). At 67.5 m in the arkosic sandstone subsequence, there is an arkose conglomerate with maximum clast diameter of 300 mm (Figures 2 and 3; Table 3).

There are more tuffaceous beds and finer-gained arkose conglomerate in measured section A01-MS02 than in A01-MS01 (Figure 2; Table 3). The lower sandstone and tuffaceous sequence consists of more tuffaceous beds than arkosic sandstone and conglomerate. The general trend of more tuffaceous material and finer-gained arkose conglomerate continues upward into the upper sandstone sequence.

Table 3 continued

Area	Way Point	Strat position (m)	Lithologic unit	Clast type	Descriptive term	Maximum long axis (ML, mm)	Comments
A06 ~MS01p	93	~17.2	ls	granitic	sandstone		
A06 MS01p	90	17.2	ls	granitic	fine to coarse-grained sandstone		First arkosic conglomerate at base of "ls"
A06	96	~36	us	tuffaceous	sandstone		Deposited on PST
A08 MS01	135	14	ls	plutonic	cobble, boulder		First arkosic conglomerate in "ls"
A08 MS01	135	19	as	granitoid		800	
A08 ~MS01	719	38	ls	plutonic and metamorphic		930	0-1 m thick, channel-fill deposit
A08 MS01	16	40	ut (PST)	plutonic		100	At top of PST basal ground layer (BGL)
A08	133	~72	us	granitic	sandstone to conglomerate		This location is projected about 65 m to the measured section MS01
A08 MS01	434	94.5	as	granitic	cobble to boulder conglomerate		0.7-m thick bed in sandstone to pebbly sandstone
A08	718B	~38	ls	plutonic		650	Tuffaceous matrix of sandstone
A08 MS02	1039	18	ls	granitoid (leucogranite)		1000	
A08 MS02	1039	18	ls	hbl diorite		700	
A08 MS02	127	52	us	plutonic		1000	
A08 MS02	1042	85	as	plutonic and metamorphic		400	
A08 MS02	1043	100	as	plutonic and metamorphic		320	
A10 MS01	1052	11.5	ls	granitoid		680	Arkosic conglomerate.
A10 ~MS01	18	38	us	volcanic + plutonic	pebbly ss		
A10 ~MS01	18	38.5	ut (PST)	plutonic		300	At top of PST basal ground layer (BGL)
A10 ~M-1	150	39.1	ut (PST)	plutonic		550	At top of PST basal ground layer (BGL)
A10 ~MS01	151	39.1	ut (PST)	plutonic		350	At top of PST basal ground layer (BGL)
A10 A01	458	80.5	as	plutonic	pebbly sandstone		
A10 MS01	1057	85	as	plutonic	conglomerate		
A15	570			granitic and metamorphic(?)		400	Tuffaceous(?) matrix of conglomerate

Beds within 4 m above the Peach Spring Tuff (PST) are tuffaceous sandstone (with various amounts of plutonic grains), and because of the amount of tuffaceous material, they are included in the upper tuffaceous sequence. At 28 m in the lower part of the upper sandstone sequence, the first arkosic sandstone and conglomerate has a 350 mm largest maximum clast diameter. Even the coarsest bed in the arkosic sandstone subsequence at 86 m is only a pebbly sandstone (in contrast to the 300 mm clast in the conglomerate in a similar stratigraphic position in section A01-MS01).

Area 15

In area 15, the Spanish Canyon Formation appears to overlie both the Alvord Peak basalt and the Clews Formation; however, the contacts are concealed beneath alluvium, terrace, or talus deposits (Figure 2). All five sequences of the Spanish Canyon

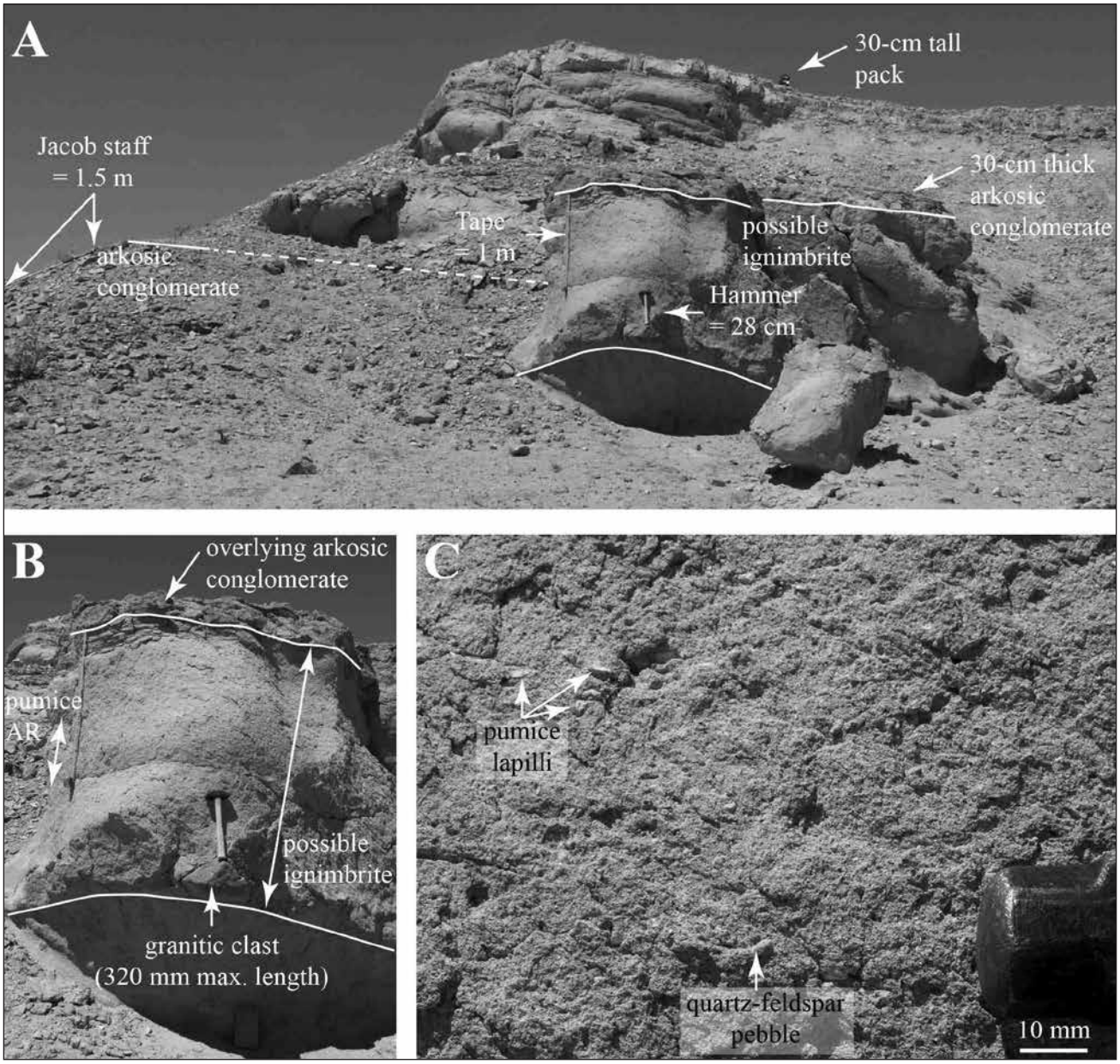

Figure 4. Photographs of the 2.4-m-thick, medium gray tuff in measured section A01-MS01 at 22.0 m in the section. (A) Possible nonwelded to partially welded ignimbrite with overlying conglomerate (contact at top and bottom or possible ignimbrite traced with white lines). Top of conglomerate (white line; solid where exposed, and dashed where partially covered by colluvium) is traced to the Jacob staff that is along measured section. Additional tuffs and tuffaceous sandstone bedsets along ridge crest. (B) Detail of possible ignimbrite with granitic clast at base. (C) Close-up of matrix with pumice (lapilli) clasts and quartz-feldspar-granitic fragments. Tape and hammer in same positions for all photographs.

formation are identified in this area, but only the lower olivine basalt flow is present in the uppermost sequence. Tuffaceous deposits dominate the lower sandstone and tuffaceous sequence and the upper sandstone sequence. In the lower sandstone and tuffaceous sequence, many beds are either pyroclastic or debris flows, and some tuffaceous beds appear to have been redeposited by stream flow. Many of the thicker beds or bedsets are 1 to 4.5 m thick. In the upper sandstone sequence, many beds appear to be redeposited tuffs, and grain size, textures, and bedforms are consistent with deposition in low-relief fluvial or possible lacustrine environments (Figure 5). There is one arkosic sandstone bedset less than 1 m thick at 38 m in the upper sandstone sequence.

Area 10

In the lower sandstone and tuffaceous sequence, parts of the arkosic sandstone and conglomerate are well exposed; however, many other parts of the arkosic sequences (including the upper sandstone

Figure 5. Tuffaceous sandstone in the upper sandstone sequence at 34 m in measured section A15-MS01.

sequence and arkosic sandstone subsequence) are obscured by alluvium or colluvium (Figure 2). From 4.5 to 11.5 m, there is a series of arkosic boulder conglomerate bedsets where the largest granitoid clast is 680 mm (Table 3). The bedsets can be traced for about 170 m along strike. The upper 15 m of the lower sandstone and tuffaceous sequence is locally exposed, and many of the rocks are plutoniclastic (with some volcaniclastic) sandstone to pebbly sandstone. From 80 to 85 m in the measured section, the arkosic sandstone subsequence contains arkosic pebbly sandstone to conglomerate; however, maximum clast sizes were not measured (Table 3).

Area 08

In Area 08, measured sections A08-MS01 and A08-MS02 are about 280 m apart, and many of the arkosic parts of the sections are covered by alluvium or colluvium (Figure 2). In both sections A08-MS01 and A08-MS02, the lowermost 8 m of the lower sandstone and tuffaceous sequence contains several arkosic conglomerate bedsets that appear to be laterally equivalent; however, individual beds are not necessarily continuous across the area. In section A08-MS01 at 19 m, a conglomerate contains a granitoid clast with the largest diameter of 880 mm, and in section A08-MS02 at 18 m, a conglomerate

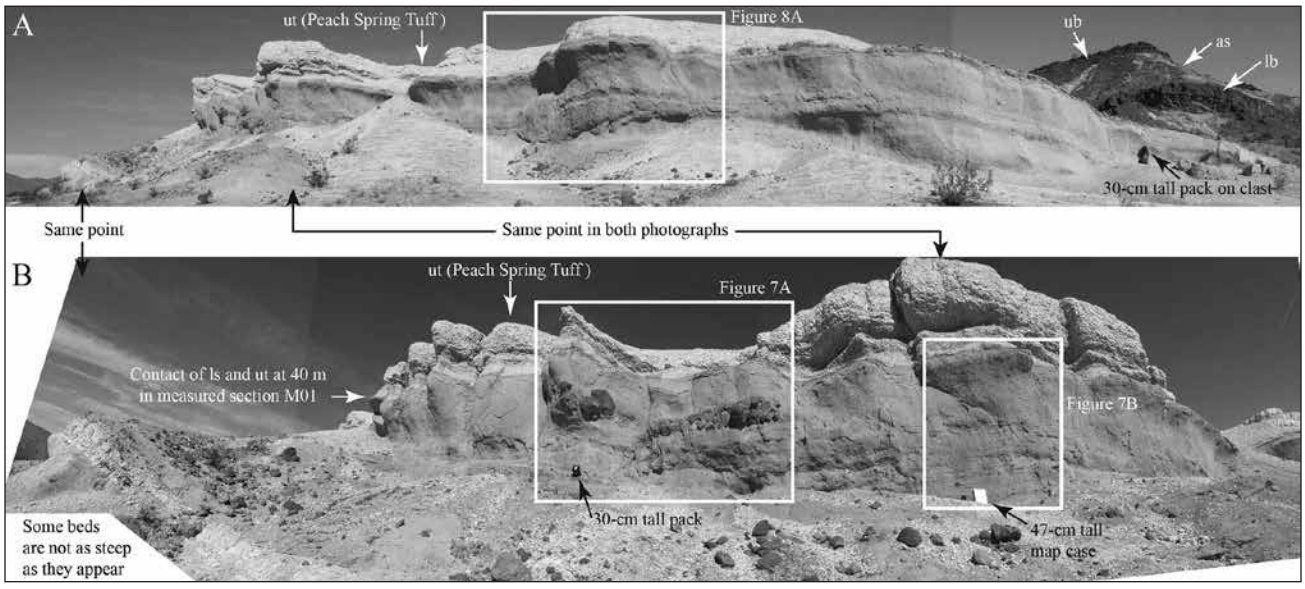

Figure 6. Photographic panoramas of the upper part of the lower sandstone and tuffaceous sequence in measured section A08-MS01 at about 38 m in the section. Symbols for sequences and subsequences are in Table 1. Note same points in both panoramas are identified for reference.

contains a granitoid clast with the largest diameter of 1000 mm and a diorite clast with the largest diameter of 700 mm (Figure 2; Table 3). In the upper part of the lower sandstone and tuffaceous sequence, tuffaceous and arkosic sandstone and conglomerate are well exposed in the northern section (A08-MS01 in Figure 2; Figure 6), but they are not as well exposed in the southern (A08-MS02) section where they appear to be sandstone with no conglomerate. In section A08-MS01 from 36.8 to 39.0 m, there are arkosic sandstone to boulder conglomerate bedsets where the granitoid clast with the largest diameter is 930 mm (Figure 7; Table 3). The A08-MS01 section from 36.8 to 39.0 m also contains (1) 20 to 50-cm thick tabular to broadly lenticular conglomerate, (2) 1.5-m thick, conglomeratic channel-fill deposits, (3) a series of cross-bedded conglomerate and sandstone bedsets that fill a 1.5-m deep channel and might represent migrating point-bar deposits, and (4) top-set beds deposited across the inter-channel and channel-fill deposits (Figures 7 and 8).

In section A08-MS01, numerous tuffaceous beds are interstratified with arkosic sandstone and conglomerate (Figure 2). At 33.0 m is a 2.9-m thick, greenish-gray to medium-gray, nonwelded to partially welded tuff (ignimbrite) that is the thickest tuff in the sequence. Based on similarities of crystal and pumice fragments, and the position just beneath the arkosic conglomerate, it is possible that this deposit also occurs in other measured sections (in particular, ~23 m in A01-MS01).

In area 08 there are variations in the abundance, and inferred lateral continuity, of arkosic conglomerate in the upper sandstone sequence and arkosic sandstone subsequence (Figure 2; Table 3). At 52 m in the upper sandstone sequence of section A08-MS02, there is a 2-m thick, arkosic conglomerate with the largest clast diameter of 1000 mm. In the upper part of the upper sandstone sequence of section A08-MS01, several arkosic sandstone to conglomerate beds are exposed, but the maximum lithic clast diameters were not measured. These exposures are about 65 m southeast of the measured section, and they project to about 72 m in the section. At 94.5 m in the arkosic sandstone subsequence of section A08-MS01, several arkosic cobble to boulder conglomerate beds are exposed, but no maximum clast sizes were measured. In the arkosic sandstone subsequence of section A08-MS02, there are two arkosic conglomerate bedsets. At 85 m is a 3.4-m thick conglomerate with the largest clast diameter of 400 mm, and at 100 m is a 2-m thick conglomerate with the largest clast diameter of 320 mm.

Area 06

In Area 06, many parts of the lower sandstone and tuffaceous sequence, upper sandstone sequence, and arkosic sandstone subsequence are covered by alluvium or colluvium (Figure 2). Descriptions of arkosic sandstone either use adjectives such as fine-grained to coarse-grained, or an adjective is not used. Two exceptions in the northern area include (1) coarse-grained arkosic conglomerate that forms the lowermost beds in the lower sandstone and tuffaceous sequence, and (2) pebbly sandstone that forms the lowermost beds in the upper sandstone sequence. The first beds deposited on top of the nonwelded, light gray, Peach Spring Tuff ignimbrite are tuffaceous sandstone or pebbly sandstone, but specific clast types (such as granitic or volcanic) were not identified. These beds could be included in the upper tuffaceous sequence, but exposures are typically less than 1 m of section, so they were not identified as a redeposited tuffaceous part of upper tuffaceous sequence.

Area 04

In Area 04, a northwest striking fault transects the area, and the Spanish Canyon Formation exposed in each structural block is distinctly different. Southwest of the fault, the Spanish Canyon Formation section dips shallowly to the southwest, and the lower tuffaceous sequence was deposited on the Alvord Peak basalt. Terrace deposits truncate much of the Spanish Canyon Formation, and several faults to the south-southwest repeat the section, so it is not clear how much of the lower tuffaceous sequence (or any of the other sequences) is exposed.

Northeast of the fault, the Spanish Canyon Formation section dips shallowly to the east-southeast. In measured section A04-MS02, the 7-m thick Peach Spring Tuff (PST) forms the upper tuffaceous sequence, and it was deposited on the Alvord Peak basalt (Figure 2). Along this part of the small ridge formed by the PST, the ignimbrite is partially welded and incipiently crystallized, probably at high temperature (Buesch, 2012). Less than 2.2 m of section at the base of the PST is covered by talus and slope wash at the measured section and along the small ridge

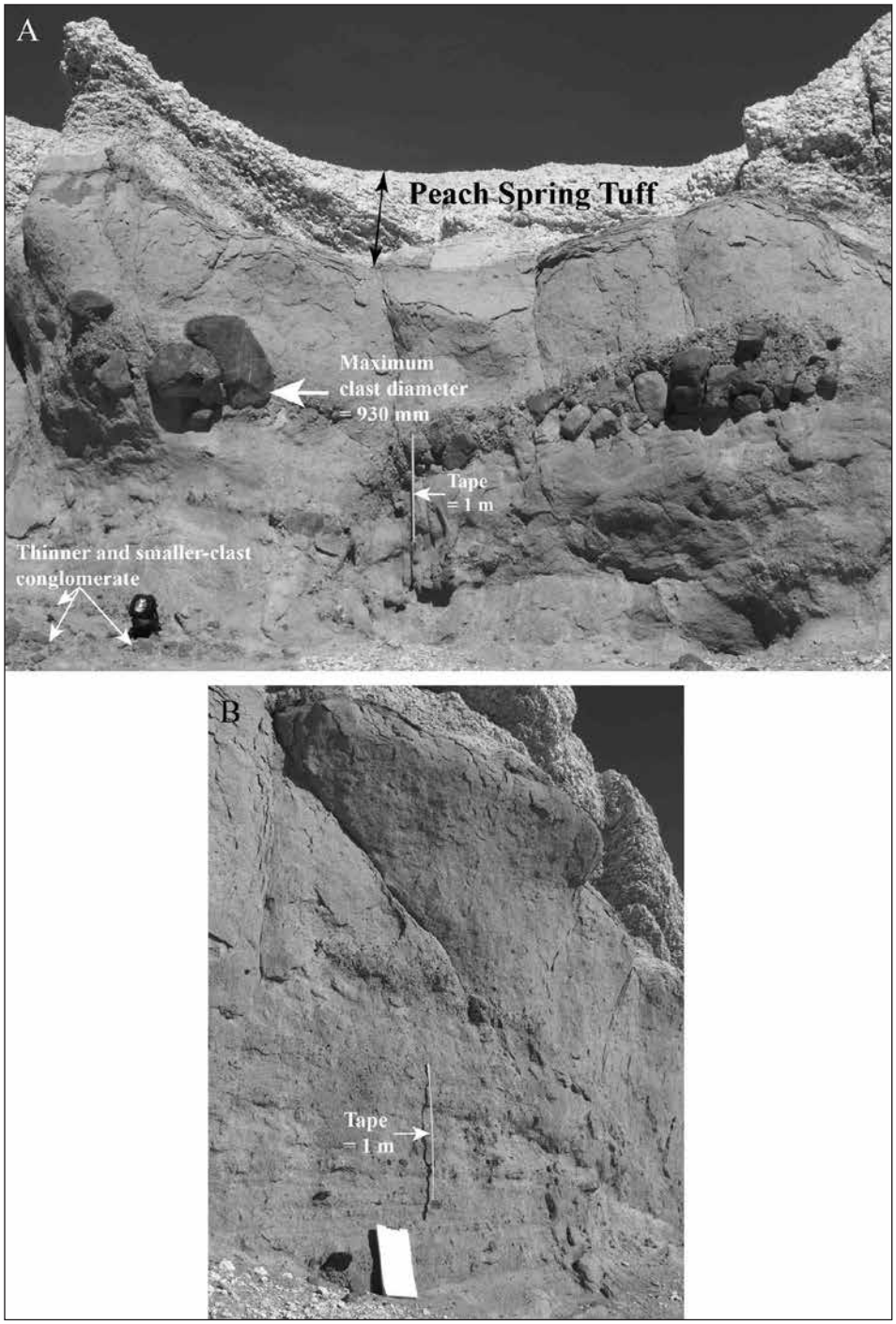

Figure 7. Photographic details in measured section A08-MS01 at 38 m in the section with (A) tabular and channel-filling conglomerate and (B) tabular to very low-relief lenticular bedding.

to the southwest of the measured section. About 10 m northeast of measured section A04-MS02, there is a pre-PST tuff that can be traced 80 m northward to where it is about 5.5 m thick. As with the PST, as much as 2 m of the base of the pre-PST tuff is covered by talus, slope wash, or young alluvium. This pre-PST bed appears to be a single deposit, and it is part of the tuffaceous component of the lower sandstone and tuffaceous sequence, but it has not been correlated to a specific bed in the southwestern structural block. Also in the northeast structural block, an olivine basalt flow is very poorly exposed between (one or more) sets of terrace deposits before the section is buried by one of the large alluvial washes in the area. Only one olivine basalt flow is exposed, and it is not known whether it is in the lower or upper basalt subsequence.

In the northeast structural block, most of the upper sandstone sequence is sandstone with very few pebbly beds. Beds in the upper sandstone sequence are locally exposed between areas covered by slightly lithified terrace deposits that contain large abundances of plutonic and metamorphic clasts. Because of shallow dips and poorly developed bedding in the upper sandstone sequence and terrace deposits, it is challenging to distinguish the two. Although the amounts of tuffaceous and arkosic materials in the upper sandstone are difficult to identify, there appear to be slightly more tuffaceous beds in the lower part of the sequence and mostly arkosic beds in the upper part.

Interpretations

In the Spanish Canyon Formation, the lower and upper tuffaceous sequences consist of fine- to coarse-grained tuffs, and the lower sandstone and tuffaceous sequence consists of interstratified sandstone and tuff. Some tuffs in all three of these sequences appear

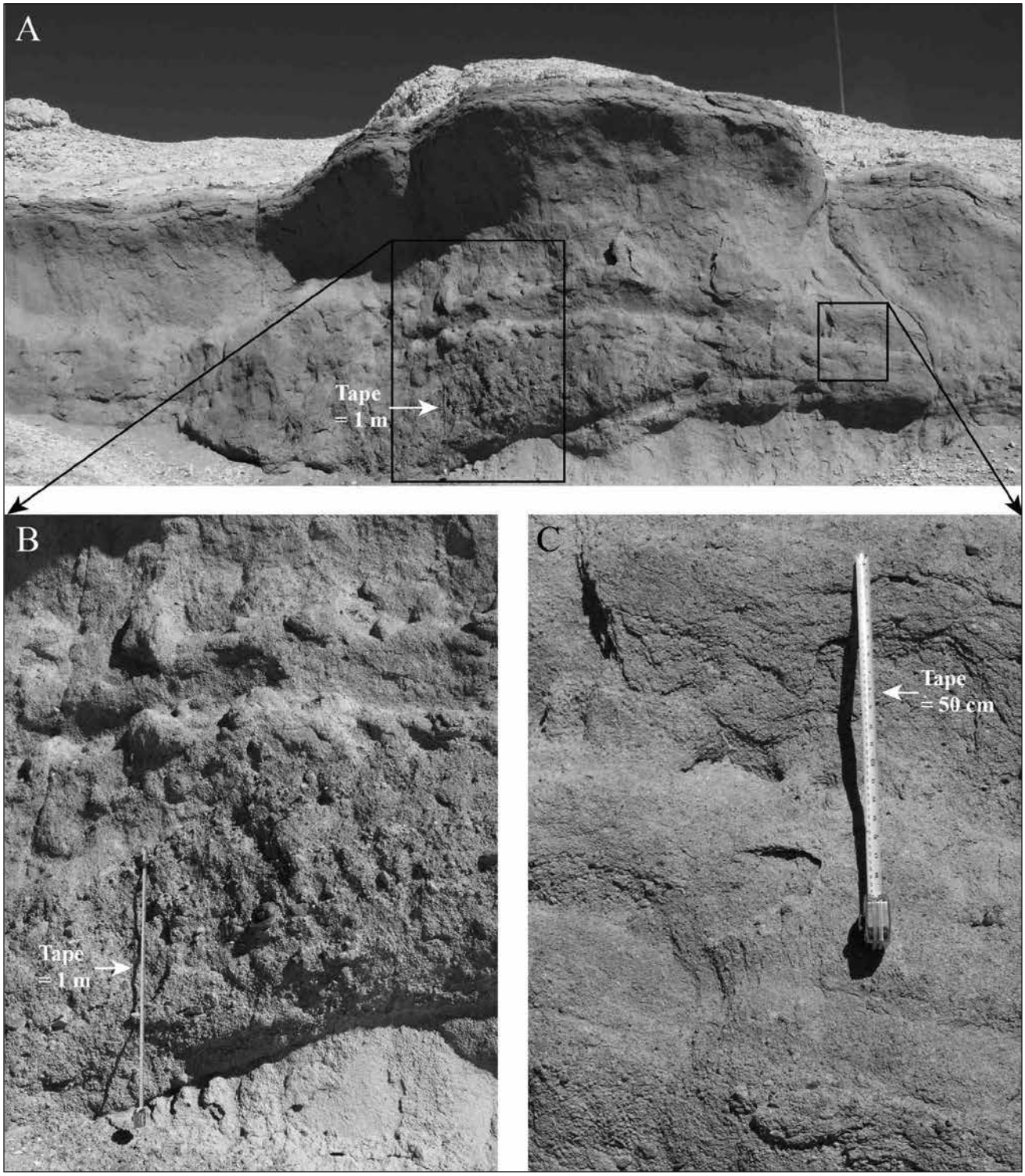

Figure 8. Photographic details in measured section A08-MS01 at 38 m with (A and B) 1.5-m tall, channel-filling, cross beds, and (C) detail of top-set beds.

to be pyroclastic flow deposits or slightly reworked and redeposited tuffs. Shortly after the initial deposition of thicker tuffs, which probably resulted from larger and higher energy events, smaller subsequent events began to erode the primary tuff giving rise to a series of beds that inherit the tuffaceous material (typically ash as matrix material and pumice as clasts), but which also contain plutoniclastic grains derived from more deeply incised pre-tuffaceous substrate or from nearby alluvial systems. Shortly after deposition of the Peach Spring Tuff in the upper tuffaceous sequence, there was again a series of beds

that were only locally deposited (typically recorded in less than a few meters of beds) where tuffaceous materials, most of which were probably derived from the Peach Spring Tuff, were mixed with arkosic sand that had been transported into the basin to form tuffaceous sandstone. The Peach Spring Tuff and the few subsequent tuffaceous sandstone deposits represent the last significant pulse of tuffaceous material into the basin during accumulation of the Spanish Canyon Formation. After this, the sandstone and conglomerate in the upper sandstone sequence became increasingly arkosic. The olivine basalt and arkosic sandstone sequence forms the upper part of the formation, where the arkosic sandstone subsequence is interstratified with the lower and upper olivine basalt subsequences. The olivine basalt flows occur through most of the eastern Alvord Mountain area, and each of the lower and upper olivine basalt subsequences contains multiple lava flows. The upper olivine basalt flows form the top of the formation.

Some nonwelded tuffaceous deposits in the lower arkosic sandstone and tuffaceous sequence (including some of the thicker beds that appear to be partially welded) might have been deposited from pyroclastic flows. However, without the development of a compaction profile (which is developed during welding in a pyroclastic flow) and the ability to trace beds to determine how they interacted with topography, the textures and structures can be similar for nonwelded pyroclastic flow and some debris flow deposits. Many tuffaceous and arkosic sandstone beds in the lower sandstone and tuffaceous sequence, including some sandstone in the upper sandstone sequence and the arkosic sandstone subsequence, have similar bedforms indicating the particles were probably transported by water during sheet-flood conditions (and possibly hyperconcentrated flows).

Many tuffaceous sandstone and arkosic sandstone and conglomerate beds have a broadly tabular geometry, and in some well-exposed sections, many are broadly lenticular. These bedforms are consistent with deposition in a low-relief, medial to distal alluvial or fluvial environment, and some of the finer grained beds might have been deposited in a lacustrine environment. Locally, channels as much as 1.5 m deep indicate more moderate amounts of relief on the paleogeomorphic surface. Some channels had steep-sided walls and were filled with very coarse grained conglomerate, and some channels were filled with cross-bedded conglomerate that is consistent with deposition along a point bar.

Interstratification of arkosic sandstone and conglomerate with the volcanic rocks of the Spanish Canyon Formation represents incursions of alluvial fans into a depocenter dominated in the lower parts by tuffaceous beds and interrupted in the upper parts by olivine basalt lava flows. The overall lateral continuity of the lithostratigraphic sequences, and the gradational changes in thickness and facies of the Peach Spring Tuff to the north-northwest (Buesch, 2012), indicates the likelihood that the Spanish Canyon Formation was deposited in only one main basin.

References

Buesch, D.C., 2012, Stratigraphy of the possible Peach Spring Tuff in the Alvord Mountain area, California; *in* Reynolds, R.E., ed.,"Searching for the Pliocene: Southern Exposures", California State University Desert Studies Consortium, p. 179-180.

Buesch, D.C., Miller, D.M., and Hillhouse, J.W., 2013, Lithology, age, and paleomagnetic characteristics of the lower tuffaceous sequence in the Spanish Canyon Formation, Alvord Mountain, California: *in* Reynolds, R.E., ed.,"Raising Questions in the Central Mojave Desert", California State University Desert Studies Consortium, p. 227.

Byers, F. M., 1960, Geology of the Alvord Mountain Quadrangle, San Bernardino County, California: U.S. Geol. Surv. Bull. 1089-A, 71 p.

Ferguson, C.A., McIntosh, W.C., and Calvin F. Miller, C.F., 2013, Silver Creek caldera—The tectonically dismembered source of the Peach Spring Tuff: Geology, v. 41, p. 3-6, first published on October 19, 2012, doi:10.1130/G33551.1.

Fillmore, R.P., 1993, Sedimentation and extensional basin evolution in a Miocene metamorphic core complex setting, Alvord Mountain, central Mojave Desert, California, USA: Sedimentology, v. 40, p. 121-142.

Hillhouse, J.W., and Miller, D.M., 2011, Magnetostratigraphy and tectonic rotation of the Miocene Spanish Canyon Formation at Alvord Mountain, California: *in* Reynolds, R.E., ed., "The Incredible Shrinking Pliocene", California State University Desert Studies Consortium, p. 49-52.

Peterson, D.W. 1979, Significance of the flattening of pumice fragments in ash-flow tuffs: Geological Society of America Special Paper 180, p. 195-203.

Possible origin of the myth that "California is falling into the ocean"

Norman Meek

Department of Geography, California State University, San Bernardino, CA 92407; nmeek@csusb.edu

Throughout my life I've heard the myth that California is falling into the ocean.[1] Many people hold that conviction strongly, and yet when asked about the supporting evidence, their responses are never clear. During the 30 years I've spent in southern California, I've developed a geography-based theory about how the idea originated, but like the origins of most myths, it is impossible to verify.

In the early history of geology, the Earth's topography was explained mostly by vertical tectonics. Mountains with thick layers of shallow marine strata were explained using concepts like the geosyncline. A geosyncline is a sedimentary trough that slowly subsides in place over millions of years (Knopf, 1948), and many varieties were eventually recognized. Mountains containing thick sequences of these types of rocks, such as the Appalachians and Alps, would then originate when the earth heaved the strata upwards in the same geographic location where the slow subsidence had previously occurred. Dickinson (2003, p. 857) describes how the geosynclines (and several other geologic ideas) turned out to be scientifically based myths themselves.

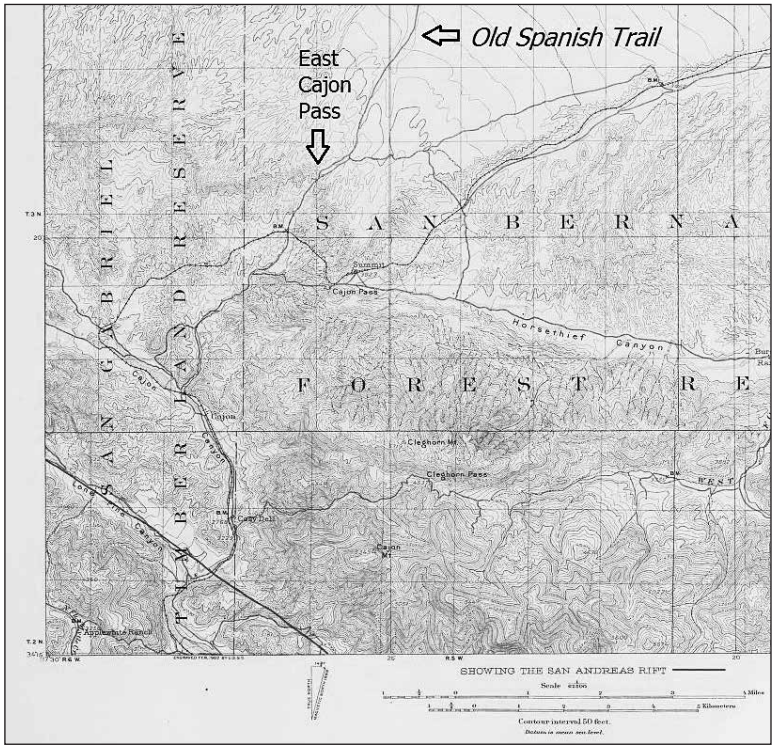

Figure 1. Typical early 20th century topographic map of southern California. This copy of the Hesperia 15' quadrangle is from the Lawson (1908) report. Note the legend label at the base: "Showing the San Andreas Rift."

The basic ideas of plate tectonics, where portions of the lithosphere move long distances horizontally, were not considered seriously at the time because no mechanism had been recognized that could drive long-distance horizontal crustal movements. Thus, in the early days of American settlement in California, it was widely believed that mountains could rise or fall, but that they could not move substantial distances horizontally.

During this same time, geologists recognized the presence of major lengthy faults in southern California, such as the San Andreas (Lawson, 1908). Because these faults defined the edges of major mountain ranges, such as the San Bernardino and San Gabriel ranges, it was clear that they were important regional features. But in an era of vertical tectonics, these faults were believed to be faults that permitted the rise or fall of the adjacent mountains; they were not recognized as features associated with mountains moving long horizontal distances. In fact, on early geologic maps of southern California, the San Andreas fault is termed a "rift zone,"

1 I have been unable to discover when the idea of California falling into the ocean originated, but the myth has been widely repeated by the public for decades. For example, the movie "2012" (released in November 2009) depicts California falling into the ocean. Moreover, because of numerous public inquiries about whether the myth is valid, portions of the USGS Multimedia Gallery website, the California Department of Conservation website, the U.C. Berkeley Seismological Lab website, and the Geotripper website have sections devoted to scientifically refuting the myth.

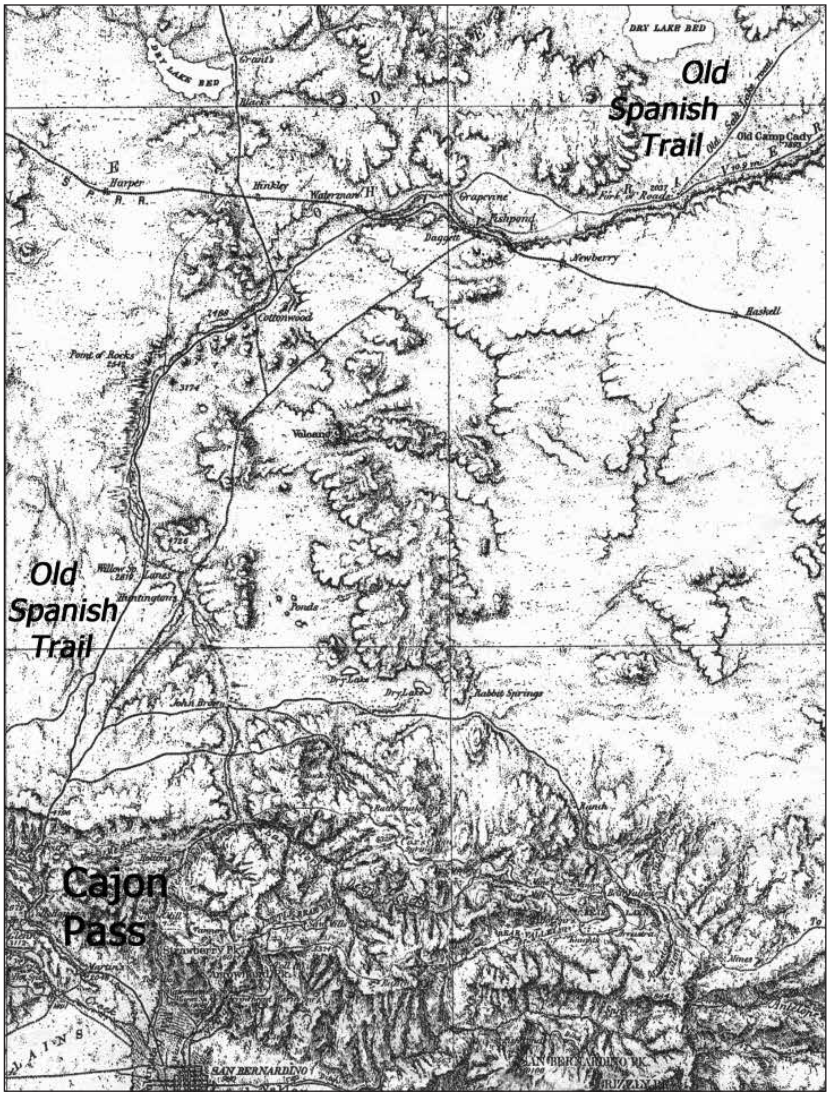

Figure 2. Map of the Old Spanish Trail route (mapped here as the Old Salt Lake road) in the Mojave Desert, California depicted by the Wheeler Survey. Part of the Sanford route to West Cajon Pass is shown in the lower left edge of the map. This map was issued on Nov. 30th, 1883.

suggesting that its primary function in southern California was allowing the adjacent crust to move vertically [the term itself was "adopted from the usage for analogous features in Palestine and Africa" (Lawson, 1908, p. 2) and the Colorado Desert "may with much plausibility be regarded as a great Rift Valley of even greater magnitude than the now famous African prototype first recognized by Suess" (Lawson, 1908, p. 52); see Fig. 1].[2]

Enter the early settlers

Getting to California overland in the days before the Transcontinental railroads was a difficult task. If one was unwilling to risk a crossing of the Sierra Nevada, the best alternative for west-bound travelers at and south of Salt Lake City was to take the Old Spanish Trail route to the Los Angeles basin before heading north to the Central Valley. The Old Spanish Trail was described and publicized after Frémont traveled it in 1844 (Frémont, 1845; Lyman and Reese, 2001). West of Camp Cady the route followed the Mojave River towards its source in the San Bernardino Mountains. The route later facilitated wagon traffic, and water and grass were fairly common (at least for the Mojave Desert) in the river valley. During the mid-19th century, the route was inland southern California's first unpaved highway and was much preferred to the rugged Sierra Nevada route as well as the southern path from Yuma across the waterless Borrego Desert.

The Old Spanish Trail left the Mojave River at Lane's Crossing near modern-day Oro Grande and traveled 17 miles upslope towards the Cajon Pass, much like I-15 does today through the nearby region. The path from Oro Grande to the lowest widely used saddle (e.g., East Cajon Pass) was accompanied by a steady 1500 foot elevation gain over the 17 miles. It must have been evident to all of the travelers who climbed this long grade that they were going up a giant alluvial fan, one known today as the Victorville fan (or sometimes Baldy Mesa). That is because they had already traversed a few alluvial fans as they crossed southern Nevada and the eastern California Desert, so they were familiar with alluvial fans and other debris wedges found on the slopes of desert mountains.

2 A manuscript reviewer suggested that reports from the 1857 earthquake on the San Andreas fault might shed light on the myth. A thorough review of those reports assembled by Agnew (2006) shows that in 1857 neither the scientists nor the general public associated regional tectonic deformation with earthquakes, even though long surface fissures were reported immediately after the earthquake. Although some vertical offsets were recognized (Agnew, 2006, p. 31-32), the cause of the large earthquake was attributed to such phenomena as earthquake weather, subterranean fires and gas releases, and incipient volcanism. When reviewing the 1857 reports, I was unable to find a single reference to a mountain range or large landmass rising, falling, or shifting laterally.

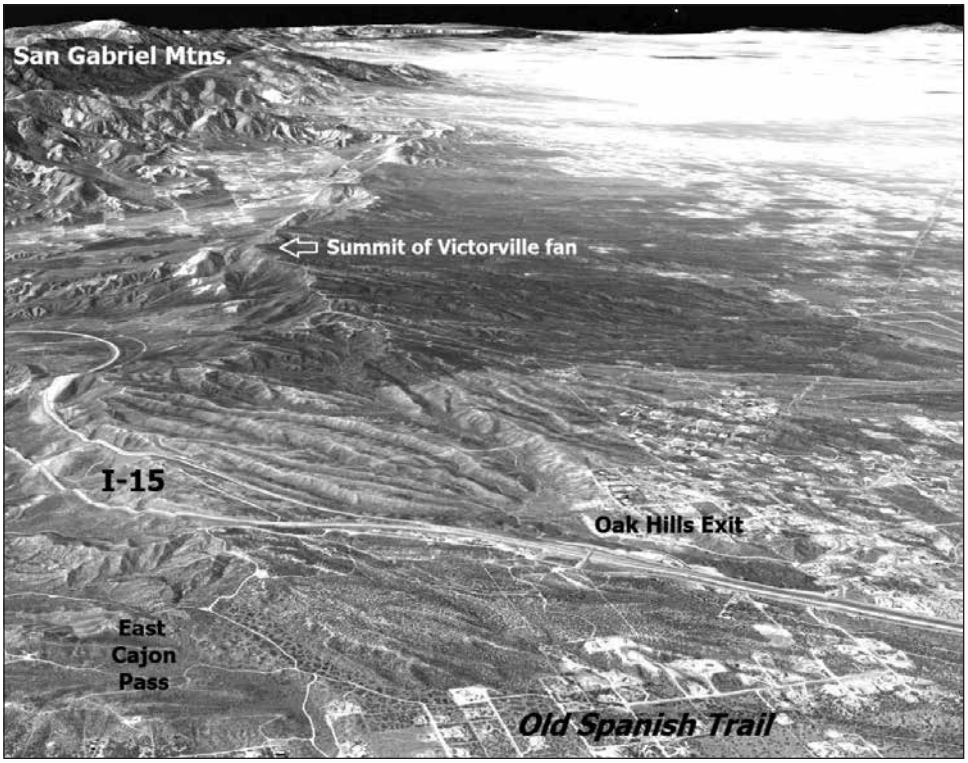

Figure 3. Oblique aerial photo (viewing NNW) showing the crest of the Victorville fan at Cajon Pass. I-15 is visible and parallels the Old Spanish Trail. Note how the fan has been cut off from its San Gabriel Mountain source. It is still connected to the mountains in the distance, but that is not visible on the ground from the fan crest near the trail. Instead, to many people it appears the mountain source has dropped into Cajon Pass. Modified Google Maps Image, 2014.

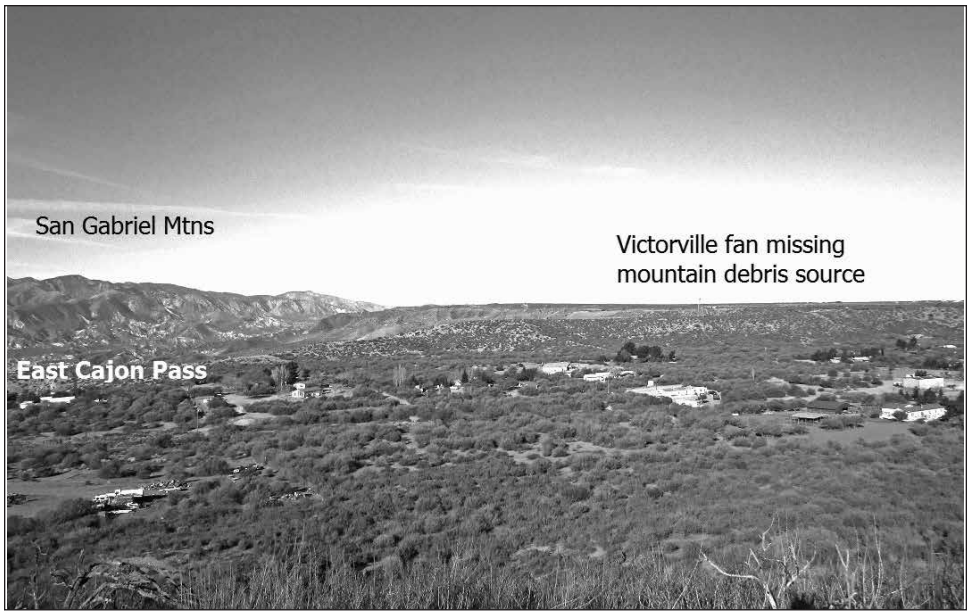

Figure 4. Ground view of the Victorville fan from an overlook near where the Old Spanish Trail crests the Victorville fan near eastern Cajon Pass. The view is towards the WNW (photo taken 1/18/14 from UTM: 11S 461323 3799259).

However, when they reached the crest of the Victorville fan after one or two days' upward march, they would have been shocked to discover that the fan was not connected to a mountain source (see Figs. 2, 3, and 4). In fact, standing on the trail crest on the Victorville fan with a panoramic view of Cajon Pass, it must have been a topic of some debate to explain what had happened to the mountains that had shed the fan. In an era of vertical tectonics it would have been reasonable for most to conclude that the mountains must have subsided downward into the pass, and thus if this continued much longer the coastal regions of California would be submerged beneath the Pacific Ocean.

Starting in 1850, the Sanford grade routes were added in western Cajon Pass to better facilitate wagon traffic (Robinson, 2005, p. 194). These alternative routes also led up the Victorville fan to its crest and would have provided similar vistas of the beheaded fan. Thus, anyone travelling through Cajon Pass was likely to witness a giant alluvial fan without a mountain debris source.

Today, when I take introductory geography students to an overlook very close to where the Old Spanish Trail crested the Victorville Fan and ask what happened to create the landscape that they see, nearly all recognize that they are at the crest of the gently sloping surface of a large alluvial fan. Then, when I ask for hypotheses about what happened to the mountain source, it is common to have one or more students suggest that

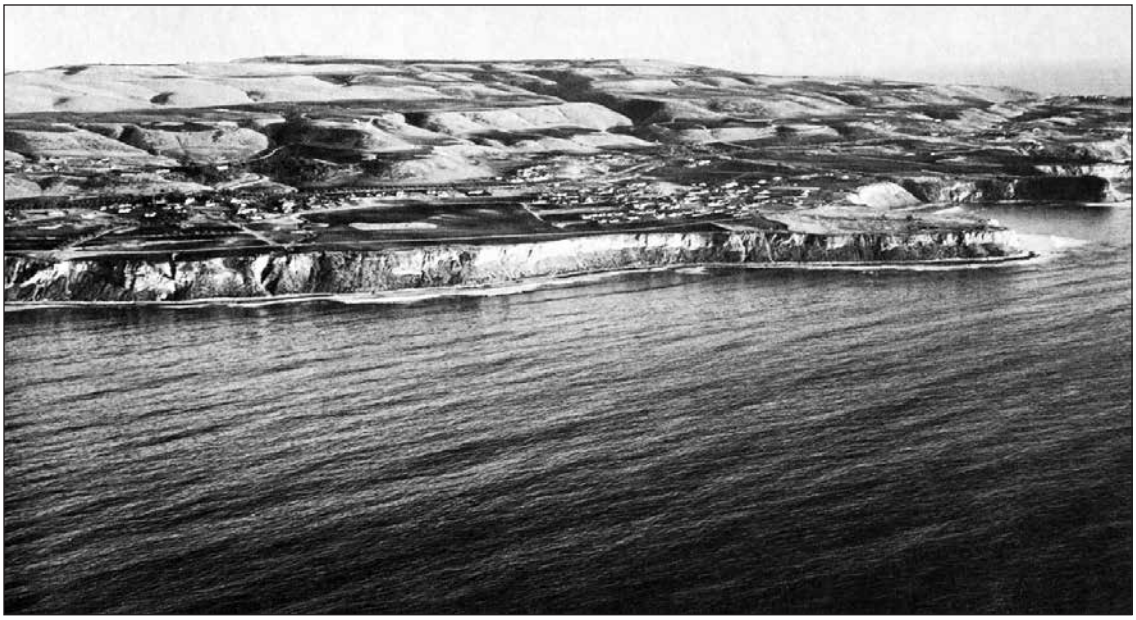

Figure 5. Multiple marine terraces indicate that coastal California is rising rapidly out of the ocean rather than subsiding into it. This image shows some of the 13 shoreline platforms once visible on Palos Verdes Hills near Long Beach, CA (from Shelton, 1966, p. 335).

the mountains have dropped into the pass, rather than moved the >15 miles horizontally that has actually happened in the last million years. In fact, it wasn't until 1926 that geologist Levi Noble proposed that the San Andreas fault in southern California might be a lateral fault, and not until 1953 before long lateral offsets along the fault were even proposed (Hill, 1981).

Most of the coastal regions of central and southern California have abundant evidence that California has, in fact, risen out of the ocean during much of the Quaternary. In addition to numerous marine platforms, there are locales with numerous Pleistocene marine shoreline platforms at Palos Verdes, the Ventura basin, and numerous other locations (see Fig. 5). Nevertheless, this type of evidence was little known to these early settlers, and prior to the first railroads in the 1870s, many early residents of southern California had experienced firsthand the absence of a mountain at the top of the long Victorville fan grade, which made it abundantly clear to them that subsidence of the crust was dominant in southern California. This idea would have remained unchallenged for about 100 years before alternatives were even suggested.

Thus, it is my proposal that we are still living with the firsthand experiences and beliefs of these early California pioneers that were established firmly in an era of vertical tectonics.

References cited

Agnew, D.C., 2006. *Reports of the Great California Earthquake of 1857*. Scripps Institute of Oceanography, 59 p. http://escholarship.org/uc/item/6zn4b4jv. Accessed 26 Feb 2014.

Dickinson, W.R., 2003. "The place and power of myth in geoscience: an associate editor's perspective," *American Journal of Science*, 303, p. 856-864.

Frémont, J.C., 1845. *Report of the exploring expedition to the Rocky Mountains in the year 1842 and to Oregon and North California in the years 1843-44*. Washington: Blair and Rives, 583 p.

Hill, M., 1981. "San Andreas fault: history of concepts," *Geological Society of America Bulletin*, 92(3): 112-131.

Knopf, A., 1948. "The Geosynclinal Theory," *Bulletin of the Geological Society of America*, 59: 649-670.

Lawson, A. C., 1908. *The California Earthquake of April 18, 1906: Report of the State Earthquake Investigation Commission*, Carnegie Institution of Washington Publication 87, 2 vols.

Lyman, L, and Reese, L., 2001. *The Arduous Road: Salt Lake to Los Angeles, the most difficult wagon road in American history*. Victorville, CA: Lyman Historical Research and Publishing Company, 107 p.

Robinson, J.W., 2005. *Gateways to southern California*. City of Industry, CA: Big Santa Anita Historical Society, 488 p.

Shelton, J.S., 1966. *Geology Illustrated*. San Francisco: W.H. Freeman and Co., 434 p.

Stream capture to form Red Pass, northern Soda Mountains, California

David M. Miller[1] and Shannon A. Mahan[2]

[1] U.S. Geological Survey, 345 Middlefield Road, Menlo Park CA 94025, dmiller@usgs.gov. [2] U.S. Geological Survey, P.O. Box 25046, Denver CO 80225

ABSTRACT: Red Pass, a narrow cut through the Soda Mountains important for prehistoric and early historic travelers, is quite young geologically. Its history of downcutting to capture streams west of the Soda Mountains, thereby draining much of eastern Fort Irwin, is told by the contrast in alluvial fan sediments on either side of the pass. Old alluvial fan deposits (>500 ka) were shed westward off an intact ridge of the Soda Mountains but by middle Pleistocene time, intermediate-age alluvial fan deposits (~100 ka) were laid down by streams flowing east through the pass into Silurian Valley. The pass was probably formed by stream capture driven by high levels of groundwater on the west side. This is evidenced by widespread wetland deposits west of the Soda Mountains. Sapping and spring discharge into Silurian Valley over millennia formed a low divide in the mountains that eventually was overtopped and incised by a stream. Lessons include the importance of groundwater levels for stream capture and the relatively youthful appearance of this ~100-200 ka feature in the slowly changing Mojave Desert landscape.

Introduction

Early trade routes, missionary roads, and mining transport routes across the Mojave Desert followed the easiest topography and balanced distance against availability of necessary resources, especially water. Through-going perennial streams such as the Mojave River were favored by many routes both for the avoidance of mountain passes and for stream and spring resources. The Old Spanish Trail, a trade route established in 1829, took advantage of Red Pass in the Soda Mountains (Figure 1), for the leg from springs in Death Valley to Bitter Springs (Hafen and Hafen, 1993). The route may have followed prehistoric trails. Red Pass was apparently named for red volcanic rocks in the steep walls of the canyon traversing it. Technically, it is not a pass (a topographic low on a mountain divide) but rather a deep, narrow canyon cutting through a former divide. The route is the active bed of an un-named east-flowing ephemeral stream that leads to the floor of Silurian Valley (Figure 1). The stream drains much of the high country of Fort Irwin.

In this paper we describe the stratigraphic and geomorphic setting of Red Pass, and provide luminescence ages for one set of deposits in the pass. We conclude that drainage directions reversed during the middle Pleistocene, indicating stream capture. This capture was probably driven by disparate groundwater levels, the level on the west side of the Soda Mountains being much higher than that on the east.

Geologic setting

Red Pass crosses the northern Soda Mountains, which at that location are comprised of two low, north-trending ridges. The Soda Mountains form the west flank of the broad Silurian Valley, suggested to be a youthful downwarp by Miller et al. (2007). The mountains are underlain by Mesozoic metavolcanic and granitic rocks (Grose, 1959) against which are faulted sedimentary rocks of probable Miocene age. The entire area is part of the tectonically active Eastern California Shear Zone, a region of strike-slip faulting (Dokka and Travis, 1990).

West of the Soda Mountains, east-trending mountains and intervening valleys ascend northward (Miller and Yount, 2003) and topography is overall much higher than that of Silurian Valley. For instance, the elevation of the floor of Silurian Valley east of Red Pass is 260 m, whereas valley floors west of Red Pass are 440, 680, and 960 m (south to north). Adjacent mountains also rise south to north: 1300,

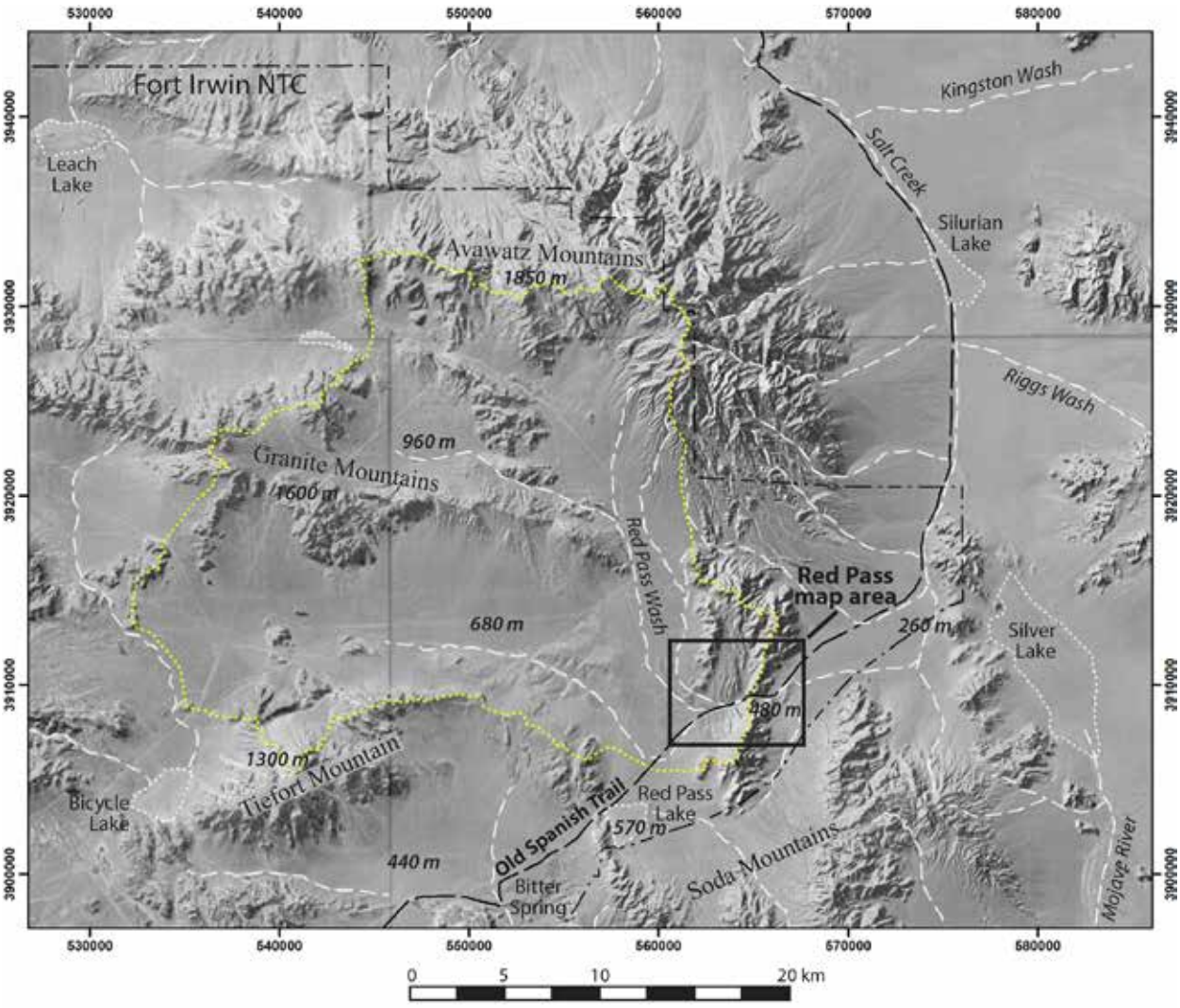

Figure 1. Location map for Red Pass in the northern Soda Mountains, showing major streams (white dashed lines), playa lakes (dotted outline), valleys, mountains, and approximate path of Old Spanish Trail. Red Pass wash watershed outlined by heavy pale dots is ~700 km^2. Red Pass map area of Figure 2 indicated by box. Approximate altitudes of valleys and mountain ranges are shown.

1600, and 1850 m. Parts of this high western terrane are internally drained to playas, parts drain south to playas (Cronese and Coyote Lakes) adjacent to the Mojave River drainage, and the remainder is drained eastward through Red Pass. The development of external drainage for this high region is significant in its geomorphic evolution, in that valleys adjacent to the east-trending mountains change from depositional basins to sediment bypass systems.

Valleys, streams, and mountain ridges are generally not named in the area of Red Pass. We will refer to Salt Creek, which drains much of Silurian Valley; "Red Pass wash" as extending from the southwest side of the Avawatz Mountains, flowing south and then east through Red Pass into Silurian Valley; and the watershed of Red Pass wash at Red Pass as "Red Pass watershed" (Figure 1). In this area, the Avawatz Mountains are the highest terrane, and probably the main contributor of runoff to the Red Pass watershed (Fig. 1) although more high mountains lie to the southwest within the watershed. Youthful tectonics in the Fort Irwin area southwest of the Avawatz Mountains (Schermer et al., 1996) may have caused changes in the configuration of the Red Pass wash during the last few million years, but this topic has not been studied.

We use the soils-geomorphic stratigraphy established by Birkeland (1990), as modified for the Mojave Desert by McFadden et al. (1987) and Reheis et al. (1989). We use the nomenclature for the Mojave Desert Quaternary deposits established by Miller et al. (2009), which uses a few categories of age that range from active to young, intermediate, and old. Active and young deposits possessing weak soils

are 0 to 14 ka and generally are inset into intermediate-age deposits that are ~30 to 220 ka, and old deposits that are >500 ka (Table 1; Miller et al., 2009). Intermediate and old deposits bear distinctive soils, surface characteristics, and geomorphic positions.

Table 1: Summary of map units for the Red Pass area, using nomenclature for Quaternary deposits of Miller et al. (2009).

Map unit	Name of deposit	Approximate Age (ka)	Description
Qya	Young alluvial fan	0-14	Poorly sorted sand and gravel with very weak soil
Qya4	Older young fan	9-14	Poorly sorted sand and gravel with stage I calcic soil
Qia2	Younger Int. fan	30-90	Poorly sorted sand and gravel with stage II calcic soil
Qia3	Older Int. fan	140-220	Poorly sorted sand and gravel with stage III calcic soil
Qoa	Old alluvial fan	500-1000	Poorly sorted sand and gravel with very strong soil
Qaw	Active wash	0-6	Moderately sorted sand and gravel of active stream bed
Qyw	Young wash	0-14	Moderately sorted sand and gravel with very weak soil
Qyw4	Older young wash	9-14	Moderately sorted sand and gravel with stage I calcic soil
Qiw	Intermediate wash	30-220	Moderately sorted sand and gravel with pronounced soil
Qigw	Intermediate GWD	140-220	Silt, sand and mud with moderate soil
Qogw	Old GWD	500-1000	Silt, sand and mud with strong soil
Ts	Sandstone	Miocene	Sandstone, siltstone, and conglomerate; rare ash beds
Jg	Granitic rocks	Jurassic	Fine to medium grained leucocratic biotite granite
Jmv	Metavolcanic rocks	Jurassic	Foliated fine grained meta-rhyolite

Geology of Red Pass area

The geologic and geomorphic framework of Red Pass is defined by the bedrock in two ridges of the northern Soda Mountains and an intervening basin (Figure 2). The eastern, taller and more continuous ridge is underlain by Mesozoic metavolcanic rocks (Grose, 1959), whereas the western, low ridge that declines in elevation southward is underlain by Mesozoic granite. Faulted in between the two ridges is a gently west-dipping section of sandstone, mudstone, and conglomerate that is probably part of the Miocene Avawatz Formation (Spencer, 1990). The two bedrock ridges serve to partition the area into three Quaternary depositional realms: eastern, central, and western.

Quaternary deposits in the *eastern* realm consist of stubby, steep alluvial fans of intermediate and young age (Figure 2). Their toes are cut by and merge with a major young alluvial fan built by Red Pass wash. A few narrow deposits of intermediate-age Qia2 fan materials are present near the head of that major fan, indicating that it started forming at least by Qia2 time (~30-90 ka), but the predominance of young alluvial deposits indicate that it has undergone significant aggradation in young fan time (since ~14 ka).

Quaternary alluvial fan deposits in the *western* realm form a complex array of fan materials ranging in age from old to young. The streams associated with these deposits flow to the southwest, parallel to the overall topography and consistent with the southward decline in altitude of the granitic ridge from which they are derived. The Qia3 deposits in these fans typically include laterally persistent lenses of medium-grained eolian sand. The fans end at the major south-draining stream of Red Pass wash. West and south of that major stream and its tributaries lies a complex of thin alluvial fan deposits draped on groundwater-discharge deposits that formed in a wetland setting (unit Qigw on Figure 2). These deposits will be described more completely below.

Quaternary deposits in the *central* realm are complex. They consist mainly of old (Qoa) deposits that can be shown by their westward dips, sedimentary structures, and clast composition (metavolcanic rocks) to have been derived from the eastern bedrock ridge. The old deposits are deeply incised by steams that flow north or south toward Red Pass wash. Lining the deeply cut stream valleys are terraces of intermediate and young age. In several valleys, narrow streams are entrenched into old alluvial fan deposits, below a widespread strath terrace topped by a Qya4 gravel veneer. The deposits in the valleys entrenched into Qoa deposits carry mixed clasts of metavolcanic and granitic rocks, indicating a different source area than the Qoa deposits. The groundwater-discharge deposits of the western realm lap around the southern end of the granite ridge and into the central realm approximately along the axis of Red Pass wash.

Deposits along the axis of Red Pass wash where it cuts through the Soda Mountains are instructive. All Red Pass wash deposits contain clasts of widely

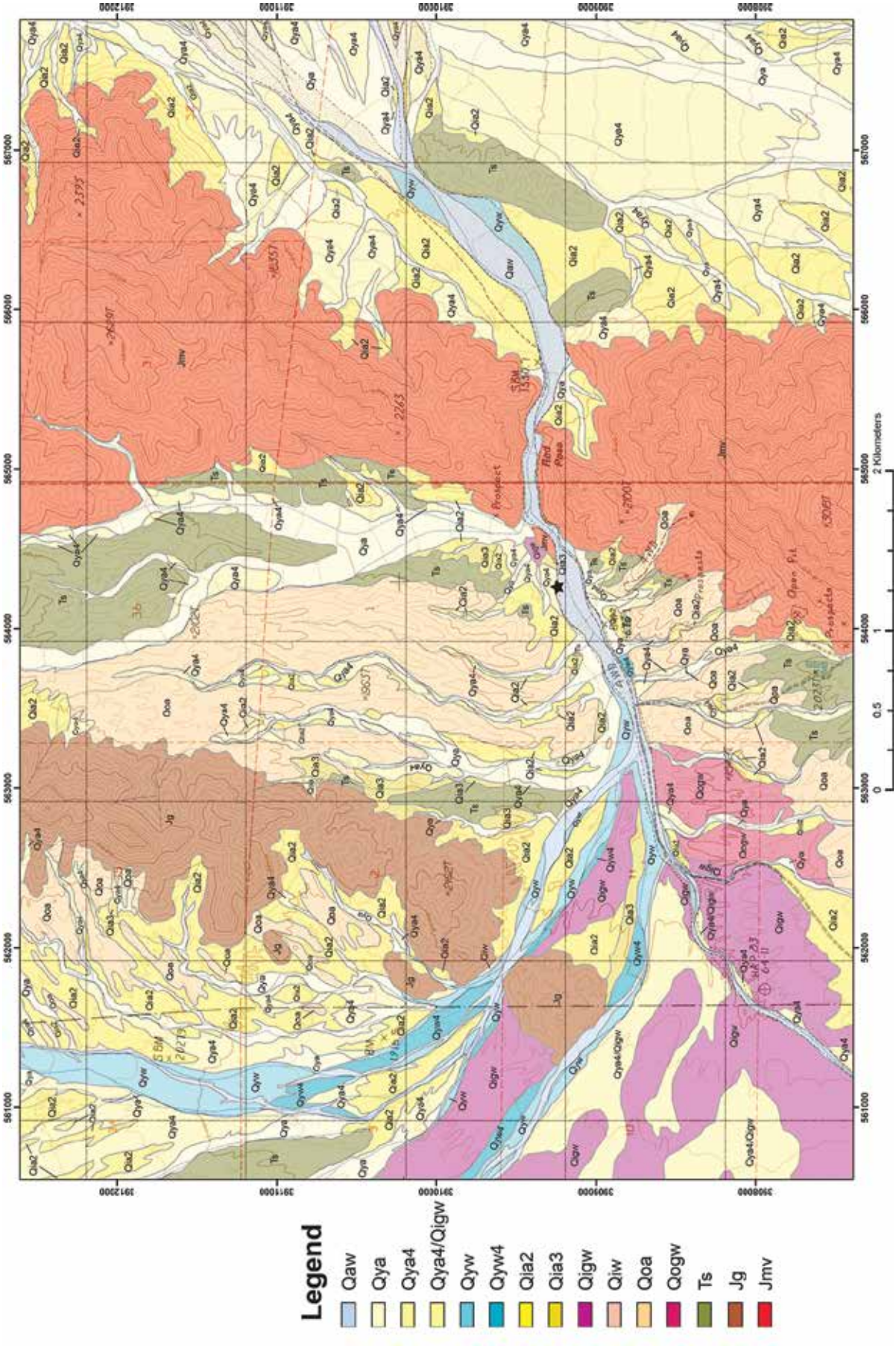

Figure 2. Geologic map of the Red Pass area. Map units for surficial materials are described in Table 1 and follow Miller et al. (2009). Location of dated sediment indicated by star.

varying rock types, including marble derived from the Avawatz Mountains. As described by Mahan et al. (2007), a perched terrace of stream deposits lies on the north side of the wash near a knob of metavolcanic rock. The upper unit of this section of stream deposits bears soils distinctive of Qya4 deposits, despite the relatively strongly developed Av horizon and pavement. This unit lies on a partly stripped set of soils associated with an underlying deposit, which rests on yet another buried soil and a third deposit. In total, this section is 6.6 m high. Shortly east of the metavolcanic rock knob, Qya3 deposits with very weak cambic development and an incipient varnish and pavement lie 2.5 m above the active wash. The heights above Red Pass wash of Qya4 and Qya3 deposits, as well as the buried Qia deposit, are much greater than similar terraces just 1 km upstream. There, typical terrace heights are: Qya3, 0.4–0.7 m; Qya4, 1.0–1.5 m; Qia2, 2.0–3.0 m.

Nearly flat-lying, fine grained deposits that we interpret as intermediate-age groundwater discharge deposits (GWD) lie near the metavolcanic knob and just above Red Pass wash level, but are much more extensive up stream to the west (Figure 2). These Qigw deposits extend over a broad lowland to the southwest which covers much of the distance to Red Pass Lake playa (Figure 1). These deposits consist of dark to medium brown, moderately to well sorted, fine to medium sand in thin laterally extensive beds, along with abundant "popcorn" calcium carbonate nodules of pale color. Less common are lenses of organic materials, beds of dark muds, and stringers of pebbles. The deposits are topped by Qia3 alluvial fan deposits and calcic horizons of the alluvial fan deposits, generally stage III, involve the underlying Qigw deposits. The overlying fan deposits in many places are erosionally truncated, as evidenced by lenses of partial soil profiles overlain by Qya4 deposits. In the area of Figure 2, these Qigw deposits and overlying thin deposits tend to dip gently eastward. In one area, mapped as old GWD (Qogw), stage IV soils lie on the GWD without any overlying fan deposits. These Qogw deposits lie directly on Qoa alluvial fan deposits and both Qoa and Qogw deposits dip gently west, discordant to deposits in Red Pass wash. We provisionally mapped these as being older than the intermediate age GWD, but we have not established this age assignment by stratigraphic or geochronologic means.

Stream profiles can provide information on capture events, which typically produce knickpoints and steep-gradient reaches. We examined gradients of Red Pass wash and its tributaries within the area shown by Figure 1 and also explored gradients to the east and west. The Red Pass wash long profile is at a nearly constant gradient of 2.3% including reaches below, within, and above Red Pass. Well to the east, near the toe of the alluvial fan that stretches toward Salt Creek, the slope declines to 2.0%; Salt Creek is very gentle (0.2%). Upstream from Red Pass, the wash branches into four main stems, which retain constant gradient for the two northern stems, but decline in gradient (1.3-1.9%) for the two southern stems that lie within GWD. Tributaries cutting into Qoa and feeding Red Pass wash immediately west of Red Pass are much steeper gradient than the wash. Tributaries lying north of the wash range in gradient from 3.9% (west) to 5.3% (east). Tributaries lying south of the wash range in gradient from 3.5% (west) to 8.8% (east). All tributaries steepen in their lowest reaches near Red Pass wash.

Geochronology

Luminescence was used to provide age control for two units in the high terrace capped by Qya4 deposits adjacent to the main stream in Red Pass. Samples were collected by auguring into the freshly cleaned face, driving a tube into the sediment, and capping the ends of the tube under shielding that protected the face from sunlight. The tubes were then placed in light-proof photographic bags until the initial processing. Samples were also collected for water content and dose rate measurements. For lab dosimetry, bulk samples were studied as described by Mahan et al. (2007) at the USGS Gamma Spectrometry facility in Denver to determine the rate at which the sediment was bombarded by charged particles resulting from radioactive decay. Cosmic-ray dose rate was estimated for each sample as a function of depth, elevation above sea level and geomagnetic latitude (Prescott and Hutton, 1988). Saturation moisture was estimated by packing dry soil into plastic tubes of known volumes, thoroughly wetting the, centrifuging the wet sediment, drawing off the water, and re-measuring the wetted volume.

Two types of luminescence dating were performed on different grain sizes and mineral fractions: quartz OSL on fine sand-size separates and IRSL (infra-red

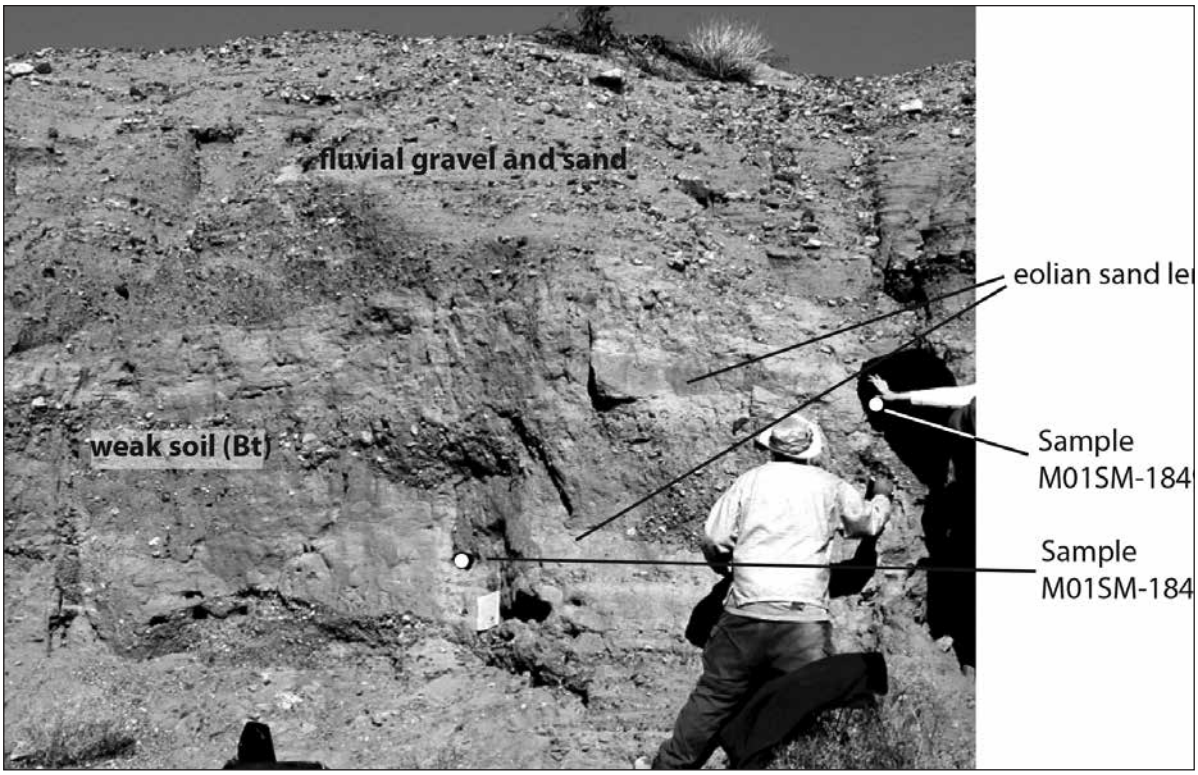

Figure 3. Photograph and diagram of the sampled section in Red Pass. After Mahan et al. (2007).

stimulation on K-feldspars) on the polymineralic fine silt fraction (4-11 μm) as described by Mahan et al. (2007). OSL samples were analyzed by single-aliquot regeneration procedures and IRSL samples were analyzed by the total-bleach multiple-aliquot additive-dose method. Ages are reported with 1σ error limits.

The sampled section is inset into deeply eroded Qoa deposits, and incorporates a different clast composition that is derived from the west and north. The deposits are several meters above the modern stream channel in Red Pass, but the surface of the deposits and sedimentary structures indicate streams and sediment flowed east, parallel to the modern drainage. The compound stream deposit is 6.6 m thick with a Qya4 (latest Pleistocene) deposit on top of two older deposits, each separated by truncated paleosols. The Qya4 alluvial deposit we dated contains a partly reworked eolian sand lens in an otherwise thin- to thick-bedded stream deposit characterized by lateral continuity of bedding and moderate grain-size sorting (Figure 3). We sampled the eolian sand lens in the Qya4 deposit, 170 cm beneath the weak desert pavement surface and 130 cm beneath a stage I calcic horizon for luminescence (sample M01SM-1849a). A lower sample in a sand lens within stream deposits under a paleosol, tentatively labeled Qia, was 90 cm deeper (sample M01SM-1849b). The upper sample yielded an average age of 12.5 ± 0.55 ka (1σ) on feldspar and 11.5 ± 0.23 ka on quartz (Table 2; see also data in Mahan et al., 2007). These two ages overlap within 2σ error limits. The lower Qia sample had one IRSL age of 21.4 ± 0.99 ka that was much younger than the other two ages of 30.9 ± 1.11 ka (IRSL) and 36.9 ± 1.29 ka (OSL). The younger IRSL age is almost certainly a result of inadequate

Table 2: Feldspar IRSL and quartz OSL ages from the Red Pass area. Errors in 1σ.

Sample ID and map unit	Equivalent Dose (Gy) (±1s%)	Age, error (yr) IRSL	Equivalent Dose (Gy) (±1s%)	N	Age, error (yr) quartz OSL
M01SM-1849a	64 ± 1	12,110 ± 590	45 ± 1	46 (48)	11,540 ± 235
Upper sand, Qya4	68 ± 1	12,790 ± 525			
M01SM-1849b	150 ± 2	30,895 ± 1,110	142 ± 3	31 (40)	36,880 ± 1,290
Lower sand, Qia1?	104 ± 2	21,420 ± 990			

or incomplete disc coverage and normalization parameters, which was addressed more robustly in the second sample. There appears to be a discrepancy between the ~31 ka feldspar age and the ~37 ka quartz age, but these ages probably represent a mixture of partially bleached grains within the sample, such that the age is somewhere between 30 ka to 38 ka.

Interpretation

We interpret the alluvial fan patterns, drainage directions, and clast compositions to indicate a change from sediment shed westward off of the metavolcanic bedrock ridge to form an adjacent alluvial fan, to deep incision of the fans and introduction of a major stream (Red Pass wash) with mixed clast compositions typical of a large drainage basin. Specifically, the small, steep fans of the eastern realm have responded to local base level rise during Qia2 and Qya time, probably as the large fan issuing from the mouth of Red Pass aggraded and buried the toes of small fans. Earlier (pre-Qia2) aggradation of the fans is hinted at by a lack of Qoa deposits, perhaps now buried. Fans of the central realm underwent a dramatic shift in drainage direction, clast composition, and base level during Qia3 time. Qia3 deposits are set into deep channels incised into Qoa deposits, carry mixed clasts, and drain south across the former west drainage pattern of Qoa deposits. Qogw and Qigw deposits indicate an area of high groundwater and poor drainage lay west of Red Pass into Qia3 time, but that wetland was incised and drained after Red Pass was cut. These data all indicate that Red Pass was cut early in Qia3 time, ~200 ka. The western realm apparently graded to an axial wash similar to Red Pass wash for the most part, but the south end of the alluvial fan shed west off of the granite ridge shows probable cut off of Qoa by younger fans that drain south and southeast.

The nearly constant gradient of Red Pass wash from >5 km west of Red Pass to 4 km east shows no knickpoints or steep reaches that sometimes accompany stream capture. This may indicate that geomorphic adjustment to stream capture is nearly complete. This implies that capture was old enough for significant geomorphic equilibration, but rates of geomorphic equilibration in deserts are poorly understood so no time constraint is available from published literature. Gentler stream gradients in upper branches of Red Pass wash passing through GWD more closely reflect gradients of the GWD, indicating that these reaches have changed little since capture. Tributary streams cutting Qoa deposits steepen eastward toward Red Pass, indicating continuing adjustment of these tributaries to the capture event. Steeper gradients in the lowest reaches of tributaries, adjacent to Red Pass wash, indicate a more youthful downcutting of the wash after the capture, and only partial adjustment by tributaries. This younger incision is possible related to the stranding of high deposits in the area where we dated sediments.

Our luminescence ages add to the chronology for difficult-to-date desert alluvial fan deposits and confirm a late incision in Red Pass. The three ~12 ka ages for Qya4 deposits conform with the 9-14 ka age range for these deposits regionally (Miller et al., 2010). The underlying Qia deposit, dated at 30 to 38 ka herein, helps to resolve a particularly difficult problem. Regionally, Qia deposits have been divided into three subunits, but the two youngest (Qia1 and Qia2) in many places are difficult to distinguish without geomorphic evidence or detailed study of soils. As a result, the two young units are typically lumped, generally denoted Qia2. This lump unit Qia2 has ages ranging from 30 to 90 ka (S. Mahan, K. Maher, D. Miller unpubl data). The apparently simple depositional system at Red Pass supports the interpretation that Qia1 deposits are ~30-38 ka.

If Red Pass was cut during Qia3 time, why are younger deposits in Red Pass perched high above the wash floor? We considered three hypotheses: 1) recent downcutting below the Qia3 level, 2) episodic filling and cutting associated with pulses of sediment, and 3) temporary base level rise and fall driven by building of GWD in the pass. The first hypothesis requires that all deposits before Qya4 graded to a much higher level than the modern wash, but Qia2 deposits in tributary channels do not grade to this hypothetical high base level. The second hypothesis explains the observations that Qia1 (~30 ka) deposits, Qya4 deposits, and Qya3 deposits all are anomalously perched near the narrows of Red Pass. Sediment pulses conceivably could have plugged the narrows, causing temporary aggradation. However, the hypothetical plugs would be most durable if composed of boulders, some of which might remain in the pass; we have observed none. The third hypothesis builds on the observations that

GWD typically are robust aggrading deposits (Quade et al., 1995; Forester et al., 2003; Pigati et al., 2011), even when they form in major washes. The shallow groundwater leads to thick growth of phreatophyte plants, which trap sediment effectively. Support for this hypothesis comes from the small patch of Qigw near the volcanic knob at Red Pass and the relatively localized perched deposits. The bedrock floor of Red Pass wash in the narrows effectively dams shallow groundwater, enhancing the possibility of forming GWD there.

If we are correct that temporary GWD caused local aggradation upstream of Red Pass, the interplay of GWD and stream sediment delivery can be examined. The Qia2 deposits near the volcanic knob at Red Pass appear to lie on and grade into the Qigw deposits, indicating that part of the pulse of Qia2 sediment coincided with GWD development. Overlying Qia2 is a soil, then Qia1—indicating abandonment of the depositional surface of Qia2 and later aggradation, perhaps without significant downcutting. The same is indicated for the Qia1-Qya4 transition: soil development indicates abandonment followed by aggradation. We cannot resolve the amount of downcutting (if any) associated with each soil development cycle, nor the length of time involved, with the limited deposits remaining in the pass. However, it appears that there is a strong association of stream sediment delivery with periods of GWD aggradation, which suggests overall wetter times for sediment delivery. Interestingly, soil development (and lack of stream activity) as constrained by our dating of Qya4 and Qia1 deposits is between about 12 and 30 ka. This period includes the last glacial maximum (ca. 24-20 ka), apparently not a significantly wet interval in the Mojave Desert.

Our data indicate that high groundwater levels west of the Soda Mountains played a direct and important role in stream capture to form Red Pass. Extensive paleo-wetlands west of the Soda Mountains are recorded by GWD deposits, indicating high water tables in the 520-570 m altitude range. Although mechanisms for stream capture have been argued for over a century, the mechanism most commonly cited is that aggressive head-cutting by a stream lowers ridge-crest altitudes, eventually allowing a stream on the other side of the ridge to overtop and incise the ridge (e.g., McKnight and Hess, 2006). Such head-cutting must be driven by either larger discharge and/or more erodible substrate. Alternatively, Pederson (2001) argued that high groundwater on one side is more commonly the driver of stream capture, by means of seeps and springs that cut into the ridge, increasing discharge on the downstream side as well as disaggregating rock, causing aggressive head-cutting. The presence of widespread GWD of the same age as the timing of stream capture strongly suggests that groundwater flow through the Soda Mountains played a key role in the stream capture event. By this hypothesis, some of the Qoa sediment would have been under the water table, and there may have been several sapping locations on the east side of the bedrock ridge. We have not found any old GWD along that ridge to support this hypothesis.

Although the processes leading to stream capture can take a long time, the final capture event is generally thought to occur very quickly (Pederson, 2001), with rapid sediment and water delivery downstream that may reach catastrophic proportions. Such an event could leave a depositional record or significant scour in the Salt Creek drainage. We estimate that at least 40 x 10^6 m^3 of rock and sediment was eroded out of Red Pass and the Qoa fans. Much of this probably constituted coarse bedload, and was deposited in the fan stretching to Salt Creek, where stream gradient lessens dramatically, but any such deposits are completely buried at present.

If the stream capture occurred about 200 ka, why does Red Pass seem so youthful, with a flat active wash surface from wall to wall and steep cliffs on both sides? Possibilities include: 1) recent large stream discharge causing recent erosion of the walls and floor; 2) very slow erosion of cliff faces; and 3) youthful tectonics causing recent erosion in response to uplift. A large flood during the last 50 years seems unlikely because no geomorphic record of such a recent event is known and historical air photos show no evidence for an event. Remnants of camp sites using technology of the 19th century can be found on low terraces adjacent to Red Pass wash, suggesting that any large floods predated the Old Spanish Trail. A large flood in prehistory, such as 2–3 centuries ago, is possible but difficult to prove. Slow rates of geomorphic change in the desert are well known but not well quantified. We have observed post-Qia2 stream capture sites that appear to be very fresh elsewhere in the desert. For example, the cutting of Afton Canyon at ~24 ka (Reheis et al., 2012) produced

an impressive feature that still looks youthful. Young tectonics may play a role, as it has been suggested that Silurian Valley is a young, possibly active, downfold (Miller et al., 2007). A downfold would steepen the gradient of Red Pass wash east of Red Pass. In contrast, the fan east of Red Pass is of same gradient west and east of the pass, showing little evidence for folding. The possibly active Soda-Avawatz fault passes through the piedmont of western Silurian Valley, but it is strike-slip and does not have an obvious scarp that would steepen stream gradients. Faults in the Soda Mountains at Red Pass do not cut Qoa deposits, and are not likely to be a tectonic cause for the youthful appearance of Red Pass. These lines of evidence, combined, suggest that the youthful appearance of Red Pass is due to slow rates of erosion in the desert environment.

Conclusions

Red Pass, part of an important historic overland route for people and goods, consists of an east-flowing ephemeral stream that is deeply cut into the Soda Mountains. Stream capture at Red Pass occurred at ~200 ka, based on a stark contrast between alluvial fan geomorphology, deposit provenance, and transport direction before and after. Also supporting the timing are widespread paleo-wetland deposits before the capture event. The capture event added a large watershed consisting of several high mountains and valleys of eastern Fort Irwin to the Silurian Valley watershed, probably significantly increasing discharge to Salt Creek. Groundwater perched at high levels on the west side of the Soda Mountains likely played an important role in the capture event, causing spring discharge and sapping that drove westward head-cutting through the Soda Mountains.

Acknowledgments

We wish to thank Dave Bedford and John Vogel for field assistance, and personnel at Fort Irwin for granting access to the National Training Center. We appreciate helpful reviews by Andy Cyr and Dave Bedford.

References

Birkeland, P. W. 1990. Soils and geomorphology. Oxford University Press, New York, New York, USA.

Dokka, R.K., and Travis, C.J., 1990, Role of the eastern California shear zone in accommodating Pacific-North American plate motion: Geophysical Research Letters, v. 17, p. 1323-1326.

Forester, R.M., Miller D.M., and Pedone, V.A., 2003, Ground water and ground-water discharge carbonate deposits in warm deserts, *in* Reynolds, R.E., ed., Land of Lost Lakes: Desert Studies Consortium, California State University, p. 27-36.

Grose, T., 1959, Structure and petrology of the northeast part of the Soda Mountains, San Bernardino County, California: Geological Society of America Bulletin, v.70, n.12, p. 1509-1548.

Hafen, L.R., and Hafen, A.W., 1993, Old Spanish Trail: University of Nebraska Press, 375 p.

Mahan, S.A., Miller, D.M., Menges, C.M., and Yount, J.C., 2007, Late Quaternary stratigraphy and luminescence geochronology of the northeastern Mojave Desert, with emphasis on the Valjean Valley area, *in* Miller, D.M. and Valin, Z.C., eds., Geomorphology and tectonics at the intersection of Silurian and Death Valleys, southern California: U.S. Geological Survey Open-File Report 2007-1424, p. 63-97.

McFadden, L.D., Ritter, J.B., and Wells, S.G., 1987, Use of multiparameter relative-age methods for age estimation and correlation of alluvial fan surfaces on a desert piedmont, eastern Mojave Desert, California: Quaternary Research, v. 32, p. 276-290.

McKnight, T.L., and Hess, D., 2006, Physical Geography: A Landscape Appreciation (8th Edition): Upper Saddle River, New Jersey: Pearson, Prentice Hall, 462 p.

Miller, D.M., and Yount, J.L., 2002, Late Cenozoic tectonic evolution of the north-central Mojave Desert inferred from fault history and physiographic evolution of the Fort Irwin area, California: Geological Society of America Memoir 195, p. 173-197.

Miller, D.M., Menges, C.M., and McMackin, M.R., 2007, Geomorphology and tectonics at the intersection of Silurian and Death Valleys, southern California: Field trip road log, *in* Miller, D.M. and Valin, Z.C., eds., Geomorphology and tectonics at the intersection of Silurian and Death Valleys, southern California: U.S. Geological Survey Open-File Report 2007-1424, p. 7-49.

Miller, D.M., Bedford, D.R, Hughson, D.L., McDonald, E.V., Robinson, S.E., Schmidt, K.M., 2009, Mapping Mojave Desert ecosystem properties with surficial geology, *in* The Mojave Desert: Ecosystem Processes and Sustainability, ed. by R.H. Webb, L.F. Fenstermaker, J.S. Heaton, D.L. Hughson, E.V. McDonald, D.M. Miller: University of Nevada Press, p. 225-251.

Miller, D.M., Schmidt, K.M., Mahan, S.A., McGeehin, J.P., Owen, L.A., Barron, J.A., Lehmkuhl, F., Lohrer, R., 2010, Holocene landscape response to seasonality of storms in the Mojave Desert: Quaternary International, v. 215, p. 45-61.

Pederson, D.T., 2001, Stream piracy revisited: A groundwater sapping solution: GSA Today, vol. 11, no. 9, p. 4-10.

Pigati, J.S., Miller, D.M., Bright, J.E., Mahan, S.A., Nekola, J.C., and Paces, J.B., 2011, Chronology, sedimentology, and microfauna of groundwater discharge deposits in the central Mojave Desert, Valley Wells, California: Geological Society of America Bulletin, v. 123, p. 2224–2239.

Prescott, J.R., and Hutton, J.T., 1988, Cosmic ray and gamma ray dosimetry for TL and ESR: Nuclear Tracks and Radiation Measurements v. 14, p. 223-230.

Quade, J., Mifflin, M.D., Pratt, W.L., McCoy, W., and Burckle, L, 1995, Fossil spring deposits in the southern Great Basin and their implications for changes in water-table levels near Yucca Mountain, Nevada, during Quaternary time: Geological Society of America Bulletin, v. 107, no. 2, p. 213-230.

Reheis, M.C., Harden, J.W., McFadden, L.D., and Shroba, R.R., 1989, Development rates of late Quaternary soils, Silver Lake playa, California: Soil Science Society of America Journal v. 53, p. 1127-1140.

Reheis, M.C., Bright, J., Lund, S.P., Miller, D.M., Skipp, G., and Fleck, R.J., 2012, A half-million year record of paleoclimate from the Lake Manix core, Mojave Desert, California: Palaeogeography, Palaeoclimatology, Palaeoecology, v. 365-366, p. 11-37.

Schermer, E.R., Luyendyk, B.P., and Cisowski, S., 1996, Late Cenozoic structure and tectonics of the northern Mojave Desert: Tectonics, v. 15, p. 905-932.

Spencer, J.E., 1990, Late Cenozoic extensional and compressional tectonism in the southern and western Avawatz Mountains, southeastern California, *in* Wernicke, B.P., ed., Basin and Range extensional tectonics near the latitude of Las Vegas, Nevada: Geological Society of America Memoir 176, p. 317-333.

The terrestrial opposition effect on desert playas

David K. Lynch
Thule Scientific, thule@earthlink.net

ABSTRACT: New observations and analyses are presented of the terrestrial opposition effect on mud cracks (mud polygons) on desert playas. The enhanced brightness (radiance) of the surface near the antisolar point has been correctly ascribed to two sources, shadow-hiding and coherent backscatter. The observations reported here suggest a third optical mechanism that may in some cases influence the TOE: some parts of the mud polygon are more strongly illuminated than others depending on the angle of incidence of sunlight. This causes the areas facing the observer and the sun to be brighter (W sr-1 cm-2) than the rest of the polygon field.

I. Introduction

The terrestrial opposition effect (TOE) is a bright spot a few degrees across seen on the ground around the antisolar point (ASP). The scattering angle at the ASP is 180°. The TOE is most often visible from an aircraft, which is high enough that its shadow is penumbral and visually undetectable (Figure 1).

The more general opposition effect (OE) has been long known on the moon, when it brightens dramatically near opposition, i.e., at full moon. Indeed, the total amount of light reflected toward Earth at first

Figure 1 (left). Terrestrial opposition effect on a grassy plain. The bright spot is elliptical and vertically elongated, typical of grassy plains. Figure 2 (right). Terrestrial opposition effect on mud polygons seen as a bright glow around the shadow of the observer's head. No shadows can be seen above the shadow of the observer's head (ASP), but they are readily visible below it.

quarter moon is only about 1/10th as much as full moon. Based on the brightening of Saturn's rings as it approaches opposition, Seeliger (1887; 1895) explained the optical mechanism as shadow-hiding (SH); when the observer's line-of-sight (LOS) is parallel to the sun's ray, no shadows can be seen.

More recently, Hapke and others (Kuga and Ishimaru (1984); Hapke (1986), Hapke et al. (1993) have shown that another optical mechanism – coherent backscatter (CB) - plays a major and sometimes dominant role in in the brightness of surfaces when viewed in backscatter.

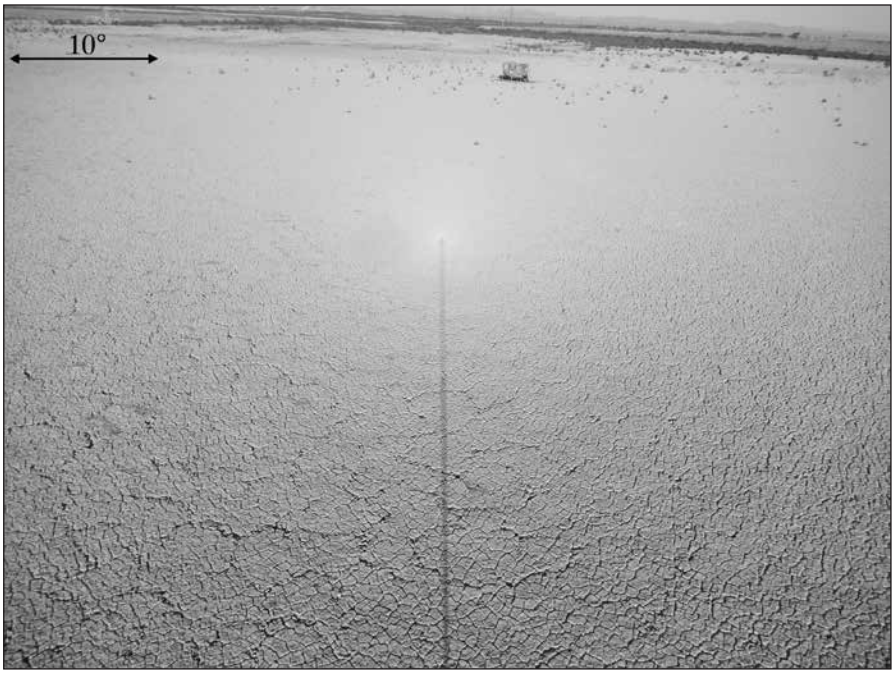

Figure 3. Terrestrial opposition effect on mud polygons with the camera placed on a six meter long pole. Compared to the same surface as Figure 2, the observer's shadow (camera shadow) is greatly reduced, allowing more complete exposure of the TOE.

The OE (or TOE) is present on every surface, natural and manmade. Its shape and brightness distribution depends primarily on the detailed geometry of the shadowers (SH), the microscopic optical properties of the sunlit surfaces of the shadowers (CB) and the scattering angle.

Studying the TOE involves three challenges: (1) The shadow of the observer's head prevents sunlight from reaching the ASP (Figure 2), and thus the observer cannot see the ASP. (2) From the air, the geometry of the surface is not known in any detail, so modeling is not possible. (3) Even from the ground when the TOE is within reach, most surfaces are inhomogeneous and therefore their backscatter characteristics are correspondingly irregular. To minimize these problems, investigators would like to make ground-based observations of a wide, flat surface that is on relatively homogeneous, and one that can be observed with the minimum possible observer shadow.

In this paper, we present new observations, a simple observing technique, and analyses of natural mud polygons ("mud cracks") and show that geometrical dilution of sunlight influences the brightness distribution of the TOE, and by extension, the OE in general.

II. Observations

In Oct 2013, a prominent TOE was observed on mud polygons on the New River delta in Imperial County, CA (Figures 2), and subsequent observations were made in Nov 2013 (Figure 3). To minimize the observer's shadow, a small point-and-shoot digital camera (Nikon AW100) was placed at the end of a 6m long extendable painter's pole. The camera's shadow was primarily penumbral with a small core of umbra. The geometry of these mud polygons is relatively simple and they can be observed *in situ* to obtain detailed shape information for modeling purposes.

Referring to Figure 3, we see that virtually no shadows can be seen above the TOE, but in the lower portion of the photograph shadows become progressively more evident as more and more shadows are exposed.

Horizontal and vertical scans through Figure 3 were made that passed as close as possible to the unobscured (by the camera shadow) ASP (Figures 4 & 5). After removing the camera's vignetting by dividing the scan by an identical scan through a flat image, the resulting scans were roughly proportional to true radiometric brightness. Pixel-to-pixel noise in the image was measured from dark images and found to be only 1-3 units out of 255. The deep vertical excursions are shadows, not noise.

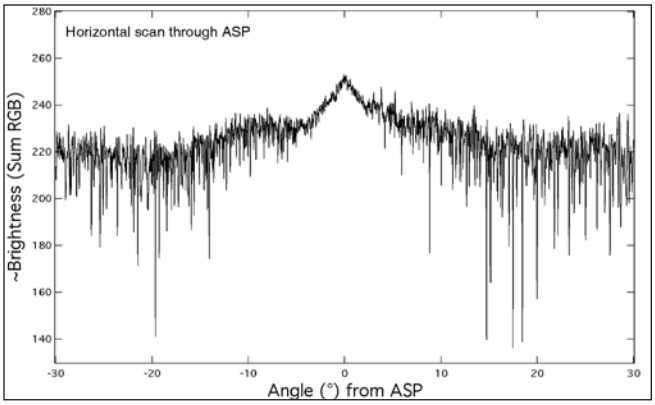

Figure 4. Horizontal scan through the ASP, after removing vignetting. The scan was done ~0.1° away from the ASP, as close as possible while still avoiding the camera's shadow. The horizontal profile quantitatively confirms the visual impression: a bright area surrounding the ASP that grows gradually fainter with angular distance from the ASP. The enhanced brightness has two components: the narrow, central triangular peak is due to CB and is about 2.7° wide (full width at half maximum - FWHM). The broader enhanced region is due to SH (FWHM ~30°). Shadow signatures appear as narrow spikes in the scan, always downward because they are dark.

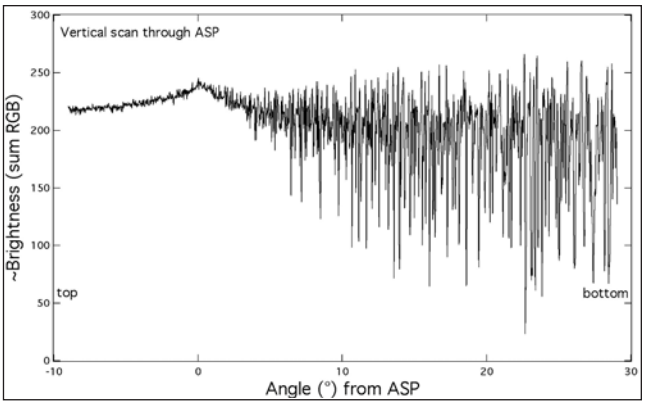

Figure 5. Vertical scan through the TOE shown in Figure 3, after removing vignetting. Coherent backscatter causes the central peak. The broader surrounding enhancement is due to shadow hiding, and to bright, sunward facing surfaces of the mud polygons (see section III). Shadows appear as dark, downward spikes in the scan. Note the ~absence of shadows near the ASP.

III. Dilution of sunlight as a function of angle of incidence.

The scan in Figure 4 agrees with visual inspection of Figure 3, but the scan in Figure 5 held a surprise. The downward spikes due to shadows in Figure 5 were expected but not the bright upward spikes, some exceeding the brightness of the TOE itself. A close examination of Figure 3 (Figure 6) reveals the explanation.

Sunlight falling on any surface is spread out and therefore diluted based on the angle between the surface normal and the incoming sunlight, the angle of incidence **i**. Dilution here is defined as cos(**i**). There is no dilution if the surface normal parallels the sunlight (**i** = 0°), i.e. dilution is 1.0 because cos(**i**) is unity. As the angle increases, dilution increase as cos(**i**), and becomes less than unity, eventually reaches zero when sunlight is parallel to the surface. This is illustrated in Figure 7.

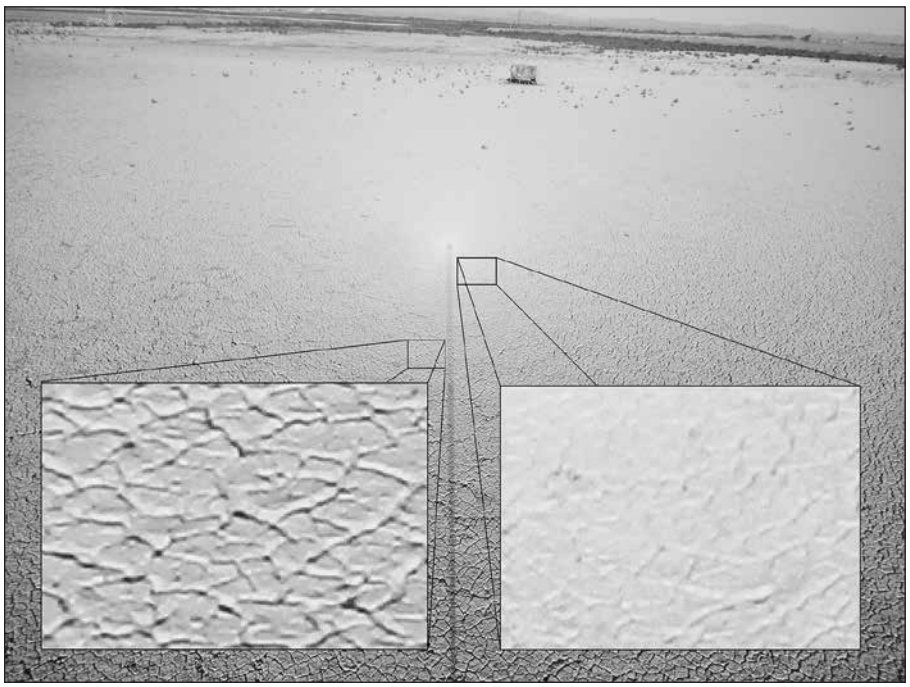

Figure 6. The brightest parts of the scene are not at the ASP but rather on some of the sunward facing parts of the mud polygons.

This explains why the brightest parts of the scene are brighter than the CB OE. For surfaces perpendicular to the incoming light, there is no dilution because cos(**i**) = unity. These are the brightest surfaces. When **i** > 0, there is more dilution because cos(**i**) < 1. Even though CB brightens the surface, it does not always brighten it as much as dilution does.

Dilution is a well-know effect but to our knowledge, it has not been discussed in the context of the TOE. The findings reported here are for one particular set of mud polygons, but other factors are expected

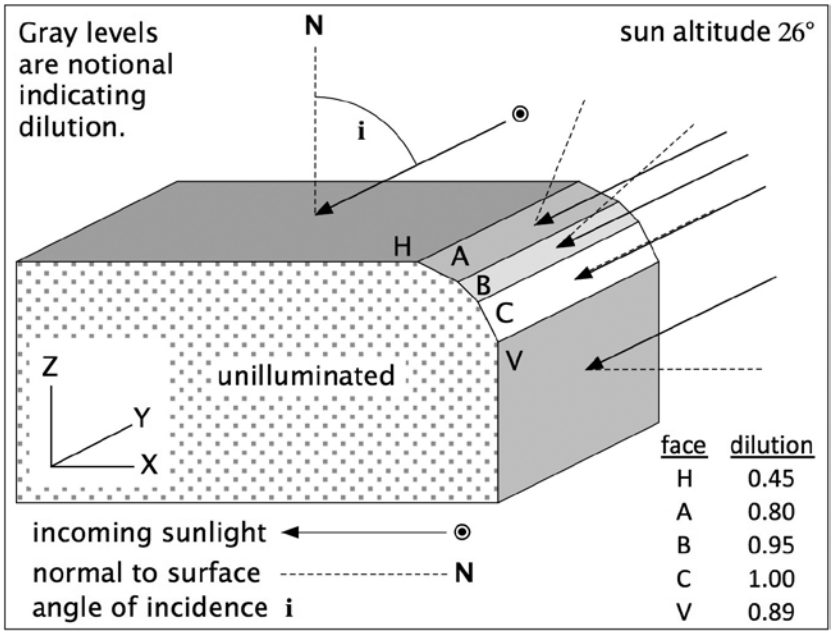

Figure 7. Drawing of a slice through a mud polygon. The observer and Sun define the vertical x-z plane. Solid lines indicate the direction of incoming sunlight, in this case with the sun at an altitude of 26°. Dashed lines are normals to each face, and **i** is the angle of incidence. Incoming sunlight reaching each face is geometrically diluted by an amount equal to cos(**i**). The brightest face is the one with its normal parallel to incoming sunlight, i.e., **i** = 0, indicated in white (face C). All other faces are darker. This explanation assumes equal reflectivity of all surfaces.

to introduce variations. The main factors are (1) the ratio of the width of the polygon to the crack width, and (2) the geometry and amount of rounding at the edge of the polygon.

Acknowledgments

The author would like to thank David S. P. Dearborn and Andrew T. Young for many useful discussions about the opposition effect.

References

Seeliger, H. (1887), Zur Theorie der Beleuchtung der grossen Planeten insbesondere des Saturn, Abhandl. Bayer. Akad. Wiss. Math-Naturw. Kl. II 16:405-516.

Seeliger, H. (1895), Theorie der Beleuchtung staubformiger kosmischen Masses insbesondere des Saturinges, Abhandl. Bayer. Akad. Wiss. Math-Naturw. Kl. II 18:1-72.

Hapke, B. (1986), Bidirectional reflectance spectroscopy, 4. The extinction coefficient and the opposition effect, Icarus 67:264-280.

Hapke, B., Nelson, R., and Smyth, W. (1993), The opposition effect of the moon: the contribution of coherent backscatter, Science 260:509-511.

Kuga, Y., and Ishimaru, A. (1984), Retroreflection from a dense distribution of spherical particles, J. Opt. Soc. Am. A1:831-835.

Abstracts from proceedings 2014 Desert Symposium

Robert E. Reynolds, editor
Redlands, California. rreynolds220@verizon.net

Invertebrate fossils from the Kidwell collection in the Anza-Borrego Desert State Park paleontology collection

Louise Bahar
Anza-Borrego Desert State Park Paleontology Society, bahar.louise@gmail.com

Dr. Susan Kidwell, assisted by graduate students, explored the Anza-Borrego Desert to study the geology and sedimentology of the area in the late 1980s. She worked under permit issued by the Park and was allowed to collect fossils and retain them for her research. After she completed the research, a group of five Anza-Borrego Desert State Park Paleontology Society volunteers traveled to Chicago in late 2009 to retrieve the specimens. They wrapped about 5000 fossil specimens for shipment to the paleontology laboratory in Anza-Borrego. An addition to the main curation area was built to house this collection. In fall of 2012, two experts in marine invertebrates arrived independently to work on identifying and describing the Kidwell fossil collection. Dr. Astrid Montiel Boehringer began a post-doctoral fellowship through Scripps Institution of Oceanography/University of California San Diego to identify and catalogue the Latrania portion of the Imperial Formation invertebrates. At the same time, the ABDSP volunteer organization, Paleontology Society, obtained funding from the Charles Stout Foundation, and other sources, to hire N. Scott Rugh to identify the fossils and describe them. Their combined experience with invertebrate marine mollusks enabled them to assign genus and species names to nearly all of the mollusks and a great majority of other marine invertebrates, such as corals, sponges, crabs and sand dollars. This joint task was completed in spring of 2013. As the identification of this collection was going on, the Anza-Borrego Desert State Park Paleontology Society organized the specimens in drawers by locality and then cataloged the specimens into their computer database. This work allows researchers to access details about the collection that would be otherwise unavailable.

Monitoring soil moisture dynamics on Mojave Desert piedmonts

David R.Bedford, David M. Miller, and Kevin M. Schmidt
U.S. Geological Survey, 345 Middlefield Rd, Menlo Park, CA 94025

Quaternary evolution of the Mojave Desert has resulted in a diverse suite of surficial deposits across piedmonts where much of the biologic activity is focused. The deposits are composed of different source rocks and are formed by different geomorphic processes, resulting in a range of sedimentary structures, soil textures, and water retention properties. Following deposition, soil development further altered soil texture, creating distinct soil horizons. These age-dependent soil horizons have different hydrologic properties. Subsequent vegetation types, patterns, and amounts characteristically track different surficial deposits; for instance underlying soils associated with desert pavements tend to support restricted vegetation cover of limited diversity, whereas young stream-channel proximal deposits tend to support large amounts of vegetation with higher diversity. Understanding the linkages between soil maturity and vegetation is key to understanding the functioning of the ecosystem and anticipating effects from human disturbance and climatic changes. Thus, we are studying the soils-vegetation-climate (aka, ecohydrology) in order to better understand desert ecosystem dynamics. Our studies have focused on the Kelso Valley watershed in the Mojave National Preserve, CA in large part because of its diversity of soils, elevation zones, and biota. At sites across the watershed we have been conducting long-term monitoring, detailed geologic and vegetation mapping, and water manipulation experiments to understand the natural and

anthropogenically disturbed (i.e. by roads) ecohydrology. Here we focus on more than seven years of soil moisture monitoring to illustrate the strong effects of soil properties on water status, and therefore available water for vegetation. We illustrate the variable response of soil moisture to precipitation pulses for six different soils. In general, small precipitation (<~6 mm) pulses wet all soils shallow (< 10 cm) depths, which often dry out rapidly. However, differential wetting is evident for larger pulses. Some soils rapidly increase in water content and later rapidly dry out within days, while others maintain elevated moisture levels for longer time periods. Older, more advanced soils have a much reduced moisture pulse relative to precipitation pulse size. Combined with surficial geologic maps that encode soil hydrologic properties, these results can be used to describe ecohydrological responses to precipitation pulses across a wide range of space and time scales.

Alpine plants as indicators of climate change

Jim and Catie Bishop
GLORIA California–Nevada Team

Alpine plants, living at elevations above treeline, face a demanding climate with very interesting adaptations (including a few similar to plants living in a desert). They are biological indicators of climate change, spanning the globe and sampling maritime/continental, and polar/mid-latitude/tropical climates. An international protocol (GLORIA, Global Observation Research Initiative in Alpine Environments) provides scientifically valid and globally comparable data. GLORIA operates with a core professional science cadre at the University of Vienna, a specific protocol, agency/academic personnel, and a lot of helpful volunteer scientists.

California was the site in 2004 of the first GLORIA Target Regions (a group of summits spanning from treeline to the highest peak) in the Western Hemisphere. The North American network is well represented in California and Nevada, with 29 summits in the Sierras and Great Basin, from classic high alpine at 14,000 feet elevation to desert alpine. Additional studies supplement the network. The baseline data is informative, and five-year repeat surveys have revealed some interesting things, although two decades of study will be needed to identify persistent climate change.

Geochemical correlation of basalts in northern Deep Springs Valley, California, by X-ray Fluorescence Spectroscopy (XRF),

Aaron J. Case
CSU Fullerton, CA aaroncasegeology@gmail.com

In northern Deep Springs Valley (DSV), between Owens Valley and Death Valley, California, Pliocene-age olivine basalts lie on the valley floor and atop the adjacent White/Inyo Mountains to the west and the Deep Springs Range to the east. Previous geologic mapping shows the DSV basalt flows and the Last Chance Range (LCR) basalts found to the southeast as the same geologic unit with a source in the White/Inyo Mountains. The basalts in northern DSV are offset ~400 m by the Deep Springs fault and have a K/Ar age of 10.8 Ma. To determine if the olivine basalts found in the region are all from the same source, four samples were collected in a linear pattern from west to east across northern DSV. The samples were powdered and analyzed for major and trace element composition by X-ray Fluorescence Spectrometer (XRF). Trace-element plots (e.g., Ba, Nb, Zr) show that the DSV basalts are similar and are likely one flow, but the DSV basalts are distinct from the LCR basalts. I interpret these data to show that the DSV and LCR basalts have different sources and should not be mapped as the same geologic unit. The likely source of the DVS basalts is in the White/Inyo Range. The geochemical correlation shows that the DSV basalts flowed NW to SE in a paleo-channel 10.8 Ma and that DSV did not exist at that time.

Mary Hunter Austin—Land of Little Rain, Country of Lost Borders

Walter Feller
walter@aeve.com

Mary Hunter Austin defines the Land of Little Rain as being "Between the high Sierras south from Yosemite—east and south over a very great assemblage of broken ranges beyond Death Valley, and on illimitably into the Mojave Desert." The Mojave she describes is still there, recognizable in many ways while disappearing into memories and stories. Her intention was not to write a guidebook, but a personal introduction to the land she loved. She gave away no secrets. She gave away no man's fondest memories. She lived in a time when white men were giving names to places previously only known to Indians, and with her prose kept those Indian names

alive, and in doing so she added a layer of authenticity and connection to times before history. By describing her home lands she found the most basic elements of character inherent to all of the Mojave and the mountain lands surrounding it. Each land is the same, but differs ever so slightly. This captures our sameness, the essence of the Mojave, and how this diversity as a whole defines us. Step by step, piece by piece, these are the things I started seeing all over the desert as I've photographed. This presentation is my interpretation of her beautifully assembled words.

Death of a tortoise: decomposition and taphonomy of a *Hesperotestudo* in the Anza-Borrego Desert

Linda Gilbert, Robert H. Keeley, and Ron Pavlu
Anza-Borrego Desert Paleontology Society

The Plio-Pleistocene Hueso Formation (2.8–0.95 Ma) in the Anza-Borrego Desert was a zone of meandering, braided stream beds, composed of locally derived sediments and sands. The sandstone, mudstone, and conglomerate remnants of that environment have yielded over 100 giant tortoise sites. The most recent site (ABDSP 3551), found in 2010, contains the most complete shell found in the last 50 years. The site lies in the fluvial Hueso Formation (Fm), stratigraphically between younger and older units of the lacustrine mudstone and siltstone of the Tapiado Fm.

The site was revealed by a scatter of fractured bone, trapped between tufts of desert grass, within an arc of exposed, thin, white bone, and embedded in yellowish sandstone. The 1.5 m site was gridded, surface bone was mapped and collected, and the nearby gully was sieved before the site was excavated. The thin arc of bone revealed a specimen lying at a dip-angle of 32 degrees, in sand, on top of a firm silt bed. The anterior of the shell faced east, perhaps aligned with the Hueso sediment transport system that trends to the ESE.

Two jackets were constructed, one containing the main carapace/plastron material and the second, a tightly packed stack of bone and dermal ossicles. The latter included: a vertebral piece of carapace; dermal ossicles, likely from the right front leg; plus fine, thin bone fragments. These were found resting on the silt bed. The jackets were removed to the Colorado Desert District Stout Research Center.

In the laboratory, the larger jacket was found to contain a sand-filled, complete plastron with partial carapace of a male *Hesperotestudo*. The outer margin of the plastron is complete and articulated with the lower 27 cm of the right wall of the carapace. Whereas the plastron and most of the carapace wall are in excellent condition, the margin of the carapace and broken edges show considerable disintegration, due possibly to prolonged near-surface chemical and physical reactions of sediments to local environmental seasonal conditions, perhaps both before original burial and after near-surface exposure.

Work on this specimen to remove the matrix filling the shell has revealed few fragments of the carapace below the layer of original surface fragments, with (so far) no skull or post-cranial elements. Abundant insect holes bored into the uppermost 6 cm of sandy matrix filling the shell probably resulted from recent insect activity.

The second jacket, containing the three additional skeletal portions, is also being prepared. Large slabs of carapace bone underlie these elements and their tightly packed condition makes for cautious progress.

Based on detailed sediment measurements taken at the site, one explanation is that the tortoise died near a flat silt overbank in a stream channel. Sometime after death, following considerable decay/scavenging/breakage, a shift in the channel or a flood brought in sand to partially fill the shell. As the presence of the shell changed the stream flow, the south side became eroded and the shell slid into the depression, leaving it at a 32 degree dip to the right. As sediments began to cover the tilted shell on the outside, sand continued to accumulate inside the shell, at 32 degrees to the plane of the plastron. Finally, the remaining exposed top and left wall of the carapace broke down and collapsed, much of it contributing to the fragments strewn downhill from the carapace.

Sediment deposits continued to bury the tortoise shell deeper and deeper until the end of local basin deposition, shortly after the end of the Jaramillo subchron at 0.99 Ma. Erosion and uplift brought the specimen back to the surface where the exposure of the thin arc of bone left its signature.

Tracking the tracks with photogrammetry

Jon Gilbert *(svcompassrose@aol.com),* Hugh Vance, and Gabriel Vogeli

As part of paleontology resources management in the Anza-Borrego Desert State Park (ABDSP), a need for locating, collecting, and storing digitized data for ephemeral tracks and trackways was identified. An instructive photogrammetry class, presented by Bureau of Land Management paleontologists at the 2013 Society of Vertebrate Paleontology conference, provided the technical means to address that need. Three volunteers from the ABDSP Paleontology Society attended, where they gained a basic knowledge of how to conduct photogrammetry. This included selecting camera equipment, taking the photos, a set of instructions, and a list of software available for processing digital images. It was then decided to conduct a practice photogrammetry project.

The practice project was conducted to prove that personnel could be effective using photographic techniques in a planned sequence with targets and adequate camera equipment to create useful digital imagery and to establish protocols appropriate for the ABDSP field and for objects in the fossil collection. The resulting digital photos were processed with Photoscan software, and clear and precise digital 3D models were produced.

The objects used for the practice project were all fossils from the ABDSP collection, and included a camel track (Camelidae) in mudstone, the beak of a terror bird (*Titanis walleri*), and a giant land tortoise (*Hesperotestudo*).

The digital 3D photos will provide data for record keeping, study, and long range monitoring of ephemeral tracks and track ways, to record deterioration and possible new nearby exposures. There are approximately 200 documented track/trackway locations in the ABDSP. The plan is that all localities will be photographed and placed in a storage data file. Then, as time permits, the data will be processed using appropriate software to effect measurements.

When the technology is available and affordable, we plan to make reproductions of selected objects using the photogrammetric data, providing input to a 3D printer/ replicator.

Geology of a Tertiary intermontane basin of the Last Chance Range, northwest Death Valley National Park, California

Christopher Johnson
Department of Geological Sciences, California State University-Fullerton, Fullerton, CA, 92834 [cjohnson107@csu.fullerton.edu]

A hypothesized Pliocene fluvial connection between Owens Valley and Death Valley that predates the course of the Pleistocene Owens River would provide a migration pathway for aquatic and other species. The mapped Tertiary sediments and basalt flows hold one key to developing an accurate model of the paleo-river during this time. Previous mapping of the Tertiary sediments and flows was limited to spatial distribution, with limited description of the deposits themselves.

In the central Last Chance Range are ~4 km^2 of Tertiary sediments and basalt flows. The Tertiary deposits crop out along a N-S trending canyon that is underlain primarily by tilted Cambrian-age carbonates of the Bonanza King and Nopah Formations. To better understand the source and nature of these Tertiary rocks, I constructed a ~1:12,000 geologic map, described the sediments, and collected two basalt samples. The basalt was powdered and analyzed by X-ray fluorescence to determine its geochemical composition.

In the north, the base of the Tertiary sediments is coarse, well-cemented, landslide debris of Bonanza King and Nopah clasts. In the south, the basal unit is debris flow deposits of quartzite boulders. Overlying these coarse deposits are yellow, tan, and gray sandstone and breccia with a basalt flow near the top of the section. The Tertiary deposits are capped by a second basalt flow. The beds are folded into a N-S trending syncline. The composition of the basalt is similar to basalts found 3 km to the north in the Last Chance Range.

The quartzite debris flows are enigmatic. Clast imbrications within the debris flows indicate NW–SE flow. The closest outcrop of quartzite to the NW is the Cambrian Zabriskie Quartzite (>2 km- and outside the present drainage basin). No outcrops of quartzite are mapped to the north, east, or south. The correlation of basalt flows between basins in the Last Chance Range combined with the exotic quartzite clasts suggest that these now isolated deposits were once part of a larger intermontane basin that

extended to the N and NW. The N–S trending fold suggests E–W-oriented compressive stresses post-Pliocene.

The advisor for this undergraduate research project was Dr. Jeffrey Knott (CSUF). Dr. Jade-Star Lackey (Pomona College) provided XRF facilities. Financial support was provided by a grant from CSUF Associated Students, Inc. and a CSUF Incentive Grant (to Knott).

Preparation and jacketing of a mammoth skull in a sand environment

Robert Keeley, Sandra Keeley, Jon Gilbert, Lyndon K. Murray, and George T. Jefferson.
Colorado Desert District Stout Research Center, Borrego Springs, CA 92004. rhkeeley@earthlink.net

A combination of uncemented, coarse sand matrix, a large specimen, and friable bone required special techniques for the preparation and jacketing of the mammoth skull discovered in the Anza-Borrego Desert State Park in 2012 (Field Number PSJ 083).

Extensive consolidation of the bone in the field, using butvar-76 (40 g of butvar-76 dissolved in 500 ml of ethanol or acetone solvent), was required to avoid total loss of structure. The slow process involved exposing a small area of bone using a light brush, applying butvar-76 to the surface, and waiting for it to dry before proceeding. Once the surface bone was consolidated, an array of 3.1 mm holes was drilled to allow injection of the butvar-76 consolidant deeper into the specimen. Approximately 152 liters of consolidant were applied to the 0.6 m^3 specimen over a period of 2 months.

In order to reduce the skull's jacket to manageable weight and dimensions, the tusks were removed by sawing approximately 30 cm beyond the end of the alveoli and were jacketed separately. To minimize distortion of the skull jacket during transport, a three layer construction was employed: a 25 mm inner plaster jacket, a 50 mm foam layer, and a 25 mm outer plaster jacket. The resulting jacket is 1.8 m long, 1.2 m wide, with an average height of 0.7 m—a volume of about 1.8 m^3

The conventional approach of rolling a specimen from its matrix pedestal after construction of the upper jacket was not feasible because the unconsolidated sediment would have flowed out of the jacket immediately upon beginning rotation. We borrowed from methods described in the literature (pallet method, Maltese, 2009; jacket support clamp, Peterson et al., 2000), creating a floor under the specimen, and then clamping the floor to the upper jacket. The floor was created by driving aluminum sheets under the specimen and then supporting the sheets with a steel frame, constructed by driving 1 x 1 inch steel square stock bars in a grid pattern under the plates and bolting them together. Once the floor was secured to the jacket with crisscrossed nylon straps, the specimen was successfully rolled using a jeep-mounted winch. The floor, at this stage facing up, was removed and a conventional plaster cap (20 mm thick) was applied. The jacket was removed with the cap up, avoiding a second roll of the specimen.

References

Maltese, A. 2009. Difficult excavation and preparation of a large *Daspletosaurus* specimen. In Methods in Fossil Preparation: Proceedings of the First Annual Fossil Preparation and Collections Symposium, pp 63-68.

Peterson, R.E., N.V. D'Andrea, and A.B. Heckert 2000. The Rondan jacket support clamp and jacket transport sled. New Mexico Museum of Natural History and Science Bulletin 16 (New Mexico's Fossil Record 2), p. 281-288. (ISSN 1524-4156) Archived in NC DOCKS with permission of the editor. The version of record is available at: http://econtent.unm.edu/.

Discovery of a *Mammuthus columbi* partial skeleton in late Pleistocene sediments of Anza-Borrego Desert State Park, southern California

Sandra Keeley, Lyndon K. Murray, George T. Jefferson, Robert Keeley, and Arnie Mroz
Colorado Desert District Stout Research Center, Borrego Springs, CA 92004, sandrakeeley@yahoo.com

In the spring of 2012, volunteer members of the Anza-Borrego Desert State Park (ABDSP) Paleontology Society surveyed a previously unstudied area of the Park, producing, among several previously unrecorded late Pleistocene taxa, the first substantial mammoth discovery in the southern half of the Park. The initial find of the *Mammuthus columbi* specimen was a small bone fragment. Subsequent excavation of the steep hillside has uncovered a concentrated but incomplete skeleton, including several limb bones plus the skull, with full dentition and both tusks in alveoli, missing the cranium above the orbits, and resting on the apparently complete mandible.

Although dating the site is in progress (radiocarbon and Uranium–Thorium), the stratigraphic location of the fossil site is in the Bow Willow beds, with an estimated age of approximately 500

ka (Dorsey et al., 2011). However, a nearby *Bison* vertebra (see Murray et al., this volume) occurs stratigraphically within a couple of meters of the mammoth, placing the age of the mammoth within the age range of *Bison* (first appearance in North America, south of 55° north latitude, between about 160 to 210 ka; Bell et al., 2004). These bones are the youngest fossils yet recovered within the Park, significantly extending the ABDSP fossil record, for the first time, into the Rancholabrean NALMA (see Murray et al., this volume).

The skull lay upon its left side, dipping downhill 40^0 against a small silt lens. Orientation of the postcranial elements is inconsistent and some bones are piled upon each other. Spiral fractures were noted on several elements. Overall, the bone preservation varies from the cortical surfaces (good) into the medullary tissue (often punky).

The specimen occurs in a cross-bedded pebbly sand lens/channel which cuts into flat lying braided stream-type coarse grained sands. The bones were found eroding out of a 28^0 ridge slope in a loosely consolidated, poorly sorted coarse sand/silt layer.

These conditions limited the number of workers onsite, and posed significant challenges for the construction and removal of jackets. The logistics of the steep sand hillside, the exposure to a public roadway, the larger size of the bones, and the uneven preservation of the bones presented numerous excavation and removal challenges (see Keeley et al. this volume).

Ancillary faunal work in the Bow Willow beds, removal of the ca. 1,750 kg (3,500-pound) jacketed skull material, and laboratory preparation of additional bones is currently in progress. The occurrence of the specimen presents a challenging taphonomic study.

References

Bell, C.J., E.L. Lundelius Jr., A.D. Barnosky, R.W. Graham, E.H. Lindsay, D.R. Ruez Jr., H.A. Semken Jr., S.D. Webb, and R.J. Zakrzewski 2004. The Blancan, Irvingtonian, and Rancholabrean Mammal Ages. In Late Cretaceous and Cenozoic Mammals of North America, edited by M.O. Woodburne, Columbia University Press pp. 232-314.

Dorsey, R.J., B.A. Housen, S.U. Janecke, C.M. Fanning, and A.L.F. Spears 2011. Stratigraphic record of basin development within the San Andreas fault system: Late Cenozoic Fish Creek-Vallecito basin, southern California. Geological Society of America Bulletin 123(5,6):771-793.

Airborne hyperspectral infrared imaging survey of the southern San Andreas Fault

David K. Lynch[1], David M. Tratt[2], Kerry N. Buckland[2], and Patrick D. Johnson[2]

[1]USGS, Pasadena, California; [2]The Aerospace Corporation, Los Angeles, Calif.

The San Andreas Fault (SAF) between Desert Hot Springs and Bombay Beach has been surveyed with *Mako*, an airborne hyperspectral imager operating across the wavelength range 7.6–13.2 μm in the thermal-infrared (TIR) spectral region. The data were acquired with a 4-km swath width centered on the SAF, and many tectonic features are recorded in the imagery. Spectral analysis using diagnostic features of minerals can identify rocks, soils, and vegetation. Mako imagery can also locate rupture zones and measure slip distances.

Designed and built by The Aerospace Corporation, the innovative and highly capable airborne imaging spectrometer used for this work enables low-noise

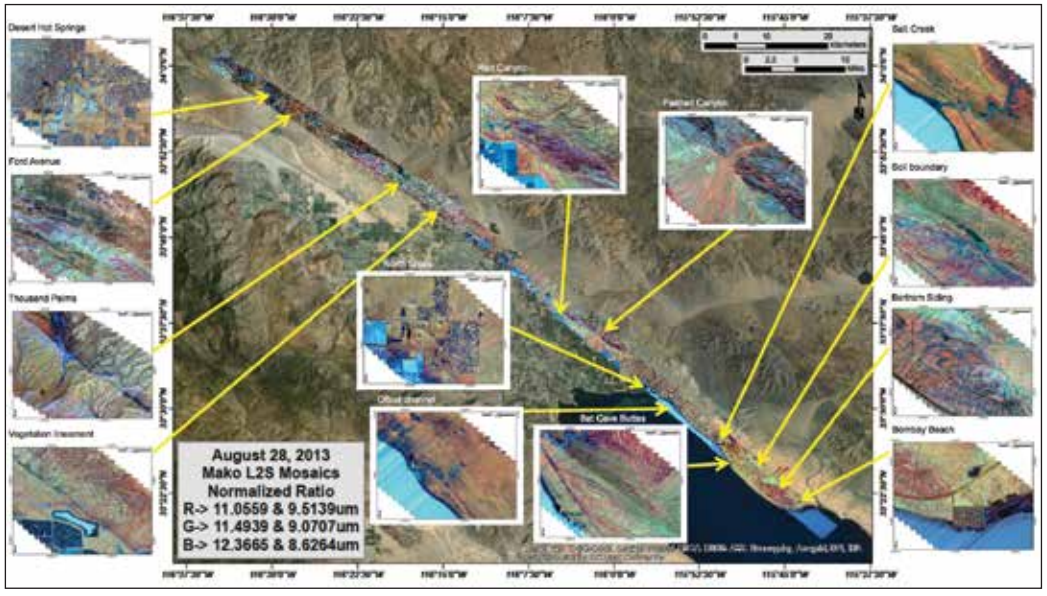

Mako image. See Lynch et al., Airborne hyperspectral infrared imaging survey of the southern San Andreas Fault.

performance (NEΔT$\lesssim$0.1 K @ 10 μm) at small pixel IFOV (0.55 mrad) and high frame rates, making possible an area-coverage rate of 20 km^2 per minute with 2-m ground resolution from 12,500 ft (3.8 km) above-ground altitude. Since its commissioning in 2010, Mako has been used in numerous studies involving other earthquake fault systems (Hector Mine, S. Bristol Mts.), mapping of surface geology, geothermal sources (fumaroles near the Salton Sea), urban surveys, and the detection, quantification, and tracking of natural and anthropogenic gaseous emission plumes.

Mako is available for airborne field studies and new applications are of particular interest. It can be flown at any altitude below 20,000 ft to achieve the desired GSD.

Holocene loess vs. modern dust in the Cima volcanic field

Marith Reheis, Shannon Mahan, Jim Budhan, and David Rhode
USGS, MS-980, Federal Center, Box 25046, Denver, CO 80225 mreheis@usgs.gov

Desert loess (eolian dust) of Holocene age is rare in the southwestern U.S., but locally has accumulated downwind of active dust sources against obstacles such as steep range fronts and in natural traps such as potholes and lava flows. Dust has also accumulated in surface soils, where it makes up the vesicular A horizon, and modern dust is ubiquitous. The Cima volcanic field, downwind of Soda Lake playa, has long been known as a site of desert loess accumulation on irregular basalt-flow surfaces during the Quaternary through the work of Les McFadden and Steve Wells, and has also been a site of modern dust studies for the past 30 years. We sampled a 1.3-m section of loess preserved in a lava tube on flow I, which is thought to be about 27 ka by ^{36}Cl exposure dating (Phillips, 2003, Geomorphology v. 53, 199-208) and ~31-37 ka by ^{3}He exposure dating (Wells et al., 1995, Geology v. 23, 613-616). Packrat middens within the lava tube yielded ages ranging from about 1300 to 12,500 cal yr B.P. (written commun., J. McGeehin, U.S.G.S.), providing a limiting age for the opening of the lava tube to the ground surface.

Deposition rates, particle size, and chemistry of the Holocene loess are similar to modern dust. The loess deposit ranges in age from ~7500 yr B.P. at the base to <2670 yr B.P. at the top, based on 7 OSL ages; all but one are in stratigraphic order. These ages combined with thickness yield a range of deposition rates averaging less than 3 g/m2/yr but with values of ~55 g/m2/yr near the base and <1 g/m2/yr at the top, with a secondary peak in deposition rate ~15 g/m2/yr from about 3500-3200 yr B.P. Modern dust rates over the last 30 years are 10–15 g/m2/yr. The loess exhibits a fining-upward pattern from basal sandy silt having a broad peak from 50-10 μm to very fine silt in the upper 30 cm having a double peak at 10 and 2 μm. All but the basal coarser loess is very similar in grain size distribution to modern dust. Carbonate and soluble-salt contents are typically <0.2% in the loess, but increase to about 0.7% in the upper 20 cm. However, modern dust has carbonate and salt contents of ~2% and 10%, respectively. This difference may suggest either that dust sources have changed since ~2000 yr B.P., or that soluble components are not completely retained in the loess. The elemental analyses also suggest differences in certain trace elements associated with anthropogenic emissions. These comparisons suggest that modern dust is generally a good analog for late Holocene loess, although the geochemistry of certain components may differ, and rates of deposition have varied by at least an order of magnitude during the past 7500 yr.

A review of the hydrological and geochemical evolution of Bristol Dry Lake

Michael R. Rosen
US Geological Survey, 2730 N. Deer Run Road, Carson City, NV 89701, mrosen@usgs.gov

Regional and surficial geologic surveys of Bristol Dry Lake have been performed since the early 1900s. The early studies suggested a connection between the Death Valley drainage and the Colorado River system at Ash Hill near Ludlow during the Late Pleistocene that could explain the similarity of fish species in rivers that are now hydrologically separated. However, recent investigations using mtDNA Divergence Time testing of desert pupfish supports a much older divergence in evolution, suggesting any hydrologic connection(s) must have existed greater than 3 mya (million years ago). The Divergence Testing agrees with stratigraphic data from 500 m long cores that indicate that Bristol Dry Lake has not been a deep lake for the past 3.65 my. The recent discovery of Bouse Formation sediments in one of the northern alluvial fans indicates that before 4

mya, Bristol Dry Lake may have been connected to the Colorado River system. However, there are no carbonate sediments, indicative of Bouse Formation, in a core collected from the margin of the basin that has a tephra age of 3.65 mya at 261 m depth with more than 200 m of alluvial sediment below it. Either Bouse Formation sediments are deeper than 500 m in the basin center and marginal core, or an alternative explanation (such as significant fault displacement, as is seen in the basin center core) for the presence of Bouse Formation sediment identified at the surface is needed.

The geochemical evolution of the basin has been the subject of considerable debate since Bristol Dry Lake was included as an end member of closed basin geochemical evolution on the "Eugster and Hardie" diagram. The Na–Ca–Cl brine, which is now mined for drilling fluids, is unusual for continental environments. One argument is that geothermal fluids are needed to create a brine of this composition; however, the basin is devoid of geothermal indicators. Another hypothesis is that during its change from an open (during Bouse Formation time) to closed (since at least 3.65 mya) system the chemical evolution of the water in the basin changed from Ca-rich Bouse Formation water to Na-rich closed basin water. This would indicate a possible mixed origin for the brine. Elevated Li concentrations, which generally indicate geothermal inputs, are also high (110 ppm Li) in Bristol Dry Lake. A simple Li/Cl ratio calculation demonstrates that if the lithium concentration were obtained solely from the evaporative concentration of meteoric groundwater, the concentration of that hypothetical source water would be between 0.11 and 0.025 ppm lithium. These values represent maximum values because there are no known lithium sinks, but the precipitation of halite is a major chloride sink. The calculated lithium value of the hypothetical source water is relatively low compared with many types of hydrothermal waters and the lower value is only slightly higher than the average value for North American rivers (0.003 ppm Li). Taking into account the massive chloride loss by the precipitation of halite, it seems possible that the lithium concentration of the brine was derived simply from the evaporation of meteoric or rain water flowing into the basin. The source of ions to the basin remains elusive and further study is warranted.

Debris flow deposits on Starvation Canyon Fan, Death Valley, California

Kelly Shaw
Department of Geological Sciences, California State University-Fullerton, Fullerton, CA 92834; kellyshaw524@csu.fullerton.edu. Faculty Advisor: Jeffrey Knott

Hunt and Mabey (1966, Fig. 48, pg. 67) mapped three debris flow lobes on the surface of the Starvation Canyon alluvial fan in western Death Valley, California with an estimated volume of 8 to 25 million cubic yards. These deposits were mapped on top of the fan indicating that they were younger than the ~70 ka Qg2 alluvial fan. In the source area, Tertiary volcanic rocks were mapped at the mouth of Starvation Canyon in the Panamint Range by Hunt and Mabey, with faulted Cambrian and Precambrian metasedimentary rocks to the west. The Precambrian Sterling Quartzite and Johnny Formations are composed of distinctive brown quartzite and purple shale. Granite at Hanaupah Canyon is 8.6 km upstream from the piedmont.

Field observations show that the northern lobe of the Qg2 deposits of the Starvation Canyon fan consists of grusified granite boulders at the surface. The debris flow deposits, which generally line a wash channel, are composed of 1-6 m diameter, varnished, but relatively unweathered, granite boulders with rare boulders of metasedimentary rock (<2%). The wash channel is incised through the Qg2 deposits with debris flow boulders overtopping the channel margins and resting atop the Qg2 deposits in the distal fan region. The southern lobe of the Starvation Canyon fan is composed of Qg3 gravels with an intervening active channel (Qg4). Both the younger and active channels are lined with large granite boulders (up to ~9 m diameter) that are unweathered with little, if any, varnish.

Based on my field observations, Hunt and Mabey were correct in their conclusion that younger, unweathered granite boulders from debris flows are found atop the Qg2 gravel. However, my observations are that the debris flow boulders are limited to the channel and channel margins. I infer that these deposits traveled along the incised channels and did not overtop the Qg2 gravels, aside from the area at the distal end of the fan. I infer that the flow volumes were significantly lower than previously thought and, based on the dominance (>98%) and size (up to ~9 m) of granite boulders these flows would have traveled

≤ 16 km before being deposited on the Starvation Canyon fan, with the origination point >8 km from the apex of the fan. My interpretation is that these debris flows were emplaced in multiple events rather than one large event. This is based on the differences in weathering of the boulders as well as the disconnected nature of the debris flow deposits. The active channel (Qg4) is composed of similar debris flow deposits as are found in the older channels. This would indicate that the same processes continued since ~70 ka with debris flows traveling 16 km down fan.

Identifying fossil logs in the Anza-Borrego Desert State Park

Tom Spinks
ABDSP paleontology volunteer, PO Box 2067, Borrego Springs, Ca. 92004 Tlspinks217@gmail.com

The Colorado Desert District Stout Research Center is the repository for paleobotany specimens collected in the Anza-Borrego Desert State Park (ABDSP), housing several hundred plant fossils, mostly tree stem material. In 2002, a study of the park's fossil logs (still in the field) was undertaken by students from the University of California, Riverside (UCR) to determine the paleo-ecological and paleo-environmental conditions that existed in the park some two to four and one half million years ago. Tasks carried out by the students included mapping where fossil logs are found, both geographically and stratigraphically, and taking samples, with the goal of identifying the kinds of trees found. The study located 77 fossil log sites whose geographic coordinates were recorded along with their relative position and orientation within the stratigraphic layers. Samples were taken from 24 of the fossil logs and thin-section slides were prepared to identify them. Work on the study ended in 2004 without being completed.

Earlier work identifying woods in the ABDSP was carried out by Park Ranger Paul Remeika. He reported at least eight different fossil wood taxa with the common names fan palm, buckeye, walnut, bay laurel, avocado, ash, cottonwood, willow, and a softwood cedar or juniper.

The UCR fossil wood study was recently revived by paleontology volunteer Tom Spinks. The previously prepared fossil log thin-sections were examined and photographed using a 50X Aven light reflecting microscope. Four of the 24 samples were identified to the family and genus level. The common names of the identified fossil trees are bay laurel, ash, walnut-type, and avocado. The new identifications support previous descriptions of the flora in this area during the Pliocene epoch.

Future work on this project includes resampling the known fossil logs, evaluation of the physical changes that have occurred to them over the last 12 years, discovery and recording of newly exposed fossil logs, and development of a map showing the distribution of various tree taxa throughout the stratigraphic record of ABDSP.

Monitoring reptile habitat preference in the East Mojave, Soda Springs area

Jason K. Wallace
CSU Desert Studies Center, jwallace@fullerton.edu

Limited quantitative data exist regarding the relative abundance and habitat associations of reptiles. The purpose of this research is to determine the effects of seasonal changes and environmental conditions on the abundance, diversity, and habitat preference of the desert reptiles residing in the East Mojave, Soda Springs area. A grid of 129 pitfall traps covering 55,000 sq meters of an alluvial fan, divided into four distinct habitat types, was used to capture reptiles. Data collected once per month over three collection periods were combined for this study (June 1991–May 1993, January 2000–December 2001, and January 2008–December 2013). Of the 20 total reptile species captured, eight were abundant enough to conduct a habitat utilization analysis. Of these eight, seven had uneven distributions. *Uta stansburiana* was the only species captured evenly across the entire trap grid. Most individual reptiles were captured in habitat type # 3 (compacted sand with small rocks; 37.1 %), more specifically in rows 11-15 (21.3 %). Results suggest the resident reptiles partition the resources available to them, at least in part, by habitat preference. Although unevenly distributed, spatial overlap between species did occur. When taking all 20 species into account, the most spatial overlap occurred in habitat type # 3 (s = 13). Recognition of natural habitats that possess characteristics suitable for many different species is very important, especially in the age of large-scale replacements of diverse natural ecosystems with less diverse managed systems. Long term, on-going data sets are important for further understanding of reptile community

dynamics. They are necessary for the effective management of land and resources and helpful for making more informed decisions ultimately assisting in the maintenance of biodiversity.

The Ash Meadows Fish Conservation Facility

Darrick Weissenfluh[1], Olin Feuerbacher[1], Lee Simons[1], and Ambre Chaudoin[2]
[1]U.S. Fish and Wildlife Service, Ash Meadows Fish Conservation Facility; [2]The Great Basin Institute, Ash Meadows Fish Conservation Facility, C/O Ash Meadows NWR, HCR 70, BOX 610Z Amargosa Valley, Nevada 89020-9632, Presenter Email**:** *chaudoin@email.arizona.edu*

The Ash Meadows Fish Conservation Facility (AMFCF) exists to help conserve imperiled aquatic species, in particular the endangered Devils Hole pupfish *Cyprinodon diabolis.* Recent lows in the *C. diabolis* population and a lack of backup populations of this species prompted the U.S. Fish and Wildlife Service, with support from numerous partners, to secure funds through the Southern Nevada Public Lands Management Act (SNPLMA) to construct the AMFCF. This state-of-the-art facility includes a propagation room with multiple recirculating aquaria systems, and a 100,000-gallon refuge tank that emulates the Devils Hole environment. The refuge tank can deliver a wide range of precisely controlled water parameters. Natural substrate resembling what is found in Devils Hole covers a shallow spawning/feeding shelf in the refuge tank. The water above this shelf is maintained at depths similar to historical (pre-pumping) levels in Devils Hole. Algae and invertebrates collected from Devils Hole are cultured in the facility's propagation room and stocked into the refuge tank; these organisms are also fed to captive larval and juvenile Devils Hole pupfish. Recovery efforts at the AMFCF have focused on collection of *C. diabolis* eggs from Devils Hole to propagate at the AMFCF, and establishment of Devils Hole invertebrate and algae cultures to create a biological community capable of sustaining *C. diabolis* in the refuge tank. The facility currently has 30 Devils Hole pupfish; all but one were hatched from eggs collected from Devils Hole during November 2013 and January 2014. AMFCF staff is currently focused on producing additional generations of pupfish in captivity. Given the wild population's precarious status, our goal is to establish two refuge populations of *C. diabolis* in systems capable of maintaining selection pressures similar to those found in Devils Hole.

—Notes—